DEPARTAMENTO DE ASTROFÍSICA

Universidad de La Laguna

Searching for and characterising the high redshift star-forming galaxy population in the early Universe

Memoria que presenta
D. Pablo Arrabal Haro
para optar al grado de
Doctor por la Universidad de La Laguna.

Trabajo dirigido por Dr. José Miguel Rodríguez Espinosa
y codirigido por Dra. Casiana Muñoz Tuñón

INSTITUTO Đ ASTROFISICA Đ CANARIAS
noviembre de 2019

Examination date: December, 2019
Thesis supervisors: Dr. José Miguel Rodríguez Espinosa and Dra. Casiana Muñoz Tuñón

Part of the material included in this document has been published in *Monthly Notices of the Royal Astronomical Society.*

Dedicado a Masco, Drugo, Lourdes, Mamua y Papua.
Ya quisieran mis galaxias brillar como lo hacéis vosotros.

Resumen

Caracterizar las propiedades de las galaxias a alto z en diferentes épocas cosmológicas es crucial para arrojar luz sobre cómo las primeras galaxias se formaron y evolucionaron, ayudando a trazar la historia del Universo a lo largo del tiempo cósmico. Esta tesis se centra en el estudio de LAEs y LBGs a z = 3.4-6.8, un periodo de tiempo entre $\sim$ 0.8-2 Gyr después del Big Bang, el cual alberga el fin de la época de la reionización. Para llegar tan profundo, hemos hecho uso del cartografiado SHARDS del campo GOODS-N, de 200 h de tiempo de exposición con GTC. Los 25 filtros consecutivos de banda media en el óptico/NIR nos han proporcionado muy buenas SEDs de estas galaxias, que hemos complementado con datos auxiliares de otras observaciones profundas previamente realizadas en el campo, permitiendo un exhaustivo análisis de ellas.

En la primera parte de este trabajo, desarrollamos sólidos criterios de selección propios, prestando especial atención al descarte de objetos intrusos. La muestra final consta de 1558 fuentes, divididas en 528 LAEs y 1030 no-LAEs/LBGs. La comparación de esta muestra con estudios previos de banda ancha ha revelado que estos últimos son propensos a introducir una cantidad no despreciable de intrusos de bajo redshift debido a la carencia de buena resolución espectral en sus SEDs. De las SEDs de nuestra muestra, hemos derivado redshifts fotométricos, EWs de Lyα, SFRs y LFs.

Con objeto de calcular edades y masas estelares de nuestras galaxias, hemos llevado a cabo un modelado de las SEDs mediante síntesis de poblaciones estelares, usando SFHs de tipo brote de formación estelar. El análisis de poblaciones estelares se centra en las diferencias entre subfamilias de LAEs y LBGs, así como en la necesidad de una o dos SPs para adecuadamente describir cada SED. Los resultados derivados del ajuste de modelos, unidos a la proporción relativa de cada subfamilia encontrada en este trabajo a cada z, apoya una relación evolutiva de LAEs de baja masa a LBGs más masivos. Con las masas derivadas de los modelos, hemos obtenido SMFs y estimado la SMD a diferentes redshifts.

También hemos llevado a cabo una búsqueda de galaxias próximas entre sí formando grupos, reportando 92 de ellos, algunos con hasta seis miembros. Muchos de estos grupos muestran estructuras en forma de cola que apuntan a una ligadura gravitacional entre sus galaxias. Además, hemos estudiado una sobredensidad a $z = 5.198 \pm 0.015$ previamente descubierta en el campo de GOODS-N, encontrando 44 nuevos candidatos dentro de nuestra muestra. Algunos de ellos han sido confirmados a través de observaciones MOS.

Si la mayoría de los nuevos candidatos que quedan son confirmados, este protocúmulo sería el más poblado hasta la fecha más allá de $z = 5$ en un rango de redshift tan ajustado.

La parte final de esta tesis está dedicada a un agrupamiento no supervisado de las SEDs usando métodos de ML, tanto de nuestra muestra como de la muestra de LAEs a alto redshift SC4K-COSMOS. Los resultados apuntan a la línea de Lyα y a la pendiente UV como los parámetros que más relevantemente condicionan la diferenciación entre clases, separando fuentes con emisión Lyα fuerte y pendiente UV azul de aquellas con pendiente más empinada y línea de emisión más débil. El estudio de las edades y masas estelares medias de los grupos apoya la hipótesis evolutiva entre subgrupos de LAEs y LBGs. Además, la clasificación con ML ha mostrado ser muy efectiva para la detección de algunos pocos intrusos que aún quedaban en ambas muestras.

Abstract

Characterising the properties of high-z galaxies at different cosmological epochs is crucial to shed light on how the first galaxies formed and evolved, helping to trace the history of the Universe over cosmic time. This thesis focuses on the study of LAEs and LBGs at $z = 3.4$-6.8, a period of time between ~ 0.8-2 Gyr after the Big Bang, hosting the end of the reionisation epoch. To reach such deep galaxies, we have made use of the SHARDS survey of the GOODS-N field, with 200 h of exposure time with GTC. The 25 consecutive medium-band filters in the optical/NIR have provided us with very good SEDs of these galaxies, which we have further completed with ancillary data from other previous deep observations of the field, allowing a comprehensive analysis of the SEDs.

In the first part of this work, we develop our own robust selection criteria, paying special attention to the interlopers rejection. The final selected sample consists of 1558 sources, divided in 528 LAEs and 1030 non-LAEs/LBGs. The comparison of this sample with previous broad-band studies has revealed that the latter are prone to introduce a non-negligible amount of low redshift interlopers due to the lack of good spectral resolution in their SEDs. From the SEDs in our sample, we have derived photometric redshifts, Lyα EWs, SFRs and LFs.

In order to calculate ages and stellar masses of our galaxies, we have carried out a SP synthesis modeling of the SEDs, using burst-like SFHs. We focus the SP analysis on differences between subfamilies of LAEs and LBGs, as well as on the need of one or two SPs to properly describe each SED. The results derived from the model fitting, joined to the relative fraction of each subfamily found at each z in this work, support an evolutionary relation from low mass LAEs to more massive LBGs. With the model-derived masses, we have built SMFs and estimated the SMD at different redshifts.

We have also performed a search for galaxies in close groups, reporting 92 of them, some with up to six members. Many of these groups show tail-like structures that point to a gravitational bound between their galaxies. Additionally, we have studied a previously discovered $z = 5.198 \pm 0.015$ overdensity in GOODS-N, finding 44 new candidates within our sample. Some of them have been further confirmed through MOS observations. If most of the remaining new candidates are confirmed, this proto-cluster would be the most populated one up to date beyond $z = 5$ in such a tight redshift range.

The final part of this thesis is dedicated to an unsupervised ML SEDs clustering of both our sample and the SC4K-COSMOS high-z LAEs sample. The results point to the Lyα line and the UV slope as the most relevant parameters

driving the classes differentiation, separating sources with strong Lyα emission and blue UV slope from those with steeper slope and fainter line emission. The study of the median ages and stellar masses of the groups supports the evolutionary hypothesis between LAEs and LBGs subgroups. Moreover, the ML classification has shown to be very effective for the detection of some few remaining interlopers in both samples.

Contents

List of Figures

List of Tables

Acronyms

ACS - *Advanced Camera for Surveys*
AGN - *Active Galactic Nuclei*
BAL - *Broad Absorption Line*
CANDELS - *Cosmic Assembly Near-infrared Deep Extragalactic Legacy Survey*
CCD - *Charge-Coupled Device*
CFHT - *Canada-France-Hawaii Telescope*
CIGALE - *Code Investigating GALaxy Emission*
CMB - *Cosmic Microwave Background*
CWL - *Central Wavelength*
DSP - *Double Stellar Population*
EAZY - *Easy and Accurate Redshifts from Yale*
EM - *Expectation-Maximisation*
EoR - *Epoch of Reionisation*
EW - *Equivalent Width*
FIR - *Far Infrared*
FOV - *Field Of View*
FWHM - *Full Width at Half Maximum*
GALEX - *GALaxy Evolution eXplorer*
GM - *Gaussian Mixture*
GOODS-N - *Great Observatories Origins Deep Survey-North*
GTC - *Gran Telescopio Canarias*
HST - *Hubble Space Telescope*
IGM - *Intergalactic Medium*
IMF - *Initial Mass Function*
INT - *Isaac Newton Telescope*
IPAC - *Infrared Processing and Analysis Center*
IR - *Infrared*

IRAC - *Infrared Array Camera*
IRAF - *Image Reduction and Analysis Facility*
ISM - *Interstellar Medium*
JWST - *James Web Space Telescope*
ΛCDM - *Λ-Cold Dark Matter*
LAE - *Lyman Alpha Emitter*
LBG - *Lyman Break Galaxy*
LePHARE - *PHotometric Analysis for Redshift Estimate*
LF - *Luminosity Function*
LSST - *Large Synoptic Survey Telescope*
MAGPHYS - *Multi-wavelength Analysis of Galaxy PHYSical properties*
MIR - *Medium Infrared*
ML - *Machine Learning*
MOIRCS - *Multi-Object Infrared Camera and Spectrograph*
MOS - *Multi-Object Spectroscopy*
NASA - *National Aeronautics and Space Administration*
NED - *NASA/IPAC Extragalactic Database*
NIR - *Near Infrared*
NOAO - *National Optical Astronomy Observatory*
OB - *Observing Block*
OSIRIS - *Optical System for Imaging and low-intermediate-Resolution Integrated Spectroscopy*
OVV - *Optically Violent Variable*
PEARS - *Probing Evolution And Reionization Spectroscopically*
PDF - *Probability Distribution Function*
QSO - *Quasi-Stellar Object*
SC4K - *Slicing COSMOS with 4K LAEs*
SED - *Spectral Energy Distribution*
SFH - *Star Formation History*
SFR - *Star Formation Rate*
SFRD - *Star Formation Rate Density*
SHARDS - *Survey for High-z Absorption Red and Dead Sources*
SMBH - *Supermassive Black Hole*
SMD - *Stellar Mass Density*
SMF - *Stellar Mass Function*
SMG - *Sub-Millimeter Galaxy*
S/N - *Signal-to-Noise ratio*
SP - *Stellar Population*
SSP - *Single Stellar Population*
TKRS - *Team Keck Treasury Redshift Survey*

TOPCAT - *Tool for OPerations on Catalogues And Tables*
UV - *Ultraviolet*
VIRCAM - *VISTA Infrared CAMera*
VISTA - *Visible and Infrared Survey Telescope for Astronomy*
WFC3 - *Wide Field Camera 3*
WIRCam - *Wide-field Infrared Camera*

1

Introduction

Mi historia comienza en mil novecientos diquitidós. Decimos "diquiti" a raíz de que el káiser nos robara la palabra "veinte". Yo fui tras el rufián para recuperarla, pero me rendí al cabo de diquitiseis kilómetros.
Abe Simpson (The Simpsons).

This first chapter contains a general introduction to the cosmic period in which this research is framed, presenting some of the main topics studied. It shows an overview of the history of the Universe, paying special attention to the different types of high-z galaxies, as well as to the most relevant physical parameters that lead us to an understanding of the high-z Universe. In the final section, we present the outline of this thesis.

Understanding the history of our Universe since its origin at the Big Bang, 13.8 billion years ago, until the galaxies we see nowadays has been one of the major scientific goals of modern astrophysics during the last century. Thanks to a plethora of comprehensive studies, astrophysicists have been able to trace a detailed path of the life of the Universe. In particular, the Λ-Cold Dark Matter model (ΛCDM) has become the most widely accepted cosmological model, as it is capable of explaining the observed accelerated expansion of the Universe thanks to the inclusion of the dark energy cosmological constant Λ (Riess et al. 1998; Perlmutter et al. 1999). This cosmological model also provides a successful explanation of the observed large-scale distribution of galaxies in voids and filaments forming the so-called "cosmic web" (Jõeveer et al. 1978; Geller & Huchra 1989).

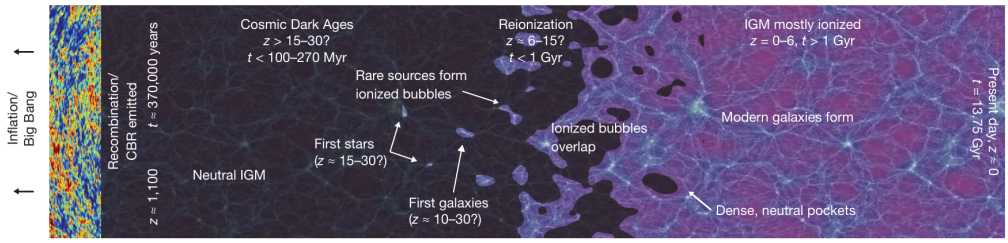

Figure 1.1: Image from Robertson et al. (2010) showing an overview of the history of the Universe from recombination to our days.

The chronology of the Universe up to our days can be divided in four main stages according to the state of the Universe in each of them. The first of these epochs corresponds to only the first few 10^{-12} s after the creation of matter and space-time in the Big Bang. This extremely short period of time encompasses the emergence of the four known fundamental interactions (gravitational, strong, weak and electromagnetic, in that order) from a single unified force (Ryden 2003), as well as the cosmic inflation (Guth 1981), *i.e.*, an extreme enlargement of the metric scale, understood as the size and geometry of space-time itself.

The first long step of the Universe would last from the end of the cosmic inflation era to $\sim$ 380 000 years after the Big Bang. This epoch is known as the "hot Universe". It started as an extremely dense and hot plasma, composed of leptons and quarks too energetic to combine into hadrons. However, the expansion of the Universe cooled down this plasma, allowing the formation of the first protons and neutrons (Allday 2002). Between $\sim$ 2-20 min after the Big Bang, the pressure and temperature of the Universe had gone down enough to allow nuclear fusion, leading to the formation of the first nuclei of hydrogen, helium and lithium in a process called "Big Bang nucleosynthesis" (Karki 2010; Kusakabe et al. 2014). Nonetheless, the temperature of the Universe at this point was still too high to allow the combination of electrons with nuclei or protons. Thus the Universe was fully ionised, and photons could only travel very short distances before interacting with ionised particles. Indeed, the Universe was opaque.

By $\sim$ 380 000 years after the Big Bang ($z \sim 1100$) the temperature had cooled sufficiently ($T \sim 4000$ K) to allow the combination of electrons and protons in what we call the "recombination era" (Peebles 1968; Zeldovich et al.

1968). This event quickly turned the Universe into neutral, drastically increasing the distances that photons could travel with very little scattering. This primordial radiation is the Cosmic Microwave Background (CMB), that nowadays is seen in the $\lambda \sim$ 1-2 mm range, due to the expansion of the Universe, equivalent to a $T \sim 2.73$ K black body emission (Penzias & Wilson 1965).

The recombination defines the beginning of the "dark ages", an epoch where, even though the Universe is neutral and transparent to radiation, there are not light-emitting objects yet (Loeb 2010). The first stars ever formed would then appear through gravitational collapse of baryonic matter inside previously collapsed dark matter halos (Silk 1977; Couchman & Rees 1986; Tegmark et al. 1997). These first stars are the so-called Population III stars. They were made of only hydrogen and helium, and they were the first objects producing ionising photons, thus starting the transition to the Epoch of "Reionisation" (EoR).

The EoR of the Universe is a specially interesting period of time, although not completely understood yet. The current belief is that the first generation of stars and galaxies formed when the Universe was $\sim$ 250 Myr old (Hashimoto et al. 2018), starting the ionisation of the Intergalactic Medium (IGM), which was a continuous process (Robertson et al. 2010; Finkelstein 2016). The prevailing theory is that the reionisation started as an inside-out phenomenon in which overdense regions of galaxies created large H II bubbles. These bubbles would expand and merge until eventually reionise the entire IGM (Barkana & Loeb 2001; Iliev et al. 2006; Alvarez et al. 2009). Currently, the accepted idea is that the bulk of ionising photons, causing the reionisation, proceeded from the star-forming galaxies at this epoch of the Universe (Stiavelli et al. 2004; Richards et al. 2006; Ouchi et al. 2009; Robertson et al. 2010; Bouwens et al. 2011; Finkelstein et al. 2012; Robertson et al. 2013; Bouwens et al. 2015; Finkelstein et al. 2015), although a possible non-negligible contribution from accreting Supermassive Black Holes (SMBHs) has also been proposed (Giallongo et al. 2015; Madau & Haardt 2015). Simulations and measures of H I absorption in distant quasar and gamma-ray burst spectra indicate that the reionisation of the Universe was completed at $z \sim$ 5.5-6 (Fan et al. 2002, 2006,b; Kawai et al. 2006; Becker et al. 2015; Inoue et al. 2018). From this point in cosmic time ($\sim$ 1 Gyr after the Big Bang), the Universe evolved in an almost fully ionised IGM until our days. Fig. 1.1 shows an overview of the chronology of the Universe.

1.1 Types of high-z galaxies

In the search for high-z galaxies, many diverse surveys have been carried out over the last decades. These works have been focused at different spectral

regions, from X-rays to radio. Depending on their internal properties and on the way they are selected, high-z galaxies can be divided as follows:

1.1.1 Lyman break galaxies

Lyman Break Galaxies (LBGs) is a term used to define those galaxies detected through the so-called Lyman-break technique (Guhathakurta et al. 1990; Steidel & Hamilton 1992, 1993; Steidel et al. 1995). This method relies in the identification of the Lyman break, an emission drop present at $\lambda = 912$ Å, corresponding to the ionisation energy of the hydrogen atom in the ground state. This emission drop is expected to be very strong in young galaxies due to interstellar H I absorption. Moreover, at the highest redshifts, the denser H I clouds produce Lyman-α (Lyα, 1216 Å) absorption resulting in a thick Lyα forest which affects the galaxy continuum in the wavelength range between $\lambda = 912$-1216 Å . This Lyα forest is so optically thick at very high-z, that it erases virtually all the galaxy emission blue-ward of Lyα in what is known as the Gunn-Peterson trough (Gunn & Peterson 1965; Rauch 1998; Fan et al. 2006c; Dunlop 2013). Taking advantage of the strong Doppler redshift effect in high-z galaxies, it is possible to measure their Lyman break in the optical and Near Infrared (NIR).

LBGs have traditionally been detected using broad-band filters (see, *e.g.*, Steidel et al. 2003; Giavalisco et al. 2004; Steidel et al. 2005; Iwata et al. 2007; McLure et al. 2009; Oesch et al. 2010; van der Burg et al. 2010; Ellis et al. 2013; Bouwens et al. 2014, 2015b; Laporte et al. 2016, among others). Observations using this kind of filters look for objects that appear in subsequent filters but suddenly disappear in the bluest filters, corresponding to the measurement of the Lyman break. Because of their detection through this emission drop, LBGs also receive the name of "drop-out" sources.

In addition to the emission drop detection, the colour between the filters in which the source is detected is also taken into account to favour the selection of galaxies presenting blue colours, as those are associated to young star-forming galaxies, expected to present low dust content at high redshift (Bouwens et al. 2009, 2010; Zafar et al. 2010; Dunlop et al. 2012; Finkelstein et al. 2012b; Schaerer et al. 2015). An example of a broad band colour selection criteria for high-z LBGs is shown in Fig. 1.2.

The big advantage of the broad-band colour selection is that it can be easily applied to large surveys, identifying candidates that are further explored with spectroscopic observations (*e.g.*, Giavalisco et al. 1994; Shapley et al. 2003). The drawback of this method comes from the low number of filters typically used and its large width, which translates in not very precise photometric

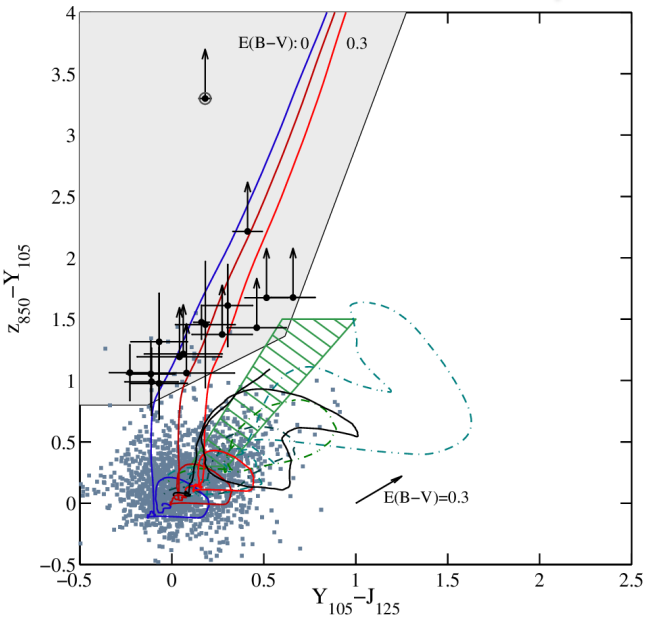

Figure 1.2: Figure from Oesch et al. (2010) showing the colour-colour diagram used for the selection of $z \sim 7$ drop-out galaxies with *HST* broad-band data. The eligible area is represented in grey. The solid and dashed lines show tracks for different types of galaxies with different obscurations.

redshift calculations ($\Delta z \sim$ 0.1-0.2). In any case, the Lyman break technique has been one of the most efficient ways of finding these high-z galaxies, specially after the launch of the *Hubble Space Telescope* (*HST*) and the development of the Advanced Camera for Surveys (ACS) and the Wide Field Camera 3 (WFC3), which allowed the acquisition of very deep optical and NIR images with an excellent spatial resolution.

The study of these sources over the last thirty years revealed that high-z LBGs are the most frequent type of star-forming galaxies in the early Universe (Dunlop 2013), with typical Star Formation Rates (SFRs) of the order of $\sim$ 10-100 $M_{\odot}$ yr^{-1} and stellar masses ($M_{\rm star}$) of $M_{\rm star} \sim 10^{9}$-10^{10} $M_{\odot}$ (Shapley et al. 2003; Erb et al. 2006; Stark et al. 2009; González et al. 2011; Duncan

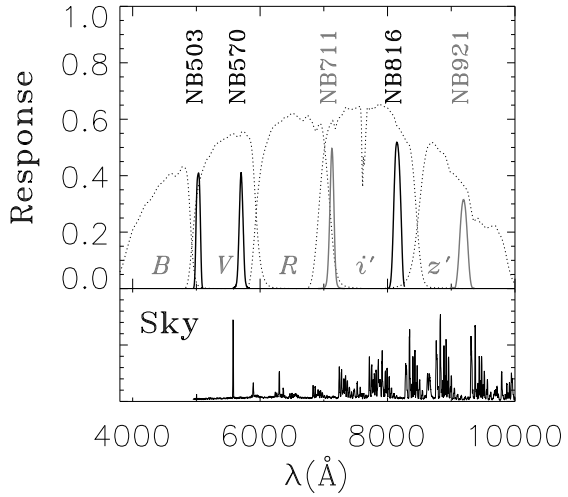

Figure 1.3: Figure from Ouchi et al. (2008) showing a narrow band configuration to detect LAEs at five different redshifts between $z = 3.1$-5.7. The upper panel presents the transmission curves of the narrow bands (solid line profiles) and the complementary broad bands (dotted line profiles). The lower panel shows a sky spectrum. Note how the narrow-band filters are specifically fitted in the gaps between sky lines.

et al. 2014; Grazian et al. 2015; Salmon et al. 2015; Song et al. 2016; Stefanon et al. 2017, among others). Finally, the size of high-z LBGs is really small in comparison with galaxies of the local Universe, with the former showing radii of only $r_{\rm eff} \sim$ 1-2 kpc (*e.g*, Bouwens et al. 2004; Oesch et al. 2010; Ono et al. 2013; Shibuya et al. 2015; Curtis-Lake et al. 2016; Ribeiro et al. 2016; Liu et al. 2017).

1.1.2 Lyman alpha emitters

Lyman Alpha Emitters (LAEs) are star-forming galaxies that present the Lyα line in emission, as their name claims. The usual method to detect these

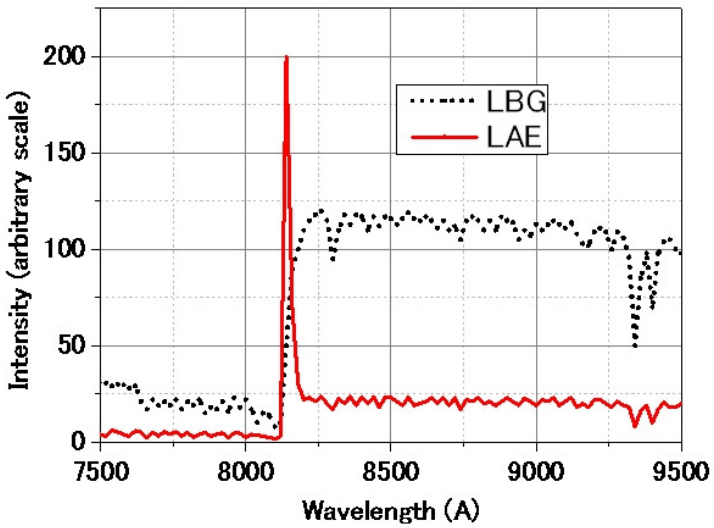

Figure 1.4: Figure from Iye (2011) showing the typical spectra of a LAE (red solid line) and a LBG (black dotted line) at an assumed $z \sim 5.7$.

galaxies is through the use of narrow-band filters (Hu et al. 1998; Rhoads et al. 2000; Ouchi et al. 2003; Malhotra & Rhoads 2004; Taniguchi et al. 2005; Iye et al. 2006; Gronwall et al. 2007; Murayama et al. 2007; Ouchi et al. 2008, 2010; Cassata et al. 2015; Matthee et al. 2015; Santos et al. 2016; Matthee et al. 2017; Sobral et al. 2017, 2018; Sobral & Matthee 2019, among others). This technique usually employs complementary broad-band filters. The comparison of the emissions detected in the narrow-band with the broad band sampling a similar wavelength makes it possible to identify emission excesses in the narrow band corresponding to the line emission. Furthermore, the search for very high-z LAEs ($z \gtrsim 4.5$) needs to carefully consider the wavelength window of the narrow bands, since the Lyα line of these objects is redshifted beyond $\lambda_{\rm obs} \sim 7000$ Å, where the sky is full of emission lines from atmospheric OH. Fig. 1.3 shows an example of a narrow band survey design.

One of the disadvantages of the classical narrow band technique is the contamination from other emission lines at lower redshifts which can only be sorted

out with additional broad-band observations or spectroscopy (Dunlop 2013). In addition, the comoving volume sampled with this method is quite small as the redshift measured with each narrow-band filter is very specific. On the other hand, the major advantage of the narrow-band technique is the capability of detecting faint continuum sources through their line emission, which otherwise would be much more difficult to detect employing the Lyman-break technique.

As LBGs, high-z LAEs are also very small galaxies, with radii of the order of $r_{\rm eff} \sim 1$ kpc (Bond et al. 2009, 2012). LAEs and LBGs are indeed very similar galaxies, their difference being mostly due to the way they are detected. LAEs are typically fainter and bluer in the ultraviolet (UV) than broad-band selected LBGs. LAEs also show lower dust content and metallicities (Finkelstein et al. 2011; Ono et al. 2012; Schaerer et al. 2015). Regarding their stellar mass, the narrow-band technique allows the detection of faint continuum sources with strong Lyα emission, which is typically associated to low masses. Indeed LAEs have masses in the range $M_{\rm star} \sim 10^8$-10^9 (Gawiser et al. 2007; Ono et al. 2010; Hagen et al. 2014). Finally, the conspicuous Lyα emission line present in LAEs is due to the strong emission produced by massive O and B type stars, and it is therefore associated to young stellar populations (SPs). A visualisation of a typical LAE and LBG spectra can be seen in Fig. 1.4.

1.1.3 Active galactic nuclei

Active Galactic Nuclei (AGN) are extremely luminous galaxies in which most of the energy is not emitted by stars, but it is produced through accretion of matter into a central SMBH (Rees 1984). These objects were first found in the form of low redshift Seyfert galaxies thanks to the identification of broad emission line profiles (Seyfert 1943). Depending on their emission in the radio region of the electromagnetic spectrum, these galaxies can be divided in radio-quiet and radio-loud AGNs, the latter typically presenting conspicuous emission jets aligned with the rotation axis of the SMBH (Penrose 1969; Hirotani et al. 2000). Independently, AGN are also separated in Type 1 or Type 2, depending on whether they present broad or narrow emission lines, respectively.

Among the AGNs family, we find the Quasi-Stellar Objects (QSOs or quasars; Matthews & Sandage 1963), whose name originally came from their stellar-like aspect in the optical. Quasars have played a key role in the estimations of the end of the reionisation epoch through the spectroscopic identification of the Gunn-Peterson effect blue-ward of the Lyα line (Fan et al. 2002, 2006,b; Kawai et al. 2006; Becker et al. 2015). Obtaining high quality spectroscopy of these objects at $z \gtrsim 6$ is only possible because of their extremely high intrinsic luminosity. Fig. 1.5 shows the spectrum of a $z = 7.05$ quasar found

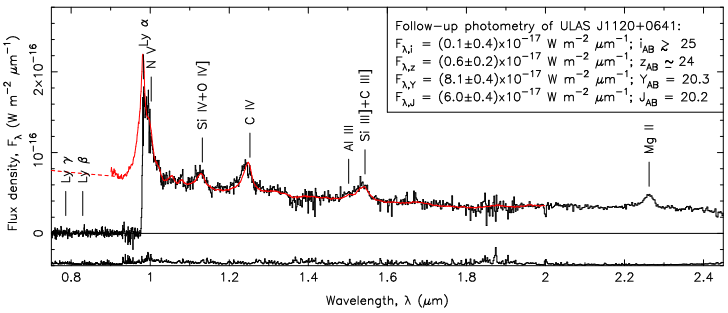

Figure 1.5: Figure from Mortlock et al. (2011) showing the spectrum of a $z = 7.085$ quasar (upper black solid line). The lower black solid line shows the 1σ noise, and the red line corresponds to a composite spectrum of a $z \sim 2.5$ quasar. Note that the extreme Gunn-Peterson trough erases any emission between the Lyman break (912 Å) and the Lyα line (1216 Å), indicating a not yet reionised IGM.

by Mortlock et al. (2011).

Apart of the already mentioned AGNs, there are other subgroups like the Broad Absorption Line quasars (BAL quasars; Weymann et al. 1991; Gibson et al. 2009; Liu et al. 2015) or the blazars, objects with quick variability and polarised optical emission that can as well be split into Optically Violent Variable quasars (OVV quasars; Kuhr et al. 1983; Webb et al. 1990; Ghisellini et al. 2009) and BL Lac objects (*e.g.*, Padovani & Giommi 1995; Urry et al. 2000).

Despite all the different type of AGNs, several studies over the past decades have claimed the unification of the AGN family (Rowan-Robinson 1977; Lawrence & Elvis 1982; Barthel 1989; Antonucci 1993; Urry & Padovani 1995, among others). According to this theory, the differences observed between different AGN subclasses, such as the appearance of broad or narrow lines, or the presence or absence of jets, could be simply explained in terms of the relative angle of observation respect to the accretion disk. However, in the last years many works have also appeared that put this unification theory to debate, claiming the existence of real internal differences in the nature of some AGN subgroups, driven by parameters like the mass accretion rate into the SMBH (*e.g.*, Tran 2001; Wu et al. 2011; Wang et al. 2012; Villarroel et al. 2017), leaving the AGN unification as a still open question.

1.1.4 Sub-millimeter galaxies

Sub-millimeter galaxies (submm galaxies or SMGs) receive their name from the spectral wavelength used for their detection. These are strongly dust obscured objects where the dust thermal emission is detected in the mm/sub-mm range. They were discovered more recently (Smail et al. 1997; Barger et al. 1998; Hughes et al. 1998; Ivison et al. 1998) and modern measurements have shown that these galaxies host the strongest starbursts known, with SFRs up to the order of 10^3 $M_\odot$ yr^{-1} (Casey et al. 2014; Riechers et al. 2014; Oteo et al. 2016; Casey et al. 2017).

SMGs are a very unusual type of galaxies, with a space density much lower than that of LAEs and LBGs at high-z. Because of this rarity and their spectral behaviour, there is the hypothesis that these sources experiment short but extremely intense starburst (Greve et al. 2005; Daddi et al. 2007) that quickly enrich their Interstellar Medium (ISM), rising the dust content and making them undetectable in the rest-frame UV and optical wavelengths. The nature of the mechanism driving such a strong SFR is yet uncertain (Swinbank et al. 2008; Michałowski et al. 2012; Narayanan et al. 2015). One hypothesis is that this violent SFRs are caused by galaxy mergers, as has been found for many SMGs at high-z (Capak et al. 2008; Ivison et al. 2013; Messias et al. 2014; Oteo et al. 2016; Riechers et al. 2017; Marrone et al. 2018, among others). On the other hand, other works based on theoretical simulations (*e.g.*, Dekel et al. 2009; Narayanan et al. 2015) propose that high SFRs in SMGs are triggered by infall of a combination of cold gas and previously ejected gas.

Most of the flux from SMGs is directly related with the absorption by dust of the UV emission from young stars. The strong dust extinction of these sources makes them impossible to detect at the rest-frame UV (Dunlop 2013). Further study of these sources at high-z in upcoming years is very important to build a complete idea of the early evolution of galaxies.

1.2 Galaxy evolution with cosmic time

The improvement of high-z observations over the past decades has meant a revolution in our view of galaxy evolution since the "dark ages" until the large variety of galaxies that we see nowadays. Thanks to numerous deep galaxy observations along different cosmic times, we are able to set robust constrains on the galaxy number density in terms of their stellar mass and luminosity, or the star formation density at each epoch of the Universe.

1.2.1 Luminosity function

The Luminosity Function (LF) is the measure of the number density of galaxies per comoving volume unit as a function of the luminosity. It can be built in terms of certain emission line luminosities or, more commonly at high-z, in terms of the rest-frame UV emission at $\lambda \sim 1500$ Å. The usual shape of the LF is modeled by the combination of an exponential term in the so-called bright-end and a potential term in the so-called faint-end. The absolute magnitude or luminosity at which the transition from one term to the other occurs is the characteristic M^* or L^*. This way of modeling the LF can be expressed in the Schechter (1976) form for both luminosity and absolute magnitude:

$$\phi(L) = \phi^* \exp(-L/L^*)(L/L^*)^{\alpha}, \tag{1.1}$$

$$\phi(M) = \phi^* \frac{\ln(10)}{2.5} \exp[-10^{0.4(M^*-M)}] 10^{0.4(M^*-M)(\alpha+1)}, \tag{1.2}$$

where ϕ is the number density at certain L or M, and ϕ^* is a normalisation factor corresponding to the characteristic number density, which measures the overall galaxy number density.

Besides providing an idea of the density of these sources at each cosmic time, the comparison of LFs with theoretical halo models is crucial for understanding how stars are formed from gas at high-z. Previous studies have shown that the observed baryonic LFs fall behind the theoretical halo ones at both the bright and faint luminosities, while being similar at the L^* knee (see Finkelstein 2016). This discrepancy suggests that the conversion of gas into stars is less efficient in those L ranges than at L^*. One hypothesis is that the discrepancies between LFs and halo models are associated to negative feedback effects produced mostly by supernovae at the faint-end and AGN SMBH accretion at the bright-end (see, *e.g.*, Somerville & Davé 2015). This feedback can heat or expel the gas of the galaxy, quenching star formation. Since these physical processes can affect the shape of the LFs, the study of the variation of this function with z is crucial to constrain these processes. Additionally, the integration of the UV LFs allows us to calculate the SFR density (SFRD), *i.e.*, the ratio at which stars are formed per unit of comoving volume, which will be further introduced in Sec. 1.2.3.

A large amount of works have recently studied the UV LF at high-z (Bouwens et al. 2007; Iwata et al. 2007; McLure et al. 2009; Castellano et al. 2010; van der Burg et al. 2010; McLure et al. 2013; Schenker et al. 2013; Tilvi et al. 2013; Oesch et al. 2014; Bowler et al. 2015; Bouwens et al. 2015b; Finkelstein et al. 2015; McLeod et al. 2015, 2016; Livermore et al. 2017; Pelló et al. 2018; Ono

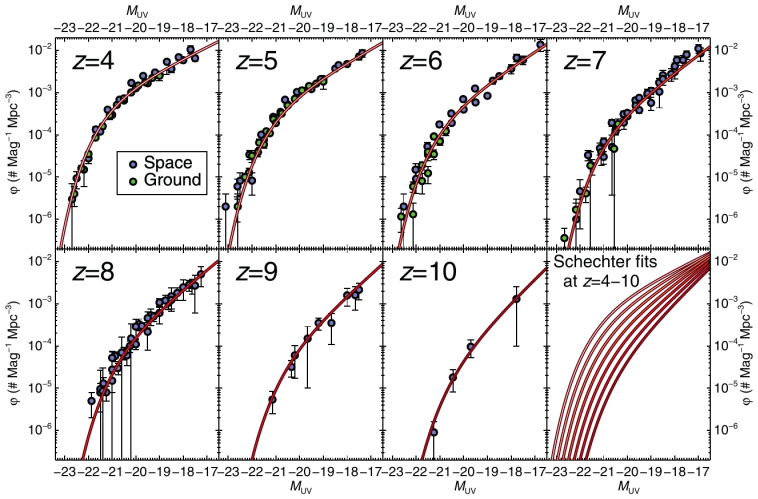

Figure 1.6: Figure from Finkelstein (2016) showing the rest-frame UV LF evolution with redshift combining both ground (green dots) and space (blue dots) observations.

et al. 2018; Bhatawdekar et al. 2019; Qiu et al. 2019, among others). Some of these studies find a constant behaviour of M^* with redshift (*e.g.*, Finkelstein et al. 2015; Bouwens et al. 2015b; Ono et al. 2018), whereas others find an slight increase of M^* with z (*e.g.*, Finkelstein 2016). In what all works do agree is in the decreasing behaviour of ϕ^* and α (steeper faint-end slopes) with redshift, associated to not only a lower amount of galaxies in the early Universe, but also a higher proportion of low luminosity sources. Fig. 1.6 shows the evolution of the LF with redshift found in Finkelstein (2016).

1.2.2 Stellar mass function

Stellar Mass Functions (SMFs) are the $M_{\rm star}$ analog to the LFs, *i.e.*, they tell the number density of galaxies per comoving volume unit as a function of $M_{\rm star}$ instead of L or M_{1500}. They are as useful as LFs. For instance, the comparison of the baryonic SMF faint-end with that of the halo models gives us information on the relevance of negative feedback in the star formation quenching in the same way as explained in Sec. 1.2.1 for the LFs.

With respect to the LF, the SMF presents the advantage of directly probing an intrinsic physical parameter of the galaxies, while its drawback comes from the fact that the stellar mass is not a directly measured parameter. Indeed, stellar masses are usually derived from SP synthesis models fitted to the Spectral Energy Distribution (SEDs) of the galaxies (Tinsley 1968, 1980; Bruzual 1983; Charlot & Bruzual 1991; Bruzual & Charlot 1993; Leitherer et al. 1999; Vazdekis 1999; Noll et al. 2009; Schaerer & de Barros 2009, 2010; Walcher et al. 2011; Conroy 2013; Schaerer et al. 2013; Boquien et al. 2019, among others), although they are sometimes estimated through the UV luminosity making use of a previously calibrated mass-to-ligth ratio (see, *e.g.*, Stark et al. 2009; González et al. 2011; Stefanon et al. 2017).

Making use of both kind of SED-derived stellar masses, a large number of authors have characterised the SMF at high-z (Pérez-González et al. 2008; Marchesini et al. 2009; Stark et al. 2009; Caputi et al. 2011; González et al. 2011; Santini et al. 2012; Duncan et al. 2014; Caputi et al. 2015; Grazian et al. 2015; Song et al. 2016; Davidzon et al. 2017; Stefanon et al. 2017), finding again a Schechter-like behaviour as follows:

$$\phi(M)dM = \phi^* \exp(-M/M^*)(M/M^*)^{\alpha} dM/M^*, \tag{1.3}$$

where this time M^* corresponds to the characteristic stellar mass at which the exponential and potential terms of the Schechter function are equally dominant.

Analogously to the LF, the integration of the SMF is a measurement of the Stellar Mass Density (SMD). The study of this magnitude at different redshifts is a direct measurement of the fraction of stellar mass existing in the Universe at a given cosmic time. SMD estimation at many different redshifts both from theoretical models (*e.g.*, Hopkins & Beacom 2006; Reddy & Steidel 2009; Behroozi et al. 2013) and SMF integration (Dickinson et al. 2003; Fontana et al. 2006; Pozzetti et al. 2007; Pérez-González et al. 2008; Kajisawa et al. 2009; Marchesini et al. 2009, 2010; González et al. 2011; Mortlock et al. 2011b; Lee et al. 2012; Santini et al. 2012; Ilbert et al. 2013; Muzzin et al. 2013; Duncan et al. 2014; Tomczak et al. 2014; Grazian et al. 2015; Song et al. 2016, among others) show a constant increase of the SMD with cosmic time (see Fig. 1.7), indicating that a much lower fraction of mass in the Universe had formed stars as we look back in time.

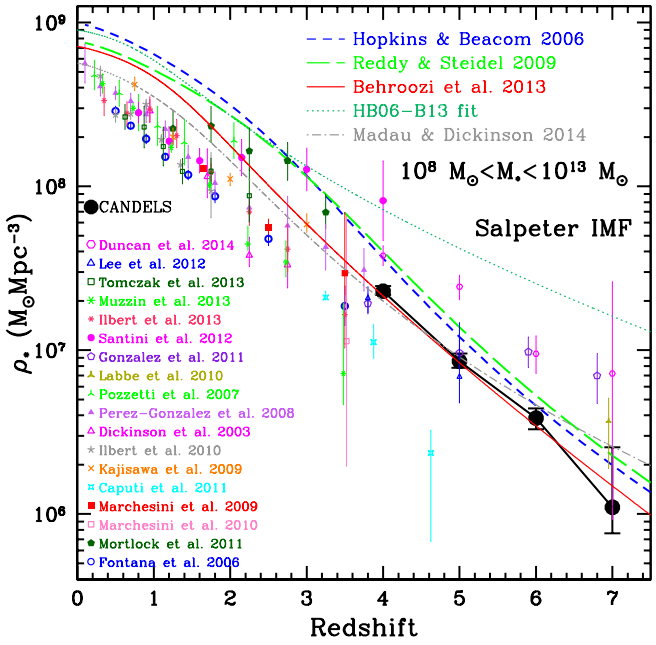

Figure 1.7: Figure from Grazian et al. (2015) showing the SMD variation with z from a compilation of both observational (points) and theoretical (lines) works.

1.2.3 Star formation rate density

SFRs of galaxies can be estimated from their luminosity in certain wavelengths (Kennicutt 1998; Madau et al. 1998; Madau & Dickinson 2014). Virtually, every observational proxy of the SFR measures the formation rate of massive stars, since, even though low mass stars dominate the SP in terms of mass, massive stars are the ones responsible of most of the emitted energy from young SPs (Madau & Dickinson 2014).

In particular, the rest-frame UV emission around $\lambda \sim 1500$ Å is the most popular tracer of the SFR at high-z. This is due to the possiblity of detecting it at high-z, in the optical/NIR range. This emission is directly linked to massive

O and B stars in young SPs with very short lifetimes ($\lesssim$ 20 Myr), and so its detection is directly related with recent star formation. However, the UV emission is strongly affected by dust absorption even in high-z LAEs and LBGs, where the dust content is very low. To correct this absorption and recover the actual UV emission of the galaxies, the development of precise dust extinction laws has been crucial (Calzetti et al. 1994, 2000; Calzetti 2001; Castellano et al. 2012).

A different way of estimating the SFR of a galaxy is through its nebular emission from excited and ionised gas in H II regions (see, *e.g.*, Kennicutt 1998). The most commonly used emission lines to calculate the SFR are the recombination lines of hydrogen, such as Lyα or Hα (6563 Å). Lines from other elements like [O II] (3727 Å) or [O III] (5007 Å) are also used to estimate SFRs, although they are more dependent on the exact ISM conditions. The issue with this method to estimate the SFR is that, at high-z, the modeling of the Lyα absorption becomes specially complicated. To the dust extinction contribution, we have to add the resonant scattering produced by H I clouds, causing a large uncertainty in the measurement of the real intrinsic Lyα emission. Because of this, Hα is considered the most reliable emission line to infer SFRs. However, at very high-z, both the Hα and oxygen lines are highly redshifted, usually falling out of the wavelength range studied. These handicaps make the nebular estimation of the SFR a less reliable option at high redshift.

Another technique for the SFR calculation is through the dust heat emission in the IR (*e.g.*, Calzetti et al. 2007; Daddi et al. 2007; Papovich et al. 2007; Magnelli et al. 2009, 2011). As previously explained in Sec. 1.1.4, the UV light absorbed by dust is thermally re-emitted in the rest-frame Medium and Far Infrared (MIR and FIR), and so we can calculate how much emission was initially emitted at shorter wavelengths. This technique works very well at low redshift, but at high redshifts, the sub-mm observations require large bolometric corrections to estimate the total IR luminosities, which strongly depend on the dust temperature (Madau & Dickinson 2014). This could add significant uncertainty to the derived IR fluxes at high-z, as well as bias the detection towards galaxies with the coldest dust.

From the integration of the UV LF (see Sec. 1.2.1) and making use of the different methodologies mentioned to estimate the SFR, the SFRD can be obtained normalising the SFR with the sampled comoving volume. In this way, the SFRD from different studies can be compared, leading to a good modeling of the star formation history of the Universe (Lilly et al. 1996; Madau et al. 1996; Behroozi et al. 2013; Madau & Dickinson 2014; Qiu et al. 2019).

According to the current SFRD picture, a peak of star formation would

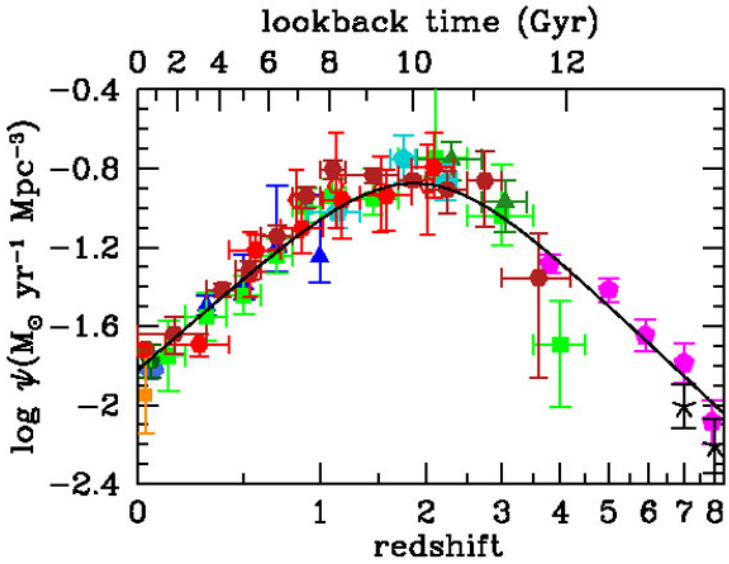

Figure 1.8: Figure from Madau & Dickinson (2014) showing the SFRD variation with redshift from a large compilation of works calculating SFRs from both rest-frame UV and IR observations.

have occurred at $z \simeq 2$, when the Universe was ~ 3.5 Gyr old (see Fig. 1.8). The star formation would have continuously risen from $z \simeq 8$ to $z \simeq 3$ following a $\propto (1+z)^{-2.9}$ trend. After its peak at $z \simeq 2$, the SFRD would have decreased with a $\propto (1+z)^{2.7}$ behaviour. There is debate about whether the observed trend remains or not beyond $z = 9$ (Coe et al. 2013; Ellis et al. 2013; Oesch et al. 2013; McLeod et al. 2015). In case that the SFRD exhibits a steep drop at some redshift, it may indicate the epoch of initial galaxy formation.

1.3 Galaxy clusters

Galaxy clusters are the most massive gravitationally bound structures in the Universe. They play a key role in the modeling of structure formation. In particular, they arise in regions of high matter density fluctuations.

The current paradigm of structures evolution claims that galaxy clusters form hierarchically, through accretion and mergers of smaller galaxies driven by dark matter gravitational wells (Press & Schechter 1974; Gott & Rees 1975; Kravtsov & Borgani 2012). Galaxy clusters at high-z are also thought to be the progenitors of low redshift elliptical galaxies as those which dominate the Virgo and Coma clusters (Lutz et al. 2001; Ivison et al. 2013; Chanchaiworawit et al. 2019). The distribution of these galaxy overdensities with z is an important tool to set constrains on the cosmological models describing the Universe (see, *e.g.*, Allen et al. 2011).

Contributions of the study of galaxy clusters to cosmology, are the discovery of dark matter in the Coma cluster (Zwicky 1933), the measurement of enhanced groups of clusters relative to isolated galaxies, supporting the model of random initial conditions maximised during the inflation (Bahcall & Soneira 1983). More recently, other contributions are the use of cluster counts or the intercluster medium mass fraction to directly constrain cosmological parameters (Voit 2005; Allen et al. 2011; Komatsu et al. 2011).

These structures have been studied in detail at low redshift ($z \simeq 1$; Pelló et al. 1996; Ellis et al. 1997; Stanford et al. 1998; Carlberg et al. 2001; Eke et al. 2004; Halliday et al. 2004; Holden et al. 2005; Pelló et al. 2009; Calvi et al. 2011; Spitler et al. 2012; Dannerbauer et al. 2014, among others), finding global masses of up to 10^{15} $M_{\odot}$ (Gonzalez et al. 2015). At $z \gtrsim 3$, however, we do not find these clusters but the so called proto-clusters (Steidel et al. 1998; Venemans et al. 2002; Shimasaku et al. 2003; Blain et al. 2004; Malhotra et al. 2005; Ouchi et al. 2005; Wang et al. 2005; Venemans et al. 2007; Daddi et al. 2009; Mancini et al. 2009; Capak et al. 2011; Toshikawa et al. 2012; Walter et al. 2012; Cucciati et al. 2014; Lee et al. 2014; Toshikawa et al. 2014; Ouchi et al. 2018; Calvi et al. 2019; Chanchaiworawit et al. 2019; Higuchi et al. 2019). High-z proto-clusters are overdense galaxy regions, in the early Universe, whose self-gravitation will eventually make them collapse creating the massive galaxy clusters we see nowadays at $z \simeq 0$ (see, *e.g.*, Chanchaiworawit et al. 2019).

It has been proven that massive sources at high-z, like QSOs or bright LAEs/LBGs, are good signposts for high-z overdensities (Venemans et al. 2007; Capak et al. 2011; Cucciati et al. 2014; Davies et al. 2014; Jiang et al. 2018). Furthermore, LAEs and LBGs at epochs prior to the reionisation ($z \gtrsim 5.5$-6) are also more easily detectable when they are in groups, as they create large enough ionisation bubbles allowing the ionising photons to escape, avoiding the resonant scatter produced by the abundant neutral hydrogen at that epoch of the Universe (Miralda-Escudé 1998; Dayal et al. 2009; Dayal & Ferrara 2011; Mortlock et al. 2011; Hutter et al. 2015).

1.4 Thesis outline

This thesis focuses on the characterisation of the LAE and LBG population at z = 3.4-6.8, a period of time where the Universe was still very young ($\sim$ 0.8-2 Gyr old), hosting the end of the EoR, and where star formation was very active, with the consequent increase of both the SFRD and the SMD.

To perform the search for these galaxies, we made use of the Survey for High-z Absorption Red and Dead Sources (SHARDS; Pérez-González et al. 2013). This survey observed the Great Observatories Origins Deep Survey North (GOODS-N) field with the 10.4m Gran Telescopio Canarias (GTC), with 25 consecutive medium-band filters in the optical/NIR range. The major advantage of the work presented here over previous ones is that SHARDS allows the simultaneous detection of both LAEs and LBGs in a uniform way, as Bina et al. (2016), Drake et al. (2017) and Drake et al. (2017b) have done on smaller fields using MUSE (Multi Unit Spectroscopic Explorer). Furthermore, the 25 medium-band filters provide more accurate SEDs than broad-band filters, facilitating the rejection of interlopers.

Since we are using both Lyα narrow-band selection and the Lyman break technique simultaneously, throughout this work we follow the approach of *e.g.*, Iye (2011), where any galaxy with Lyα emission line detected with the SHARDS filters is called a LAE. On the other side, the term LBG is reserved for galaxies showing the Lyman break and a well defined rest-frame UV continuum detected in SHARDS at redder wavelengths. Note that an object can simultaneously be a LAE and a LBG (hereinafter LAEs/LBGs). In fact, all LAEs should be LBGs. However, for many LAEs, their SFR and/or stellar masses are sufficiently low that their continuum is not detected with the Lyman break dropout technique (Trainor et al. 2015, 2016). For this reason, we will observationally call pure LAEs to those emitters with a prominent Lyα line and a very faint UV continuum that is not detected in SHARDS.

This work is structured as follows: Chapter 2 presents the SHARDS data and the ancillary GOODS-N data used, describing our own high-z LAEs and LBGs selection criteria. The rejection of interlopers is also sown in detail. Furthermore, the main direct physical parameters are calculated. We built LFs at different redshifts and compare those with similar ones from previous broad-band works in the same field. Chapter 3 carries out a SP modeling of the sample, paying special attention to differences between the three observational subclasses we define, suggesting a possible evolutionary relation between them. We also study the SMF and the SFR-$M_{\rm star}$ relation at different redshifts. Chapter 4 is dedicated to the search for and analysis of sources forming pairs or close groups. In particular, we study a previously reported $z \sim 5.2$ overdensity,

finding 44 new candidates. Subsequent Multi Object Spectroscopic (MOS) observation is also presented in this chapter, as well as the results derived from the spectra obtained. In Chapter 5, we carry out an unsupervised Machine Learning (ML) classification of the SEDs of both our sample and the high-z LAEs SC4K-COSMOS (Slicing COSMOS with 4k LAEs) sample (Sobral et al. 2018), with the aim of finding relevant physical differences between the classes obtained.

Finally, the main conclusions of this work, as well as possible future projects related with them, are presented in Chapter 6. All calculations are made adopting a Λ-dominated flat universe with $H_0 = 68$ km s^{-1} Mpc^{-1}, $\Omega_M = 0.3$ and $\Omega_\Lambda = 0.7$ (Planck Collaboration et al. 2016) and a Salpeter (1955) Initial Mass Function (IMF). All magnitudes are expressed in the AB system (Oke & Gunn 1983) and all physical distances refer to comoving distances.

2

High-z galaxies selection

¡Atención, señores! ¡Estoy detectando en la pantalla un gigantesco anfibio! ¡Mide 80 m y se dirige hacia aquí! ¡Oh, oh, Dios mío, está en mi zapato!... es una ranita. [...] Un momento, este no es el monstruómetro, es el exagerador de ranas.

Profesor Frink buscando al monstruo del lago Ness (The Simpsons).

This chapter describes the process carried out to build up a sample of high-z galaxies, highlighting the differences found with respect to similar samples obtained in previous broad band studies. We present the data used in this search for high-z galaxies as well as the selection criteria derived for the task. We describe the process followed to reject low z interlopers and the estimation of the magnitude completeness of the final sample. Some physical parameters directly derived from the SEDs are also shown, including LFs to complete the comparison of our selection criteria with previous broad band ones.

The work shown in this chapter is published in Arrabal Haro et al. (2018).

2.1 Data description

One of the main motivations for the work we endeavour in this thesis is given by the accessibility to very deep and spectrally resolved modern data. They open the study of far away galaxies in a new way, representing great improvements with respect to the traditional methods employed in high-z galaxy detection in past years. In this respect, we take advantage of the SHARDS survey (Pérez-González et al. 2013), which constitutes our main source of data, as well as ancillary public data from the Rainbow Cosmological Surveys Database[1]

[1]Operated by the Universidad Complutense de Madrid (UCM), partnered with the University of California Observatories at Santa Cruz (UCO/Lick, UCSC).
`http://rainbowx.fis.ucm.es/Rainbow_navigator_public/`.

(Barro et al. 2011,b, 2019).

SHARDS is an ESO/GTC deep optical spectro-photometric survey of the GOODS-N field. This survey was acquired with 200 hours of observing time with the Optical System for Imaging and low-intermediate-Resolution Integrated Spectroscopy (OSIRIS) instrument (Cepa 2010), on the 10.4 m GTC. The surveyed area covers ∼130 arcmin^2, split into two pointings, almost covering the entire GOODS-N field, as shown in Fig. 2.1. This survey provides very deep photometry ($m \lesssim$ 26.5-27.0 AB mag, at the 3σ level) in 25 consecutive optical/NIR medium-band filters, from 500 nm to 941 nm. The first 22 filters have a Full Width at Half Maximum (FWHM) of $\sim$ 17 nm, while the last three have a FWHM of 35, 25 and 33 nm, respectively.

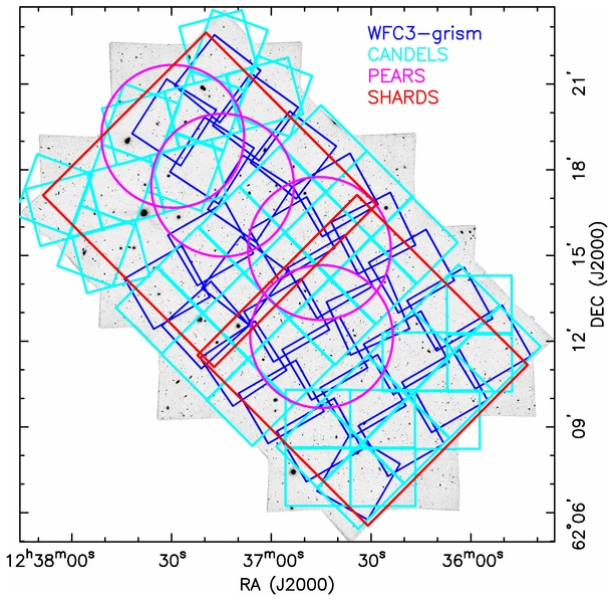

Figure 2.1: Image from Pérez-González et al. (2013) showing the footprint of the SHARDS data superimposed on the ACS images for the GOODS-N field. The footprints of the *HST* grism surveys carried out with ACS (PEARS) and WFC3 and the CANDELS coverage of GOODS-N are also shown. SHARDS covers a total surveyed area of $\sim$ 130 arcmin^2 divided into two pointings.

The main purpose of SHARDS was to provide SEDs with good enough spectral resolution to study red and passive galaxies up to redshift $z \sim 2$. Nonetheless, it can be used to detect line emitting sources that otherwise would not be detected using broader filters (Rodriguez Espinosa et al. 2014; Cava et al. 2015; Hernán-Caballero et al. 2017; Lumbreras-Calle et al. 2019), as well as drop-out sources that can be well characterised by the many consecutive filters. Indeed, the relative narrowness of the SHARDS filters and large number of them result in good spectrally resolved SEDs ($R \sim 50$). This is what makes SHARDS an excellent survey to search and study LAEs and LBGs at redshifts between 3.4 and 6.8, whose Lyα emission line or Lyman break fall within the wavelength range of SHARDS. A comparison of the central transmission curves of the 25 SHARDS filters with that of the *HST*/ACS F606W filter is presented in Fig. 2.2, giving an idea of the large amount of consecutive photometric points covering the optical/NIR wavelength range. This makes the spectrally resolved SHARDS SEDs much better than typical broad band SEDs. The SHARDS data reduction and calibration was not made in this work but it is explained in great detail in Pérez-González et al. (2013).

We carry out additional data processing before starting our high-z LAEs and LBGs search. First, we limit the effective search field to the common area of all the SHARDS images for each pointing, as each SHARDS image samples a slightly displaced area with respect to the others. To take this into account, we extract the right ascension and declination of every pixel above zero counts in all our SHARDS images. Then a match of all the coordinates is made with the Tool for OPerations on Catalogues And Tables (TOPCAT, Taylor 2005), obtaining an intersection image of all the different SHARDS filter images for each of the two pointings. The edges of these two effective images are then analytically fitted to define an effective spatial region of 128.4 arcmin^2 for which we have information in all the SHARDS filters. This field trimming becomes specially important when looking for the LAEs and LBGs we are interested in, as the selection criteria (see Sec. 2.2) is based on emission drops along the SED. Thus, not limiting the search to the common area of all filters would lead to many false detections near the borders of the frame. In this cases, the selection code would indeed identify emission drop-outs for sources that are not sampled in all the filters, whose emission drop is not linked to a real non detection but to the absence of data in that filters.

We also need to take into consideration existing variations in the effective Central Wavelength (CWL) within the SHARDS filters, which depends on the particular position of each source in the Field Of View (FOV). This is a pure geometrical effect, as a result of the angle of incidence of the GTC/OSIRIS light beam on the filter. Objects in the same SHARDS image are detected with sim-

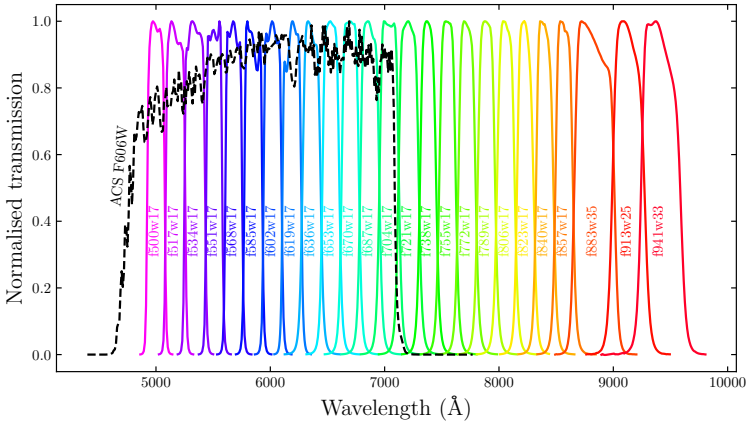

Figure 2.2: Normalised transmission curves of the 25 medium band SHARDS filters. The superposed black dashed line corresponds to the transmission curve of the F606W *HST*/ACS broad band. The differences in bandwidth give us an idea of how much better the spectral resolution of the SHARDS SEDs is with respect to traditional broad band measurements.

ilar effective wavelengths but not exactly the same, depending on their distance to the optical axis, *i.e.*, the exact filter transmission curve experimented by each object is not the nominal one, but it is shifted depending on their position in the FOV. Fortunately, this is an effect already calibrated (see Pérez-González et al. 2013), so we can get the exact CWL for each object in each filter directly from the SHARDS catalogue. Thus, the exact CWL experimented by a source in the FOV follows:

$$\mathrm{CWL}(X,Y) = A + B[(X - X_0)^2 + (Y - Y_0)^2], \tag{2.1}$$

where X and Y are the pixel positions in the OSIRIS FOV, and X_0 and Y_0 are the pixel position of the optical axis. A and B are the coefficients of the quadratic fit. An example of the calibration of the f687w17 filter is shown in Fig. 2.3. The exact FWHM of the band sampling each CWL is also considered, as this slightly varies from one filter to the other even though most of them have ~ 17 nm widths, except for the last three filters, as previously mentioned.

In order to further extend our wavelength coverage, we have also made

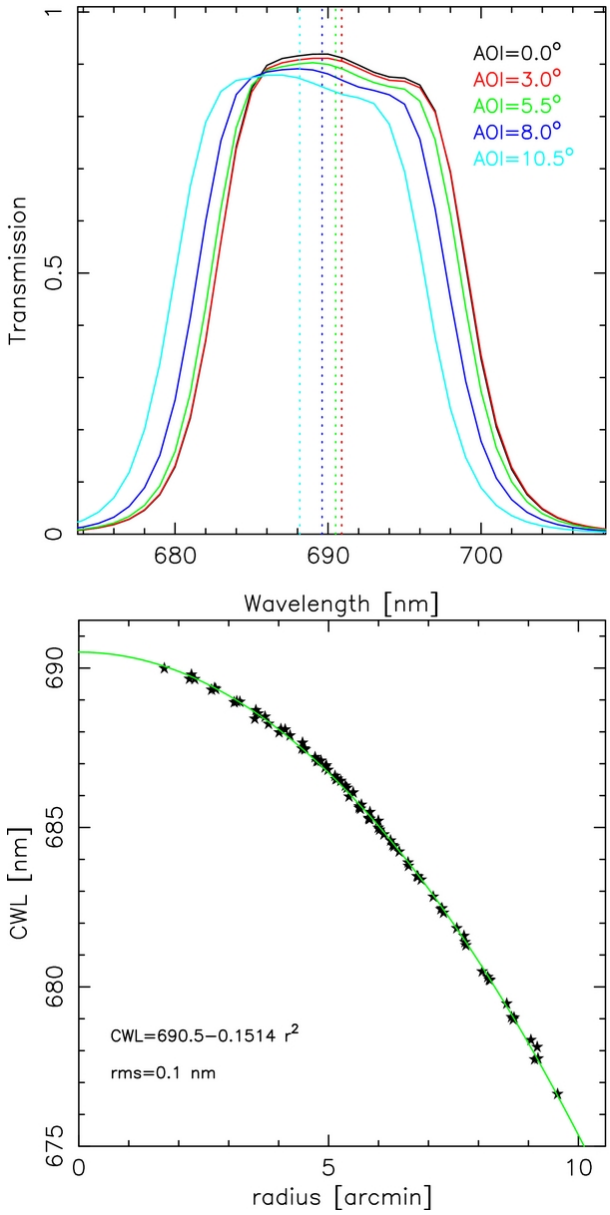

Figure 2.3: Image from Pérez-González et al. (2013) showing the calibration of the SHARDS f687w17 filter as a function of the angle of incidence (*top*) as well as the spatial variation of the CWL along the OSIRIS FOV (*bottom*).

use of additional public data from *HST*/ACS (Giavalisco et al. 2004b; Riess et al. 2007), *HST*/WFC3 (Grogin et al. 2011; Koekemoer et al. 2011), *GALEX* (Bianchi 2014), Subaru/Suprime-Cam (as a part of the Hawaii Hubble Deep Field North project, Capak et al. 2004), Subaru/MOIRCS (Kajisawa et al. 2011), CFHT/WIRCam (Lin et al. 2012; Hsu et al. 2019) and *Spitzer*/IRAC (Fazio et al. 2004; Pérez-González et al. 2005, 2008; Ashby et al. 2015) as compiled in the Rainbow Cosmological Surveys Database (Barro et al. 2011,b, 2019). We have therefore added valuable data in wavelengths beyond the SHARDS range. This is important to ensure that our candidates do not present significant emission blue-ward of the Lyman break, and, in general, to more robustly discard interlopers. The summary of the main characteristics of filters profile, atmospheric seeing and depth of the images used are shown in Table 2.1 and 2.2 for both SHARDS and the ancillary Rainbow data used, respectively.

2.2 Sample selection

Here we explain in detail the process to search for the candidate sources in the SHARDS catalogue. SHARDS contains 44752 sources in the GOODS-N field, and for each object there is information on its flux in the SHARDS filters, plus the ancillary data available in Rainbow (see Section 2.1).

2.2.1 Preselection criteria

A first preselection is made taking advantage of the photometric redshifts available in the Rainbow Database for 35445 of the SHARDS objects in the CANDELS/GOODS-N field. These redshifts were obtained by Barro et al. (2019, hereinafter Ba19), through SED fitting with Easy and Accurate Redshifts from Yale (EAZY, Brammer et al. 2008), using SHARDS combined with the WFC3 102 and 141 grisms and additional data from *HST*, Subaru, *Spitzer* and others. These detailed SED characterisation leads to an accurate redshift calculation $\Delta z/(1+z_{\rm spec}) \sim 0.0032$ (see also Ferreras et al. 2014; Domínguez Sánchez et al. 2016). From this sample, 1078 $z = 3.4$-6.8 candidates are preselected using their redshift estimation.

For the 9307 objects in the SHARDS catalogue without photometric redshift in Ba19, a selection criterion based on colour excesses between filters was designed. Since we are interested in detecting both Lyα in emission and/or the Lyman break feature, we first build colour-magnitude diagrams using consecutive filters. Thus we are able to detect all relevant flux changes from one filter to the next (regardless of whether they were emission lines or drop-outs). In order to only select objects with reliable flux changes, we study the dependence of

Table 2.1: Main parameters of the SHARDS filter set and observations.

Filter	CWL (Å)	Width (Å)	A (Å)	B (10^{-5} pix^{-2})	X_0 (pix)	Y_0 (pix)	$m_{3\sigma}$ (AB mag)		Seeing (arcsec)	
							P1	P2	P1	P2
(1)	(2)	(3)	(4)	(5)	(6)	(7)	(8)	(9)	(10)	(11)
F500W17	5000	150	5033.7	-1.323	-315.7	1003.7	26.9	26.6	0.96	0.94
F517W17	5170	165	5203.1	-1.304	-430.5	991.6	26.3	27.0	0.79	0.93
F534W17	5340	177	5385.1	-1.379	-370.3	1053.0	27.0	27.2	0.92	0.81
F551W17	5510	138	5550.1	-2.060	-255.8	988.1	26.6	26.6	0.83	0.78
F568W17	5680	144	5721.1	-2.117	-289.8	1008.8	26.6	26.7	0.83	0.82
F585W17	5850	151	5886.9	-2.327	-123.2	1024.7	26.7	26.8	0.97	0.89
F602W17	6020	155	6057.5	-2.277	-212.5	1001.2	26.6	27.0	0.88	0.89
F619W17	6190	158	6231.4	-2.404	-202.3	984.8	26.9	27.1	0.85	0.90
F636W17	6360	162	6413.7	-2.589	-116.3	985.8	26.9	26.9	0.79	0.92
F653W17	6530	154	6560.1	-2.636	-151.1	998.6	27.1	27.3	0.98	1.00
F670W17	6700	160	6718.6	-2.602	-183.3	1037.2	26.7	27.0	0.79	1.07
F687W17	6870	172	6912.2	-2.366	-383.2	946.8	27.2	27.0	0.84	0.93
F704W17	7040	179	7077.8	-2.725	-209.3	1027.9	26.9	26.8	0.89	0.92
F721W17	7210	185	7231.2	-2.972	-94.5	960.0	26.7	26.7	0.93	1.02
F738W17	7380	149	7418.0	-2.413	-328.0	1050.3	26.5	26.5	0.86	0.90
F755W17	7550	153	7581.2	-2.662	-228.4	1033.5	26.9	26.5	0.92	0.93
F772W17	7720	159	7746.2	-2.931	-122.0	1026.0	26.7	26.6	0.94	1.04
F789W17	7890	160	7912.2	-3.089	-123.4	994.3	26.3	26.2	0.97	0.92
F806W17	8060	161	8094.2	-2.941	-200.1	932.8	26.6	26.6	0.96	0.99
F823W17	8230	147	8291.5	-3.058	-152.7	888.0	26.7	26.9	0.82	0.91
F840W17	8400	156	8435.7	-3.104	-236.7	992.2	26.4	26.5	0.88	0.91
F857W17	8570	159	8599.7	-2.895	-249.3	1002.1	27.0	26.5	0.73	0.95
F883W35	8830	336	8853.3	-2.892	-285.2	977.5	26.4	26.4	0.93	1.02
F913W25	9130	278	9136.4	-4.055	-60.4	975.4	27.1	27.0	0.77	0.85
F941W33	9410	333	9440.4	-3.406	-165.0	1067.1	25.9	26.0	0.91	0.99

(1) SHARDS filter name. (2) Nominal central wavelength. (3) Filter width. (4) Coefficient A for exact CWL calibration (from equation 2.1). (5) Coefficient B for CWL calibration (from equation 2.1). (6) X_0 coordinate for the OSIRIS optical center. (7) Y_0 coordinate for the OSIRIS optical center. (8) and (9) Sensitivity limits at the 3σ level for pointings 1 and 2, respectively. (10) and (11) Average seeing for pointings 1 and 2, respectively. The data in this table has been taken from `https://guaix.fis.ucm.es/~pgperez/SHARDS/Filters/TAB_filters/TAB_filters.html`.

Table 2.2: Main parameters of the ancillary images used from previous observations in the GOODS-N field.

Filter	Telescope/Instrument	CWL (Å)	FWHM (Å)	$m_{5\sigma}$ (AB mag)	Seeing (arcsec)
(1)	(2)	(3)	(4)	(5)	(6)
FUV	*GALEX*	1526	228	25.0	4.5
NUV	*GALEX*	2329	796	25.0	5.4
F435W	*HST*/ACS	4349	939	27.1	0.10
B	Subaru/Suprime-Cam	4367	1083	27.01	0.71
V	Subaru/Suprime-Cam	5435	993	26.40	0.71
F606W	*HST*/ACS	5926	2323	27.7	0.10
R	Subaru/Suprime-Cam	6241	1426	26.96	1.11
F775W	*HST*/ACS	7754	1511	27.2	0.11
I	Subaru/Suprime-Cam	7671	1553	25.85	0.72
F814W	*HST*/ACS	7976	1856	28.1	0.11
F850LP	*HST*/ACS	8907	1209	26.9	0.11
z	Subaru/Suprime-Cam	9193	1404	25.54	0.67
F105W	*HST*/WFC3	10531	2917	26.4	0.18
F125W	*HST*/WFC3	12496	3005	27.5	0.18
J	CFHT/WIRCam	12541	1588	24.7	0.8
F140W	*HST*/WFC3	13976	3941	26.9	0.18
F160W	*HST*/WFC3	15433	2874	27.3	0.19
MOIRCS-K_s	Subaru/MOIRCS	21461	3100	24.7	0.6
K_s	CFHT/WIRCam	21500	3270	24.4	0.6
IRAC1	*Spitzer*/IRAC	35466	7432	24.5	1.7
IRAC2	*Spitzer*/IRAC	45024	10097	24.6	1.7
IRAC3	*Spitzer*/IRAC	57157	13912	22.8	1.9
IRAC4	*Spitzer*/IRAC	78556	28312	22.7	2.0

(1) Filter name. (2) Telescope/Instrument. (3) CWL. (4) Filter FWHM. (5) Sensitivity limit at the 5σ level for a 2 arcsec aperture. (6) Average seeing.

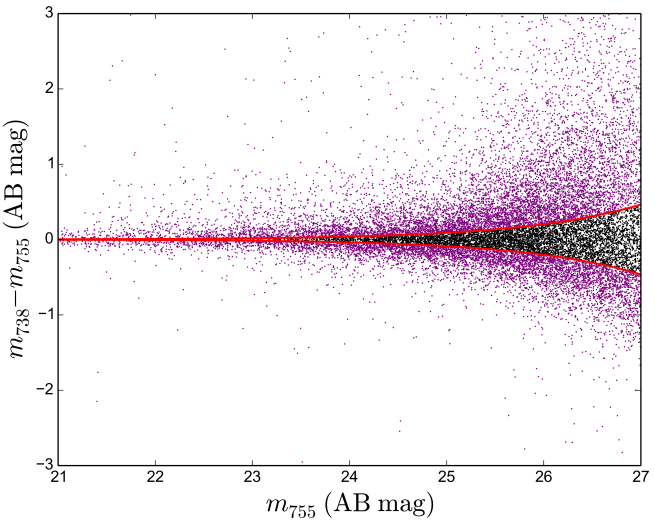

Figure 2.4: Example of a colour-magnitude diagram for the filters f738w17 and f755w17. The red lines represent 1σ errors for each magnitude, so they limit the objects we consider having a relevant emission change in these filters. Purple points above the upper red line have higher magnitude in the f738w17 filter and therefore they show a reliable emission drop with respect to the f755w17. Similar diagrams were built for every pair of consecutive filters.

magnitude errors with magnitude in the SHARDS catalogue for each one of the filters. We then estimate the mean error for a given magnitude and determine whether a flux change between filters is large enough. If, on the contrary, this error is within the expected errors for that magnitude, we discard the source. The procedure uses logarithmic fits of the magnitude error for each filter. We use 1σ error limits to identify relevant emission changes (see Fig. 2.4).

SHARDS SEDs are then built for the objects that satisfy the colour-magnitude criterion, and with them we start a more selective filtering. For this purpose we implement a code that analyses the SEDs of the objects and selects candidates according to the following criteria:

$$\delta \leq \langle m_{j<i} \rangle - m_i \wedge \Delta m_i < \langle m_{j<i} \rangle - m_i, \tag{2.2}$$

where m_i is the AB apparent magnitude of the emission filter just after the break, Δm_i, its error, $m_{j<i}$ are the magnitudes of all the bluer filters before m_i. Finally, δ is an adjustable magnitude difference for the break, which we kept above the 1σ level of the colour-magnitude diagram limits. In other words, our code looks for a source in filter i whose emission is at least δ AB magnitudes brighter than its mean magnitude in all the non-zero emission filters blue-ward of the given filter i (first term of Eq. [2.2]). The code keeps only those cases where the emission gap is larger than the errors in the magnitude of the brightest filter defining the break (second term of Eq. [2.2]). We compare each filter detection with the mean detection of all the filters which are bluer than it to make sure that what we detect is a spectral break, and not other absorption features affecting only one of the SHARDS bands. This method produces a large number of high-z candidate SEDs (1642), but a number that we can visually check. As expected, many of the detections ($\sim 70\%$) are either spurious objects, high slope red galaxies/stars or other emission line galaxies, not LAEs nor LBGs. Nonetheless, this turns out to be a good method to get a first cut of objects, while not imposing such a restrictive constrain as to discard valid candidates.

The last step is to visually inspect all the candidate objects, not only looking at their SEDs but also directly viewing the images. In this process we mainly use images from GTC/SHARDS, *HST*/ACS, and *HST*/WFC3, though we also use other images available in the Rainbow Database from Subaru/Suprime-Cam and *Spitzer*/IRAC. The SEDs are further completed with useful data at other wavelengths available in Rainbow (see Section 2.1). Finally, we visually discard those objects which are deemed either spurious or present strong emission blue-ward of their supposed Lyman break wavelength. This check is necessary since lower z objects with a high slope SED could match our SHARDS preselection criteria when their emission in one of the redder filters is substantially higher than the average emission in the filters blue-ward of that one.

The whole process is iterated many times, identifying the wavelength where the Lyman break appears for each object, paying special attention to galaxies with photometric redshift estimations from previous authors, making sure we do not skip possible candidates while not including unwanted objects. Using this last method we add 492 new objects. These together with the 1078 selected objects from Ba19 mentioned before constitute our final selection, consisting of 1570 well characterised candidates, pending a final interlopers screening.

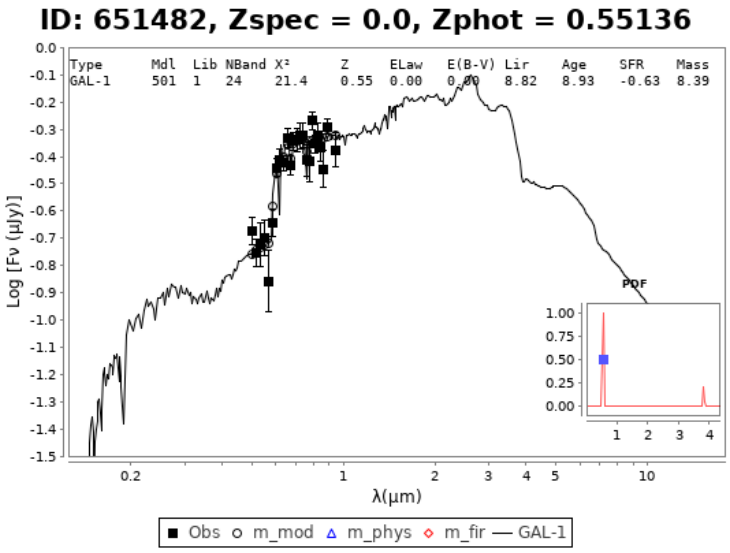

Figure 2.5: LePHARE best fit for one of the 12 preselected sources finally discarded. The black squares correspond to the SHARDS photometry, while the solid line represents the LePHARE best-fitting theoretical spectrum. The inner frame shows the redshift Probability Distribution Function (PDF). Note that there is a small peak at $z \sim 4$ suggesting that the emission drop-out of the SED could correspond to the Lyman break. However, the clear peak of the PDF at low redshift indicates that we are more probably sampling the Balmer jump in a lower z galaxy.

2.2.2 Interlopers rejection

Once the first selection is finished, we carry out additional theoretical models fits to our SEDs to make a further test on those objects that have met our selection criteria but could still be lower z interlopers. In the search for high-z LBGs the main interlopers are low-z galaxies where the D4000 break is wrongly identified as the Lyman break. Additionally, M, L, and T dwarf stars with a very steep slope can be mistakenly taken as drop-outs. In these, it is possible to measure an abrupt flux change, specially with broad band filters. However,

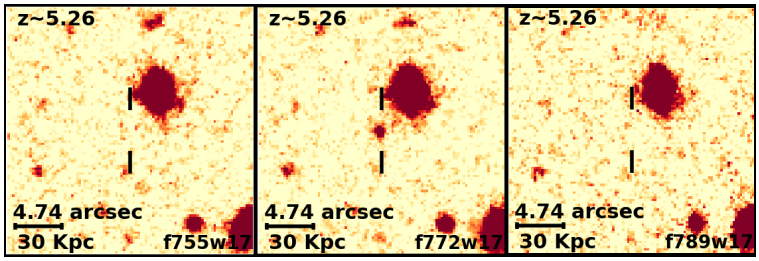

Figure 2.6: Mosaic of three consecutive SHARDS filters sampling the Lyα emission of the $z \sim 5.26$ pure LAE SHARDS J123720.02+621200.6 (within vertical marks). The central filter of the image shows the Lyα line in emission. There is no detection at shorter wavelengths, but neither red-ward of the central filter, as the UV continuum is below the SHARDS detection limit. This source shows a weak continuum detection in *HST*/ACS images red-ward of Lyα, though our definition of pure LAE is based on the SHARDS images as reference. North is up, East is left.

these last cases are in general easily recognisable when using many narrow-band filters. Hence we do not expect an important number of them among our interlopers. The fitting process was made with the code LePHARE (Photometric Analysis for Redshift Estimate, Arnouts et al. 1999; Ilbert et al. 2006). We use different galaxy models (*e.g.,* Coleman et al. 1980; Kinney et al. 1996; Bruzual & Charlot 2003), assuming a Salpeter (1955) IMF and a Calzetti extinction law (Calzetti et al. 1994). For the stars rejection, we use SEDs from Bohlin et al. (1995), Kinney et al. (1996) and Chabrier et al. (2000), with special attention to cold M, L and T stars from Pickles (1998), Burgasser et al. (2004), Cruz et al. (2004), Burgasser & McElwain (2006), Chiu et al. (2006), Reid et al. (2006), Burgasser (2007), Looper et al. (2007), Burgasser et al. (2008), Burgasser et al. (2010) and Kirkpatrick et al. (2010).

As in every other survey, we do not get good SED fitting for all the 1570 candidate galaxies in our sample, but only for 644 (with $\chi^2 \lesssim 40$). Therefore, we expect some unwanted objects within the worst fitted sources of the sample. Only 12 out of the well fitted part of the sample are found to be lower z interlopers. None of them are found to be steep red-slope stars, but low-z galaxies. An example of one of the interlopers is shown in Fig. 2.5. To estimate the final interloper fraction in our high-z galaxy selection we extrapolate the interloper fraction found for the well fitted sample to the whole sample, obtaining a $\sim 2\%$

fraction of interlopers in our final selection. Thus, after eliminating the identified interlopers, our final sample consists of 1558 high-z galaxies, classified as 528 LAEs and 1030 LBGs with no emission line (hereinafter non-LAEs/LBGs). Among the emitters, 124 of them are pure LAEs with no continuum detected in SHARDS (see Fig. 2.6 for an example), although they could be detected in the *HST*/ACS broad band images, while the rest (404) are LBGs with Lyα line emission (LAEs/LBGs). Figs. 2.7 and 2.8 show the SED and the SHARDS images of a good LAE/LBG candidate, respectively.

2.3 Completeness estimation

In order to compare our sample selection with previous ones and, in particular, to properly correct the calculations of our LFs, we need an estimation of the sample completeness. However, a handicap of our selection criteria is that it requires visual inspection of the large amount of candidates preselected with the Eq. 2.2 condition. This makes a usual calculation of the magnitude completeness through galaxies simulation/recovery very inefficient and time consuming, so we opt for a simpler and presumably more conservative estimation of the magnitude limit of our sample. To achieve this, we take the rest-frame UV magnitude at 1500 Å as the reference magnitude. The selection of this particular magnitude is due to the fact that the completeness will be used for corrections at the time of building the UV LFs (see Sec. 2.5.2). We study the behaviour of the logarithm of the cumulative number of LBGs with m_{1500} below each apparent magnitude (see Fig. 2.9). Our assumption here is that, as we do not reach the faint-end of the classical Schechter (1976) LF, our selection will be mostly dominated by the exponential term of the Schechter function. It is thus reasonable to assume that we can calculate our completeness looking at the m_{1500} at which the slope of the logarithmic cumulative distribution starts decreasing. In this way we obtain the value beyond which we start missing candidate objects. This value indicates our completeness apparent magnitude.

In practical terms, we fit a linear function to the bright magnitude region of the cumulative logarithm function, between the magnitudes where the slope does not vary. In this step we adopt a magnitude bin of 0.25 mag to preserve the statistical information in the brightest bins, avoiding stochastic variations and obtaining a representative and monotonically increasing behaviour of the magnitude cumulative curve. Once we have fitted the non-changing slope region of the logarithmic cumulative curve, we extrapolate it to compare it with the actual curve as we move towards fainter magnitudes. The magnitude value at which the actual curve becomes a certain percentage of the theoretical extrapolation indicates the corresponding significance completeness limit of the

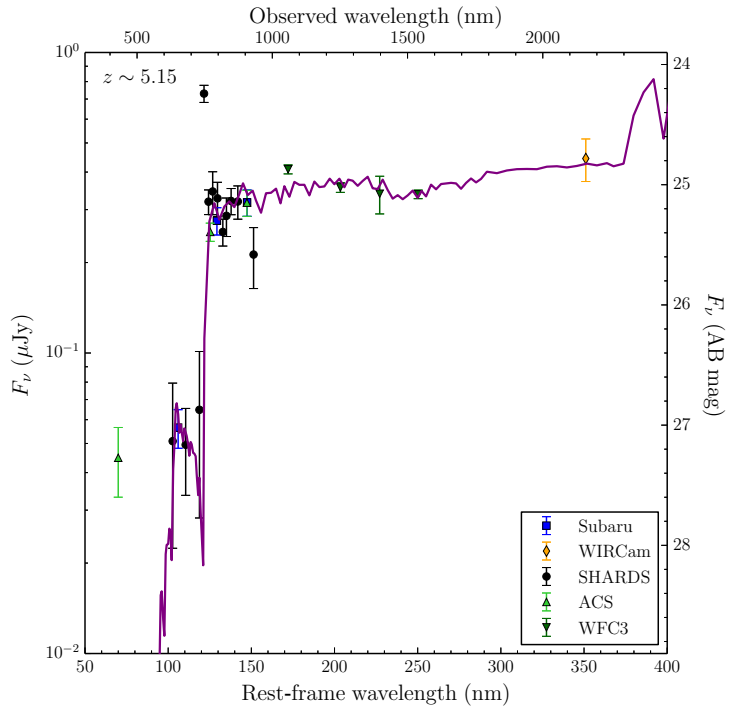

Figure 2.7: SED of the candidate SHARDS J123655.49+621532.7, a LAE/LBG with emission line at 747.5 nm corresponding to the Lyα line at redshift $z \sim 5.15$. To make this SED we made use of all the data available in the Rainbow Database with reliable information on this galaxy. Notice that all emission blue-ward of the line goes down abruptly, while to the red, the UV continuum can be easily detected. The purple line is a template of a $z \sim 5.15$ model. A mosaic with the detection of this object in all the 25 SHARDS filters is shown in Fig. 2.8.

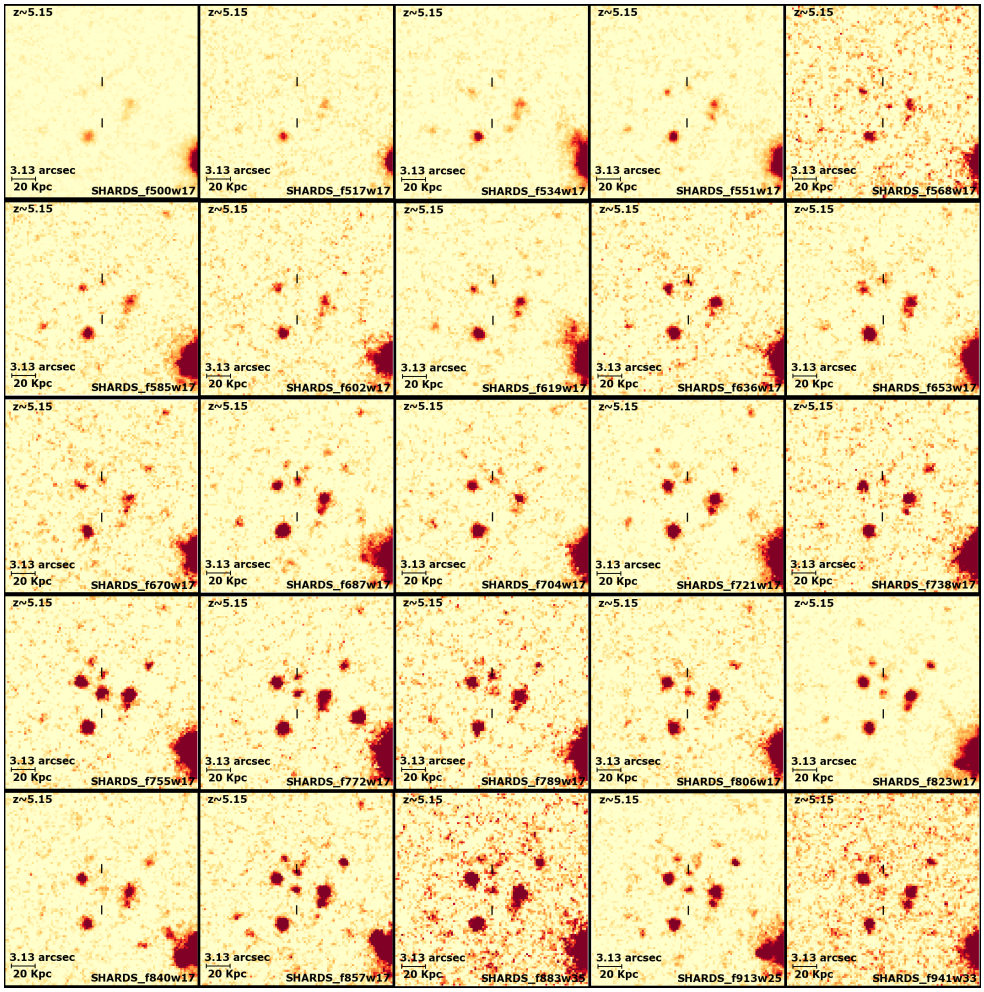

Figure 2.8: Mosaic made with the images of the 25 SHARDS filters from bluer (*top left*) to redder (*bottom right*) of the candidate source SHARDS J123655.49+621532.7 (enclosed between two vertical marks). Its SED is shown in Fig. 2.7. The strongest emission, corresponding to the Lyα line, can be clearly appreciated in filter f755w17. Redder filters show fainter emission, corresponding to the UV rest-frame continuum, while shorter wavelengths filters do not show any emission at all at the object position. North is up, East is left.

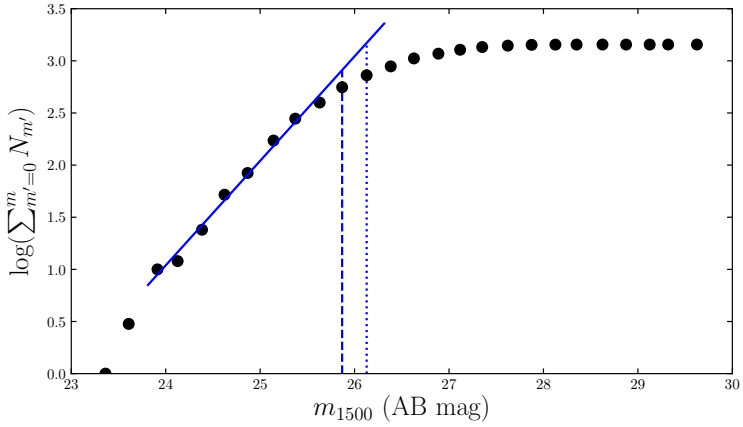

Figure 2.9: Logarithmic cumulative curve measuring the amount of sources in terms of the apparent AB magnitude at 1500 Å rest-frame for the LBG candidates using a 0.25 AB mag bin. Assuming the real distribution is exponential, the point where the slope changes indicates the magnitude at which we start missing objects. The blue solid line is a fit to the slope of the complete region while the dashed and dotted lines indicate the magnitudes at which we reach 90% and 50% completeness level according to that fit, which in our case correspond to ~ 25.87 and ~ 26.13 AB mag, respectively.

sample. We obtain a 90% completeness at magnitude $m_{1500} \sim 25.87 \pm 0.25$ AB mag and a 50% completeness at 26.13 ± 0.25 AB mag, although our faintest sources reach up to $m_{1500} \sim 28$ AB mag. This completeness value corresponds to different M_{1500} absolute magnitudes at each different redshift, as summarised in Table 2.3, and will limit the depth up to which our calculations are robust.

Table 2.3: Mean UV absolute magnitude completeness at each redshift range.

$< z >$	$< M_{1500}$ 90% completeness>	$< M_{1500}$ 50% completeness>
4	-20.22	-19.96
5	-20.59	-20.33
6	-20.89	-20.63

2.4 Physical parameters of the sample

Once we have a well defined sample, in this section we present the first basic physical parameters directly obtained from the SEDs of the sample.

2.4.1 Redshifts

Section 2.2 showed how the SED of each object was used to identify the filter wavelength at which that object presents either an emission line or a continuum drop. The main assumptions for obtaining the redshift of the objects are that the line is indeed Lyα and the emission drop is the Lyman break. These premises are supported by the selection criteria described in Sections 2.2.1 and 2.2.2. With these assumptions, we get their line/break wavelength, taking into account the precise position of the source in the FOV to correct the CWL shift effect described in Section 2.1. Previous calculations pointed out that this effect is quite relevant when the object is located far from the central region and therefore from the optical axis. We also take care of using the appropriate filter width corresponding to the pre-break filter at the time of estimating our photometric redshift uncertainties. It is important to clarify that the Lyman break wavelength used for the redshift calculation when no Lyα line is detected, is not 912 Å, but just 1215.67 Å. This is because the Lyα forest, due to intergalactic absorption, mostly erases any continuum emission blue-ward of Lyα at high redshifts (Rauch 1998; Fan et al. 2006c; Dunlop 2013).

To prove the goodness of our photometric redshifts we check every case where a spectroscopic redshift is available either in the Rainbow Database or in the NASA/IPAC Extragalactic Database (NED)[2]. We end up with 156 spectroscopic redshifts from Steidel et al. (2003), Kakazu et al. (2007), Barger et al. (2008), Kajino et al. (2009), Adams et al. (2011), Conselice et al. (2011), Shim et al. (2011), Stark et al. (2011), Stark et al. (2013) and Schenker et al. (2013b). The comparison of these spectroscopic redshift with our photometric redshifts is shown in Fig. 2.10. We find a good agreement between the values, with none of our spectroscopically confirmed objects beyond an assumed outliers threshold of $|\Delta z|/(1 + z_{\rm spec}) = 0.15$, as in Ba19. The excellent correlation indicates that we can trust the calculated redshifts for our candidates with an average error of around $\Delta z = 0.07$ (0.14 for objects above $z \sim 6.2$, where the filters measuring the Lyman break are wider).

The redshift distribution of our LAE and LBG candidates is shown in Fig. 2.11. The number of LBGs decreases with z. This may be partly due to the lower number of SHARDS filters providing relevant information in the

[2] https://ned.ipac.caltech.edu/.

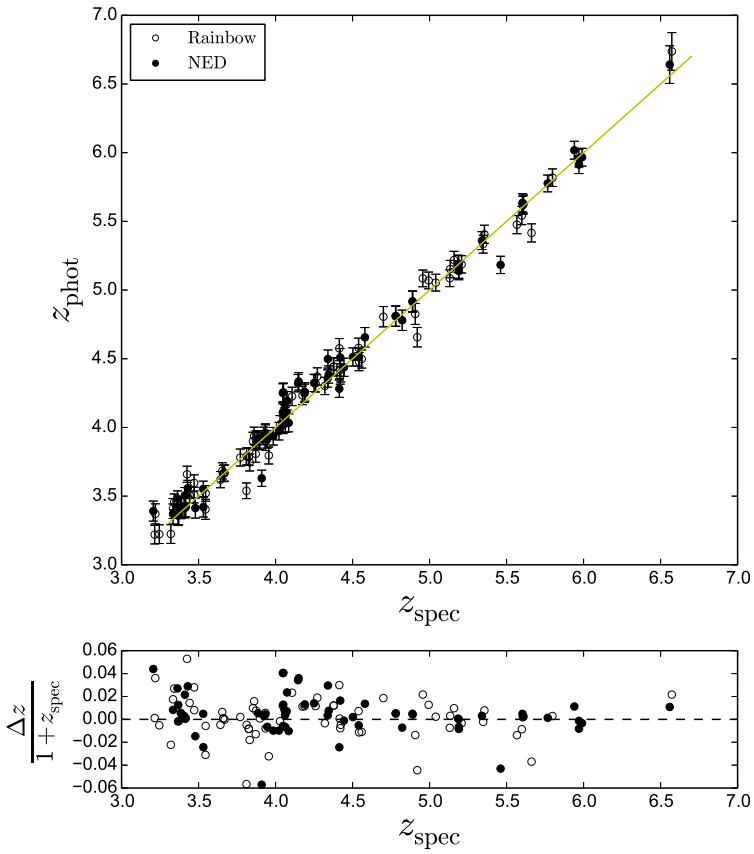

Figure 2.10: Comparison between our photometric redshifts with the spectroscopic ones for those candidates with spectroscopic z available in Rainbow or NED. Black dots are extracted from NED while empty circles are from Rainbow. In case the same object has spectroscopic z in both databases we plot the NED one only to avoid redundancy (after checking that the value is the same). The solid yellow line is the one-to-one line. Notice that none of the spectroscopically confirmed objects of our sample has a calculated photo-z over the $|\Delta z|/(1+z_{\rm spec}) = 0.15$ outliers threshold. The excellent correlation indicates that both our selection criteria and redshift calculations are very robust and accurate.

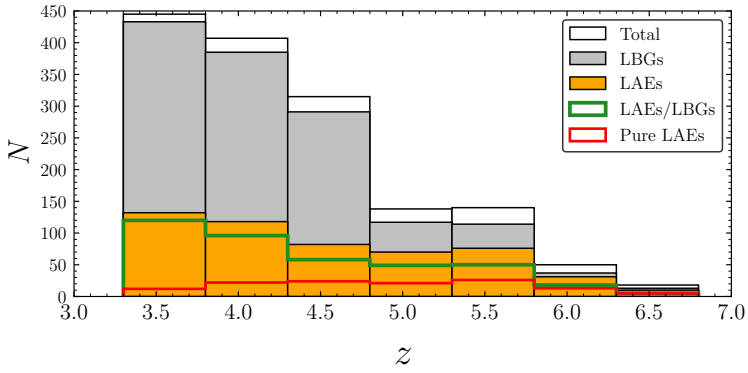

Figure 2.11: Redshift distribution of the sample. In grey we plot the LBGs (including both LAEs/LBGs and non-LAEs/LBGs). In orange, the LAEs. These last ones are divided in LAEs/LBGs with UV continuum detection in SHARDS, represented in green, and pure LAEs with no continuum detection in SHARDS, in red.

red part of the spectrum and the fact that farther away objects are fainter and so we miss more of them (Malmquist bias). We also notice that the relative number of LAEs is larger beyond $z \sim 5.0$-5.5. The fraction of pure LAEs and LBGs and their behaviour with z are discussed in depth in Chapter 3. The complete list of redshifts is given in Table 2.4.

2.4.2 Star Formation Rates

Traditionally, two different methods have been used to obtain SFRs for the LAEs and LBGs. The emitters SFR can be obtained from the Lyα line emission following Kennicutt (1998), who assumed case B recombination (Brocklehurst 1971) and a Salpeter (1955) IMF over a 0.1-100 $M_\odot$ mass range:

$$\mathrm{SFR}\ (M_\odot\ \mathrm{yr}^{-1}) = \frac{L(\mathrm{H}\alpha)\ (\mathrm{erg\ s}^{-1})}{1.26 \times 10^{41}}, \tag{2.3}$$

where $L(\mathrm{H}\alpha) = L(\mathrm{Ly}\alpha)/8.7$.

The other method is based on the UV continuum luminosity density at 1500 Å (L_{1500}) with the assumptions of solar metallicity and a Salpeter IMF,

as in Madau et al. (1998):

$$\text{SFR } (M_\odot \text{ yr}^{-1}) = 1.25 \times 10^{-28} L_{1500} \text{ (erg s}^{-1} \text{ Hz}^{-1}). \quad (2.4)$$

To correct for galactic dust extinction, A_λ values from the Schlafly & Finkbeiner (2011) dust maps are used. The internal dust extinction is calculated following Calzetti et al. (1994), Calzetti et al. (2000) and Castellano et al. (2012), assuming $F_\lambda \propto \lambda^\beta$, where β is the UV slope. This β slope is estimated via linear fit to the magnitudes measured in the filters sampling the rest-frame UV wavelength from 1300 Å through to 2600 Å:

$$m_i = -2.5(\beta + 2.0)\log(\lambda_i) + C, \quad (2.5)$$

where m_i is the magnitude measured in the filter centred in λ_i and C is a constant. The UV opacity is then calculated through:

$$A_{\text{UV}} = 2.31(\beta - \beta_0), \quad (2.6)$$

where β_0 is the intrinsic UV spectral slope, fixed at $\beta_0 = -2.1$ for $\beta > -1.4$ or $\beta_0 = -2.35$ for lower measured UV slopes, as prescribed in Calzetti et al. (2000). The mean β values obtained at $z \sim 4$ ($3.5 \leq z < 4.5$), $z \sim 5$ ($4.5 \leq z < 5.5$) and $z \sim 6$ ($5.5 \leq z < 6.5$) are -1.85 ± 0.49, -1.98 ± 0.57 and -2.19 ± 0.66, respectively. These β values are consistent with the literature (see, *e.g.*, Dunlop et al. 2012, and references therein).

A problem with the Kennicutt method is that the Lyα line is very sensitive to both H I resonant scattering and dust absorption. Therefore the actual Lyα emission of the galaxy can be greatly affected. Indeed, the Lyα photon escape fraction (f_{esc}) is very uncertain. Many recent works have estimated it at high-z finding very different results between $f_{\text{esc}} = 0.02$-0.5 (Robertson et al. 2010; Hayes et al. 2010, 2011; Matthee et al. 2016; Sobral et al. 2017, 2018b), which certainly adds a large, and difficult to quantify, uncertainty to the SFRs derived through the Lyα emission in our sample. On the other hand, the continuum is much less affected by absorption and scattering due to neutral gas so we assume that SFRs calculated using the rest-frame UV continuum luminosity at 1500 Å are more reliable. In those cases where we have LBGs with emission line we can compare their SFRs calculated via one method and the other. For all the LAEs/LBGs, the SFRs calculated using Eq. (2.4) are much larger, reaching differences of even three orders of magnitude

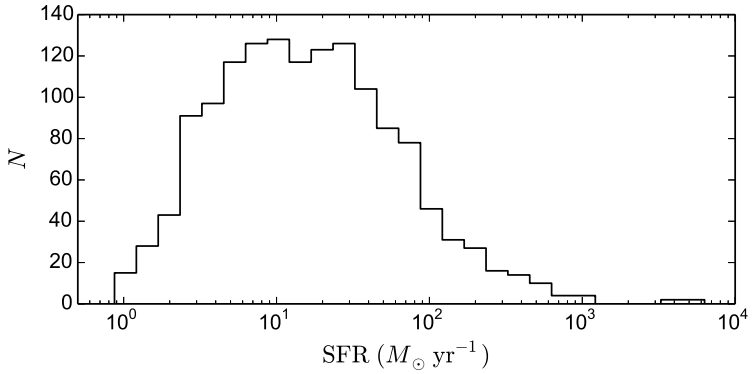

Figure 2.12: LBGs UV-derived SFR histogram. Calculated through the L_{1500} (Eq. 2.4). The sample presents an average and median value of 58 ± 7 $M_\odot$ yr^{-1} and 15 ± 9 $M_\odot$ yr^{-1}, respectively, with seven objects above 10^3 $M_\odot$ yr^{-1}.

for 11 candidates (2.7% of the LAEs/LBGs subsample) with bright M_{1500} but a small Lyα line. This large difference can be due to: 1) the uncertainties in measuring the Lyα line due to scattering and extinction effects, and 2) the fact that the continuum measurement integrates not only the current starburst but also the recent previous history of star formation of that source (Salim et al. 2009; Salmon et al. 2015). Moreover, for these LBGs with Lyα emission line, the exact ratio between the two SFRs, despite the line-derived one being always lower, seems to be stochastic. This is probably due to the fact that the intensity of the line emission relative to the continuum heavily depends on the strength of the current starburst, which quickly decays within a few Myr, as will be further discussed in Chapter 3. Thus, the ratio between SFRs, measured with the Kennicutt and the Madau methods, will mostly depend on the current stage of the young starburst and the number of former recent starbursts undergone by a given source, apart from extinction.

The SFRs, corrected for extinction following the above prescription, are given in Table 2.4, where we show the SFR based on L(Lyα) and/or L_{1500} depending on whether the galaxy presents emission line or continuum emission. As expected for these early galaxies, the SFRs are fairly high (*e.g.,* Bouwens et al. 2007, 2015b; Mashian et al. 2016; Casey et al. 2017), with those calculated with L_{1500} being 58 ± 7 $M_\odot$ yr^{-1} on average, with a median of 15 ± 9 $M_\odot$ yr^{-1}. The complete LBGs SFR distribution can be seen in Fig. 2.12. There are 7

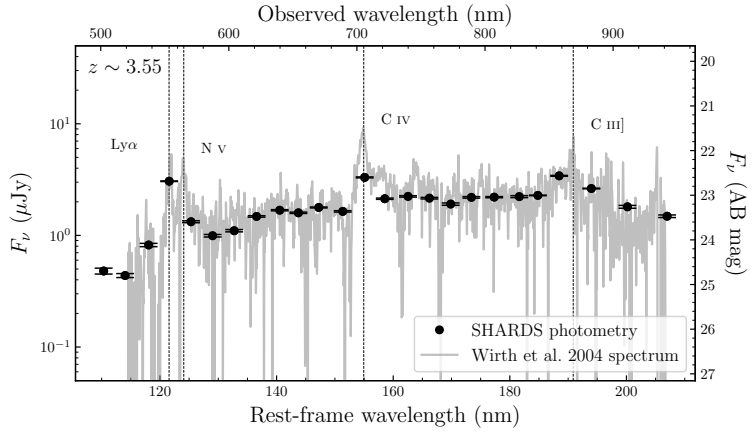

Figure 2.13: SED of the object SHARDS J123723.72+622113.0, a very bright dusty AGN with $\beta = -0.71 \pm 0.40$, resulting in $A_{\rm UV} = 3.22 \pm 0.93$ mag and a dust corrected SFR of $1.11 \pm 0.08 \times 10^3\ M_\odot\ {\rm yr}^{-1}$. Overlapped in grey, we show the spectrum available in the Team Keck Treasury Redshift Survey (TKRS) from Wirth et al. (2004). Lyα, N V, C IV and C III] lines are identified.

objects forming stars at a rate above $10^3\ M_\odot\ {\rm yr}^{-1}$. These galaxies are reported AGNs or very dusty star-forming galaxies (see Casey et al. 2017) whose SEDs present a very red UV slope. An example of this is given in Fig. 2.13.

2.4.3 Equivalent Widths

The EW of the Lyα line tells us the relative strength of the young star formation burst. It relates the line emission due to the current starburst to the continuum produced by the more evolved population of the galaxy. For every LBG with line emission we obtain the EW measuring the continuum either in the adjacent SHARDS filter or, if this filter has a large uncertainty, calculating a weighted mean of the fluxes in nearby filters. If it is not possible to get a continuum from the SHARDS filters, the continuum is obtained from *HST* broad band data. To establish a minimum reliably detected line flux we impose that the filter measuring the line emission should be at least 1σ above the continuum flux level. Applying this, we reach a minimum measured rest-frame EW of 5.1 ± 4.7 Å.

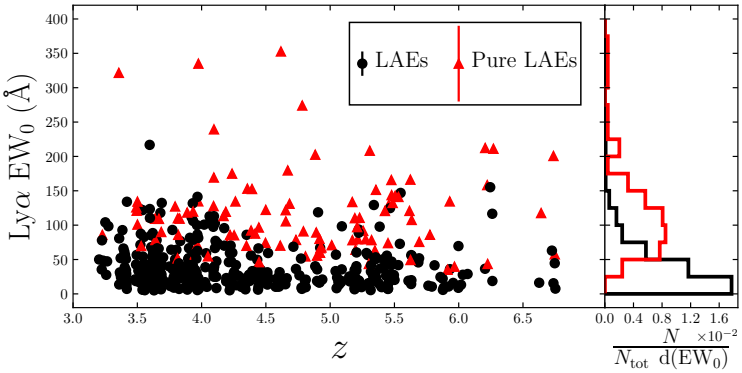

Figure 2.14: Rest-frame EW of the Lyα source candidates with emission line. Red triangles show the pure LAEs while the black circles are the LAEs/LBGs. Error bars are omitted for convenience, but they are given in Table 2.4. Median error bars are shown in the legend. The EW$_0$ probability density distribution independent of z is shown in the right panel. Pure LAEs show larger EWs than LAEs/LBGs. Moreover, the number of sources increases at lower EWs for both populations.

Measuring a continuum for pure LAEs is difficult as these objects are characterised by having very low or no detectable continuum emission in SHARDS. In some of these cases we can use broad band data but there are a few ones (28) where we cannot reliably measure their continua and therefore we cannot calculate the EW. As expected, pure LAEs have larger EWs than the rest of LAEs, although their uncertainties are also larger, since their continuum is much fainter. In our sample, the pure LAEs rest-frame EWs are in the range 35-353 Å, with a median value of 109.1 ± 7.6 Å, while those of the LBGs/LAEs are in the range 5.1-217 Å, with a median of 27.8 ± 2.0 Å. Nonetheless, the number of sources decreases as we move to higher EWs (see right panel in Fig. 2.14). Notice that for the LBGs we plot only those 404 that are also LAEs, which means that there are 1030 additional non-LAEs/LBGs with no emission line detected, *i.e.*, with Lyα EW$_0 < 5.1$ Å.

In this work we have detected LAEs up to quite low EWs. However, in order to compare with previous studies, we have analysed the fraction of them (respect to the complete LAEs and LBGs sample) with EW$_0$ larger than a

standard commonly used value of Lyα EW$_0 > 25$ Å. The comparison is done with various authors at different redshifts (Pentericci et al. 2011; Stark et al. 2011; Curtis-Lake et al. 2012; Ono et al. 2012; Treu et al. 2013; Schenker et al. 2014; Tilvi et al. 2014; Cassata et al. 2015; De Barros et al. 2017; Caruana et al. 2018). Results are shown in Fig. 2.15, where we divided the sample into two brightness groups. Our fraction of LAEs with EW$_0 > 25$ Å ($X_{\mathrm{Ly}\alpha}$) matches well those previously obtained, although we register a slightly smaller fraction of the faintest sources at $z \sim 4$ and $z \sim 5$. The decrease of $X_{\mathrm{Ly}\alpha}$ beyond $z \sim 6$ found by other authors (*e.g.*, Caruana et al. 2014; Schenker et al. 2014) suggests an increase of the H I abundance as we move to a non-fully reionised Universe (see, *e.g.*, Fan et al. 2006), which would strongly affect the scattering of the Lyα line.

2.5 Comparison with previous high-z galaxy samples

After obtaining the basic physical parameters of our sample presented in Sec. 2.4, we are in position to build LFs at different redshifts and compare the number density of selected sources with those selected in previous broad band selections.

2.5.1 Differences with traditional broad band selection criteria

Keeping in mind our magnitude completeness estimation from Sec. 2.3, we compare our high-z galaxy sample results with previous works. As reference, we take the large multi-field survey carried out by Bouwens et al. (2015b, hereinafter B15). In that work the LBGs search is made using *HST* broad band colour criteria. They find a much higher number of objects than we do. Indeed, in the GOODS-N field, B15 found 3917 LBGs, out of which 3455 fall within our redshift range according to their classification. Instead, we only selected 1558 objects. To understand this discrepancy we analyse in further detail the B15 GOODS-N sample.

First of all we remove the GOODS-N B15 objects that fall out of our field of view. Their images survey 133.7 arcmin^2 in the GOODS-N field, while our effective search field is only $\sim$ 128.4 arcmin^2 (see Sec. 2.1). Moreover, the centring and exact shape of the two fields differ slightly. Thus, we miss 405 galaxies (11.4%) just because of these effects, leaving still 3050 objects to explain. However, only 2757 of them have photometric detection in at least one of the SHARDS filters. This means we are missing 293 sources, or equivalently, 9.6% of the B15 sample falling within our field, with no detections in SHARDS.

Another effect to consider is the loss of sources due to neighbour contamination. This is so because of the higher spatial resolution of the *HST* in

Table 2.4: Main relevant parameters of the sample. The full version of this table is shown in Appendix A.

Object Name	R.A.	Dec.	z	$L_{Ly\alpha}$	m_{1500}	$SFR_{L_{Ly\alpha}}$	$SFR_{L_{1500}}$	EW_0
	(J2000)	(J2000)		(10^{42} erg s^{-1})	(AB mag)	($M_\odot$ yr^{-1})	($M_\odot$ yr^{-1})	(Å)
(1)	(2)	(3)	(4)	(5)	(6)	(7)	(8)	(9)
SHARDS20010117	12:35:48.07	62:12:02.39	4.28±0.06	-	27.5±0.6	-	1.7±0.9	-
SHARDS20007539	12:35:48.12	62:12:03.78	5.38±0.07	0.9±0.2	25.8±0.2	0.8±0.2	11.2±1.7	15± 3
SHARDS20012481	12:35:50.89	62:11:58.49	5.69±0.06	-	26.2±0.1	-	10.7±1.3	-
SHARDS20005927	12:35:51.53	62:12:16.49	3.22±0.07	-	26.4±0.2	-	27.4±4.9	-
SHARDS20005405	12:35:51.63	62:12:12.66	4.03±0.07	-	25.6±0.2	-	36.8±7.9	-
SHARDS20008074	12:35:52.15	62:11:20.83	5.53±0.07	0.5±0.2	26.2±0.1	0.4±0.2	8.0±1.0	42±31
SHARDS20008444	12:35:53.20	62:10:32.94	4.01±0.07	-	26.8±0.6	-	2.8±1.5	-
SHARDS20010810	12:35:53.38	62:10:23.25	5.12±0.06	-	27.2±0.3	-	6.2±1.5	-
SHARDS20005669	12:35:54.09	62:10:32.87	3.36±0.07	0.2±0.2	26.4±0.3	0.2±0.2	137.1±36.3	14±10
SHARDS20011405	12:35:54.26	62:10:18.83	5.37±0.07	-	25.9±0.2	-	9.9±2.0	-
SHARDS20006420	12:35:54.43	62:10:33.80	3.88±0.06	-	26.0±0.3	-	37.5±11.3	-
SHARDS20006258	12:35:54.54	62:12:14.59	3.48±0.06	0.3±0.2	25.7±0.1	0.3±0.2	12.9±1.8	21±12
SHARDS20013727	12:35:55.03	62:12:04.79	5.96±0.07	0.3±0.2	26.2±0.2	0.3±0.2	160.5±33.0	16±10
SHARDS20009009	12:35:55.19	62:11:25.40	3.89±0.06	-	26.7±0.3	-	16.7±5.1	-
SHARDS20006827	12:35:55.65	62:10:19.00	4.28±0.06	-	26.2±0.2	-	5.5±1.2	-
SHARDS20008662	12:35:55.79	62:10:28.94	4.17±0.07	-	26.9±0.6	-	2.9±1.6	-
SHARDS20008870	12:35:55.83	62:12:32.05	4.19±0.07	-	27.1±0.5	-	4.0±2.0	-
SHARDS20010887	12:35:56.17	62:11:45.41	5.14±0.06	-	26.2±0.3	-	76.2±23.6	-
SHARDS20010975	12:35:56.63	62:11:43.25	5.40±0.07	0.2±0.2	26.8±0.5	0.2±0.2	10.7±5.4	11± 9
...	...	...	...	...	...	...	...	...

(1) Name of the object using the SHARDS identification. (2) Right ascension. (3) Declination. (4) Photometric redshift. (5) Lyα luminosity (in case the Lyα emission line is detected). (6) Apparent magnitude measured at a rest-frame wavelength of 1500 Å (not measurable in some pure LAEs). (7) SFR derived from the Lyα emission. (8) SFR derived from the rest-frame UV continuum at 1500 Å. (9) Rest-frame Lyα EW.

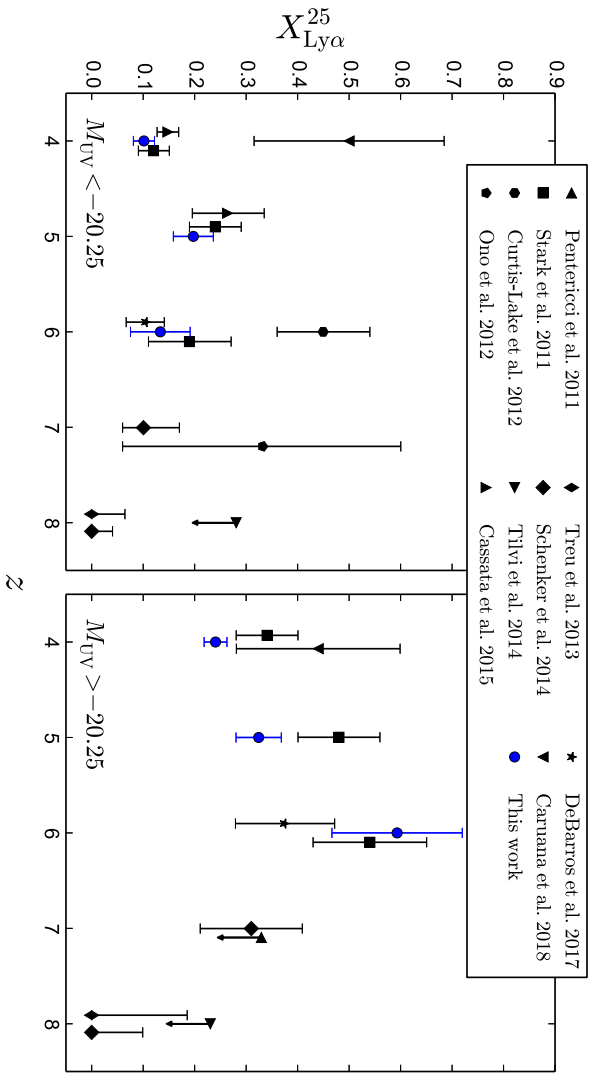

Figure 2.15: Fraction of objects with rest-frame Lyα EW > 25 Å versus redshift. *Left*: galaxies brighter than $M_{\mathrm{UV}} = -20.25$. *Right*: galaxies fainter than $M_{\mathrm{UV}} = -20.25$. A slight offset in redshift is introduced to improve clarity. We show results from Pentericci et al. (2011), Stark et al. (2011), Curtis-Lake et al. (2012), Ono et al. (2012), Treu et al. (2013), Schenker et al. (2014), Tilvi et al. (2014), Cassata et al. (2015), De Barros et al. (2017) and Caruana et al. (2018).

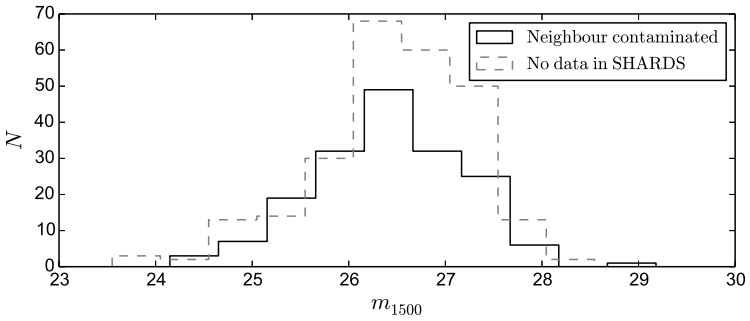

Figure 2.16: Rest-frame m_{1500} distribution of the objects present in the B15 sample that are missed in this work because of non-detection or seeing issues. The m_{1500} was measured using *HST* broad band photometry.

comparison to our ground-based GTC/OSIRIS resolution. To quantify this effect, we mask the stars and other large objects in the SHARDS images and analyse how many of the B15 candidates would be affected by these large objects in our SHARDS images. For the smaller objects, we assume that any B15 galaxy with a brighter neighbour (or at most 0.5 mag fainter) at a distance of $\theta = 0.9$ arcsec or less (typical SHARDS seeing) is at least partially contaminated in our images, and therefore we could be missing it. We find 192 objects (7%) affected by this issue. The m_{1500} distribution of the objects missed because of non-detection or neighbour contamination is shown in Fig. 2.16. At this point, there are still 2565 galaxies of the B15 that should be detected.

We then limit the remaining B15 sample to those objects that should be in our selection. That is, sources brighter than our completeness magnitude, within our field, not affected by proximity contamination and whose redshifts fall in the range we can measure with our 25 SHARDS filters. Since we will exclude galaxies falling outside our m_{1500} completeness limit, we first calculate the wavelength corresponding to 1500 Å rest-frame for each B15 object, which depends on z, to identify the *HST* filter that better samples that wavelength in each case. Then we look for every object in its corresponding filter in the *HST*/ACS catalogue to check whether or not we should detect it with the SHARDS data. Up to $m_{1500} = 25.87$ AB, there are 575 sources meeting all our limiting conditions. However, out of these, 115 (20.0%) are not actually high-z galaxies neither in our study nor according to the photometric redshifts calculated in Ba19.

Table 2.5: Broad band low-z interlopers fraction in GOODS-N objects from B15. The redshift distribution of these objects can be seen in Fig. 2.17

m_{1500} limit (1)	N in B15 (total) (2)		N in B15 (interlopers) (3)		Interlopers fraction (%) (4)	
	θ=0.9″	θ=1.2″	θ=0.9″	θ=1.2″	θ=0.9″	θ=1.2″
25.50	329	311	68	55	20.67	17.68
25.87	575	539	115	92	20.00	17.07
26.00	666	628	133	108	19.97	17.20
26.13	762	721	151	126	19.82	17.48
26.50	1133	1074	234	201	20.65	18.72
27.00	1674	1582	359	316	21.45	19.97
27.50	2077	1959	463	416	22.29	21.24

Each cell shows the amount of sources matching both the brightness limit imposed in each case and two different spatial resolution limits (isolation distance to be considered not contaminated by neighbours in the SHARDS images). (1) Apparent magnitude at 1500 Å. Only sources brighter than this limit are considered for each row. (2) Total amount of objects labeled as $z \simeq$ 3.4-6.8 in B15. (3) Amount of them considered low z interlopers according to the SHARDS photometry in both this work and Ba19. (4) Fraction of low-z interlopers.

We are conscious that the magnitude limit and spatial resolution in our search cause a loss of sources. Nevertheless, even considering these effects, we still find a non-negligible fraction of objects in the B15 sample that meet our limiting magnitude condition but are not selected applying our criteria. These missing sources are visually revised in the SHARDS images to confirm they are bright and isolated enough not to be contaminated by any neighbour. We find that these 115 sources do not look like high-z LBGs when seen with our higher spectral resolution. Instead, those objects seem to be either lower z Balmer break galaxies, cool stars or just red galaxies. Indeed, when these sources are seen through a few broad band filters, they could be easily misclassified as high-z LBGs, as they may present a reasonable flux drop from one broad filter to the next.

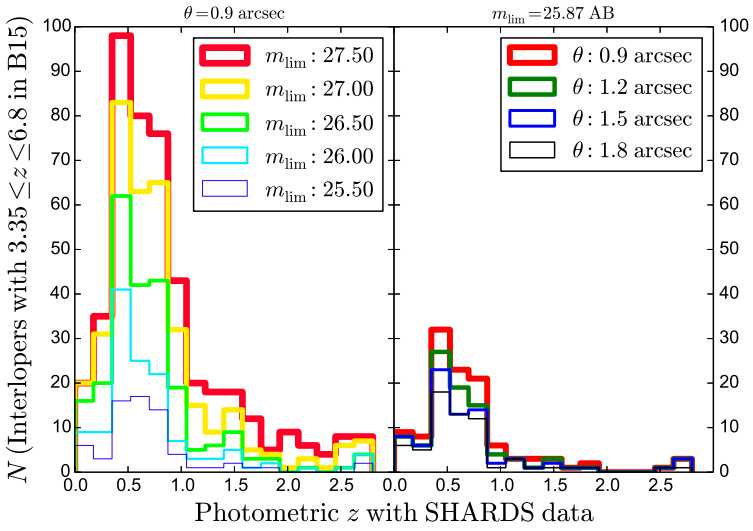

Figure 2.17: Redshift distribution of the objects in the B15 sample that appear as interlopers according to both our selection criteria and the photometric fits with SHARDS data from Ba19. On the left, different colours correspond to different m_{1500} limits with a fixed isolating distance (0.9 arcsec). On the right, different isolating distances with a fixed m_{1500} limit of 25.87 AB mag, corresponding to our 90% completeness. The shape of the distribution is practically the same in all cases. The peak around $z \sim 0.5$ suggests a wrong identification of the Balmer break as the Lyman break.

Note that we have not recomputed photometric redshifts for objects that are not in our sample. However, since they have not been selected with our criteria, they are considered lower z sources. In order to study the redshift distribution of these not selected sources, we make use of the redshifts calculated in Ba19. In addition, we repeat the analysis previously described in this section using different values of magnitude limit and flux contamination distance (seeing). The number of B15 galaxies that meet our limiting conditions but whose SHARDS photometric z is much lower than that given in B15 is shown in Table 2.5. In this Table, we use both 0.9 arcsec (corresponding to the typical SHARDS seeing) and 1.2 arcsec (a bit above that seeing) as the

minimum distance between objects at which they can be considered isolated. There is little change in the interloper fraction for limiting magnitudes up to $\sim$ 26.13 AB, mostly constant at $\sim$ 20%. Beyond that, this fraction slightly increases (up to 22.3% at $\sim$ 27.5 AB), which makes sense since fainter objects are more difficult to characterise and identify as either good galaxy candidates or interlopers.

Therefore we conclude that $\sim$ 20% of the B15 sample, up to $m_{1500} \sim 25.87$ AB, is actually misclassified as high-z LBGs (quite above the $\sim$ 2-6% found by Vulcani et al. 2017). It is interesting to see the redshift distribution of these misidentified objects. Figure 2.17 is a histogram representing them as a function of redshift for different $m_{\rm lim}$ and isolation distances. We find a clear concentration of sources at very precise redshifts. Moreover, the shape of the interlopers redshift distribution is practically the same independently of the depth and seeing considered. This implies that these interlopers are not due to seeing or brightness issues, but to the spectral resolution quality. In fact, the distribution peaks around $z \sim 0.5$, and a large fraction ($\sim$70%) of the misclassified sources are distributed between z = 0.3-0.9, corresponding to a range between $z \sim$ 3-5 if the Balmer break is mistakenly taken as the Lyman break. We would actually expect a similar fraction of interlopers in other broad band studies with similar colour selection criteria. Fig. 2.18 shows an example of one of these misidentified objects selected in B15.

Finally, for some galaxies in the B15 sample that also meet our selection criteria, the redshift assigned in B15 does not match ours within a $\Delta z = 0.3$ error (approximately twice our highest photo-z error). An example of this is shown in Fig. 2.19. To better characterise this discrepancy, we study the subsample of objects with photo-z calculated both in B15, Ba19 and this work, consisting on 933 galaxies. The B15 redshift of 138 of these sources ($\sim$ 15%) are found to differ from both Ba19 and our calculated redshifts. We consider our redshift determination much more accurate since we have a much better spectral resolution in our data, and our redshifts are in an excellent agreement with spectroscopic values as shown in Fig. 2.10. Indeed, the photo-z obtained with broad band filters show a considerable uncertainty.

Interestingly, there are other 312 objects in our sample that are not selected by B15. Of them, 121 are placed in two little gaps of the B15 GOODS-N field, as shown in Fig. 2.20. Of the remaining 191, 17 have spectroscopic z available in Rainbow and/or NED that matches the photo-z calculated in this work. A closer look to their SEDs does not give us any conclusive hint about why they are not selected using broad band filters. An example of these objects is shown in Fig. 2.21. Some of these galaxies are pure LAEs with strong line emission and a very faint continuum that could have been missed with broad band filters.

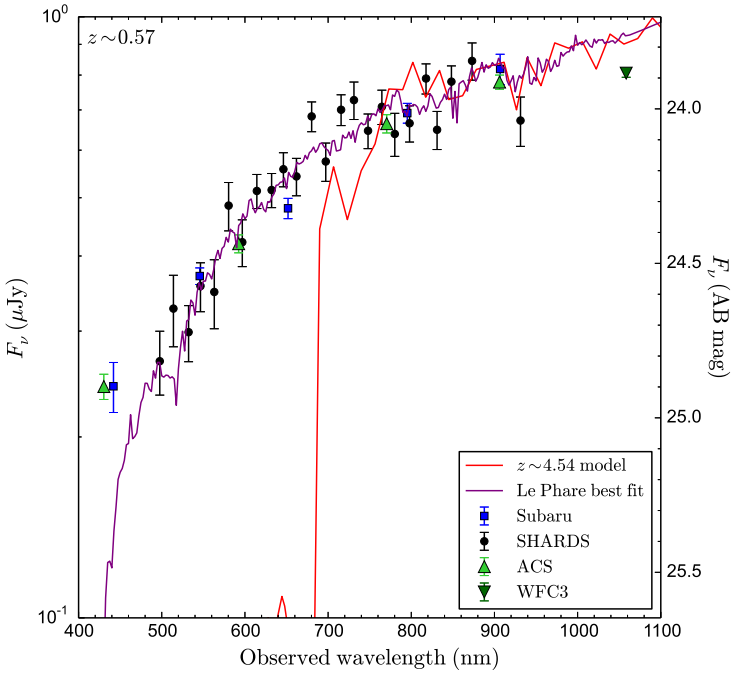

Figure 2.18: SED of the object SHARDS J123659.36+621518.7, wrongly selected as a $z \sim 4.54$ LBG using broad band criteria. The information as given by the green triangles (ACS and WFC3 data) can lead to an incorrect Lyman break detection. A LePHARE fit with the complete SHARDS data (purple line) shows that this is a $z \sim 0.57$ object. The red line shows where the break would appear if this were a $z \sim 4.54$ galaxy.

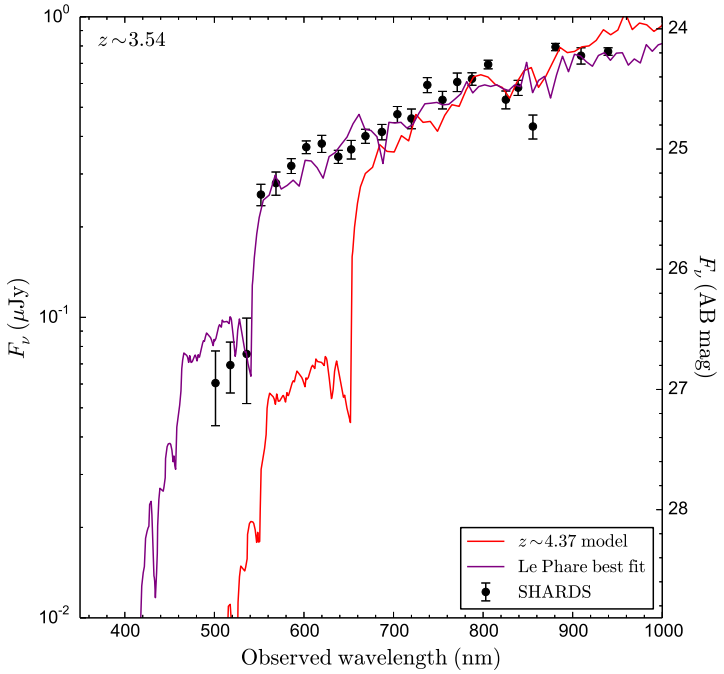

Figure 2.19: SED of the source SHARDS J123643.53+621121.4, one of our LBGs at $z \sim 3.54$ wrongly selected as an object at $z = 4.37$ using broad band criteria. At that redshift we should see the Lyman Break around 640 nm, which is clearly not the case when observed with the higher SHARDS resolution. Our z matches fairly well the LePHARE fit (purple line). The red line shows where the Lyman Break would be if it were at $z = 4.37$.

This explanation is however valid for just 16 objects out of the 191. We do not know why the rest are not selected with the broad band criteria.

Summarising, from the 3455 objects detected by B15 in GOODS-N within our z range, after considering limiting brightness difference, small field of view differences and possible neighbouring light contamination, we would expect to detect 575 of them up to our 90% completeness magnitude. Of them, 115 are not selected and are classified as low z objects, implying that $\sim 20\%$ of the B15 broad band selected sample up to $m_{1500} = 25.87$ AB mag seem to be interlopers. On the other hand, we have further found 191 galaxies that we consider good candidates and were not selected in B15.

2.5.2 Luminosity Functions

We proceed now to build the LBGs LFs, which are shown in Fig. 2.22. The 90% completeness absolute magnitude limit for each redshift is marked with a dashed vertical line. A correction for those objects that we miss, either because of non-detection in the SHARDS images or because of neighbouring light contamination of their SEDs, is considered for each z range, based on their m_{1500} distribution (see Fig. 2.16). The magnitude values are measured using *HST* photometry. To correct the data in the faint region of the LF, we use the $V/V_{\rm max}$ correction (Schmidt 1968) to adequately consider the effective volume sampled by each detected source. We divide the sample in three main redshift bins to facilitate comparing with the literature, namely $z \sim 4$ ($3.5 \leq z < 4.5$), $z \sim 5$ ($4.5 \leq z < 5.5$) and $z \sim 6$ ($5.5 \leq z < 6.5$). A Schechter function (Schechter 1976) is used to fit the data:

$$\phi(M) = \phi^* \frac{\ln(10)}{2.5} \exp[-10^{0.4(M^*-M)}] 10^{0.4(M^*-M)(\alpha+1)}. \quad (2.7)$$

Since we are missing a fair number of the faintest objects, we cannot get information about the power-law term of the Schechter function. Therefore, the α parameter cannot be directly calculated, so we fix its value to a value consistent with the literature. In particular, we set it at each redshift to the mean value obtained from the following authors: Bouwens et al. (2007), van der Burg et al. (2010) and B15 at $z \sim 4$, Bouwens et al. (2007), Iwata et al. (2007), McLure et al. (2009), van der Burg et al. (2010) and B15 at $z \sim 5$ and Bouwens et al. (2007), McLure et al. (2009), Bouwens et al. (2012), Bowler et al. (2015) and B15 at $z \sim 6$. It is important to note that the α values derived from the literature may be overestimated according to the large interloper fraction we find in typical surveys made through broad band observations. The bright region

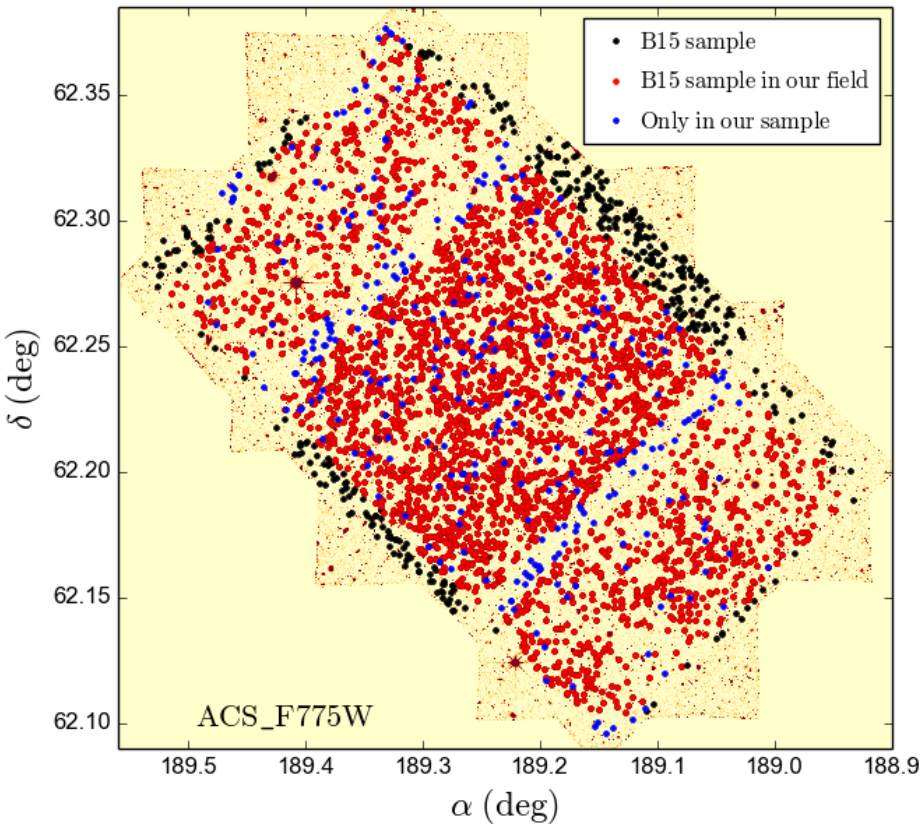

Figure 2.20: Spatial differences between the GOODS-N field sampled in B15 and the one sampled with SHARDS. The black dots are included in the B15 sample, but not in ours. The red dots are those within the SHARDS effective field. The blue dots are objects selected in our sample but not in B15. Small gaps of the B15 GOODS-N field contain 121 of them, but there are still 191 more within their effective field.

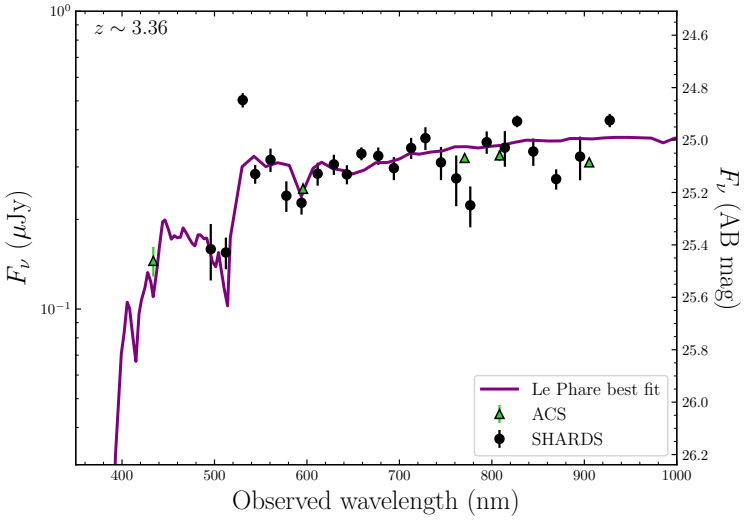

Figure 2.21: SED of the object SHARDS J123646.68+621517.1, selected with our criteria but not with the broad band selection criteria used in B15. The best LePHARE fit is shown in purple.

can be fitted with the exponential term of the Schechter function to estimate ϕ^* and M^*. The results are listed in Table 2.6. Furthermore, we notice that the brightest points of our LFs tend to be slightly over their fitted Schechter function. This is in agreement with recent large field studies that propose a power-law behaviour for the bright region of the LFs, instead of the classical Schechter function (Sobral et al. 2017, 2018). Nonetheless, our field is not large enough to claim conclusive results in this regard.

A cosmic variance calculator, developed by Trenti & Stiavelli (2008) using halo models, is also considered to evaluate the effect of cosmic variance and Poisson counts errors, as done *e.g.*, in B15, Conselice et al. (2016) and Vulcani et al. (2017). We thus calculate that the number counts at $z \sim 4$, $z \sim 5$ and $z \sim 6$ has a fractional error due to cosmic variance of 16%, 20% and 28%, respectively, added to the error bars. These uncertainties are relatively large in our study as we are limited to a relatively small field (128.4 arcmin^2).

At $z \sim 6$ we have large uncertainties, due to low-number statistics, cosmic

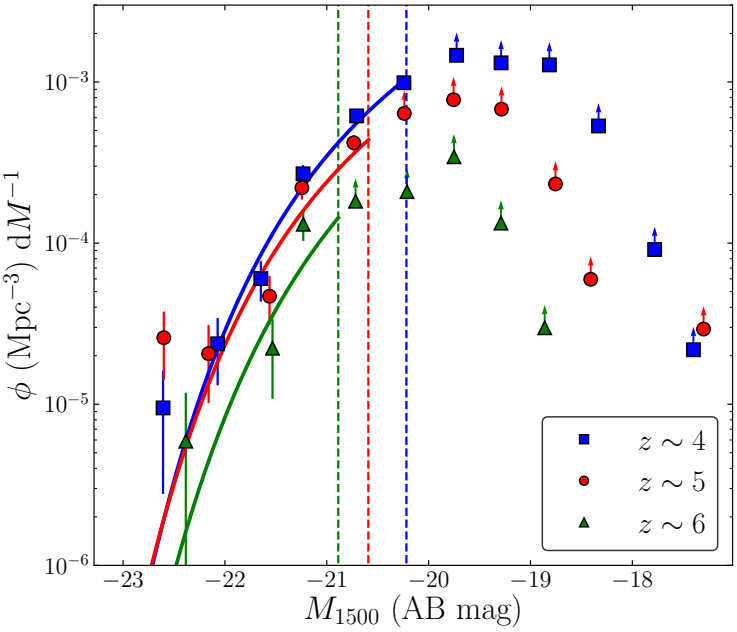

Figure 2.22: LFs of the LBG sample divided in three z ranges: $z \sim 4$ ($3.5 \leq z < 4.5$), $z \sim 5$ ($4.5 \leq z < 5.5$) and $z \sim 6$ ($5.5 \leq z < 6.5$). The solid lines correspond to the best-fitting Schechter function obtained at each z, while the dashed vertical lines show the 90% completeness absolute magnitude at each redshift.

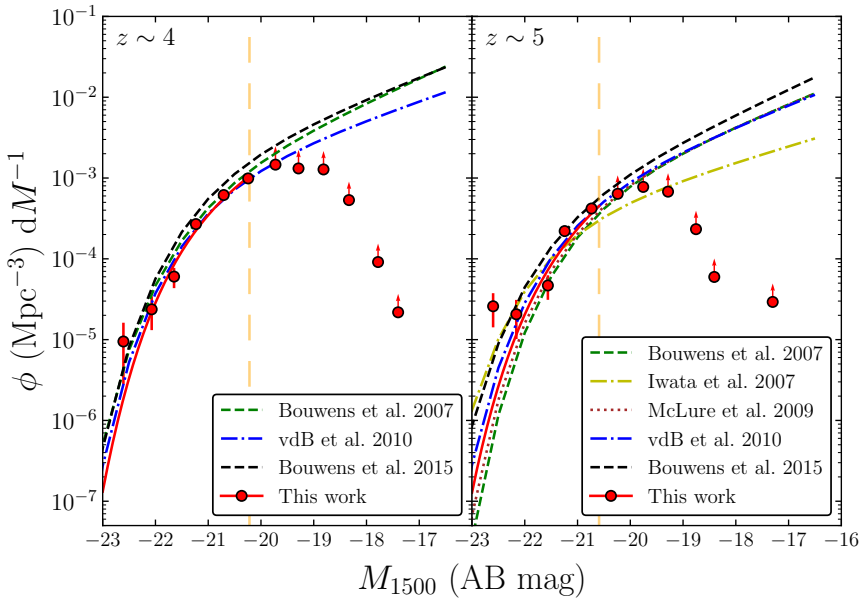

Figure 2.23: LFs of the most populated redshift ranges of our study ($z \sim 4$ and $z \sim 5$) overlaid with LFs from previous works (Bouwens et al. 2007; Iwata et al. 2007; McLure et al. 2009; van der Burg et al. 2010; Bouwens et al. 2015b). The dashed faded orange vertical line indicates our 90% completeness magnitude limit. Our LFs fit well previous studies in the bright region. However, they keep systematically below a previous broad band survey in our field (B15). We associate this to interlopers issues in broad band selection criteria. For this same reason, we expect the faint-end of the LF to be below previously estimated values, although our survey lacks the capability of sampling it.

Table 2.6: Best-fitting Schechter parameters for the LFs at $z \sim 4$, $z \sim 5$ and $z \sim 6$.

$\langle z \rangle$	M^*_{1500}	ϕ^* (10^{-3} Mpc^{-3})	α[1]
4	-20.75±0.13	1.55±0.31	-1.64±0.04
5	-20.85±0.26	0.90±0.34	-1.64±0.04
6	-20.74±0.58	0.54±0.61	-1.79±0.03

[1] Fixed to the mean value given in the literature referred in the text.

variance effects and Poissonian errors. For the other two redshift ranges, the results are comparable to previous studies (see Fig. 2.23). Notice that both at $z = 4$ and 5, our LF estimations fit the bright-end fairly well, decaying quickly as we move to fainter magnitudes.

We do match previous studies in the bright region. Nevertheless, even in this region our LFs are always below that from B15, with whom we share the GOODS-N field. We are indeed missing candidates because of seeing contamination in this region, but this effect is already corrected, though not enough to explain the difference we find, since the seeing contamination only affects a $\sim$ 7% of the cases, as described in Section 2.5.1. On the other hand, the reliability of our candidates is very high, suggesting that the reason for the discrepancy is not only due to a lack of faint objects in our sample, but to an overestimation in the detection of high-z LBGs when the selection is made with broad band filters. We cannot estimate the precise effect that the interloper fraction produces at magnitudes beyond our completeness limit, but we expect it to increase according to the trend shown in Table 2.5, implying an uncertain calculation of the Schechter α parameter in surveys done with broad band photometry. We would like to stress the importance of having good spectral resolution for building a high-z galaxy sample free from interlopers. As an estimation, we would expect the "real" LF to be somewhere between ours and that given in previous *HST* works, to account for the seeing and limiting magnitude difference. Our study supports that previous broad band LFs should be downscaled by a factor $\sim$ 20%, which could be even more important at fainter magnitudes. This would lead to a decrease in the faint end slope of the LFs.

2.6 Conclusions

We have used the SHARDS survey to carry out a search for high-z LAEs and LBGs. The narrow/medium width of the 25 SHARDS filters and their com-

pleteness in the 500-941 nm wavelength range have allowed us to develop very precise SEDs in the optical/NIR. We have therefore sampled the high-z galaxy population from $z \sim 3.4$ to $z \sim 6.8$ in a uniform way. The special characteristics of the filters have allowed us to simultaneously detect both LAEs and LBGs, using a robust strategy based on the identification of the Lyman break via colour excesses and photometric fits to the SEDs. The SED information has been complemented using additional data from *HST*/ACS, *HST*/WFC3, Subaru/Suprime-Cam, Subaru/MOIRCS, CFHT/WIRCam, *Spitzer*/IRAC and *GALEX*. We built a sample consisting of 1558 candidates, separated in 124 pure LAEs with barely any continuum detected in SHARDS, 404 LAEs/LBGs and 1030 non-LAEs/LBGs with no Lyα emission line. For the entire sample we have calculated redshifts, SFRs, Lyα EWs and $X_{\mathrm{Ly}\alpha}$. Finally, we have studied the LFs, comparing them with the literature. The main conclusions are:

(a) The characterisation of the high-z LAEs and LBGs population ideally needs both a very good spectral resolution, as achieved with SHARDS, and a extremely good depth and spatial resolution only achievable with *HST*, and the *James Webb Space Telescope* (*JWST*) in the near future. The main advantage of our work is the robustness of the high-z sample. We reach our 90% and 50% completeness limits at 25.87 and 26.13 AB mag, respectively, with a seeing of ~ 0.9 arcsec. The LFs obtained in this chapter are therefore a solid lower limit of the galaxy density distribution. They should be very close to the real LFs, which we estimate must be somewhere between ours and those given in previous broad band *HST* studies, as the latter are affected by a non-negligible fraction of interlopers.

(b) The high-z candidates selection is more reliable with a large set of consecutive narrow/medium band filters than with broad band filters, as the higher spectral resolution is crucial in rejecting interlopers. We have found that, from the objects previously selected in GOODS-N within our z range and magnitude limit and not affected by seeing issues, $\sim 20\%$ do not pass our selection criteria and are in fact low-z interlopers. This is in disagreement with the previous estimation of broad band interlopers ($\sim$ 2-6%) from Vulcani et al. (2017). We also show that this interlopers ratio slightly increases for fainter sources, from $\sim$ 26.13 AB mag up to the magnitudes we can reliably measure with SHARDS ($\sim$ 27.0 AB mag), expecting that it will be even higher for fainter magnitudes.

(c) Within the objects selected in this work, some redshift inconsistencies are found between our photometric redshifts and those obtained from a

colour selection criteria using broad band filters. These inconsistencies affect $\sim 15\%$ of the common sub-sample, highlighting the importance of good spectral information when estimating photometric redshifts.

(d) Thanks to the simultaneous detection of a large number of LAEs and LBGs we have been able to obtain very good statistics of $X_{\mathrm{Ly}\alpha}$ as a function of z. Using a Lyα EW$_0$ threshold of 25 Å, the results are in good agreement with previous works, showing an increase of the fraction of high-EW objects up to $z \sim 5.5$-6. Beyond that redshift, $X_{\mathrm{Ly}\alpha}$ decreases, probably because the reionisation is not completed at that epoch, thus, the increasing abundance of H I scatters the Lyα emission line.

(e) The ϕ^* and M^* Schechter parameters of the LFs found in this work at $z \sim 4$ and $z \sim 5$ are consistent with previous studies, since they dominate the bright region of the LFs. We are aware that we cannot build complete LFs of these populations, since we are missing the faintest sources. Therefore, our own α parameters cannot be derived. Nonetheless, we claim that the interloper fraction obtained using broad band surveys is sufficiently important that will incur in a small decrease in the slope of the faint-end of previous LFs.

3

Stellar population modelling

Ahora que soy el hombre más anciano de la ciudad, caigo en la cuenta de que ya no soy joven.
C. Montgomery Burns (The Simpsons).

This chapter compares the various observationally defined subfamilies we distinguished in the sample of high-z LAEs and LBGs. To that end, we use stellar population synthesis models to fit the SEDs of the sources. We look for differences in ages and stellar masses between the three observationally defined subfamilies in the sample. Our results point to a possible evolutionary relation between them. SMFs are also studied at each z, as well as the SFR-$M_{\rm star}$ relation. The SMD at each redshift is also estimated through integration of the SMF.

The work shown in this chapter will be published in Arrabal Haro et al. (2019, submitted).

3.1 Methodology

This chapter attempts to fit theoretical SP models to the individual galaxies of the high-z LAEs and LBGs sample (see Chapter 2). We remind that the sample consisted of 1558 sources at z = 3.4-6.8, distributed into 1434 LBGs (404 of them showing Lyα emission line with EW$_0$ > 5.1 Å), and 124 pure LAEs ($m_{1500} \gtrsim$ 27.0 AB; Lyα EW$_0$ > 35Å), as summarised in Table 3.1. We pay special attention to whether or not two separated SPs are needed to model the SEDs of these galaxies as well as to significant differences between the three different observationally defined subgroups. Additionally, to further extend our SEDs beyond the SHARDS wavelength range while preserving the good seeing and photometric depth, we also make use of ancillary broad band GOODS-N data from *HST*/ACS (Giavalisco et al. 2004b; Riess et al. 2007), *HST*/WFC3

Table 3.1: Sample distribution among the three different observationally defined subfamilies.

Type	N	Defining observational criteria
Non-LAEs/LBGs	1030	$m_{1500} \lesssim 27$ AB; $\mathrm{EW_{Ly\alpha}} \lesssim 5$ Å
LAEs/LBGs	404	$m_{1500} \lesssim 27$ AB; $\mathrm{EW_{Ly\alpha}} \gtrsim 5$ Å
Pure LAEs	124	$m_{1500} \gtrsim 27$ AB; $\mathrm{EW_{Ly\alpha}} \gtrsim 35$ Å

(Grogin et al. 2011; Koekemoer et al. 2011) and *Spitzer*/IRAC (Fazio et al. 2004; Pérez-González et al. 2005, 2008; Ashby et al. 2015), from the Rainbow database. The NIR data is particularly relevant when modelling these galaxies, since it provides more robust estimations of the ages and stellar masses of any significant older SP. Likewise, the non-detection in these NIR bands is typically linked to young and/or low mass galaxies.

In order to shed light into the nature and evolution of LAEs and LBGs, we use the Code Investigating GALaxy Emission (CIGALE, Noll et al. 2009; Boquien et al. 2019). This python software builds stellar populations from synthetic models combined with various Star Formation Histories (SFHs). CIGALE calculates the emission from gas ionised by massive stars, applying an attenuation law to both the ionised gas and the stars with a differential attenuation between young and old stars. The energy absorbed is re-emitted by the dust at MIR/FIR wavelengths. Combining all the input parameters given, CIGALE creates a grid of models that are compared with the observed data, checking their likelihood and selecting the best fit for each object. This best-fitting model is then used to derive the main physical parameters. For more details about CIGALE, we refer to Noll et al. (2009) and Boquien et al. (2019).

3.1.1 The models

We use the commonly adopted exponentially declining SFH to model our SPs, as in, *e.g.*, Papovich et al. (2001), Pérez-González et al. (2003), Pérez-González et al. (2008), Serra et al. (2011), Rodriguez Espinosa et al. (2014) and Grazian et al. (2015) but see also Carnall et al. (2019) and Leja et al. (2019) for further discussions on SFHs. For this purpose, CIGALE allows the use of a double exponential SFH consisting in a first decaying exponential corresponding to the long-term star formation responsible of the bulk of stellar mass, plus a second exponential that models a recent burst of star formation. The combined SFHs can be expressed as follows:

$$\mathrm{SFR}(t) \propto \begin{cases} \exp(-t/\tau_0) & \text{if } t < t_0 - t_1 \\ \exp(-t/\tau_0) + k \cdot \exp(-t/\tau_1) & \text{if } t \geq t_0 - t_1, \end{cases} \tag{3.1}$$

where τ_0 and τ_1 are the e-folding times of the old and young exponential SPs, respectively, and k is a constant indicating the relative strength of the young burst. The time t_1 is the age of the young population, while t_0 is so for the old one. Furthermore, the fraction of stars formed in the young SP relative to the total stellar mass is given by the burst strength f, which can be expressed using discrete integrals, since CIGALE computes the SFH with a period of 1 Myr:

$$f = \frac{k \sum_{t=t_0-t_1-1}^{t_0-1} \exp(-t/\tau_1)}{\sum_{t=0}^{t_0-1} \exp(-t/\tau_0) + k \sum_{t=t_0-t_1-1}^{t_0-1} \exp(-t/\tau_1)}. \tag{3.2}$$

With this definition, k can be written in the following way:

$$k = \frac{f}{1-f} \cdot \frac{\sum_{t=0}^{t_0-1} \exp(-t/\tau_0)}{\sum_{t=t_0-t_1-1}^{t_0-1} \exp(-t/\tau_1)}, \tag{3.3}$$

which indeed leads to the classical case of a single exponential model when $f = 0$.

Using this SFH, the models are computed with the Bruzual & Charlot (2003) stellar emission library, adding nebular templates based on Inoue (2011). A Salpeter (1955) IMF is assumed as well as a Calzetti et al. (2000) dust extinction law. In order to avoid degeneracy and save computational time, we take the following approximations to constrain some of the many possible input physical parameters:

- To better resemble the SPs to short bursts of star formation, the e-folding time is limited to low values ($\tau \leq 5$ Myr). With this assumption, we avoid adopting completely instantaneous starbursts while making the SFH quickly decay with time. Note that these short τ values are consistent with previous works modelling high-z galaxies as, *e.g.*, Rodriguez Espinosa et al. (2014) and Hernán-Caballero et al. (2017), where the τ adopted very low values in spite being let free.

- The Lyα escape fraction is set to 0.15, consistent with previous calculations at high-z (Mas-Hesse et al. 2003; Robertson et al. 2010; Hayes et al.

2011; Otí-Floranes et al. 2014; Rodriguez Espinosa et al. 2014; Matthee et al. 2016; Sobral et al. 2017, 2018b). Very different escape fraction values are estimated in most recent works. Sobral et al. (2018b) show that the Lyα escape fraction for luminous $z \sim$ 2-3 LAEs is very high ($f_{\rm esc} \sim 0.5$). The Lyα escape fraction for common LAEs at $z = 2.23$ is also relatively high according to Sobral et al. (2017), who measured a $f_{\rm esc} \sim 0.37$ by directly measuring Hα and Lyα for these LAEs. On the other side, Matthee et al. (2016) also studied the escape fraction at $z = 2.23$ for more massive, star forming and dusty Hα emitters, reporting much lower values ($f_{\rm esc} \sim 0.02 - 0.05$). The cosmic average of the Lyα escape fraction is estimated around $f_{\rm esc} \sim 0.05 - 0.15$ (Hayes et al. 2010; Sobral et al. 2017).

- For the dust correction, the colour excess is assumed to be relatively low for these high-z sources, up to $\mathrm{E}(B-V) = 0.12$. This agrees with the values of this parameter calculated using the mean β slopes, and the $A_{\rm uv}$ obtained in Sec. 2.4.2 in the z range of study.

- For the Single Stellar Population (SSP) fits (burst strength $f = 0$), the age is let free within a logarithmic time range from 3 to 1500 Myr. On the other hand, the Double Stellar Population (DSP) models have the age of their burst limited to a maximum of 50 Myr, while the age of the underlying population can vary in a logarithmic range from that age to 1500 Myr. Several tests with different age ranges were made to constrain these values. Those carried out with maximum ages below 1500 Myr showed a peak and an abrupt cut at the maximum allowed age, specially at the lowest redshifts. At the same time, no galaxies presented ages above 1500 Myr when the maximum age limit was further extended, which was expected since this value is close to the age of the Universe at our lowest redshifts. None of the old SPs from the DSP models were neither younger than 50 Myr when this lower limit was extended.

- The relative strength of the young starburst in the DSP models is limited between a minimum burst strength of $f = 0.025$ and a maximum of $f = 0.5$, which means that the stellar mass of the young population should represent at least a 2.5% of the total stellar mass of the galaxy in the DSP best fits.

- We allow the metallicity to vary from $Z = 10^{-4}$ up to $Z = Z_{\odot}$.

Additionally, we make use of a CIGALE feature that allows us to specify a prior for the integrated Lyα line flux, measured in Sec. 2.4.3. Using that feature, the Lyα line is weighted more heavily than a single data-point. Thereby, we make sure that the Lyα line is well modelled in those galaxies presenting it, avoiding low χ^2 solutions where the SED is well fitted except for the filter detecting the line, which otherwise would be selected as best-fitting solutions but that actually do not represent the Lyα emission well. In case of the 1030 non-LAEs/LBGs, to avoid imposing too strong constrains in the non-detected Lyα emission, we provide them with a common negligible input Lyα flux value, while assigning large enough errors to reach the integrated flux of the faintest Lyα line flux measured in the LAEs sample with the SHARDS filters in Sec. 2.4.3 ($F_{\mathrm{Ly}\alpha,\mathrm{min}} \simeq 1.3^{+2.0}_{-1.3} \times 10^{-19}$ erg s^{-1} cm^{-2}).

3.1.2 Single and double stellar population considerations

Since we want to determine whether a second SP is actually needed to model our SHARDS high-z galaxies, both SSP and DSP models are run separately, and their best solutions compared.

To discriminate between the two approaches, we make use of the Bayesian Information Criterion (BIC, Schwarz 1978) as explained in Liddle (2007) and applied in, *e.g.*, Méndez-Abreu et al. (2018):

$$\mathrm{BIC} = \chi^2 + q \ln(m), \tag{3.4}$$

where q is the number of free parameters of the model used and m, the number of independent data points available.

The advantage of using this Bayesian indicator over the χ^2 when comparing results from different models is that the BIC penalises the addition of extra free parameters in a stronger way than the normal or even the reduced χ^2 does. Defining the BIC difference between SSP and DSP models as $\Delta\mathrm{BIC} \equiv \mathrm{BIC}_{1\mathrm{SP}} - \mathrm{BIC}_{2\mathrm{SP}}$, there is a ΔBIC threshold from which higher ΔBIC values correspond to scenarios where the additional free parameters (in this case, an extra SP) are needed to properly model the galaxies.

To calibrate our ΔBIC and obtain the threshold value, a set of theoretical models created with one and two SPs are all fitted with CIGALE using SSP and DSP models in a separate way in order to compare their ΔBIC distributions, following the method used in Méndez-Abreu et al. (2018). In particular, we take the best-fitting SSP model and the best-fitting DSP model of each one of

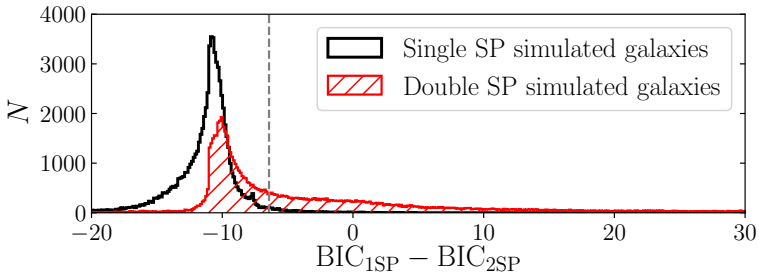

Figure 3.1: ΔBIC distribution of the mock galaxies. The vertical dashed line marks the threshold ΔBIC = −6.42 beyond which a source requires a DSP model. There is a majority of galaxies for which the SSP and DSP best solutions have similar χ^2, resulting in ΔBIC $\simeq -10$ for $q_1 = 5$, $q_2 = 8$ at a typical number of independent SED points of $m \sim 30$ (see Eq. 3.4). For objects with ΔBIC < -6.42, SSP models are preferred over double ones.

the actual galaxies, convolve them with our photometric filters and use Monte Carlo simulations to create 50 new mock samples by perturbing the convolved photometry with Gaussian noise in accordance with the photometric error of each point. In this way, we obtain ∼155800 mock SEDs whose origin is known (half of them are product of SSP models and the other half come from DSP models). Moreover, these mock SEDs provide a good representation of our observed high-z galaxy sample as they are perturbations of the convolution of the best models fitted to the actual sample.

They are then modelled both with single and double SP in order to compare the resulting ΔBIC distribution. The obtained histogram of ΔBIC values for the mock galaxies is shown in Fig. 3.1. The limit from which 95.45% (2σ significance) of the models come from DSP simulations is given by ΔBIC = −6.42. Those cases for which ΔBIC > −6.42 can therefore be selected as our *bona-fide* DSP galaxies. Note that sources with ΔBIC < −6.42 might still be DSP galaxies. However, we cannot precisely discern the best way of modelling each one of those individual sources in terms of their ΔBIC, and so the simplest model is favoured over the more complex one. That is, the best SSP fit is taken as the best model for galaxies with ΔBIC < −6.42, while for those with ΔBIC > −6.42 the best DSP model is taken.

3.2 SP differences between families

With the caveats mentioned in Sec. 3.1.1, we obtained good CIGALE solutions for all the sources in the sample except four very faint ones whose SEDs lack detection in many filters and present large uncertainties in the measurements. In this section we present the results of the model fitting, highlighting the most significant differences found between the three observational classes in the sample. Even though many physical parameters are computed by CIGALE during the model fitting, we will focus here only in the ages and stellar masses of our sample. We note that there is a well known degeneracy between age, dust and metallicity, and therefore age values should be taken with care in an absolute sense.

In Table 3.2 we present the IDs, coordinates, ages and stellar masses (split into young and old SP when we select a DSP synthetic spectrum) derived for our 1554 well modelled galaxies. The median age and $M_{\rm star}$ of each subgroup are shown in Table 3.3.

3.2.1 Stellar populations required

We apply the calibrated ΔBIC criterion explained in Sec. 3.1.2 to get the model that best fit each individual galaxy in our sample with either one or two SPs, finding that in most cases (71.3%), these high-z galaxies do not require the addition of an extra SP to model their SEDs. The frequency distribution of ΔBIC for the three families is shown in Fig. 3.2. Even though the three groups clearly present their peaks within the SSP ΔBIC range, it is worth noticing that the LAEs/LBGs family is wider and the one that more likely tends towards higher ΔBIC values. Specifically, only 22.0% and 29.2% of the non-LAEs/LBGs and pure LAEs need of a second SP in their fits, respectively, while this occurs for 45.5% of the LAEs/LBGs (see Table 3.4).

3.2.2 Age differences

The need of a second SP in almost half of the LAEs/LBGs is well reflected in the ages of the sample. Looking at the age distribution in Fig. 3.3, a large difference can be appreciated between pure LAEs and non-LAEs/LBGs, where the first ones are much younger, with a median age of 20^{+37}_{-19} Myr, while that of the non-LAEs/LBGs is 70 ± 12 Myr. On the other hand, the LAEs/LBGs age distribution shows a dichotomy, presenting two differentiated peaks associated to the inherent nature of the models fitting those objects, *i.e.*, the first and younger peak corresponds to SSP galaxies while the older one is associated to DSP scenarios. Following this result, the LAEs/LBGs class could

Table 3.2: Main physical parameters derived from the best models fitted to each source. A full version of this table is available in Appendix A.

Object Name	R.A.	Dec.	z	$M_{\rm star,m}$	$\rm Age_m$	$\tau_{\rm m}$	$M_{\rm star,b}$	$\rm Age_b$	$\tau_{\rm b}$
	(J2000)	(J2000)		($10^9\,M_\odot$)	(Myr)	(Myr)	($10^9\,M_\odot$)	(Myr)	(Myr)
(1)	(2)	(3)	(4)	(5)	(6)	(7)	(8)	(9)	(10)
SHARDS20010117	12:35:48.1	62:12:02.4	4.28 ± 0.06	1.7 ± 1.1	68 ± 39	2.7 ± 1.4	-	-	-
SHARDS20007539	12:35:48.1	62:12:03.8	5.38 ± 0.07	9.7 ± 4.1	766 ± 240	3.0 ± 1.6	$1.1^{+1.5}_{-1.0}$	16 ± 6	2.5 ± 1.6
SHARDS20012481	12:35:50.9	62:11:58.5	5.69 ± 0.06	2.6 ± 1.4	59 ± 27	2.6 ± 1.3	-	-	-
SHARDS20005927	12:35:51.5	62:12:16.5	3.22 ± 0.07	2.9 ± 0.5	48 ± 8	2.8 ± 1.4	-	-	-
SHARDS20005405	12:35:51.6	62:12:12.7	4.03 ± 0.07	6.7 ± 1.4	74 ± 20	2.8 ± 1.4	-	-	-
SHARDS20008074	12:35:52.2	62:11:20.8	5.53 ± 0.07	0.6 ± 0.3	20 ± 7	2.1 ± 1.3	-	-	-
SHARDS20008444	12:35:53.2	62:10:32.9	4.01 ± 0.07	5.7 ± 4.3	860 ± 450	3.0 ± 1.6	$0.8^{+1.0}_{-0.7}$	32 ± 13	1.7 ± 1.3
SHARDS20010810	12:35:53.4	62:10:23.3	5.12 ± 0.06	1.3 ± 0.8	64 ± 39	2.6 ± 1.4	-	-	-
SHARDS20005669	12:35:54.1	62:10:32.9	3.36 ± 0.07	10.0 ± 5.9	318 ± 218	3.0 ± 1.6	$0.5^{+0.7}_{-0.4}$	24 ± 10	2.5 ± 1.5
SHARDS20011405	12:35:54.3	62:10:18.8	5.37 ± 0.07	3.5 ± 1.4	73 ± 34	2.8 ± 1.4	-	-	-
SHARDS20006420	12:35:54.4	62:10:33.8	3.88 ± 0.06	6.6 ± 2.4	98 ± 46	2.9 ± 1.4	-	-	-
SHARDS20006258	12:35:54.5	62:12:14.6	3.48 ± 0.06	1.0 ± 0.4	16 ± 8	2.0 ± 1.2	-	-	-
SHARDS20013727	12:35:55.0	62:12:04.8	5.96 ± 0.07	20.0 ± 10.0	298 ± 199	3.0 ± 1.6	1.1 ± 1.4	24 ± 11	2.6 ± 1.5
SHARDS20009009	12:35:55.2	62:11:25.4	3.89 ± 0.06	1.6 ± 0.5	61 ± 25	2.7 ± 1.4	-	-	-
SHARDS20006827	12:35:55.7	62:10:19.0	4.28 ± 0.06	1.8 ± 0.6	38 ± 12	2.0 ± 1.1	-	-	-
...	...	...	...	...	...	...	...	...	...

(1) Name of the object using the SHARDS identification. (2) Right ascension. (3) Declination. (4) Photometric redshift. (5) Stellar mass of the main SP. (6) Age of the main SP. (7) e-folding time of the main SP. (8) Stellar mass of the young SP. (9) Age of the young SP. (10) e-folding time of the young SP. The last three columns are left empty when the best solution does not require a second SP.

Table 3.3: Median age and stellar mass for each group and subgroup in our sample.

Type	Age (Myr)	$M_{\rm star}$ (10^9 $M_\odot$)
Non-LAEs/LBGs	70 ± 12	3.7 ± 0.7
LAEs/LBGs	54 ± 26	2.8 ± 1.4
Pure LAEs	20^{+37}_{-19}	$0.42^{+0.88}_{-0.41}$
SSP LAEs/LBGs	22 ± 8	0.68 ± 0.59
DSP LAEs/LBGs	721 ± 30	10 ± 3

The estimations for the pure LAEs show large errors due to the lower number of sources within this group. Nonetheless, both the age and $M_{\rm star}$ of this group are significantly low compared to the other two subgroups. Indeed the median $M_{\rm star}$ of the pure LAEs is an order of magnitude below that of the non-LAEs/LBGs.

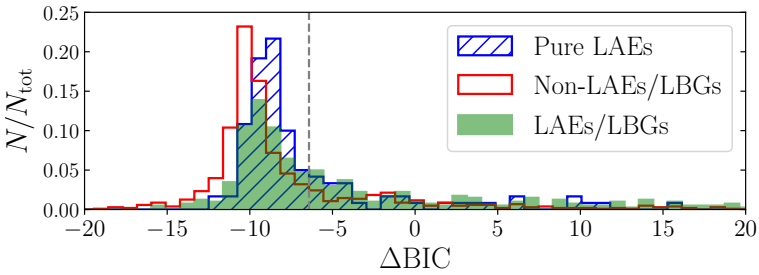

Figure 3.2: ΔBIC distribution of pure LAEs (blue diagonals), LBGs with no Lyα emission line (red unfilled) and LAEs/LBGs (solid green) weighted by the amount of objects within each class. The $\Delta{\rm BIC} = -6.42$ value from which two SPs are needed is depicted by a vertical dashed line. It can be appreciated that the majority of objects (71.3%) are well modelled using a SSP model. Thus, pure LAEs and non-LAEs/LBGs are proportionally much less represented in the DSP models ΔBIC range than LAEs/LBGs, whose distribution is wider and more extended towards high ΔBIC values.

Table 3.4: Number and fraction of sources within each family that require two SPs to model their SEDs according to the ΔBIC criterion.

Type	$N_{\rm DSP}$ (%)
Non-LAEs/LBGs	227 (22.0%)
LAEs/LBGs	184 (45.5%)
Pure LAEs	35 (29.2%)
Complete sample	446 (28.7%)

as well be split into two different subgroups: 1) the SSP LAEs/LBGs, corresponding to very young galaxies (median age $\sim$ 22 Myr) with large enough $M_{\rm star}$ to show a prominent UV continuum detectable in SHARDS, and 2) the DSP LAEs/LBGs, representing more evolved galaxies with an older underlying massive SP suffering a recent star-forming episode, thus the additional young SP.

To shed light on whether the SSP age difference between non-LAEs/LBGs and LAEs/LBGs is only driven by the detection of the Lyα line or not, SSP LAEs/LBGs are fitted a second time omitting the Lyα line contribution from their SEDs by replacing the flux in the filter sampling the Lyα line with an estimation of the continuum emission from the adjacent SHARDS filters or the broad band *HST*/ACS when needed. The new Lyα-removed photometry is then refitted with and without the integrated Lyα flux prior used for the non-LAEs/LBGs (see Sec. 3.1.1). In both cases, the median age obtained for the SSP LAEs/LBGs in this second run is only $\sim$ 6-8 Myr younger than that of the SSP non-LAEs/LBGs, thus being equal within errors. This highlights that the youthfulness of the SSP LAEs/LBGs in the models comes from the Lyα emission line, also implying that some non-LAEs/LBGs for which the intrinsic Lyα line remains undetected because of scattering or dust extinction could be equally young as well, adding an extra difficulty in the characterisation of this last subgroup.

3.2.3 Stellar mass differences

Regarding the stellar mass, the distribution presented in Fig. 3.4 shows again a clear difference between pure LAEs (median $M_{\rm star} \sim 4.2^{+8.8}_{-4.1} \times 10^8\ M_\odot$) and non-LAEs/LBGs (median $M_{\rm star} \sim 3.7 \pm 0.7 \times 10^9\ M_\odot$), with $M_{\rm star}$ an order of magnitude higher for the latter ones. Notice also that the LAEs/LBGs present a smooth $M_{\rm star}$ distribution along a wider $M_{\rm star}$ range, with a median value of $2.8 \pm 1.4 \times 10^9\ M_\odot$, in between of the other two families. However, when we split

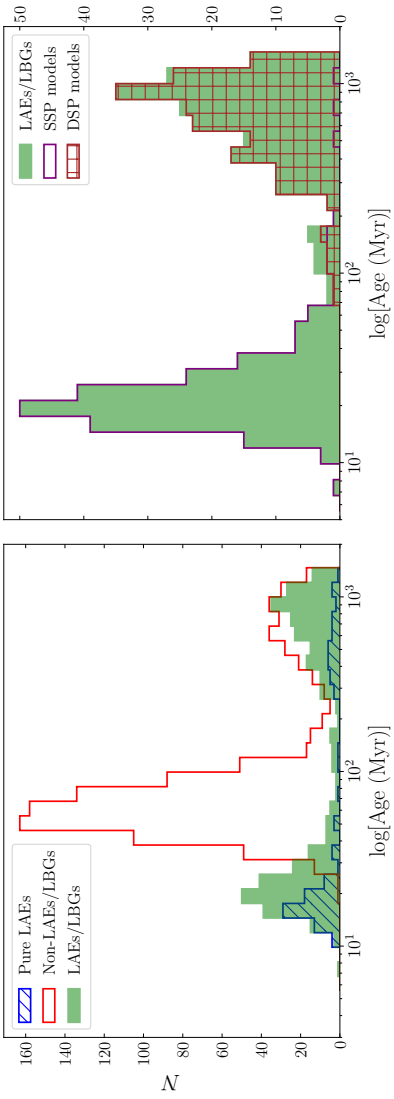

Figure 3.3: *Left*: Age distribution for the pure LAEs (blue diagonals), LAEs/LBGs (solid green) and no Lyα line LBGs (unfilled red). Notice that most pure LAEs show low ages (65% below 50 Myr), while the non-LAEs/LBGs are typically older, peaking at $\sim$ 70 Myr and presenting a secondary peak at the oldest ages. *Right*: LAEs/LBGs age distribution in more detail. In this case, there is a clear separation with a fraction (45.5%) of the sources requiring a DSP (squared brown pattern), while in the rest of the sources a SSP model is preferred (unfilled purple). The two peaks observed in the distribution can be explained by the underlying nature of the best fitting models. The first one corresponds to models of relatively young galaxies where the Lyα emission is still present while being massive enough to show some UV continuum. For the second peak, SSP models are unable to properly model the Lyα emission and simultaneously reach a bright UV continuum, making a second old SP necessary. Examples of this last scenario are shown in Fig. 3.7. The same two peaks are also found for the other two subfamilies. However, we do emphasise the LAEs/LBGs distribution as they are proportionally much more represented in the DSP best-fitting models (45.5%).

this group into the two subgroups already differentiated in the age distribution it can be seen that the more massive side of the $M_{\rm star}$ distribution is driven by the DSP LAEs/LBGs while the low side of the mass distribution corresponds to the SSP ones. This result is not surprising once we take into account that, according with Fig. 3.3, the DSP LAEs/LBGs are much older and therefore have typically been forming stars for a much longer time, becoming more massive on average. These last objects could be understood as non-LAEs/LBGs that see their star formation increased by some triggering physical mechanism (mergers or neighbour gravitational interaction, instabilities, large cosmic web gas accretion, etc.), becoming LAEs/LBGs.

3.2.4 Burst strength

For the 446 galaxies better fitted using DSP models, a study of the relevance of each population in terms of mass is done by looking at the burst strength parameter f, whose distribution is shown in Fig. 3.5. We find a clear peak of 78 objects at burst strength $f < 0.03$. This distribution shows that even in the cases where a DSP modelling is better, these galaxies are still dominated in terms of stellar mass by the main old SP. Furthermore, the $M_{\rm star}$ of the young SP is almost negligible. However, it is important to highlight that the relevance of this young population comes with the conspicuous Lyα emission line and UV luminosity, which could not be reproduced using only a single old SP. No significant differences of the burst strength distribution were noticed among the three observational subgroups and no trend with redshift was neither found.

3.2.5 Evolutionary relation between subclasses?

From the ages and stellar masses derived with CIGALE in this work we can build up some relations between the different observational families previously defined. As highlighted at the beginning of Sec. 3.2, the age values are uncertain due to the existing degeneracy between dust extinction, metallicity and the age itself, and so the absolute values should be carefully considered. Nevertheless, on equal conditions, we can use them to trace age differences between the fitted LAEs and LBGs.

On one side, we have the pure LAEs, defined as objects with strong Lyα line emission but a faint UV continuum ($m_{1500} \gtrsim 27$ AB). These sources typically present low stellar masses in their young SP (median $M_{\rm star} = 4.2^{+8.8}_{-4.1} \times 10^8\ M_\odot$). Additionally, the presence of strong Lyα emission quickly decays with time as it is only produced by O and B stars with $M > 10\ M_\odot$ and lifetimes of a few Myr. Therefore, it is an indicator of recent star formation. Besides, the low

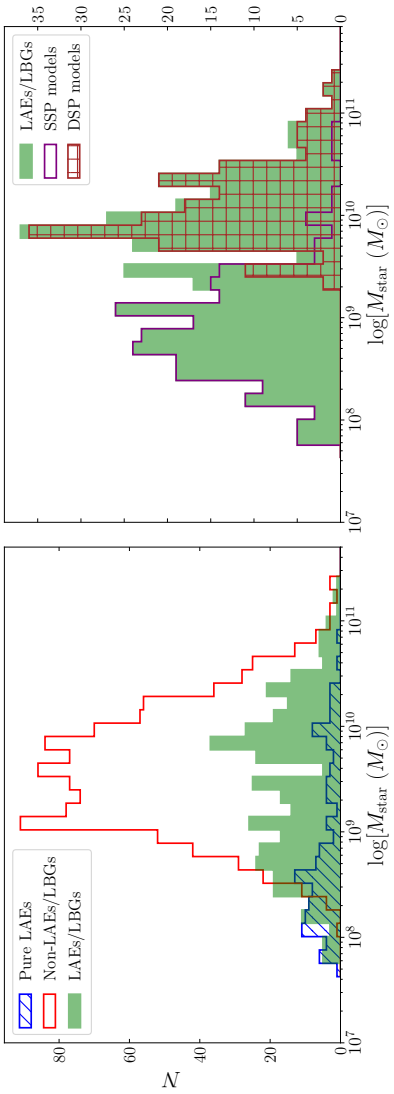

Figure 3.4: *Left:* Stellar mass distribution of pure LAEs (blue diagonals), LAEs/LBGs (solid green) and non-LAEs/LBGs (unfilled red). Notice that both LBGs families show substantially higher $M_{\rm star}$ than the pure LAEs. *Right:* Split of the LAEs/LBGs $M_{\rm star}$ distribution into SSP (unfilled purple) and DSP (squared brown) models. The DSP galaxies present much larger masses than those modelled by a SSP, with median values of $1.0 \pm 0.3 \times 10^{10}\ M_\odot$ for the former and $6.8 \pm 5.9 \times 10^{8}\ M_\odot$ for the later. This, joined to the age dichotomy mentioned in Fig. 3.3 (right panel) points to two different subgroups within the LAEs/LBGs: young low-intermediate mass sources modelled by a SSP and old massive galaxies experimenting a recent star-forming episode, which are better explained using two SPs.

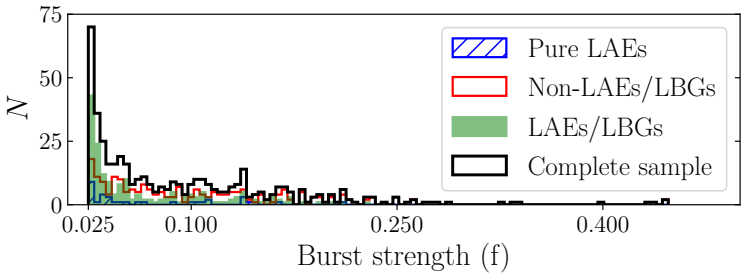

Figure 3.5: Distribution of the burst strength in the sources better approached by DSP models. The large peak at the minimum burst strength value indicates that even though two SPs are needed to properly model these objects, their SEDs are mostly the product of a main massive dominant old SP, with the young SP being almost irrelevant if not for the UV luminosity.

$M_{\rm star}$ indicates that these galaxies also have to be typically young, since they are currently undergoing a starburst, but they have not been forming stars long enough to accumulate larger stellar masses. This hypothesis is confirmed by the median age obtained with the CIGALE fitting for this family (20^{+37}_{-19} Myr). According to that, many of these sources could indeed be experimenting one of their first episodes of star formation, or at least one strong enough to overtake all the older stars in luminosity. Furthermore, we also find that most of these objects can be explained using a single decaying exponential SFH. An example of this is shown in Fig. 3.6, where the Lyα emission line, together with the absence of strong UV continuum photometric points in the SED leads to model these pure LAEs in terms of a single young and low mass SP.

For the LAEs/LBGs, the dichotomy found in their age and $M_{\rm star}$ distributions shown in the right panels of Figs. 3.3 and 3.4 set a clear differentiation between SSP LAEs/LBGs and DSP LAEs/LBGs when modeling them with burst-like SFHs. The objects of this family that can be fitted using a SSP are the youngest and less massive within the LAEs/LBGs. These cases do not present any strong emission at longer wavelengths and can therefore be reproduced by a young SP (median age of 22 ± 8 Myr) with Lyα line in emission and a fairly flat UV continuum. According to the description given in the previous paragraph for the pure LAEs, the SSP LAEs/LBGs would just be the most massive members of that same class: young galaxies well modelled by a SSP, with the only difference that SSP LAEs/LBGs present a massive enough

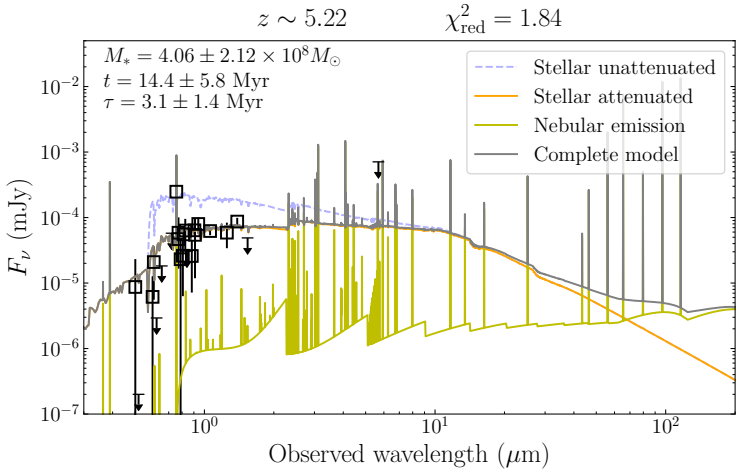

Figure 3.6: Best model for the pure LAE SHARDS J123640.20+621228.8. The black squares are the photometric points used in the fit. The whole final model (grey line) is decomposed into the attenuated stellar emission (orange line) and the nebular emission (yellow line). The unattenuated stellar emission is also represented by the dashed bluish line. The SED presents a clear Lyα emission line, but the absence of strong continuum points at the longest sampled wavelengths makes it possible to well fit it with a single young and not so massive SP.

young SP (median $M_{\rm star} = 6.8 \pm 5.9 \times 10^8$ $M_\odot$) to show an UV continuum detectable in SHARDS, preventing the pure LAEs observational classification but actually belonging to the same kind of objects. On the other side, the DSP LAEs/LBGs are much older and more massive. The need of a second SP to understand the SEDs of this subgroup comes from the presence of the Lyα emission line plus some bright IRAC points. Both emission features cannot be simultaneously fitted by a SSP (as in, *e.g.*, Rodriguez Espinosa et al. 2014). In Fig. 3.7, we present two examples to illustrate what happens when we try to fit some of these objects SEDs with a SSP that either fits well the Lyα line but not the continuum at the longest sampled wavelengths or the other way around. The CIGALE best solutions for this subgroup suggest that the DSP LAEs/LBGs can be understood as evolved galaxies with an old SP that raises

the continuum emission at the longest wavelengths, currently experimenting a recent star-forming episode triggered by accretion of new gas or by mergers.

On the opposite side, we have the non-LAEs/LBGs, understood as galaxies selected through their Lyman break in the UV continuum emission, but without Lyα line emission detected in the SHARDS photometry. This family is the oldest and most massive of the SSP models of the three predefined observational families, with a median stellar mass almost an entire order of magnitude above that of the pure LAEs ($M_{\rm star} = 3.7\pm0.7\times10^9\ M_\odot$). The absence of a detectable Lyα line should not be taken as a secure indicator of the relative faintness of the most recent star formation in these objects, since the real Lyα emission of the galaxy can be strongly affected by dust extinction and resonant scattering through the interstellar medium. Indeed, dust extinction affects strongly both the Lyα line and the rest-frame UV continuum. Hence, there is an intrinsic selection effect towards galaxies with low internal extinction. Lyα photons scattering by neutral gas, on the other hand, plays an important role in the fraction of LBGs with and without Lyα emission. Regarding Lyα H I resonant scattering, recent works estimate different escape fraction values depending on the galaxy population, as mentioned in Sec. 3.1.1, from large $f_{\rm esc} \sim 0.5$ for bright $z \sim$ 2-3 LAEs (Sobral et al. 2018b) and typical LAEs (Sobral et al. 2017; Sobral & Matthee 2019) to very low $f_{\rm esc} \sim 0.02 - 0.05$ for more massive and dusty $z = 2.23$ Hα emitters (Matthee et al. 2016). In any case, these Lyα destruction or scattering phenomena are very difficult to quantify with our data so the discussion of this non-LAEs/LBGs family aims to give a general overview of the class, even though there could be particular cases not matching it.

Thus, the results from the CIGALE SED fitting point to non-LAEs/LBGs typically being in a more evolved stage after previous episodes of star formation. They would have formed a large amount of stars and therefore show larger stellar masses and stronger continuum emission supported by old long-living stars. The need of a second SP to model this class is another problem difficult to handle. If these more massive sources have undergone many previous star-forming episodes, it could be thought that the most reasonable way of approaching them should be using more than one SP. However, the emission patterns that more easily differentiate young SP from old ones (as the nebular emission) are not conspicuous in these sources. This indicates that these sources do not have a really young SP ($\lesssim$ 25 Myr). Nonetheless, it exists a degeneracy in the number of relatively old SPs with different ages (understood as different star-forming episodes) that could produce the actual observed SEDs, which, on the other side, can usually be reproduced by a single one (see Fig. 3.8). As we adopted the BIC as a good indicator to estimate whether a second SP is needed in our models, the majority of situations where both the SSP and DSP approaches

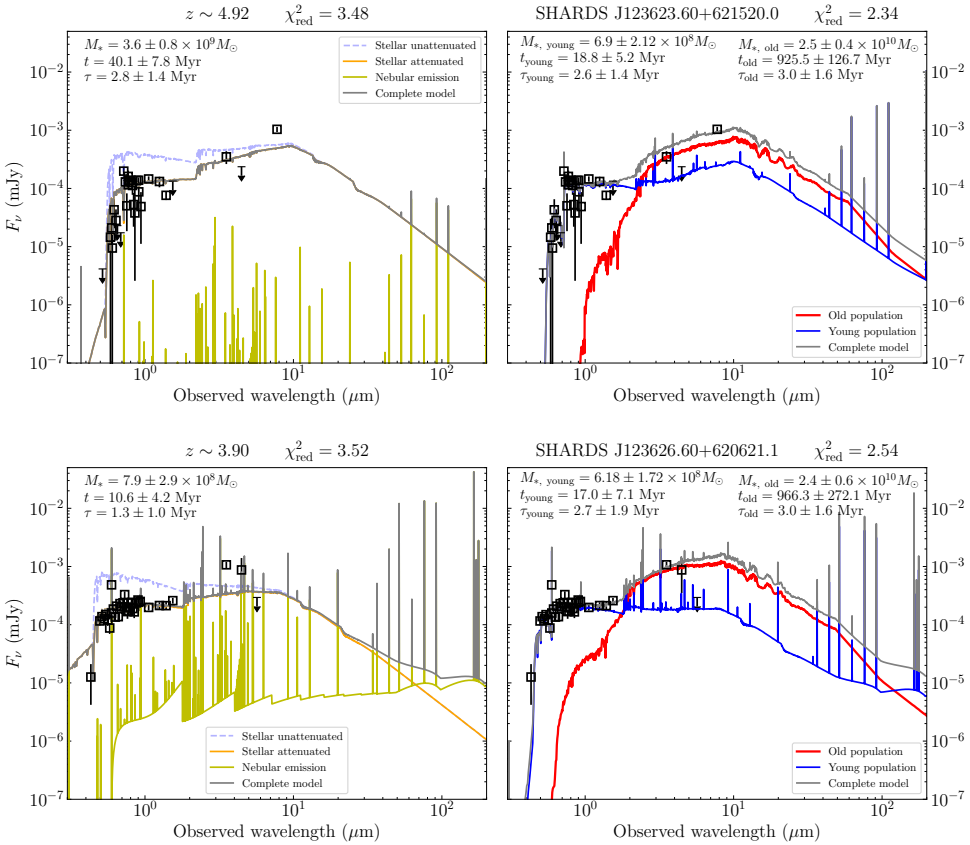

Figure 3.7: Best SSP and DSP solutions for two LAEs/LBGs better modelled with two SPs. The objects SHARDS J123623.60+621520.0 and SHARDS J123626.60+620621.1 are shown in the upper and lower panels, respectively. In each case, the left frame shows the best SSP fit. The black squares are the photometric points of the SED, the yellow line shows the nebular emission, the stellar attenuated emission is represented in orange and the stellar unattenuated emission is plotted with a dashed bluish line, with the grey line being the complete model. On the other side, the right frames correspond to the best DSP fits, where the different components of the emission have been omitted for clarity and the contributions of the old and young SPs are represented in red and blue, respectively. For the upper source, the best SSP model matches relatively well the continuum but it is not able to reproduce the Lyα emission line. The addition of a second SP becomes necessary to not only match that Lyα emission, but even improve the continuum fit in IRAC. The opposite scenario can be seen in the lower source, where the best SSP fit manages to well reproduce the line emission at the cost of leaving the reddest points unfitted. This time, the second population added is an old one that contributes to raise the continuum emission in the IRAC range.

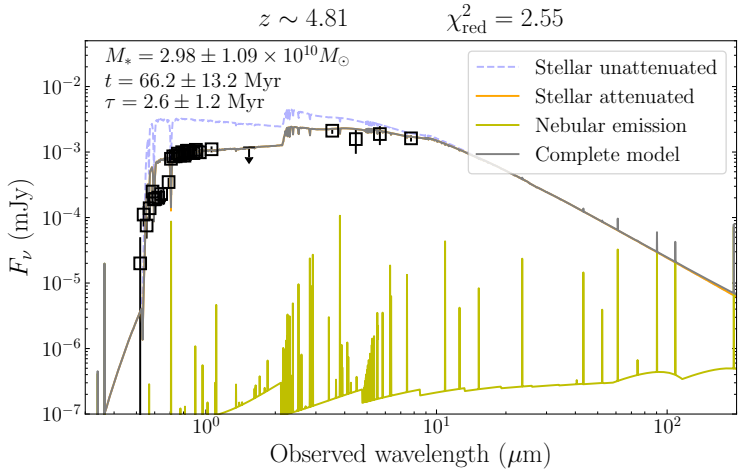

Figure 3.8: SSP model taken as the best solution for the non-LAE/LBG SHARDS J123757.50+621718.7. The absence of Lyα emission line makes it possible to fit the continuum of the SED even up to the IRAC measurements using a single relatively old, massive stellar population. Note that the nebular emission is so low that the complete spectrum practically corresponds to the attenuated stellar emission.

give similar χ^2 solutions end up favouring the simplest model. Thus only a 22% of the non-LAEs/LBGs do need the extra SP. Furthermore, since the UV continuum close to Lyα is driven by the most recent SF episodes the SEDs of these sources are most of the time (74.9%) fitted by SSPs in the range of 30-150 Myr, still older than those typically fitted to the pure LAEs and the SSP LAEs/LBGs, but certainly younger than what they could be if they were actually hosting an underlying old SP. What we want to emphasise here is that even though those objects are well modelled by a SSP, that does not mean there could not be some other faint and much older extra SPs. As we are adopting the simplest model in these situations, we should be aware of a possible bias towards younger ages for this particular family of non-LAEs/LBGs.

Knowing that the Lyα emission quickly decays within the first few Myr, we would expect to see a small fraction of objects presenting strong Lyα line emission among the LAEs/LBGs population, which actually matches the EW

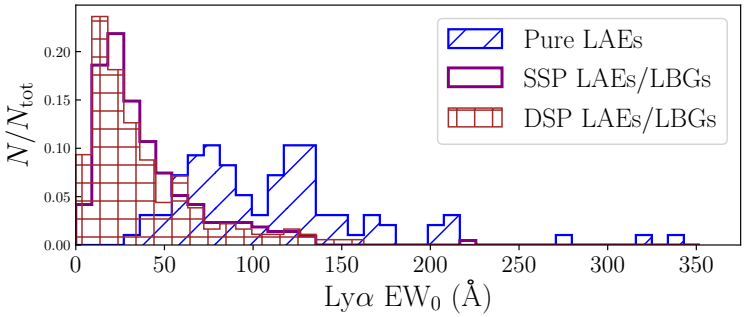

Figure 3.9: Rest-frame Lyα EW distribution of pure LAEs (blue diagonals), SSP LAEs/LBGs (unfilled purple) and DSP LAEs/LBGs (brown squares) weighted by the total amount of objects belonging to each subclass. No relation is found between Lyα EW and the need of a second SP when modelling the SEDs of LAEs/LBGs.

distribution of this sample presented in Fig. 2.14. This is also the reason why we find only 404, out of 1434, continuum sources with emission line. Indeed, we have detected 1030 sources with no emission line, which would correspond to evolved galaxies with no significant young starburst at present. This represents the most common state of this type of high-z galaxies, with the strong Lyα line emission being a recurrent and transiting episode in their lives. Nonetheless, it is also possible that in some sources, specially beyond $z \sim 5$, the Lyα photons are destroyed by scattering through a dense neutral medium as discussed in Hayes et al. (2010). Furthermore, a closer look to the Lyα EW of the LAEs (see Fig. 3.9) reveals no relation between that and the need of any extra SP for the LAEs/LBGs, suggesting that the requirement of DSP models for these high-z galaxies is given not only by their Lyα emission but by the relation between this and their emission at longer wavelengths, as also shown in Fig. 3.7. The Lyα EW would thus be an indicator of the age in the SSP models, or of the relative strength of the young SP respect to the old one in the DSP models. On the other side, pure LAEs do show larger Lyα EWs, as expected from their observational definition. Additionally, the relative number of young LAEs increases with z (see Fig. 3.10), while that of the old LBGs decreases, which also supports the scenario of an evolution from the pure LAE to the LBG stage, with a larger proportion of sources in the younger stage at higher redshifts, decreasing as more evolved galaxies form and accumulate as we move to lower redshifts.

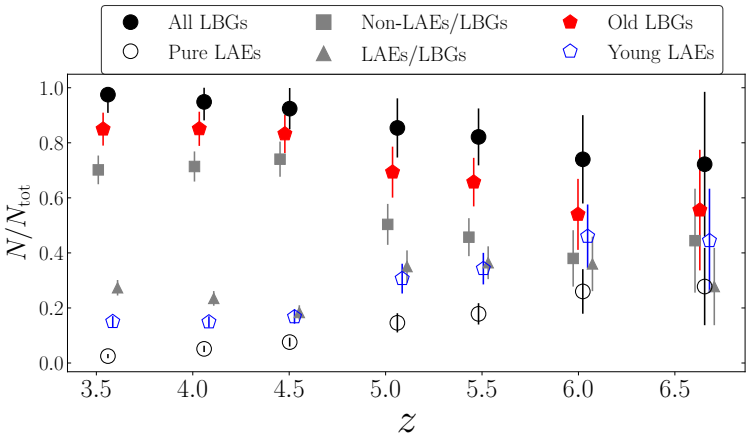

Figure 3.10: Amount of sources of each subgroup respect to the total number of sources at each z bin. The three observationally defined families are represented by empty circles (pure LAEs), grey squares (non-LAEs/LBGs) and grey triangles (LAEs/LBGs). The sum of non-LAEs/LBGs and LAEs/LBGs is also represented by the black filled circles. The two most relevant groups summarising the results derived from the SED fitting are also shown: old LBGs (red filled pentagons), conformed by the non-LAEs/LBGs and the DSP LBGs; and young LAEs (blue empty pentagons), representing the pure LAEs and SSP LAEs/LBGs. Slight offsets in the z axis have been introduced for clarity. The trend of these last two main groups is consistent with an evolutionary scenario between them.

This behaviour is also consistent with the study of the SFRD carried out by Sobral et al. (2018), who found an increasing trend with z of the $\mathrm{SFRD_{Ly\alpha}/SFRD_{UV}}$ ratio.

3.3 Stellar mass functions

The stellar masses derived from the best-fitting SP models are used to build SMFs at each redshift up to our stellar mass completeness. The completeness $M_{\rm star,lim}$ is estimated using the technique employed in *e.g.*, Pozzetti et al. (2010) and Davidzon et al. (2017) to calculate the stellar mass limit for a survey

limited in magnitude. This method consists on taking the masses derived in each redshift bin and rescaling them to the magnitude limit of our survey:

$$\log(M_{\rm star,resc}) = \log(M_{\rm star}) + 0.4(m - m_{\rm lim}). \tag{3.5}$$

We adopt $m_{\rm lim} \sim 27$ AB mag as an approximation of the average 3σ limit detection in the SHARDS filters. The $M_{\rm star,lim}$ is then defined as the 90th percentile of the $M_{\rm star,rec}$ distribution. With this method, we estimate an average $M_{\rm star,lim} \sim 6.6 \times 10^9\ M_\odot$ for our stellar mass sample. This $M_{\rm star}$ completeness limit means that our SMFs are dominated by the LBGs population, as the majority of pure LAEs present masses below that limit (see Fig. 3.4). Additionally, a $V_{\rm max}$ correction (Schmidt 1968) is considered when building our SMFs. The advantage of the $V_{\rm max}$ correction is that it directly provides the normalisation of the SMF. To model the SMF, we make use of the widely used Schechter (1976) function:

$$\phi(M)dM = \phi^* \exp(-M/M^*)(M/M^*)^\alpha dM/M^*, \tag{3.6}$$

which can be better expressed in the $\log M$ space when working with SMFs:

$$\begin{aligned}\phi(M)d\log M = \phi^* \ln 10 \exp(-10^{\log M - \log M^*}) \\ \times\ (10^{\log M - \log M^*})^{\alpha+1} d\log M.\end{aligned} \tag{3.7}$$

The resulting SMFs are shown in Fig. 3.11 as well as the best Schechter fits and their 1σ and 3σ confidence intervals derived from Monte Carlo simulations perturbing the points themselves as well as the $M_{\rm star}$ bin sizes and centres, as explained in more detail in Appendix B. The error bars of our points correspond to the Poissonian uncertainties. The few points available at $z \sim 6$ up to our stellar mass completeness makes it very difficult to estimate the α slope at this z, hence the large uncertainty derived from the fitting. Moreover, the calculated $M_{\rm star,lim} \sim 8.3 \times 10^9\ M_\odot$ at $z \sim 6$ seems to be slightly underestimated as it includes incomplete SMF points close to the M^* knee for certain perturbations of the $M_{\rm star}$ bins, which end up in positive α values. To avoid this issue, we constrain the α fitting to $-2.8 < \alpha < -1.0$ at $z \sim 6$ and limit the SMF points to those strictly increasing up to our $M_{\rm star,lim}$ as we consider that further ones are actually incomplete. Note that this approach could be slightly biasing the obtained α values towards more negative values at $z \sim 6$ as it is also reflected

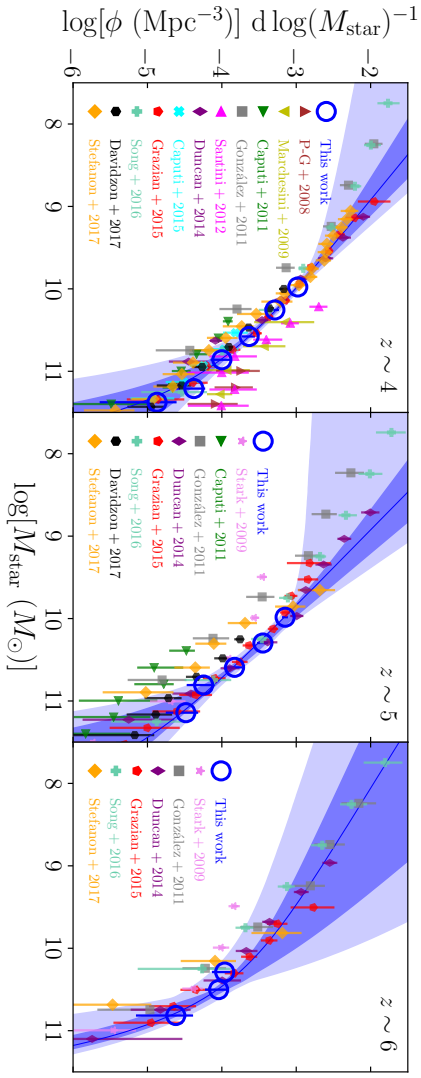

Figure 3.11: SMF at $z \sim 4$, $z \sim 5$ and $z \sim 6$. The Monte Carlo best fit is indicated by the solid blue line, while the darker and lighter blue contours correspond to the 68% and 99.7% confidence intervals, respectively. For comparison, we also show previous SMF calculations from Pérez-González et al. (2008) ($3.5 < z < 4.0$), Marchesini et al. (2009) ($3.0 < z < 4.0$), Stark et al. (2009), Caputi et al. (2011), González et al. (2011), Santini et al. (2012), Duncan et al. (2014), Caputi et al. (2015), Grazian et al. (2015), Song et al. (2016), Davidzon et al. (2017) and Stefanon et al. (2017). All SMFs have been rescaled to a Salpeter IMF for comparison.

in the error bars obtained with the Monte Carlo simulations for that z. More details on the fitting process, as well as the significance contours of the fitted Schechter parameters at each redshift are given in Appendix B. The best-fitting Schechter parameters are summarised in Table 3.5.

Even though the obtained SMFs shown in Fig. 3.11 are in good agreement with previous estimations from similar studies where the stellar masses were derived through SED fitting, a non-negligible discrepancy can be noticed respect to other works where the UV luminosity was used to derive the $M_{\rm star}$ through the estimation of a tight mass-to-light ratio (Stark et al. 2009; González et al. 2011; Stefanon et al. 2017). This discrepancy between SED-fitted and $M_{\rm UV}$-derived $M_{\rm star}$ could appear due to small differences in the calculated M/L relation, as discussed in Grazian et al. (2015). Our SMF best-fitting Schechter parameters presented in Table 3.5 show a decreasing of the SMF with z. We find that the characteristic stellar mass M^* shifts towards higher masses with cosmic time, as also found by Grazian et al. (2015). No significant change is found for the low-mass slope, from $\alpha = -1.88^{+0.20}_{-0.17}$ at $z \sim 4$ to $\alpha = -1.86^{+0.22}_{-0.22}$ at $z \sim 5$ with a slight increase to $-1.68^{+0.17}_{-0.63}$ at $z \sim 6$. However, the large uncertainty of this last measurement makes the α slope consistent with little to no change within our redshift range. In any case, our α values are much steeper than those found at low redshift, in agreement with previous estimations (*e.g*, Santini et al. 2012; Duncan et al. 2014; Grazian et al. 2015; Song et al. 2016; Davidzon et al. 2017; Stefanon et al. 2017, among others).

The characterisation of the SMF has allowed us to estimate the SMD at each redshift by integrating the SMF from 10^8 to 10^{13} $M_\odot$ (as in, *e.g.*, Duncan et al. 2014; Grazian et al. 2015; Song et al. 2016). The obtained SMDs values at each z are presented in Table 3.5, and a comparison of our estimations with previous works is also shown in Fig. 3.12, where it can be appreciated that our calculations follow the general evolution with cosmic time reported by previous authors, presenting a specially large uncertainty at $z \sim 6$ due to the already mentioned lack of information in the low mass regime of our SMF at that redshift and the corresponding uncertainty of the estimated α slope.

Apart from the large errors of the SMD estimation at $z \sim 6$, it is worth noticing that the decrease of SMD between $z \sim$ 4-5 is softer than that between $z \sim$ 5-6, suggesting that the SMD at $z \sim 5$ obtained in our field could be larger than expected following the general SMD-z trend at $z =$ 4-6. This could be linked to the presence of a reported $z \sim 5.2$ overdensity in the GOODS-N field (Walter et al. 2012; Arrabal Haro et al. 2018), as further exposed in Chapter 4.

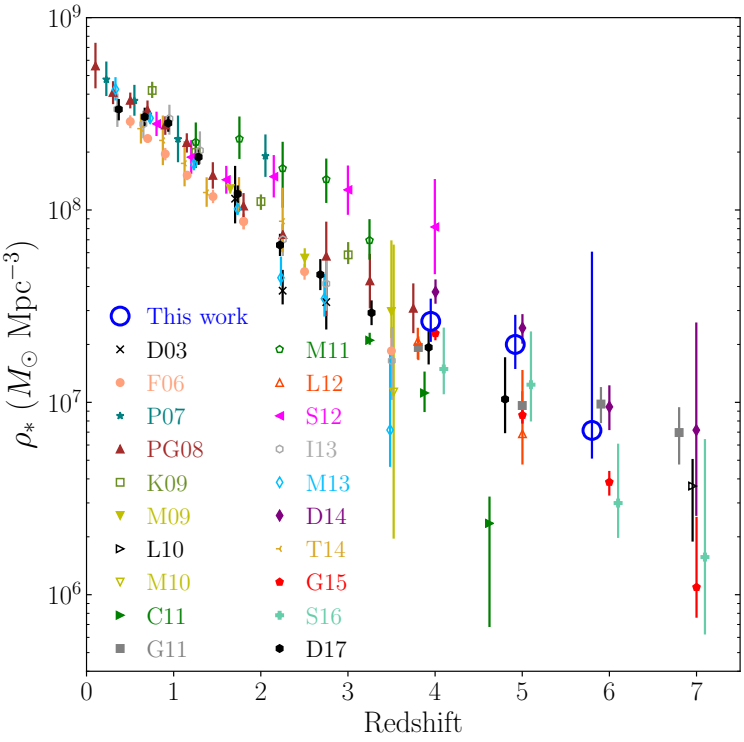

Figure 3.12: SMD obtained by integration of the SMFs at each z. To give a global view of the SMD evolution with z, we show previous estimations from Dickinson et al. (2003, D03), Fontana et al. (2006, F06), Pozzetti et al. (2007, P07), Pérez-González et al. (2008, PG08), Kajisawa et al. (2009, K09), Marchesini et al. (2009, M09), Marchesini et al. (2010, M10), Labbé et al. (2010, L10), Caputi et al. (2011, C11), González et al. (2011, G11), Mortlock et al. (2011b, M11), Lee et al. (2012, L12), Santini et al. (2012, S12), Ilbert et al. (2013, I13), Muzzin et al. (2013, M13), Duncan et al. (2014, D14), Tomczak et al. (2014, T14), Grazian et al. (2015, G15), Song et al. (2016, S16) and Davidzon et al. (2017, D17). All SMDs are rescaled to a Salpeter IMF.

Table 3.5: SMF best-fitting Schechter parameters and the corresponding SMD obtained by integration of the SMF from 10^8 to 10^{13} $M_\odot$. The shown SMD uncertainties correspond to 1σ significance.

z	$\log M^*$	$\log \phi^*$	α	$\log \rho_*$
4	$11.01^{+0.49}_{-0.33}$	$-4.21^{+0.48}_{-0.69}$	$-1.88^{+0.20}_{-0.17}$	$7.42^{+0.12}_{-0.11}$
5	$10.76^{+0.68}_{-0.14}$	$-4.02^{+0.24}_{-1.00}$	$-1.86^{+0.22}_{-0.22}$	$7.30^{+0.15}_{-0.13}$
6	$10.55^{+0.04}_{-0.12}$	$-4.06^{+0.12}_{-0.03}$	$-1.68^{+0.17}_{-0.63}$	$6.85^{+0.93}_{-0.15}$

3.4 SFR-$M_{\rm star}$ relation

To build SFR-$M_{\rm star}$ relations at each z and compare them with previous estimations, we make use of the SFRs calculated for this sample in Sec. 2.4.2 using the Kennicutt (1998) and Madau et al. (1998) prescriptions after correcting for both galactic and internal dust extinction following Schlafly & Finkbeiner (2011) and Calzetti et al. (2000), respectively. As explained in Sec. 2.4.2, the SFRs were calculated through the Lyα emission line for the pure LAEs and through the UV luminosity for the LBGs. To avoid using multiple different SFR indicators, we only make use of the SFRs estimated through L_{1500}, which allows us to better compare our results with previous works studying this relation in a similar way as, *e.g*, Salmon et al. (2015). Moreover, the SFRs derived through the Lyα line luminosity can be strongly affected by resonant scattering. The so-called SFR-$M_{\rm star}$ "main sequence" (Fig. 3.13) is modelled using the common linear approach between the logarithm of these magnitudes (*e.g.*, Salmon et al. 2015):

$$\log[\mathrm{SFR}\ (M_\odot\ \mathrm{yr}^{-1})] = \beta \log[M_{\rm star}\ (M_\odot)] + C. \tag{3.8}$$

The error bars shown in Fig. 3.13 correspond to the standard error of the median SFR at each $M_{\rm star}$ bin. To fit the slope and zero point of the relation we applied Monte Carlo methods not only perturbing the points within the errors, but also the $M_{\rm star}$ bin centres and sizes in a range of 0.1-0.5 dex. To compare our results, we use data from semi-empirical models (Behroozi et al. 2013), hydrodynamic simulations (Davé et al. 2013) and observational data from Salmon et al. (2015). Note that the distribution of these observational data matches ours very well, with the trend of the theoretical models being slightly steeper. The best-fitted values of β and C are given in Table 3.6. It can be noticed that the slope of the SFR-$M_{\rm star}$ remains invariable with z within the errors, as it has been previously reported in the literature (Stark et al. 2009;

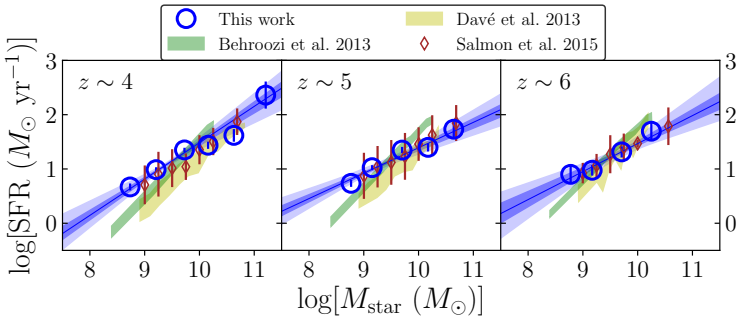

Figure 3.13: SFR-M_{star} relation measured at each redshift using the UV-derived SFRs. The error bars of our data (blue circles) are associated to the standard error of the median SFR at each M_{star} bin. The blue solid line corresponds to the best fit and the darker and lighter blue regions delimit the 1σ and 3σ confidence intervals of the fit, respectively. Theoretical predictions from Behroozi et al. (2013, faded green) and Davé et al. (2013, faded yellow) show slightly steeper slopes than the observational data from Salmon et al. (2015) and from our sample. The slope of the SFR-M_{star} relation does not show a significant change with z.

González et al. 2010; Papovich et al. 2011; Salmon et al. 2015).

The SFRs of the pure LAEs are only estimated through their Lyα luminosity (see Sec. 2.4.2). In order to study the distribution of the different subclasses along this main sequence employing the same SFR estimator for all of them, we make use of the main sequence built up with the SFRs derived from the best-fitting SSP CIGALE models (Fig. 3.14). Note that the different nature of the SFR estimators makes their absolute values incomparable as they can differ a lot. Typical SFR estimators tend to have strong assumptions on the SFH that can be broken when using burst-like SFHs as the ones employed for high-z galaxies in this work. For more details on differences in SFR calculation, see Boquien et al. (2014) or Boquien et al. (2016), among others. The reason to study the SFR-M_{star} using the SFRs from the models is, apart from having an additional measure of the main sequence slope, to analyse differences between subclasses from a common SFR estimation. The best-fitting parameters of this model-derived SFR-M_{star} relation are also shown in Table 3.6. The slope obtained in this second case is slightly steeper than the one obtained employing the UV-derived SFRs, getting closer to that theoretically predicted by Behroozi

Table 3.6: best-fitting parameters for the SFR-$M_{\rm star}$ main sequence built up using UV-derived SFRs (second and third columns) and model-derived SFRs (last two columns).

z	$\beta_{L_{1500}}$	$C_{L_{1500}}$	$\beta_{\rm mod}$	$C_{\rm mod}$
4	$0.67^{+0.15}_{-0.19}$	$-5.21^{+1.75}_{-1.40}$	$0.76^{+0.03}_{-0.04}$	$-5.30^{+0.33}_{-0.31}$
5	$0.47^{+0.13}_{-0.13}$	$-3.29^{+1.22}_{-1.21}$	$0.72^{+0.06}_{-0.06}$	$-4.94^{+0.41}_{-0.56}$
6	$0.52^{+0.22}_{-0.18}$	$-3.69^{+1.73}_{-2.13}$	$0.76^{+0.09}_{-0.09}$	$-5.32^{+0.81}_{-0.82}$

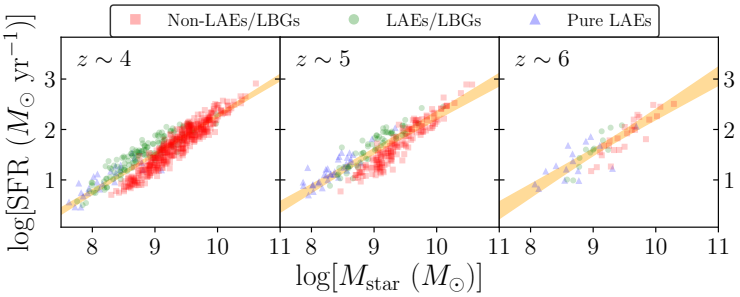

Figure 3.14: SFR-$M_{\rm star}$ main sequence measured at each redshift using the SFRs given by the best-fitting SSP CIGALE models. The orange region delimit the 3σ confidence interval of the fit. The slope of the SFR-$M_{\rm star}$ relation does not change with z within our redshift range.

et al. (2013) and Davé et al. (2013). Furthermore, the SFR-$M_{\rm star}$ relation derived from the best-fitting SSP models also remains constant between z = 4-6, reinforcing this result.

Regarding the different subgroups distribution, it can be appreciated that pure LAEs occupy the left end of the main sequence, corresponding to lower stellar masses and SFRs, while LBGs conform the bulk at intermediate and large masses. Note that both LAEs/LBGs and pure LAEs appear in the upper side of the main sequence, in agreement with the idea of these sources experimenting a recent star-forming episode, while non-LAEs/LBGs are placed in the bottom-middle side of it.

Several authors have previously studied the SFR-$M_{\rm star}$ relation (Stark et al. 2009; González et al. 2010; Papovich et al. 2011; Salmon et al. 2015) also finding

the same lack of evolution on its slope between $4 \lesssim z \lesssim 6$ (see Figs. 3.13 and 3.14). The low scatter of this relation suggests that galaxies at this epoch form stars at a higher rate the more massive they are. This supports the hypothesis of a constant pristine gas income over the evolution of these high-z galaxies, leaving violent starburst episodes due to mergers or instabilities in a secondary role in the stellar mass growth of these galaxies. However, this stochastic events still likely alter the smooth increase of the $M_{\rm star}$, as also suggested in González et al. (2010) and Papovich et al. (2011). Our study is in agreement with the scenario of a smooth neutral gas infall driving the growth of galaxies at $4 \lesssim z \lesssim 6$ altered by episodic SF processes. It should be noticed that the SFRs derived from the L_{1500} are the SFRs averaged over the last 30-100 Myr it takes to the UV luminosity to change after SFR variations (*e.g.*, Salim et al. 2009; Salmon et al. 2015). In this way, galaxies which are brighter in the UV do show higher SFRs according to the smooth growth scenario suggested by the SFR-$M_{\rm star}$ main sequence. Nevertheless, these UV brighter and more massive sources are not necessarily presenting the strongest Lyα emission lines, indicator of the current ($\lesssim$ 25 Myr) SF. We do actually find a majority of sources (1030) with undetected Lyα line in our sample. This is consistent with a scenario of most of the sources at z = 4-6 constantly accreting pristine gas and presenting faint Lyα emission lines, with those showing high Lyα EWs being suffering a stochastic episode of SF on top of that. In fact, studying the SFR-$M_{\rm star}$ main sequence derived from the best-fitting SSP models (Fig. 3.14) we find that both pure LAEs and LAEs/LBGs are placed above the mean main sequence, indicating that they are indeed experimenting a recent star-forming episode.

3.5 Conclusions.

We have used CIGALE to model the sample of high-z LAEs and LBGs selected in Chapter 2, consisting of 1558 sources at $3.4 < z < 6.8$ in the GOODS-N field. Special attention is given to the differences between the three different subfamilies observationally defined in terms of their Lyα line and UV continuum emission. Single and double burst-like SP models are used to fit every SED, making use of a BIC calibration to decide in which situations an extra SP is really needed. With the stellar masses derived from the models, we have studied the SMF, SMD and SFR-$M_{\rm star}$ relation at each z, as well as the evolution of the fraction of sources from each subclass. The main conclusions are the following:

(a) The majority ($\sim 71\%$) of the high-z LAEs and LBGs are well explained by a SSP. The cases better described with a DSP are still strongly dominated

by the older population in terms of $M_{\rm star}$. However, the young SP is essential in terms of luminosity to properly fit the Lyα and rest-frame UV emission of these SEDs.

(b) The relative amount of objects from each of the subfamilies that need an additional SP is not the same. We find that the LAEs/LBGs require DSP models in $\sim 46\%$ of the cases, in comparison with $\sim 22\%$ and $\sim 29\%$ found for the non-LAEs/LBGs and pure LAEs, respectively. The need of two populations in a significant fraction of the LAEs/LBGs is due to the presence of a strong Lyα emission line combined with a bright continuum at the longest sampled wavelengths (IRAC) that cannot be simultaneously fitted well by a single stellar population, as in, *e.g.*, Rodriguez Espinosa et al. (2014).

(c) Pure LAEs can be understood as very young and very low mass galaxies with a median age of ~ 20 Myr and a median $M_{\rm star}$ of $\sim 4.2 \times 10^8$ $M_\odot$, presenting high Lyα EWs (indicative of very high Lyα escape fractions; Sobral & Matthee 2019) and experimenting one of their first star-forming episodes. The increasing fraction of these objects with z in our sample, consistent with Sobral et al. (2018b), supports the hypothesis of these pure LAEs being an initial and transitional stage on the evolution of high-z galaxies.

(d) LAEs/LBGs can be split into two subgroups clearly differentiated in age and stellar mass properties. SSP LAEs/LBGs seem to be very young (median age of $\sim$ 22 Myr; $M_{\rm star} \sim 6.8 \times 10^8$ $M_\odot$) but slightly more massive on average than the pure LAEs. The similarities with the pure LAEs subclass suggests that these are members of the same kind of young galaxies, but with different SFRs and stellar masses. The relative number of young LAEs follows the same trend with z than the pure LAEs one, supporting the idea of them being the same kind of galaxies.

(e) DSP LAEs/LBGs are fitted by much older and more massive models (median age $\sim$ 721 Myr; median $M_{\rm star} \sim 10^{10}$ $M_\odot$) featuring a young and much less massive population causing the bulk of the Lyα emission. According to this, multiple SP LAEs/LBGs seem to be galaxies much more massive and evolved (at this z), undergoing an episodic star-forming episode.

(f) Non-LAEs/LBGs are the most difficult subclass to model, as they do not show emission patterns that strongly help to constrain their ages in the rest-frame wavelength range sampled in this work at these redshifts.

This creates a degeneracy in the combinations of SPs that could lead to a good fit of their SEDs with negligible variations in the χ^2. Moreover, some of these galaxies could actually host a very young SP whose Lyα line is not detected because of resonant scattering and dust extinction. Furthermore, the use of the BIC for the SSP-DSP discrimination could be biasing the calculated ages for this family towards younger values, so we only aim at modelling these sources in a general way, in the understanding that the description of the class may not match all the individual cases.

(g) With the caveats just mentioned, the results derived from CIGALE show that non-LAEs/LBGs lack a really young SP ($\lesssim$ 25 Myr). Furthermore, the absence of strong Lyα emission indicates that these sources are not in a current star-forming episode, but forming stars in a smooth way (or have extremely low escape fractions). They are older and much more massive than pure LAEs or SSP LAEs/LBGs, with a median $M_{\rm star}$ of $\sim 3.7 \times 10^9$ $M_\odot$. These results suggest that non-LAEs/LBGs are a more evolved stage of high-z galaxies that have been forming stars for a longer time, developing a larger $M_{\rm star}$ and presenting brighter continuum emission at the longest wavelengths. The evolution of the registered fraction of these objects with z also supports the idea of non-LAEs/LBGs being more evolved star-forming sources, more common the lower the z is.

(h) We report a decreasing evolution of the characteristic M^* of the SMFs with z, as in *e.g.*, Grazian et al. (2015), finding $\log(M^*/M_\odot) = 11.01^{+0.49}_{-0.33}$, $10.76^{+0.68}_{-0.14}$ and $10.55^{+0.04}_{-0.12}$ at $z \sim 4$, 5 and 6, respectively. The low-mass slopes found are steeper than those typically found at low redshift. No significant evolution is found between z = 4-5, with a small increase at $z \sim 6$ ($\alpha = -1.88^{+0.20}_{-0.17}$, $-1.86^{+0.22}_{-0.22}$ and $-1.68^{+0.17}_{-0.63}$ at $z \sim 4$, 5 and 6, respectively). However, the α estimated at $z \sim 6$ has to be carefully considered, as we do not have much information covering the $M_{\rm star}$ region corresponding to the potential term of the Schechter SMF at that redshift.

(i) The SMD is estimated by integration of the SMF at each redshift. Our results are in agreement with the SMD-z trend reported at these redshifts by previous authors (Labbé et al. 2010; González et al. 2011; Lee et al. 2012; Duncan et al. 2014; Grazian et al. 2015; Song et al. 2016). The SMD obtained at $z \sim 5$, although consistent with the general trend, is slightly larger than expected if we follow the mean slope of the SMD-z relation at high-z, which could be linked to the presence of a previously reported $z \sim 5.2$ overdensity in GOODS-N (Walter et al. 2012; Arrabal Haro et al.

2018). Additional research is being pursued to further characterise this overdensity.

(j) The slope values found for the SFR $\propto M_{\rm star}^{\beta}$ relation are $\beta = 0.67^{+0.15}_{-0.19}$, $0.47^{+0.13}_{-0.13}$, $0.52^{+0.22}_{-0.18}$ at $z \sim 4$, 5 and 6, respectively, for the UV-derived SFRs and $\beta = 0.76^{+0.03}_{-0.04}$, $0.72^{+0.06}_{-0.06}$, $0.76^{+0.09}_{-0.09}$ at $z \sim 4$, 5 and 6, respectively, for the model-derived SFRs, both of them consistent with little to no redshift evolution of that slope within that redshift range, in agreement with previous works. The existence of such tight relation between these two magnitudes and its invariability within this z range point to the hypothesis of a smooth pristine gas infall as the main mechanism responsible of the mass growth of these galaxies along their lives, as suggested before (*e.g.*, Stark et al. 2009; González et al. 2010; Papovich et al. 2011; Salmon et al. 2015). Nevertheless, the best-fitting models obtained in this work together with the fact that LAEs appear above the SFR-$M_{\rm star}$ main sequence, also support the existence of stochastic star-forming events due to mergers and other instabilities that alter the increase of the stellar mass in a secondary way, as also suggested in González et al. (2010) and Papovich et al. (2011).

4

High-z grouping and overdensities

- Qué rabia cuando se quedan dos tortitas unidas.
- Las buenas tortitas siempre se quedan unidas.
Conversación de bar que hace que Marge Simpson no abandone a su amiga (The Simpsons).

In this chapter we present a search for high-z sources in groups within our previously selected sample. Several close groups of up to six members have been found. Physical differences with respect to isolated galaxies are analysed. We also study an already known $z \sim 5.2$ GOODS-N overdensity, finding a large number of new galaxies possibly belonging to this overdensity, making it one of the largest ones at high-z. This is important as it may show clues to be considered in models of large structure formation. This chapter also presents the preparation, reduction and preliminary results of multi object spectroscopy observations of some of these proto-cluster candidates.

Part of the content of this chapter is published in Arrabal Haro et al. (2018) or will be published in Calvi, Arrabal Haro et al. (2020, in prep.).

4.1 Close pairs

We carried out a search for groups of neighbouring galaxies in the sample of high-z sources selected in the GOODS-N field in Chapter 2, aiming to explore whether there are any physical differences between the sources in groups and those that are isolated galaxies at these redshifts.

To find objects with close neighbours, we look for galaxies at the same redshift (within our photometric redshift errors) that are inside a 30 comoving kpc radius circular region, assuming that objects farther away would not be part of the group, as considered, *e.g.*, in Mundy et al. (2017). The distance between objects in the group is calculated from their angular separation using

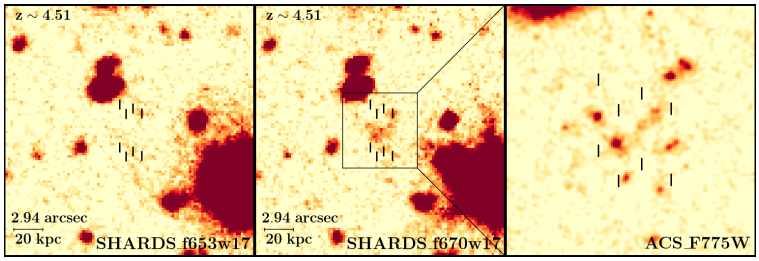

Figure 4.1: Images of the G6 $z \sim 4.51$ quartet in two consecutive SHARDS filters spanning the Lyman break (f653w17 in the left panel and f670w17 in the middle one). North is up, East is left. Note that the sources between marks do not appear in the bluer filter. The right-hand panel shows a zoomed image of the objects in the F775W *HST*/ACS image. A little plume can be appreciated in the westernmost source, which points to gravitational interaction between the objects of the group.

the angular diameter distance $D_{\rm A}$ at their redshift as it appears in Hogg (1999). It is worth noticing here that the distance limit adopted to consider that two sources are neighbours is a physical comoving distance and not an angular one. This is so because $D_{\rm A}$ drastically changes with z and so the angular separation between two objects corresponds to very different comoving separations between them depending on the z they share.

We find that 202 of the candidates are in 92 close groups of two or more galaxies, which represent $\sim 13\%$ of the total sample. In particular, we register 79 pairs, 10 trios, 2 quartets and a sextet. The remaining sources are isolated. This is in agreement with previous works looking for pairs or very close groups at these redshifts, which find similar fractions of grouped sources (Conselice & Arnold 2009; Mundy et al. 2017).

Table 4.1 lists the groups we found with their assigned names, indicating the distance between pairs or, in the case of groups with more members, the largest distance between the central object and the rest. The images of the quartet (G6) in the SHARDS bands sampling the Lyman break are shown in Fig. 4.1.

The distances between the objects in these groups vary from 59 kpc to 3.26 kpc. Almost half of them (48) are pairs separated by longer distances than the rest ($\sim$ 40-60 kpc), though they could still be interacting sources according to the typical distances given in Duc et al. (2014). In the other 44 groups, the

Table 4.1: Overview of the galaxies found in close groups. A full version of this table is available in Appendix A.

Group	Source ID	R.A. (J2000)	Dec. (J2000)	Distance (kpc)	Redshift
(1)	(2)	(3)	(4)	(5)	(6)
G1	SHARDS10005314	12:37:24.06	62:18:33.45	6.57±0.09	3.42±0.07
	SHARDS10008105	12:37:24.01	62:18:32.67		3.42±0.07
	SHARDS10013381	12:37:24.10	62:18:34.25		3.42±0.07
G2	SHARDS10004588	12:37:17.72	62:19:04.59	45.65±2.85	3.96±0.06
	SHARDS10007056	12:37:17.21	62:18:59.31		3.96±0.06
G3	SHARDS20005310	12:36:28.03	62:09:01.82	5.86±0.08	3.92±0.06
	SHARDS20011181	12:36:28.14	62:09:01.52		3.92±0.06
G4	SHARDS20005660	12:36:50.68	62:09:32.47	30.26±1.13	4.24±0.07
	SHARDS20009490	12:36:51.10	62:09:35.58		4.24±0.07
G5	SHARDS10006493	12:37:44.84	62:18:17.25	20.56±0.73	5.09±0.06
	SHARDS10008700	12:37:44.98	62:18:20.28		5.09±0.06
G6	SHARDS10009103	12:37:39.15	62:17:34.59	9.15±0.13	4.51±0.07
	SHARDS10007188	12:37:39.38	62:17:34.55		4.51±0.07
	SHARDS10007963	12:37:39.47	62:17:35.47		4.51±0.07
	SHARDS10014515	12:37:39.28	62:17:35.06		4.51±0.07
G7	SHARDS20009174	12:37:01.39	62:09:09.95	50.23±4.24	4.35±0.06
	SHARDS20006656	12:37:01.04	62:09:16.78		4.35±0.06
G8	SHARDS20006276	12:36:04.10	62:09:21.99	18.50±0.35	3.75±0.06
	SHARDS20005680	12:36:04.40	62:09:23.37		3.75±0.06
...	...	...	...	...	...

(1) Group identification. (2) SHARDS identification. (3) Right ascension. (4) Declination. (5) Distance between the objects in the group. In case of more than two objects in a group, the distance shown is the largest between the central object and the rest. (6) Photometric redshift.

galaxies are separated by distances of around 30 kpc or less (3.90-4.72 arcsec, depending on redshift). Three of the trios and one of the quartets are confined in a quite small area of around 20 kpc diameter. Many of the other trios are formed by a very close pair separated by a larger distance from the third object of the group. Something similar happens with the sextet (G55), which looks like four very close objects (one of which even seems to be three different non-resolved sources) in a $\sim$ 14 kpc region, with the fifth and sixth sources somewhat more separated, but showing a large and conspicuous tail between the more compact ones (see Fig. 4.2).

For these very close sources it is difficult to distinguish whether they are independent galaxies or star-forming knots in a single clumpy galaxy (Elmegreen et al. 2013). However, the SED fitting carried out in Chapter 3 gives us stellar masses of the order of $\log(M_{\rm star}/M_{\odot}) \sim$ 8-11 for the grouped galaxies (see Fig. 4.5), pointing towards these objects being high-z galaxies rather than clumps. Note that the theoretical model fitting used SEDs including *HST*/ACS and *HST*/WFC3 data, with very good spatial resolution (see Table 2.2). Additionally, the typical size of these objects is $\sim$ 0.4 arcsec, which is consistent with typical sizes of high-z galaxies as found by (Bouwens et al. 2004; Oesch et al. 2010; Ono et al. 2013; Shibuya et al. 2015; Holwerda et al. 2015; Curtis-Lake et al. 2016; Ribeiro et al. 2016; Liu et al. 2017). Moreover, luminous clumps in clumpy galaxies are usually surrounded by a common isophote, embedding the entire galaxy, below the bright level of the clumps but above the background sky (see Hinojosa-Goñi et al. 2016). This effect is not observed in these groups. For these reasons, the objects identified herein as companion sources are more probably individual galaxies in compact groups. Unfortunately, discerning whether the southernmost object of the G55 sextet is a single clumpy galaxy with three prominent star forming regions or three different merging galaxies is something that escapes the spatial resolution of our capabilities.

In particular, the group G5 (shown in Fig. 4.3) is an already spectroscopically confirmed pair of galaxies at $z \sim 5.1$ in which the northern source shows a nebulosity around it that could be either a tidal tail caused by the interaction with the other galaxy or the remnant of a recent merger with a third object (Rodriguez Espinosa et al. 2014). We find similar tail-like morphologies in most of our groups (*e.g.,* the westernmost object of G6 shown in Fig. 4.1). These structures support the hypothesis that our groups are gravitationally bounded systems. In addition to the tidal tails we also notice some other little spots near the trios and one more near G6 in the *HST*/ACS images that could be additional members of their respective groups. However, these extra objects do not appear either in the SHARDS or the ACS catalogues nor in the Rainbow database, and they cannot be resolved in the GTC images, so we do not have

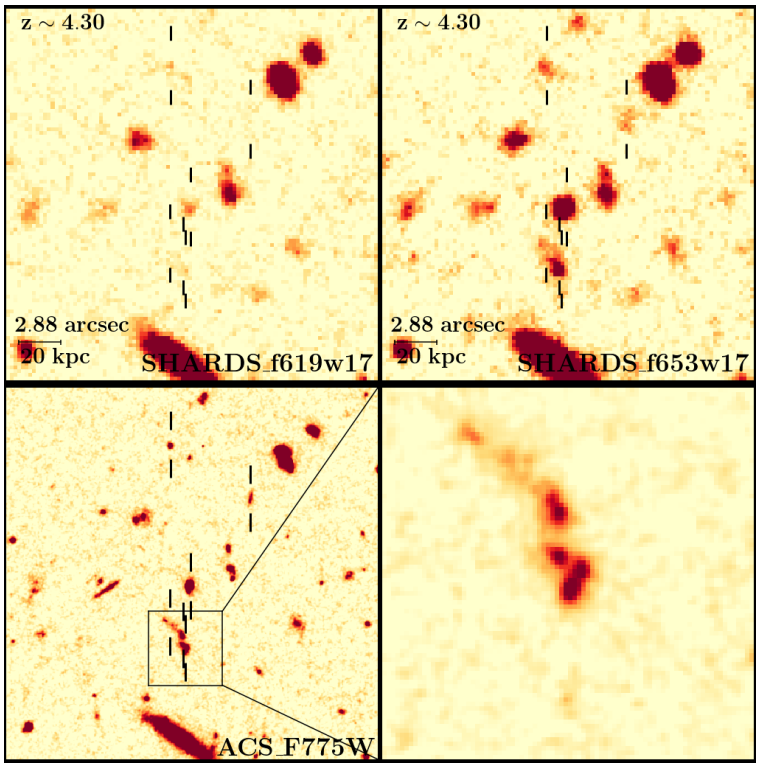

Figure 4.2: Images of the G55 sextet in two SHARDS filters spanning the Lyman break (f619w17 in the left upper panel and f653w17 in the right upper one). North is up, East is left. Note that the sources between marks do not appear in the bluer filter. The bottom-left panel presents an equally scaled view of the objects in the F775W *HST*/ACS image. The bottom-right panel shows a zoomed image in the same ACS filter with the contrast modified to better appreciate the sources in the long tail. Note that, at this resolution, the southernmost source seems to actually be formed by three different clumps.

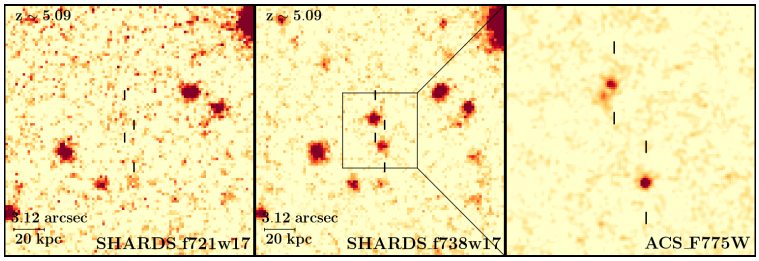

Figure 4.3: View of the G5 $z \sim 5.09$ pair of galaxies in the two consecutive SHARDS filters sampling their Lyman break. The right-hand frame corresponds to a zoomed image of the pair in the F775W *HST*/ACS image. Note the presence of a clear nebulosity around the northern source, pointing to a gravitational interaction between these two galaxies.

conclusive photometric information for them.

Note that the number of groups found, though significant, is not large enough to warrant studies of their dependence on redshift. They seem to follow a similar z distribution as the whole sample (see Fig. 4.4), finding a higher proportion of grouped sources in the $z \sim 4.3$-4.8 range. No significant differences are found when comparing the $M_{\rm star}$, age and SFR (Fig. 4.5).

4.2 GOODS-N $z \sim 5.2$ overdensity

In addition to the very close groups mentioned in Sec. 4.1, we also explore two already reported overdensities in the GOODS-N field at $z = 4.05$ (Daddi et al. 2009) and $z = 5.198$ (Walter et al. 2012). We find 87 and 55 objects possibly belonging (within our photo-z errors) to the $z = 4.05$ and the $z = 5.198$ overdensities, respectively. Unfortunately, the absence of a public list of coordinates of the reported $z = 4.05$ overdensity members makes it not possible for us to determine which of our selected candidates are new discoveries and which had already been found. The sources reported in Walter et al. (2012) for the $z = 5.198$ are not only well identified, but also constrained in a thinner redshift range of $z = 5.198 \pm 0.015$. Additionally, this second overdensity is located farther away in time, closer to the reionisation epoch, which gives it additional interest of study. For the reasons mentioned, we focus our work in characterizing the candidates that could belong to the $z \sim 5.2$ overdensity.

For this $z \sim 5.2$ proto-cluster, Walter et al. (2012) found 13 objects at

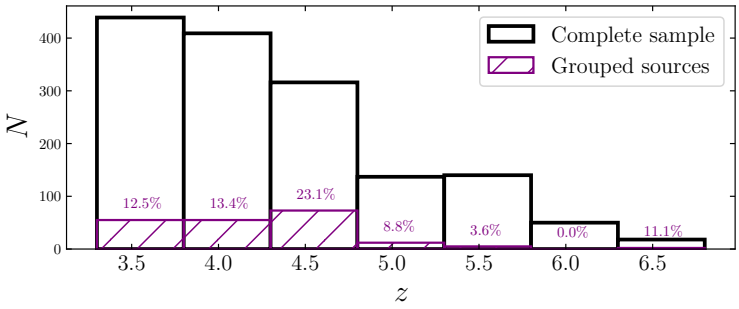

Figure 4.4: Redshift distribution of the grouped galaxies (purple diagonals) compared to the global sample (black line). We find a higher proportion of grouped sources at $z \sim 4.3$-4.8. However, we cannot guarantee a robust claim with the statistics we have.

$z = 5.198 \pm 0.015$ in the GOODS-N field, 11 of which are also detected by us. Of the two not detected, one is too faint to be robustly selected with our selection criteria and the other, HDF850.1, is a strongly dust-obscured galaxy and was detected via cold molecular gas lines in the milimetric (Walter et al. 2012), not showing any emission in the optical/NIR. We have further detected 44 additional sources whose redshifts are compatible with $z = 5.198 \pm 0.015$. They are all detected with the Lyα line/break in the f755w17 SHARDS filter and have an estimated redshift error of $\Delta z \sim 0.07$. This increases by a factor of ~ 4 the number of sources previously found for the $z = 5.198$ overdensity. A total of 55 possible cluster members for a single proto-cluster is something unseen beyond $z = 5$ (*e.g.*, Capak et al. 2011; Toshikawa et al. 2012, 2014; Higuchi et al. 2019). If confirmed, this proto-cluster at $z \sim 5.2$ will be the richest one found at high redshift within such short z range. Even though our photo-z calculations are very accurate, their uncertainties are still too large to confidently assign all these candidates to an overdensity confined in a redshift range of $\Delta z \sim 0.015$. To confirm whether our candidates do actually belong to the $z \sim 5.2$ proto-cluster, we design a MOS observation of them using the GTC/OSIRIS instrument.

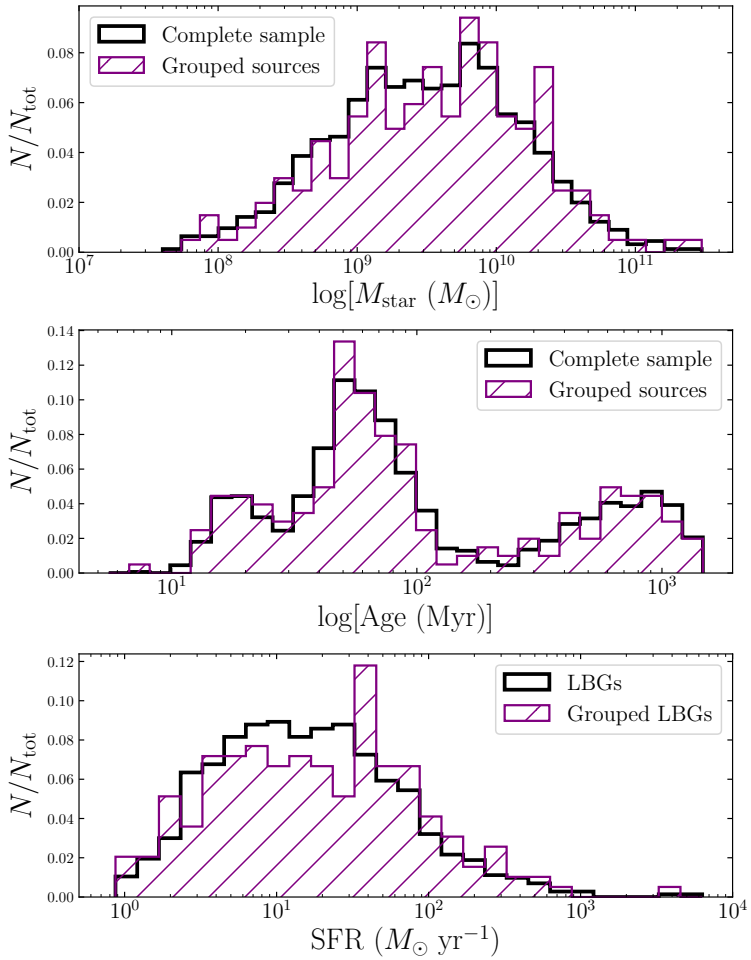

Figure 4.5: Normalised $M_{\rm star}$ (*top*), age (*middle*) and SFR (*bottom*) distributions of the grouped galaxies (purple diagonals) compared to the global sample (black line). Only UV-derived SFRs are compared. No significant differences are appreciated.

4.2.1 MOS mask design

The spectroscopic follow up of our candidates is prepared for OSIRIS (Cepa 2010) in service mode. The total FOV is 7.5×6.0 arcmin^2 in MOS mode. We use the R2500I grism, which covers the spectral range between 7330-10000 Å, producing a spectral resolution of 2.7 Å at $\lambda_{\rm obs} = 7450$ Å, with a 2×2 binning, so the pixels scale is 0.254 arcsec/pix.

The design of the mask is focused on including the maximum amount of new candidates possibly belonging to the $z \sim 5.2$ overdensity. The brightest objects among them get the highest priority to reduce the required integration time. We give a secondary priority to the not previously reported fainter objects, including as a last priority the sources previously reported in Walter et al. (2012). Finally, we fill the available slits with other galaxies of our sample for which the Lyα line/break is measurable with the R2500I grism employed in the observation. Once we have a general idea of the best mask orientation and the target distribution within it, the final configuration of the mask is carried out with the OSIRIS Mask Designer tool[1]. Special care is put in shifting the slits of nearby sources to avoid overlapping of the dispersed light along the spectral direction. We also take into account the direction in which each wavelength is dispersed to ensure that the region of every spectrum corresponding to the wavelengths where we expect to find the Lyα line is not dispersed out of the CCD (Charge-Coupled Device) detectors.

The final design of the MOS observation includes 24 targets, among which 4 are already reported in Walter et al. (2012) and 7 are mask fillers. That is, we include 13 new candidates. Four fiducial stars are also included to facilitate the best alignment of the mask during the observations. The final configuration of the MOS mask is shown in Figs. 4.6 and 4.7.

4.2.2 MOS reduction

The observations were taken in two different days during a single run on February 2019, obtaining 9 Observing Blocks (OBs). Each OB consists of two frames (one per CCD), with an exposure time of 1368 seconds. The long exposure time takes into account the OSIRIS CCDs inefficiency at these long wavelengths. The widths of the rectangular slits were 1.2 arcsecs, and the seeing those nights ranged from 0.7 to 1.0 arcsec.

The data reduction and calibration process of the observed MOS images follow the standard prescriptions using the Image Reduction and Analysis Facility (IRAF, Tody 1986). The bias subtraction and flat normalisation are done for

[1] http://www.gtc.iac.es/instruments/osiris/osirisMOS.php#Step_by_step

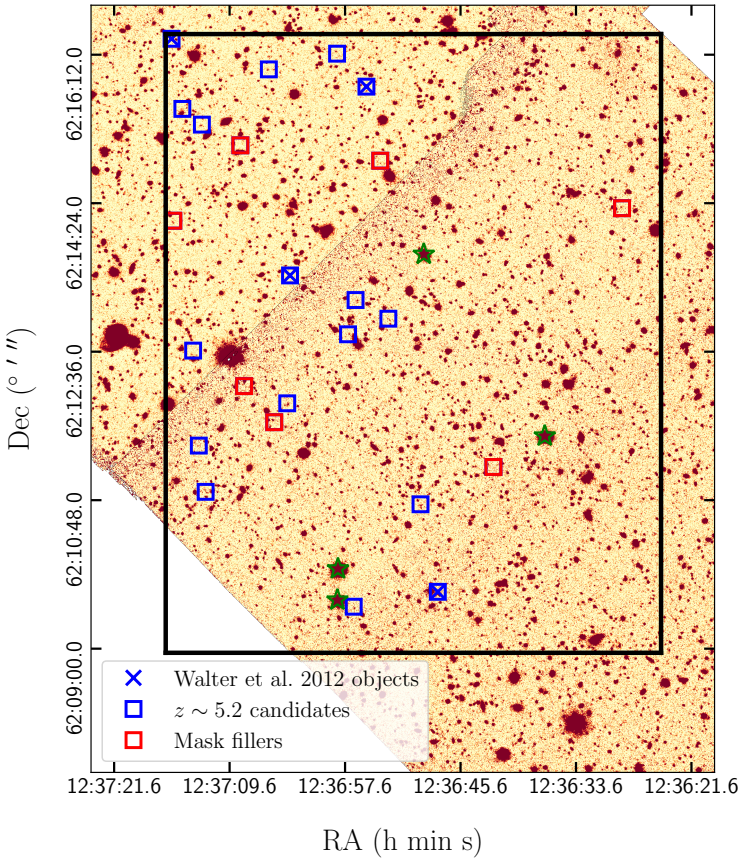

Figure 4.6: MOS mask configuration over the SHARDS f755w17 reference image. The big black frame corresponds to the 7.5×6 arcmin^2 FOV of the MOS mask. The blue squares show the position of the 17 $z \sim 5.2$ candidates, out of which 4 have already been reported (blue crosses). Seven filler sources are marked with red squares, and the four green stars indicate the position of the fiducial stars used for the pointing.

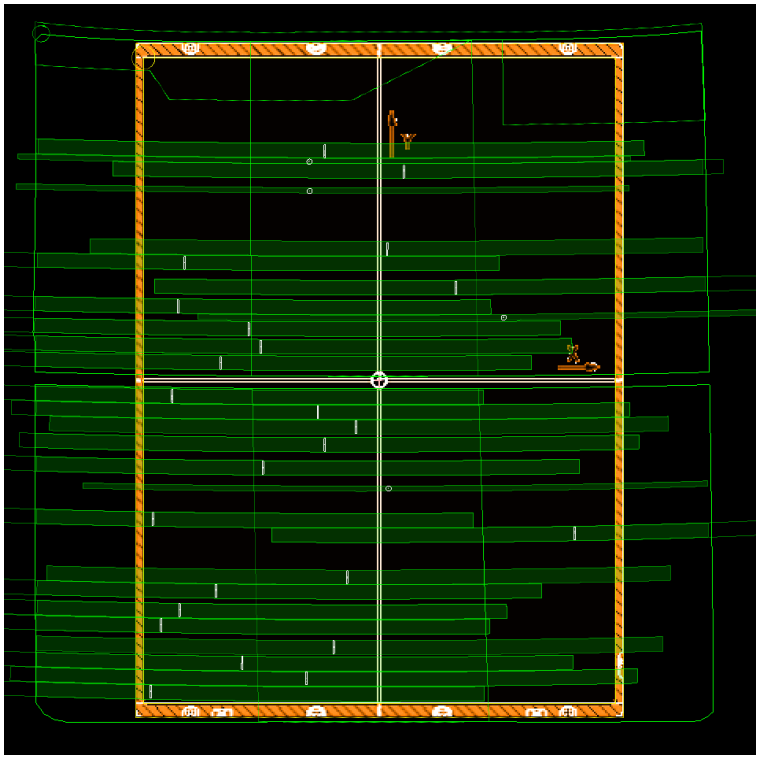

Figure 4.7: Overview of the final mask design for the MOS observation of $z \sim 5.2$ overdensity candidates. The orange vertical rectangle corresponds to the physical dimensions of the mask and so it limits the region where the slits can be placed. The two big parallel horizontal empty rectangles with green borders represent the two OSIRIS CCDs and they limit the region where the dispersed light can be measured. Note that two small regions at the top of the upper CCD need to be removed from the effective detection area because they are affected by vignetting produced by internal components of the OSIRIS instrument. The little vertical white rectangles represent the 24 slit positions, and each horizontal filled green rectangle shows the measurable light from each slit after being dispersed by the R2500I grism. Special care needs to be taken with the slits placed near the edges of the mask to ensure that the exact wavelengths where we expect the Lyα emission do not fall out of the CCDs. The four white circles correspond to brighter fiducial stars to guarantee a good pointing and orientation of the mask during the observation.

each individual OB. We use a reference flat for each CCD to remove geometrical distortions. Afterwards, the science images are combined using an average Signal-to-Noise (S/N) rejecting algorithm to get rid of possible cosmic rays. Slits spectra are then trimmed to individually perform the wavelength calibration. For that, we make use of sky emission lines in the 6400-10500 Å range as calibrators[2]. Using IRAF-NOAO (National Optical Astronomy Observatory) package tasks, we identify the corresponding sky emission lines within our slit frames. Fourth-order Chebyshev polynomials are fit along the spatial direction in some near sky region to provide a smooth sky model to subtract from the 2D spectrum.

We focus in the search for conspicuous emission features during the 2D and 1D visual inspection in the wavelength range of 7300-7800 Å, which is the wavelength range probed by the SHARDS f755w17 filter where the candidates were previously detected. If a Lyα emission in the mentioned wavelength range is clearly identified, we assign an A flag to the object, corresponding to a secure detection. On the opposite, if from visual inspection we are not able to observe a clear detection, we perform a second iteration of sky subtraction to look for significant peaks in the 2D spectrum. Sources detected in this way are flagged with the letter B, indicating that they are relatively weak detections. The C flag is assigned to non-detections, while an F indicates that the object was a mask filler introduced to optimise the use of the observing time, but that are not meant to be members of the $z \sim 5.2$ overdensity. We detect 10 sources with very good S/N, plus 3 additional sources with a reasonable but more uncertain S/N.

Spectra are flux calibrated using a spectroscopic standard star observed during the same observing run. The spectroscopic standard is used to determine the response curve of the spectrograph, and in turn can be used to flux-calibrate the spectra of our targets. First, we reduce and perform the wavelength calibration of the spectroscopic standard star in the same way as done with the science frames. However, since the standard star was taken with a wider slit (2.5 arcsec), specific flat frames corresponding to the standard star are used. The 1D spectrum of the standard is extracted using the IRAF *apall* task. Knowing the exposure time and the extinction correction, we match the 1D spectrum of the spectroscopic standard in units of ADU s^{-1} to the available flux density Oke (1990) catalogue, tabulated in the IRAF *onedstds* directory. Thus, we obtain the flux transformation from ADU s^{-1} to erg s^{-1} cm^{-2} $Å^{-1}$ to calibrate the science frames. The final calibrated spectra of some A and B

[2]We used the LRIS catalog of sky emission lines from `http://www.astrossp.unam.mx/~resast/standards/NightSky/skylines.html`.

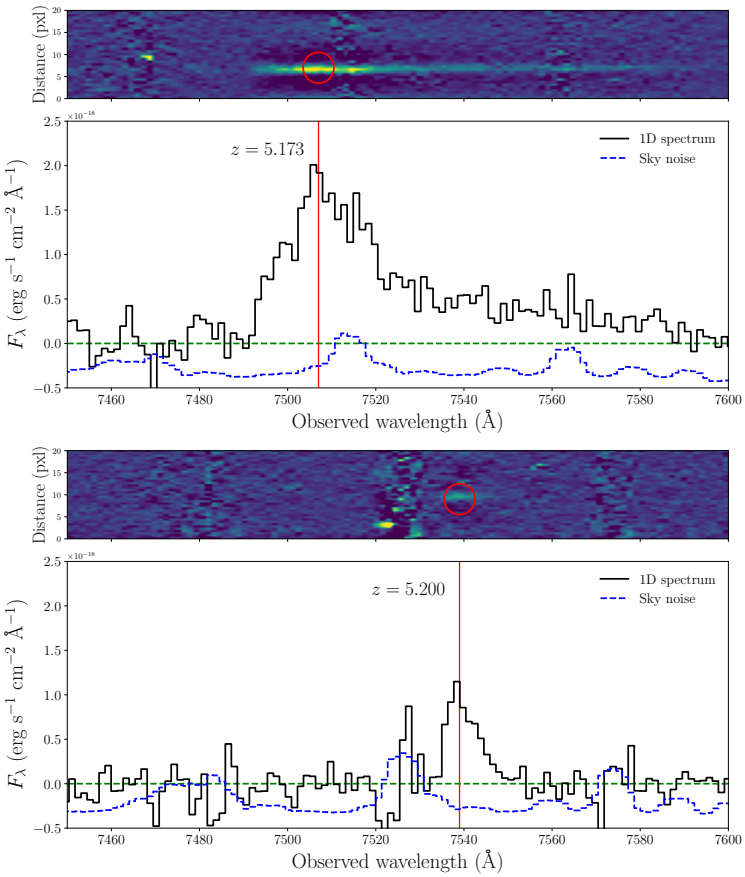

Figure 4.8: 2D and 1D spectra of two A sources classified as secure detections. The black histogram corresponds to the collapsed 1D spectra. The solid red line indicates the peak center of the Lyα emission line. The dashed blue histogram shows the sky lines spectra scaled down so they do not interfere with the actual spectra of the sources. The zero flux is indicated by the horizontal dashed green line. The SHARDS20004537 source shown in the upper spectrum is the brightest object measured in our MOS observation and was previously found in Walter et al. (2012), although we detect it at a slightly lower redshift. On the other side, the SHARDS10011501 galaxy shown in the lower spectrum is a newly discovered object just in the middle of the overdensity z range. Note the asymmetry of the measured line, which gives even more robustness to the Lyα detection of these sources.

.

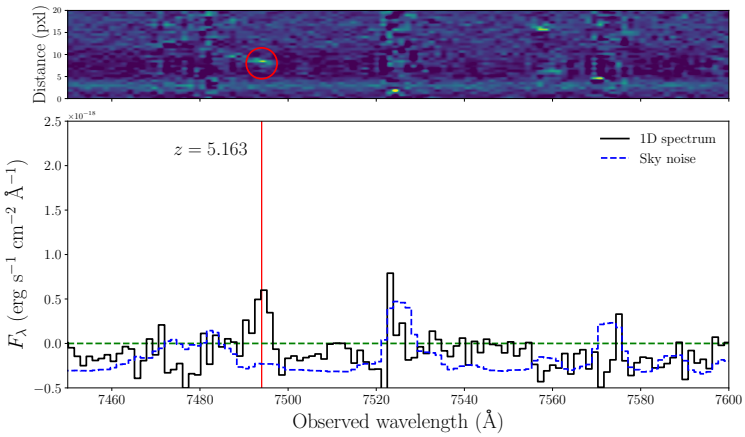

Figure 4.9: 2D and 1D spectra of one of the three B sources classified as uncertain detections. The solid red line indicates the peak center of the Lyα emission line. The dashed blue histogram shows the sky lines spectra scaled down so they do not interfere with the actual spectra of the sources. The zero flux is indicated by the horizontal dashed green line. Note that this object presents a spectroscopic z slightly below the proto-cluster one, so not belonging to it even though its $z_{\rm spec}$ is in good agreement with its previously estimated $z_{\rm phot}$ within their errors (see Table 4.2).

.

flagged galaxies can be seen in Figs. 4.8 and 4.9, respectively. The upper object shown in Fig. 4.8 is indeed a very bright source ($m_{\rm Ly\alpha} = 22.74 \pm 0.014$ AB mag, in the SHARDS f755w17 filter) reported in Walter et al. (2012) and previous broad band searches (Cristiani et al. 2004; Fontanot et al. 2007; Iwata et al. 2007). In fact, Cristiani et al. (2004) and Fontanot et al. (2007) classified it as a QSO. This is, however, the first time that a spectrum of this source is published, making it specially valuable. The strong emission observed in the spectrum, both in Lyα and in the UV continuum, points to this source being a QSO, indeed. Additionally, the small peak presented by the source blue-ward of Lyα suggests that this galaxy could also be a high-z Lyman continuum leaker in an ionised gas bubble (Vanzella et al. 2015; De Barros et al. 2016; Shapley et al. 2016; Bian et al. 2017; Vanzella et al. 2018). The 2D and 1D spectra of all the sources can be seen in Appendix C.

4.2.3 MOS results

The final spectroscopic redshifts measured for the objects in the mask are shown in Table 4.2, as well as their detection quality according to the classification mentioned in Sec. 4.2.2. The error in redshift is obtained from the typical FWHM of the Lyα line measured in our spectra ($\sim$ 13 Å) which translates into $\Delta z_{\rm spec} \sim 0.005$. According to the new spectroscopic redshifts, we find 7 sources compatible with $z = 5.198 \pm 0.015$ within their errors, *i.e.*, belonging to the proto-cluster. Among them, only one was previously reported in Walter et al. (2012). However, we find two Walter sources at a slightly lower spectroscopic redshift than the one previously reported (5.170 and 5.173 $\pm$0.005, respectively). This makes us think that the overdensity width could actually be extended to $z = 5.20 \pm 0.03$, in which case we would include these two Walter sources which indeed are supposed to belong to the proto-cluster, plus another newly found galaxy, making a total of 11 proto-cluster members (8 new ones) out of the 17 observed initial candidates, as summarised in Table 4.3.

In addition to the overdensity candidates, 4 out of the 7 mask fillers are also detected, finding a good agreement between their photometric and spectroscopic redshifts for all but one of them. The issue with this last object is that it is located in a specially noisy region in the reddest SHARDS images, which could have affected its identification and posterior photo-z calculation. Apart from that, the MOS results show a very good redshift agreement, highlighting the high quality of the SHARDS photometric redshifts. A comparison of the photometric and spectroscopic z of all the MOS detected galaxies is shown in Fig. 4.10.

Additionally, preliminary calculations from Calvi, Arrabal Haro et al. (2020, in prep.) using Friends-of-Friends algorithms with all the objects detected in our MOS observation suggest that these galaxies could be distributed into two close and differentiated virialised groups. The Friends-of-Friends algorithm used follows the Huchra & Geller (1982) method developed to search for groups and clusters in a magnitude limited survey. An iterative procedure is used, according to which we built a cylinder centred on each galaxy. For this analysis a projected mutual distance of $D_L = 1$ Mpc is adopted as well as a line of sight V_L equal to three times the velocity dispersion, fixed at 500 km/s rest-frame. This assumptions follow a similar approach of that used to identify groups at low (McGee et al. 2008; Calvi et al. 2011) and high redshift (White et al. 2005; Halliday et al. 2004; Poggianti et al. 2006; Milvang-Jensen et al. 2008). Two close gravitationally interacting groups are found, with 4 and 9 objects, respectively.

Table 4.2: Sources included in the GTC/OSIRIS MOS observation.

ID	R.A. (J2000)	Dec. (J2000)	$z_{\rm phot}$ ($\pm$0.07)	$z_{\rm spec}$ ($\pm$0.005)	Detection flag
(1)	(2)	(3)	(4)	(5)	(6)
SHARDS20008777	12:36:56.70	62:09:30.52	5.19	5.181	A
SHARDS20004537[1]	12:36:47.96	62:09:41.36	5.19	5.173	A
SHARDS20013107	12:36:49.76	62:10:45.01	5.21	5.179	A
SHARDS20008702	12:37:12.09	62:10:54.06	5.21	5.155	A
SHARDS20007667	12:36:42.18	62:11:12.14	5.48	5.323	F
SHARDS10006522	12:37:12.80	62:11:27.70	5.22	5.218	B
SHARDS20011722	12:37:04.96	62:11:44.72	5.36	5.335	F
SHARDS20013448	12:37:03.61	62:11:58.46	5.22	5.224	A
SHARDS20006636	12:37:08.09	62:12:10.95	5.36	–	F
SHARDS10005737	12:37:13.39	62:12:36.80	5.26	–	C
SHARDS20008932	12:36:57.29	62:12:48.65	5.23	–	C
SHARDS20011455	12:36:53.10	62:13:00.00	5.23	–	C
SHARDS20010724	12:36:56.51	62:13:13.57	5.23	5.188	A
SHARDS20007459[1]	12:37:03.32	62:13:31.45	5.27	5.217	A
SHARDS10006852	12:37:15.45	62:14:11.26	4.45	–	F
SHARDS20010811	12:36:28.81	62:14:20.36	5.79	–	F
SHARDS20013642	12:36:53.94	62:14:54.90	5.82	5.800	F
SHARDS10008970	12:37:08.48	62:15:06.10	5.88	5.336	F
SHARDS10018196	12:37:12.48	62:15:21.15	5.17	5.195	A
SHARDS10008210	12:37:14.51	62:15:32.57	5.18	5.162	B
SHARDS10008850[1]	12:36:55.38	62:15:48.77	5.15	-	C
SHARDS10011501	12:37:05.52	62:16:01.33	5.17	5.200	A
SHARDS10010385	12:36:58.43	62:16:12.75	5.16	5.195	A
SHARDS10006357[1]	12:37:15.63	62:16:23.58	5.19	5.170	B

[1] Object previously reported in Walter et al. (2012).
(1) SHARDS identification. (2) Right ascension. (3) Declination. (4) Photometric redshift from the SHARDS SEDs. (5) Derived spectroscopic redshift from the MOS spectra. (6) Spectroscopic detection flag: A, secure detection. B, moderate detection. C, no detection. F, mask filler.

Table 4.3: $z \sim 5.2$ MOS results summary. Note that those galaxies detected but not belonging to the overdensity are still in good agreement with their photometric redshifts within the errors.

	Observed candidates	Detected, in the overdensity	Detected, not in the overdensity	Not detected
In Walter et al. (2012)	4	3	-	1
New candidates	13	8	2	3

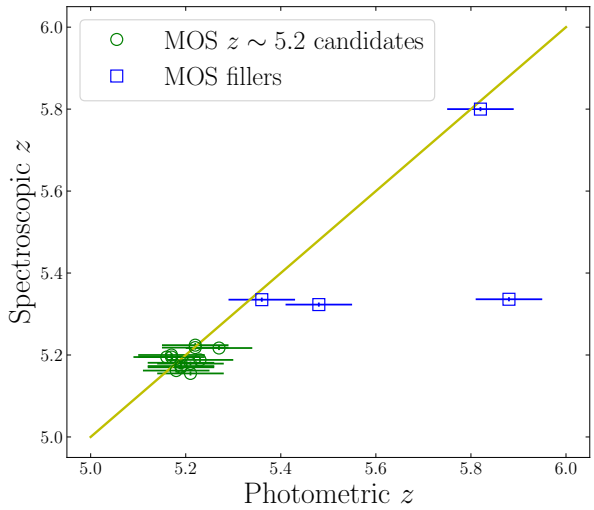

Figure 4.10: Comparison of the photometric and spectroscopic redshifts of all the sources detected in the MOS observation. The green circles indicate the candidates to belong to the overdensity, while the blue squares correspond to the filler sources. The one-to-one line is shown in yellow. Good agreement is found except for one object.

.

Further study of these structures is in process and will be available in Calvi, Arrabal Haro et al. (2020, in prep.). Moreover, given the success of this first MOS observation, three new OSIRIS masks are being prepared to observe as many as possible of the remaining 31 new $z \sim 5.2$ candidates from our sample yet spectroscopically unobserved.

4.3 Conclusions

We have carried out a search for groups of high-z neighbouring galaxies in the GOODS-N field, imposing that all objects in those groups share a common photometric redshift and are separated no more than 60 comoving kpc. Additionally, we have studied an already known GOODS-N $z = 5.198 \pm 0.015$ overdensity (Walter et al. 2012) composed of 13 galaxies, finding 44 new candidates within our sample. A MOS observation has been designed to study 13 of these new proto-cluster candidates, detecting 10, of which 8 are confirmed as overdensity members. The main results are:

(a) We find 202 galaxies ($\sim 13\%$ of the total sample) in 92 groups of two or more objects: 79 pairs, 10 trios, 2 quartets and a sextet.

(b) In 44 of the groups, the sources are separated by less than 30 kpc, presenting small tail-like structures between them, which suggests that they are probably gravitationally interacting galaxies.

(c) We do not find any significant difference in the stellar mass, age or SFR distributions of the sources grouped in these compact groups with respect to the global sample.

(d) We report 55 objects compatible with $z = 5.198 \pm 0.015$ within their photo-z errors. If most of the 44 new proposed sources are confirmed the number of galaxies in that overdensity would virtually quadruplicate, making it the richest one beyond $z = 5$ up to date in such a tight redshift range.

(e) From the MOS of 13 new $z \sim 5.2$ proto-cluster candidates, 10 of them are detected and 8 confirmed as members of the overdensity. The overdensity z range has been widened to $z = 5.20 \pm 0.03$ because of the finding of two proto-cluster members from Walter et al. (2012) at slightly shifted redshifts. The success of this first MOS observation has led to the preparation of three new MOS masks to observe as many non-observed new candidates as possible, with the intention of completely characterise this interesting proto-cluster.

(f) The spectroscopic redshifts derived with the MOS observations are in very good agreement with those previously estimated from the SHARDS SEDs, highlighting once again the excellent quality of the photometric redshifts obtained for our medium/narrow band selected sample.

5

Machine learning SED clustering

¿Cómo que me lo ha perdido? Ha podido caerse en una de esas máquinas. Ay, Dios mío, su gorra roja de la suerte... ¡En una caja! ¡Mi hijo convertido en caja! ¡Maldición! ¡Es una caja!
Homer Simpson en la fábrica de cajas (The Simpsons).

This chapter discusses the SED clustering of two high-z LAEs and LBGs samples using machine learning algorithms. We show the results of the application of Gaussian mixture models to the SEDs in both the SHARDS sample of LAEs and LBGs and the SC4K-COSMOS high-z LAEs sample (Sobral et al. 2018). The main purpose of this unsupervised clustering methodology is to find significant physical differences that may exist between the various clusters.

The content of this chapter shows results of a work that will be published in Arrabal Haro et al. (2020, in prep.).

5.1 Machine learning algorithm description

Aiming to find relevant differences in the energy distribution of high-z galaxies, we carry out an unsupervised classification of high-z SEDs making use of ML algorithms. Particularly, the clustering of the sample is implemented using Gaussian Mixture (GM) models. This algorithm presents clear advantages over the more classical k-means, in which each object can exclusively belong to a single cluster, only depending on the distance to the cluster center. On the contrary, the GM method assigns a different probability of belonging to each cluster to every object. This allows the overlapping of clusters, indicating that two different families of objects could present similar physical observables despite belonging to different groups. Additionally, the GM is much more

flexible in terms of cluster covariance, while that can only be spherical for the k-means model (unless using non-euclidean distances), which translates in poorer determinations of which cluster each object belongs to.

As indicated by its name, the GM method tries to model the SEDs as a mixture of multidimensional Gaussian distributions. For one dimension, the Gaussian probability density function can be expressed as:

$$G(X|\mu,\sigma) = \frac{\exp[-(x-\mu)^2/2\sigma^2]}{\sigma\sqrt{2\pi}}, \tag{5.1}$$

where μ and σ^2 are the mean and variance of the distribution, respectively. If we extend Eq. 5.1 for a d-variate Gaussian distribution, the probability density function is given by:

$$G(X|\mu,\Sigma) = \frac{\exp[-\frac{1}{2}(X-\mu)^T\Sigma^{-1}(X-\mu)]}{\sqrt{2\pi|\Sigma|}}, \tag{5.2}$$

where μ is not a single scalar mean now, but a d-dimensional mean vector and Σ is the covariance matrix.

Assuming there are K clusters within our SED sample, we can define π_k as the mixing coefficient of the k-th distribution. This coefficient gives us the probability of observing a data point from the Gaussian distribution k. The probability density can be then defined as a linear combination of the densities of all K distributions as follows:

$$p(X) = \sum_{k=1}^{K} \pi_k G(X|\mu_k,\Sigma_k). \tag{5.3}$$

To estimate the characteristic parameters of the K Gaussian distributions using the maximum log-likelihood method, we compute the natural logarithm of the probability density:

$$\ln p(X|\mu,\Sigma,\pi) = \sum_{i=1}^{N} \ln p(X_i) = \sum_{i=1}^{N} \ln \sum_{k=1}^{K} \pi_k G(X_i|\mu_k,\Sigma_k), \tag{5.4}$$

with N being the total amount of SEDs of our sample. We can now define $\gamma_k(X) = p(k|X)$ such that $\sum_{n=1}^{N}\gamma_k(x_n)$ corresponds to the total number of SEDs in the k-th cluster. Therefore, from Bayes' theorem,

$$\gamma_k(X) = \frac{p(X|k)p(k)}{\sum_{k=1}^{K} p(k)p(X|k)} = \frac{p(X|k)\pi_k}{\sum_{k=1}^{K}\pi_k p(X|k)}. \tag{5.5}$$

In order to maximise the log-likelihood function (Eq. 5.4), the derivative of $p(X|\mu, \Sigma, \pi)$ with respect to μ, Σ and π have to be equal to zero, thus the following equations:

$$\mu_k = \frac{\sum_{n=1}^{N} \gamma_k(x_n) x_n}{\sum_{n=1}^{N} \gamma_k(x_n)}, \tag{5.6}$$

$$\Sigma_k = \frac{\sum_{n=1}^{N} \gamma_k(x_n)(x_n - \mu_k)(x_n - \mu_k)^T}{\sum_{n=1}^{N} \gamma_k(x_n)}, \tag{5.7}$$

$$\pi_k = \frac{1}{N} \sum_{n=1}^{N} \gamma_k(x_n). \tag{5.8}$$

As the estimation of these parameters cannot be done in a closed form, we make use of the Expectation-Maximisation (EM) algorithm (Dempster et al. 1977) to determine them. This algorithm is an iterative method to find maximum-likelihood solutions when the data is incomplete or has some hidden variables. It consists on two iterable steps, the expectation one and the maximisation one, as its name claims. During the first step, the algorithm initialises the parameters μ_k, Σ_k and π_k using random seeds or by some preliminary clustering results. Then, the γ_k are estimated for those parameter values. In the maximisation step, the algorithm carries out a new estimation of the Gaussian distributions parameters with the current γ_k and computes the log-likelihood function (Eq. 5.4). The whole process (except for the initial random seeds estimation) is iterated until the log-likelihood converges. It is worth noticing that the EM algorithm finds a local optimal point which might not be the global one and so the final classification may slightly vary depending on the starting conditions. To solve this issue, we carry out several GM runs using a hundred different initial seeds.

Additionally, in order to explore all the different natures of the SEDs clustering, we compute the GM both initializing the iterative process via random seeds and via a previous k-means estimation. In every case, four different kind of cluster covariances are used to compare the results. The best covariance and number of clusters modelling our SED sample is determined in terms of the BIC (Eq. 3.4), as employed in the SP modelling of the SHARDS sample (Sec. 3.1.1). It is possible that the BIC trend with the number of clusters does not reach a clear minimum, and therefore the exact optimal number of clusters is not obvious. In this cases, a common approach consists on evaluating not the BIC itself, but its gradient, to identify beyond which number of clusters

an increase in the amount of them does not translate into a substantial BIC improvement, and therefore we may be overfitting our data.

Once the best number of clusters has been estimated, we make use of the silhouette coefficient (see Rousseeuw 1987) to select the best GM among all the different runs resulting in that optimal number of clusters. This coefficient gives us a measure of how differentiated are the clusters from each other. Keeping the assumption that we have K clusters, for a SED x_i belonging to the cluster C_k, we can define the mean distance between x_i and all the other SEDs in the same cluster as:

$$a(x_i) = \frac{1}{|C_k| - 1} \sum_{j \in C_k, i \neq j} d(x_i, x_j), \tag{5.9}$$

where $d(x_i, x_j)$ is the distance between the SEDs x_i and x_j in the cluster C_k. Eq. 5.9 gives us a an indication of how well the SED x_i is assigned to its cluster. We can also define the minimum distance between x_i and all the other SEDs within the other clusters:

$$b(x_i) = \min_{k' \neq k} \frac{1}{|C_{k'}|} \sum_{j \in C_{k'}} d(x_i, x_j). \tag{5.10}$$

The silhouette score of the SED x_i can now be defined as:

$$s(x_i) = \begin{cases} \frac{b(x_i) - a(x_i)}{\max\{a(x_i), b(x_i)\}} & \text{if } |C_k| > 1 \\ 0 & \text{if } |C_k| = 1. \end{cases} \tag{5.11}$$

By definition, $-1 \leq s(x_i) \leq 1$. For those SEDs whose silhouette score is close to 1, it can be inferred that $a(x_i) \ll b(x_i)$, indicating that the SED belongs to its assigned cluster with a high probability. On the contrary, a silhouette score close to -1 implies that the SED might belong to the neighbour cluster rather than the one assigned to it. To analyse the mean silhouette score of a whole cluster, we just take the mean $s(C_k)$ of all the SEDs within that cluster. This can be extended to a mean silhouette score of the entire sample, which gives an idea of how well differentiated are the clusters, hence the quality of the overall classification. By taking the GM run with largest silhouette score among all the GMs for which we obtain the optimal number of clusters K (previously estimated with the BIC), we make sure to select the GM classification with the best defined clusters.

5.2 SEDs sample preparation

The main purpose of our ML classification is to automatically identify emission variations between SEDs which lead to physical differences between clusters. These might be associated to some kind of evolution from one to another. Hence we first normalise all the SEDs to their Lyα emission. In this way, we get rid of the absolute F_ν value of the SEDs, avoiding the clustering algorithm to separate the sample in terms of brightness or stellar mass. Instead, it will do so in terms of differences in the intrinsic SED shape, more linked to age, EWs, metallicity and extinction variations. Of course, to also avoid a classification conditioned by the wavelength placement of the Lyα line/break, and therefore the redshift, during the ML process we will work with the UV rest-framed SEDs.

A first consideration we have to take into account when doing a ML classification, is the need of having information of each object in every single point of the parameter space used. This means that we cannot run the GM algorithm leaving the photometric non-detections untouched, otherwise those points would represent drastic changes in the SEDs, leading to physically unreal clusters driven by non available data. Not only information in every point is needed, but also the exact wavelength value of each photometric point in the SEDs has to be the same in order to be compared for the whole sample. This second requirement is not trivial when working with the SHARDS filters due to the shift of their effective CWL with the position in the FOV, as discussed in Sec. 2.1.

To solve the absence of detection in certain filters for some of the objects, we limit our SEDs to only the SHARDS points, leaving apart any ancillary data where many of the sources in our sample are not detected due to either depth or spatial resolution of the images. In addition, the wavelength range of the SHARDS SEDs is limited to only include three filters blue-ward of Lyα, since many of these points after the Lyman break lack relevant emission in most of our galaxies just because of their nature. Pure LAEs are also removed from the sample, as this kind of objects do not present reliable continuum emission in SHARDS by definition.

It is important to note here that the fact that we are working with rest-frame SEDs implies that the wavelength coverage, as well as the rest-frame spectral resolution, will be different depending on the redshift of each source. This complicates even more the choice of a common parameter space for the GM. In this sense, higher z objects will be sampled with better spectral resolution, but only up to lower maximum wavelengths, and vice-versa. To compare our SHARDS SEDs in the most possible uniform way, we divide the sample into the

three broad redshift ranges used in previous chapters, namely, $z \sim 4$, 5 and 6. In this way, we do not miss longer wavelengths information in a $z \sim 3.5$ source because of the rest-frame wavelength cap imposed by $z \sim 6.5$ galaxies while also not wasting the higher rest-frame spectral resolution in the later ones.

The last step in the preparation of our data for the GM algorithms consists on a SED interpolation to replace remaining non-detections in some SHARDS filters with the expected flux density value interpolated from its SED continuum. At the same time, this interpolation is used to set the exact same rest-frame wavelength points for the whole sample within each redshift bin. To achieve this, we select a well sampled fiducial galaxy for each redshift range and take its rest-frame wavelengths as the reference one for all the galaxies in that redshift bin. The three reference galaxies are taken with redshifts very close to the central one of their respective z bin to be representative of the average rest-frame wavelength coverage at that redshifts. We allow the flux interpolation to a reference wavelength (or in case of non-detection in a filter) only in those cases where there are reliable measurements in nearby filters at no more than $40/(1+z)$ nm red- and blue-ward of that reference wavelength (slightly beyond the width of two consecutive SHARDS filters). The filter sampling the Lyα emission line is never used in any interpolation. If it is not possible to find two valid points to interpolate, we look for a good detection in a single filter closer than $17/(1+z)$ nm (standard SHARDS filter width) and adopt its photometry as we assume that filter is sampling the emission of the object at the corresponding reference wavelength. At the end of the process, we reject any galaxy not fully sampled in the whole parameter space, ending up with 406 sources at $z \sim 4$, 111 at $z \sim 5$ and 24 at $z \sim 6$.

5.2.1 The SC4K-COSMOS sample

To further complement the results of a ML classification of high-z SEDs, in addition to our SHARDS selected sample, we also apply the same GM algorithms to the SC4K-COSMOS LAEs sample. This $z \sim$ 2-6 galaxy sample was selected by Sobral et al. (2018) using both narrow, medium and broad band data from the Subaru Telescope and the Isaac Newton Telescope (INT) in the $\sim$2 deg^2 COSMOS field. Apart from the two INT narrow bands and the COSMOS Archive[1] narrow, medium and broad band data (Capak et al. 2007; Taniguchi et al. 2007), there is also ancillary measurements of these sources in the NIR with VISTA/VIRCAM (McCracken et al. 2012) and *Spitzer*/IRAC (Sanders et al. 2007; Steinhardt et al. 2014), which help us to extend the SEDs included

[1] https://irsa.ipac.caltech.edu/data/COSMOS/images/

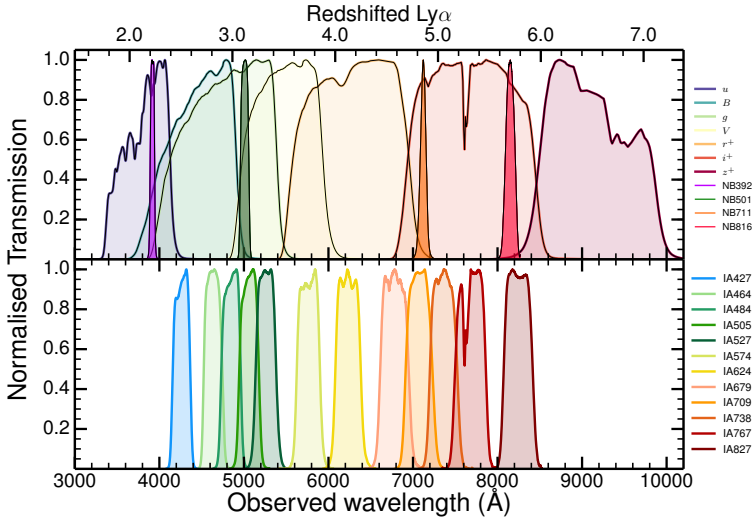

Figure 5.1: Figure from Sobral et al. (2018) showing the transmission curves of the filters used in their selection criteria. Narrow- and broad-band filters are shown in the upper panel, while the bottom one corresponds to the medium bands.

in the ML classification towards longer wavelengths. A summary of the general properties of the filters used in the GM clustering for this sample is presented in Table 5.1.

The 3908 LAEs of this sample were identified by Sobral et al. (2018) with a selection criteria following the Lyman break technique and looking for emission excesses in the narrow- and medium-band filters employed, dividing the sample in 16 redshift slices. The broad bands were used to estimate the continuum emission of the sources. The normalised transmission curves of the different width filters employed in their selection criteria are shown in Fig. 5.1. Sources with very red colours red-ward of the emission line were removed as possible lower redshift interlopers. For more detailed information about this sample selection and properties, we refer to Sobral et al. (2018). The spatial distribution of the final SC4K-COSMOS objects in each redshift slice can be seen in Fig. 5.2.

Table 5.1: Overview of the SC4K-COSMOS photometric filters.

Filter	Telescope/Instrument	$\lambda_{\rm eff}$ (Å)	FWHM (Å)	$m_{3\sigma}$ (AB mag)
(1)	(2)	(3)	(4)	(5)
u	CFHT/MegaCam	3911.0	538.0	27.8
IA427	Subaru/Suprime-Cam	4256.3	206.5	27.0
B	Subaru/Suprime-Cam	4439.6	806.7	28.3
IA464	Subaru/Suprime-Cam	4633.3	218.0	26.9
g^+	Subaru/Suprime-Cam	4728.3	1162.9	27.6
IA484	Subaru/Suprime-Cam	4845.9	228.5	27.0
IA505	Subaru/Suprime-Cam	5060.7	230.5	26.8
IA527	Subaru/Suprime-Cam	5258.9	242.0	27.1
V	Subaru/Suprime-Cam	5448.9	934.8	27.6
IA574	Subaru/Suprime-Cam	5762.1	271.5	26.8
IA624	Subaru/Suprime-Cam	6230.0	300.5	26.8
r^+	Subaru/Suprime-Cam	6231.8	1348.8	27.7
IA679	Subaru/Suprime-Cam	6778.8	336.0	26.7
IA709	Subaru/Suprime-Cam	7070.7	315.5	26.8
NB711	Subaru/Suprime-Cam	7119.6	72.5	25.9
IA738	Subaru/Suprime-Cam	7358.7	323.5	26.5
i^+	Subaru/Suprime-Cam	7629.1	1489.4	27.2
IA767	Subaru/Suprime-Cam	7681.2	364.0	26.5
NB816	Subaru/Suprime-Cam	8149.0	119.5	26.6
IA827	Subaru/Suprime-Cam	8240.9	343.5	26.5
z^+	Subaru/Suprime-Cam	9086.6	955.3	26.8
Y	VISTA/VIRCAM	10211.2	930.0	26.2
J	VISTA/VIRCAM	12540.9	172.0	25.8
H	VISTA/VIRCAM	16463.7	2910	26.1
K_s	VISTA/VIRCAM	21487.7	3090	25.8
IRAC1	*Spitzer*/IRAC	35262.5	7412	25.6
IRAC2	*Spitzer*/IRAC	44606.7	10113	25.5
IRAC3	*Spitzer*/IRAC	56764.4	13499	22.6
IRAC4	*Spitzer*/IRAC	77030.1	28397	22.5

(1) Filter name. (2) Telescope and instrument used for the observations. (3) Effective wavelength. (4) Filter FWHM. (5) 3σ magnitude depth measured in a 2 arcsec aperture.

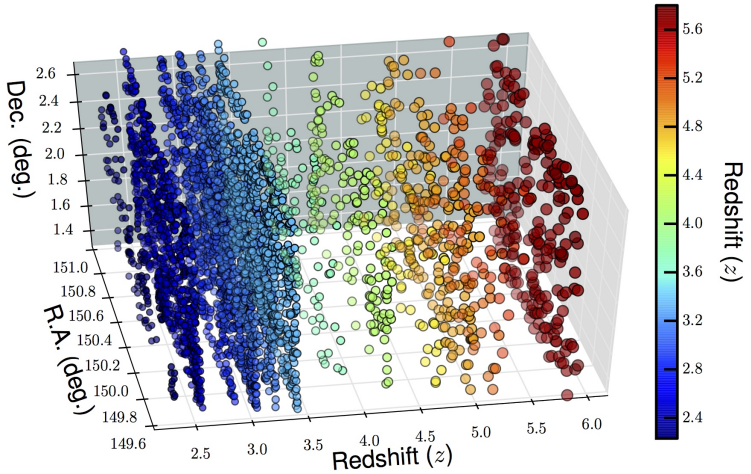

Figure 5.2: Figure from Sobral et al. (2018) showing the 3D spatial distribution of the SC4K-COSMOS sample, divided in 16 redshift slices.

One of the advantages of using this large high-z LAEs sample is that the FOV observed with it is very large (~ 2 deg^2), which reduces the cosmic variance and allows a good characterisation of the brightest sources. Indeed, the LAEs present in SC4K-COSMOS are typically brighter than those of our high-z SHARDS sample. Thus, a much larger fraction of them are well detected at the longest wavelengths, adding a valuable extra spectral range to the SEDs used for the ML classification.

The preparation of the SC4K sample for the GM algorithm follows the process described at the beginning of this section for the SHARDS sample, except that the redshift bins used include a $z \sim 3$ range ($2.5 < z < 3.5$). Furthermore, the interpolation of the reference wavelength and non-detections is made through photometric points located up at a wavelength difference proportional to the width of the filter associated to each reference wavelength. Notice that this was not necessary when using only SHARDS filters. After discarding not fully sampled SEDs, we ended up with an effective SC4K-COSMOS sample of 2811 LAEs at $z \sim 3$, 233 at $z \sim 4$, 303 at $z \sim 5$ and 100 at $z \sim 6$.

5.3 Machine learning derived classes

5.3.1 Best clustering

Determining the number of classes and the particular best clustering model derived for each sample and redshift interval follows the BIC and silhouette score optimisation described in Sec. 5.1. A first test is done to check differences in the resulting BIC when varying the type of covariance matrix used. We find that only for a spherical and diagonal covariance matrices, the BIC decreases with the amount of clusters. Between these two covariances, the lowest BIC values are found when using a diagonal covariance matrix, hence that will be the preferred type for our GM classification. A comparison of the BIC trend obtained for the four different covariance matrices tested at $z \sim 4$ for the SHARDS sample is shown in Fig. 5.3. The same result is found for every redshift bin.

After selecting our best modeling covariance matrix, we carry out the final GM clustering employing 100 initial random seeds and a diagonal covariance. The BIC distributions for the SHARDS and SC4K-COSMOS samples are shown in Figs. 5.4 and 5.5, respectively. The SHARDS sample presents two well defined BIC minimums at $z \sim 4$ and 5, whose distributions show a valley-like, decreasing-increasing, trend. However, at $z \sim 6$, the BIC does not converge, but it starts at a local minimum for the simplest assumption of two clusters and increases from there to start decreasing again beyond five clusters. We consider that the low amount of fully sampled $z \sim 6$ galaxies in the SHARDS sample (24) makes it unreasonable to select models producing more than five different classes, as they would be poorly populated. Thus, we favour the two classes classification, although keeping in mind that this value is probably driven by the low amount of SEDs available for the GM algorithm to work with at this redshift. On the other hand, the SC4K-COSMOS BIC dependence with the number of clusters follows a smooth trend, although, for some redshifts, it does not show a clear minimum nor a stable number of clusters beyond which the BIC remains constant. In those situations, we analyse the variation of the slope between points as an approximation of the second derivative of the BIC trend. In particular, we look for the first number of clusters beyond the third one for which the slope changes towards a flatter slope and this change is larger than all previous slope variations. This method gives us a best amount of clusters consistent with the redshift bins for which we do obtain a clearer BIC minimum. The final best number of classes for both samples at each redshift is summarised in Table 5.2.

Note that the optimal number of clusters obtained for the SC4K sample

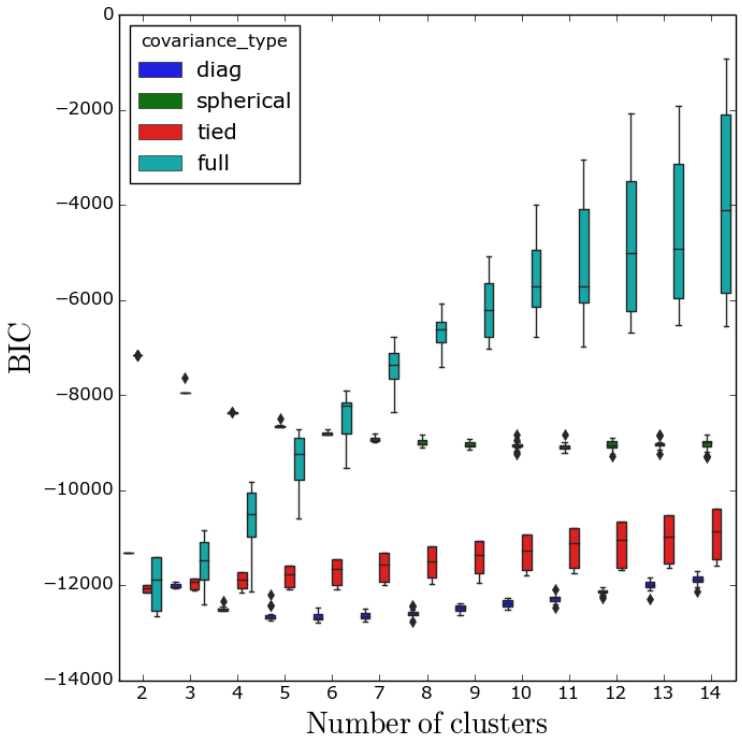

Figure 5.3: BIC variation with the number of clusters identified in terms of the different covariances tested for the SHARDS sample at $z \sim 4$. The horizontal markers within each rectangle indicates the BIC median value among the models resulting in each number of clusters. The BIC quartiles are represented by the coloured rectangles, while the complete error bars show the entire range of BIC values. Outliers models are determined in terms of the inter-quartile range and are marked with black diamonds. A slight offset in the number of clusters axis is introduced for clarity. Only the spherical and diagonal covariance matrices show a converging behaviour, with the diagonal one showing lower BIC values, which is consistent, since the spherical covariance is a specific case of the more general diagonal covariance.

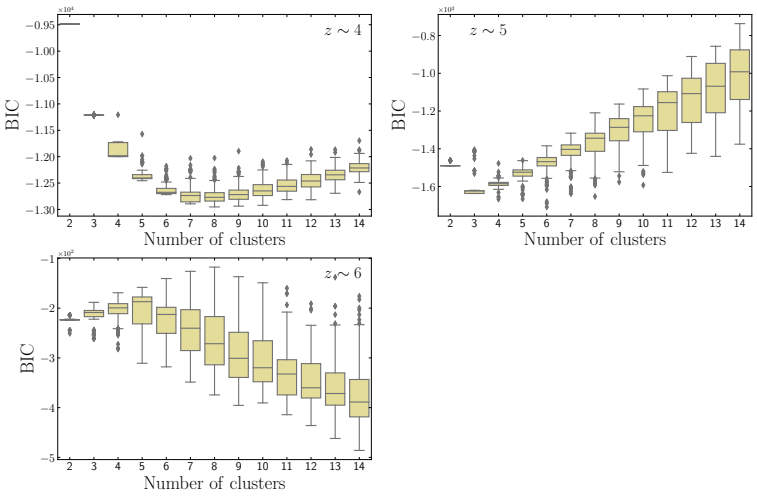

Figure 5.4: BIC variation with the number of classes derived in the GM classification for the SHARDS sample at each redshift range. The horizontal markers within each rectangle indicates the BIC median value among the models resulting in each number of clusters. The BIC quartiles are shown by the beige rectangles, while the complete error bars show the entire range of BIC values. Outliers models are determined in terms of the inter-quartile range and are marked with the black diamonds. From these distributions, we estimate a best number of clusters of 7, 3 and 2 for the SHARDS sample at $z \sim 4$, 5 and 6, respectively. Note, however, that the $z \sim 6$ BIC minimum corresponds with the simplest division into two groups and grows up from there, which suggests that the GM clustering at this redshift is not very representative, probably due to the low amount of fully sampled galaxies.

Table 5.2: Optimal number of classes derived via GM clustering for the SHARDS and SC4K-COSMOS samples at each redshift range.

	GM optimal number of clusters			
	$z \sim 3$	$z \sim 4$	$z \sim 5$	$z \sim 6$
SHARDS	-	7	3	2
SC4K-COSMOS	7	7	6	7

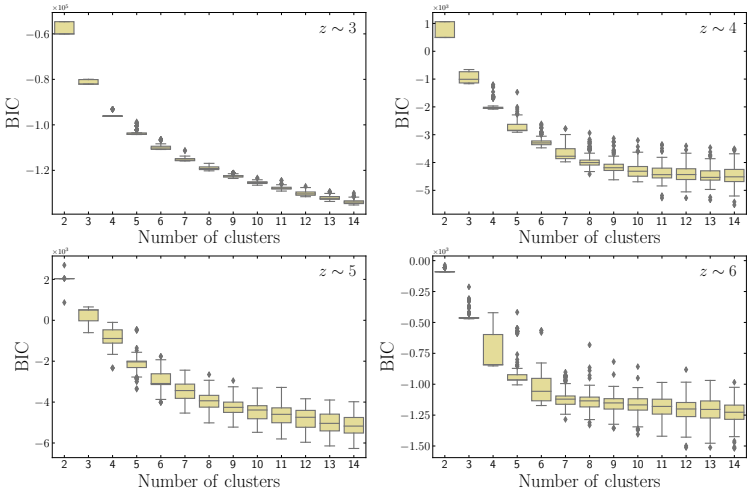

Figure 5.5: BIC variation with the number of classes derived in the GM classification for the SC4K-COSMOS sample at each redshift range. The horizontal markers within each rectangle indicates the BIC median value among the models resulting in each number of clusters. The BIC quartiles are shown by the beige rectangles, while the complete error bars show the entire range of BIC values. Outliers models are determined in terms of the inter-quartile range and are marked with the black diamonds. From these distributions, we estimate a best number of clusters of 7, 7, 6 and 7 for the SC4K sample at $z \sim 3$, 4, 5 and 6, respectively.

remains almost constant at all redshifts and is also consistent with the most populated SHARDS z range ($z \sim 4$). At $z \sim 5$, however, the SHARDS best clustering drastically decreases down to 3. A possible reason for this effect could be that the SEDs wavelength range in the SHARDS sample are shorter than that of the SC4K one. Indeed the very limited rest-frame UV region used makes finding class defining patterns more difficult.

5.3.2 Classes interpretation

Once we have obtained the best GM model at each redshift, we study the physical properties of the individual classes. Our analysis focuses in relevant

differences in age, stellar mass, UV slope β and Lyα emission between classes. For each cluster, we compute the median of these physical properties of all the objects belonging to the cluster. For the SHARDS sample, we make use of the β slopes and Lyα EW calculated in Chapter 2 and the ages and $M_{\rm star}$ obtained in Chapter 3. For the SC4K sample, β slopes and Lyα fluxes are taken from Sobral et al. (2018), while the ages and $M_{\rm star}$ are obtained using CIGALE, following the same methodology described in Chapter 3 for the SHARDS sample. Furthermore, a reference SED for each obtained class is calculated from the mean SED of all the galaxies belonging to that class. This average SEDs are useful to get a visual idea of the most relevant shape differences between groups. For simplicity, the best GM classification obtained for all the redshift bins in both samples are shown in Appendix D, as well as tables with the median physical parameters of all of them.

Since the differences between clusters seem to follow a similar nature in all the redshift ranges, we start our analysis with the best statistically characterised classes. These lead to conclusions that can be extrapolated to the worse characterised redshift bins. In particular, for the SHARDS sample, the derived classes at $z \sim 4$ are shown in Fig. 5.6. A first look to the mean SEDs of these clusters suggests that the most relevant differentiating factors are given by the relative strength of the Lyα emission with respect to the continuum and/or the UV slope in a secondary plane. Furthermore, we find a cluster composed by only three members (cl.2) with a non very LBG-like shape of their UV continuum, presenting an absorption pattern around 1600 Å. This class could be actually showing us possible remaining low redshift interlopers in our sample. The median physical parameters of the $z \sim 4$ clusters are presented in Table 5.3.

Additionally, we look for differences in the fraction of LAEs present in each class. In this regard, excluding the already mentioned cl.2, we find two groups (cl.0 and cl.5) conformed by only LAEs. Moreover, the separation between these two clusters is given by the Lyα EW_0, which, despite being high for both classes, is practically double in the first class (114.8±11.8 Å and 59.6±10.9 Å, respectively). On the other hand, two other different classes (cl.1 and cl.4) only include non-LAEs/LBGs among their members. In addition to these last two groups, there is another (cl.3) formed by a majority of non-LAEs/LBGs (72%) plus the LAEs/LBGs presenting the lowest Lyα EWs. Comparing the LAEs clusters with the non-LAEs clusters, a difference in their median β can also be inferred. In particular, we find β=-1.55±0.12, -1.62±0.07, -1.69±0.05 for cl.1, cl.3 and cl.4, respectively, versus β=-2.23±0.23, -2.26±0.25 for cl.0 and cl.5, respectively. These UV slopes are steeper in the non-LAEs groups, which

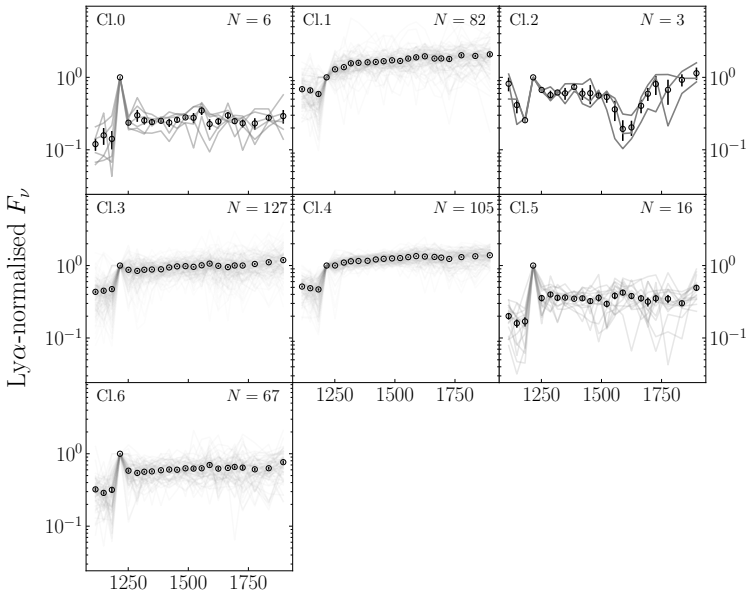

Figure 5.6: Best GM model clustering the SHARDS $z \sim 4$ sample. The open circles show the mean SED of the objects in the cluster. The error bars of the circles correspond to the standard error of the mean. Every individual SED belonging to each class is represented by a grey line faded in proportion to the number of objects within the class.

Table 5.3: Median physical properties of the sources within each ML-derived class for the SHARDS sample at $z \sim 4$. The errors shown correspond to the standard error of the median.

Cluster ID	$M_{\rm star}$ (10^9 $M_\odot$)	Age (Myr)	Lyα EW$_0$ (Å)	β	LAEs fraction	N
0	3.6 ± 5.0	296 ± 236	114.8 ± 11.8	-2.23 ± 0.23	1.0	6
1	5.6 ± 4.1	80 ± 36	0.0 ± 0.0	-1.55 ± 0.12	0.0	82
2	2.7 ± 1.2	52 ± 325	16.6 ± 1.5	-1.76 ± 0.13	1.0	3
3	3.4 ± 2.3	61 ± 42	0.0 ± 1.3	-1.62 ± 0.07	0.28	127
4	5.5 ± 0.8	67 ± 34	0.0 ± 0.0	-1.69 ± 0.05	0.0	105
5	1.3 ± 1.1	23 ± 157	59.6 ± 10.9	-2.26 ± 0.25	1.0	16
6	2.3 ± 6.3	60 ± 66	24.4 ± 2.8	-1.87 ± 0.10	0.85	67

is also related with the fact that LAEs host young SPs producing the Lyα emission and rising the UV emission close to that line, as discussed in more detail in Chapter 3. This emission is produced by the most massive O and B stars and quickly decays with time, specially at the shortest wavelengths, hence the appearance of steeper median UV slopes in the non-LAEs groups.

There is still a last class (cl.6) for which no clear defining properties are found. It is composed by a large majority of LAEs (85%) with low Lyα EWs (24.4±2.8 Å). In this sense, cl.6 is similar to cl.3, two hybrid classes, with the difference that the median β is more negative in the former (-1.87±0.10), and therefore including a larger amount of LAEs. The difference can also be understood if we note that the ML algorithm is including objects with larger Lyα EWs in class cl.6 than in class cl.3. However, both of them include objects with EWs equal to zero, so the UV slope seems to be a more relevant parameter driving the membership of these particular two groups.

No relevant differences are found in the stellar mass beyond the fact already studied in Chapter 3 that the groups with higher fraction of LAEs show slightly lower median masses. In any case, no special $M_{\rm star}$ differences between groups were meant to be found after normalising the SEDs, since we are focusing the ML classification in terms of the SED shapes and not in terms of their intrinsic brightness, as mentioned in Sec. 5.2. Finally, the differences in the median age of the groups are not reliable enough because the standard deviations of the values within each class are very large, preventing any significant conclusion in this regard.

At $z \sim 5$, the SHARDS sample is separated in a simpler but similar way to $z \sim 4$, with two classes with a majority of LAEs and a third one domi-

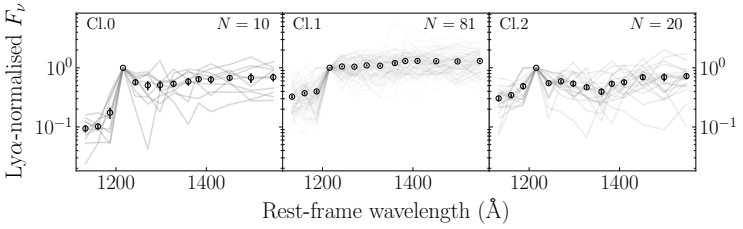

Figure 5.7: Best GM model clustering the SHARDS $z \sim 5$ sample. The open circles show the mean SED of the objects in the cluster. The error bars of the circles correspond to the standard error of the mean. Every individual SED belonging to each class is represented by a grey line faded in proportion to the number of objects within the class.

nated by non-LAEs/LBGs. The two LAEs clusters show similar median Lyα EW_0 (16.4±11.2 Å and 20.8±8.0 Å) and β slope (-2.07±0.29 and -2.04±0.24). Nonetheless, a look to the mean SED of these two groups suggests that the difference between them is given by the relative strength of the emission drop of the Lyman break (see Fig. 5.7). Not much can be said about the SHARDS $z \sim 6$ clustering, as only 24 sources are available and the two clusters models taken do not seem to be very representative, as only two objects are separated from the rest. Moreover, the standard deviation of the SEDs within the two groups is large. This is probably due to the low number of sources and the fact that only a very short rest-frame wavelength coverage is sampled by the GM classification at this z (up to only $\lambda \sim 1400$ Å), not even allowing a reliable characterisation of the β differences.

Regarding the SC4K sample, the best clustering model for this sample at $z \sim 3$ is shown in Fig. 5.8, with the median physical parameters of its clusters presented in Table 5.4. Similar conclusions can be inferred for this sample as for the SHARDS sample at $z \sim 4$. This time, from the 7 resulting classes, we can differentiate three (cl.0, cl.3 and cl.5) presenting declining median UV slopes (β=-2.44±0.01, -2.44±0.04 and -2.44±0.11, respectively). The fact that these three clusters show the exact same median β value is a consequence of a hard upper limit on the IMF present in the MAGPHYS (Multi-wavelength Analysis of Galaxy PHYSical properties) models used to estimate the UV slope. Indeed, if we compute the mean β values instead of the median values, we obtain similar but not equal UV slopes for these three groups ($\langle\beta\rangle$=-2.35±0.01, -2.23±0.03 and -2.13±0.09, respectively). A look at the average SEDs of the same three groups

Table 5.4: Median physical properties of the sources within each ML-derived class for the SC4K-COSMOS sample at $z \sim 3$. The errors shown correspond to the standard error of the medians.

Cluster ID	$M_{\rm star}$ (10^9 $M_\odot$)	Age (Myr)	$F_{\rm Ly\alpha}$ (10^{-17} erg s^{-1} cm^{-2})	β	N
0	0.3 ± 6.1	8 ± 12	0.1 ± 38.6	-2.44 ± 0.01	548
1	3.7 ± 9.0	263 ± 10	8.2 ± 97.4	-2.00 ± 0.02	656
2	9.6 ± 6.4	217 ± 15	7.8 ± 1.3	-1.57 ± 0.12	324
3	1.1 ± 6.0	150 ± 10	8.7 ± 50.9	-2.44 ± 0.04	745
4	5.1 ± 4.4	267 ± 24	0.1 ± 3.9	-1.89 ± 0.24	248
5	0.1 ± 42.0	7 ± 18	8.4 ± 31.9	-2.44 ± 0.11	284
6	20.9 ± 561	282 ± 157	7.6 ± 68.5	-2.12 ± 0.99	6

(Fig. 5.8) suggests that the difference between them is given by the relative strength of the Lyα emission. However, the dispersion of the median values obtained for $F_{\rm Ly\alpha}$ is too large to extract a robust conclusion. Next, we have two other classes (cl.2 and cl.4) showing steep median UV slopes (β=-1.57±0.12 and -1.89±0.24, respectively). In this second case, it can be said that there is a small but reliable difference in the median $F_{\rm Ly\alpha}$ values of these two clusters within their errors ($F_{\rm Ly\alpha}$=7.8±1.3×10^{-17} and 0.1±3.9×10^{-17} erg s^{-1} cm^{-2}, respectively). This difference can be directly appreciated in the average SEDs shown in Fig. 5.8.

Of the remaining two groups of the 7 classes derived for the SC4K sample at $z \sim 3$, cl.1 appears as the most neutral in terms of the UV slope, with a completely flat median one (β=-2.00±0.02). Finally, the last group is specially interesting, since it is conformed by only 6 members. The SED shape of this cluster does not correspond to a LAE, and so the GM algorithms have found the subclass hosting the few interlopers of the SC4K sample at this z. Note that the SC4K sample is a LAEs sample, and therefore these few sources, despite being interlopers, are not necessarily low redshift galaxies, since they could just be high-z non-LAEs/LBGs where the Lyman break was identified as an emission excess in some filter during the sample selection carried out by Sobral et al. (2018).

Furthermore, stellar mass differences can be appreciated between some of the clusters obtained for the SC4K sample at $z \sim 3$, despite the fact that the standard deviation of this value is too large in many groups. Because of this, these $M_{\rm star}$ differences have to be carefully considered in a qualitative way. In particular, we could say that the median $M_{\rm star}$ of the cl.0, cl.3 and cl.5 groups,

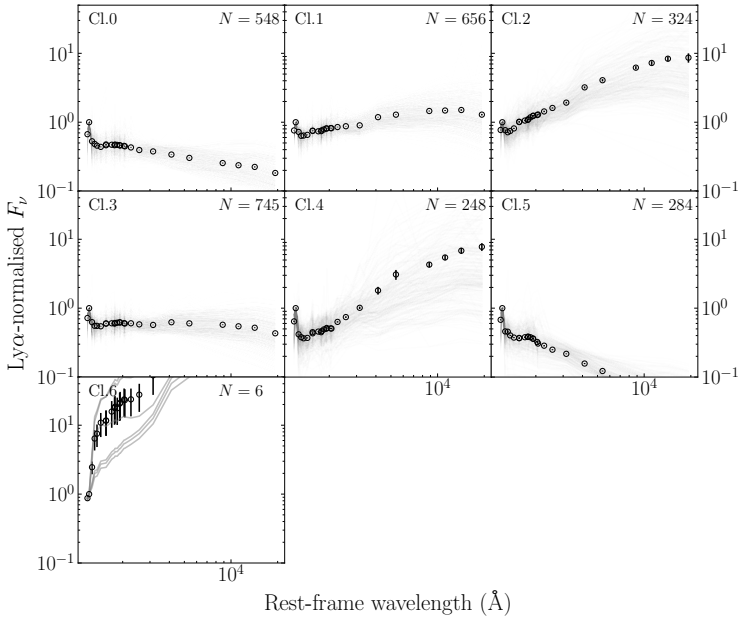

Figure 5.8: Best GM clustering model for the SC4K-COSMOS sample at $z \sim 3$. The open circles show the mean SED of the objects in the cluster. The error bars of the circles correspond to the standard error of the mean. Every individual SED belonging to each class is represented by a grey line faded in proportion to the number of objects within the class. The class cl.6, with only six sources, likely groups the few remaining interlopers.

the classes presenting bluer UV slopes, are lower than the rest. Moreover, the median age of cl.0 and cl.5 are significantly younger than in the other clusters, suggesting that these two groups could be made out of galaxies in the initial stages of their lives. On the contrary, those presenting the highest median $M_{\rm star}$ and ages are classes whose galaxies show steeper UV slopes, resulting in brighter emission at longer wavelengths, associated with older SPs (see Chapter 3).

Similar results to the ones obtained at $z \sim 3$ for the SC4K-COSMOS sample clustering can be obtained at the other redshift ranges. The mean SED and median physical parameters of all the best-modeling clusters at all the z intervals are shown in Appendix D. In particular, for all the SC4K redshift bins we find a small class composed by the few non-LAEs galaxies among the sample. This result highlights the value of using ML algorithms at the time of finding sources presenting unintended SED shapes.

It is important to note here that we have run a ML classification over two sample of galaxies previously selected by their colours and emission patterns. Hence, the samples used here have already been defined by some common properties. The interesting fact is that the ML algorithms have been able to find differences between galaxies that were previously selected by their similarities, finding, at the same time, the few remaining interloper sources. From the results observed in this work, it can be derived that the application of these kind of unsupervised methods to blind samples of galaxies could be really useful in future automatised galaxy searches in big surveys, such as, for instance, those carried out with the LSST (Large Synoptic Survey Telescope).

5.4 Conclusions

We have made use of Gaussian mixtures algorithms to carry out an unsupervised machine learning classification of the SEDs in both our SHARDS sample and the SC4K-COSMOS LAEs sample (Sobral et al. 2018). To focus in the search for possible evolutionary relations between clusters, we have run the GM methods over the normalised rest-frame SEDs at different redshifts bins. In this way, we prevent the GM models from creating the clusters in terms of the own redshift or brightness of the SEDs, but of their shape differences. A minimisation of the BIC has been used to determine the best number of clusters in each case. The best-fitting model among those resulting in the optimal number of classes has been selected through the silhouette score (see Rousseeuw 1987). The median Lyα EWs, UV slopes, ages and stellar masses of each cluster have been calculated to establish relevant differences between them. Further study of the obtained classes and their physical differences is work in progress. The main results are the following:

(a) We have tested different covariance matrices for the multi-variate Gaussian distributions employed in the GM algorithm. The best SED clustering (in terms of the lowest BIC) found at every z range is achieved when using a diagonal covariance type.

(b) The optimal number of clusters found for the SC4K-COSMOS sample is almost the same at all redshifts: 7 classes at $z \sim 3$, 4, 6, and 6 classes at $z \sim 5$. This is also in agreement with the 7 groups found for the SHARDS sample at $z \sim 4$. However, the best number of clusters for the SHARDS SEDs goes down to 3 and 2 at $z \sim 5$ and 6, respectively. This decrease is probably due to the combination of a low number statistic and the shorter rest-frame wavelength coverage of the SHARDS SEDs used with respect to the SC4K ones.

(c) The physical parameters analysed for each group show significant differences in the Lyα emission and the UV slope. These two parameters seem to be the most relevant ones for the unsupervised clustering process. Some less significant differences are also found in the median ages and stellar masses of the groups. Nonetheless, the standard deviation of these two magnitudes within the groups does not allow us to extract robust conclusions in most cases.

(d) For both SHARDS at $z \sim 4$ and SC4K at all its redshift bins, we always find a low represented group with the few objects presenting a somewhat different SED. This particular cluster corresponds to the few remaining interlopers of the samples. Finding them through GM models highlights the efficiency of these algorithms at the time of identifying objects showing SEDs not in concordance with the common of the whole sample.

(e) For the SHARDS sample, we have studied the fraction of LAEs within each cluster. In particular, at $z \sim 4$ we find two clusters fully represented by LAEs and another two only containing non-LAEs/LBGs. Moreover, apart from the obvious Lyα EW_0 differences between these LAEs and non-LAEs groups, the median UV slopes of the LAEs clusters are also significantly bluer than the non-LAEs/LBGs ones, hence the good separation of these kind of objects. Among the two remaining groups, there is one conformed by a majority of non-LAEs/LBGs plus the LAEs presenting the lowest Lyα EWs, with a median β slope in accordance with the previous two non-LAEs/LBGs groups. The last cluster corresponds to the intermediate group, hosting a majority of LAEs with intermediate median Lyα EWs and UV slopes with respect to the other classes.

(f) Similar results are found for the SC4K sample. Particularly, for the best sampled z bin of this work (2811 galaxies at $z \sim 3$), we find two clusters presenting steep UV slopes, with the difference between them being the relative strength of the Lyα flux. A third cluster corresponds to the galaxies presenting a neutral UV slope, with a median value exactly flat. The three remaining classes show very blue β values and seem to also show differences in terms of the Lyα emission, although the dispersion is too high this time to conclude anything. Furthermore, the three bluest clusters seem to also correspond to the younger and less massive galaxies, such as galaxies in the initial stages of their lives. Nevertheless, this point has to be taken with a bit of salt, since the standard deviation of the age and $M_{\rm star}$ is too high in many cases.

(g) The ML classification carried out in this work has been implemented over two samples of galaxies already belonging to the very particular subgroup of high-z LAEs and LBGs. This kind of galaxies, already share certain characteristic emission features and were previously selected because of them. The fact that the GM algorithms used in this work have been able to extract some thin differences between the galaxies in these samples, finding, at the same time, the few interlopers there could be, makes ML algorithms look very promising for blind searches in future large extragalactic surveys.

6

Conclusions

- Me parece que he entendido la película. ¿La policía sabía que los de asuntos internos les tendían una trampa?
- ¿Qué dice? Aquí nadie ha hablado de esas cosas.
- Es que si me aburro, yo me las invento, mi capacidad de atención es reducida.
Conversación entre Homer Simpson y un sectario (The Simpsons).

This chapter presents the main conclusions of our research as well as possible future projects aiming to take advantage of these results and/or extend them.

6.1 Main results

In this thesis we have undertaken a comprehensive characterisation of the high-z LAEs and LBGs population in the GOODS-N field. This has been achieved making use of the SHARDS survey (Pérez-González et al. 2013), whose good depth in 25 consecutive medium-band filters in the optical/NIR has allowed the simultaneous detection of LAEs and LBGs in the $z \sim 3.4$-6.8 range. Ancillary data from previous observations of the GOODS-N field with *HST*, *Spitzer*, Subaru, CFHT and *GALEX* have also been used to complement our data.

We have made use of the stellar population synthesis code CIGALE to fit burst-like theoretical models to the SEDs in our sample, paying special attention to differences between the three subfamilies observationally defined in terms of their Lyα line and UV continuum emission. Single and double SP models have been fitted to the galaxies, calibrating a Bayesian information criterion to decide under which situations the extra SP is really needed.

The spatial distribution of the sample has also been analysed, looking for groups of galaxies sharing a common redshift and separated by short comoving distances. Special focus has been put into a previously reported GOODS-N $z \sim 5.2$ overdensity (Walter et al. 2012), for which we have found a large amount of newly discovered candidates. Furthermore, some of these candidates have been confirmed with a GTC/OSIRIS MOS observation.

Finally, a machine learning classification of the SEDs of both our sample and the SC4K-COSMOS $z \sim$ 2-6 LAEs sample (Sobral et al. 2018) has been implemented via Gaussian Mixture algorithms, deriving the most relevant differences between the obtained clusters at each z.

For the entire sample, we have calculated photometric redshifts, comoving distances, SFRs, Lyα EWs, $X_{\mathrm{Ly}\alpha}$, ages and stellar masses. In addition, LFs, SMFs, SMDs and SFR-M_{star} relations have also been studied at each redshift.

The main results of our work are summarised below:

(a) We have developed our own high-z LAEs and LBGs selection criteria based on the identification of the Lyα line and/or the Lyman break via emission excesses, photometric fits to the SEDs and visual inspection of the candidates. This selection criteria has proven to be very robust when comparing our derived photometric redshifts with the available spectroscopy.

(b) The sample built consists of 1558 candidates, observationally separated in 124 pure LAEs with strong Lyα emission ($\mathrm{EW}_0 > 35$ Å) and barely any continuum detected in SHARDS, 404 LAEs/LBGs with Lyα line and well detected continuum emission in SHARDS and 1030 non-LAEs/LBGs with no observed Lyα emission line.

(c) We claim that the characterisation of high-z LAEs and LBGs in wide wavelength ranges requires well spectrally resolved SEDs, which are only achievable in photometry using consecutive sets of narrow/medium-band filters like SHARDS. We have shown that the broad band colour selection criteria used to build LBG samples are prone to introduce a non-negligible amount of low redshift interlopers (up to ~ 20 %). Moreover, the photometric redshift estimation is also much poorer in broad band selected samples, since they lack good spectral resolution.

(d) The best-fitting Schechter ϕ^* and M^* parameters found for the LF at $z \sim 4$ and $z \sim 5$ are consistent with previous studies. In any case, our LFs lands slightly below those from the broad band study of the same field compared in this work. We cannot, however, extend our LFs to

the faint end since we miss the faintest sources, not allowing our own estimation of the α slope.

(e) We report a fraction of LAEs with $EW_0 > 25$ Å as a function of z in agreement with previous works. An increase of the fraction of high-EW_0 objects up to $z \sim 5.5$-6 is found, followed by a decrease of $X_{Ly\alpha}$ at higher redshifts. This behaviour of the fraction of high-EW_0 LAEs is associated to the fact that the reionisation is not complete beyond $z \sim 5.5$-6, with the consequent scatter of the Lyα emission produced by the increasing abundance of H I with lookback time.

(f) Regarding the SP models fitting, using SPs with low τ values representing strong star-forming episodes similar to instantaneous starbursts, we find that a majority of our LAEs and LBGs are well modeled by a single SP. The LAEs/LBGs appears as the group that more frequently needs the addition of a second SP. This is due to the presence of a strong Lyα line combined with bright continuum emission at longer wavelengths that cannot be simultaneously well fitted by a single burst-like SP.

(g) The M_{star} and ages obtained from the SP modeling show that, on average, pure LAEs are young and very low mass galaxies presenting strong Lyα emission and experimenting one of their first star-forming episodes. LAEs/LBGs fitted with a single SP are the most massive members of that same kind of galaxies. On the other hand, LAEs/LBGs requiring a second SP are relatively evolved and massive galaxies, with the Lyα line being produced by an undergoing episode of star formation. For the non-LAEs/LBGs, the absence of strong emission patterns that help to constrain their ages causes a degeneracy in the combination of SPs that could be used to model them, making their characterisation more uncertain. Furthermore, it would be possible that some of the non-LAEs/LBGs are hosting young SPs whose Lyα line is not detected because of dust extinction and resonant scattering, adding even more uncertainty to this observational class. In any case, we infer that non-LAEs/LBGs lack a really young SP and are typically older and more massive than LAEs. Finally, the evolution of the fraction of these three observational families with z supports the idea of pure LAEs and SSP LAEs/LBGs being young stages of the high-z galaxy population. These kind of sources are more common the higher the z is. On the contrary, the non-LAEs/LBGs and DSP LAEs/LBGs correspond to more evolved star-forming sources, more common the lower the z is.

(h) We report a decreasing evolution of the characteristic stellar mass M^* of the SMFs with z, in agreement with other works. No significant evolution of the α slope is found between $z = 4$-5, with a small increase at $z \sim 6$, which has to be carefully taken, as we lack information at the low mass end of the SMF at $z \sim 6$. From the derived SMFs we have estimated SMDs in agreement with the combined SMD-z trend from previous studies.

(i) The analysis of the SFR-$M_{\rm star}$ relation using either UV-derived SFRs and model-derived ones show little to no evolution between $z \sim 4$-6, as reported by several authors. The fact that LAEs appear above the SFR-$M_{\rm star}$ main sequence indicates that these galaxies are indeed forming stars at higher rates than average, supporting the hypothesis that they are experimenting a strong star-forming episode.

(j) In our spatial group analysis, we have found 202 galaxies ($\sim 13\%$ of the total sample) in 92 groups of two or more members: 79 pairs, 10 trios, 2 quartets and a sextet. Many of these close groups show tail-like structures suggesting gravitational interaction between them. No significant differences in age, $M_{\rm star}$ nor SFR have been found for these grouped sources respect to the general sample.

(k) We report 55 objects compatible with an overdensity at $z = 5.198 \pm 0.015$ (Walter et al. 2012) within their photo-z errors, 44 of them new candidates, which means almost quadruplicating the amount of previously reported sources in that overdensity (13). A MOS observation targeting 13 new candidates ended up with the detection of 10 of them and the confirmation of 8 new members of the overdensity. If the ratio of confirmation keeps similar in future observations, this would be the richest galaxy proto-cluster known up to date beyond $z = 5$ with such a tight redshift constrain.

(l) Relevant differences have been found between the different SED clusters obtained after the application of GM algorithms to both our sample and the SC4K sample. The UV slope and the Lyα line turn out to be the most relevant parameters driving this unsupervised classification. We find the sources with the strongest Lyα emission and the bluest UV slopes clearly separated from those showing steeper UV slopes and fainter Lyα lines. In particular, LAEs and LBGs appear well differentiated between clusters for the SHARDS sample. Some link could also be made between the groups

in terms of stellar mass and age, whose median values are typically lower for the bluer UV slope groups.

(m) The machine learning classification has resulted very useful for identifying the few interlopers still existent in both the SHARDS and SC4K samples, highlighting the promising possibilities of the implementation of this methods in the search for different kind of galaxies in future large surveys.

6.2 Future work

The results of this research open the door to several interesting projects that could lead to an improvement or an extension of the questions presented here. The high quality of the SHARDS data make it an incredibly valuable tool for the study of the farthest away galaxies in the Universe, as shown in this work. Some of the future projects here proposed are already in progress, and some others are more ambitious and will require more dedication in the future if they are considered of interest:

- One of the improvements that we are already working on is an extension of the stellar population modeling of our LAEs and LBGs sample. We will explore the results of using a delayed SFH and varying the e-folding time towards higher values, to simulate a more constant SFH. This is in contrast with the starburst-like models employed in Chapter 3. This increase in τ will probably help us to solve the current age dichotomy found in our work for the quickly declining model. In addition, we are also testing the results of using a Small Magellanic Cloud-like dust extinction law, steeper than the currently used Calzetti law. We will compare the results of these changes and see how they match or change the vision of high-z LAEs and LBGs presented in this work. The new results will be included in Arrabal Haro et al. (2019, submitted) to address some of the already received referee's comments.

- Another work in progress is the final analysis of the ML-derived SED clusters. In particular, we plan to check the results of denormalising the mean SEDs obtained for each group through the average brightness of its members and fitting it with CIGALE using the same prescriptions as for the general sample. This might result in clearer differences that could support those already found. Additionally the use of GM algorithms allows us to make an analysis of the different membership probabilities of each individual galaxy to each cluster, which could highlight which

clusters are better and worse defined. Another option could also be to repeat the same analysis carried out using a different ML method and compare the results with the presented GM clustering. This ML analysis will be fully presented in Arrabal Haro et al. (2020, in prep.).

- One of the main results of this work is the discovery of 44 new candidates for a $z \sim 5.2$ proto-cluster. Eight of them have already been spectroscopically confirmed with a single GTC/OSIRIS MOS observation, as presented in this work. Now we have completed the phase two of a new observation program targeting as many of the remaining candidates as possible. We have GTC time for three MOS observations in which we plan to observe more new candidates. A preliminary preview of these new masks orientation is shown in Fig. 6.1. If the results of these observations are as successful as for the first one presented in this work, we would study the large majority of the new candidates found in this work, confirming the relevance of this proto-cluster. Even though, additional MOS observations would still be needed to characterise all of the newly found candidates, specially the faintest. The final complete study of the already available MOS will be published in Calvi, Arrabal Haro et al. (2020, in prep.).

- During the study of our sample, we serendipitously found an interesting emission blob slightly displaced from the central position of a $z \sim 3.5$ galaxy. This displaced emission is only present in the SHARDS f511w17 filter, not appearing at all in other SHARDS filters nor in the *HST*/ACS images (see Fig. 6.2), which makes us think that could correspond to a strong star-forming region of the galaxy whose Lyα emission is only detected in that SHARDS filter because of its narrowness. Preliminary surface brightness calculations showed that this blob emission concentrated in such a narrow wavelength range would indeed get diluted in the broad ACS F606W filter, making it invisible in the current *HST* images. A long slit spectroscopic observation of this object could shed some light on its nature.

- Another interesting project could be the implementation of a ML algorithm trained to select high-z LAEs and LBGs with high confidence. We have proven that the selection criteria for this kind of objects developed in this work is very good. However, it has the inconvenience of the need of visual inspection of the SEDs and images, which impedes its complete automation and makes much more difficult any kind of simulation-recovery process of interest to, for example, estimate the completeness limits of

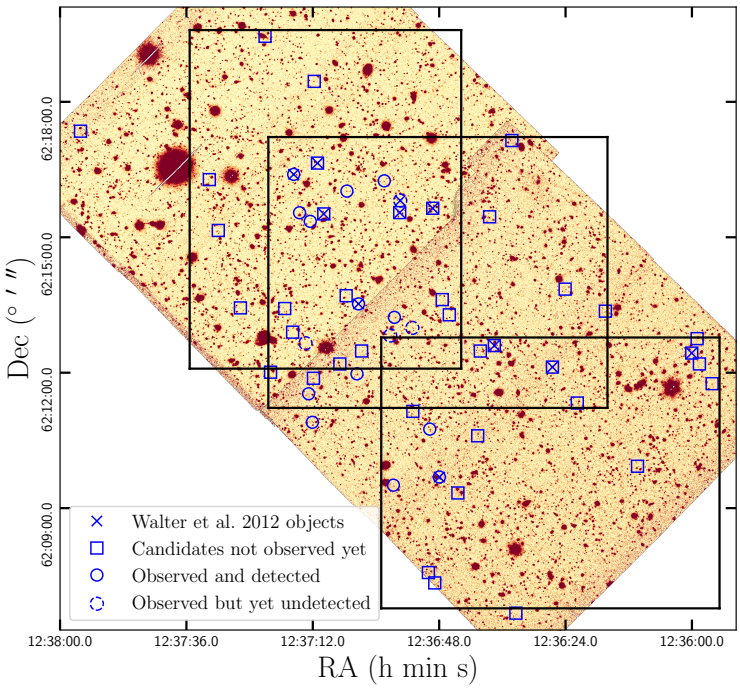

Figure 6.1: Preview of the three upcoming GTC/OSIRIS MOS observations targeting possible $z = 5.198$ overdensity members from our sample. The black rectangles correspond to the OSIRIS mask size on the field. The sources previously reported in Walter et al. (2012) are marked with blue crosses. The empty squares indicate the position of candidates from our sample not spectroscopically observed yet. The blue empty circles show those detected in the first MOS observation, while the dashed empty circles represent those observed but not yet detected with the available observing time.

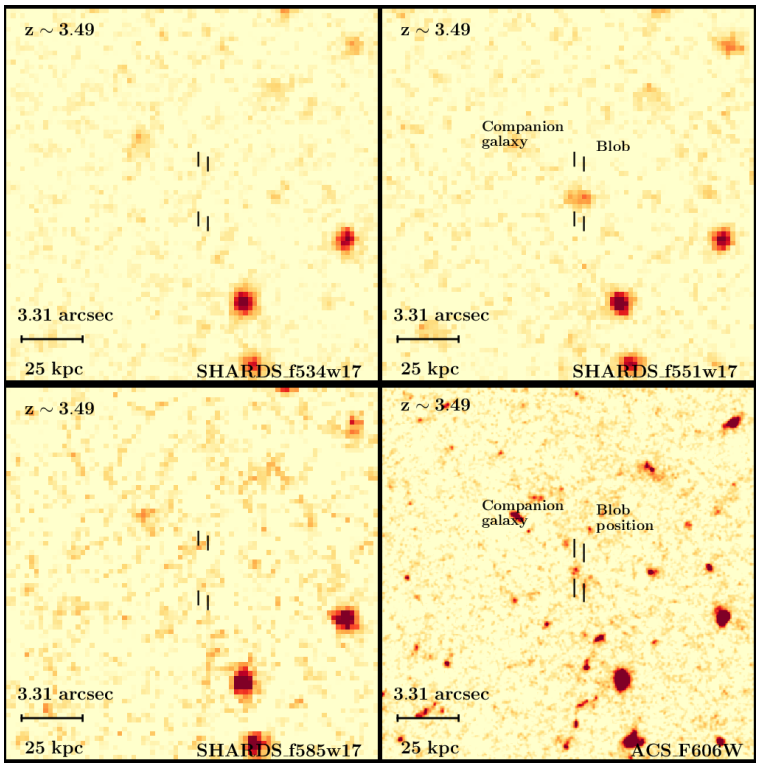

Figure 6.2: View of a conspicuous $z \sim 3.49$ pure LAE presenting an emission blob slightly displaced from the central position of the galaxy. The upper right panel shows the detection in the f551w17 filter, the only SHARDS filter where it can be appreciated. Two other SHARDS images blue-ward (upper left) and red-ward (lower left) are also shown for comparison. The lower right panel presents the view in the ACS F606W broad band image. Note that the companion galaxy is clearly detected in the ACS image, but not so the emission blob.

the selected sample. We could take advantage of our robust LAEs and LBGs sample to train a ML algorithm able to automatically identify these sources in future similar multi-wavelength narrow/medium-band surveys.

Bibliography

- Y yo voy a recordarle... la de Mateo... 21:17.
- ¿Y dejándole, salió de la ciudad, se fue a Betania y allí pasó la noche?
- Sí... Medite.
Conversación entre Homer Simpson y el reverendo Lovejoy (The Simpsons).

Adams, J. J., Blanc, G. A., Hill, G. J., et al. 2011, ApJS, 192, 5

Allday, J. 2002, Quarks, Leptons and the Big Bang (Bristol; Institute of Physics)

Allen, S. W., Evrard, A. E., & Mantz, A. B. 2011, ARA&A, 49, 409

Alvarez, M. A., Busha, M., Abel, T., & Wechsler, R. H. 2009, ApJ, 703, L167

Antonucci, R. 1993, ARA&A, 31, 473

Arnouts, S., Cristiani, S., Moscardini, L., et al. 1999, MNRAS, 310, 540

Arrabal Haro, P., Rodríguez Espinosa, J. M., Muñoz-Tuñón, C., et al. 2018, MNRAS, 478, 3740

—. 2019, submitted, MNRAS

Arrabal Haro, P., Sobral, D., Rodríguez Espinosa, J. M., et al. 2020, in prep., MNRAS

Ashby, M. L. N., Willner, S. P., Fazio, G. G., et al. 2015, ApJS, 218, 33

Bahcall, N. A., & Soneira, R. M. 1983, ApJ, 270, 20

Barger, A. J., Cowie, L. L., Sanders, D. B., et al. 1998, Nature, 394, 248

Barger, A. J., Cowie, L. L., & Wang, W. H. 2008, ApJ, 689, 687

Barkana, R., & Loeb, A. 2001, Phys. Rep., 349, 125

Barro, G., Pérez-González, P. G., Gallego, J., et al. 2011, ApJS, 193, 13

—. 2011b, ApJS, 193, 30

Barro, G., Pérez-González, P. G., Cava, A., et al. 2019, ApJS, 243, 22

Barthel, P. D. 1989, ApJ, 336, 606

Becker, G. D., Bolton, J. S., Madau, P., et al. 2015, MNRAS, 447, 3402

Behroozi, P. S., Wechsler, R. H., & Conroy, C. 2013, ApJ, 770, 57

Bhatawdekar, R., Conselice, C. J., Margalef-Bentabol, B., & Duncan, K. 2019, MNRAS, 486, 3805

Bian, F., Fan, X., McGreer, I., Cai, Z., & Jiang, L. 2017, ApJ, 837, L12

Bianchi, L. 2014, Ap&SS, 354, 103

Bina, D., Pelló, R., Richard, J., et al. 2016, A&A, 590, A14

Blain, A. W., Chapman, S. C., Smail, I., & Ivison, R. 2004, ApJ, 611, 725

Bohlin, R. C., Colina, L., & Finley, D. S. 1995, AJ, 110, 1316

Bond, N. A., Gawiser, E., Gronwall, C., et al. 2009, ApJ, 705, 639

Bond, N. A., Gawiser, E., Guaita, L., et al. 2012, ApJ, 753, 95

Boquien, M., Buat, V., & Perret, V. 2014, A&A, 571, A72

Boquien, M., Kennicutt, R., Calzetti, D., et al. 2016, A&A, 591, A6

Boquien, M., Burgarella, D., Roehlly, Y., et al. 2019, A&A, 622, A103

Bouwens, R. J., Illingworth, G. D., Blakeslee, J. P., Broadhurst, T. J., & Franx, M. 2004, ApJ, 611, L1

Bouwens, R. J., Illingworth, G. D., Franx, M., & Ford, H. 2007, ApJ, 670, 928

Bouwens, R. J., Illingworth, G. D., Bradley, L. D., et al. 2009, ApJ, 690, 1764

Bouwens, R. J., Illingworth, G. D., Oesch, P. A., et al. 2010, ApJ, 708, L69

Bouwens, R. J., Illingworth, G. D., Labbe, I., et al. 2011, Nature, 469, 504

Bouwens, R. J., Illingworth, G. D., Oesch, P. A., et al. 2012, ApJ, 752, L5

Bouwens, R. J., Bradley, L., Zitrin, A., et al. 2014, ApJ, 795, 126

Bouwens, R. J., Illingworth, G. D., Oesch, P. A., et al. 2015, ApJ, 811, 140

—. 2015b, ApJ, 803, 34

Bowler, R. A. A., Dunlop, J. S., McLure, R. J., et al. 2015, MNRAS, 452, 1817

Brammer, G. B., van Dokkum, P. G., & Coppi, P. 2008, ApJ, 686, 1503

Brocklehurst, M. 1971, MNRAS, 153, 471

Bruzual, G. 1983, ApJ, 273, 105

Bruzual, G., & Charlot, S. 1993, ApJ, 405, 538

—. 2003, MNRAS, 344, 1000

Burgasser, A. J., McElwain, M. W., Kirkpatrick, J. D., et al. 2004, AJ, 127, 2856

Burgasser, A. J., & McElwain, M. W. 2006, AJ, 131, 1007

Burgasser, A. J. 2007, ApJ, 659, 655

Burgasser, A. J., Liu, M. C., Ireland, M. J., Cruz, K. L., & Dupuy, T. J. 2008, ApJ, 681, 579

Burgasser, A. J., Cruz, K. L., Cushing, M., et al. 2010, ApJ, 710, 1142

Calvi, R., Poggianti, B. M., & Vulcani, B. 2011, MNRAS, 416, 727

Calvi, R., Rodríguez Espinosa, J. M., Mas-Hesse, J. M., et al. 2019, MNRAS, 2183

Calvi, R., Arrabal Haro, P., Dannerbauer, H., Rodríguez Espinosa, J. M., & Muñoz-Tuñón, C. 2020, in prep., MNRAS

Calzetti, D., Kinney, A. L., & Storchi-Bergmann, T. 1994, ApJ, 429, 582

Calzetti, D., Armus, L., Bohlin, R. C., et al. 2000, ApJ, 533, 682

Calzetti, D. 2001, PASP, 113, 1449

Calzetti, D., Kennicutt, R. C., Engelbracht, C. W., et al. 2007, ApJ, 666, 870

Capak, P., Cowie, L. L., Hu, E. M., et al. 2004, AJ, 127, 180

Capak, P., Aussel, H., Ajiki, M., et al. 2007, ApJS, 172, 99

Capak, P., Carilli, C. L., Lee, N., et al. 2008, ApJ, 681, L53

Capak, P. L., Riechers, D., Scoville, N. Z., et al. 2011, Nature, 470, 233

Caputi, K. I., Cirasuolo, M., Dunlop, J. S., et al. 2011, MNRAS, 413, 162

Caputi, K. I., Ilbert, O., Laigle, C., et al. 2015, ApJ, 810, 73

Carlberg, R. G., Yee, H. K. C., Morris, S. L., et al. 2001, ApJ, 552, 427

Carnall, A. C., Leja, J., Johnson, B. D., et al. 2019, ApJ, 873, 44

Caruana, J., Bunker, A. J., Wilkins, S. M., et al. 2014, MNRAS, 443, 2831

Caruana, J., Wisotzki, L., Herenz, E. C., et al. 2018, MNRAS, 473, 30

Casey, C. M., Narayanan, D., & Cooray, A. 2014, Phys. Rep., 541, 45

Casey, C. M., Cooray, A., Killi, M., et al. 2017, ApJ, 840, 101

Cassata, P., Tasca, L. A. M., Le Fèvre, O., et al. 2015, A&A, 573, A24

Castellano, M., Fontana, A., Boutsia, K., et al. 2010, A&A, 511, A20

Castellano, M., Fontana, A., Grazian, A., et al. 2012, A&A, 540, A39

Cava, A., Pérez-González, P. G., Eliche-Moral, M. C., et al. 2015, ApJ, 812, 155

Cepa, J. 2010, Astrophysics and Space Science Proceedings, 14, 15

Chabrier, G., Baraffe, I., Allard, F., & Hauschildt, P. 2000, ApJ, 542, 464

Chanchaiworawit, K., Guzmán, R., Salvador-Solé, E., et al. 2019, ApJ, 877, 51

Charlot, S., & Bruzual, G. 1991, ApJ, 367, 126

Chiu, K., Fan, X., Leggett, S. K., et al. 2006, AJ, 131, 2722

Coe, D., Zitrin, A., Carrasco, M., et al. 2013, ApJ, 762, 32

Coleman, G. D., Wu, C. C., & Weedman, D. W. 1980, ApJS, 43, 393

Conroy, C. 2013, ARA&A, 51, 393

Conselice, C. J., & Arnold, J. 2009, MNRAS, 397, 208

Conselice, C. J., Bluck, A. F. L., Buitrago, F., et al. 2011, MNRAS, 413, 80

Conselice, C. J., Wilkinson, A., Duncan, K., & Mortlock, A. 2016, ApJ, 830, 83

Couchman, H. M. P., & Rees, M. J. 1986, MNRAS, 221, 53

Cristiani, S., Alexander, D. M., Bauer, F., et al. 2004, ApJ, 600, L119

Cruz, K. L., Burgasser, A. J., Reid, I. N., & Liebert, J. 2004, ApJ, 604, L61

Cucciati, O., Zamorani, G., Lemaux, B. C., et al. 2014, A&A, 570, A16

Curtis-Lake, E., McLure, R. J., Pearce, H. J., et al. 2012, MNRAS, 422, 1425

Curtis-Lake, E., McLure, R. J., Dunlop, J. S., et al. 2016, MNRAS, 457, 440

Daddi, E., Dickinson, M., Morrison, G., et al. 2007, ApJ, 670, 156

Daddi, E., Dannerbauer, H., Stern, D., et al. 2009, ApJ, 694, 1517

Dannerbauer, H., Kurk, J. D., De Breuck, C., et al. 2014, A&A, 570, A55

Davé, R., Katz, N., Oppenheimer, B. D., Kollmeier, J. A., & Weinberg, D. H. 2013, MNRAS, 434, 2645

Davidzon, I., Ilbert, O., Laigle, C., et al. 2017, A&A, 605, A70

Davies, L. J. M., Bremer, M. N., Stanway, E. R., et al. 2014, MNRAS, 438, 2732

Dayal, P., Ferrara, A., Saro, A., et al. 2009, MNRAS, 400, 2000

Dayal, P., & Ferrara, A. 2011, MNRAS, 417, L41

De Barros, S., Vanzella, E., Amorín, R., et al. 2016, A&A, 585, A51

De Barros, S., Pentericci, L., Vanzella, E., et al. 2017, A&A, 608, A123

Dekel, A., Birnboim, Y., Engel, G., et al. 2009, Nature, 457, 451

Dempster, A. P., Laird, N. M., & Rubin, D. B. 1977, Journal of the Royal Statistical Society. Series B (Methodological), 39, 1

Dickinson, M., Papovich, C., Ferguson, H. C., & Budavári, T. 2003, ApJ, 587, 25

Domínguez Sánchez, H., Pérez-González, P. G., Esquej, P., et al. 2016, MNRAS, 457, 3743

Drake, A. B., Guiderdoni, B., Blaizot, J., et al. 2017, MNRAS, 471, 267

Drake, A. B., Garel, T., Wisotzki, L., et al. 2017b, A&A, 608, A6

Duc, P.-A., Paudel, S., McDermid, R. M., et al. 2014, MNRAS, 440, 1458

Duncan, K., Conselice, C. J., Mortlock, A., et al. 2014, MNRAS, 444, 2960

Dunlop, J. S., McLure, R. J., Robertson, B. E., et al. 2012, MNRAS, 420, 901

Dunlop, J. S. 2013, in Astrophysics and Space Science Library, Vol. 396, The First Galaxies, ed. T. Wiklind, B. Mobasher, & V. Bromm, 223

Eke, V. R., Frenk, C. S., Baugh, C. M., et al. 2004, MNRAS, 355, 769

Ellis, R. S., Smail, I., Dressler, A., et al. 1997, ApJ, 483, 582

Ellis, R. S., McLure, R. J., Dunlop, J. S., et al. 2013, ApJ, 763, L7

Elmegreen, B. G., Elmegreen, D. M., Sánchez Almeida, J., et al. 2013, ApJ, 774, 86

Erb, D. K., Steidel, C. C., Shapley, A. E., et al. 2006, ApJ, 646, 107

Fan, X., Narayanan, V. K., Strauss, M. A., et al. 2002, AJ, 123, 1247

Fan, X., Strauss, M. A., Becker, R. H., et al. 2006, AJ, 132, 117

Fan, X., Carilli, C. L., & Keating, B. 2006b, ARA&A, 44, 415

Fan, X., Strauss, M. A., Richards, G. T., et al. 2006c, AJ, 131, 1203

Fazio, G. G., Ashby, M. L. N., Barmby, P., et al. 2004, ApJS, 154, 39

Ferreras, I., Trujillo, I., Mármol-Queraltó, E., et al. 2014, MNRAS, 444, 906

Finkelstein, S. L., Hill, G. J., Gebhardt, K., et al. 2011, ApJ, 729, 140

Finkelstein, S. L., Papovich, C., Ryan, R. E., et al. 2012, ApJ, 758, 93

Finkelstein, S. L., Papovich, C., Salmon, B., et al. 2012b, ApJ, 756, 164

Finkelstein, S. L., Ryan, Russell E., J., Papovich, C., et al. 2015, ApJ, 810, 71

Finkelstein, S. L. 2016, Publ. Astron. Soc. Aust., 33, e037

Fontana, A., Salimbeni, S., Grazian, A., et al. 2006, A&A, 459, 745

Fontanot, F., Cristiani, S., Monaco, P., et al. 2007, A&A, 461, 39

Gawiser, E., Francke, H., Lai, K., et al. 2007, ApJ, 671, 278

Geller, M. J., & Huchra, J. P. 1989, Science, 246, 897

Ghisellini, G., Foschini, L., Volonteri, M., et al. 2009, MNRAS, 399, L24

Giallongo, E., Grazian, A., Fiore, F., et al. 2015, A&A, 578, A83

Giavalisco, M., Steidel, C. C., & Szalay, A. S. 1994, ApJ, 425, L5

Giavalisco, M., Dickinson, M., Ferguson, H. C., et al. 2004, ApJ, 600, L103

Giavalisco, M., Ferguson, H. C., Koekemoer, A. M., et al. 2004b, ApJ, 600, L93

Gibson, R. R., Jiang, L., Brandt, W. N., et al. 2009, ApJ, 692, 758

González, V., Labbé, I., Bouwens, R. J., et al. 2010, ApJ, 713, 115

—. 2011, ApJ, 735, L34

Gonzalez, A. H., Decker, B., Brodwin, M., et al. 2015, ApJ, 812, L40

Gott, J. R., I., & Rees, M. J. 1975, A&A, 45, 365

Grazian, A., Fontana, A., Santini, P., et al. 2015, A&A, 575, A96

Greve, T. R., Bertoldi, F., Smail, I., et al. 2005, MNRAS, 359, 1165

Grogin, N. A., Kocevski, D. D., Faber, S. M., et al. 2011, ApJS, 197, 35

Gronwall, C., Ciardullo, R., Hickey, T., et al. 2007, ApJ, 667, 79

Guhathakurta, P., Tyson, J. A., & Majewski, S. R. 1990, ApJ, 357, L9

Gunn, J. E., & Peterson, B. A. 1965, ApJ, 142, 1633

Guth, A. H. 1981, Phys. Rev. D, 23, 347

Hagen, A., Ciardullo, R., Gronwall, C., et al. 2014, ApJ, 786, 59

Halliday, C., Milvang-Jensen, B., Poirier, S., et al. 2004, A&A, 427, 397

Hashimoto, T., Laporte, N., Mawatari, K., et al. 2018, Nature, 557, 392

Hayes, M., Östlin, G., Schaerer, D., et al. 2010, Nature, 464, 562

Hayes, M., Schaerer, D., Östlin, G., et al. 2011, ApJ, 730, 8

Hernán-Caballero, A., Pérez-González, P. G., Diego, J. M., et al. 2017, ApJ, 849, 82

Higuchi, R., Ouchi, M., Ono, Y., et al. 2019, ApJ, 879, 28

Hinojosa-Goñi, R., Muñoz-Tuñón, C., & Méndez-Abreu, J. 2016, A&A, 592, A122

Hirotani, K., Iguchi, S., Kimura, M., & Wajima, K. 2000, ApJ, 545, 100

Hogg, D. W. 1999, arXiv e-prints, astro

Holden, B. P., Blakeslee, J. P., Postman, M., et al. 2005, ApJ, 626, 809

Holwerda, B. W., Bouwens, R., Oesch, P., et al. 2015, ApJ, 808, 6

Hopkins, A. M., & Beacom, J. F. 2006, ApJ, 651, 142

Hsu, L.-T., Lin, L., Dickinson, M., et al. 2019, The Astrophysical Journal, 871, 233

Hu, E. M., Cowie, L. L., & McMahon, R. G. 1998, ApJ, 502, L99

Huchra, J. P., & Geller, M. J. 1982, ApJ, 257, 423

Hughes, D. H., Serjeant, S., Dunlop, J., et al. 1998, Nature, 394, 241

Hutter, A., Dayal, P., & Müller, V. 2015, MNRAS, 450, 4025

Ilbert, O., Arnouts, S., McCracken, H. J., et al. 2006, A&A, 457, 841

Ilbert, O., McCracken, H. J., Le Fèvre, O., et al. 2013, A&A, 556, A55

Iliev, I. T., Mellema, G., Pen, U. L., et al. 2006, MNRAS, 369, 1625

Inoue, A. K. 2011, MNRAS, 415, 2920

Inoue, A. K., Hasegawa, K., Ishiyama, T., et al. 2018, PASJ, 70, 55

Ivison, R. J., Smail, I., Le Borgne, J. F., et al. 1998, MNRAS, 298, 583

Ivison, R. J., Swinbank, A. M., Smail, I., et al. 2013, ApJ, 772, 137

Iwata, I., Ohta, K., Tamura, N., et al. 2007, MNRAS, 376, 1557

Iye, M., Ota, K., Kashikawa, N., et al. 2006, Nature, 443, 186

Iye, M. 2011, Proceedings of the Japan Academy. Series B, Physical and biological sciences, 87, 575—586

Jiang, L., Wu, J., Bian, F., et al. 2018, Nature Astronomy, 2, 962

Jõeveer, M., Einasto, J., & Tago, E. 1978, MNRAS, 185, 357

Kajino, H., Ohta, K., Iwata, I., et al. 2009, ApJ, 704, 117

Kajisawa, M., Ichikawa, T., Tanaka, I., et al. 2009, ApJ, 702, 1393

—. 2011, PASJ, 63, 379

Kakazu, Y., Cowie, L. L., & Hu, E. M. 2007, ApJ, 668, 853

Karki, R. 2010, Himalayan Physics, 1, doi:10.3126/hj.v1i0.5186

Kawai, N., Kosugi, G., Aoki, K., et al. 2006, Nature, 440, 184

Kennicutt, Robert C., J. 1998, ApJ, 498, 541

Kinney, A. L., Calzetti, D., Bohlin, R. C., et al. 1996, ApJ, 467, 38

Kirkpatrick, J. D., Looper, D. L., Burgasser, A. J., et al. 2010, ApJS, 190, 100

Koekemoer, A. M., Faber, S. M., Ferguson, H. C., et al. 2011, ApJS, 197, 36

Komatsu, E., Smith, K. M., Dunkley, J., et al. 2011, ApJS, 192, 18

Kravtsov, A. V., & Borgani, S. 2012, ARA&A, 50, 353

Kuhr, H., Liebert, J. W., Strittmatter, P. A., Schmidt, G. D., & Mackay, C. 1983, ApJ, 275, L33

Kusakabe, M., Kim, K. S., Cheoun, M.-K., et al. 2014, ApJS, 214, 5

Labbé, I., González, V., Bouwens, R. J., et al. 2010, ApJ, 716, L103

Laporte, N., Infante, L., Troncoso Iribarren, P., et al. 2016, ApJ, 820, 98

Lawrence, A., & Elvis, M. 1982, ApJ, 256, 410

Lee, K.-S., Ferguson, H. C., Wiklind, T., et al. 2012, ApJ, 752, 66

Lee, K.-G., Hennawi, J. F., Stark, C., et al. 2014, ApJ, 795, L12

Leitherer, C., Schaerer, D., Goldader, J. D., et al. 1999, ApJS, 123, 3

Leja, J., Carnall, A. C., Johnson, B. D., Conroy, C., & Speagle, J. S. 2019, ApJ, 876, 3

Liddle, A. R. 2007, MNRAS, 377, L74

Lilly, S. J., Le Fevre, O., Hammer, F., & Crampton, D. 1996, ApJ, 460, L1

Lin, L., Dickinson, M., Jian, H.-Y., et al. 2012, ApJ, 756, 71

Liu, W.-J., Zhou, H., Ji, T., et al. 2015, ApJS, 217, 11

Liu, C., Mutch, S. J., Poole, G. B., et al. 2017, MNRAS, 465, 3134

Livermore, R. C., Finkelstein, S. L., & Lotz, J. M. 2017, ApJ, 835, 113

Loeb, A. 2010, How Did the First Stars and Galaxies Form?, Princeton frontiers in physics (Princeton University Press)

Looper, D. L., Kirkpatrick, J. D., & Burgasser, A. J. 2007, AJ, 134, 1162

Lumbreras-Calle, A., Muñoz-Tuñón, C., Méndez-Abreu, J., et al. 2019, A&A, 621, A52

Lutz, D., Dunlop, J. S., Almaini, O., et al. 2001, A&A, 378, 70

Madau, P., Ferguson, H. C., Dickinson, M. E., et al. 1996, MNRAS, 283, 1388

Madau, P., Pozzetti, L., & Dickinson, M. 1998, ApJ, 498, 106

Madau, P., & Dickinson, M. 2014, ARA&A, 52, 415

Madau, P., & Haardt, F. 2015, ApJ, 813, L8

Magnelli, B., Elbaz, D., Chary, R. R., et al. 2009, A&A, 496, 57

—. 2011, A&A, 528, A35

Malhotra, S., & Rhoads, J. E. 2004, ApJ, 617, L5

Malhotra, S., Rhoads, J. E., Pirzkal, N., et al. 2005, ApJ, 626, 666

Mancini, C., Matute, I., Cimatti, A., et al. 2009, A&A, 500, 705

Marchesini, D., van Dokkum, P. G., Förster Schreiber, N. M., et al. 2009, ApJ, 701, 1765

Marchesini, D., Whitaker, K. E., Brammer, G., et al. 2010, ApJ, 725, 1277

Marrone, D. P., Spilker, J. S., Hayward, C. C., et al. 2018, Nature, 553, 51

Mas-Hesse, J. M., Kunth, D., Tenorio-Tagle, G., et al. 2003, ApJ, 598, 858

Mashian, N., Oesch, P. A., & Loeb, A. 2016, MNRAS, 455, 2101

Matthee, J., Sobral, D., Santos, S., et al. 2015, MNRAS, 451, 400

Matthee, J., Sobral, D., Oteo, I., et al. 2016, MNRAS, 458, 449

Matthee, J., Sobral, D., Darvish, B., et al. 2017, MNRAS, 472, 772

Matthews, T. A., & Sandage, A. R. 1963, ApJ, 138, 30

McCracken, H. J., Milvang-Jensen, B., Dunlop, J., et al. 2012, A&A, 544, A156

McGee, S. L., Balogh, M. L., Henderson, R. D. E., et al. 2008, MNRAS, 387, 1605

McLeod, D. J., McLure, R. J., Dunlop, J. S., et al. 2015, MNRAS, 450, 3032

McLeod, D. J., McLure, R. J., & Dunlop, J. S. 2016, MNRAS, 459, 3812

McLure, R. J., Cirasuolo, M., Dunlop, J. S., Foucaud, S., & Almaini, O. 2009, MNRAS, 395, 2196

McLure, R. J., Dunlop, J. S., Bowler, R. A. A., et al. 2013, MNRAS, 432, 2696

Méndez-Abreu, J., Aguerri, J. A. L., Falcón-Barroso, J., et al. 2018, MNRAS, 474, 1307

Messias, H., Dye, S., Nagar, N., et al. 2014, A&A, 568, A92

Michałowski, M. J., Dunlop, J. S., Cirasuolo, M., et al. 2012, A&A, 541, A85

Milvang-Jensen, B., Noll, S., Halliday, C., et al. 2008, A&A, 482, 419

Miralda-Escudé, J. 1998, ApJ, 501, 15

Mortlock, D. J., Warren, S. J., Venemans, B. P., et al. 2011, Nature, 474, 616

Mortlock, A., Conselice, C. J., Bluck, A. F. L., et al. 2011b, MNRAS, 413, 2845

Mundy, C. J., Conselice, C. J., Duncan, K. J., et al. 2017, MNRAS, 470, 3507

Murayama, T., Taniguchi, Y., Scoville, N. Z., et al. 2007, ApJS, 172, 523

Muzzin, A., Marchesini, D., Stefanon, M., et al. 2013, ApJ, 777, 18

Narayanan, D., Turk, M., Feldmann, R., et al. 2015, Nature, 525, 496

Noll, S., Burgarella, D., Giovannoli, E., et al. 2009, A&A, 507, 1793

Oesch, P. A., Bouwens, R. J., Illingworth, G. D., et al. 2010, ApJ, 709, L16

—. 2013, ApJ, 773, 75

—. 2014, ApJ, 786, 108

Oke, J. B., & Gunn, J. E. 1983, ApJ, 266, 713

Oke, J. B. 1990, AJ, 99, 1621

Ono, Y., Ouchi, M., Shimasaku, K., et al. 2010, MNRAS, 402, 1580

Ono, Y., Ouchi, M., Mobasher, B., et al. 2012, ApJ, 744, 83

Ono, Y., Ouchi, M., Curtis-Lake, E., et al. 2013, ApJ, 777, 155

Ono, Y., Ouchi, M., Harikane, Y., et al. 2018, PASJ, 70, S10

Oteo, I., Ivison, R. J., Dunne, L., et al. 2016, ApJ, 827, 34

Otí-Floranes, H., Mas-Hesse, J. M., Jiménez-Bailón, E., et al. 2014, A&A, 566, A38

Ouchi, M., Shimasaku, K., Furusawa, H., et al. 2003, ApJ, 582, 60

Ouchi, M., Shimasaku, K., Akiyama, M., et al. 2005, ApJ, 620, L1

—. 2008, ApJS, 176, 301

Ouchi, M., Ono, Y., Egami, E., et al. 2009, ApJ, 696, 1164

Ouchi, M., Shimasaku, K., Furusawa, H., et al. 2010, ApJ, 723, 869

Ouchi, M., Harikane, Y., Shibuya, T., et al. 2018, PASJ, 70, S13

Padovani, P., & Giommi, P. 1995, MNRAS, 277, 1477

Papovich, C., Dickinson, M., & Ferguson, H. C. 2001, ApJ, 559, 620

Papovich, C., Rudnick, G., Le Floc'h, E., et al. 2007, ApJ, 668, 45

Papovich, C., Finkelstein, S. L., Ferguson, H. C., Lotz, J. M., & Giavalisco, M. 2011, MNRAS, 412, 1123

Peebles, P. J. E. 1968, ApJ, 153, 1

Pelló, R., Miralles, J. M., Le Borgne, J. F., et al. 1996, A&A, 314, 73

Pelló, R., Rudnick, G., De Lucia, G., et al. 2009, A&A, 508, 1173

Pelló, R., Hudelot, P., Laporte, N., et al. 2018, A&A, 620, A51

Penrose, R. 1969, Nuovo Cimento Rivista Serie, 1, 252

Pentericci, L., Fontana, A., Vanzella, E., et al. 2011, ApJ, 743, 132

Penzias, A. A., & Wilson, R. W. 1965, ApJ, 142, 419

Pérez-González, P. G., Gil de Paz, A., Zamorano, J., et al. 2003, MNRAS, 338, 508

Pérez-González, P. G., Rieke, G. H., Egami, E., et al. 2005, ApJ, 630, 82

Pérez-González, P. G., Rieke, G. H., Villar, V., et al. 2008, ApJ, 675, 234

Pérez-González, P. G., Cava, A., Barro, G., et al. 2013, ApJ, 762, 46

Perlmutter, S., Aldering, G., Goldhaber, G., et al. 1999, ApJ, 517, 565

Pickles, A. J. 1998, PASP, 110, 863

Planck Collaboration, Ade, P. A. R., Aghanim, N., et al. 2016, A&A, 594, A13

Poggianti, B. M., von der Linden, A., De Lucia, G., et al. 2006, ApJ, 642, 188

Pozzetti, L., Bolzonella, M., Lamareille, F., et al. 2007, A&A, 474, 443

Pozzetti, L., Bolzonella, M., Zucca, E., et al. 2010, A&A, 523, A13

Press, W. H., & Schechter, P. 1974, ApJ, 187, 425

Qiu, Y., Mutch, S. J., da Cunha, E., Poole, G. B., & Wyithe, J. S. B. 2019, MNRAS, 489, 1357

Rauch, M. 1998, ARA&A, 36, 267

Reddy, N. A., & Steidel, C. C. 2009, ApJ, 692, 778

Rees, M. J. 1984, ARA&A, 22, 471

Reid, I. N., Lewitus, E., Burgasser, A. J., & Cruz, K. L. 2006, ApJ, 639, 1114

Rhoads, J. E., Malhotra, S., Dey, A., et al. 2000, ApJ, 545, L85

Ribeiro, B., Le Fèvre, O., Tasca, L. A. M., et al. 2016, A&A, 593, A22

Richards, G. T., Strauss, M. A., Fan, X., et al. 2006, AJ, 131, 2766

Riechers, D. A., Carilli, C. L., Capak, P. L., et al. 2014, ApJ, 796, 84

Riechers, D. A., Leung, T. K. D., Ivison, R. J., et al. 2017, ApJ, 850, 1

Riess, A. G., Filippenko, A. V., Challis, P., et al. 1998, AJ, 116, 1009

Riess, A. G., Strolger, L.-G., Casertano, S., et al. 2007, ApJ, 659, 98

Robertson, B. E., Ellis, R. S., Dunlop, J. S., McLure, R. J., & Stark, D. P. 2010, Nature, 468, 49

Robertson, B. E., Furlanetto, S. R., Schneider, E., et al. 2013, ApJ, 768, 71

Rodriguez Espinosa, J. M., Gonzalez-Martin, O., Castro-Rodriguez, N., et al. 2014, MNRAS, 444, L68

Rousseeuw, P. J. 1987, Journal of Computational and Applied Mathematics, 20, 53

Rowan-Robinson, M. 1977, ApJ, 213, 635

Ryden, B. 2003, Introduction to Cosmology (Addison-Wesley)

Salim, S., Dickinson, M., Michael Rich, R., et al. 2009, ApJ, 700, 161

Salmon, B., Papovich, C., Finkelstein, S. L., et al. 2015, ApJ, 799, 183

Salpeter, E. E. 1955, ApJ, 121, 161

Sanders, D. B., Salvato, M., Aussel, H., et al. 2007, ApJS, 172, 86

Santini, P., Fontana, A., Grazian, A., et al. 2012, A&A, 538, A33

Santos, S., Sobral, D., & Matthee, J. 2016, MNRAS, 463, 1678

Schaerer, D., & de Barros, S. 2009, A&A, 502, 423

—. 2010, A&A, 515, A73

Schaerer, D., de Barros, S., & Sklias, P. 2013, A&A, 549, A4

Schaerer, D., Boone, F., Zamojski, M., et al. 2015, A&A, 574, A19

Schechter, P. 1976, ApJ, 203, 297

Schenker, M. A., Robertson, B. E., Ellis, R. S., et al. 2013, ApJ, 768, 196

Schenker, M. A., Ellis, R. S., Konidaris, N. P., & Stark, D. P. 2013b, ApJ, 777, 67

—. 2014, ApJ, 795, 20

Schlafly, E. F., & Finkbeiner, D. P. 2011, ApJ, 737, 103

Schmidt, M. 1968, ApJ, 151, 393

Schwarz, G. E. 1978, Ann. Stat., 6, 461

Serra, P., Amblard, A., Temi, P., et al. 2011, ApJ, 740, 22

Seyfert, C. K. 1943, ApJ, 97, 28

Shapley, A. E., Steidel, C. C., Pettini, M., & Adelberger, K. L. 2003, ApJ, 588, 65

Shapley, A. E., Steidel, C. C., Strom, A. L., et al. 2016, ApJ, 826, L24

Shibuya, T., Ouchi, M., & Harikane, Y. 2015, ApJS, 219, 15

Shim, H., Chary, R.-R., Dickinson, M., et al. 2011, ApJ, 738, 69

Shimasaku, K., Ouchi, M., Okamura, S., et al. 2003, ApJL, 586, L111

Silk, J. 1977, ApJ, 211, 638

Smail, I., Ivison, R. J., & Blain, A. W. 1997, ApJ, 490, L5

Sobral, D., Matthee, J., Best, P., et al. 2017, MNRAS, 466, 1242

Sobral, D., Santos, S., Matthee, J., et al. 2018, MNRAS, 476, 4725

Sobral, D., Matthee, J., Darvish, B., et al. 2018b, MNRAS, 477, 2817

Sobral, D., & Matthee, J. 2019, A&A, 623, A157

Somerville, R. S., & Davé, R. 2015, ARA&A, 53, 51

Song, M., Finkelstein, S. L., Ashby, M. L. N., et al. 2016, ApJ, 825, 5

Spitler, L. R., Labbé, I., Glazebrook, K., et al. 2012, ApJ, 748, L21

Stanford, S. A., Eisenhardt, P. R., & Dickinson, M. 1998, ApJ, 492, 461

Stark, D. P., Ellis, R. S., Bunker, A., et al. 2009, ApJ, 697, 1493

Stark, D. P., Ellis, R. S., & Ouchi, M. 2011, ApJ, 728, L2

Stark, D. P., Schenker, M. A., Ellis, R., et al. 2013, ApJ, 763, 129

Stefanon, M., Bouwens, R. J., Labbé, I., et al. 2017, ApJ, 843, 36

Steidel, C. C., & Hamilton, D. 1992, AJ, 104, 941

—. 1993, AJ, 105, 2017

Steidel, C. C., Pettini, M., & Hamilton, D. 1995, AJ, 110, 2519

Steidel, C. C., Adelberger, K. L., Dickinson, M., et al. 1998, ApJ, 492, 428

Steidel, C. C., Adelberger, K. L., Shapley, A. E., et al. 2003, ApJ, 592, 728

—. 2005, ApJ, 626, 44

Steinhardt, C. L., Speagle, J. S., Capak, P., et al. 2014, ApJ, 791, L25

Stiavelli, M., Fall, S. M., & Panagia, N. 2004, ApJ, 610, L1

Swinbank, A. M., Lacey, C. G., Smail, I., et al. 2008, MNRAS, 391, 420

Taniguchi, Y., Ajiki, M., Nagao, T., et al. 2005, PASJ, 57, 165

Taniguchi, Y., Scoville, N., Murayama, T., et al. 2007, ApJS, 172, 9

Taylor, M. B. 2005, in Astronomical Society of the Pacific Conference Series, Vol. 347, Astronomical Data Analysis Software and Systems XIV, ed. P. Shopbell, M. Britton, & R. Ebert, 29

Tegmark, M., Silk, J., Rees, M. J., et al. 1997, ApJ, 474, 1

Tilvi, V., Papovich, C., Tran, K. V. H., et al. 2013, ApJ, 768, 56

Tilvi, V., Papovich, C., Finkelstein, S. L., et al. 2014, ApJ, 794, 5

Tinsley, B. M. 1968, ApJ, 151, 547

—. 1980, Fund. Cosmic Phys., 5, 287

Tody, D. 1986, in Society of Photo-Optical Instrumentation Engineers (SPIE) Conference Series, Vol. 627, Proc. SPIE, ed. D. L. Crawford, 733

Tomczak, A. R., Quadri, R. F., Tran, K.-V. H., et al. 2014, ApJ, 783, 85

Toshikawa, J., Kashikawa, N., Ota, K., et al. 2012, ApJ, 750, 137

Toshikawa, J., Kashikawa, N., Overzier, R., et al. 2014, ApJ, 792, 15

Trainor, R. F., Steidel, C. C., Strom, A. L., & Rudie, G. C. 2015, ApJ, 809, 89

Trainor, R. F., Strom, A. L., Steidel, C. C., & Rudie, G. C. 2016, ApJ, 832, 171

Tran, H. D. 2001, ApJ, 554, L19

Trenti, M., & Stiavelli, M. 2008, ApJ, 676, 767

Treu, T., Schmidt, K. B., Trenti, M., Bradley, L. D., & Stiavelli, M. 2013, ApJ, 775, L29

Urry, C. M., & Padovani, P. 1995, PASP, 107, 803

Urry, C. M., Scarpa, R., O'Dowd, M., et al. 2000, ApJ, 532, 816

Vanzella, E., de Barros, S., Castellano, M., et al. 2015, A&A, 576, A116

Vanzella, E., Nonino, M., Cupani, G., et al. 2018, MNRAS, 476, L15

Vazdekis, A. 1999, ApJ, 513, 224

Venemans, B. P., Kurk, J. D., Miley, G. K., et al. 2002, ApJ, 569, L11

Venemans, B. P., Röttgering, H. J. A., Miley, G. K., et al. 2007, A&A, 461, 823

Villarroel, B., Nyholm, A., Karlsson, T., et al. 2017, ApJ, 837, 110

Voit, G. M. 2005, Reviews of Modern Physics, 77, 207

Vulcani, B., Trenti, M., Calvi, V., et al. 2017, ApJ, 836, 239

Walcher, J., Groves, B., Budavári, T., & Dale, D. 2011, Ap&SS, 331, 1

Walter, F., Decarli, R., Carilli, C., et al. 2012, Nature, 486, 233

Wang, J. X., Malhotra, S., & Rhoads, J. E. 2005, ApJ, 622, L77

Wang, J.-M., Du, P., Baldwin, J. A., et al. 2012, ApJ, 746, 137

Webb, J. R., Carini, M. T., Clements, S., et al. 1990, AJ, 100, 1452

Weymann, R. J., Morris, S. L., Foltz, C. B., & Hewett, P. C. 1991, ApJ, 373, 23

White, S. D. M., Clowe, D. I., Simard, L., et al. 2005, A&A, 444, 365

Wirth, G. D., Willmer, C. N. A., Amico, P., et al. 2004, AJ, 127, 3121

Wu, Y.-Z., Zhang, E.-P., Liang, Y.-C., Zhang, C.-M., & Zhao, Y.-H. 2011, ApJ, 730, 121

Zafar, T., Watson, D. J., Malesani, D., et al. 2010, A&A, 515, A94

Zeldovich, Y. B., Kurt, V. G., & Syunyaev, R. A. 1968, Zhurnal Eksperimentalnoi i Teoreticheskoi Fiziki, 55, 278

Zwicky, F. 1933, Helvetica Physica Acta, 6, 110

van der Burg, R. F. J., Hildebrandt, H., & Erben, T. 2010, A&A, 523, A74

A

Sample catalog and main derived physical parameters.

This appendix presents the sample catalog with the main physical parameters of the GOODS-N high-z LAEs and LBGs sample selected in this work.

In Table A.1, we present the 1558 sources selected at z = 3.4-6.8, with the main physical parameters directly derived from the SEDs: photometric redshifts, Lyα luminosities and EWs, rest-frame UV fluxes and SFRs derived from both Lyα and L_{1500}. A complete electronic version of this table is available in the online version of Arrabal Haro et al. (2018).

Table A.2 collects the main physical parameters obtained with the CIGALE SP synthesis model fitting of the SEDs, namely, stellar masses, ages and e-folding times of the main SP and the additional SP (when needed according to the BIC calibration presented in Sec. 3.1.2). A complete electronic version of this table will be available in the online version of Arrabal Haro et al. (2019, submitted).

Finally, the 202 sources found in 92 close groups are presented in Table A.3, showing the common photometric redshift of each group and the maximum comoving distance from its central object to the furthest away one. A complete electronic version of this table is available in the online version of Arrabal Haro et al. (2018).

Table A.1: Main relevant parameters of the sample. (1) Name of the object using the SHARDS identification. (2) Right ascension. (3) Declination. (4) Photometric redshift. (5) Lyα luminosity (in case the Lyα emission line is detected). (6) Apparent magnitude measured at a rest-frame wavelength of 1500 Å (not measurable in some pure LAEs). (7) SFR derived from the Lyα emission. (8) SFR derived from the rest-frame UV continuum at 1500 Å. (9) Rest-frame Lyα EW.

Object Name	R.A.	Dec.	z	$L_{Ly\alpha}$	m_{1500}	$SFR_{L_{Ly\alpha}}$	$SFR_{L_{1500}}$	EW_0
	(J2000)	(J2000)		(10^{42} erg s^{-1})	(AB mag)	($M_\odot$ yr^{-1})	($M_\odot$ yr^{-1})	(Å)
	(2)	(3)	(4)	(5)	(6)	(7)	(8)	(9)
SHARDS20010117	12:35:48.07	62:12:02.39	4.28 ± 0.06	–	27.5 ± 0.6	–	1.7 ± 0.9	–
SHARDS20007539	12:35:48.12	62:12:03.78	5.38 ± 0.07	0.9 ± 0.2	25.8 ± 0.2	0.8 ± 0.2	11.2 ± 1.7	15 ± 3
SHARDS20012481	12:35:50.89	62:11:58.49	5.69 ± 0.06	–	26.2 ± 0.1	–	10.7 ± 1.3	–
SHARDS20005927	12:35:51.53	62:12:16.49	3.22 ± 0.07	–	26.4 ± 0.2	–	27.4 ± 4.9	–
SHARDS20005405	12:35:51.63	62:12:12.66	4.03 ± 0.07		25.6 ± 0.2		36.8 ± 7.9	
SHARDS20008074	12:35:52.15	62:11:20.83	5.53 ± 0.07	0.5 ± 0.2	26.2 ± 0.1	0.4 ± 0.2	8.0 ± 1.0	42 ± 31
SHARDS20008444	12:35:53.20	62:10:32.94	4.01 ± 0.07	–	26.8 ± 0.6	–	2.8 ± 1.5	–
SHARDS20010810	12:35:53.38	62:10:23.25	5.12 ± 0.06	–	27.2 ± 0.3	–	6.2 ± 1.5	–
SHARDS20005669	12:35:54.09	62:10:32.87	3.36 ± 0.07	0.2 ± 0.2	26.4 ± 0.3	0.2 ± 0.2	137.1 ± 36.3	14 ± 10
SHARDS20011405	12:35:54.26	62:10:18.83	5.37 ± 0.07	–	25.9 ± 0.2	–	9.9 ± 2.0	–
SHARDS20006420	12:35:54.43	62:10:33.80	3.88 ± 0.06	–	26.0 ± 0.3	–	37.5 ± 11.3	–
SHARDS20006258	12:35:54.54	62:12:14.59	3.48 ± 0.06	0.3 ± 0.2	25.7 ± 0.1	0.3 ± 0.2	12.9 ± 1.8	21 ± 12
SHARDS20013727	12:35:55.03	62:12:04.79	5.96 ± 0.07	0.3 ± 0.2	26.2 ± 0.2	0.3 ± 0.2	160.5 ± 33.0	16 ± 10
SHARDS20009009	12:35:55.19	62:11:25.40	3.89 ± 0.06	–	26.7 ± 0.3	–	16.7 ± 5.1	–
SHARDS20006827	12:35:55.65	62:10:19.00	4.28 ± 0.06		26.2 ± 0.2		5.5 ± 1.2	
SHARDS20008662	12:35:55.79	62:10:28.94	4.17 ± 0.07	–	26.9 ± 0.6	–	2.9 ± 1.6	–
SHARDS20008870	12:35:55.83	62:12:32.05	4.19 ± 0.07	–	27.1 ± 0.5	–	4.0 ± 2.0	–
SHARDS20010887	12:35:56.17	62:11:45.41	5.14 ± 0.06	–	26.2 ± 0.3	–	76.2 ± 23.6	–
SHARDS20010975	12:35:56.63	62:11:43.25	5.40 ± 0.07	0.2 ± 0.2	26.8 ± 0.5	0.2 ± 0.2	10.7 ± 5.4	11 ± 9
SHARDS20005559	12:35:57.22	62:10:38.99	4.17 ± 0.07	–	25.9 ± 0.2	–	90.9 ± 18.0	–
SHARDS20003293	12:35:57.47	62:12:24.01	3.90 ± 0.06	–	26.3 ± 0.4	–	11.5 ± 4.0	–
SHARDS20004834	12:35:57.72	62:11:30.02	3.37 ± 0.07	–	25.2 ± 0.1	–	50.5 ± 5.6	–
SHARDS20004871	12:35:58.19	62:11:05.55	3.62 ± 0.06	–	24.7 ± 0.1	–	44.2 ± 3.9	–
SHARDS20009905	12:35:58.58	62:12:11.66	5.28 ± 0.07	1.2 ± 0.2	–	1.1 ± 0.2	–	80 ± 22
SHARDS20012586	12:35:58.86	62:10:17.25	5.69 ± 0.06	0.8 ± 0.3	–	0.8 ± 0.3	–	76 ± 89
SHARDS20010376	12:35:59.01	62:12:45.29	5.15 ± 0.06	–	25.1 ± 0.2	–	229.4 ± 49.9	–
SHARDS20005220	12:35:59.52	62:09:49.69	4.29 ± 0.06		25.1 ± 0.1		107.7 ± 10.7	
SHARDS20005503	12:36:00.04	62:12:26.09	5.15 ± 0.06	0.6 ± 0.2	25.2 ± 0.1	0.6 ± 0.2	38.4 ± 5.0	18 ± 7
SHARDS20010137	12:36:00.58	62:12:20.02	4.20 ± 0.07		27.5 ± 0.7		1.7 ± 1.1	
SHARDS20011116	12:36:00.61	62:12:59.63	4.45 ± 0.07	0.3 ± 0.2	26.0 ± 0.2	0.2 ± 0.2	19.3 ± 4.4	22 ± 17
SHARDS20005166	12:36:00.84	62:12:52.37	3.50 ± 0.06	–	25.5 ± 0.1	–	31.2 ± 3.7	–
SHARDS20005022	12:36:01.16	62:12:52.33	3.50 ± 0.06	–	25.1 ± 0.1	–	72.5 ± 7.0	–
SHARDS20005185	12:36:01.25	62:12:53.70	3.50 ± 0.06		25.6 ± 0.1		15.3 ± 1.9	
SHARDS20005390	12:36:01.25	62:13:18.92	3.91 ± 0.06	0.4 ± 0.2	25.9 ± 0.2	0.4 ± 0.2	30.3 ± 6.2	13 ± 7
SHARDS20005748	12:36:01.39	62:09:44.72	3.61 ± 0.06	0.8 ± 0.7	25.8 ± 0.2	0.7 ± 0.7	22.0 ± 4.0	68 ± 57
SHARDS20005027	12:36:01.47	62:09:43.12	3.36 ± 0.07	–	25.2 ± 0.1	–	39.2 ± 4.7	–
SHARDS20006671	12:36:01.58	62:12:24.87	3.50 ± 0.06	–	25.4 ± 0.1	–	87.1 ± 10.3	–

Continued on next page

Table A.1 – *Continued from previous page*

Object Name	R.A. (J2000)	Dec. (J2000)	z	$L_{Ly\alpha}$ (10^{42} erg s^{-1})	m_{1500} (AB mag)	$SFR_{L_{Ly\alpha}}$ ($M_\odot$ yr^{-1})	$SFR_{L_{1500}}$ ($M_\odot$ yr^{-1})	EW$_0$ (Å)
SHARDS20005412	12:36:01.65	62:11:18.84	3.90 ± 0.06	–	25.4 ± 0.1	–	55.2 ± 8.1	–
SHARDS20004739	12:36:03.14	62:10:23.35	3.90 ± 0.06	–	24.7 ± 0.1	–	77.5 ± 7.2	–
SHARDS20006276	12:36:04.10	62:09:21.99	3.75 ± 0.06	–	25.9 ± 0.3	–	75.2 ± 19.4	–
SHARDS20005680	12:36:04.40	62:09:23.37	3.75 ± 0.06	0.5 ± 0.2	26.5 ± 0.4	0.4 ± 0.2	23.9 ± 9.6	40 ± 23
SHARDS20015119	12:36:04.61	62:12:27.76	5.73 ± 0.06	–	25.9 ± 0.2	–	86.1 ± 18.6	–
SHARDS20005970	12:36:05.22	62:10:19.71	4.30 ± 0.06	–	25.5 ± 0.1	–	62.9 ± 6.9	–
SHARDS20007405	12:36:05.28	62:13:23.58	4.06 ± 0.07	–	26.4 ± 0.4	–	16.7 ± 6.7	–
SHARDS20005279	12:36:06.08	62:08:56.31	4.42 ± 0.07	–	25.3 ± 0.2	–	67.1 ± 15.3	–
SHARDS20011135	12:36:06.60	62:14:04.05	3.65 ± 0.06	–	26.7 ± 0.4	–	726.2 ± 262.3	–
SHARDS20009951	12:36:06.75	62:09:32.83	3.76 ± 0.06	0.1 ± 0.1	26.4 ± 0.3	0.1 ± 0.1	3.8 ± 1.2	11 ± 12
SHARDS20004883	12:36:07.39	62:13:40.07	3.65 ± 0.06	–	25.0 ± 0.1	–	79.0 ± 8.2	–
SHARDS20008937	12:36:07.43	62:10:18.05	3.77 ± 0.06	–	27.1 ± 0.6	–	4.5 ± 2.6	–
SHARDS20012287	12:36:07.53	62:11:05.39	3.77 ± 0.06	–	26.7 ± 0.4	–	2.9 ± 1.2	–
SHARDS20010275	12:36:07.74	62:12:26.09	3.64 ± 0.06	0.3 ± 0.1	26.5 ± 0.3	0.3 ± 0.1	30.5 ± 8.6	35 ± 20
SHARDS20005404	12:36:07.94	62:09:30.14	3.62 ± 0.06	–	25.5 ± 0.1	–	20.8 ± 2.8	–
SHARDS20005835	12:36:07.98	62:11:20.91	4.87 ± 0.08	–	26.1 ± 0.2	–	27.7 ± 4.5	–
SHARDS20006747	12:36:08.13	62:10:07.15	3.37 ± 0.07	0.3 ± 0.2	26.8 ± 0.3	0.2 ± 0.2	5.7 ± 1.7	24 ± 18
SHARDS20011097	12:36:08.41	62:09:57.63	4.58 ± 0.07	–	26.9 ± 0.6	–	3.4 ± 2.0	–
SHARDS20008956	12:36:08.44	62:09:01.71	3.89 ± 0.06	0.8 ± 0.2	–	0.8 ± 0.2	–	118 ± 35
SHARDS20010119	12:36:08.51	62:10:16.29	3.90 ± 0.06	–	26.2 ± 0.3	–	4.7 ± 1.3	–
SHARDS20007130	12:36:08.59	62:08:40.57	3.75 ± 0.06	–	26.3 ± 0.4	–	31.7 ± 12.3	–
SHARDS20006314	12:36:08.60	62:10:18.71	4.59 ± 0.07	–	25.4 ± 0.2	–	103.7 ± 16.8	–
SHARDS20008067	12:36:09.27	62:11:20.52	3.50 ± 0.06	1.2 ± 0.3	–	1.1 ± 0.2	–	134 ± 64
SHARDS20005577	12:36:09.28	62:10:04.95	3.49 ± 0.06	1.1 ± 0.2	25.6 ± 0.1	1.0 ± 0.2	13.8 ± 1.7	43 ± 9
SHARDS20008093	12:36:09.49	62:14:03.54	4.22 ± 0.07	–	25.9 ± 0.2	–	7.4 ± 1.4	–
SHARDS20005473	12:36:09.53	62:11:15.84	5.42 ± 0.07	0.5 ± 0.3	25.1 ± 0.1	0.5 ± 0.2	40.6 ± 5.5	11 ± 4
SHARDS20002083	12:36:09.70	62:11:10.69	3.91 ± 0.06	–	24.8 ± 0.1	–	24.9 ± 2.6	–
SHARDS20008357	12:36:10.34	62:09:55.67	5.15 ± 0.06	–	26.1 ± 0.3	–	38.9 ± 9.8	–
SHARDS20005273	12:36:10.36	62:09:09.87	3.89 ± 0.06	1.1 ± 0.2	25.8 ± 0.2	1.0 ± 0.1	49.2 ± 9.2	39 ± 8
SHARDS20013907	12:36:10.37	62:14:23.50	3.52 ± 0.06	–	28.0 ± 0.4	–	1.7 ± 0.6	–
SHARDS20007147	12:36:10.44	62:08:56.64	3.75 ± 0.06	–	26.0 ± 0.2	–	274.0 ± 60.3	–
SHARDS20017520	12:36:10.56	62:08:47.60	3.61 ± 0.06	–	26.1 ± 0.2	–	5712.4 ± 1331	–
SHARDS20006199	12:36:10.74	62:12:42.73	3.79 ± 0.06	–	26.1 ± 0.3	–	27.7 ± 7.6	–
SHARDS20006058	12:36:10.80	62:14:15.22	4.22 ± 0.07	–	25.6 ± 0.2	–	27.3 ± 4.3	–
SHARDS20007027	12:36:11.17	62:13:40.04	4.77 ± 0.07	–	26.3 ± 0.2	–	30.5 ± 5.8	–
SHARDS20008071	12:36:11.23	62:08:23.11	4.02 ± 0.07	–	25.7 ± 0.3	–	41.8 ± 10.8	–
SHARDS20015907	12:36:11.38	62:11:52.01	4.46 ± 0.07	0.4 ± 0.2	26.2 ± 0.4	0.3 ± 0.2	16.2 ± 6.0	20 ± 10
SHARDS20006779	12:36:11.44	62:09:55.77	3.77 ± 0.06	–	25.7 ± 0.2	–	9.7 ± 1.7	–
SHARDS20001077	12:36:11.49	62:09:31.14	3.37 ± 0.07	–	24.5 ± 0.0	–	38.9 ± 3.7	–
SHARDS20007575	12:36:11.54	62:12:43.90	3.65 ± 0.06	0.2 ± 0.1	26.5 ± 0.3	0.2 ± 0.1	24.9 ± 6.9	16 ± 9
SHARDS20004820	12:36:11.88	62:09:10.52	4.30 ± 0.06	–	24.9 ± 0.1	–	129.8 ± 10.7	–
SHARDS20007747	12:36:11.91	62:14:38.52	5.45 ± 0.07	0.5 ± 0.2	25.7 ± 0.1	0.5 ± 0.2	13.2 ± 1.1	14 ± 6
SHARDS20010570	12:36:11.93	62:12:36.86	5.31 ± 0.07	0.4 ± 0.3	26.9 ± 0.6	0.3 ± 0.2	4.0 ± 2.1	16 ± 10
SHARDS20005294	12:36:12.00	62:09:59.69	3.91 ± 0.06	–	25.2 ± 0.1	–	73.6 ± 9.2	–
SHARDS20010722	12:36:12.05	62:14:11.31	4.34 ± 0.06	–	27.9 ± 0.9	–	1.2 ± 1.0	–
SHARDS20011388	12:36:12.16	62:09:54.97	4.59 ± 0.07	0.2 ± 0.2	27.5 ± 1.0	0.2 ± 0.2	1.9 ± 1.7	11 ± 11
SHARDS20007085	12:36:12.16	62:10:24.87	5.29 ± 0.07	–	25.7 ± 0.2	–	11.9 ± 2.2	–
SHARDS20007508	12:36:12.32	62:10:20.89	3.63 ± 0.06	0.2 ± 0.1	26.6 ± 0.3	0.2 ± 0.1	10.6 ± 3.3	18 ± 11

Continued on next page

Table A.1 – *Continued from previous page*

Object Name	R.A. (J2000)	Dec. (J2000)	z	$L_{Ly\alpha}$ (10^{42} erg s^{-1})	m_{1500} (AB mag)	$\mathrm{SFR}_{L_{Ly\alpha}}$ ($M_\odot$ yr^{-1})	$\mathrm{SFR}_{L_{1500}}$ ($M_\odot$ yr^{-1})	EW$_0$ (Å)
SHARDS20011200	12:36:12.44	62:17:49.49	4.23 ± 0.07	–	27.1 ± 0.2	–	2.4 ± 0.4	–
SHARDS20005700	12:36:12.63	62:09:40.16	5.41 ± 0.07	–	25.3 ± 0.2	–	141.4 ± 21.6	–
SHARDS20013688	12:36:12.64	62:13:47.65	5.32 ± 0.07	0.3 ± 0.3	26.8 ± 0.5	0.3 ± 0.3	4.4 ± 2.2	33 ± 26
SHARDS20009678	12:36:12.73	62:14:53.08	4.48 ± 0.07	0.3 ± 0.2	26.3 ± 0.4	0.3 ± 0.2	8.4 ± 3.3	21 ± 15
SHARDS20013577	12:36:13.17	62:13:32.66	4.62 ± 0.07	–	26.3 ± 0.3	–	166.3 ± 49.4	–
SHARDS20013579	12:36:13.18	62:14:20.65	4.08 ± 0.07	–	27.0 ± 0.7	–	2.5 ± 1.7	–
SHARDS20009536	12:36:13.21	62:10:15.86	4.23 ± 0.07	–	26.0 ± 0.1	–	28.9 ± 4.0	–
SHARDS20009758	12:36:13.30	62:10:38.09	3.72 ± 0.06	–	26.8 ± 0.6	–	6.6 ± 3.5	–
SHARDS20005311	12:36:13.30	62:09:07.02	3.76 ± 0.06	–	25.4 ± 0.1	–	9.6 ± 1.4	–
SHARDS20005356	12:36:13.47	62:09:35.74	4.19 ± 0.07	–	25.2 ± 0.1	–	49.2 ± 5.4	–
SHARDS20004106	12:36:13.48	62:09:31.03	3.77 ± 0.06	–	27.0 ± 0.6	–	2.2 ± 1.2	–
SHARDS20011916	12:36:13.75	62:10:11.02	5.57 ± 0.07	–	26.6 ± 0.3	–	34.0 ± 9.1	–
SHARDS20007396	12:36:13.87	62:14:21.36	5.38 ± 0.07	0.2 ± 0.3	25.9 ± 0.0	0.2 ± 0.2	27.3 ± 1.8	6 ± 7
SHARDS20007841	12:36:13.97	62:12:59.26	3.62 ± 0.06	0.2 ± 0.3	27.0 ± 0.7	0.2 ± 0.2	11.2 ± 4.1	6 ± 5
SHARDS20011637	12:36:14.09	62:09:32.79	3.91 ± 0.06	–	25.6 ± 0.1	–	149.0 ± 15.0	–
SHARDS20015984	12:36:14.11	62:09:38.26	4.30 ± 0.07	–	25.6 ± 0.2	–	71.3 ± 8.3	–
SHARDS20007199	12:36:14.30	62:13:46.04	3.90 ± 0.06	–	25.9 ± 0.2	–	103.8 ± 6.6	–
SHARDS20008483	12:36:14.43	62:10:30.94	3.78 ± 0.06	–	25.9 ± 0.2	–	46.2 ± 6.6	–
SHARDS20005148	12:36:14.51	62:11:49.82	3.73 ± 0.06	–	25.7 ± 0.1	–	6.6 ± 2.2	–
SHARDS20005356	12:36:14.57	62:10:40.84	3.85 ± 0.07	–	25.3 ± 0.1	–	18.9 ± 2.4	–
SHARDS20008246	12:36:14.60	62:11:40.40	3.22 ± 0.07	0.1 ± 0.2	26.2 ± 0.3	0.1 ± 0.2	42.7 ± 4.8	5 ± 7
SHARDS20010502	12:36:15.01	62:13:52.20	3.24 ± 0.07	–	26.2 ± 0.3	–	5.5 ± 1.7	–
SHARDS20006670	12:36:15.06	62:13:15.49	4.20 ± 0.08	0.2 ± 0.2	27.5 ± 0.5	0.2 ± 0.2	5.9 ± 1.4	36 ± 31
SHARDS20004964	12:36:15.30	62:11:10.44	4.21 ± 0.07	–	25.4 ± 0.1	–	2.2 ± 1.1	–
SHARDS20006780	12:36:15.33	62:15:07.58	4.63 ± 0.07	–	25.3 ± 0.1	–	201.1 ± 2.5	–
SHARDS20005125	12:36:15.46	62:09:49.27	3.67 ± 0.06	–	26.4 ± 0.5	–	72.1 ± 7.3	–
SHARDS20009668	12:36:15.44	62:13:28.74	3.97 ± 0.06	–	25.1 ± 0.1	–	141.1 ± 5.9	–
SHARDS20007258	12:36:15.51	62:08:38.24	4.80 ± 0.08	–	27.0 ± 1.4	–	543.0 ± 475.2	–
SHARDS20007556	12:36:15.66	62:15:08.23	4.25 ± 0.08	–	25.4 ± 0.1	–	3.2 ± 4.2	–
SHARDS20011087	12:36:15.62	62:15:09.33	3.23 ± 0.07	–	26.7 ± 0.4	–	68.0 ± 7.3	–
SHARDS20006191	12:36:15.63	62:10:52.23	3.99 ± 0.07	–	27.1 ± 0.4	–	8.3 ± 3.3	–
SHARDS20009704	12:36:16.08	62:14:56.83	3.42 ± 0.06	–	26.7 ± 0.9	–	24.8 ± 8.9	–
SHARDS20008109	12:36:16.09	62:09:56.82	4.50 ± 0.07	0.2 ± 0.2	26.1 ± 0.2	0.2 ± 0.2	5.7 ± 4.8	32 ± 25
SHARDS20009709	12:36:16.17	62:09:46.30	4.39 ± 0.06	–	26.9 ± 0.3	–	4.6 ± 7.3	–
SHARDS20006259	12:36:16.29	62:13:29.77	5.12 ± 0.06	0.1 ± 0.2	26.9 ± 0.4	0.1 ± 0.2	25.9 ± 6.9	12 ± 14
SHARDS20008909	12:36:16.74	62:09:36.89	4.20 ± 0.07	0.3 ± 0.3	26.7 ± 0.3	0.2 ± 0.3	185.0 ± 9.4	7 ± 8
SHARDS20008737	12:36:17.15	62:15:11.74	4.64 ± 0.07	–	26.5 ± 0.2	–	44.0 ± 3.1	–
SHARDS20008636	12:36:17.31	62:09:00.14	4.59 ± 0.07	–	25.4 ± 0.1	–	3.8 ± 10.2	–
SHARDS20004861	12:36:17.33	62:14:56.46	3.53 ± 0.06	1.3 ± 0.2	27.4 ± 0.9	1.2 ± 0.1	59.8 ± 2.5	51 ± 10
SHARDS20010163	12:36:17.38	62:10:22.38	3.30 ± 0.06	–	26.1 ± 0.3	–	22.3 ± 2.5	–
SHARDS20007156	12:36:17.54	62:13:16.31	3.66 ± 0.06	0.3 ± 0.3	26.4 ± 0.3	0.3 ± 0.2	20.7 ± 2.0	–
SHARDS20004728	12:36:17.98	62:14:21.93	4.24 ± 0.07	–	24.6 ± 0.1	–	40.7 ± 9.6	16 ± 13
SHARDS20013550	12:36:18.09	62:14:34.68	4.24 ± 0.07	0.3 ± 0.1	–	0.3 ± 0.1	8.6 ± 2.5	–
SHARDS20006793	12:36:18.14	62:11:26.48	4.34 ± 0.06	0.2 ± 0.2	26.0 ± 0.2	0.2 ± 0.2	251.5 ± 22.3	175 ± 77
SHARDS20006476	12:36:18.19	62:10:21.85	5.58 ± 0.07	–	24.8 ± 0.1	–	6.9 ± 1.1	13 ± 10
							195.9 ± 15.7	

Continued on next page

Table A.1 – *Continued from previous page*

Object Name	R.A. (J2000)	Dec. (J2000)	z	$L_{Ly\alpha}$ (10^{42} erg s^{-1})	m_{1500} (AB mag)	$SFR_{L_{Ly\alpha}}$ ($M_\odot$ yr^{-1})	$SFR_{L_{1500}}$ ($M_\odot$ yr^{-1})	EW$_0$ (Å)
SHARDS20008202	12:36:18.55	62:08:14.31	4.30 ± 0.06	–	27.8 ± 0.8	–	1.3 ± 0.9	–
SHARDS20006130	12:36:18.64	62:14:21.42	4.36 ± 0.06	–	26.1 ± 0.2	–	6.2 ± 1.1	–
SHARDS20008283	12:36:18.65	62:13:11.40	4.08 ± 0.07	–	26.1 ± 0.4	–	49.5 ± 17.7	–
SHARDS20007309	12:36:18.78	62:12:00.90	4.90 ± 0.08	0.3 ± 0.3	25.2 ± 0.1	0.3 ± 0.3	17.3 ± 1.6	19 ± 16
SHARDS20006868	12:36:18.83	62:11:23.97	4.22 ± 0.07	–	25.5 ± 0.1	–	83.3 ± 11.4	–
SHARDS20002379	12:36:18.88	62:11:33.33	3.93 ± 0.06	–	24.7 ± 0.1	–	21.3 ± 2.1	–
SHARDS20008952	12:36:18.90	62:12:24.82	5.05 ± 0.06	0.1 ± 0.2	26.4 ± 0.4	0.1 ± 0.2	27.4 ± 10.6	8 ± 12
SHARDS20006498	12:36:18.98	62:08:36.80	3.37 ± 0.07	–	26.1 ± 0.2	–	60.7 ± 11.2	–
SHARDS20006720	12:36:18.99	62:13:59.08	3.95 ± 0.06	–	26.0 ± 0.3	–	28.6 ± 7.5	–
SHARDS20009000	12:36:19.02	62:10:58.34	5.44 ± 0.07	0.5 ± 0.2	26.0 ± 0.1	0.5 ± 0.2	9.7 ± 1.1	56 ± 29
SHARDS20006040	12:36:19.04	62:09:32.39	3.91 ± 0.06	–	25.4 ± 0.1	–	50.1 ± 7.0	–
SHARDS20015457	12:36:19.13	62:08:30.78	5.96 ± 0.07	1.2 ± 0.3	–	1.1 ± 0.2	–	–
SHARDS20007567	12:36:19.16	62:10:49.67	4.33 ± 0.06	0.1 ± 0.2	27.0 ± 0.4	0.1 ± 0.2	3.9 ± 1.4	11 ± 11
SHARDS20016360	12:36:19.16	62:15:23.27	6.72 ± 0.14	–	26.0 ± 0.2	–	37.3 ± 6.5	–
SHARDS20009201	12:36:19.17	62:15:08.83	3.95 ± 0.06	0.3 ± 0.2	26.5 ± 0.1	0.3 ± 0.1	8.6 ± 0.8	59 ± 59
SHARDS20006003	12:36:19.21	62:08:47.39	3.77 ± 0.06	–	25.9 ± 0.2	–	26.9 ± 5.7	–
SHARDS20010699	12:36:19.24	62:15:19.44	4.49 ± 0.07	–	26.4 ± 0.3	–	5.0 ± 1.6	–
SHARDS20009747	12:36:19.35	62:08:39.23	3.90 ± 0.06	0.3 ± 0.2	26.1 ± 0.2	0.3 ± 0.1	5.1 ± 1.2	15 ± 8
SHARDS20013231	12:36:19.40	62:08:27.91	5.71 ± 0.06	–	27.1 ± 0.2	–	10.6 ± 1.8	–
SHARDS20007548	12:36:19.43	62:10:49.55	4.07 ± 0.07	–	25.7 ± 0.2	–	9.5 ± 2.0	–
SHARDS20007432	12:36:19.58	62:10:50.89	4.34 ± 0.06	–	26.1 ± 0.2	–	6.0 ± 1.0	–
SHARDS20014504	12:36:19.75	62:15:25.00	3.26 ± 0.07	–	28.5 ± 0.5	–	1.1 ± 0.6	–
SHARDS20016872	12:36:19.83	62:12:21.85	3.40 ± 0.07	–	27.7 ± 0.6	–	256.5 ± 151.6	–
SHARDS20005235	12:36:19.85	62:14:04.36	3.95 ± 0.06	–	25.1 ± 0.1	–	21.8 ± 2.6	–
SHARDS20018850	12:36:20.14	62:14:13.67	5.33 ± 0.07	–	26.8 ± 0.1	–	4.4 ± 0.5	–
SHARDS20013817	12:36:20.25	62:07:40.89	3.75 ± 0.06	–	27.0 ± 0.7	–	4.4 ± 2.8	–
SHARDS20005304	12:36:20.27	62:12:11.20	4.08 ± 0.07	–	25.4 ± 0.2	–	13.5 ± 2.2	–
SHARDS20006306	12:36:20.29	62:13:59.32	3.81 ± 0.06	–	25.9 ± 0.2	–	7.1 ± 1.6	–
SHARDS20008408	12:36:20.39	62:13:58.54	3.81 ± 0.06	–	25.9 ± 0.2	–	779.1 ± 168.6	–
SHARDS20001139	12:36:20.43	62:09:37.08	3.50 ± 0.06	–	24.3 ± 0.0	–	66.4 ± 5.0	–
SHARDS20007599	12:36:20.48	62:12:45.42	4.91 ± 0.08	1.6 ± 0.3	26.5 ± 0.1	1.5 ± 0.3	10.3 ± 1.2	119 ± 60
SHARDS20007866	12:36:20.61	62:15:32.56	4.91 ± 0.08	–	26.6 ± 0.2	–	5.0 ± 1.1	–
SHARDS20010067	12:36:20.71	62:08:57.88	5.28 ± 0.07	0.8 ± 0.3	26.6 ± 0.7	0.7 ± 0.3	38.2 ± 23.0	59 ± 39
SHARDS20006845	12:36:20.72	62:15:30.57	4.91 ± 0.08	0.3 ± 0.3	27.3 ± 0.5	0.3 ± 0.3	3.6 ± 1.6	17 ± 14
SHARDS20004366	12:36:20.74	62:14:07.82	3.95 ± 0.06	–	25.3 ± 0.1	–	25.5 ± 3.3	–
SHARDS20008363	12:36:20.75	62:08:29.48	4.04 ± 0.07	–	26.1 ± 0.3	–	10.1 ± 3.2	–
SHARDS20006203	12:36:20.93	62:15:05.67	3.41 ± 0.07	–	26.5 ± 0.2	–	2.9 ± 0.7	–
SHARDS20007883	12:36:21.32	62:13:54.84	3.81 ± 0.06	–	26.4 ± 0.4	–	3.7 ± 1.4	–
SHARDS20012642	12:36:21.33	62:09:02.67	4.20 ± 0.07	–	26.3 ± 0.2	–	5.0 ± 1.2	–
SHARDS20013414	12:36:21.38	62:09:04.41	5.73 ± 0.06	–	26.4 ± 0.2	–	12.1 ± 2.1	–
SHARDS20008503	12:36:21.50	62:13:38.89	4.09 ± 0.07	–	26.3 ± 0.5	–	4.8 ± 2.1	–
SHARDS20007440	12:36:21.59	62:12:04.11	3.52 ± 0.06	0.9 ± 0.1	26.4 ± 0.2	0.8 ± 0.1	15.3 ± 3.5	71 ± 22
SHARDS20004772	12:36:21.77	62:11:19.72	5.18 ± 0.06	–	24.0 ± 0.0	–	57.2 ± 3.6	–
SHARDS20006586	12:36:21.85	62:14:30.92	4.09 ± 0.07	–	26.0 ± 0.3	–	18.2 ± 5.7	–
SHARDS20007581	12:36:21.86	62:08:14.23	4.72 ± 0.07	–	26.7 ± 0.5	–	4.0 ± 1.7	–
SHARDS20005050	12:36:21.94	62:15:16.80	4.92 ± 0.08	–	24.7 ± 0.1	–	129.9 ± 10.7	–
SHARDS20012959	12:36:22.03	62:15:13.45	5.78 ± 0.06	0.9 ± 0.2	–	0.8 ± 0.2	–	86 ± 54
SHARDS20005914	12:36:22.12	62:09:57.51	4.33 ± 0.06	–	25.8 ± 0.1	–	82.4 ± 10.9	–

Continued on next page

Table A.1 – *Continued from previous page*

Object Name	R.A. (J2000)	Dec. (J2000)	z	$L_{Ly\alpha}$ (10^{42} erg s^{-1})	m_{1500} (AB mag)	$SFR_{L_{Ly\alpha}}$ ($M_\odot$ yr^{-1})	$SFR_{L_{1500}}$ ($M_\odot$ yr^{-1})	EW$_0$ (Å)
SHARDS20011578	12:36:22.16	62:15:49.38	4.36 ± 0.06	—	27.1 ± 0.4	—	41.9 ± 16.7	—
SHARDS20011882	12:36:22.17	62:09:42.25	3.78 ± 0.06	0.5 ± 0.1	25.7 ± 0.2	0.5 ± 0.1	10.0 ± 1.7	16 ± 4
SHARDS20009497	12:36:22.26	62:15:57.72	4.30 ± 0.07	0.4 ± 0.2	25.5 ± 0.5	0.4 ± 0.2	12.5 ± 5.8	26 ± 14
SHARDS20004970	12:36:22.37	62:13:36.22	4.36 ± 0.06	—	25.4 ± 0.1	—	70.8 ± 7.8	—
SHARDS20012600	12:36:22.44	62:19:51.74	3.21 ± 0.06	0.2 ± 0.1	25.8 ± 0.1	0.2 ± 0.1	17.7 ± 2.4	28 ± 21
SHARDS20012090	12:36:22.52	62:07:53.68	3.26 ± 0.07	0.2 ± 0.1	27.4 ± 0.3	0.2 ± 0.1	3.0 ± 0.8	—
SHARDS20007245	12:36:22.52	62:07:12.90	3.36 ± 0.07	0.2 ± 0.2	26.3 ± 0.3	0.2 ± 0.2	12.6 ± 29.4	28 ± 21
SHARDS20013383	12:36:22.74	62:09:02.85	4.32 ± 0.06	0.2 ± 0.2	26.3 ± 0.2	0.2 ± 0.2	7.7 ± 1.5	12 ± 9
SHARDS20006244	12:36:22.76	62:14:21.67	3.34 ± 0.07	—	25.7 ± 0.1	—	29.3 ± 4.0	—
SHARDS20005080	12:36:22.87	62:14:22.02	3.75 ± 0.06	—	26.7 ± 0.5	—	4.0 ± 1.9	—
SHARDS20005700	12:36:22.93	62:10:02.08	3.79 ± 0.06	1.0 ± 0.2	25.2 ± 0.1	0.9 ± 0.2	74.7 ± 9.6	54 ± 11
SHARDS20006645	12:36:23.06	62:15:56.46	4.51 ± 0.08	—	—	—	—	—
SHARDS20005265	12:36:23.23	62:12:35.48	4.36 ± 0.06	5.2 ± 0.2	26.3 ± 0.2	4.7 ± 0.2	18.5 ± 3.8	153 ± 16
SHARDS20015060	12:36:23.33	62:13:10.72	4.49 ± 0.06	—	27.8 ± 0.5	—	1.5 ± 0.7	—
SHARDS20013787	12:36:23.44	62:16:03.33	5.07 ± 0.06	—	26.7 ± 0.3	—	4.7 ± 2.4	—
SHARDS20013017	12:36:23.44	62:10:53.22	3.65 ± 0.06	—	27.2 ± 0.3	—	4.7 ± 1.3	—
SHARDS20004838	12:36:23.46	62:08:47.47	3.38 ± 0.07	—	25.0 ± 0.1	—	35.5 ± 13.3	—
SHARDS20006466	12:36:23.56	62:15:12.66	3.92 ± 0.08	0.3 ± 0.3	26.1 ± 0.2	0.3 ± 0.3	22.1 ± 8.6	17 ± 14
SHARDS20005566	12:36:23.83	62:14:11.09	3.54 ± 0.06	—	25.8 ± 0.5	—	23.9 ± 3.9	—
SHARDS20012395	12:36:24.01	62:13:43.37	4.65 ± 0.07	—	25.6 ± 0.1	—	13.7 ± 2.0	—
SHARDS20012079	12:36:24.08	62:13:53.06	4.25 ± 0.06	0.6 ± 0.3	25.8 ± 0.1	0.6 ± 0.3	15.0 ± 6.9	40 ± 32
SHARDS20013820	12:36:24.13	62:11:51.24	5.61 ± 0.07	—	26.4 ± 0.2	—	33.4 ± 4.4	—
SHARDS20009710	12:36:24.19	62:09:16.20	4.62 ± 0.06	—	26.4 ± 0.2	—	6.8 ± 1.3	—
SHARDS20013919	12:36:24.21	62:09:20.61	4.32 ± 0.06	—	26.2 ± 0.2	—	5.3 ± 1.0	—
SHARDS20013534	12:36:24.39	62:14:24.61	5.79 ± 0.07	0.5 ± 0.5	25.7 ± 0.1	0.4 ± 0.5	12.5 ± 1.4	91 ± 139
SHARDS20007585	12:36:24.46	62:09:21.26	3.85 ± 0.07	—	26.3 ± 0.2	—	11.1 ± 2.1	—
SHARDS20009337	12:36:24.47	62:15:17.06	3.92 ± 0.06	0.2 ± 0.2	27.3 ± 0.8	0.1 ± 0.1	40.3 ± 43.6	12 ± 11
SHARDS20007133	12:36:24.54	62:10:24.37	3.94 ± 0.06	0.2 ± 0.2	27.3 ± 0.8	0.1 ± 0.1	13.3 ± 2.3	—
SHARDS20005602	12:36:24.67	62:07:39.48	4.30 ± 0.06	2.1 ± 0.3	25.4 ± 0.1	1.9 ± 0.3	13.4 ± 1.4	87 ± 20
SHARDS20007542	12:36:24.70	62:07:39.37	4.53 ± 0.06	0.3 ± 0.3	25.2 ± 0.1	0.3 ± 0.3	354.4 ± 43.0	17 ± 17
SHARDS20010634	12:36:24.70	62:13:50.67	3.06 ± 0.06	—	26.3 ± 0.6	—	30.8 ± 16.2	—
SHARDS20009655	12:36:24.77	62:12:34.77	3.81 ± 0.06	—	26.1 ± 0.3	—	15.7 ± 4.8	—
SHARDS20005714	12:36:25.34	62:11:34.71	4.23 ± 0.07	—	25.4 ± 0.1	—	49.0 ± 6.4	—
SHARDS20006463	12:36:25.42	62:09:05.58	4.32 ± 0.07	—	25.3 ± 0.1	—	34.2 ± 3.3	—
SHARDS20010781	12:36:25.53	62:11:19.80	5.34 ± 0.07	0.4 ± 0.2	—	0.4 ± 0.2	—	78 ± 55
SHARDS20014346	12:36:25.53	62:13:22.13	5.43 ± 0.07	—	27.2 ± 0.2	—	3.1 ± 0.5	—
SHARDS20014826	12:36:25.53	62:15:34.08	5.38 ± 0.07	0.2 ± 0.2	27.0 ± 0.2	0.2 ± 0.2	15.3 ± 2.4	29 ± 27
SHARDS20009609	12:36:25.57	62:07:06.54	3.54 ± 0.07	1.3 ± 0.2	26.6 ± 0.2	1.2 ± 0.2	5.2 ± 0.8	98 ± 32
SHARDS20010591	12:36:25.57	62:15:07.40	3.54 ± 0.06	—	26.2 ± 0.2	—	7.7 ± 1.5	—
SHARDS20010751	12:36:25.59	62:13:10.49	3.95 ± 0.06	0.3 ± 0.2	27.2 ± 0.2	0.3 ± 0.2	3.0 ± 0.5	35 ± 30
SHARDS20004745	12:36:25.75	62:14:36.18	3.45 ± 0.07	—	25.7 ± 0.1	—	75.0 ± 8.0	—
SHARDS20008284	12:36:25.85	62:14:58.87	4.23 ± 0.07	—	25.4 ± 0.1	—	8.5 ± 1.3	—
SHARDS20007379	12:36:25.86	62:07:40.41	4.25 ± 0.07	—	26.4 ± 0.4	—	5.6 ± 1.8	—
SHARDS20008577	12:36:25.86	62:16:10.28	3.68 ± 0.06	0.7 ± 0.1	26.7 ± 0.6	0.7 ± 0.1	8.6 ± 4.9	118 ± 50
SHARDS20000859	12:36:25.92	62:09:03.62	4.32 ± 0.06	—	23.7 ± 0.0	—	110.3 ± 7.1	—
SHARDS20008112	12:36:25.95	62:13:19.37	3.81 ± 0.06	—	26.5 ± 0.4	—	5.7 ± 2.0	—

Continued on next page

Table A.1 – *Continued from previous page*

Object Name	R.A. (J2000)	Dec. (J2000)	z	$L_{Ly\alpha}$ (10^{42} erg s^{-1})	m_{1500} (AB mag)	$SFR_{L_{Ly\alpha}}$ ($M_\odot$ yr^{-1})	$SFR_{L_{1500}}$ ($M_\odot$ yr^{-1})	EW$_0$ (Å)
SHARDS20004779	12:36:25.97	62:08:59.41	4.32 ± 0.06	–	24.4 ± 0.0	–	309.3 ± 22.9	–
SHARDS20005242	12:36:25.99	62:09:00.29	4.32 ± 0.06	–	25.1 ± 0.1	–	109.3 ± 11.6	–
SHARDS20005536	12:36:26.11	62:09:13.23	4.21 ± 0.07	–	25.7 ± 0.1	–	8.7 ± 1.3	–
SHARDS20007108	12:36:26.12	62:09:01.16	4.32 ± 0.06	–	25.3 ± 0.1	–	76.9 ± 9.6	–
SHARDS20014466	12:36:26.16	62:13:38.13	4.65 ± 0.07	–	26.7 ± 0.6	–	21.4 ± 12.1	–
SHARDS20009028	12:36:26.20	62:10:32.55	5.45 ± 0.07	0.4 ± 0.2	26.4 ± 0.3	0.4 ± 0.2	15.5 ± 4.7	28 ± 15
SHARDS20008717	12:36:26.48	62:13:31.59	5.34 ± 0.07	1.0 ± 0.3	26.0 ± 0.1	0.9 ± 0.2	28.7 ± 4.1	129 ± 86
SHARDS20022686	12:36:26.49	62:12:07.43	5.20 ± 0.06	0.2 ± 0.2	25.8 ± 0.2	0.1 ± 0.2	38.9 ± 7.0	23 ± 30
SHARDS20007321	12:36:26.57	62:13:20.93	4.50 ± 0.07	0.9 ± 0.2	–	0.8 ± 0.2	–	74 ± 28
SHARDS20007074	12:36:26.61	62:06:21.09	3.60 ± 0.06	2.0 ± 0.3	26.1 ± 0.5	1.9 ± 0.2	4.6 ± 2.0	217 ± 106
SHARDS20003814	12:36:26.65	62:16:18.82	3.82 ± 0.06	–	26.9 ± 0.5	–	2.9 ± 1.5	–
SHARDS20005090	12:36:26.81	62:08:25.37	3.91 ± 0.06	–	25.2 ± 0.1	–	16.2 ± 2.0	–
SHARDS20005401	12:36:26.81	62:11:03.69	3.25 ± 0.07	–	25.7 ± 0.1	–	49.4 ± 6.0	–
SHARDS20007167	12:36:26.92	62:10:06.22	5.04 ± 0.06	–	25.8 ± 0.2	–	17.1 ± 3.9	–
SHARDS20008172	12:36:26.94	62:13:59.53	3.68 ± 0.06	–	26.6 ± 0.3	–	461.6 ± 145.0	–
SHARDS20015413	12:36:27.02	62:14:50.52	4.92 ± 0.08	–	26.8 ± 0.3	–	26.7 ± 7.3	–
SHARDS20007619	12:36:27.14	62:15:17.86	4.65 ± 0.07	–	26.3 ± 0.1	–	8.5 ± 1.0	–
SHARDS20008187	12:36:27.15	62:12:41.64	4.36 ± 0.06	–	26.7 ± 0.4	–	218.2 ± 75.4	–
SHARDS20007579	12:36:27.22	62:15:17.25	4.50 ± 0.07	0.2 ± 0.2	25.9 ± 0.2	0.2 ± 0.2	12.6 ± 3.0	19 ± 18
SHARDS20012340	12:36:27.22	62:13:39.59	5.07 ± 0.06	–	26.5 ± 0.5	–	26.2 ± 12.6	–
SHARDS20012246	12:36:27.40	62:16:01.87	4.65 ± 0.07	–	27.4 ± 0.4	–	8.6 ± 3.1	–
SHARDS20015624	12:36:27.56	62:13:27.96	6.47 ± 0.11	–	26.1 ± 0.1	–	77.9 ± 7.5	–
SHARDS20011533	12:36:27.66	62:14:32.13	4.10 ± 0.07	–	26.6 ± 0.5	–	7.8 ± 3.9	–
SHARDS20014180	12:36:27.68	62:14:02.77	5.07 ± 0.06	0.3 ± 0.1	–	0.3 ± 0.1	–	–
SHARDS20018314	12:36:27.78	62:14:32.87	3.54 ± 0.06	0.2 ± 0.2	28.3 ± 0.4	0.2 ± 0.1	30.8 ± 12.8	37 ± 41
SHARDS20010477	12:36:27.79	62:12:46.60	4.09 ± 0.07	0.9 ± 0.2	–	0.9 ± 0.1	–	128 ± 50
SHARDS20006528	12:36:27.93	62:14:56.75	3.41 ± 0.07	–	26.7 ± 0.3	–	16.7 ± 4.6	–
SHARDS20005310	12:36:28.03	62:09:01.82	3.92 ± 0.06	0.5 ± 0.2	25.0 ± 0.1	0.4 ± 0.1	40.2 ± 4.4	15 ± 5
SHARDS20011786	12:36:28.07	62:13:19.46	5.34 ± 0.07	–	26.9 ± 0.4	–	4.1 ± 1.4	–
SHARDS20011181	12:36:28.14	62:09:01.52	3.92 ± 0.06	–	25.3 ± 0.2	–	45.7 ± 10.7	–
SHARDS20006518	12:36:28.23	62:09:07.84	4.33 ± 0.06	–	25.9 ± 0.1	–	9.4 ± 1.3	–
SHARDS20008735	12:36:28.26	62:08:50.89	4.21 ± 0.07	–	26.6 ± 0.3	–	102.1 ± 31.5	–
SHARDS20017018	12:36:28.33	62:12:40.94	5.07 ± 0.06	–	26.0 ± 0.2	–	8.4 ± 1.3	–
SHARDS20003920	12:36:28.36	62:15:37.23	3.41 ± 0.07	–	27.1 ± 0.4	–	2.4 ± 0.9	–
SHARDS20010361	12:36:28.42	62:14:16.19	4.92 ± 0.08	0.8 ± 0.2	–	0.8 ± 0.2	–	66 ± 15
SHARDS20007629	12:36:28.58	62:14:10.50	5.34 ± 0.07	–	25.9 ± 0.1	–	10.6 ± 1.4	–
SHARDS20008303	12:36:28.60	62:08:51.41	4.32 ± 0.06	0.1 ± 0.2	25.8 ± 0.1	0.1 ± 0.2	8.0 ± 1.1	13 ± 17
SHARDS20011098	12:36:28.65	62:13:51.70	3.96 ± 0.06	–	27.1 ± 0.6	–	2.1 ± 1.3	–
SHARDS20009271	12:36:28.67	62:14:23.76	5.63 ± 0.07	–	25.6 ± 0.4	–	14.1 ± 5.0	–
SHARDS20005784	12:36:28.67	62:12:29.16	4.09 ± 0.07	–	25.5 ± 0.2	–	383.5 ± 77.3	–
SHARDS20009880	12:36:28.71	62:14:18.75	5.48 ± 0.07	0.5 ± 0.2	25.7 ± 0.1	0.4 ± 0.2	12.6 ± 1.6	24 ± 11
SHARDS20008943	12:36:28.73	62:16:26.97	4.10 ± 0.07	–	26.8 ± 0.6	–	6.5 ± 3.7	–
SHARDS20017665	12:36:28.73	62:16:15.26	3.54 ± 0.06	0.1 ± 0.1	27.3 ± 0.4	0.1 ± 0.1	4.0 ± 1.5	54 ± 66
SHARDS20004921	12:36:28.75	62:12:45.42	4.25 ± 0.07	–	24.8 ± 0.1	–	49.1 ± 4.9	–
SHARDS20010811	12:36:28.81	62:14:19.16	5.79 ± 0.06	–	26.6 ± 0.1	–	6.3 ± 0.5	–
SHARDS20009052	12:36:28.84	62:14:45.19	3.68 ± 0.06	0.2 ± 0.2	27.0 ± 0.5	0.2 ± 0.1	2.1 ± 0.9	21 ± 13
SHARDS20005934	12:36:28.95	62:12:00.28	4.36 ± 0.06	–	25.4 ± 0.1	–	21.2 ± 2.6	–
SHARDS20004937	12:36:29.02	62:06:05.44	4.55 ± 0.07	–	24.8 ± 0.2	–	29.1 ± 6.2	–

Continued on next page

Table A.1 – *Continued from previous page*

Object Name	R.A. (J2000)	Dec. (J2000)	z	$L_{Ly\alpha}$ (10^{42} erg s^{-1})	m_{1500} (AB mag)	$SFR_{L_{Ly\alpha}}$ ($M_\odot$ yr^{-1})	$SFR_{L_{1500}}$ ($M_\odot$ yr^{-1})	EW$_0$ (Å)
SHARDS20012975	12:36:29.16	62:12:38.33	4.92 ± 0.08	–	27.0 ± 0.4	–	3.4 ± 1.3	–
SHARDS20015609	12:36:29.28	62:15:40.74	6.74 ± 0.14	1.5 ± 0.2	–	1.3 ± 0.2	–	201 ± 38
SHARDS20014011	12:36:29.28	62:15:12.99	3.68 ± 0.06	1.0 ± 0.2	23.7 ± 0.1	0.9 ± 0.2	506.9 ± 50.2	7 ± 1
SHARDS20014663	12:36:29.44	62:14:48.30	3.25 ± 0.07	–	26.1 ± 0.2	–	27.4 ± 5.3	–
SHARDS20006963	12:36:29.47	62:14:02.84	3.41 ± 0.07	0.5 ± 0.2	26.5 ± 0.2	0.5 ± 0.2	9.8 ± 2.3	34 ± 12
SHARDS20015840	12:36:29.52	62:12:55.61	3.48 ± 0.07	0.4 ± 0.1	–	0.4 ± 0.1	–	166 ± 95
SHARDS20011428	12:36:29.72	62:12:45.97	4.10 ± 0.07	–	26.7 ± 0.3	–	12.3 ± 3.1	–
SHARDS20014051	12:36:29.73	62:14:45.21	4.59 ± 0.07	–	27.6 ± 0.3	–	1.4 ± 0.4	–
SHARDS20013937	12:36:29.78	62:14:55.23	4.93 ± 0.08	–	26.7 ± 0.3	–	4.5 ± 1.1	–
SHARDS20009067	12:36:29.80	62:14:31.97	5.48 ± 0.07	0.6 ± 0.2	25.8 ± 0.1	0.5 ± 0.2	15.8 ± 2.0	44 ± 19
SHARDS20009220	12:36:29.84	62:09:48.46	4.76 ± 0.07	0.3 ± 0.3	26.1 ± 0.2	0.2 ± 0.1	7.4 ± 1.2	27 ± 29
SHARDS20008664	12:36:29.96	62:12:33.96	3.64 ± 0.06	0.3 ± 0.2	26.3 ± 0.3	0.2 ± 0.1	11.1 ± 2.2	25 ± 17
SHARDS20006940	12:36:29.96	62:16:56.01	4.39 ± 0.07	0.5 ± 0.2	25.4 ± 0.3	0.5 ± 0.2	13.2 ± 3.5	33 ± 13
SHARDS20008724	12:36:29.96	62:16:31.70	4.36 ± 0.07	–	26.2 ± 0.3	–	5.9 ± 1.6	–
SHARDS20007258	12:36:29.96	62:06:21.49	3.56 ± 0.06	–	26.9 ± 0.5	–	3.2 ± 2.5	–
SHARDS20007915	12:36:30.03	62:15:45.14	3.74 ± 0.06	–	27.1 ± 0.5	–	9.9 ± 4.2	–
SHARDS20012785	12:36:30.14	62:16:29.46	4.37 ± 0.07	0.2 ± 0.3	27.4 ± 0.5	0.2 ± 0.2	2.0 ± 1.0	30 ± 43
SHARDS20006234	12:36:30.18	62:14:45.89	4.75 ± 0.07	0.2 ± 0.3	26.3 ± 0.1	0.2 ± 0.2	6.0 ± 0.8	9 ± 8
SHARDS20006371	12:36:30.20	62:15:05.88	3.68 ± 0.06	0.6 ± 0.2	26.2 ± 0.8	0.6 ± 0.1	32.0 ± 2.8	39 ± 12
SHARDS20007936	12:36:30.21	62:13:06.97	3.95 ± 0.07	–	25.1 ± 0.1	–	5.2 ± 4.1	–
SHARDS20011499	12:36:30.22	62:14:14.84	5.63 ± 0.07	0.2 ± 0.2	25.6 ± 0.1	0.2 ± 0.2	23.6 ± 2.7	14 ± 13
SHARDS20006583	12:36:30.27	62:06:15.94	4.11 ± 0.07	0.7 ± 0.2	26.2 ± 0.2	0.7 ± 0.2	11.5 ± 1.1	70 ± 35
SHARDS20008593	12:36:30.38	62:09:59.21	4.18 ± 0.06	–	26.2 ± 0.3	–	29.2 ± 6.6	–
SHARDS20007608	12:36:30.44	62:06:45.08	4.34 ± 0.06	–	26.8 ± 0.3	–	14.0 ± 4.5	–
SHARDS20007578	12:36:30.49	62:06:15.82	3.48 ± 0.07	–	25.7 ± 0.2	–	7.8 ± 1.2	–
SHARDS20006377	12:36:30.53	62:15:41.06	3.32 ± 0.06	–	26.7 ± 0.3	–	4.0 ± 1.1	–
SHARDS20013370	12:36:30.58	62:13:27.90	3.37 ± 0.06	–	26.0 ± 0.1	–	22.1 ± 3.4	–
SHARDS20013497	12:36:30.61	62:16:36.69	3.26 ± 0.07	–	27.1 ± 0.3	–	2.8 ± 0.8	–
SHARDS20009182	12:36:30.70	62:09:21.43	4.15 ± 0.08	–	27.3 ± 1.0	–	4.8 ± 4.5	–
SHARDS20006461	12:36:30.75	62:14:46.51	4.18 ± 0.07	0.3 ± 0.3	27.2 ± 0.4	0.3 ± 0.3	5.1 ± 2.1	40 ± 49
SHARDS20014141	12:36:30.77	62:14:26.61	4.62 ± 0.07	–	26.7 ± 0.6	–	3.4 ± 1.8	–
SHARDS20009549	12:36:30.93	62:15:53.05	3.62 ± 0.07	0.2 ± 0.1	–	0.2 ± 0.1	–	49 ± 26
SHARDS20011794	12:36:30.96	62:12:16.70	3.59 ± 0.07	0.2 ± 0.3	27.3 ± 0.7	0.4 ± 0.2	1.3 ± 0.9	50 ± 41
SHARDS20003443	12:36:31.06	62:12:15.59	3.54 ± 0.06	0.2 ± 0.2	26.1 ± 0.5	0.2 ± 0.2	9.4 ± 4.0	36 ± 49
SHARDS20005365	12:36:31.16	62:16:52.21	3.56 ± 0.06	–	25.3 ± 0.1	–	67.0 ± 6.6	–
SHARDS20001522	12:36:31.23	62:10:17.49	3.46 ± 0.06	0.4 ± 0.2	25.8 ± 0.2	0.4 ± 0.1	39.2 ± 6.4	16 ± 6
SHARDS20007926	12:36:31.25	62:08:58.50	3.06 ± 0.07	0.7 ± 0.2	25.4 ± 0.4	0.6 ± 0.2	12.2 ± 1.7	103 ± 77
SHARDS20005124	12:36:31.31	62:10:38.67	3.54 ± 0.07	–	25.3 ± 0.1	–	149.9 ± 18.2	–
SHARDS20005442	12:36:31.45	62:15:43.90	4.43 ± 0.08	–	25.6 ± 0.2	–	20.7 ± 2.7	–
SHARDS20008033	12:36:31.47	62:16:13.18	4.23 ± 0.08	–	27.3 ± 0.6	–	34.7 ± 8.3	–
SHARDS20009733	12:36:31.56	62:10:35.27	4.25 ± 0.07	–	26.3 ± 0.3	–	3.1 ± 1.8	–
SHARDS20008713	12:36:31.65	62:12:33.13	4.23 ± 0.07	0.2 ± 0.2	26.7 ± 0.6	0.1 ± 0.2	237.3 ± 66.6	–
SHARDS20008610	12:36:31.69	62:09:23.82	5.30 ± 0.07	–	25.6 ± 0.2	–	3.4 ± 1.5	29 ± 36
SHARDS20010033	12:36:31.89	62:12:23.15	4.50 ± 0.07	–	25.7 ± 0.2	–	10.5 ± 4.2	–
SHARDS20005557	12:36:31.89	62:16:05.15	3.82 ± 0.06	0.2 ± 0.2	27.0 ± 0.6	0.2 ± 0.2	22.8 ± 9.6	44 ± 79
SHARDS20011759	12:36:31.97	62:13:39.03	4.37 ± 0.06	0.1 ± 0.2	26.7 ± 0.3	0.1 ± 0.2	214.3 ± 61.0	19 ± 31
SHARDS20008719	12:36:32.00							

Continued on next page

Table A.1 – *Continued from previous page*

Object Name	R.A. (J2000)	Dec. (J2000)	z	$L_{Ly\alpha}$ (10^{42} erg s^{-1})	m_{1500} (AB mag)	$SFR_{L_{Ly\alpha}}$ ($M_\odot$ yr^{-1})	$SFR_{L_{1500}}$ ($M_\odot$ yr^{-1})	EW$_0$ (Å)
SHARDS20003435	12:36:32.03	62:12:11.26	3.41 ± 0.07	–	25.0 ± 0.1	–	76.5 ± 8.6	–
SHARDS20015534	12:36:32.09	62:14:41.94	6.05 ± 0.07	0.3 ± 0.1	–	0.2 ± 0.1	–	–
SHARDS20009699	12:36:32.13	62:16:33.62	3.96 ± 0.06	–	27.7 ± 1.6	–	1.3 ± 1.9	–
SHARDS20004892	12:36:32.15	62:14:32.75	3.69 ± 0.06	–	25.2 ± 0.1	–	78.2 ± 8.7	–
SHARDS20014601	12:36:32.21	62:16:07.35	3.55 ± 0.06	–	25.1 ± 0.1	–	211.7 ± 25.4	–
SHARDS20001223	12:36:32.24	62:09:46.44	3.65 ± 0.06	0.5 ± 0.1	25.3 ± 0.1	0.5 ± 0.1	52.7 ± 6.3	15 ± 4
SHARDS20008098	12:36:32.26	62:06:23.05	4.28 ± 0.06	–	26.0 ± 0.1	–	6.9 ± 1.0	–
SHARDS20003820	12:36:32.28	62:16:20.46	3.59 ± 0.06	0.7 ± 0.4	25.2 ± 0.1	0.7 ± 0.3	25.2 ± 2.6	16 ± 7
SHARDS20015345	12:36:32.31	62:14:49.39	5.63 ± 0.07	–	26.7 ± 0.1	–	24.8 ± 2.9	–
SHARDS20005143	12:36:32.34	62:16:07.04	3.83 ± 0.06	0.3 ± 0.2	24.6 ± 0.1	0.3 ± 0.2	155.4 ± 15.2	7 ± 5
SHARDS20007115	12:36:32.50	62:13:31.31	5.35 ± 0.07	–	25.3 ± 0.1	–	18.3 ± 1.7	–
SHARDS20010860	12:36:32.62	62:12:17.31	3.54 ± 0.06	0.1 ± 0.1	27.0 ± 0.4	0.1 ± 0.1	8.8 ± 3.4	31 ± 26
SHARDS20006942	12:36:32.62	62:14:45.42	3.83 ± 0.06	0.3 ± 0.1	26.2 ± 0.3	0.3 ± 0.1	9.3 ± 2.6	22 ± 9
SHARDS20007420	12:36:32.69	62:11:30.52	5.33 ± 0.07	0.8 ± 0.3	26.7 ± 0.4	0.7 ± 0.3	5.1 ± 1.9	26 ± 10
SHARDS20007442	12:36:32.73	62:08:56.45	4.21 ± 0.07	–	27.3 ± 0.6	–	4.1 ± 2.4	–
SHARDS20006041	12:36:32.88	62:16:44.23	3.87 ± 0.06	0.3 ± 0.2	25.6 ± 0.2	0.3 ± 0.2	21.2 ± 3.4	22 ± 13
SHARDS20014837	12:36:32.93	62:15:38.32	5.63 ± 0.07	0.7 ± 0.1	–	0.6 ± 0.0	–	108 ± 45
SHARDS20006098	12:36:33.06	62:09:13.45	4.22 ± 0.07	–	25.4 ± 0.1	–	11.8 ± 1.4	–
SHARDS20004876	12:36:33.07	62:12:30.30	3.54 ± 0.06	–	25.0 ± 0.1	–	185.8 ± 17.7	–
SHARDS20006745	12:36:33.17	62:05:54.30	4.01 ± 0.07	–	25.6 ± 0.3	–	8.9 ± 2.1	–
SHARDS20009074	12:36:33.18	62:15:04.40	3.69 ± 0.06	–	25.8 ± 0.3	–	26.8 ± 7.9	–
SHARDS20018848	12:36:33.20	62:13:11.47	4.25 ± 0.07	0.3 ± 0.1	–	0.3 ± 0.1	–	85 ± 49
SHARDS20005122	12:36:33.35	62:09:06.98	4.33 ± 0.06	–	25.1 ± 0.1	–	274.2 ± 24.2	–
SHARDS20017954	12:36:33.36	62:12:32.35	4.79 ± 0.07	–	27.9 ± 0.8	–	3.2 ± 2.3	–
SHARDS20013652	12:36:33.41	62:14:15.85	5.49 ± 0.07	–	26.9 ± 0.3	–	11.2 ± 3.4	–
SHARDS20014367	12:36:33.43	62:12:40.76	5.48 ± 0.07	–	26.9 ± 0.1	–	21.9 ± 2.7	–
SHARDS20007475	12:36:33.43	62:06:40.43	5.12 ± 0.06	–	26.2 ± 0.7	–	73.4 ± 46.1	–
SHARDS20004846	12:36:33.50	62:14:18.13	3.42 ± 0.07	–	25.1 ± 0.1	–	14.9 ± 1.6	–
SHARDS20011204	12:36:33.56	62:15:02.17	3.42 ± 0.07	–	27.4 ± 0.2	–	1.3 ± 0.3	–
SHARDS20006430	12:36:33.70	62:10:53.74	5.05 ± 0.06	0.7 ± 0.2	25.7 ± 0.2	0.7 ± 0.2	43.2 ± 9.5	24 ± 9
SHARDS20006329	12:36:33.74	62:12:30.87	3.54 ± 0.06	0.1 ± 0.2	26.2 ± 0.2	0.1 ± 0.2	14.5 ± 3.1	6 ± 7
SHARDS20003862	12:36:33.81	62:16:50.35	3.60 ± 0.06	–	24.9 ± 0.1	–	64.2 ± 6.1	–
SHARDS20007523	12:36:33.87	62:14:33.83	4.11 ± 0.07	–	23.9 ± 0.1	–	225.0 ± 21.5	–
SHARDS20018734	12:36:33.91	62:14:04.51	3.69 ± 0.06	0.4 ± 0.1	–	0.4 ± 0.1	–	90 ± 57
SHARDS20010324	12:36:33.97	62:11:25.02	5.62 ± 0.07	1.5 ± 0.3	–	1.4 ± 0.2	–	121 ± 75
SHARDS20011652	12:36:34.03	62:15:30.25	4.83 ± 0.08	0.4 ± 0.0	–	0.3 ± 0.0	–	–
SHARDS20007910	12:36:34.20	62:17:08.55	5.22 ± 0.06	0.1 ± 0.2	25.8 ± 0.1	0.1 ± 0.2	22.4 ± 2.1	10 ± 17
SHARDS20016606	12:36:34.22	62:12:28.22	3.41 ± 0.07	–	27.6 ± 0.6	–	42.3 ± 24.7	–
SHARDS20010727	12:36:34.37	62:15:56.35	3.42 ± 0.07	–	27.9 ± 0.8	–	2.4 ± 1.9	–
SHARDS20014645	12:36:34.38	62:10:47.54	5.61 ± 0.07	–	26.5 ± 0.2	–	36.4 ± 7.3	–
SHARDS20005159	12:36:34.40	62:05:46.52	3.59 ± 0.06	1.0 ± 0.3	24.8 ± 0.1	0.9 ± 0.2	95.4 ± 14.1	27 ± 7
SHARDS20007099	12:36:34.43	62:13:15.61	4.10 ± 0.07	0.6 ± 0.2	26.0 ± 0.3	0.5 ± 0.1	23.8 ± 7.0	103 ± 52
SHARDS20009822	12:36:34.44	62:15:23.10	3.97 ± 0.06	0.2 ± 0.1	–	0.2 ± 0.1	–	72 ± 38
SHARDS20008016	12:36:34.46	62:16:49.98	4.28 ± 0.06	–	26.6 ± 0.3	–	4.2 ± 1.2	–
SHARDS20014022	12:36:34.53	62:14:18.27	4.38 ± 0.06	–	27.4 ± 0.3	–	2.0 ± 0.5	–
SHARDS20004907	12:36:34.85	62:07:47.34	4.31 ± 0.06	–	24.9 ± 0.1	–	40.4 ± 3.4	–
SHARDS20009487	12:36:34.87	62:12:45.35	4.37 ± 0.06	–	26.6 ± 0.1	–	20.6 ± 2.9	–
SHARDS20018593	12:36:34.88	62:13:27.45	4.66 ± 0.07	–	27.1 ± 0.3	–	2.7 ± 0.8	–

Continued on next page

Table A.1 – *Continued from previous page*

Object Name	R.A. (J2000)	Dec. (J2000)	z	$L_{Ly\alpha}$ (10^{42} erg s^{-1})	m_{1500} (AB mag)	$SFR_{L_{Ly\alpha}}$ ($M_\odot$ yr^{-1})	$SFR_{L_{1500}}$ ($M_\odot$ yr^{-1})	EW$_0$ (Å)
SHARDS20013502	12:36:34.96	62:15:51.29	5.35 ± 0.07	0.4 ± 0.3	26.5 ± 0.2	0.3 ± 0.2	35.3 ± 8.1	53 ± 57
SHARDS20008208	12:36:35.12	62:13:15.27	3.41 ± 0.07	0.4 ± 0.2	26.8 ± 0.1	0.4 ± 0.2	2.3 ± 0.3	29 ± 12
SHARDS20005147	12:36:35.13	62:16:10.46	3.55 ± 0.06	—	25.6 ± 0.3	—	31.5 ± 9.4	—
SHARDS20005244	12:36:35.13	62:12:55.24	4.25 ± 0.07	—	25.9 ± 0.1	—	49.2 ± 12.3	—
SHARDS20002745	12:36:35.14	62:07:29.75	3.89 ± 0.06	—	24.3 ± 0.0	—	164.2 ± 22.8	—
SHARDS20005761	12:36:35.23	62:07:43.65	4.37 ± 0.06	—	25.4 ± 0.1	—	20.5 ± 2.1	—
SHARDS20005801	12:36:35.28	62:15:04.02	3.37 ± 0.06	0.2 ± 0.1	25.3 ± 0.6	0.1 ± 0.1	25.8 ± 3.5	6 ± 4
SHARDS20008841	12:36:35.41	62:06:45.04	5.39 ± 0.07	0.7 ± 0.2	26.1 ± 0.2	0.6 ± 0.2	8.9 ± 4.9	37 ± 12
SHARDS20006033	12:36:35.44	62:13:51.02	4.38 ± 0.06	—	26.0 ± 0.2	—	7.7 ± 1.3	—
SHARDS20006253	12:36:35.49	62:13:49.96	4.51 ± 0.07	—	26.4 ± 0.4	—	14.7 ± 6.0	—
SHARDS20005252	12:36:35.52	62:13:12.89	4.10 ± 0.07	0.9 ± 0.2	24.8 ± 0.1	0.8 ± 0.1	149.6 ± 16.2	67 ± 17
SHARDS20007856	12:36:35.57	62:14:16.38	3.74 ± 0.07	1.1 ± 0.2	26.7 ± 0.1	1.0 ± 0.1	4.4 ± 0.5	—
SHARDS20007051	12:36:35.70	62:15:26.10	3.33 ± 0.06	0.3 ± 0.2	26.0 ± 0.2	0.3 ± 0.1	107.4 ± 17.1	34 ± 20
SHARDS20008325	12:36:35.83	62:14:26.07	3.63 ± 0.08	—	25.2 ± 0.2	—	22.9 ± 4.1	—
SHARDS20005944	12:36:35.84	62:12:20.77	3.95 ± 0.07	0.7 ± 0.1	25.8 ± 0.2	0.7 ± 0.1	61.2 ± 3.6	39 ± 9
SHARDS20009748	12:36:35.86	62:13:54.72	3.35 ± 0.07	0.4 ± 0.3	25.9 ± 0.1	0.4 ± 0.2	24.5 ± 3.0	26 ± 17
SHARDS20005134	12:36:36.08	62:11:54.16	3.74 ± 0.07	—	25.6 ± 0.1	—	229.7 ± 30.0	—
SHARDS20005504	12:36:36.10	62:08:02.17	3.91 ± 0.06	—	25.1 ± 0.1	—	17.8 ± 2.3	—
SHARDS20005728	12:36:36.13	62:06:01.44	3.91 ± 0.06	—	25.4 ± 0.1	—	16.1 ± 2.3	—
SHARDS20017781	12:36:36.21	62:15:50.45	3.65 ± 0.07	—	26.6 ± 0.2	—	5.2 ± 0.8	—
SHARDS20010035	12:36:36.29	62:12:47.02	3.64 ± 0.06	1.1 ± 0.1	26.0 ± 0.2	1.0 ± 0.1	31.3 ± 5.5	122 ± 22
SHARDS20006167	12:36:36.40	62:16:20.70	3.94 ± 0.07	2.3 ± 0.2	26.3 ± 0.5	2.1 ± 0.2	4.6 ± 2.2	101 ± 15
SHARDS20005480	12:36:36.45	62:07:34.79	4.19 ± 0.07	0.7 ± 0.2	27.2 ± 0.1	0.6 ± 0.2	16.9 ± 1.7	18 ± 5
SHARDS20017750	12:36:36.48	62:07:34.72	4.75 ± 0.14	0.5 ± 0.2	27.2 ± 0.5	0.4 ± 0.2	25.8 ± 11.3	45 ± 18
SHARDS20009692	12:36:36.69	62:05:55.70	3.67 ± 0.06	—	26.4 ± 0.3	—	5.3 ± 2.4	—
SHARDS20007149	12:36:36.79	62:06:42.47	3.62 ± 0.06	0.5 ± 0.1	26.4 ± 0.3	0.4 ± 0.1	7.3 ± 1.8	54 ± 22
SHARDS20009506	12:36:36.92	62:16:47.49	3.25 ± 0.06	—	25.9 ± 0.2	—	35.8 ± 6.4	—
SHARDS20010086	12:36:37.02	62:14:32.87	3.55 ± 0.06	—	26.4 ± 0.2	—	19.2 ± 4.2	—
SHARDS20009072	12:36:37.04	62:14:58.89	3.09 ± 0.06	0.2 ± 0.3	26.6 ± 0.5	0.1 ± 0.2	5.2 ± 2.4	19 ± 34
SHARDS20013821	12:36:37.15	62:14:48.38	4.64 ± 0.07	—	27.9 ± 1.6	—	1.6 ± 0.9	—
SHARDS20007136	12:36:37.16	62:15:47.49	4.04 ± 0.07	—	27.3 ± 1.0	—	2.2 ± 2.0	—
SHARDS20012571	12:36:37.18	62:15:51.62	3.36 ± 0.07	—	27.0 ± 0.6	—	5.9 ± 3.4	—
SHARDS20008722	12:36:37.21	62:07:41.08	4.26 ± 0.07	—	25.7 ± 0.2	—	25.1 ± 4.2	—
SHARDS20018981	12:36:37.22	62:15:32.41	4.67 ± 0.07	—	27.7 ± 1.1	—	1.5 ± 0.2	—
SHARDS20013416	12:36:37.23	62:15:34.70	4.16 ± 0.07	—	27.6 ± 1.1	—	3.0 ± 3.1	—
SHARDS20016990	12:36:37.27	62:17:01.26	6.49 ± 0.11	—	26.9 ± 0.1	—	26.2 ± 2.9	—
SHARDS20005023	12:36:37.33	62:16:10.49	4.09 ± 0.07	—	26.1 ± 0.2	—	554.2 ± 98.9	—
SHARDS20010716	12:36:37.34	62:11:51.53	5.62 ± 0.07	—	27.0 ± 0.2	—	4.0 ± 0.4	—
SHARDS20012087	12:36:37.50	62:14:06.96	3.97 ± 0.06	0.5 ± 0.2	27.1 ± 0.1	0.4 ± 0.1	467.3 ± 68.2	63 ± 37
SHARDS20009737	12:36:37.52	62:12:36.02	3.21 ± 0.06	—	26.5 ± 0.1	—	18.8 ± 1.7	—
SHARDS20011958	12:36:37.64	62:11:51.78	5.63 ± 0.07	—	25.6 ± 0.1	—	42.0 ± 3.4	—
SHARDS20010441	12:36:37.71	62:13:39.20	4.17 ± 0.07	0.4 ± 0.2	26.8 ± 0.1	0.3 ± 0.2	2.9 ± 0.3	77 ± 65
SHARDS20006108	12:36:37.76	62:06:22.18	4.57 ± 0.07	—	26.0 ± 0.1	—	25.6 ± 3.1	—
SHARDS20011333	12:36:37.79	62:16:25.00	5.69 ± 0.06	0.5 ± 0.2	26.6 ± 0.1	0.4 ± 0.2	25.9 ± 0.5	46 ± 27
SHARDS20010952	12:36:37.79	62:10:33.40	5.78 ± 0.06	—	25.8 ± 0.1	—	12.5 ± 0.8	—
SHARDS20011853	12:36:37.84	62:15:33.46	3.55 ± 0.06	—	27.5 ± 0.7	—	3.0 ± 1.8	—

Continued on next page

Table A.1 – *Continued from previous page*

Object Name	R.A. (J2000)	Dec. (J2000)	z	$L_{Ly\alpha}$ (10^{42} erg s^{-1})	m_{1500} (AB mag)	$SFR_{L_{Ly\alpha}}$ ($M_\odot$ yr^{-1})	$SFR_{L_{1500}}$ ($M_\odot$ yr^{-1})	EW_0 (Å)
SHARDS20010554	12:36:37.96	62:14:42.71	3.55 ± 0.06	–	26.1 ± 0.2	–	31.3 ± 5.9	–
SHARDS20018746	12:36:37.98	62:16:42.32	6.26 ± 0.14	0.6 ± 0.2	27.8 ± 0.1	0.5 ± 0.2	2.2 ± 0.4	117 ± 41
SHARDS20011004	12:36:38.02	62:12:57.49	3.55 ± 0.06	0.2 ± 0.1	27.3 ± 0.5	0.2 ± 0.1	10.2 ± 4.9	36 ± 30
SHARDS20000132	12:36:38.17	62:06:55.71	3.62 ± 0.06	–	23.9 ± 0.0	–	204.1 ± 15.0	–
SHARDS20016319	12:36:38.18	62:16:01.73	4.41 ± 0.06	–	26.1 ± 0.3	–	6.3 ± 1.8	–
SHARDS20005393	12:36:38.30	62:07:16.68	3.76 ± 0.06	–	25.2 ± 0.1	–	26.6 ± 3.4	–
SHARDS20013533	12:36:38.42	62:15:27.18	5.22 ± 0.06	–	27.9 ± 1.0	–	11.2 ± 9.8	–
SHARDS20008360	12:36:38.45	62:16:34.43	4.03 ± 0.07	0.1 ± 0.2	26.7 ± 0.1	0.1 ± 0.2	3.1 ± 0.3	17 ± 23
SHARDS20015718	12:36:38.59	62:07:10.07	3.90 ± 0.06	–	26.3 ± 0.3	–	55.9 ± 16.2	–
SHARDS20009925	12:36:38.60	62:11:38.23	3.82 ± 0.06	0.3 ± 0.1	–	0.3 ± 0.1	–	86 ± 80
SHARDS20012961	12:36:38.76	62:15:24.93	4.67 ± 0.07	–	27.4 ± 0.3	–	5.0 ± 1.3	–
SHARDS20006289	12:36:38.84	62:16:26.35	4.29 ± 0.07	–	26.1 ± 0.2	–	26.0 ± 5.4	–
SHARDS20008424	12:36:38.87	62:08:31.22	3.78 ± 0.06	–	26.4 ± 0.4	–	58.6 ± 20.2	–
SHARDS20016074	12:36:38.92	62:15:49.71	6.26 ± 0.14	–	25.3 ± 0.1	–	79.5 ± 10.0	–
SHARDS20016977	12:36:39.18	62:14:16.21	4.67 ± 0.07	–	26.9 ± 0.2	–	31.9 ± 5.7	–
SHARDS20009701	12:36:39.19	62:12:32.87	4.66 ± 0.07	0.2 ± 0.2	26.8 ± 0.1	0.1 ± 0.2	8.0 ± 1.0	21 ± 31
SHARDS20006131	12:36:39.24	62:11:02.15	4.24 ± 0.07	–	25.7 ± 0.2	–	26.7 ± 6.2	–
SHARDS20011505	12:36:39.25	62:14:40.11	4.51 ± 0.07	–	26.9 ± 0.2	–	3.7 ± 0.7	–
SHARDS20007965	12:36:39.26	62:13:26.42	3.97 ± 0.06	0.6 ± 0.2	26.2 ± 0.4	0.6 ± 0.2	7.6 ± 2.6	86 ± 60
SHARDS10010677	12:36:39.27	62:17:51.27	4.43 ± 0.07	–	27.6 ± 0.2	–	1.9 ± 0.4	–
SHARDS20006502	12:36:39.27	62:09:03.22	4.22 ± 0.07	1.1 ± 0.2	25.6 ± 0.2	1.0 ± 0.1	49.3 ± 7.7	59 ± 16
SHARDS20008538	12:36:39.35	62:12:16.16	3.68 ± 0.06	0.4 ± 0.2	27.7 ± 0.9	0.4 ± 0.1	3.2 ± 2.8	39 ± 15
SHARDS20025308	12:36:39.37	62:17:30.11	3.62 ± 0.06	–	26.3 ± 0.3	–	6.8 ± 1.7	–
SHARDS20005445	12:36:39.57	62:12:30.50	3.41 ± 0.07	–	26.2 ± 0.2	–	83.1 ± 16.7	–
SHARDS10016190	12:36:39.60	62:18:00.67	6.64 ± 0.14	–	26.6 ± 0.1	–	17.0 ± 2.0	–
SHARDS20011322	12:36:39.66	62:14:06.76	5.08 ± 0.06	0.2 ± 0.2	27.0 ± 0.7	0.2 ± 0.2	3.6 ± 2.5	17 ± 19
SHARDS20006896	12:36:39.72	62:11:47.35	4.10 ± 0.07	–	26.2 ± 0.4	–	23.7 ± 8.7	–
SHARDS20018364	12:36:39.79	62:11:07.78	4.92 ± 0.08	0.9 ± 0.4	–	0.8 ± 0.4	–	80 ± 82
SHARDS20014454	12:36:39.92	62:13:55.54	3.55 ± 0.06	0.1 ± 0.1	27.7 ± 0.2	0.1 ± 0.1	116.3 ± 25.1	21 ± 33
SHARDS20005752	12:36:40.03	62:11:11.80	4.37 ± 0.06	–	26.3 ± 0.3	–	20.6 ± 5.4	–
SHARDS20007090	12:36:40.04	62:07:38.84	4.05 ± 0.07	–	25.8 ± 0.3	–	13.8 ± 3.3	–
SHARDS20013998	12:36:40.09	62:16:04.11	5.94 ± 0.07	–	27.5 ± 0.1	–	4.5 ± 0.6	–
SHARDS20009272	12:36:40.13	62:12:01.21	4.50 ± 0.07	–	27.3 ± 0.8	–	2.6 ± 1.9	–
SHARDS10007510	12:36:40.17	62:18:01.73	4.43 ± 0.07	0.2 ± 0.1	–	0.2 ± 0.1	–	–
SHARDS20011183	12:36:40.18	62:12:28.78	5.21 ± 0.06	0.8 ± 0.3	–	0.7 ± 0.3	–	80 ± 75
SHARDS20012102	12:36:40.21	62:14:22.20	4.51 ± 0.07	–	26.6 ± 0.4	–	9.8 ± 3.7	–
SHARDS20013477	12:36:40.27	62:09:36.73	5.32 ± 0.07	0.4 ± 0.2	26.6 ± 0.5	0.4 ± 0.2	7.4 ± 3.2	41 ± 27
SHARDS20012613	12:36:40.32	62:13:54.01	4.51 ± 0.07	–	26.5 ± 0.4	–	5.2 ± 1.8	–
SHARDS20015077	12:36:40.32	62:13:51.09	3.42 ± 0.07	–	29.3 ± 0.6	–	4.2 ± 2.4	–
SHARDS20018778	12:36:40.45	62:11:33.02	5.48 ± 0.07	0.4 ± 0.1	–	0.4 ± 0.1	–	144 ± 92
SHARDS20007281	12:36:40.47	62:10:43.17	3.53 ± 0.06	–	26.0 ± 0.2	–	32.1 ± 6.2	–
SHARDS20006527	12:36:40.59	62:06:33.75	3.89 ± 0.06	0.3 ± 0.2	25.2 ± 0.1	0.2 ± 0.1	36.4 ± 4.8	13 ± 7
SHARDS20008030	12:36:40.68	62:10:36.13	5.20 ± 0.06	0.7 ± 0.3	–	0.6 ± 0.3	–	64 ± 64
SHARDS20015721	12:36:40.71	62:16:37.44	5.92 ± 0.06	0.1 ± 0.1	28.0 ± 0.2	0.0 ± 0.1	2.5 ± 0.5	11 ± 14
SHARDS20006417	12:36:40.76	62:16:38.26	4.99 ± 0.06	–	25.2 ± 0.2	–	97.4 ± 17.8	–
SHARDS20005144	12:36:40.77	62:16:54.82	3.76 ± 0.06	–	25.4 ± 0.1	–	69.7 ± 8.8	–
SHARDS20009559	12:36:40.77	62:09:17.88	4.76 ± 0.07	–	25.8 ± 0.1	–	9.4 ± 1.2	–
SHARDS20011570	12:36:40.78	62:15:10.53	4.85 ± 0.08	–	27.1 ± 0.1	–	2.9 ± 0.4	–

Continued on next page

Table A.1 – *Continued from previous page*

Object Name	R.A. (J2000)	Dec. (J2000)	z	$L_{Ly\alpha}$ (10^{42} erg s^{-1})	m_{1500} (AB mag)	$SFR_{L_{Ly\alpha}}$ ($M_\odot$ yr^{-1})	$SFR_{L_{1500}}$ ($M_\odot$ yr^{-1})	EW$_0$ (Å)
SHARDS20008514	12:36:40.82	62:17:36.45	3.69 ± 0.06	—	26.1 ± 0.2	—	6.3 ± 1.4	—
SHARDS20006201	12:36:40.83	62:17:28.66	3.37 ± 0.07	—	25.9 ± 0.1	—	37.6 ± 5.5	—
SHARDS20005243	12:36:40.90	62:16:42.07	4.34 ± 0.07	—	25.2 ± 0.1	—	67.8 ± 7.7	—
SHARDS20012597	12:36:40.91	62:15:16.92	4.34 ± 0.06	—	26.8 ± 0.3	—	15.1 ± 4.6	—
SHARDS20002926	12:36:40.96	62:09:25.38	3.39 ± 0.07	—	24.6 ± 0.0	—	72.7 ± 7.2	—
SHARDS20002829	12:36:41.08	62:17:00.04	3.37 ± 0.07	—	25.3 ± 0.1	—	38.4 ± 4.1	—
SHARDS20002853	12:36:41.22	62:17:50.01	3.62 ± 0.06	0.3 ± 0.2	27.4 ± 0.3	0.3 ± 0.2	17.6 ± 5.6	62 ± 64
SHARDS20012856	12:36:41.25	62:16:39.96	3.62 ± 0.06	0.3 ± 0.2	27.4 ± 0.2	0.3 ± 0.2	2.0 ± 0.4	62 ± 64
SHARDS20002639	12:36:41.37	62:09:25.33	3.32 ± 0.07	—	26.3 ± 0.4	—	7.0 ± 2.4	—
SHARDS20006219	12:36:41.44	62:16:41.57	4.18 ± 0.07	—	25.8 ± 0.2	—	7.5 ± 1.5	—
SHARDS10012055	12:36:41.47	62:18:22.55	3.49 ± 0.06	0.3 ± 0.2	26.6 ± 0.3	0.3 ± 0.2	3.8 ± 0.9	19 ± 10
SHARDS20002821	12:36:41.52	62:17:47.22	3.40 ± 0.07	0.3 ± 0.2	25.5 ± 0.3	0.3 ± 0.2	28.5 ± 7.8	19 ± 10
SHARDS20008022	12:36:41.52	62:06:54.43	4.59 ± 0.07	—	26.9 ± 0.2	—	17.3 ± 3.2	—
SHARDS20013063	12:36:41.67	62:11:58.47	4.50 ± 0.07	—	26.5 ± 0.4	—	19.8 ± 7.3	—
SHARDS20017407	12:36:41.67	62:17:45.95	3.90 ± 0.07	2.1 ± 0.1	27.5 ± 0.7	1.9 ± 0.1	2.9 ± 1.9	42 ± 17
SHARDS20008308	12:36:41.68	62:18:47.24	3.19 ± 0.06	0.4 ± 0.1	27.6 ± 0.3	0.3 ± 0.1	9.5 ± 2.6	42 ± 17
SHARDS10005829	12:36:41.89	62:17:27.41	4.25 ± 0.07	—	27.9 ± 0.2	—	4.8 ± 0.6	—
SHARDS20013579	12:36:41.96	62:18:14.65	4.25 ± 0.14	1.0 ± 0.2	27.9 ± 0.2	0.9 ± 0.2	20.4 ± 3.2	155 ± 46
SHARDS20005917	12:36:42.03	62:07:34.62	6.16 ± 0.06	—	25.7 ± 0.1	—	15.7 ± 1.8	—
SHARDS20016077	12:36:42.03	62:16:36.16	3.76 ± 0.14	—	25.7 ± 0.2	—	20.3 ± 6.1	—
SHARDS20019075	12:36:42.06	62:07:01.17	3.76 ± 0.06	—	26.4 ± 0.3	—	14.2 ± 6.6	—
SHARDS20014836	12:36:42.14	62:16:30.96	3.88 ± 0.06	—	27.0 ± 0.1	—	14.2 ± 9.4	—
SHARDS20007667	12:36:42.15	62:16:10.97	5.48 ± 0.07	1.0 ± 0.2	25.6 ± 0.1	0.9 ± 0.2	80.9 ± 9.4	42 ± 13
SHARDS20004867	12:36:42.17	62:15:23.01	3.25 ± 0.06	—	24.6 ± 0.1	—	185.2 ± 20.9	—
SHARDS10006528	12:36:42.23	62:17:28.05	3.37 ± 0.07	—	27.1 ± 0.3	—	4.7 ± 1.5	—
SHARDS20011685	12:36:42.40	62:09:10.61	3.59 ± 0.07	—	26.6 ± 0.1	—	9.1 ± 3.0	—
SHARDS20010845	12:36:42.47	62:09:06.21	5.09 ± 0.06	—	27.0 ± 1.2	—	9.1 ± 5.3	—
SHARDS20008900	12:36:42.51	62:15:10.22	4.62 ± 0.06	—	26.2 ± 0.5	—	8.6 ± 0.6	—
SHARDS20008670	12:36:42.60	62:15:04.38	4.62 ± 0.07	0.2 ± 0.2	25.6 ± 0.5	0.2 ± 0.1	22.6 ± 13.2	8 ± 5
SHARDS20015099	12:36:42.69	62:13:55.38	4.50 ± 0.11	—	27.1 ± 0.1	—	24.9 ± 3.7	—
SHARDS20016040	12:36:42.73	62:07:25.18	5.30 ± 0.06	—	27.3 ± 0.2	—	24.5 ± 3.8	—
SHARDS20006187	12:36:42.87	62:09:58.14	3.67 ± 0.06	—	24.3 ± 0.1	—	43.5 ± 683.3	—
SHARDS20005617	12:36:42.98	62:09:57.91	3.67 ± 0.06	—	25.6 ± 0.2	—	153.1 ± 25.0	—
SHARDS20022667	12:36:42.96	62:10:18.35	4.75 ± 0.07	0.6 ± 0.2	25.6 ± 0.2	0.6 ± 0.2	6.8 ± 1.4	27 ± 10
SHARDS20017639	12:36:43.00	62:16:33.20	4.75 ± 0.14	—	26.2 ± 0.2	—	74.2 ± 17.8	—
SHARDS20006281	12:36:43.03	62:17:35.20	4.69 ± 0.07	0.2 ± 0.3	25.8 ± 0.2	0.2 ± 0.3	26.8 ± 9.9	8 ± 10
SHARDS10007206	12:36:43.03	62:17:33.10	5.49 ± 0.07	0.5 ± 0.2	26.0 ± 0.4	0.5 ± 0.2		29 ± 11
SHARDS20007272	12:36:43.04	62:07:10.09	4.19 ± 0.07	1.8 ± 0.0		1.7 ± 0.0		
SHARDS20006911	12:36:43.05	62:07:12.60	4.04 ± 0.07	—	25.8 ± 0.2	—	15.5 ± 2.6	—
SHARDS20003769	12:36:43.06	62:16:35.96	3.48 ± 0.06	—	26.2 ± 0.4	—	16.6 ± 5.9	—
SHARDS20007839	12:36:43.10	62:10:44.76	4.56 ± 0.07	—	24.6 ± 0.1	—	68.2 ± 5.6	—
SHARDS20005338	12:36:43.12	62:11:05.05	3.67 ± 0.06	—	25.5 ± 0.2	—	4.1 ± 0.6	—
SHARDS10005604	12:36:43.20	62:17:29.05	3.90 ± 0.06	0.4 ± 0.2	25.6 ± 0.1	0.4 ± 0.1	15.9 ± 3.9	13 ± 5
SHARDS20007846	12:36:43.31	62:14:17.46	3.83 ± 0.06	0.8 ± 0.1	26.6 ± 0.4	0.8 ± 0.1	3.8 ± 2.2	77 ± 21
SHARDS20025361	12:36:43.38	62:16:56.06	3.40 ± 0.07	0.2 ± 0.2	26.5 ± 0.2	0.2 ± 0.2	26.4 ± 4.3	10 ± 12
SHARDS10005410	12:36:43.48	62:18:56.89	4.40 ± 0.07	0.5 ± 0.2	25.2 ± 0.2	0.4 ± 0.2	10.4 ± 2.6	10 ± 4
SHARDS10016909	12:36:43.44	62:18:10.46	4.44 ± 0.07	0.5 ± 0.2	25.2 ± 0.2	0.4 ± 0.2	14.6 ± 4.5	66 ± 46
SHARDS20004706	12:36:43.54	62:11:21.40	3.54 ± 0.06	—	27.2 ± 1.1	—	1131.1 ± 99.0	

Continued on next page

Table A.1 – *Continued from previous page*

Object Name	R.A. (J2000)	Dec. (J2000)	z	$L_{Ly\alpha}$ (10^{42} erg s^{-1})	m_{1500} (AB mag)	$SFR_{L_{Ly\alpha}}$ ($M_\odot$ yr^{-1})	$SFR_{L_{1500}}$ ($M_\odot$ yr^{-1})	EW_0 (Å)
SHARDS20017692	12:36:43.64	62:13:53.69	3.97 ± 0.06	–	26.7 ± 0.4	–	3.2 ± 1.3	–
SHARDS20004872	12:36:43.85	62:12:41.55	4.51 ± 0.07	–	25.1 ± 0.1	–	35.3 ± 4.2	–
SHARDS10011362	12:36:43.94	62:18:31.67	4.59 ± 0.07	0.2 ± 0.3	26.8 ± 0.2	0.2 ± 0.2	9.3 ± 2.1	19 ± 25
SHARDS20008756	12:36:43.98	62:15:07.31	3.75 ± 0.06	–	25.8 ± 0.2	–	6.4 ± 1.3	–
SHARDS20013486	12:36:44.04	62:13:14.23	5.64 ± 0.07	–	27.0 ± 0.1	–	3.9 ± 0.4	–
SHARDS10008371	12:36:44.17	62:17:09.32	4.19 ± 0.07	0.6 ± 0.1	–	0.6 ± 0.1	–	119 ± 38
SHARDS20011466	12:36:44.19	62:07:00.43	4.19 ± 0.07	–	27.9 ± 1.1	–	1.2 ± 1.1	–
SHARDS10033454	12:36:44.20	62:17:41.38	3.38 ± 0.07	–	25.1 ± 0.1	–	40.4 ± 4.1	–
SHARDS20006730	12:36:44.26	62:11:17.56	3.96 ± 0.06	–	25.6 ± 0.2	–	40.7 ± 7.1	–
SHARDS20014151	12:36:44.31	62:11:44.77	5.35 ± 0.07	0.5 ± 0.3	–	0.5 ± 0.3	–	63 ± 49
SHARDS20012331	12:36:44.34	62:16:23.86	4.43 ± 0.07	0.3 ± 0.2	25.7 ± 0.2	0.3 ± 0.2	100.0 ± 17.3	35 ± 25
SHARDS20005215	12:36:44.38	62:10:03.66	3.81 ± 0.06	–	24.8 ± 0.1	–	831.0 ± 88.9	–
SHARDS20000232	12:36:44.44	62:07:22.69	4.20 ± 0.07	–	25.0 ± 0.1	–	64.8 ± 7.4	–
SHARDS20018507	12:36:44.45	62:09:20.15	5.18 ± 0.06	0.3 ± 0.3	26.5 ± 0.4	0.2 ± 0.3	5.9 ± 2.1	24 ± 30
SHARDS20010705	12:36:44.45	62:15:17.40	4.29 ± 0.06	–	26.4 ± 0.2	–	4.8 ± 1.0	–
SHARDS20013762	12:36:44.47	62:14:19.55	3.42 ± 0.07	–	27.2 ± 0.4	–	1.8 ± 0.8	–
SHARDS20008158	12:36:44.50	62:07:04.36	4.19 ± 0.07	–	26.2 ± 0.2	–	5.6 ± 1.2	–
SHARDS20014762	12:36:44.55	62:12:36.14	5.36 ± 0.07	–	27.0 ± 0.4	–	3.8 ± 1.3	–
SHARDS20011334	12:36:44.65	62:10:40.00	3.54 ± 0.06	0.3 ± 0.2	26.3 ± 0.3	0.2 ± 0.2	21.0 ± 6.2	39 ± 37
SHARDS20005176	12:36:44.67	62:11:50.54	4.66 ± 0.07	–	24.7 ± 0.1	–	216.0 ± 24.5	–
SHARDS20008534	12:36:44.69	62:13:52.46	3.42 ± 0.07	–	27.2 ± 0.5	–	3.9 ± 1.7	–
SHARDS20018297	12:36:44.73	62:12:18.91	5.91 ± 0.06	0.3 ± 0.1	27.6 ± 0.3	0.3 ± 0.1	2.6 ± 0.6	–
SHARDS10008064	12:36:44.80	62:17:05.69	3.77 ± 0.06	–	27.0 ± 0.5	–	4.4 ± 2.1	–
SHARDS20006062	12:36:45.00	62:07:42.89	3.78 ± 0.06	0.3 ± 0.1	26.0 ± 0.2	0.3 ± 0.1	78.6 ± 17.2	35 ± 16
SHARDS20011766	12:36:45.02	62:14:20.84	4.62 ± 0.07	–	26.7 ± 0.2	–	25.1 ± 4.5	–
SHARDS20005942	12:36:45.13	62:11:06.78	4.10 ± 0.07	0.4 ± 0.2	25.8 ± 0.3	0.4 ± 0.2	52.1 ± 13.2	39 ± 18
SHARDS20010821	12:36:45.15	62:14:16.28	4.39 ± 0.06	–	27.4 ± 0.2	–	1.9 ± 0.4	–
SHARDS20009923	12:36:45.18	62:11:14.59	3.82 ± 0.06	–	26.7 ± 0.1	–	8.0 ± 1.0	–
SHARDS20009185	12:36:45.19	62:09:32.16	3.94 ± 0.06	–	26.7 ± 0.3	–	3.2 ± 0.8	–
SHARDS20005675	12:36:45.20	62:09:33.70	4.35 ± 0.06	1.0 ± 0.2	26.2 ± 0.3	0.9 ± 0.2	7.7 ± 1.9	86 ± 39
SHARDS20008968	12:36:45.22	62:09:58.04	3.25 ± 0.07	0.5 ± 0.1	26.5 ± 0.2	0.4 ± 0.1	46.2 ± 9.1	104 ± 47
SHARDS20005675	12:36:45.24	62:09:34.08	4.35 ± 0.06	–	25.9 ± 0.2	–	10.6 ± 2.0	–
SHARDS10006879	12:36:45.24	62:17:07.39	3.22 ± 0.07	–	26.1 ± 0.2	–	34.3 ± 5.8	–
SHARDS20022705	12:36:45.32	62:16:11.68	5.54 ± 0.07	–	26.5 ± 0.1	–	6.3 ± 0.6	–
SHARDS10012658	12:36:45.39	62:18:02.37	5.42 ± 0.07	0.2 ± 0.2	26.1 ± 0.3	0.2 ± 0.2	13.1 ± 4.3	38 ± 47
SHARDS20010734	12:36:45.68	62:14:11.77	3.97 ± 0.06	0.4 ± 0.1	–	0.3 ± 0.1	–	135 ± 115
SHARDS10009632	12:36:45.71	62:17:53.70	3.77 ± 0.06	0.4 ± 0.2	27.3 ± 0.7	0.3 ± 0.2	2.8 ± 1.8	93 ± 84
SHARDS20004663	12:36:45.75	62:14:21.86	3.42 ± 0.07	–	24.7 ± 0.0	–	91.6 ± 8.9	–
SHARDS20012625	12:36:45.91	62:11:58.27	5.63 ± 0.07	0.7 ± 0.2	26.5 ± 0.1	0.6 ± 0.2	6.4 ± 0.6	55 ± 36
SHARDS20009303	12:36:45.94	62:11:11.13	4.65 ± 0.07	–	26.3 ± 0.4	–	16.5 ± 6.5	–
SHARDS20009104	12:36:46.01	62:15:36.93	4.27 ± 0.07	–	26.7 ± 0.1	–	13.2 ± 1.9	–
SHARDS20007885	12:36:46.07	62:14:48.87	3.75 ± 0.06	–	26.0 ± 0.5	–	74.5 ± 35.1	–
SHARDS20015308	12:36:46.08	62:13:16.95	5.22 ± 0.06	–	26.6 ± 0.2	–	9.0 ± 2.0	–
SHARDS20004843	12:36:46.16	62:07:01.52	4.44 ± 0.07	–	25.0 ± 0.1	–	43.1 ± 4.9	–
SHARDS10017518	12:36:46.19	62:16:40.90	3.22 ± 0.07	0.2 ± 0.2	26.6 ± 0.3	0.2 ± 0.2	8.8 ± 2.7	36 ± 29
SHARDS10009131	12:36:46.20	62:17:28.52	3.91 ± 0.06	–	27.3 ± 0.1	–	1.7 ± 0.2	–
SHARDS20008584	12:36:46.26	62:11:34.47	3.41 ± 0.07	–	26.6 ± 0.3	–	5.1 ± 1.3	–
SHARDS10005302	12:36:46.26	62:16:12.63	3.62 ± 0.06	–	25.0 ± 0.1	–	70.5 ± 7.4	–

Continued on next page

Table A.1 – *Continued from previous page*

Object Name	R.A. (J2000)	Dec. (J2000)	z	$L_{Ly\alpha}$ (10^{42} erg s^{-1})	m_{1500} (AB mag)	$\mathrm{SFR}_{L_{Ly\alpha}}$ ($M_\odot$ yr^{-1})	$\mathrm{SFR}_{L_{1500}}$ ($M_\odot$ yr^{-1})	EW$_0$ (Å)
SHARDS20009371	12:36:46.36	62:15:10.22	4.29 ± 0.06	–	26.7 ± 0.1	–	3.7 ± 0.5	–
SHARDS20012762	12:36:46.38	62:15:04.07	4.61 ± 0.06	0.4 ± 0.2	–	0.4 ± 0.2	–	113 ± 79
SHARDS20005762	12:36:46.39	62:15:13.44	4.03 ± 0.07	1.0 ± 0.2	25.7 ± 0.3	0.9 ± 0.2	9.5 ± 2.6	39 ± 10
SHARDS20017660	12:36:46.41	62:15:01.08	4.88 ± 0.08	0.6 ± 0.1	–	0.5 ± 0.1	–	203 ± 63
SHARDS20015606	12:36:46.44	62:15:47.96	3.32 ± 0.07	–	26.5 ± 0.2	–	172.5 ± 37.9	–
SHARDS20004611	12:36:46.49	62:17:58.42	4.20 ± 0.07	0.9 ± 0.2	–	0.9 ± 0.2	–	72 ± 40
SHARDS20004965	12:36:46.67	62:17:30.08	3.33 ± 0.06	0.6 ± 0.1	–	0.5 ± 0.1	–	109 ± 54
SHARDS20007442	12:36:46.69	62:15:17.12	3.36 ± 0.07	1.1 ± 0.2	25.1 ± 0.1	1.0 ± 0.2	32.4 ± 3.3	31 ± 7
SHARDS20007344	12:36:46.74	62:16:28.28	4.33 ± 0.06	–	26.4 ± 0.2	–	5.6 ± 1.1	–
SHARDS20002930	12:36:46.84	62:17:07.52	3.22 ± 0.07	–	24.7 ± 0.0	–	94.8 ± 9.0	–
SHARDS20005039	12:36:46.85	62:07:02.48	3.90 ± 0.06	–	26.7 ± 0.3	–	8.5 ± 2.6	–
SHARDS20005095	12:36:46.87	62:16:59.23	3.31 ± 0.07	–	25.4 ± 0.1	–	91.6 ± 10.9	–
SHARDS20006693	12:36:46.87	62:07:27.26	4.27 ± 0.07	0.1 ± 0.2	25.2 ± 0.3	0.1 ± 0.2	0.9 ± 0.3	13 ± 15
SHARDS20010364	12:36:46.89	62:07:08.71	4.31 ± 0.07	0.2 ± 0.2	25.4 ± 0.7	0.1 ± 0.2	17.6 ± 11.2	10 ± 9
SHARDS20000366	12:36:46.99	62:07:18.07	3.23 ± 0.07	–	25.0 ± 0.1	–	17.6 ± 1.9	–
SHARDS20006145	12:36:47.02	62:07:46.80	3.43 ± 0.07	–	25.3 ± 0.1	–	20.2 ± 2.3	–
SHARDS20005856	12:36:47.03	62:16:48.71	3.44 ± 0.07	–	25.6 ± 0.1	–	27.4 ± 3.8	–
SHARDS20007155	12:36:47.04	62:13:43.17	3.95 ± 0.06	–	25.9 ± 0.2	–	39.9 ± 4.7	–
SHARDS20016717	12:36:47.07	62:07:58.08	3.20 ± 0.06	0.9 ± 0.3	26.8 ± 0.2	0.9 ± 0.3	6.8 ± 1.5	57 ± 23
SHARDS20007641	12:36:47.13	62:07:53.98	3.24 ± 0.07	0.5 ± 0.2	26.3 ± 0.3	0.4 ± 0.2	4.6 ± 2.0	50 ± 35
SHARDS10010013	12:36:47.26	62:16:04.40	3.41 ± 0.07	–	25.9 ± 0.3	–	10.3 ± 2.5	–
SHARDS20010356	12:36:47.30	62:15:17.40	3.68 ± 0.06	–	27.2 ± 0.2	–	5.9 ± 1.1	–
SHARDS20010488	12:36:47.37	62:16:13.06	3.01 ± 0.07	–	26.5 ± 0.3	–	3.2 ± 0.9	–
SHARDS20016530	12:36:47.38	62:13:36.07	4.23 ± 0.06	1.1 ± 0.2	–	1.0 ± 0.2	–	169 ± 77
SHARDS10006930	12:36:47.42	62:13:37.80	3.23 ± 0.06	–	26.7 ± 0.1	–	23.4 ± 2.8	–
SHARDS20009832	12:36:47.42	62:16:00.25	3.64 ± 0.06	–	26.3 ± 0.3	–	6.0 ± 1.5	–
SHARDS20005249	12:36:47.45	62:11:50.64	3.94 ± 0.06	–	27.1 ± 0.5	–	113.2 ± 47.8	–
SHARDS20015243	12:36:47.47	62:10:53.79	3.40 ± 0.07	0.2 ± 0.3	–	0.2 ± 0.3	–	35 ± 83
SHARDS20006335	12:36:47.66	62:15:02.07	4.52 ± 0.07	–	25.2 ± 0.1	–	46.9 ± 5.8	–
SHARDS10018017	12:36:47.69	62:17:16.93	4.32 ± 0.06	–	27.9 ± 1.6	–	1.4 ± 2.0	–
SHARDS20008709	12:36:47.70	62:17:06.33	4.57 ± 0.06	–	27.1 ± 0.4	–	2.5 ± 0.9	–
SHARDS20005017	12:36:47.74	62:15:09.17	3.54 ± 0.06	–	25.8 ± 0.1	–	33.9 ± 4.0	–
SHARDS20007137	12:36:47.75	62:09:35.59	3.04 ± 0.06	–	25.4 ± 0.5	–	44.3 ± 4.9	–
SHARDS20004537	12:36:47.99	62:09:43.35	5.18 ± 0.06	6.9 ± 0.3	23.5 ± 0.0	6.3 ± 0.3	228.2 ± 13.1	35 ± 3
SHARDS20011372	12:36:48.00	62:12:40.25	4.93 ± 0.06	0.6 ± 0.3	23.8 ± 0.0	0.5 ± 0.3	8.2 ± 3.6	68 ± 55
SHARDS20009288	12:36:48.06	62:13:45.72	4.52 ± 0.08	–	–	–	–	–
SHARDS10010985	12:36:48.06	62:19:02.53	3.64 ± 0.06	0.7 ± 0.2	26.9 ± 0.6	0.6 ± 0.2	6.7 ± 3.7	63 ± 29
SHARDS20008788	12:36:48.13	62:15:33.99	3.54 ± 0.07	1.0 ± 0.3	26.6 ± 0.3	0.9 ± 0.3	7.2 ± 1.0	73 ± 53
SHARDS20007738	12:36:48.15	62:14:33.55	3.56 ± 0.06	–	26.7 ± 0.1	–	36.9 ± 4.0	–
SHARDS10012429	12:36:48.22	62:16:37.43	3.38 ± 0.07	–	26.9 ± 0.4	–	1.6 ± 0.5	–
SHARDS10013979	12:36:48.25	62:16:30.67	3.63 ± 0.06	–	27.2 ± 0.6	–	8.2 ± 4.3	–
SHARDS20015260	12:36:48.25	62:09:39.44	4.63 ± 0.07	–	27.1 ± 0.3	–	2.7 ± 0.7	–
SHARDS20009821	12:36:48.33	62:13:20.43	3.56 ± 0.06	0.1 ± 0.1	27.2 ± 0.5	0.1 ± 0.1	5.1 ± 2.2	44 ± 46
SHARDS20018558	12:36:48.32	62:15:03.75	3.93 ± 0.06	0.3 ± 0.2	–	0.3 ± 0.1	–	134 ± 77
SHARDS20008926	12:36:48.36	62:15:31.10	3.76 ± 0.06	–	26.7 ± 0.4	–	9.6 ± 3.3	–
SHARDS20009870	12:36:48.38	62:12:17.29	3.36 ± 0.07	–	27.0 ± 0.4	–	16.3 ± 5.8	–
SHARDS20017589	12:36:48.38	62:09:45.55	3.33 ± 0.06	–	26.7 ± 0.4	–	962.6 ± 370.1	–

Continued on next page

Table A.1 – *Continued from previous page*

Object Name	R.A. (J2000)	Dec. (J2000)	z	$L_{Ly\alpha}$ (10^{42} erg s^{-1})	m_{1500} (AB mag)	$SFR_{L_{Ly\alpha}}$ ($M_\odot$ yr^{-1})	$SFR_{L_{1500}}$ ($M_\odot$ yr^{-1})	EW_0 (Å)
SHARDS10005025	12:36:48.41	62:16:42.96	4.19 ± 0.07	–	24.6 ± 0.1	–	102.3 ± 9.9	–
SHARDS10007239	12:36:48.50	62:19:05.66	4.61 ± 0.07	0.3 ± 0.2	26.2 ± 0.1	0.3 ± 0.2	11.4 ± 1.6	32 ± 32
SHARDS10010315	12:36:48.55	62:18:13.55	3.50 ± 0.06	0.3 ± 0.1	–	0.3 ± 0.1	–	101 ± 101
SHARDS20012717	12:36:48.60	62:11:20.03	4.66 ± 0.07	1.2 ± 0.3	–	1.1 ± 0.3	–	106 ± 49
SHARDS10016735	12:36:48.62	62:16:31.85	6.65 ± 0.14	–	27.3 ± 0.1	–	4.2 ± 0.7	–
SHARDS20013849	12:36:48.73	62:15:16.74	4.04 ± 0.07	–	27.2 ± 0.1	–	1.9 ± 0.3	–
SHARDS20007005	12:36:48.74	62:08:10.32	4.88 ± 0.08	–	25.3 ± 0.1	–	89.1 ± 9.1	–
SHARDS20019079	12:36:48.79	62:11:25.25	4.25 ± 0.07	–	27.1 ± 0.6	–	2.4 ± 1.2	–
SHARDS20014914	12:36:48.84	62:07:20.62	5.15 ± 0.06	0.3 ± 0.3	26.7 ± 0.4	0.3 ± 0.3	12.5 ± 4.3	23 ± 24
SHARDS20016700	12:36:48.84	62:07:40.74	6.19 ± 0.14	–	25.8 ± 0.2	–	77.1 ± 17.5	–
SHARDS20009301	12:36:48.87	62:12:44.45	4.67 ± 0.07	–	27.3 ± 0.9	–	2.2 ± 1.9	–
SHARDS20011033	12:36:48.89	62:11:25.80	4.66 ± 0.07	–	26.5 ± 0.5	–	9.1 ± 4.6	–
SHARDS10003033	12:36:48.90	62:18:25.50	3.38 ± 0.07	–	25.3 ± 0.1	–	27.9 ± 3.0	–
SHARDS20006572	12:36:48.93	62:09:08.90	3.66 ± 0.06	0.5 ± 0.1	26.1 ± 0.2	0.4 ± 0.1	22.9 ± 4.9	54 ± 21
SHARDS10008432	12:36:48.93	62:18:53.77	4.89 ± 0.08	1.2 ± 0.2	–	1.1 ± 0.1	–	89 ± 12
SHARDS20006140	12:36:48.96	62:11:52.88	4.66 ± 0.07	–	26.8 ± 0.6	–	9.0 ± 4.7	–
SHARDS20011008	12:36:48.98	62:15:22.31	4.52 ± 0.07	–	27.6 ± 0.5	–	1.6 ± 0.7	–
SHARDS20007006	12:36:49.10	62:13:30.59	4.39 ± 0.06	–	26.4 ± 0.2	–	21.7 ± 4.8	–
SHARDS20011601	12:36:49.11	62:10:22.14	3.81 ± 0.06	0.2 ± 0.1	–	0.2 ± 0.1	–	52 ± 46
SHARDS20025409	12:36:49.13	62:15:52.01	3.90 ± 0.06	–	27.6 ± 0.1	–	1.3 ± 0.2	–
SHARDS20010215	12:36:49.20	62:09:47.18	3.94 ± 0.06	–	26.5 ± 0.5	–	39.9 ± 18.1	–
SHARDS20005370	12:36:49.23	62:15:38.56	5.14 ± 0.06	–	25.9 ± 0.1	–	18.2 ± 2.4	–
SHARDS20010078	12:36:49.32	62:07:34.66	5.02 ± 0.06	–	25.9 ± 0.3	–	9.7 ± 2.7	–
SHARDS20005850	12:36:49.49	62:14:21.22	3.36 ± 0.07	2.1 ± 0.3	25.4 ± 0.1	1.9 ± 0.3	16.3 ± 1.9	81 ± 16
SHARDS20011401	12:36:49.59	62:08:55.75	3.52 ± 0.06	–	26.6 ± 0.3	–	21.0 ± 5.4	–
SHARDS20006378	12:36:49.60	62:07:57.85	4.88 ± 0.08	–	26.1 ± 0.2	–	20.0 ± 3.4	–
SHARDS20006571	12:36:49.60	62:15:24.42	4.18 ± 0.07	–	26.0 ± 0.2	–	6.8 ± 1.5	–
SHARDS20013746	12:36:49.62	62:10:39.01	5.79 ± 0.06	0.4 ± 0.1	25.9 ± 0.1	0.3 ± 0.1	66.9 ± 4.5	–
SHARDS10009609	12:36:49.65	62:18:13.26	3.23 ± 0.07	0.3 ± 0.2	26.9 ± 0.3	0.3 ± 0.2	3.9 ± 1.2	48 ± 38
SHARDS20002756	12:36:49.66	62:13:28.74	3.42 ± 0.07	–	25.5 ± 0.1	–	27.3 ± 3.5	–
SHARDS20013107	12:36:49.79	62:10:45.01	5.21 ± 0.06	0.9 ± 0.3	26.5 ± 0.1	0.8 ± 0.3	5.7 ± 0.8	60 ± 40
SHARDS10008730	12:36:49.79	62:15:52.02	4.30 ± 0.06	–	26.4 ± 0.1	–	8.0 ± 1.1	–
SHARDS20011530	12:36:49.87	62:12:47.71	5.36 ± 0.07	–	25.2 ± 0.1	–	126.7 ± 11.3	–
SHARDS10008171	12:36:49.87	62:18:24.07	3.64 ± 0.06	–	26.6 ± 0.3	–	22.2 ± 7.0	–
SHARDS20008753	12:36:49.88	62:08:05.02	3.65 ± 0.06	–	25.8 ± 0.2	–	455.5 ± 75.7	–
SHARDS20011732	12:36:49.92	62:09:30.09	5.46 ± 0.07	–	25.6 ± 0.2	–	13.4 ± 2.2	–
SHARDS20014293	12:36:49.97	62:13:55.66	5.81 ± 0.06	0.5 ± 0.3	26.7 ± 0.1	0.5 ± 0.2	5.3 ± 0.5	42 ± 34
SHARDS20008210	12:36:49.97	62:09:53.61	5.33 ± 0.07	0.8 ± 0.4	25.6 ± 0.2	0.7 ± 0.3	42.4 ± 6.7	55 ± 32
SHARDS20008207	12:36:50.05	62:07:34.37	5.16 ± 0.06	–	26.3 ± 0.2	–	6.7 ± 1.4	–
SHARDS10012647	12:36:50.05	62:18:00.52	3.50 ± 0.06	–	27.3 ± 0.3	–	2.7 ± 0.7	–
SHARDS20010714	12:36:50.08	62:14:33.82	3.61 ± 0.06	0.4 ± 0.2	27.1 ± 0.6	0.4 ± 0.2	3.3 ± 1.7	85 ± 86
SHARDS10006314	12:36:50.17	62:16:25.21	3.38 ± 0.07	–	26.4 ± 0.2	–	5.4 ± 1.0	–
SHARDS20006375	12:36:50.22	62:11:19.14	3.96 ± 0.06	–	26.3 ± 0.3	–	8.4 ± 2.5	–
SHARDS10008675	12:36:50.30	62:16:23.20	4.05 ± 0.07	–	–	0.4 ± 0.1	–	55 ± 34
SHARDS20009900	12:36:50.32	62:12:26.14	5.49 ± 0.07	–	26.5 ± 0.2	–	7.5 ± 1.6	–
SHARDS10007578	12:36:50.42	62:18:57.95	4.21 ± 0.07	0.2 ± 0.2	27.2 ± 0.7	0.2 ± 0.1	76.0 ± 48.1	46 ± 48
SHARDS20011638	12:36:50.48	62:12:50.42	4.38 ± 0.06	0.4 ± 0.1	–	0.4 ± 0.1	–	92 ± 79
SHARDS10017724	12:36:50.55	62:18:16.87	3.64 ± 0.06	–	26.6 ± 0.3	–	2.9 ± 0.9	–

Continued on next page

Table A.1 – *Continued from previous page*

Object Name	R.A.	Dec.	z	$L_{\mathrm{Ly}\alpha}$	m_{1500}	$\mathrm{SFR}_{L_{\mathrm{Ly}\alpha}}$	$\mathrm{SFR}_{L_{1500}}$	EW_0
	(J2000)	(J2000)		(10^{42} erg s^{-1})	(AB mag)	($M_\odot$ yr^{-1})	($M_\odot$ yr^{-1})	(Å)
SHARDS20012497	12:36:50.61	62:10:52.38	4.92 ± 0.08	0.3 ± 0.3	26.1 ± 0.2	0.3 ± 0.2	47.4 ± 8.5	67 ± 78
SHARDS20005660	12:36:50.68	62:09:32.47	4.24 ± 0.07	–	25.9 ± 0.2	–	36.6 ± 7.1	–
SHARDS20010568	12:36:50.85	62:11:08.32	4.37 ± 0.06	0.2 ± 0.2	26.6 ± 0.2	0.2 ± 0.2	4.9 ± 0.8	28 ± 26
SHARDS20011030	12:36:50.85	62:11:26.61	3.82 ± 0.06	–	27.4 ± 0.1	–	1.6 ± 0.2	–
SHARDS20007436	12:36:50.86	62:09:04.67	3.80 ± 0.06	–	26.4 ± 0.4	–	371.1 ± 128.3	–
SHARDS20007244	12:36:50.93	62:08:49.50	3.52 ± 0.06	–	26.4 ± 0.2	–	3.8 ± 0.8	–
SHARDS10012082	12:36:50.94	62:19:15.26	4.61 ± 0.07	0.3 ± 0.2	–	0.3 ± 0.2	–	70 ± 89
SHARDS20007645	12:36:51.03	62:13:38.76	3.98 ± 0.06	0.3 ± 0.2	25.8 ± 0.2	0.2 ± 0.1	13.6 ± 2.5	23 ± 16
SHARDS20011342	12:36:51.07	62:08:43.06	3.79 ± 0.06	0.3 ± 0.1	26.1 ± 0.2	0.3 ± 0.1	76.1 ± 17.9	50 ± 29
SHARDS20009490	12:36:51.10	62:09:35.58	4.24 ± 0.07	–	26.7 ± 0.1	–	3.6 ± 0.4	–
SHARDS10011621	12:36:51.14	62:18:48.01	3.79 ± 0.06	–	27.5 ± 0.7	–	1.6 ± 1.1	–
SHARDS20011536	12:36:51.15	62:09:20.94	4.77 ± 0.07	0.4 ± 0.3	27.3 ± 0.2	0.4 ± 0.3	2.4 ± 0.5	51 ± 64
SHARDS20012099	12:36:51.19	62:15:24.15	3.62 ± 0.06	0.4 ± 0.1	27.4 ± 0.1	0.3 ± 0.1	1.5 ± 0.2	88 ± 35
SHARDS20009241	12:36:51.20	62:15:00.01	4.71 ± 0.07	0.6 ± 0.3	25.4 ± 0.2	0.5 ± 0.2	275.2 ± 48.5	69 ± 44
SHARDS20007340	12:36:51.25	62:14:53.23	4.52 ± 0.07	–	26.4 ± 0.2	–	16.9 ± 3.0	–
SHARDS10003147	12:36:51.26	62:18:14.84	3.51 ± 0.06	–	24.5 ± 0.0	–	61.1 ± 4.7	–
SHARDS20005336	12:36:51.32	62:14:59.51	4.58 ± 0.07	0.3 ± 0.2	25.4 ± 0.1	0.2 ± 0.2	54.5 ± 5.0	10 ± 8
SHARDS20007294	12:36:51.40	62:08:56.57	5.45 ± 0.07	1.7 ± 0.2	–	1.5 ± 0.2	–	74 ± 24
SHARDS10010803	12:36:51.42	62:19:04.77	4.33 ± 0.06	0.1 ± 0.1	26.9 ± 0.2	0.1 ± 0.1	17.5 ± 3.9	19 ± 24
SHARDS20006072	12:36:51.51	62:11:48.98	3.96 ± 0.06	–	25.8 ± 0.2	–	22.4 ± 4.3	–
SHARDS10005640	12:36:51.61	62:16:37.21	3.91 ± 0.06	0.3 ± 0.2	25.4 ± 0.1	0.3 ± 0.2	58.5 ± 7.0	17 ± 9
SHARDS10012394	12:36:51.69	62:19:11.30	3.79 ± 0.06	–	27.1 ± 0.5	–	6.0 ± 3.0	–
SHARDS20008477	12:36:51.69	62:12:15.10	3.97 ± 0.06	–	26.4 ± 0.3	–	10.4 ± 3.2	–
SHARDS10013447	12:36:51.73	62:19:07.97	4.61 ± 0.07	0.2 ± 0.1	–	0.1 ± 0.1	–	–
SHARDS20010543	12:36:51.73	62:13:26.27	3.98 ± 0.06	1.5 ± 0.2	–	1.3 ± 0.1	–	335 ± 243
SHARDS20009191	12:36:51.78	62:11:11.29	5.63 ± 0.07	0.3 ± 0.2	26.0 ± 0.0	0.2 ± 0.2	46.5 ± 3.2	20 ± 20
SHARDS10004575	12:36:51.79	62:19:05.83	3.39 ± 0.07	–	24.6 ± 0.0	–	99.8 ± 9.5	–
SHARDS10006854	12:36:51.80	62:19:10.38	3.93 ± 0.06	0.2 ± 0.2	26.6 ± 0.3	0.2 ± 0.2	12.5 ± 4.0	13 ± 9
SHARDS20004816	12:36:51.85	62:15:15.71	3.37 ± 0.07	1.8 ± 0.2	24.6 ± 0.0	1.6 ± 0.2	54.6 ± 5.3	28 ± 3
SHARDS20006419	12:36:51.88	62:15:14.53	3.37 ± 0.07	0.6 ± 0.2	25.7 ± 0.1	0.6 ± 0.2	31.6 ± 4.0	52 ± 20
SHARDS20009653	12:36:51.89	62:12:55.60	4.67 ± 0.07	–	26.9 ± 0.7	–	4.9 ± 3.1	–
SHARDS20006542	12:36:52.03	62:11:04.69	3.96 ± 0.06	–	27.3 ± 0.8	–	2.1 ± 1.6	–
SHARDS20007868	12:36:52.04	62:11:44.86	5.35 ± 0.07	–	25.7 ± 0.1	–	37.0 ± 4.6	–
SHARDS10009061	12:36:52.15	62:15:46.21	4.19 ± 0.07	0.2 ± 0.2	26.2 ± 0.3	0.2 ± 0.1	5.4 ± 1.4	23 ± 19
SHARDS10006579	12:36:52.17	62:18:31.45	3.24 ± 0.07	–	26.2 ± 0.2	–	22.8 ± 4.0	–
SHARDS20024707	12:36:52.28	62:15:25.19	4.43 ± 0.07	0.3 ± 0.1	27.2 ± 0.3	0.3 ± 0.1	2.4 ± 0.6	50 ± 38
SHARDS20007044	12:36:52.29	62:08:43.96	3.93 ± 0.06	0.4 ± 0.2	25.8 ± 0.2	0.4 ± 0.1	17.0 ± 3.1	41 ± 22
SHARDS10007560	12:36:52.34	62:16:05.12	5.29 ± 0.07	–	26.2 ± 0.3	–	32.4 ± 10.0	–
SHARDS20002671	12:36:52.41	62:13:37.81	3.56 ± 0.06	–	25.0 ± 0.1	–	80.7 ± 7.6	–
SHARDS10003357	12:36:52.46	62:17:50.93	3.79 ± 0.06	–	25.1 ± 0.1	–	49.3 ± 5.5	–
SHARDS10011513	12:36:52.49	62:18:17.70	4.75 ± 0.07	–	27.0 ± 0.6	–	3.0 ± 1.8	–
SHARDS10013390	12:36:52.50	62:16:01.72	3.38 ± 0.07	–	25.6 ± 0.1	–	26.6 ± 3.2	–
SHARDS20009536	12:36:52.57	62:15:04.67	4.58 ± 0.07	–	27.0 ± 0.3	–	5.7 ± 1.4	–
SHARDS20006394	12:36:52.68	62:11:37.99	4.66 ± 0.07	–	26.5 ± 0.6	–	6.1 ± 3.1	–
SHARDS20006394	12:36:52.71	62:11:37.34	3.96 ± 0.06	–	26.2 ± 0.3	–	11.9 ± 3.7	–
SHARDS20002663	12:36:52.75	62:13:39.11	3.42 ± 0.07	–	25.4 ± 0.1	–	17.4 ± 2.0	–
SHARDS20006425	12:36:52.78	62:09:24.78	3.53 ± 0.06	–	26.8 ± 0.4	–	355.5 ± 136.8	–
SHARDS10006082	12:36:52.92	62:17:24.04	4.06 ± 0.07	1.6 ± 0.2	26.6 ± 0.5	1.4 ± 0.1	3.6 ± 1.7	113 ± 28

Continued on next page

Table A.1 – *Continued from previous page*

Object Name	R.A. (J2000)	Dec. (J2000)	z	$L_{Ly\alpha}$ (10^{42} erg s^{-1})	m_{1500} (AB mag)	$SFR_{L_{Ly\alpha}}$ ($M_\odot$ yr^{-1})	$SFR_{L_{1500}}$ ($M_\odot$ yr^{-1})	EW_0 (Å)
SHARDS20013378	12:36:53.00	62:11:08.62	5.21 ± 0.06	0.2 ± 0.2	26.8 ± 0.3	0.2 ± 0.2	20.5 ± 6.6	14 ± 14
SHARDS20015076	12:36:53.05	62:11:53.63	3.42 ± 0.07	–	27.2 ± 0.2	–	7.0 ± 1.7	–
SHARDS10012815	12:36:53.08	62:15:43.33	3.49 ± 0.06	–	27.9 ± 0.9	–	3.8 ± 3.0	–
SHARDS20011455	12:36:53.09	62:12:59.54	5.23 ± 0.06	0.4 ± 0.3	26.1 ± 0.2	0.4 ± 0.3	11.2 ± 1.7	19 ± 14
SHARDS20005331	12:36:53.14	62:13:31.73	3.56 ± 0.06	–	25.8 ± 0.1	–	29.3 ± 4.3	–
SHARDS20012201	12:36:53.26	62:11:12.27	3.96 ± 0.06	–	26.9 ± 0.5	–	2.7 ± 1.2	–
SHARDS10008463	12:36:53.29	62:18:44.88	3.93 ± 0.06	–	26.4 ± 0.3	–	4.1 ± 1.0	–
SHARDS10009196	12:36:53.30	62:18:33.48	4.22 ± 0.07	–	26.5 ± 0.4	–	27.2 ± 9.1	–
SHARDS20018112	12:36:53.37	62:13:10.16	3.84 ± 0.06	–	26.8 ± 0.5	–	10.7 ± 5.0	–
SHARDS20008406	12:36:53.45	62:08:44.90	3.66 ± 0.06	–	25.8 ± 0.2	–	6.4 ± 1.1	–
SHARDS20011830	12:36:53.46	62:14:53.13	4.58 ± 0.07	–	26.8 ± 0.2	–	10.1 ± 2.4	–
SHARDS20011676	12:36:53.54	62:11:49.96	4.66 ± 0.07	–	27.3 ± 0.2	–	2.8 ± 0.5	–
SHARDS10012561	12:36:53.65	62:17:35.95	4.75 ± 0.07	–	27.7 ± 1.2	–	1.6 ± 1.8	–
SHARDS20013642	12:36:53.94	62:14:55.86	5.82 ± 0.06	–	26.4 ± 0.1	–	7.7 ± 1.1	–
SHARDS10017061	12:36:53.97	62:19:00.13	3.51 ± 0.06	–	27.3 ± 0.5	–	1.6 ± 0.7	78 ± 72
SHARDS20004616	12:36:54.05	62:08:55.14	4.23 ± 0.07	0.3 ± 0.1	27.4 ± 0.5	0.2 ± 0.1	339.6 ± 152.2	–
SHARDS10014221	12:36:54.04	62:15:33.74	3.23 ± 0.07	–	24.3 ± 0.0	–	130.6 ± 10.7	–
SHARDS20000798	12:36:54.07	62:08:56.09	3.94 ± 0.06	0.2 ± 0.2	25.9 ± 0.2	0.2 ± 0.2	10.7 ± 2.5	11 ± 7
SHARDS10003545	12:36:54.10	62:17:33.82	3.65 ± 0.06	–	25.3 ± 0.1	–	37.6 ± 4.8	–
SHARDS20024156	12:36:54.12	62:15:06.34	4.58 ± 0.07	–	26.6 ± 0.2	–	17.4 ± 3.5	–
SHARDS20024137	12:36:54.20	62:15:06.97	4.30 ± 0.06	–	26.2 ± 0.2	–	17.8 ± 3.9	–
SHARDS20012559	12:36:54.23	62:13:19.63	5.50 ± 0.07	0.1 ± 0.2	27.1 ± 0.4	0.1 ± 0.2	14.0 ± 5.3	20 ± 29
SHARDS10005446	12:36:54.25	62:16:12.70	3.91 ± 0.06	–	25.3 ± 0.1	–	29.0 ± 3.5	–
SHARDS10011651	12:36:54.27	62:16:21.07	4.45 ± 0.07	–	27.4 ± 0.2	–	10.5 ± 2.5	–
SHARDS10008601	12:36:54.31	62:15:30.78	4.44 ± 0.07	–	26.7 ± 0.2	–	3.7 ± 0.6	–
SHARDS20011498	12:36:54.32	62:12:42.90	5.92 ± 0.06	–	26.0 ± 0.1	–	59.8 ± 4.2	–
SHARDS20007869	12:36:54.51	62:08:24.88	4.76 ± 0.07	–	26.1 ± 0.2	–	7.1 ± 1.1	–
SHARDS20022948	12:36:54.56	62:14:58.39	4.72 ± 0.07	–	26.2 ± 0.3	–	10.7 ± 3.0	–
SHARDS20023901	12:36:54.59	62:15:05.23	4.58 ± 0.07	–	25.9 ± 0.1	–	33.7 ± 3.9	–
SHARDS20025282	12:36:54.62	62:15:12.02	3.49 ± 0.06	–	25.6 ± 0.2	–	42.0 ± 5.2	–
SHARDS10022257	12:36:54.65	62:16:26.91	3.78 ± 0.06	–	25.9 ± 0.2	–	10.5 ± 1.9	–
SHARDS10007859	12:36:54.68	62:16:22.13	3.91 ± 0.06	–	27.1 ± 0.6	–	6.0 ± 3.5	–
SHARDS20012408	12:36:54.70	62:13:52.86	4.70 ± 0.07	–	26.1 ± 0.1	–	61.5 ± 8.7	–
SHARDS20009233	12:36:54.81	62:08:30.23	4.76 ± 0.07	–	27.0 ± 0.3	–	4.0 ± 1.0	–
SHARDS20010396	12:36:54.83	62:08:27.03	4.62 ± 0.07	–	25.8 ± 0.2	–	9.4 ± 2.0	–
SHARDS20016398	12:36:54.93	62:12:14.44	6.75 ± 0.14	1.0 ± 0.2	–	0.9 ± 0.2	–	57 ± 11
SHARDS10008547	12:36:54.98	62:16:27.34	4.60 ± 0.07	–	26.2 ± 0.1	–	19.5 ± 2.6	–
SHARDS10011476	12:36:54.98	62:19:01.15	3.52 ± 0.06	–	28.2 ± 0.5	–	3.1 ± 1.3	–
SHARDS20022974	12:36:55.07	62:14:59.75	3.49 ± 0.06	–	27.8 ± 0.3	–	3.0 ± 0.8	–
SHARDS10013862	12:36:55.12	62:19:49.92	3.52 ± 0.06	–	26.8 ± 0.4	–	10.7 ± 3.7	–
SHARDS20022674	12:36:55.16	62:10:34.05	4.37 ± 0.06	–	26.3 ± 0.2	–	6.8 ± 1.3	–
SHARDS20022647	12:36:55.16	62:10:36.18	4.25 ± 0.07	–	25.6 ± 0.1	–	15.4 ± 2.1	–
SHARDS20004751	12:36:55.37	62:12:13.39	5.08 ± 0.06	–	23.9 ± 0.0	–	60.4 ± 3.9	–
SHARDS20007964	12:36:55.38	62:10:18.38	4.09 ± 0.07	–	26.7 ± 0.7	–	5.3 ± 3.4	–
SHARDS10002758	12:36:55.38	62:17:07.34	3.51 ± 0.06	–	25.2 ± 0.1	–	54.8 ± 5.5	–
SHARDS10008850	12:36:55.39	62:15:48.77	5.15 ± 0.06	–	26.2 ± 0.3	–	12.5 ± 3.5	–
SHARDS20025422	12:36:55.45	62:15:08.40	5.97 ± 0.07	0.4 ± 0.2	–	0.3 ± 0.1	–	40 ± 15
SHARDS10005512	12:36:55.50	62:15:32.78	5.15 ± 0.06	1.3 ± 0.3	26.2 ± 0.3	1.2 ± 0.3	55.2 ± 17.5	25 ± 8

Continued on next page

Table A.1 – *Continued from previous page*

Object Name	R.A. (J2000)	Dec. (J2000)	z	$L_{Ly\alpha}$ (10^{42} erg s^{-1})	m_{1500} (AB mag)	$SFR_{L_{Ly\alpha}}$ ($M_\odot$ yr^{-1})	$SFR_{L_{1500}}$ ($M_\odot$ yr^{-1})	EW$_0$ (Å)
SHARDS20009588	12:36:55.61	62:14:12.90	3.70 ± 0.06	—	26.9 ± 0.4	—	6.8 ± 2.8	—
SHARDS20006499	12:36:55.64	62:15:56.34	3.89 ± 0.07	—	26.1 ± 0.2	—	37.2 ± 6.2	—
SHARDS20010446	12:36:55.74	62:17:50.10	3.92 ± 0.06	0.3 ± 0.2	27.1 ± 0.5	0.2 ± 0.1	7.6 ± 3.8	34 ± 25
SHARDS20007020	12:36:55.74	62:17:26.10	3.98 ± 0.06	0.3 ± 0.2	27.9 ± 1.4	0.2 ± 0.2	1.0 ± 1.3	7 ± 5
SHARDS20006479	12:36:55.77	62:13:51.01	3.98 ± 0.06	—	27.0 ± 0.1	—	38.5 ± 5.0	—
SHARDS20010482	12:36:55.77	62:19:18.74	3.24 ± 0.07	—	25.6 ± 0.1	—	14.5 ± 2.4	—
SHARDS20010877	12:36:55.78	62:15:01.40	4.36 ± 0.06	0.3 ± 0.2	27.0 ± 0.2	0.3 ± 0.2	46 ± 41	46 ± 41
SHARDS20006029	12:36:55.81	62:15:58.75	3.45 ± 0.07	—	—	—	20.1 ± 3.5	—
SHARDS20005986	12:36:55.86	62:08:46.05	3.89 ± 0.06	—	25.6 ± 0.2	—	17.6 ± 2.3	—
SHARDS20005923	12:36:55.91	62:11:46.62	3.42 ± 0.07	—	25.5 ± 0.1	—	262.7 ± 23.9	—
SHARDS20005744	12:36:55.94	62:14:12.43	4.03 ± 0.07	—	24.0 ± 0.1	—	2.4 ± 0.5	—
SHARDS20004979	12:36:55.96	62:16:38.91	4.33 ± 0.06	—	27.1 ± 0.2	—	10.3 ± 3.8	—
SHARDS20004261	12:36:56.01	62:11:57.42	3.75 ± 0.06	—	27.0 ± 0.4	—	21.3 ± 9.7	—
SHARDS20003743	12:36:56.06	62:18:12.67	4.76 ± 0.07	—	27.2 ± 0.5	—	42.7 ± 4.7	—
SHARDS20002578	12:36:56.07	62:15:40.70	3.67 ± 0.07	—	25.4 ± 0.1	—	22.7 ± 2.1	—
SHARDS20002742	12:36:56.12	62:09:24.79	3.97 ± 0.06	—	24.6 ± 0.2	—	27.0 ± 5.4	18 ± 15
SHARDS20007101	12:36:56.23	62:09:26.38	3.94 ± 0.06	0.2 ± 0.1	25.7 ± 0.2	0.2 ± 0.1	200.8 ± 53.9	—
SHARDS20010961	12:36:56.33	62:15:31.89	3.24 ± 0.07	—	26.7 ± 0.3	—	20.6 ± 1.4	—
SHARDS10008567	12:36:56.36	62:19:20.97	3.56 ± 0.06	—	25.6 ± 0.0	—	3.5 ± 1.0	—
SHARDS10007601	12:36:56.44	62:13:39.90	3.32 ± 0.06	—	26.5 ± 0.3	—	20.9 ± 3.4	—
SHARDS20007191	12:36:56.49	62:09:22.83	3.67 ± 0.07	—	26.2 ± 0.2	—	4.2 ± 1.0	—
SHARDS20007330	12:36:56.50	62:08:42.89	3.67 ± 0.06	—	26.2 ± 0.3	—	65.2 ± 8.8	—
SHARDS20004758	12:36:56.50	62:13:46.58	3.25 ± 0.06	1.0 ± 0.5	25.6 ± 0.1	0.9 ± 0.5	—	111 ± 71
SHARDS20010724	12:36:56.51	62:17:13.56	4.07 ± 0.07	—	—	—	—	—
SHARDS20006822	12:36:56.52	62:17:34.50	3.39 ± 0.07	0.4 ± 0.2	26.4 ± 0.5	0.3 ± 0.2	21.3 ± 9.2	66 ± 46
SHARDS10009023	12:36:56.58	62:17:58.54	4.34 ± 0.06	—	27.7 ± 0.3	—	1.3 ± 0.6	—
SHARDS10009462	12:36:56.68	62:14:40.47	4.19 ± 0.06	1.2 ± 0.2	27.1 ± 0.3	1.1 ± 0.2	2.5 ± 0.6	110 ± 23
SHARDS20008777	12:36:56.70	62:09:36.26	4.23 ± 0.07	—	—	—	—	—
SHARDS20006367	12:36:56.73	62:13:06.04	4.27 ± 0.14	—	25.9 ± 0.2	—	10.7 ± 2.2	—
SHARDS20016256	12:36:56.82	62:13:16.47	3.27 ± 0.06	—	25.4 ± 0.1	—	556.9 ± 66.1	—
SHARDS20009828	12:36:56.84	62:14:20.76	3.83 ± 0.06	—	25.7 ± 0.1	—	3.1 ± 0.3	—
SHARDS20010968	12:36:56.85	62:14:04.63	3.89 ± 0.07	—	26.0 ± 0.2	—	7.2 ± 1.3	—
SHARDS20006102	12:36:56.98	62:12:41.85	3.42 ± 0.07	0.2 ± 0.2	26.4 ± 0.2	0.1 ± 0.2	6.8 ± 1.5	7 ± 7
SHARDS20014909	12:36:57.00	62:13:51.95	3.93 ± 0.06	0.2 ± 0.2	26.3 ± 0.2	0.2 ± 0.2	10.1 ± 0.8	36 ± 49
SHARDS20006946	12:36:57.00	62:13:40.96	3.69 ± 0.06	1.3 ± 0.2	26.1 ± 0.2	1.2 ± 0.1	7.0 ± 1.5	132 ± 35
SHARDS20005479	12:36:57.03	62:17:06.77	4.07 ± 0.06	—	26.4 ± 0.5	—	18.4 ± 7.9	—
SHARDS20005345	12:36:57.03	62:14:05.70	4.87 ± 0.07	—	27.2 ± 0.1	—	3.7 ± 0.4	—
SHARDS20013891	12:36:57.09	62:16:56.70	4.16 ± 0.06	0.3 ± 0.2	25.9 ± 0.3	0.3 ± 0.1	28.8 ± 7.2	25 ± 12
SHARDS20005588	12:36:57.16	62:08:13.16	4.76 ± 0.07	—	25.4 ± 0.2	—	45.4 ± 7.8	—
SHARDS20005741	12:36:57.17	62:12:34.40	3.46 ± 0.07	—	25.2 ± 0.1	—	81.7 ± 10.3	—
SHARDS10012500	12:36:57.17	62:16:46.83	3.42 ± 0.07	—	26.2 ± 0.5	—	5.8 ± 2.5	—
SHARDS10008187	12:36:57.19	62:18:58.52	3.59 ± 0.06	0.1 ± 0.2	27.5 ± 0.6	0.1 ± 0.1	7.4 ± 3.3	18 ± 19
SHARDS20008432	12:36:57.25	62:11:33.76	4.66 ± 0.07	—	27.6 ± 1.8	—	2.4 ± 3.8	—
SHARDS20009044	12:36:57.27	62:11:35.53	4.80 ± 0.07	—	28.2 ± 0.2	—	42.1 ± 7.5	—
SHARDS20008932	12:36:57.29	62:12:49.40	4.23 ± 0.06	0.4 ± 0.3	26.3 ± 0.9	0.4 ± 0.3	6.6 ± 2.7	12 ± 8
SHARDS20025450	12:36:57.31	62:14:55.06	4.33 ± 0.06	—	26.7 ± 0.4	—	6.9 ± 1.5	—
SHARDS20006088	12:36:57.31	62:12:56.28	3.56 ± 0.06	—	27.4 ± 0.1	—	51.6 ± 6.0	—
SHARDS20017397	12:36:57.35	62:13:08.45	3.98 ± 0.06	—	25.4 ± 0.2	—	11.9 ± 0.3	—
SHARDS20005313	12:36:57.39	62:11:52.86	3.42 ± 0.07	—	25.3 ± 0.1	—	55.7 ± 6.6	—

Continued on next page

Table A.1 – *Continued from previous page*

Object Name	R.A. (J2000)	Dec. (J2000)	z	$L_{Ly\alpha}$ (10^{42} erg s^{-1})	m_{1500} (AB mag)	$SFR_{L_{Ly\alpha}}$ ($M_\odot$ yr^{-1})	$SFR_{L_{1500}}$ ($M_\odot$ yr^{-1})	EW_0 (Å)
SHARDS20008481	12:36:57.44	62:10:12.14	3.67 ± 0.06	—	27.8 ± 1.1	—	1.0 ± 1.0	—
SHARDS10007458	12:36:57.50	62:16:50.53	4.61 ± 0.07	0.2 ± 0.2	25.7 ± 0.2	0.2 ± 0.2	29.2 ± 7.0	13 ± 12
SHARDS20009578	12:36:57.57	62:11:39.01	3.27 ± 0.07	—	27.1 ± 0.2	—	11.9 ± 2.2	—
SHARDS20005956	12:36:57.74	62:09:17.87	4.08 ± 0.07	—	25.5 ± 0.3	—	44.1 ± 10.9	—
SHARDS20006837	12:36:57.77	62:14:25.03	3.37 ± 0.07	—	26.7 ± 0.2	—	3.3 ± 0.7	—
SHARDS20007749	12:36:57.77	62:10:45.18	4.50 ± 0.07	—	26.0 ± 0.2	—	7.3 ± 1.7	—
SHARDS10006061	12:36:57.78	62:15:02.63	4.44 ± 0.07	0.1 ± 0.2	26.4 ± 0.4	0.1 ± 0.1	4.8 ± 1.9	6 ± 6
SHARDS20018568	12:36:57.80	62:14:33.50	5.96 ± 0.07	—	27.0 ± 0.2	—	6.2 ± 0.9	—
SHARDS10001620	12:36:57.84	62:15:34.29	3.50 ± 0.06	—	25.3 ± 0.1	—	49.6 ± 5.3	—
SHARDS10006084	12:36:57.88	62:15:24.89	4.44 ± 0.07	—	25.9 ± 0.3	—	48.6 ± 13.6	—
SHARDS10007794	12:36:57.89	62:18:04.89	4.34 ± 0.06	—	26.3 ± 0.2	—	5.1 ± 1.2	—
SHARDS20009778	12:36:57.98	62:13:50.29	4.18 ± 0.07	1.0 ± 0.2	26.9 ± 0.1	1.0 ± 0.2	7.7 ± 0.8	96 ± 32
SHARDS10007538	12:36:58.08	62:17:39.16	3.65 ± 0.06	—	26.3 ± 0.3	—	8.3 ± 2.3	—
SHARDS20006121	12:36:58.11	62:11:14.76	4.51 ± 0.07	—	25.2 ± 0.1	—	69.3 ± 9.5	—
SHARDS10010421	12:36:58.17	62:15:10.34	4.05 ± 0.07	—	26.3 ± 0.1	—	189.8 ± 21.4	—
SHARDS20009401	12:36:58.21	62:12:06.65	4.67 ± 0.07	—	26.0 ± 0.3	—	20.4 ± 5.2	—
SHARDS10013643	12:36:58.25	62:15:11.50	3.23 ± 0.07	—	28.3 ± 0.6	—	85.9 ± 45.5	—
SHARDS20007501	12:36:58.25	62:11:20.44	3.96 ± 0.06	1.4 ± 0.2	27.1 ± 0.6	1.2 ± 0.1	2.1 ± 1.3	100 ± 29
SHARDS10017054	12:36:58.28	62:14:58.16	3.63 ± 0.06	—	27.3 ± 0.2	—	2.7 ± 0.5	—
SHARDS20009570	12:36:58.28	62:11:17.39	3.41 ± 0.07	—	26.6 ± 0.2	—	168.8 ± 39.5	—
SHARDS10010385	12:36:58.43	62:16:14.96	5.16 ± 0.06	0.4 ± 0.3	25.7 ± 0.2	0.4 ± 0.3	36.1 ± 7.0	26 ± 22
SHARDS10001876	12:36:58.51	62:15:55.64	3.50 ± 0.06	—	25.2 ± 0.1	—	23.2 ± 2.2	—
SHARDS20014339	12:36:58.57	62:12:44.13	6.27 ± 0.14	1.4 ± 0.2	—	1.2 ± 0.2	—	211 ± 46
SHARDS20014001	12:36:58.60	62:10:11.81	4.92 ± 0.08	—	26.4 ± 0.2	—	7.4 ± 1.5	—
SHARDS10010637	12:36:58.62	62:17:06.66	4.22 ± 0.07	—	27.0 ± 0.1	—	2.5 ± 0.3	—
SHARDS10011777	12:36:58.76	62:17:53.69	3.65 ± 0.06	0.3 ± 0.2	27.6 ± 0.2	0.3 ± 0.2	1.2 ± 0.2	66 ± 65
SHARDS10007531	12:36:58.82	62:17:10.41	4.46 ± 0.07	0.4 ± 0.1	26.8 ± 0.1	0.3 ± 0.1	10.6 ± 1.4	—
SHARDS20011706	12:36:58.93	62:09:17.61	5.46 ± 0.07	0.1 ± 0.1	27.2 ± 0.1	0.1 ± 0.1	19.8 ± 2.9	20 ± 20
SHARDS20006444	12:36:58.95	62:12:29.13	4.52 ± 0.07	1.1 ± 0.2	26.0 ± 0.2	1.0 ± 0.2	8.9 ± 2.0	59 ± 17
SHARDS20011056	12:36:59.06	62:13:35.70	3.21 ± 0.07	—	27.0 ± 0.3	—	16.8 ± 4.9	—
SHARDS20005661	12:36:59.10	62:09:25.63	3.53 ± 0.06	—	25.6 ± 0.1	—	24.5 ± 3.2	—
SHARDS20005706	12:36:59.10	62:12:23.71	4.12 ± 0.07	0.7 ± 0.2	25.9 ± 0.3	0.6 ± 0.2	22.3 ± 6.4	47 ± 16
SHARDS10007348	12:36:59.34	62:17:22.91	4.22 ± 0.07	—	26.5 ± 0.1	—	4.0 ± 0.4	—
SHARDS10005590	12:36:59.38	62:19:05.39	3.80 ± 0.06	—	25.4 ± 0.1	—	98.8 ± 14.4	—
SHARDS10013023	12:36:59.48	62:15:01.52	3.63 ± 0.06	—	27.3 ± 0.3	—	8.4 ± 2.0	—
SHARDS10005569	12:36:59.51	62:15:14.37	3.38 ± 0.07	—	25.8 ± 0.1	—	30.0 ± 3.9	—
SHARDS20007303	12:36:59.66	62:14:27.88	3.76 ± 0.06	—	26.4 ± 0.3	—	12.0 ± 3.2	—
SHARDS10009008	12:36:59.69	62:14:54.39	5.56 ± 0.07	—	25.6 ± 0.0	—	26.6 ± 1.8	—
SHARDS10005202	12:36:59.77	62:18:54.33	3.94 ± 0.06	—	25.0 ± 0.1	—	26.5 ± 2.9	—
SHARDS10006208	12:36:59.78	62:15:13.13	4.20 ± 0.07	—	25.5 ± 0.2	—	54.0 ± 8.7	—
SHARDS20006282	12:36:59.81	62:12:18.86	5.36 ± 0.07	—	24.4 ± 0.0	—	366.9 ± 24.3	—
SHARDS10014349	12:36:59.83	62:16:36.22	3.39 ± 0.07	—	27.6 ± 0.5	—	1.1 ± 0.6	—
SHARDS20009598	12:36:59.83	62:11:37.62	4.11 ± 0.07	—	26.1 ± 0.3	—	5.5 ± 1.7	—
SHARDS10007109	12:36:59.89	62:14:58.27	4.59 ± 0.07	—	26.6 ± 0.2	—	11.1 ± 2.1	—
SHARDS20015155	12:36:59.90	62:10:12.66	4.65 ± 0.07	—	27.0 ± 0.3	—	12.3 ± 3.2	—
SHARDS10014300	12:37:00.21	62:18:03.54	4.23 ± 0.07	0.3 ± 0.2	27.6 ± 0.2	0.3 ± 0.1	1.5 ± 0.3	70 ± 68
SHARDS20012043	12:37:00.22	62:11:13.38	5.35 ± 0.07	—	27.3 ± 0.2	—	7.9 ± 1.8	—
SHARDS20008701	12:37:00.24	62:10:08.41	3.95 ± 0.06	0.2 ± 0.2	26.8 ± 0.5	0.2 ± 0.1	15.6 ± 6.9	21 ± 14

Continued on next page

Table A.1 – *Continued from previous page*

Object Name	R.A. (J2000)	Dec. (J2000)	z	$L_{Ly\alpha}$ (10^{42} erg s^{-1})	m_{1500} (AB mag)	$\mathrm{SFR}_{L_{Ly\alpha}}$ ($M_\odot$ yr^{-1})	$\mathrm{SFR}_{L_{1500}}$ ($M_\odot$ yr^{-1})	EW$_0$ (Å)
SHARDS001475[illegible]	12:37:00.26	62:14:47.23	3.49 ± 0.06	—	27.9 ± 0.4	—	2.9 ± 0.7	—
SHARDS001335[illegible]	12:37:00.27	62:16:54.14	4.31 ± 0.07	—	27.0 ± 0.1	—	4.8 ± 0.6	—
SHARDS001355[illegible]	12:37:00.33	62:16:36.66	5.31 ± 0.07	0.6 ± 0.0		0.5 ± 0.0		208 ± 81
SHARDS001359[illegible]	12:37:00.41	62:13:41.77	4.42 ± 0.07	—	26.3 ± 0.5	—	5.7 ± 2.5	—
SHARDS001312[illegible]	12:37:00.53	62:18:04.48	4.47 ± 0.07	—	26.6 ± 0.5	—	11.2 ± 5.3	—
SHARDS001312[illegible]	12:37:00.60	62:16:56.09	3.54 ± 0.06	—	24.5 ± 0.1	—	136.3 ± 11.1	—
SHARDS001335[illegible]	12:37:00.65	62:16:58.63	4.22 ± 0.07	—	26.5 ± 0.4	—	4.1 ± 1.4	—
SHARDS001335[illegible]	12:37:00.76	62:17:56.02	4.23 ± 0.07	1.7 ± 0.5	25.2 ± 0.1	1.5 ± 0.5	48.5 ± 6.0	158 ± 149
SHARDS001475[illegible]	12:37:00.72	62:18:58.24	4.22 ± 0.14				150.4 ± 76.5	
SHARDS001475[illegible]	12:37:00.80	62:14:46.95	3.49 ± 0.06	0.6 ± 0.2	28.2 ± 0.5	0.5 ± 0.2	3.1 ± 0.7	39 ± 14
SHARDS001335[illegible]	12:37:00.90	62:09:28.28	3.40 ± 0.07	—	26.4 ± 0.2	—	6.6 ± 1.9	—
SHARDS001335[illegible]	12:37:00.95	62:17:32.43	3.26 ± 0.07	—	26.9 ± 0.3	—	14.8 ± 2.6	—
SHARDS001335[illegible]	12:37:00.98	62:17:16.90	3.52 ± 0.06	—	26.2 ± 0.2	—		121 ± 62
SHARDS001335[illegible]	12:37:01.00	62:16:39.70	6.43 ± 0.07	0.4 ± 0.2		0.4 ± 0.2		
SHARDS001335[illegible]	12:37:01.01	62:16:58.71	4.33 ± 0.07	—	26.9 ± 0.2	—	34.1 ± 7.1	—
SHARDS001335[illegible]	12:37:01.04	62:09:16.78	4.35 ± 0.06	—	26.2 ± 0.2	—	13.1 ± 2.3	—
SHARDS001335[illegible]	12:37:01.14	62:20:26.47	3.24 ± 0.07	—	27.6 ± 0.6	—	1.0 ± 0.5	—
SHARDS001335[illegible]	12:37:01.15	62:09:36.34	3.23 ± 0.07	0.4 ± 0.2	25.8 ± 0.2	0.4 ± 0.2	88.6 ± 16.9	23 ± 9
SHARDS001335[illegible]	12:37:01.17	62:11:39.36	3.36 ± 0.07	—	27.0 ± 0.9	—	58.2 ± 10.0	—
SHARDS001335[illegible]	12:37:01.36	62:10:32.24	3.95 ± 0.06	—	27.8 ± 0.1	—	1.7 ± 1.4	—
SHARDS001335[illegible]	12:37:01.37	62:09:05.45	4.35 ± 0.06	—	25.4 ± 0.1	—	10.7 ± 0.5	—
SHARDS001335[illegible]	12:37:01.39	62:09:30.25	4.37 ± 0.06	—	27.2 ± 0.4	—	2.4 ± 0.9	—
SHARDS001335[illegible]	12:37:01.40	62:13:38.15	4.35 ± 0.07	—	25.7 ± 0.1	—	25.6 ± 3.1	—
SHARDS001335[illegible]	12:37:01.41	62:13:57.21	3.77 ± 0.07	—	25.7 ± 0.1	—	38.5 ± 3.1	—
SHARDS001335[illegible]	12:37:01.46	62:12:51.24	3.62 ± 0.07	—	25.4 ± 0.2	—	137.0 ± 24.2	—
SHARDS001335[illegible]	12:37:01.54	62:12:11.40	3.48 ± 0.06	—	24.4 ± 0.2	—	7.0 ± 3.3	—
SHARDS001335[illegible]	12:37:01.63	62:13:46.48	4.43 ± 0.07	—	26.8 ± 0.5	—	20.6 ± 6.8	—
SHARDS001335[illegible]	12:37:01.65	62:15:45.69	4.46 ± 0.07	0.2 ± 0.1	26.2 ± 0.3	0.2 ± 0.1	3.8 ± 1.0	28 ± 22
SHARDS001335[illegible]	12:37:01.70	62:19:16.62	4.46 ± 0.07	0.2 ± 0.2	27.7 ± 0.3	0.2 ± 0.2	40.8 ± 4.0	28 ± 34
SHARDS001335[illegible]	12:37:01.98	62:12:25.35	4.35 ± 0.06	—	26.3 ± 0.3	—	30.5 ± 8.2	—
SHARDS001335[illegible]	12:37:01.97	62:17:32.61	3.42 ± 0.06	—	24.7 ± 0.1	—	29.9 ± 3.1	—
SHARDS001335[illegible]	12:37:02.09	62:10:37.84	3.96 ± 0.06	—	26.7 ± 0.4	—	3.1 ± 1.0	—
SHARDS001241[illegible]	12:37:02.07	62:18:11.04	4.35 ± 0.06	—	25.8 ± 0.2	—	16.3 ± 3.1	—
SHARDS001335[illegible]	12:37:02.19	62:20:56.31	3.63 ± 0.06	—	26.2 ± 0.3	—	3.3 ± 0.8	—
SHARDS001335[illegible]	12:37:02.24	62:15:07.03	3.53 ± 0.06	0.7 ± 0.3	25.2 ± 0.1	0.6 ± 0.2	14.8 ± 66.2	30 ± 11
SHARDS001150[illegible]	12:37:02.30	62:20:12.76	4.04 ± 0.07	—	27.4 ± 0.2	—	352.4 ± 66.2	—
SHARDS001335[illegible]	12:37:02.30	62:16:10.53	3.54 ± 0.06	—	25.3 ± 0.5	—	3.4 ± 1.7	—
SHARDS001335[illegible]	12:37:02.31	62:12:39.05	4.09 ± 0.07	—	25.6 ± 0.6	—	3.4 ± 1.8	—
SHARDS001335[illegible]	12:37:02.31	62:13:40.01	3.88 ± 0.06	0.2 ± 0.2	25.6 ± 0.3	0.2 ± 0.2	19.7 ± 4.9	11 ± 10
SHARDS001335[illegible]	12:37:02.34	62:19:21.44	4.09 ± 0.07	—	25.2 ± 0.1	—	86.6 ± 8.5	—
SHARDS001335[illegible]	12:37:02.36	62:11:32.96	4.35 ± 0.07	—	27.8 ± 1.6	—	5.7 ± 8.2	—
SHARDS001335[illegible]	12:37:02.37	62:11:09.44	4.65 ± 0.06	—	26.2 ± 0.2	—	8.8 ± 3.5	—
SHARDS001335[illegible]	12:37:02.44	62:17:13.36	3.65 ± 0.06	—	26.3 ± 0.4	—	13.6 ± 3.4	—
SHARDS001335[illegible]	12:37:02.47	62:18:07.01	4.23 ± 0.07	0.1 ± 0.2	26.4 ± 0.1	0.1 ± 0.2	8.2 ± 1.7	10 ± 15
SHARDS001335[illegible]	12:37:02.49	62:17:25.13	3.93 ± 0.06	0.2 ± 0.2	27.1 ± 0.2	0.2 ± 0.1		47 ± 47
SHARDS001335[illegible]	12:37:02.53	62:13:58.00	3.37 ± 0.06	0.9 ± 0.2		0.8 ± 0.2		120 ± 56
SHARDS001335[illegible]	12:37:02.53	62:11:54.97	3.83 ± 0.06	—	27.1 ± 0.2	—	4.7 ± 0.7	—
SHARDS001335[illegible]	12:37:02.53	62:11:54.97	3.83 ± 0.06	—	26.2 ± 0.3	—	30.5 ± 8.1	—

Continued on next page

Table A.1 – *Continued from previous page*

Object Name	R.A. (J2000)	Dec. (J2000)	z	$L_{Ly\alpha}$ (10^{42} erg s^{-1})	m_{1500} (AB mag)	$SFR_{L_{Ly\alpha}}$ ($M_\odot$ yr^{-1})	$SFR_{L_{1500}}$ ($M_\odot$ yr^{-1})	EW$_0$ (Å)
SHARDS10009504	12:37:02.54	62:16:05.81	5.43 ± 0.07	0.4 ± 0.2	25.7 ± 0.2	0.4 ± 0.2	12.8 ± 2.3	26 ± 18
SHARDS10015291	12:37:02.56	62:16:38.13	6.21 ± 0.14	–	26.4 ± 0.1	–	67.5 ± 8.7	–
SHARDS20001613	12:37:02.59	62:10:27.45	3.41 ± 0.07	–	26.4 ± 0.2	–	3.3 ± 0.7	–
SHARDS10008415	12:37:02.68	62:17:02.19	4.22 ± 0.07	0.4 ± 0.2	26.5 ± 0.3	0.3 ± 0.1	4.3 ± 1.4	12 ± 4
SHARDS10010885	12:37:02.68	62:18:21.53	3.40 ± 0.07	0.4 ± 0.2	26.6 ± 0.2	0.4 ± 0.2	2.7 ± 0.6	61 ± 31
SHARDS20012654	12:37:02.72	62:13:55.10	5.55 ± 0.07	1.1 ± 0.1	27.1 ± 0.1	1.0 ± 0.1	3.5 ± 0.4	147 ± 32
SHARDS20023318	12:37:02.73	62:12:28.85	5.24 ± 0.07	0.2 ± 0.3	24.0 ± 0.0	0.2 ± 0.3	59.8 ± 3.6	10 ± 14
SHARDS20011267	12:37:02.81	62:11:41.66	5.36 ± 0.07	0.5 ± 0.2	–	0.4 ± 0.1	–	–
SHARDS20010427	12:37:02.85	62:09:15.54	3.94 ± 0.06	–	25.9 ± 0.2	–	12.9 ± 2.7	–
SHARDS20005951	12:37:02.90	62:13:06.65	4.29 ± 0.06	–	26.7 ± 0.4	–	22.9 ± 8.7	–
SHARDS10005684	12:37:02.91	62:16:13.35	3.79 ± 0.06	0.5 ± 0.2	25.4 ± 0.1	0.5 ± 0.2	155.3 ± 20.2	18 ± 7
SHARDS10009682	12:37:02.97	62:15:03.11	4.74 ± 0.07	–	27.3 ± 0.8	–	2.5 ± 1.8	–
SHARDS10010010	12:37:02.99	62:20:44.35	3.67 ± 0.06	0.1 ± 0.1	27.3 ± 0.6	0.1 ± 0.1	10.5 ± 5.9	37 ± 36
SHARDS20009724	12:37:03.09	62:11:37.87	3.55 ± 0.06	0.6 ± 0.1	27.0 ± 0.4	0.6 ± 0.1	2.7 ± 1.0	83 ± 20
SHARDS10008872	12:37:03.11	62:16:08.10	4.61 ± 0.07	–	27.4 ± 0.4	–	3.6 ± 1.2	–
SHARDS10008355	12:37:03.14	62:17:53.96	4.23 ± 0.07	–	26.3 ± 0.1	–	6.0 ± 0.7	–
SHARDS20012491	12:37:03.24	62:10:25.40	4.10 ± 0.07	–	27.0 ± 0.2	–	214.4 ± 33.2	–
SHARDS20057736	12:37:03.28	62:13:00.55	4.29 ± 0.06	–	26.0 ± 0.2	–	6.6 ± 1.6	–
SHARDS20007270	12:37:03.29	62:10:06.43	4.37 ± 0.06	–	26.5 ± 0.3	–	4.2 ± 1.0	–
SHARDS20007459	12:37:03.31	62:13:31.46	5.27 ± 0.07	–	25.5 ± 0.1	–	14.7 ± 1.4	–
SHARDS10006713	12:37:03.37	62:17:03.22	3.93 ± 0.06	–	26.4 ± 0.3	–	8.1 ± 2.0	–
SHARDS10006271	12:37:03.39	62:16:16.20	3.93 ± 0.06	0.2 ± 0.2	26.7 ± 0.4	0.2 ± 0.2	4.5 ± 1.5	17 ± 14
SHARDS10007662	12:37:03.39	62:19:21.92	3.81 ± 0.06	–	26.7 ± 0.4	–	3.1 ± 1.3	–
SHARDS20024698	12:37:03.53	62:14:29.70	4.31 ± 0.06	–	26.8 ± 0.4	–	16.7 ± 6.2	–
SHARDS20004993	12:37:03.55	62:14:22.72	3.37 ± 0.07	–	25.4 ± 0.1	–	118.7 ± 12.9	–
SHARDS20013448	12:37:03.61	62:11:58.46	5.22 ± 0.06	1.9 ± 0.4	25.6 ± 0.3	1.7 ± 0.4	72.0 ± 23.3	89 ± 38
SHARDS20006714	12:37:03.61	62:12:53.55	4.41 ± 0.06	–	25.7 ± 0.2	–	12.6 ± 2.2	–
SHARDS10010365	12:37:03.65	62:17:05.96	3.52 ± 0.06	–	27.1 ± 0.4	–	326.4 ± 127.6	–
SHARDS10006438	12:37:03.69	62:14:54.51	4.20 ± 0.07	–	26.0 ± 0.2	–	29.2 ± 6.3	–
SHARDS20011532	12:37:03.69	62:10:46.61	3.82 ± 0.06	–	27.5 ± 0.9	–	3.6 ± 3.1	–
SHARDS20012876	12:37:03.71	62:11:57.72	5.22 ± 0.06	1.1 ± 0.2	26.1 ± 0.2	1.0 ± 0.1	23.3 ± 4.1	94 ± 16
SHARDS20025317	12:37:03.71	62:14:30.34	4.20 ± 0.07	–	25.6 ± 0.2	–	54.1 ± 9.8	–
SHARDS20010300	12:37:03.78	62:10:06.22	4.10 ± 0.07	2.8 ± 0.2	–	2.6 ± 0.1	–	239 ± 50
SHARDS20024717	12:37:03.80	62:14:29.54	4.44 ± 0.06	–	27.0 ± 0.3	–	2.8 ± 0.7	–
SHARDS20011816	12:37:03.80	62:13:30.64	4.04 ± 0.06	0.4 ± 0.2	26.6 ± 0.6	0.4 ± 0.2	21.3 ± 11.6	59 ± 56
SHARDS10007523	12:37:03.87	62:15:02.89	4.45 ± 0.07	0.3 ± 0.2	27.0 ± 0.8	0.3 ± 0.1	2.9 ± 2.0	20 ± 11
SHARDS20002484	12:37:03.87	62:11:41.75	3.55 ± 0.06	–	24.9 ± 0.1	–	96.1 ± 9.0	–
SHARDS10012723	12:37:03.88	62:14:52.08	4.45 ± 0.07	0.3 ± 0.2	25.5 ± 0.1	0.3 ± 0.2	3725.5 ± 479.7	14 ± 8
SHARDS20006129	12:37:03.95	62:12:32.99	5.79 ± 0.06	0.5 ± 0.2	25.4 ± 0.0	0.4 ± 0.2	26.5 ± 1.5	11 ± 5
SHARDS20004933	12:37:03.99	62:11:57.52	3.42 ± 0.07	4.1 ± 0.2	25.6 ± 0.1	3.8 ± 0.2	42.2 ± 5.4	134 ± 14
SHARDS10011163	12:37:04.03	62:18:00.13	4.35 ± 0.06	–	26.5 ± 0.2	–	31.7 ± 6.6	–
SHARDS10007044	12:37:04.03	62:20:49.29	4.24 ± 0.07	–	26.4 ± 0.3	–	30.3 ± 9.1	–
SHARDS20012005	12:37:04.12	62:13:40.23	3.62 ± 0.06	0.1 ± 0.2	27.3 ± 0.6	0.1 ± 0.2	63.4 ± 35.3	16 ± 22
SHARDS20009776	12:37:04.16	62:09:43.57	4.64 ± 0.07	–	27.6 ± 1.3	–	1.7 ± 2.1	–
SHARDS10017960	12:37:04.21	62:16:36.06	3.79 ± 0.06	0.5 ± 0.1	–	0.4 ± 0.1	–	127 ± 49
SHARDS10007812	12:37:04.26	62:15:59.34	5.03 ± 0.06	–	25.9 ± 0.4	–	57.6 ± 19.8	–
SHARDS20002017	12:37:04.35	62:11:04.81	3.27 ± 0.07	0.2 ± 0.1	26.8 ± 0.3	0.2 ± 0.1	2.1 ± 0.6	47 ± 53
SHARDS10008370	12:37:04.38	62:16:19.37	4.34 ± 0.06	–	26.7 ± 0.3	–	5.5 ± 1.8	–

Continued on next page

Table A.1 – *Continued from previous page*

Object Name	R.A. (J2000)	Dec. (J2000)	z	$L_{Ly\alpha}$ (10^{42} erg s^{-1})	m_{1500} (AB mag)	$SFR_{L_{Ly\alpha}}$ ($M_\odot$ yr^{-1})	$SFR_{L_{1500}}$ ($M_\odot$ yr^{-1})	EW$_0$ (Å)
SHARDS20007025	12:37:04.38	62:12:26.59	3.88 ± 0.06	0.4 ± 0.2	25.9 ± 0.3	0.3 ± 0.2	6.8 ± 1.5	33 ± 20
SHARDS20011495	12:37:04.39	62:14:54.05	3.70 ± 0.06	—	26.0 ± 0.1	—	46.7 ± 6.9	—
SHARDS10008598	12:37:04.52	62:17:20.14	4.77 ± 0.07	—	26.0 ± 0.1	—	13.5 ± 1.9	—
SHARDS20012579	12:37:04.52	62:13:54.69	3.68 ± 0.06	—	27.1 ± 0.2	—	5.9 ± 0.8	—
SHARDS20007077	12:37:04.61	62:12:47.70	3.60 ± 0.06	0.5 ± 0.2	25.9 ± 0.2	0.4 ± 0.2	8.4 ± 1.6	26 ± 13
SHARDS20007051	12:37:04.61	62:10:46.16	3.41 ± 0.06	0.4 ± 0.2	26.5 ± 0.3	0.3 ± 0.2	11.3 ± 2.8	51 ± 35
SHARDS20027722	12:37:04.80	62:14:17.56	3.39 ± 0.06	0.2 ± 0.2	26.9 ± 0.1	0.2 ± 0.1	2.5 ± 0.3	36 ± 28
SHARDS10006774	12:37:04.82	62:15:04.12	4.23 ± 0.07	—	26.5 ± 0.1	—	4.3 ± 0.5	—
SHARDS10006795	12:37:04.85	62:15:00.05	4.45 ± 0.07	0.6 ± 0.1	26.8 ± 0.4	0.6 ± 0.1	12.2 ± 4.6	—
SHARDS20026753	12:37:04.87	62:14:23.04	3.77 ± 0.06	—	25.4 ± 0.1	—	39.1 ± 4.7	—
SHARDS10006417	12:37:04.91	62:15:44.06	3.61 ± 0.06	0.3 ± 0.2	25.2 ± 0.1	0.3 ± 0.2	15.4 ± 1.3	11 ± 7
SHARDS20015794	12:37:04.94	62:15:05.69	4.60 ± 0.07	1.1 ± 0.2		1.0 ± 0.2		151 ± 32
SHARDS20017122	12:37:04.95	62:11:44.72	3.56 ± 0.06		26.3 ± 0.3		20.1 ± 5.5	
SHARDS20015118	12:37:04.99	62:13:45.38	3.47 ± 0.06	0.2 ± 0.1	27.3 ± 0.4	0.2 ± 0.1	3.2 ± 1.3	25 ± 25
SHARDS10003566	12:37:05.01	62:17:32.20	3.94 ± 0.06		24.8 ± 0.1		128.5 ± 12.3	
SHARDS20007955	12:37:05.02	62:13:07.85	4.47 ± 0.07	—	25.2 ± 0.1	—	16.7 ± 1.6	—
SHARDS20015240	12:37:05.04	62:13:17.80	4.29 ± 0.06	—	25.8 ± 0.1	—	10.8 ± 1.6	—
SHARDS20006378	12:37:05.07	62:16:43.55	3.64 ± 0.06	0.1 ± 0.1	26.8 ± 0.4	0.1 ± 0.1	14.1 ± 5.3	7 ± 6
SHARDS10004141	12:37:05.10	62:20:09.89	3.67 ± 0.06	0.3 ± 0.2	26.1 ± 0.2	0.2 ± 0.2	23.6 ± 4.5	17 ± 11
SHARDS20010628	12:37:05.29	62:22:23.48	3.97 ± 0.07		25.9 ± 0.2		7.4 ± 1.3	
SHARDS20007116	12:37:05.29	62:12:16.40	3.47 ± 0.07	0.3 ± 0.2	25.9 ± 0.1	0.3 ± 0.2	14.4 ± 2.2	19 ± 11
SHARDS20017828	12:37:05.33	62:16:09.68	3.46 ± 0.07	—	27.4 ± 0.3	—	2.0 ± 0.5	—
SHARDS10006400	12:37:05.36	62:13:11.03	4.46 ± 0.07	—	26.1 ± 0.4	—	8.1 ± 3.4	—
SHARDS20008799	12:37:05.42	62:16:13.25	4.47 ± 0.08	—	26.6 ± 0.1	—	13.3 ± 1.8	—
SHARDS10006400	12:37:05.45	62:16:10.07	4.37 ± 0.07	—	26.0 ± 0.5	—	61.5 ± 27.3	—
SHARDS10007002	12:37:05.45	62:20:54.07	3.75 ± 0.06	0.9 ± 0.0	25.8 ± 0.1	0.8 ± 0.0	53.9 ± 8.1	134 ± 20
SHARDS10011501	12:37:05.52	62:16:54.99	3.57 ± 0.06		24.6 ± 0.0		56.0 ± 4.5	
SHARDS20002483	12:37:05.53	62:11:41.65	3.55 ± 0.06	—	26.1 ± 0.3	—	8.2 ± 2.0	—
SHARDS20006027	12:37:05.54	62:20:40.01	4.24 ± 0.07	—	25.9 ± 0.2	—	24.6 ± 5.1	—
SHARDS20006560	12:37:05.56	62:16:03.92	4.21 ± 0.14	1.0 ± 0.6	26.7 ± 0.0	0.9 ± 0.6	11.8 ± 1.3	37 ± 32
SHARDS10007840	12:37:05.58	62:13:40.81	3.62 ± 0.06	0.5 ± 0.2	26.4 ± 0.3	0.4 ± 0.2	7.4 ± 2.3	55 ± 26
SHARDS10007944	12:37:05.60	62:20:38.03	3.81 ± 0.06	—	26.4 ± 0.2	—	22.9 ± 6.1	—
SHARDS20008105	12:37:05.61	62:11:34.31	4.27 ± 0.07	—	25.5 ± 0.2	—	27.4 ± 5.8	—
SHARDS20009084	12:37:05.66	62:18:46.65	4.09 ± 0.07	—	25.2 ± 0.1	—	19.1 ± 0.3	—
SHARDS10009208	12:37:05.88	62:12:52.01	3.36 ± 0.07	1.2 ± 0.3	27.7 ± 0.2	1.1 ± 0.2	2.1 ± 0.3	98 ± 56
SHARDS20003652	12:37:05.96	62:09:17.69	3.67 ± 0.06		25.7 ± 0.1		29.9 ± 3.8	
SHARDS20007226	12:37:06.10	62:10:00.07	3.54 ± 0.06	0.4 ± 0.2	25.6 ± 0.4	0.3 ± 0.1	5.9 ± 2.2	66 ± 41
SHARDS20005167	12:37:06.13	62:16:21.25	3.93 ± 0.06	0.6 ± 0.2	25.8 ± 0.1	0.6 ± 0.2	27.0 ± 3.3	—
SHARDS10002183	12:37:06.18	62:09:41.96	3.06 ± 0.06		26.0 ± 0.3		41.2 ± 13.3	
SHARDS20009961	12:37:06.21	62:11:44.91	6.50 ± 0.11	0.5 ± 0.3		0.4 ± 0.3		33 ± 12
SHARDS20017868	12:37:06.24	62:20:21.04	4.21 ± 0.07		26.6 ± 0.2		4.9 ± 0.9	—
SHARDS10009642	12:37:06.37	62:16:55.80	4.34 ± 0.06	0.4 ± 0.1		0.3 ± 0.1		—
SHARDS10014162	12:37:06.37	62:11:56.31	4.67 ± 0.07		27.0 ± 0.7		3.1 ± 1.9	—
SHARDS20018366	12:37:06.42	62:13:20.53	3.62 ± 0.06	0.7 ± 0.2	25.4 ± 0.1	0.6 ± 0.2	16.1 ± 2.0	45 ± 17
SHARDS20007435	12:37:06.47	62:15:22.83	5.30 ± 0.07	1.2 ± 0.0	–	1.1 ± 0.0		
SHARDS10006812	12:37:06.47	62:15:22.83	5.30 ± 0.07	1.2 ± 0.0	–	1.1 ± 0.0		

Continued on next page

Table A.1 – *Continued from previous page*

Object Name	R.A. (J2000)	Dec. (J2000)	z	$L_{Ly\alpha}$ (10^{42} erg s^{-1})	m_{1500} (AB mag)	$SFR_{L_{Ly\alpha}}$ ($M_\odot$ yr^{-1})	$SFR_{L_{1500}}$ ($M_\odot$ yr^{-1})	EW_0 (Å)
SHARDS10001631	12:37:06.55	62:15:35.41	3.51 ± 0.06	1.6 ± 0.2	25.1 ± 0.1	1.4 ± 0.1	15.0 ± 1.5	34 ± 4
SHARDS20004742	12:37:06.64	62:13:49.03	3.22 ± 0.07	–	24.9 ± 0.1	–	57.5 ± 5.7	–
SHARDS20006584	12:37:06.71	62:13:48.26	3.37 ± 0.07	–	25.1 ± 0.1	–	21.4 ± 2.3	–
SHARDS20008740	12:37:06.79	62:11:10.46	3.55 ± 0.06	–	26.2 ± 0.2	–	9.0 ± 1.7	–
SHARDS20010093	12:37:06.82	62:10:28.46	3.82 ± 0.06	–	26.7 ± 0.1	–	4.0 ± 0.4	–
SHARDS20011103	12:37:06.86	62:11:51.39	4.11 ± 0.07	–	27.0 ± 0.8	–	2.4 ± 1.7	–
SHARDS20012384	12:37:06.87	62:12:11.59	5.24 ± 0.07	–	26.1 ± 0.2	–	8.2 ± 1.4	–
SHARDS20010764	12:37:06.87	62:10:49.83	3.96 ± 0.06	–	27.0 ± 0.1	–	2.3 ± 0.3	–
SHARDS20009601	12:37:06.93	62:10:38.31	3.41 ± 0.07	–	26.4 ± 0.2	–	6.1 ± 1.2	–
SHARDS20005013	12:37:07.06	62:10:32.66	3.54 ± 0.06	–	25.2 ± 0.1	–	109.6 ± 11.3	–
SHARDS10006050	12:37:07.07	62:15:07.37	3.38 ± 0.07	–	25.8 ± 0.1	–	10.3 ± 1.3	–
SHARDS10011034	12:37:07.14	62:17:21.55	3.80 ± 0.06	–	27.0 ± 0.2	–	2.1 ± 0.4	–
SHARDS10013254	12:37:07.15	62:15:00.85	3.64 ± 0.06	0.2 ± 0.1	–	0.2 ± 0.1	–	78 ± 94
SHARDS10010974	12:37:07.15	62:17:23.35	3.80 ± 0.06	0.3 ± 0.2	27.1 ± 0.5	0.3 ± 0.2	2.1 ± 1.0	64 ± 49
SHARDS10017890	12:37:07.20	62:15:10.87	4.21 ± 0.07	0.2 ± 0.1	–	0.1 ± 0.1	–	–
SHARDS20008006	12:37:07.27	62:13:31.09	3.90 ± 0.06	–	26.8 ± 0.1	–	24.5 ± 2.4	–
SHARDS10016620	12:37:07.27	62:16:04.55	4.47 ± 0.07	–	27.4 ± 0.3	–	2.0 ± 0.6	–
SHARDS20007684	12:37:07.35	62:11:24.57	4.11 ± 0.07	–	26.9 ± 0.7	–	4.8 ± 3.3	–
SHARDS20004680	12:37:07.35	62:13:53.37	3.63 ± 0.06	0.4 ± 0.2	24.5 ± 0.1	0.4 ± 0.2	103.5 ± 8.5	7 ± 3
SHARDS20008879	12:37:07.44	62:13:34.56	4.04 ± 0.07	0.1 ± 0.2	26.6 ± 0.5	0.1 ± 0.1	8.9 ± 4.3	10 ± 14
SHARDS20007333	12:37:07.55	62:11:25.18	3.83 ± 0.06	–	25.6 ± 0.2	–	22.1 ± 3.5	–
SHARDS20017009	12:37:07.60	62:12:38.09	4.29 ± 0.06	0.2 ± 0.1	27.1 ± 0.7	0.2 ± 0.1	2.5 ± 1.5	26 ± 20
SHARDS10007935	12:37:07.70	62:16:35.25	3.93 ± 0.06	0.7 ± 0.2	26.3 ± 0.2	0.7 ± 0.1	5.1 ± 1.2	79 ± 31
SHARDS10014265	12:37:07.73	62:15:37.44	5.86 ± 0.06	0.3 ± 0.2	26.1 ± 0.1	0.3 ± 0.2	44.4 ± 3.6	25 ± 22
SHARDS20014756	12:37:07.79	62:10:35.35	3.41 ± 0.07	0.1 ± 0.2	26.9 ± 0.3	0.1 ± 0.2	2.1 ± 0.6	26 ± 31
SHARDS20018464	12:37:07.80	62:14:02.76	3.49 ± 0.06	0.5 ± 0.2	–	0.4 ± 0.1	–	126 ± 128
SHARDS20006889	12:37:08.01	62:10:33.95	3.68 ± 0.06	0.1 ± 0.2	26.1 ± 0.2	0.1 ± 0.1	7.2 ± 1.6	8 ± 7
SHARDS20006636	12:37:08.04	62:12:10.95	5.50 ± 0.07	0.7 ± 0.6	25.2 ± 0.1	0.6 ± 0.6	100.1 ± 7.5	27 ± 30
SHARDS10009030	12:37:08.05	62:15:47.71	4.22 ± 0.07	–	26.5 ± 0.1	–	12.3 ± 1.3	–
SHARDS10006921	12:37:08.12	62:14:34.93	4.60 ± 0.07	0.3 ± 0.2	27.3 ± 0.4	0.3 ± 0.2	3.7 ± 1.3	25 ± 18
SHARDS10010910	12:37:08.28	62:14:40.34	3.23 ± 0.07	–	27.3 ± 0.4	–	2.6 ± 1.1	–
SHARDS10015239	12:37:08.29	62:17:14.97	6.02 ± 0.07	0.2 ± 0.2	27.3 ± 0.3	0.1 ± 0.2	10.2 ± 3.0	13 ± 13
SHARDS10010100	12:37:08.40	62:21:14.48	3.68 ± 0.06	0.1 ± 0.2	27.6 ± 0.8	0.1 ± 0.2	1.2 ± 0.9	11 ± 12
SHARDS10008970	12:37:08.48	62:15:05.10	5.30 ± 0.07	0.6 ± 0.2	–	0.6 ± 0.2	–	44 ± 14
SHARDS20013235	12:37:08.49	62:09:52.59	3.81 ± 0.06	–	25.9 ± 0.2	–	6.4 ± 1.4	–
SHARDS20009681	12:37:08.56	62:13:33.22	4.19 ± 0.07	–	26.7 ± 0.5	–	23.8 ± 10.0	–
SHARDS10009981	12:37:08.63	62:14:26.28	3.91 ± 0.06	1.0 ± 0.2	25.0 ± 0.1	0.9 ± 0.2	15.1 ± 1.8	28 ± 6
SHARDS20009051	12:37:08.68	62:09:51.63	4.24 ± 0.07	–	27.0 ± 0.1	–	2.7 ± 0.3	–
SHARDS10017359	12:37:08.76	62:14:17.41	4.45 ± 0.07	0.7 ± 0.2	–	0.6 ± 0.2	–	97 ± 73
SHARDS20006923	12:37:08.81	62:12:03.61	3.74 ± 0.06	0.4 ± 0.2	25.7 ± 0.4	0.3 ± 0.2	11.7 ± 4.1	17 ± 7
SHARDS20013188	12:37:08.85	62:10:42.66	3.96 ± 0.06	0.3 ± 0.2	27.0 ± 0.1	0.3 ± 0.1	2.3 ± 0.3	51 ± 45
SHARDS20008463	12:37:08.86	62:11:39.70	3.42 ± 0.07	–	26.6 ± 0.3	–	9.0 ± 2.3	–
SHARDS10003587	12:37:08.96	62:17:29.45	3.67 ± 0.06	0.6 ± 0.2	25.3 ± 0.1	0.5 ± 0.2	10.4 ± 1.1	32 ± 11
SHARDS20012347	12:37:09.08	62:10:11.19	4.65 ± 0.07	0.2 ± 0.2	27.2 ± 0.2	0.1 ± 0.2	2.6 ± 0.5	14 ± 17
SHARDS10006899	12:37:09.09	62:15:18.73	4.61 ± 0.07	–	26.2 ± 0.1	–	6.1 ± 0.8	–
SHARDS10007913	12:37:09.10	62:18:01.48	3.81 ± 0.06	–	26.8 ± 0.5	–	18.9 ± 9.0	–
SHARDS10008659	12:37:09.19	62:15:15.94	4.46 ± 0.07	–	26.2 ± 0.4	–	14.2 ± 5.4	–
SHARDS20009757	12:37:09.19	62:10:41.59	4.37 ± 0.06	–	26.5 ± 0.2	–	7.1 ± 1.6	–

Continued on next page

Table A.1 – *Continued from previous page*

Object Name	R.A.	Dec.	z	$L_{\mathrm{Ly}\alpha}$	m_{1500}	$\mathrm{SFR}_{L_{\mathrm{Ly}\alpha}}$	$\mathrm{SFR}_{L_{1500}}$	EW_0
	(J2000)	(J2000)		(10^{42} erg s^{-1})	(AB mag)	($M_\odot$ yr^{-1})	($M_\odot$ yr^{-1})	(Å)
SHARDS20009608	12:37:09.26	62:13:29.70	3.62 ± 0.06	0.3 ± 0.2	26.4 ± 0.3	0.3 ± 0.2	5.3 ± 1.4	30 ± 20
SHARDS10014616	12:37:09.28	62:16:18.49	5.87 ± 0.06	0.5 ± 0.1	–	0.4 ± 0.1	–	–
SHARDS10007012	12:37:09.29	62:16:00.67	3.93 ± 0.06	0.9 ± 0.2	25.6 ± 0.1	0.8 ± 0.2	8.4 ± 1.2	132 ± 69
SHARDS10010257	12:37:09.43	62:19:04.74	4.93 ± 0.08	–	27.8 ± 0.6	–	7.7 ± 4.6	–
SHARDS20008657	12:37:09.47	62:13:42.44	4.31 ± 0.06	–	26.6 ± 0.3	–	18.0 ± 5.5	–
SHARDS20009024	12:37:09.48	62:09:56.41	4.65 ± 0.07	–	26.3 ± 0.4	–	30.0 ± 12.1	–
SHARDS10001262	12:37:09.55	62:14:57.00	3.64 ± 0.06	0.3 ± 0.2	25.3 ± 0.1	0.3 ± 0.2	116.6 ± 14.9	13 ± 7
SHARDS20002042	12:37:09.56	62:11:07.29	3.42 ± 0.07	–	25.1 ± 0.1	–	70.6 ± 7.5	–
SHARDS10004461	12:37:09.69	62:21:07.13	3.96 ± 0.06	1.8 ± 0.2	24.8 ± 0.1	1.6 ± 0.2	55.4 ± 4.9	29 ± 3
SHARDS20001516	12:37:09.74	62:10:16.48	3.41 ± 0.07	–	24.8 ± 0.1	–	39.3 ± 4.0	–
SHARDS10009342	12:37:09.75	62:20:35.72	3.41 ± 0.07	–	27.0 ± 0.3	–	100.0 ± 26.4	–
SHARDS10011820	12:37:09.76	62:14:09.52	3.91 ± 0.06	0.4 ± 0.2	26.5 ± 0.3	0.4 ± 0.1	12.8 ± 3.6	82 ± 66
SHARDS20024692	12:37:09.78	62:14:00.30	3.63 ± 0.06	0.2 ± 0.2	25.3 ± 0.1	0.2 ± 0.2	26.2 ± 3.1	5 ± 5
SHARDS10010161	12:37:09.79	62:16:07.16	4.62 ± 0.07	–	26.0 ± 0.1	–	7.6 ± 0.9	–
SHARDS10005946	12:37:09.83	62:21:11.32	5.07 ± 0.06	–	25.2 ± 0.2	–	88.8 ± 16.9	–
SHARDS10001004	12:37:09.83	62:14:29.39	3.38 ± 0.07	–	24.5 ± 0.0	–	126.6 ± 12.0	–
SHARDS20025321	12:37:09.83	62:14:01.94	3.91 ± 0.06	0.6 ± 0.2	25.4 ± 0.1	0.5 ± 0.2	15.7 ± 2.0	24 ± 7
SHARDS10005528	12:37:09.84	62:14:39.37	4.32 ± 0.06	–	25.6 ± 0.1	–	106.2 ± 15.3	–
SHARDS10011670	12:37:09.92	62:15:31.05	5.17 ± 0.06	–	26.4 ± 0.3	–	6.0 ± 1.8	–
SHARDS10013088	12:37:09.94	62:16:08.90	3.65 ± 0.06	–	27.3 ± 0.2	–	414.7 ± 68.9	–
SHARDS20008110	12:37:10.01	62:13:48.27	3.63 ± 0.06	–	26.7 ± 0.4	–	20.1 ± 7.0	–
SHARDS10013903	12:37:10.04	62:15:39.40	3.65 ± 0.06	0.1 ± 0.2	27.9 ± 1.1	0.1 ± 0.2	5.4 ± 5.2	18 ± 29
SHARDS10010039	12:37:10.04	62:20:47.95	4.92 ± 0.08	–	25.9 ± 0.1	–	110.7 ± 14.5	–
SHARDS10006603	12:37:10.16	62:20:00.99	4.25 ± 0.07	–	26.3 ± 0.3	–	12.5 ± 3.9	–
SHARDS20015541	12:37:10.18	62:12:18.26	5.69 ± 0.06	0.7 ± 0.3	27.4 ± 0.1	0.6 ± 0.3	2.8 ± 0.3	52 ± 28
SHARDS10010350	12:37:10.20	62:16:50.47	4.63 ± 0.07	–	27.0 ± 0.3	–	2.9 ± 0.7	–
SHARDS10009059	12:37:10.41	62:14:48.60	3.78 ± 0.06	0.2 ± 0.2	27.0 ± 0.5	0.2 ± 0.2	5.3 ± 2.2	24 ± 20
SHARDS20024706	12:37:10.48	62:13:58.50	4.59 ± 0.07	0.3 ± 0.1	–	0.3 ± 0.1	–	–
SHARDS20009275	12:37:10.50	62:11:58.05	4.02 ± 0.07	–	26.1 ± 0.4	–	5.7 ± 2.0	–
SHARDS20009738	12:37:10.61	62:10:27.61	4.50 ± 0.07	0.9 ± 0.2	–	0.8 ± 0.2	–	122 ± 90
SHARDS10005835	12:37:10.62	62:14:52.57	3.64 ± 0.06	–	25.8 ± 0.2	–	29.0 ± 4.6	–
SHARDS20004928	12:37:10.66	62:12:38.99	3.83 ± 0.06	–	24.9 ± 0.0	–	623.1 ± 51.1	–
SHARDS10005433	12:37:10.66	62:16:010.0	4.62 ± 0.07	–	24.9 ± 0.0	–	60.5 ± 4.6	–
SHARDS10001648	12:37:10.85	62:15:36.83	3.51 ± 0.06	–	25.9 ± 0.2	–	5.8 ± 1.0	–
SHARDS20001484	12:37:10.86	62:10:13.40	3.41 ± 0.07	–	25.1 ± 0.1	–	42.0 ± 5.1	–
SHARDS10005647	12:37:10.95	62:20:59.82	4.25 ± 0.07	–	26.7 ± 0.4	–	23.9 ± 9.9	–
SHARDS20001899	12:37:10.96	62:10:54.78	3.41 ± 0.07	–	25.7 ± 0.1	–	17.2 ± 2.3	–
SHARDS10010091	12:37:11.06	62:15:34.91	4.47 ± 0.07	–	27.0 ± 0.8	–	22.0 ± 15.6	–
SHARDS10008299	12:37:11.11	62:16:38.59	5.19 ± 0.06	0.3 ± 0.1	25.8 ± 0.1	0.2 ± 0.1	58.5 ± 4.6	–
SHARDS10006279	12:37:11.11	62:15:04.73	4.46 ± 0.07	–	26.7 ± 0.6	–	3.9 ± 2.0	–
SHARDS20022683	12:37:11.11	62:12:43.55	3.89 ± 0.06	0.2 ± 0.2	25.9 ± 0.2	0.1 ± 0.2	197.2 ± 44.8	6 ± 6
SHARDS10005969	12:37:11.12	62:16:14.05	3.52 ± 0.06	1.5 ± 0.2	25.7 ± 0.1	1.4 ± 0.1	6.3 ± 0.8	124 ± 38
SHARDS10006745	12:37:11.47	62:20:20.75	4.25 ± 0.07	–	25.9 ± 0.2	–	54.8 ± 10.6	–
SHARDS10004929	12:37:11.48	62:21:55.50	4.10 ± 0.07	–	24.4 ± 0.1	–	207.0 ± 23.2	–
SHARDS10012240	12:37:11.57	62:20:54.16	3.82 ± 0.06	–	26.7 ± 0.4	–	22.8 ± 7.9	–
SHARDS20024273	12:37:11.59	62:12:54.35	4.42 ± 0.07	–	26.7 ± 0.2	–	10.4 ± 1.8	–
SHARDS10007484	12:37:11.68	62:15:07.23	4.46 ± 0.07	0.2 ± 0.2	26.4 ± 0.1	0.2 ± 0.1	4.9 ± 0.6	35 ± 34
SHARDS10008124	12:37:11.73	62:18:27.22	5.20 ± 0.06	–	25.7 ± 0.2	–	20.1 ± 3.1	–

Continued on next page

Table A.1 – *Continued from previous page*

Object Name	R.A. (J2000)	Dec. (J2000)	z	$L_{Ly\alpha}$ (10^{42} erg s^{-1})	m_{1500} (AB mag)	$SFR_{L_{Ly\alpha}}$ ($M_\odot$ yr^{-1})	$SFR_{L_{1500}}$ ($M_\odot$ yr^{-1})	EW_0 (Å)
SHARDS20010003	12:37:11.87	62:11:52.59	5.22 ± 0.06	0.2 ± 0.4	26.3 ± 0.2	0.2 ± 0.4	7.0 ± 1.3	20 ± 37
SHARDS10005600	12:37:11.89	62:14:35.01	4.45 ± 0.07	–	25.9 ± 0.3	–	38.4 ± 10.2	–
SHARDS20007787	12:37:11.92	62:10:02.86	4.49 ± 0.07	–	26.3 ± 0.3	–	22.4 ± 6.6	–
SHARDS20008760	12:37:11.95	62:11:36.96	4.80 ± 0.07	0.2 ± 0.3	26.7 ± 0.3	0.2 ± 0.3	4.4 ± 1.3	19 ± 23
SHARDS20008702	12:37:12.09	62:10:54.06	5.21 ± 0.06	1.1 ± 0.2	–	1.0 ± 0.2	–	97 ± 47
SHARDS10006628	12:37:12.09	62:20:39.61	3.96 ± 0.06	0.2 ± 0.2	26.2 ± 0.1	0.2 ± 0.1	17.0 ± 2.5	14 ± 12
SHARDS10006574	12:37:12.25	62:14:36.07	4.33 ± 0.06	0.4 ± 0.2	26.5 ± 0.3	0.3 ± 0.1	4.4 ± 1.1	22 ± 10
SHARDS10006858	12:37:12.32	62:14:16.52	4.60 ± 0.07	–	26.2 ± 0.1	–	6.5 ± 0.9	–
SHARDS10008529	12:37:12.33	62:16:25.95	4.35 ± 0.06	0.8 ± 0.1	–	0.7 ± 0.1	–	70 ± 21
SHARDS10007096	12:37:12.33	62:15:32.88	3.65 ± 0.06	–	26.3 ± 0.2	–	4.6 ± 1.1	–
SHARDS10005562	12:37:12.33	62:16:07.60	4.08 ± 0.07	–	25.7 ± 0.2	–	10.3 ± 2.3	–
SHARDS10014170	12:37:12.43	62:18:28.10	6.24 ± 0.14	2.1 ± 0.1	–	1.9 ± 0.1	–	–
SHARDS10018196	12:37:12.48	62:15:21.15	5.17 ± 0.06	0.7 ± 0.2	–	0.7 ± 0.2	–	78 ± 52
SHARDS20011614	12:37:12.51	62:10:23.54	3.54 ± 0.06	0.9 ± 0.1	27.3 ± 0.5	0.8 ± 0.1	2.9 ± 1.4	122 ± 28
SHARDS10007175	12:37:12.58	62:21:37.71	4.37 ± 0.06	0.3 ± 0.1	26.1 ± 0.3	0.3 ± 0.1	6.4 ± 1.7	28 ± 14
SHARDS10005464	12:37:12.62	62:21:59.28	4.65 ± 0.07	–	25.3 ± 0.4	–	105.1 ± 35.5	–
SHARDS10009762	12:37:12.63	62:15:04.16	6.00 ± 0.07	0.5 ± 0.2	26.0 ± 0.1	0.4 ± 0.2	82.3 ± 6.1	70 ± 57
SHARDS10012105	12:37:12.65	62:14:53.21	3.51 ± 0.06	–	26.9 ± 0.4	–	2.2 ± 0.8	–
SHARDS20008527	12:37:12.67	62:10:48.82	4.66 ± 0.07	–	26.7 ± 0.6	–	25.7 ± 14.2	–
SHARDS10006379	12:37:12.76	62:16:58.69	4.36 ± 0.06	–	26.5 ± 0.3	–	6.7 ± 1.9	–
SHARDS20007254	12:37:12.80	62:11:31.99	5.10 ± 0.06	–	25.7 ± 0.3	–	22.1 ± 6.4	–
SHARDS10006522	12:37:12.83	62:21:27.28	4.25 ± 0.07	–	25.7 ± 0.2	–	8.7 ± 1.5	–
SHARDS10006064	12:37:12.94	62:21:36.73	3.41 ± 0.07	–	25.8 ± 0.1	–	38.7 ± 4.9	–
SHARDS10005830	12:37:12.96	62:21:42.37	3.68 ± 0.06	–	26.0 ± 0.2	–	28.5 ± 5.5	–
SHARDS10005728	12:37:13.01	62:20:26.84	3.26 ± 0.07	–	25.9 ± 0.1	–	31.1 ± 4.3	–
SHARDS10005007	12:37:13.04	62:21:11.16	4.25 ± 0.07	–	24.5 ± 0.1	–	170.6 ± 15.2	–
SHARDS20016918	12:37:13.07	62:12:06.08	6.61 ± 0.14	–	27.3 ± 0.1	–	77.4 ± 11.8	–
SHARDS10006384	12:37:13.10	62:16:06.73	3.94 ± 0.06	0.6 ± 0.2	25.0 ± 0.1	0.5 ± 0.2	187.3 ± 18.9	18 ± 5
SHARDS10011694	12:37:13.13	62:18:24.13	4.25 ± 0.07	–	27.6 ± 0.9	–	3.6 ± 3.1	–
SHARDS10007072	12:37:13.20	62:18:44.64	3.68 ± 0.06	–	27.0 ± 0.4	–	12.3 ± 5.0	–
SHARDS20007630	12:37:13.20	62:11:08.90	4.26 ± 0.07	–	25.8 ± 0.2	–	16.5 ± 2.7	–
SHARDS10006128	12:37:13.22	62:21:21.36	4.25 ± 0.07	–	26.2 ± 0.3	–	19.2 ± 5.1	–
SHARDS10005324	12:37:13.22	62:15:47.83	4.62 ± 0.07	–	25.1 ± 0.1	–	231.2 ± 18.8	–
SHARDS10010954	12:37:13.26	62:16:06.36	3.52 ± 0.06	–	25.5 ± 0.1	–	96.0 ± 11.4	–
SHARDS10005737	12:37:13.38	62:12:39.24	5.26 ± 0.07	–	25.0 ± 0.1	–	22.5 ± 1.8	–
SHARDS10007421	12:37:13.70	62:21:02.92	3.26 ± 0.07	–	26.5 ± 0.2	–	8.2 ± 1.7	–
SHARDS10007446	12:37:13.76	62:18:48.82	4.50 ± 0.07	–	27.5 ± 1.2	–	3.8 ± 4.3	–
SHARDS10014567	12:37:13.77	62:15:58.72	4.35 ± 0.06	–	27.9 ± 0.5	–	1.2 ± 0.5	–
SHARDS20002400	12:37:13.81	62:11:35.16	3.60 ± 0.06	1.2 ± 0.4	24.8 ± 0.1	1.1 ± 0.3	29.3 ± 3.7	41 ± 18
SHARDS10011875	12:37:13.99	62:14:14.14	3.64 ± 0.06	0.3 ± 0.1	–	0.3 ± 0.1	–	109 ± 63
SHARDS20010744	12:37:13.99	62:11:35.05	4.27 ± 0.07	–	27.0 ± 0.1	–	7.5 ± 1.1	–
SHARDS10007654	12:37:14.01	62:18:39.18	3.96 ± 0.06	–	26.5 ± 0.2	–	19.1 ± 3.4	–
SHARDS10007983	12:37:14.02	62:16:51.60	4.63 ± 0.07	–	26.1 ± 0.1	–	34.3 ± 4.3	–
SHARDS10011747	12:37:14.12	62:14:45.75	3.79 ± 0.06	0.2 ± 0.1	27.0 ± 0.1	0.2 ± 0.1	13.3 ± 1.8	42 ± 30
SHARDS10010712	12:37:14.14	62:15:51.95	4.47 ± 0.07	–	28.0 ± 0.3	–	1.1 ± 0.3	–
SHARDS20004852	12:37:14.22	62:11:03.79	3.82 ± 0.06	–	25.1 ± 0.1	–	67.5 ± 8.4	–
SHARDS10009188	12:37:14.27	62:17:09.69	4.24 ± 0.07	–	26.5 ± 0.3	–	4.1 ± 1.1	–
SHARDS20022641	12:37:14.39	62:12:18.12	3.75 ± 0.06	–	26.7 ± 0.4	–	2.9 ± 1.0	–

Continued on next page

Table A.1 – *Continued from previous page*

Object Name	R.A. (J2000)	Dec. (J2000)	z	$L_{Ly\alpha}$ (10^{42} erg s^{-1})	m_{1500} (AB mag)	$\mathrm{SFR}_{L_{Ly\alpha}}$ ($M_\odot$ yr^{-1})	$\mathrm{SFR}_{L_{1500}}$ ($M_\odot$ yr^{-1})	EW$_0$ (Å)
SHARDS10007197	12:37:14.42	62:15:18.92	4.34 ± 0.06		26.2 ± 0.2		14.5 ± 3.0	
SHARDS10007532	12:37:14.43	62:19:48.93	5.35 ± 0.07	0.5 ± 0.3	25.5 ± 0.2	0.5 ± 0.3	15.3 ± 2.4	50 ± 37
SHARDS10008210	12:37:14.50	62:15:32.45	5.16 ± 0.06	—	26.2 ± 0.3	—	13.4 ± 4.0	—
SHARDS10013225	12:37:14.58	62:13:18.96	3.56 ± 0.07		26.6 ± 0.1		28.8 ± 2.3	
SHARDS10005207	12:37:14.63	62:14:33.46	3.78 ± 0.06	0.2 ± 0.2	25.6 ± 0.1	0.2 ± 0.2	28.6 ± 4.3	9 ± 7
SHARDS10010754	12:37:14.68	62:18:39.40	3.41 ± 0.07	0.3 ± 0.2	25.9 ± 0.1	0.3 ± 0.2	130.9 ± 17.5	12 ± 6
SHARDS10009576	12:37:14.83	62:20:14.77	3.48 ± 0.07	—	27.0 ± 0.6	—	12.6 ± 7.5	—
SHARDS10004652	12:37:14.84	62:15:25.85	3.24 ± 0.07		27.2 ± 0.4		4.8 ± 1.9	
SHARDS10004826	12:37:15.02	62:19:25.33	3.62 ± 0.06	—	27.3 ± 0.1	—	66.8 ± 7.7	—
SHARDS20007944	12:37:15.08	62:11:38.24	3.60 ± 0.06	0.4 ± 0.2	26.5 ± 0.3	0.4 ± 0.2	11.6 ± 3.6	110 ± 141
SHARDS10007280	12:37:15.09	62:13:42.48	4.44 ± 0.06	—	27.5 ± 1.2	—	6.0 ± 6.5	—
SHARDS10003901	12:37:15.10	62:18:31.01	3.68 ± 0.06		25.9 ± 0.1		195.0 ± 10.2	
SHARDS10008506	12:37:15.10	62:20:05.21	4.61 ± 0.07	—	26.2 ± 0.4	—	5.1 ± 2.0	—
SHARDS20000907	12:37:15.10	62:20:40.40	4.63 ± 0.07	—	25.4 ± 0.1	—	117.7 ± 10.7	—
SHARDS20009005	12:37:15.20	62:21:10.91	4.58 ± 0.07	1.7 ± 0.3	—	1.6 ± 0.3	—	131 ± 72
SHARDS20016925	12:37:15.20	62:12:03.09	4.53 ± 0.07	1.0 ± 0.3		0.9 ± 0.3		141 ± 179
SHARDS10005309	12:37:15.24	62:19:14.55	3.37 ± 0.06		26.2 ± 0.2		38.3 ± 8.0	
SHARDS10013708	12:37:15.33	62:13:35.26	3.45 ± 0.07	0.2 ± 0.2	26.0 ± 0.2	0.2 ± 0.2	17.1 ± 2.6	7 ± 8
SHARDS10006852	12:37:15.45	62:14:01.64	4.03 ± 0.07	—	26.5 ± 0.5	—	27.4 ± 12.3	—
SHARDS20022634	12:37:15.63	62:16:28.69	4.13 ± 0.06		26.2 ± 0.1		13.8 ± 1.1	
SHARDS20006357	12:37:15.63	62:16:22.76	4.16 ± 0.06	0.2 ± 0.3	25.8 ± 0.2	0.2 ± 0.3	22.3 ± 4.2	9 ± 12
SHARDS10006577	12:37:15.65	62:15:47.76	4.36 ± 0.06	—	26.6 ± 0.3	—	15.8 ± 4.9	—
SHARDS10012212	12:37:15.70	62:16:49.78	4.45 ± 0.07	—	26.5 ± 0.5	—	11.6 ± 5.1	—
SHARDS20010736	12:37:15.72	62:15:57.15	3.54 ± 0.06	0.2 ± 0.1	27.5 ± 0.3	0.2 ± 0.1	2.7 ± 0.7	22 ± 18
SHARDS20012220	12:37:15.83	62:12:52.36	3.27 ± 0.07	—	26.7 ± 0.2	—	16.5 ± 2.9	—
SHARDS10007252	12:37:15.84	62:16:47.40	4.24 ± 0.07		26.7 ± 0.4		3.5 ± 1.4	
SHARDS10005443	12:37:15.84	62:18:29.47	4.09 ± 0.07	—	25.9 ± 0.3	—	7.2 ± 1.8	—
SHARDS10006107	12:37:15.95	62:19:22.57	4.25 ± 0.06	—	25.2 ± 0.1	—	13.4 ± 1.6	—
SHARDS10006353	12:37:16.13	62:19:50.73	3.54 ± 0.06	—	25.2 ± 0.2	—	60.3 ± 10.8	—
SHARDS20008439	12:37:16.17	62:13:35.48	3.41 ± 0.07	—	27.5 ± 0.5	—	2.5 ± 1.3	—
SHARDS10009411	12:37:16.21	62:13:37.04	3.41 ± 0.06	0.6 ± 0.2		0.5 ± 0.2		71 ± 75
SHARDS10010911	12:37:16.26	62:14:59.54	4.76 ± 0.07		26.5 ± 0.4		5.1 ± 2.0	
SHARDS20015851	12:37:16.28	62:14:32.47	4.20 ± 0.06	0.9 ± 0.1		0.8 ± 0.1		—
SHARDS20014767	12:37:16.33	62:13:32.26	4.20 ± 0.06		27.4 ± 0.8		22.7 ± 17.3	
SHARDS10007889	12:37:16.34	62:22:17.20	3.42 ± 0.07	0.2 ± 0.2	25.8 ± 0.1	0.2 ± 0.2	40.5 ± 5.1	15 ± 11
SHARDS10006459	12:37:16.36	62:16:56.45	3.42 ± 0.07	0.7 ± 0.2	26.5 ± 0.2	0.7 ± 0.2	4.9 ± 1.0	57 ± 20
SHARDS10015417	12:37:16.36	62:14:55.84	6.20 ± 0.14	1.1 ± 0.2		1.0 ± 0.2		212 ± 73
SHARDS10007736	12:37:16.48	62:20:07.31	4.80 ± 0.07		25.6 ± 0.1	—	59.7 ± 6.3	—
SHARDS10011638	12:37:16.55	62:15:51.95	3.94 ± 0.06		26.3 ± 0.3	—	4.4 ± 1.2	—
SHARDS10005186	12:37:16.61	62:13:53.40	3.50 ± 0.06		24.3 ± 0.1	—	45.7 ± 3.9	—
SHARDS10007051	12:37:16.68	62:19:22.19	3.54 ± 0.06		26.3 ± 0.2	—	26.0 ± 5.1	—
SHARDS20022719	12:37:16.68	62:12:07.08	4.57 ± 0.07		24.9 ± 0.0	—	20.7 ± 1.7	—
SHARDS10008600	12:37:16.70	62:16:17.72	3.66 ± 0.06	0.4 ± 0.2	24.6 ± 0.3	0.4 ± 0.2	16.6 ± 4.8	23 ± 10
SHARDS10007105	12:37:16.70	62:17:49.07	3.95 ± 0.06		25.9 ± 0.2	—	46.0 ± 4.1	—
SHARDS20011741	12:37:16.74	62:11:16.56	3.73 ± 0.06		27.2 ± 0.1	—	4.8 ± 0.2	—
SHARDS10005719	12:37:16.82	62:20:44.74	3.83 ± 0.06	0.9 ± 0.2	25.6 ± 0.1	0.8 ± 0.2	18.7 ± 2.5	39 ± 8
SHARDS10006981	12:37:16.87	62:14:00.49	3.29 ± 0.07	—	25.6 ± 0.2	—	104.6 ± 18.2	—
SHARDS10008733	12:37:16.99	62:21:44.82	3.55 ± 0.06	—	27.1 ± 0.4	—	2.4 ± 0.9	—

Continued on next page

Table A.1 – *Continued from previous page*

Object Name	R.A. (J2000)	Dec. (J2000)	z	$L_{Ly\alpha}$ (10^{42} erg s^{-1})	m_{1500} (AB mag)	$SFR_{L_{Ly\alpha}}$ ($M_\odot$ yr^{-1})	$SFR_{L_{1500}}$ ($M_\odot$ yr^{-1})	EW_0 (Å)
SHARDS10003104	12:37:17.13	62:18:19.83	3.68 ± 0.06	–	25.3 ± 0.1	–	281.0 ± 33.8	–
SHARDS10003900	12:37:17.14	62:21:10.28	3.27 ± 0.07	–	24.8 ± 0.1	–	82.7 ± 8.0	–
SHARDS20011164	12:37:17.19	62:11:01.55	4.25 ± 0.07	–	26.8 ± 0.5	–	3.2 ± 1.4	–
SHARDS10007056	12:37:17.21	62:18:59.31	3.96 ± 0.06	0.4 ± 0.2	26.5 ± 0.3	0.4 ± 0.1	3.9 ± 1.0	31 ± 12
SHARDS10014408	12:37:17.24	62:14:59.79	4.22 ± 0.07	0.7 ± 0.3	–	0.7 ± 0.2	–	86 ± 48
SHARDS10007661	12:37:17.30	62:20:05.89	4.38 ± 0.06	–	26.7 ± 0.1	–	11.0 ± 1.6	–
SHARDS10007224	12:37:17.31	62:14:02.45	3.92 ± 0.06	–	26.5 ± 0.3	–	7.2 ± 2.1	–
SHARDS10008525	12:37:17.34	62:13:25.30	5.15 ± 0.06	–	25.2 ± 0.1	–	19.4 ± 2.5	–
SHARDS10005633	12:37:17.47	62:16:38.50	4.49 ± 0.07	–	25.2 ± 0.2	–	61.3 ± 9.5	–
SHARDS10005716	12:37:17.57	62:19:26.28	4.11 ± 0.07	–	26.2 ± 0.3	–	64.2 ± 21.1	–
SHARDS10006402	12:37:17.57	62:13:28.12	3.50 ± 0.06	0.8 ± 0.2	26.2 ± 0.2	0.8 ± 0.1	4.6 ± 0.8	57 ± 18
SHARDS10000432	12:37:17.61	62:13:09.67	3.37 ± 0.07	–	26.8 ± 0.2	–	4.8 ± 1.1	–
SHARDS10003772	12:37:17.69	62:21:49.41	3.27 ± 0.07	–	24.8 ± 0.0	–	72.8 ± 6.9	–
SHARDS10004588	12:37:17.72	62:19:04.59	3.96 ± 0.06	–	24.7 ± 0.1	–	42.5 ± 3.7	–
SHARDS10007493	12:37:17.72	62:20:30.68	3.83 ± 0.06	–	25.6 ± 0.1	–	66.8 ± 9.1	–
SHARDS10005275	12:37:17.84	62:13:04.08	4.31 ± 0.06	–	25.2 ± 0.1	–	42.4 ± 4.4	–
SHARDS10012747	12:37:17.87	62:15:40.76	5.88 ± 0.06	0.2 ± 0.1	26.7 ± 0.1	0.2 ± 0.1	12.5 ± 1.2	22 ± 14
SHARDS10010884	12:37:17.89	62:17:59.06	5.62 ± 0.07	0.9 ± 0.2	–	0.8 ± 0.1	–	166 ± 98
SHARDS10005406	12:37:17.95	62:17:15.56	4.25 ± 0.07	–	25.6 ± 0.2	–	60.2 ± 13.4	–
SHARDS20025351	12:37:18.02	62:11:57.33	4.17 ± 0.07	0.8 ± 0.1	–	0.7 ± 0.1	–	113 ± 43
SHARDS10007010	12:37:18.05	62:13:09.71	4.31 ± 0.06	–	26.4 ± 0.1	–	4.6 ± 0.4	–
SHARDS10005802	12:37:18.07	62:16:41.33	4.78 ± 0.07	0.3 ± 0.3	25.2 ± 0.1	0.2 ± 0.2	48.9 ± 4.4	7 ± 6
SHARDS10009075	12:37:18.11	62:20:14.05	4.66 ± 0.07	–	27.0 ± 0.6	–	3.1 ± 1.8	–
SHARDS10007498	12:37:18.26	62:15:47.07	4.48 ± 0.07	–	26.9 ± 0.8	–	25.1 ± 18.2	–
SHARDS20007547	12:37:18.29	62:10:59.62	3.35 ± 0.07	–	26.9 ± 0.4	–	2.9 ± 1.1	–
SHARDS10001627	12:37:18.33	62:15:35.22	3.40 ± 0.07	–	24.9 ± 0.0	–	23.0 ± 2.2	–
SHARDS10008374	12:37:18.38	62:18:19.22	3.82 ± 0.06	–	27.7 ± 0.9	–	1.2 ± 1.0	–
SHARDS10006456	12:37:18.48	62:22:27.74	4.11 ± 0.07	–	26.0 ± 0.3	–	23.2 ± 6.6	–
SHARDS10006488	12:37:18.65	62:22:28.07	4.50 ± 0.07	0.6 ± 0.2	25.7 ± 0.3	0.6 ± 0.1	17.9 ± 4.8	22 ± 6
SHARDS20025355	12:37:18.66	62:11:56.42	4.17 ± 0.07	–	27.3 ± 0.1	–	1.9 ± 0.2	–
SHARDS10006597	12:37:18.78	62:15:22.74	5.45 ± 0.07	0.3 ± 0.2	25.1 ± 0.1	0.3 ± 0.2	155.0 ± 18.3	8 ± 5
SHARDS10006000	12:37:18.84	62:12:19.42	3.89 ± 0.06	0.5 ± 0.2	25.4 ± 0.1	0.5 ± 0.2	28.6 ± 3.4	37 ± 14
SHARDS10006145	12:37:18.85	62:15:17.52	3.93 ± 0.06	2.4 ± 0.2	25.9 ± 0.2	2.2 ± 0.1	6.8 ± 1.1	106 ± 17
SHARDS10005595	12:37:18.98	62:22:29.66	4.25 ± 0.07	–	25.5 ± 0.1	–	67.8 ± 9.5	–
SHARDS10004376	12:37:19.00	62:19:53.52	4.26 ± 0.07	–	24.4 ± 0.1	–	43.7 ± 3.7	–
SHARDS10016379	12:37:19.07	62:12:49.86	4.30 ± 0.06	–	26.0 ± 0.2	–	32.3 ± 5.9	–
SHARDS10005784	12:37:19.16	62:19:47.94	3.42 ± 0.07	–	26.0 ± 0.1	–	19.8 ± 2.9	–
SHARDS10006640	12:37:19.30	62:14:15.70	3.38 ± 0.07	–	25.9 ± 0.1	–	20.6 ± 2.7	–
SHARDS10005279	12:37:19.45	62:17:26.97	4.10 ± 0.07	–	25.3 ± 0.2	–	77.8 ± 14.1	–
SHARDS10009329	12:37:19.56	62:17:29.86	4.37 ± 0.06	–	27.4 ± 0.2	–	2.9 ± 0.6	–
SHARDS10008605	12:37:19.63	62:16:55.18	5.47 ± 0.07	0.6 ± 0.2	25.9 ± 0.2	0.5 ± 0.2	10.3 ± 2.1	46 ± 27
SHARDS10006108	12:37:19.65	62:22:36.14	4.25 ± 0.07	–	25.8 ± 0.3	–	9.5 ± 2.3	–
SHARDS10005808	12:37:19.69	62:15:42.50	4.48 ± 0.07	–	25.2 ± 0.2	–	87.9 ± 16.1	–
SHARDS10006734	12:37:19.72	62:22:23.44	4.66 ± 0.07	–	26.3 ± 0.4	–	6.0 ± 2.0	–
SHARDS10012165	12:37:19.75	62:16:02.91	5.88 ± 0.06	0.1 ± 0.1	26.8 ± 0.1	0.1 ± 0.1	13.2 ± 1.4	9 ± 9
SHARDS10000880	12:37:19.75	62:14:13.29	3.24 ± 0.07	–	25.5 ± 0.1	–	117.4 ± 13.8	–
SHARDS10017072	12:37:19.80	62:13:21.06	3.23 ± 0.07	0.3 ± 0.1	–	0.2 ± 0.1	–	86 ± 73
SHARDS10008388	12:37:19.80	62:19:58.69	4.38 ± 0.06	–	27.1 ± 0.1	–	6.4 ± 0.9	–

Continued on next page

Table A.1 – *Continued from previous page*

Object Name	R.A. (J2000)	Dec. (J2000)	z	$L_{Ly\alpha}$ (10^{42} erg s^{-1})	m_{1500} (AB mag)	$SFR_{L_{Ly\alpha}}$ ($M_\odot$ yr^{-1})	$SFR_{L_{1500}}$ ($M_\odot$ yr^{-1})	EW$_0$ (Å)
SHARDS10011201	12:37:19.81	62:18:58.65	3.42 ± 0.07	—	27.0 ± 0.3	—	5.7 ± 1.5	—
SHARDS10008895	12:37:19.86	62:19:55.79	3.83 ± 0.06	—	26.9 ± 0.4	—	19.9 ± 8.3	—
SHARDS10010667	12:37:20.02	62:19:00.63	4.26 ± 0.07	1.5 ± 0.3	—	1.4 ± 0.3	—	92 ± 38
SHARDS10010967	12:37:20.02	62:18:53.44	4.00 ± 0.07	0.3 ± 0.0	—	0.2 ± 0.0	—	—
SHARDS10006578	12:37:20.04	62:21:23.83	4.93 ± 0.08	—	25.3 ± 0.1	—	46.6 ± 4.3	—
SHARDS10006672	12:37:20.15	62:21:23.55	3.63 ± 0.06	—	27.7 ± 0.9	—	1.1 ± 0.9	—
SHARDS10005499	12:37:20.23	62:21:47.01	3.79 ± 0.14	0.1 ± 0.2	26.6 ± 0.3	0.1 ± 0.2	3.3 ± 1.0	15 ± 18
SHARDS10015428	12:37:20.32	62:17:10.06	3.72 ± 0.06	1.6 ± 0.9	26.4 ± 0.3	1.5 ± 0.9	8.8 ± 2.3	63 ± 36
SHARDS10006144	12:37:20.35	62:18:35.29	3.68 ± 0.06	—	27.9 ± 0.5	—	12.0 ± 5.4	—
SHARDS10005080	12:37:20.39	62:17:55.74	4.10 ± 0.07	—	26.3 ± 0.2	—	7.6 ± 1.4	—
SHARDS10007090	12:37:20.45	62:22:14.86	4.26 ± 0.07	—	25.1 ± 0.1	—	121.6 ± 16.1	—
SHARDS10007596	12:37:20.50	62:17:33.04	3.41 ± 0.07	—	27.3 ± 0.4	—	16.0 ± 6.0	—
SHARDS20014592	12:37:20.58	62:17:05.77	4.40 ± 0.07	—	24.2 ± 0.1	—	68.9 ± 7.5	—
SHARDS10007449	12:37:20.60	62:17:51.36	3.67 ± 0.06	—	27.3 ± 0.3	—	4.7 ± 2.4	—
SHARDS10005156	12:37:20.60	62:18:46.71	3.55 ± 0.06	0.3 ± 0.2	26.0 ± 0.2	0.3 ± 0.2	13.1 ± 2.4	44 ± 32
SHARDS10005301	12:37:20.71	62:18:40.71	3.59 ± 0.06	—	25.9 ± 0.1	—	174.6 ± 15.7	—
SHARDS10009199	12:37:20.78	62:17:12.86	3.61 ± 0.07	0.1 ± 0.2	26.7 ± 0.5	0.1 ± 0.2	5.1 ± 6.1	17 ± 26
SHARDS10007282	12:37:20.82	62:18:29.30	4.24 ± 0.07	—	25.9 ± 0.2	—	12.7 ± 2.2	—
SHARDS10005491	12:37:20.84	62:18:23.83	4.63 ± 0.07	—	26.7 ± 0.6	—	26.0 ± 13.3	—
SHARDS10009434	12:37:20.85	62:17:07.59	3.24 ± 0.07	0.3 ± 0.3	25.4 ± 0.1	0.3 ± 0.2	105.2 ± 8.6	56 ± 92
SHARDS10005753	12:37:20.89	62:18:07.29	3.64 ± 0.07	—	25.5 ± 0.1	—	27.7 ± 3.3	—
SHARDS10016150	12:37:20.89	62:14:07.72	3.63 ± 0.14	0.2 ± 0.4	27.2 ± 0.2	0.1 ± 0.4	24.3 ± 3.5	16 ± 43
SHARDS10011730	12:37:20.94	62:15:51.76	5.61 ± 0.07	0.3 ± 0.3	26.1 ± 0.2	0.3 ± 0.2	9.5 ± 2.1	19 ± 19
SHARDS20008177	12:37:21.02	62:15:56.44	3.60 ± 0.06	0.6 ± 0.2	25.8 ± 0.2	0.6 ± 0.2	8.8 ± 1.4	123 ± 81
SHARDS20014441	12:37:21.02	62:15:56.65	3.46 ± 0.06	0.6 ± 0.1	—	0.6 ± 0.1	—	—
SHARDS10015520	12:37:21.07	62:19:56.07	5.22 ± 0.06	1.8 ± 0.3	26.4 ± 0.4	1.7 ± 0.3	10.8 ± 4.4	12 ± 2
SHARDS10013980	12:37:21.13	62:22:21.00	4.03 ± 0.07	—	26.6 ± 0.9	—	4.4 ± 3.6	—
SHARDS10000066	12:37:21.17	62:21:45.93	4.11 ± 0.07	—	26.4 ± 0.5	—	8.1 ± 3.4	—
SHARDS20010936	12:37:21.18	62:17:17.22	4.91 ± 0.08	—	26.6 ± 0.1	—	3.5 ± 0.4	—
SHARDS20012627	12:37:21.19	62:13:59.28	3.36 ± 0.07	—	26.9 ± 0.3	—	24.0 ± 6.6	—
SHARDS20015171	12:37:21.25	62:15:05.68	3.36 ± 0.08	0.6 ± 0.1	—	0.6 ± 0.1	—	322 ± 130
SHARDS20005603	12:37:21.28	62:13:10.25	3.38 ± 0.07	0.1 ± 0.2	25.7 ± 0.1	0.1 ± 0.2	47.3 ± 5.7	22 ± 33
SHARDS10009097	12:37:21.29	62:17:38.74	4.38 ± 0.07	—	26.2 ± 0.7	—	10.2 ± 1.5	—
SHARDS10006728	12:37:21.43	62:17:38.13	3.63 ± 0.06	—	26.7 ± 0.7	—	8.9 ± 5.8	—
SHARDS10000371	12:37:21.45	62:21:59.60	3.53 ± 0.06	—	24.4 ± 0.1	—	62.6 ± 5.3	—
SHARDS10005492	12:37:21.48	62:18:41.94	3.78 ± 0.06	—	25.3 ± 0.2	—	42.7 ± 4.4	—
SHARDS10007376	12:37:21.49	62:13:00.07	3.63 ± 0.06	—	26.7 ± 0.2	—	12.2 ± 2.8	—
SHARDS10008057	12:37:21.57	62:19:11.95	3.26 ± 0.07	0.2 ± 0.3	26.8 ± 0.6	0.2 ± 0.3	7.2 ± 3.8	24 ± 34
SHARDS10009068	12:37:21.59	62:17:23.42	3.36 ± 0.07	—	27.6 ± 0.6	—	1.6 ± 0.9	—
SHARDS10014866	12:37:21.58	62:16:33.38	3.67 ± 0.06	—	26.9 ± 0.2	—	2.4 ± 0.5	—
SHARDS10008856	12:37:21.71	62:13:16.97	3.50 ± 0.06	0.5 ± 0.1	—	0.5 ± 0.1	—	121 ± 29
SHARDS10010894	12:37:21.74	62:15:05.04	3.04 ± 0.06	0.3 ± 0.1	25.9 ± 0.4	0.3 ± 0.1	302.4 ± 103.5	33 ± 17
SHARDS10010379	12:37:21.78	62:14:41.41	5.34 ± 0.07	—	26.9 ± 0.5	—	4.0 ± 1.9	—
SHARDS10011292	12:37:21.98	62:19:01.09	4.66 ± 0.07	—	26.7 ± 0.5	—	19.4 ± 8.8	—
SHARDS10010964	12:37:22.02	62:14:37.37	3.79 ± 0.06	—	25.9 ± 0.2	—	12.0 ± 2.2	—
SHARDS10007478	12:37:22.06	62:13:55.42	5.99 ± 0.07	—	26.2 ± 0.1	—	9.4 ± 0.8	—

Continued on next page

Table A.1 – *Continued from previous page*

Object Name	R.A. (J2000)	Dec. (J2000)	z	$L_{Ly\alpha}$ (10^{42} erg s^{-1})	m_{1500} (AB mag)	$SFR_{L_{Ly\alpha}}$ ($M_\odot$ yr^{-1})	$SFR_{L_{1500}}$ ($M_\odot$ yr^{-1})	EW$_0$ (Å)
SHARDS10003185	12:37:22.09	62:18:12.36	3.68 ± 0.06	–	25.5 ± 0.1	–	49.3 ± 6.3	–
SHARDS10006133	12:37:22.13	62:13:57.93	3.38 ± 0.07	1.6 ± 0.2	26.2 ± 0.1	1.5 ± 0.2	3.9 ± 0.6	93 ± 17
SHARDS10009690	12:37:22.13	62:15:53.82	4.92 ± 0.08	0.4 ± 0.1	–	0.3 ± 0.1	–	60 ± 23
SHARDS10007821	12:37:22.14	62:15:46.24	5.46 ± 0.07	–	26.6 ± 0.5	–	21.3 ± 9.4	–
SHARDS10007626	12:37:22.26	62:21:47.29	3.97 ± 0.06	0.8 ± 0.2	26.6 ± 0.2	0.7 ± 0.2	7.4 ± 1.7	141 ± 78
SHARDS10007454	12:37:22.45	62:14:14.80	3.79 ± 0.06	–	26.4 ± 0.3	–	3.7 ± 1.1	–
SHARDS10016659	12:37:22.75	62:12:28.39	3.62 ± 0.06	0.3 ± 0.2	27.6 ± 0.2	0.2 ± 0.2	4.3 ± 0.7	51 ± 52
SHARDS10008257	12:37:22.85	62:21:43.84	4.93 ± 0.08	–	27.3 ± 0.4	–	8.4 ± 3.4	–
SHARDS10005822	12:37:22.93	62:18:11.51	3.54 ± 0.06	–	25.7 ± 0.1	–	40.1 ± 5.0	–
SHARDS10010177	12:37:22.99	62:14:03.86	3.92 ± 0.06	0.4 ± 0.2	26.6 ± 0.3	0.4 ± 0.1	3.4 ± 1.0	112 ± 94
SHARDS10008652	12:37:23.01	62:14:11.91	6.00 ± 0.07	0.1 ± 0.2	25.4 ± 0.0	0.1 ± 0.2	48.4 ± 2.7	9 ± 13
SHARDS10007803	12:37:23.04	62:11:57.66	4.71 ± 0.07	–	26.1 ± 0.3	–	42.2 ± 11.4	–
SHARDS10005889	12:37:23.14	62:15:17.40	4.08 ± 0.07	–	25.8 ± 0.1	–	11.1 ± 0.9	–
SHARDS10006109	12:37:23.21	62:14:00.74	4.33 ± 0.06	–	26.0 ± 0.2	–	41.3 ± 7.9	–
SHARDS10009361	12:37:23.38	62:12:10.40	3.37 ± 0.07	–	26.5 ± 0.2	–	2.9 ± 0.5	–
SHARDS10009152	12:37:23.41	62:13:49.73	4.21 ± 0.07	–	25.5 ± 0.1	–	67.1 ± 10.2	–
SHARDS10015293	12:37:23.46	62:14:59.52	6.01 ± 0.07	0.4 ± 0.1	–	0.4 ± 0.1	–	–
SHARDS10011610	12:37:23.54	62:14:29.09	4.22 ± 0.07	0.1 ± 0.2	26.6 ± 0.1	0.1 ± 0.1	3.6 ± 0.4	17 ± 22
SHARDS10005473	12:37:23.58	62:20:38.39	4.51 ± 0.07	0.7 ± 0.2	25.3 ± 0.2	0.7 ± 0.1	25.4 ± 3.9	22 ± 5
SHARDS10000941	12:37:23.62	62:14:21.17	3.51 ± 0.06	–	25.4 ± 0.1	–	45.8 ± 5.3	–
SHARDS10006333	12:37:23.65	62:13:29.38	3.38 ± 0.07	–	25.6 ± 0.1	–	50.0 ± 6.2	–
SHARDS10003916	12:37:23.72	62:21:13.00	3.55 ± 0.06	6.6 ± 0.2	23.4 ± 0.0	6.0 ± 0.2	1107.3 ± 75.4	40 ± 2
SHARDS10000377	12:37:23.77	62:13:00.56	3.38 ± 0.07	–	25.3 ± 0.1	–	44.4 ± 4.9	–
SHARDS10007352	12:37:23.79	62:16:27.08	4.49 ± 0.07	–	25.8 ± 0.3	–	1207.9 ± 289.4	–
SHARDS10006257	12:37:23.87	62:18:15.02	3.41 ± 0.07	–	25.4 ± 0.1	–	13.6 ± 1.5	–
SHARDS10006257	12:37:23.92	62:18:15.43	3.42 ± 0.07	0.4 ± 0.3	25.4 ± 0.1	0.4 ± 0.3	43.1 ± 6.8	13 ± 8
SHARDS10011421	12:37:23.95	62:15:56.36	3.67 ± 0.06	0.5 ± 0.2	–	0.5 ± 0.2	–	109 ± 87
SHARDS10008105	12:37:24.01	62:18:32.67	3.42 ± 0.07	–	26.5 ± 0.2	–	99.0 ± 20.6	–
SHARDS10010331	12:37:24.05	62:11:45.39	4.42 ± 0.07	0.3 ± 0.1	–	0.3 ± 0.1	–	88 ± 46
SHARDS10005314	12:37:24.06	62:18:33.45	3.42 ± 0.07	–	25.2 ± 0.1	–	304.5 ± 35.8	–
SHARDS10013381	12:37:24.10	62:18:34.25	3.42 ± 0.07	–	25.1 ± 0.1	–	241.0 ± 31.9	–
SHARDS10009011	12:37:24.23	62:12:37.56	3.76 ± 0.06	0.3 ± 0.2	27.7 ± 1.0	0.2 ± 0.2	2.6 ± 2.3	64 ± 58
SHARDS10008696	12:37:24.46	62:12:54.29	3.77 ± 0.06	–	26.4 ± 0.3	–	36.1 ± 9.7	–
SHARDS10006700	12:37:24.49	62:19:35.36	4.11 ± 0.07	0.6 ± 0.2	26.0 ± 0.1	0.5 ± 0.1	10.1 ± 1.5	25 ± 7
SHARDS10007705	12:37:24.51	62:12:25.81	4.72 ± 0.07	–	26.0 ± 0.3	–	7.8 ± 2.1	–
SHARDS10011003	12:37:24.58	62:14:57.99	3.66 ± 0.06	–	26.9 ± 0.5	–	3.4 ± 1.5	–
SHARDS10007395	12:37:24.63	62:12:54.06	3.63 ± 0.06	–	26.3 ± 0.3	–	3.8 ± 0.9	–
SHARDS10006160	12:37:24.69	62:18:50.54	3.69 ± 0.06	–	25.4 ± 0.1	–	34.5 ± 4.2	–
SHARDS10008695	12:37:24.95	62:14:07.76	4.22 ± 0.07	–	26.4 ± 0.3	–	4.5 ± 1.4	–
SHARDS10009285	12:37:25.20	62:18:45.34	5.64 ± 0.07	–	25.8 ± 0.1	–	31.4 ± 3.8	–
SHARDS10010541	12:37:25.25	62:13:19.30	3.64 ± 0.06	–	26.5 ± 0.3	–	6.5 ± 1.9	–
SHARDS10012056	12:37:25.34	62:18:45.32	5.36 ± 0.07	–	25.8 ± 0.4	–	38.8 ± 15.6	–
SHARDS10006159	12:37:25.40	62:20:48.08	3.55 ± 0.06	–	25.8 ± 0.1	–	36.7 ± 4.8	–
SHARDS10010265	12:37:25.43	62:11:58.62	4.03 ± 0.07	–	26.5 ± 0.1	–	3.8 ± 0.4	–
SHARDS10018093	12:37:25.52	62:15:25.66	6.22 ± 0.14	0.1 ± 0.2	–	0.1 ± 0.2	–	44 ± 56
SHARDS10007020	12:37:25.52	62:13:33.25	4.06 ± 0.07	–	27.4 ± 1.1	–	8.9 ± 8.6	–
SHARDS10005179	12:37:25.52	62:13:39.20	3.78 ± 0.06	–	25.2 ± 0.1	–	60.6 ± 7.1	–
SHARDS10015064	12:37:25.65	62:17:43.16	6.74 ± 0.14	0.7 ± 0.5	25.4 ± 0.1	0.6 ± 0.5	139.7 ± 18.4	15 ± 9

Continued on next page

Table A.1 – *Continued from previous page*

Object Name	R.A. (J2000)	Dec. (J2000)	z	$L_{Ly\alpha}$ (10^{42} erg s^{-1})	m_{1500} (AB mag)	$SFR_{L_{Ly\alpha}}$ ($M_\odot$ yr^{-1})	$SFR_{L_{1500}}$ ($M_\odot$ yr^{-1})	EW$_0$ (Å)
SHARDS10005968	12:37:25.66	62:20:47.95	3.69 ± 0.06	—	25.8 ± 0.2	—	34.0 ± 6.3	—
SHARDS10013230	12:37:25.75	62:13:26.43	3.16 ± 0.06	—	27.1 ± 0.2	—	8.9 ± 1.8	—
SHARDS10007410	12:37:25.92	62:20:07.80	4.51 ± 0.07	—	26.7 ± 0.1	—	14.1 ± 1.6	118 ± 156
SHARDS10006857	12:37:25.99	62:22:27.54	3.64 ± 0.14	1.9 ± 2.7	—	1.8 ± 2.4	—	—
SHARDS10009349	12:37:26.02	62:21:07.39	3.67 ± 0.06	—	25.7 ± 0.2	—	64.0 ± 11.4	—
SHARDS10007242	12:37:26.20	62:17:34.11	4.67 ± 0.06	—	26.3 ± 0.3	—	26.9 ± 8.3	—
SHARDS10013238	12:37:26.46	62:20:17.24	3.68 ± 0.06	—	26.3 ± 0.3	—	27.4 ± 6.9	—
SHARDS10008581	12:37:26.47	62:14:21.76	4.07 ± 0.07	—	26.9 ± 0.6	—	14.7 ± 7.7	—
SHARDS10006259	12:37:26.47	62:15:27.20	3.93 ± 0.06	—	27.1 ± 0.5	—	2.1 ± 1.0	—
SHARDS10006481	12:37:26.47	62:20:15.96	3.46 ± 0.07	—	25.7 ± 0.2	—	12.3 ± 2.2	—
SHARDS10010774	12:37:26.48	62:18:36.33	4.64 ± 0.08	0.6 ± 0.1	25.7 ± 0.1	0.6 ± 0.1	44.3 ± 5.1	—
SHARDS10010247	12:37:26.52	62:12:36.46	3.49 ± 0.06	—	26.1 ± 0.2	—	115.0 ± 17.9	—
SHARDS10008937	12:37:26.53	62:14:41.33	3.32 ± 0.07	—	25.2 ± 0.1	—	18.4 ± 0.7	—
SHARDS10005725	12:37:26.54	62:13:53.96	4.36 ± 0.07	—	27.9 ± 0.4	—	2.0 ± 0.7	—
SHARDS10010263	12:37:26.57	62:13:03.06	4.98 ± 0.08	0.4 ± 0.0	25.7 ± 0.1	0.4 ± 0.0	32.8 ± 4.0	56 ± 7
SHARDS10013791	12:37:26.62	62:13:58.99	4.49 ± 0.07	—	—	—	—	—
SHARDS10009297	12:37:26.72	62:13:08.11	4.73 ± 0.07	0.8 ± 0.1	25.8 ± 0.2	0.8 ± 0.1	11.9 ± 2.2	78 ± 13
SHARDS10005481	12:37:26.73	62:13:34.26	3.73 ± 0.06	—	—	—	—	—
SHARDS10016008	12:37:26.79	62:17:39.69	4.70 ± 0.14	—	25.2 ± 0.1	—	28.4 ± 2.8	—
SHARDS10006956	12:37:26.80	62:14:32.07	5.04 ± 0.06	0.8 ± 0.2	26.2 ± 0.3	—	93.9 ± 23.8	—
SHARDS10008381	12:37:26.89	62:16:07.07	4.94 ± 0.08	0.3 ± 0.1	26.9 ± 0.7	0.7 ± 0.2	4.7 ± 3.3	57 ± 28
SHARDS10006163	12:37:26.97	62:28:21.54	3.84 ± 0.08	—	26.9 ± 0.3	0.3 ± 0.1	6.7 ± 1.3	—
SHARDS10008662	12:37:26.98	62:15:24.34	4.03 ± 0.07	—	25.5 ± 0.1	—	25.6 ± 3.3	—
SHARDS10015434	12:37:27.08	62:17:49.46	4.91 ± 0.07	—	27.2 ± 0.2	—	6146.7 ± 883.9	—
SHARDS10009532	12:37:27.32	62:17:54.46	4.62 ± 0.06	—	26.9 ± 0.2	—	4.5 ± 1.0	—
SHARDS10011078	12:37:27.43	62:14:23.70	4.58 ± 0.06	—	27.0 ± 0.2	—	11.5 ± 1.9	—
SHARDS10005931	12:37:27.47	62:12:05.49	3.68 ± 0.06	0.3 ± 0.2	25.7 ± 0.1	0.3 ± 0.2	4.9 ± 0.8	27 ± 17
SHARDS10006478	12:37:27.48	62:17:20.29	3.67 ± 0.06	—	25.7 ± 0.3	—	12.9 ± 3.0	—
SHARDS10008318	12:37:27.51	62:14:35.02	4.36 ± 0.07	—	26.4 ± 0.3	—	11.7 ± 2.3	—
SHARDS10006234	12:37:27.58	62:16:05.01	4.67 ± 0.06	—	26.0 ± 0.2	—	9.8 ± 2.3	—
SHARDS10009572	12:37:27.67	62:16:55.21	4.65 ± 0.07	0.9 ± 0.2	25.5 ± 0.1	0.9 ± 0.2	39.9 ± 4.8	180 ± 63
SHARDS10005472	12:37:27.67	62:12:34.22	3.90 ± 0.06	1.9 ± 0.2	—	1.7 ± 0.1	—	66 ± 9
SHARDS10005516	12:37:27.73	62:12:34.66	3.49 ± 0.06	—	25.3 ± 0.1	—	17.1 ± 1.9	—
SHARDS10006777	12:37:28.16	62:20:18.96	3.39 ± 0.06	—	26.3 ± 0.2	—	3.1 ± 0.7	—
SHARDS10007497	12:37:28.20	62:24:30.42	3.59 ± 0.06	—	27.3 ± 0.6	—	11.3 ± 6.3	—
SHARDS10008558	12:37:28.21	62:14:30.35	3.64 ± 0.06	0.4 ± 0.2	26.4 ± 0.2	0.4 ± 0.2	44.4 ± 3.9	62 ± 44
SHARDS10010843	12:37:28.32	62:18:14.55	4.34 ± 0.06	—	28.3 ± 0.5	—	16.4 ± 3.8	—
SHARDS10005254	12:37:28.37	62:17:35.40	4.26 ± 0.07	—	25.2 ± 0.1	—	51.2 ± 2.5	—
SHARDS10009498	12:37:28.37	62:20:12.45	4.39 ± 0.06	—	27.0 ± 0.5	—	12.2 ± 3.4	—
SHARDS10001215	12:37:28.47	62:14:52.40	3.66 ± 0.06	—	24.6 ± 0.1	—	4.1 ± 1.3	—
SHARDS10010951	12:37:28.62	62:14:12.32	3.76 ± 0.06	0.1 ± 0.2	26.5 ± 0.1	0.1 ± 0.2	116.3 ± 10.3	—
SHARDS10006613	12:37:28.73	62:15:03.94	3.52 ± 0.06	—	26.8 ± 0.3	—	6.8 ± 0.6	12 ± 15
SHARDS10006221	12:37:28.79	62:14:17.06	3.62 ± 0.06	—	25.3 ± 0.2	—	12.1 ± 3.6	—
SHARDS10000918	12:37:28.84	62:14:17.88	3.52 ± 0.06	—	25.3 ± 0.1	—	12.3 ± 7.1	—
SHARDS10008196	12:37:28.88	62:14:19.65	3.52 ± 0.06	—	25.2 ± 0.1	—	65.3 ± 7.0	—
SHARDS10007842	12:37:29.00	62:19:13.06	3.27 ± 0.07	—	25.4 ± 0.5	—	220.3 ± 22.9	—
SHARDS10010134	12:37:29.13	62:12:07.98	4.43 ± 0.07	0.2 ± 0.2	27.4 ± 0.2	0.2 ± 0.2	2.7 ± 0.3	24 ± 22

Continued on next page

Table A.1 – *Continued from previous page*

Object Name	R.A. (J2000)	Dec. (J2000)	z	$L_{Ly\alpha}$ (10^{42} erg s^{-1})	m_{1500} (AB mag)	$SFR_{L_{Ly\alpha}}$ ($M_\odot$ yr^{-1})	$SFR_{L_{1500}}$ ($M_\odot$ yr^{-1})	EW$_0$ (Å)
SHARDS10000943	12:37:29.19	62:14:22.22	3.65 ± 0.06	–	24.6 ± 0.1	–	126.8 ± 11.5	–
SHARDS10007953	12:37:29.23	62:15:03.20	3.66 ± 0.06	0.1 ± 0.2	27.2 ± 0.6	0.1 ± 0.2	3.7 ± 2.0	23 ± 33
SHARDS10010123	12:37:29.25	62:14:02.55	3.51 ± 0.06	–	27.3 ± 0.2	–	1.4 ± 0.3	–
SHARDS10006758	12:37:29.34	62:18:04.39	4.66 ± 0.07	0.3 ± 0.2	26.0 ± 0.2	0.3 ± 0.2	22.3 ± 5.3	23 ± 15
SHARDS10007431	12:37:29.35	62:14:16.06	3.39 ± 0.07	–	26.8 ± 0.2	–	4.9 ± 1.1	–
SHARDS10013955	12:37:29.46	62:13:16.01	3.64 ± 0.06	–	27.6 ± 0.1	–	12.5 ± 1.8	–
SHARDS10000864	12:37:29.65	62:14:11.24	3.51 ± 0.06	–	24.6 ± 0.0	–	56.9 ± 4.5	–
SHARDS10004019	12:37:29.72	62:20:33.14	3.42 ± 0.07	–	25.3 ± 0.1	–	28.8 ± 3.0	–
SHARDS10010203	12:37:29.77	62:13:34.54	3.78 ± 0.06	–	27.5 ± 0.8	–	6.8 ± 5.0	–
SHARDS10010812	12:37:29.77	62:19:41.09	4.27 ± 0.07	–	27.4 ± 0.8	–	1.9 ± 1.4	–
SHARDS10000761	12:37:29.84	62:13:58.44	3.79 ± 0.06	–	25.4 ± 0.1	–	14.6 ± 1.8	–
SHARDS10009339	12:37:29.89	62:13:40.38	3.39 ± 0.07	–	27.0 ± 0.3	–	1.8 ± 0.5	–
SHARDS10002620	12:37:29.91	62:16:56.39	3.26 ± 0.07	–	25.0 ± 0.1	–	48.1 ± 4.8	–
SHARDS10009193	12:37:29.95	62:15:09.08	5.19 ± 0.06	0.2 ± 0.0	–	0.2 ± 0.0	–	–
SHARDS10005513	12:37:30.10	62:12:16.80	3.90 ± 0.06	1.6 ± 0.2	25.6 ± 0.2	1.5 ± 0.2	14.9 ± 3.0	52 ± 8
SHARDS10005930	12:37:30.10	62:12:18.34	4.19 ± 0.07	–	25.9 ± 0.2	–	15.3 ± 3.5	–
SHARDS10007860	12:37:30.12	62:17:58.45	3.69 ± 0.06	0.3 ± 0.2	25.9 ± 0.2	0.3 ± 0.2	738.1 ± 123.7	23 ± 14
SHARDS10008400	12:37:30.39	62:13:23.83	3.64 ± 0.06	0.1 ± 0.2	27.1 ± 0.5	0.1 ± 0.2	6.2 ± 3.0	20 ± 30
SHARDS10009893	12:37:30.43	62:14:48.84	4.23 ± 0.07	–	27.2 ± 0.1	–	2.1 ± 0.3	–
SHARDS10011676	12:37:30.45	62:19:39.29	4.39 ± 0.06	–	27.1 ± 0.5	–	42.8 ± 18.6	–
SHARDS10007584	12:37:30.64	62:13:07.89	3.38 ± 0.07	–	26.4 ± 0.2	–	11.6 ± 2.0	–
SHARDS10015342	12:37:30.86	62:15:32.78	6.23 ± 0.14	–	26.2 ± 1.3	–	9.6 ± 11.3	–
SHARDS10006394	12:37:30.89	62:15:22.70	3.53 ± 0.06	–	26.3 ± 0.2	–	41.0 ± 9.1	–
SHARDS10005836	12:37:30.94	62:14:03.21	3.93 ± 0.06	–	25.4 ± 0.1	–	45.1 ± 6.1	–
SHARDS10010822	12:37:31.03	62:12:54.23	4.73 ± 0.07	0.3 ± 0.2	27.4 ± 0.9	0.3 ± 0.2	2.6 ± 2.1	36 ± 35
SHARDS10007062	12:37:31.06	62:15:25.94	3.95 ± 0.06	0.5 ± 0.3	–	0.5 ± 0.2	–	57 ± 44
SHARDS10007336	12:37:31.07	62:17:24.37	4.94 ± 0.08	0.3 ± 0.2	25.6 ± 0.1	0.3 ± 0.2	72.6 ± 7.6	21 ± 14
SHARDS10008585	12:37:31.21	62:15:11.35	4.92 ± 0.08	0.5 ± 0.1	26.6 ± 0.4	0.5 ± 0.1	5.0 ± 1.9	–
SHARDS10012285	12:37:31.40	62:15:31.85	5.47 ± 0.07	0.9 ± 0.2	25.8 ± 0.2	0.8 ± 0.2	11.3 ± 2.1	125 ± 83
SHARDS10008216	12:37:31.44	62:13:31.35	3.64 ± 0.06	0.2 ± 0.2	26.7 ± 0.3	0.2 ± 0.2	2.8 ± 0.9	26 ± 26
SHARDS10009535	12:37:31.45	62:17:08.29	5.35 ± 0.07	–	27.0 ± 0.2	–	3.9 ± 0.9	–
SHARDS10012794	12:37:31.65	62:16:16.67	5.20 ± 0.06	0.2 ± 0.2	25.7 ± 0.2	0.2 ± 0.2	11.9 ± 2.0	34 ± 33
SHARDS10006716	12:37:31.68	62:12:46.77	3.23 ± 0.07	–	27.0 ± 0.4	–	9.0 ± 3.1	–
SHARDS10008779	12:37:31.86	62:15:40.98	3.40 ± 0.07	–	26.3 ± 0.2	–	23.3 ± 4.6	–
SHARDS10006433	12:37:31.89	62:20:31.65	4.39 ± 0.06	–	26.2 ± 0.2	–	9.8 ± 2.3	–
SHARDS10008612	12:37:32.00	62:17:08.89	4.66 ± 0.07	–	26.6 ± 0.4	–	21.9 ± 8.6	–
SHARDS10005576	12:37:32.03	62:16:43.34	4.65 ± 0.07	–	25.5 ± 0.2	–	197.6 ± 30.9	–
SHARDS10011819	12:37:32.13	62:15:01.24	3.25 ± 0.07	–	27.8 ± 0.3	–	8.7 ± 2.9	–
SHARDS10008639	12:37:32.27	62:15:02.25	5.61 ± 0.07	–	25.5 ± 0.2	–	82.8 ± 15.9	–
SHARDS10014561	12:37:32.28	62:18:48.25	3.42 ± 0.07	–	27.4 ± 0.4	–	622.8 ± 234.6	–
SHARDS10011091	12:37:32.30	62:15:44.50	4.24 ± 0.07	–	26.5 ± 0.1	–	33.0 ± 4.8	–
SHARDS10010895	12:37:32.56	62:13:57.26	3.65 ± 0.06	0.3 ± 0.2	27.4 ± 0.7	0.3 ± 0.2	3.5 ± 2.3	78 ± 94
SHARDS10008703	12:37:32.62	62:12:47.02	3.63 ± 0.06	0.4 ± 0.2	26.3 ± 0.2	0.4 ± 0.2	17.9 ± 4.3	45 ± 27
SHARDS10013032	12:37:32.67	62:14:16.22	6.01 ± 0.07	–	25.5 ± 0.1	–	59.4 ± 4.7	–
SHARDS10009870	12:37:32.80	62:12:39.58	3.63 ± 0.06	–	27.6 ± 0.9	–	1.2 ± 0.9	–
SHARDS10008186	12:37:32.84	62:14:11.94	4.47 ± 0.07	–	26.5 ± 0.2	–	5.6 ± 0.9	–
SHARDS10018257	12:37:32.87	62:14:42.08	3.66 ± 0.06	–	26.8 ± 0.4	–	81.7 ± 28.1	–
SHARDS10008154	12:37:33.09	62:14:23.20	4.34 ± 0.06	–	26.8 ± 0.4	–	4.9 ± 1.6	–

Continued on next page

Table A.1 – *Continued from previous page*

Object Name	R.A. (J2000)	Dec. (J2000)	z	$L_{Ly\alpha}$ (10^{42} erg s^{-1})	m_{1500} (AB mag)	$\mathrm{SFR}_{L_{Ly\alpha}}$ ($M_\odot$ yr^{-1})	$\mathrm{SFR}_{L_{1500}}$ ($M_\odot$ yr^{-1})	EW$_0$ (Å)
SHARDS10013675	12:37:33.12	62:18:04.17	6.26 ± 0.14	0.5 ± 0.6	25.4 ± 0.1	0.5 ± 0.6	21.6 ± 3.4	19 ± 24
SHARDS10006501	12:37:33.20	62:17:47.79	3.79 ± 0.06	—	25.5 ± 0.1	—	24.7 ± 3.2	
SHARDS10010081	12:37:33.20	62:17:51.51	4.51 ± 0.07	0.3 ± 0.1	27.4 ± 0.3	0.3 ± 0.1	2.0 ± 0.5	27 ± 14
SHARDS10006285	12:37:33.22	62:17:40.02	4.31 ± 0.07	—	26.1 ± 0.3	—	269.3 ± 82.2	
SHARDS10006326	12:37:33.23	62:17:40.42	4.34 ± 0.06	—	27.3 ± 0.2	—	4.9 ± 1.0	—
SHARDS10008332	12:37:33.24	62:14:07.02	4.34 ± 0.06	—	25.3 ± 0.1	—	18.6 ± 2.5	—
SHARDS10006308	12:37:33.30	62:14:44.62	3.46 ± 0.07	0.1 ± 0.2	25.3 ± 0.1	0.1 ± 0.2	29.5 ± 2.5	12 ± 13
SHARDS10006810	12:37:33.41	62:14:07.08	3.65 ± 0.06	—	25.2 ± 0.2	—	48.6 ± 6.7	—
SHARDS10006184	12:37:33.82	62:19:44.08	3.42 ± 0.07	—	25.5 ± 0.1	—	48.6 ± 5.5	—
SHARDS10015108	12:37:33.94	62:15:19.22	3.25 ± 0.07	—	27.3 ± 0.5	—	130.1 ± 58.7	—
SHARDS10009338	12:37:34.09	62:20:16.53	4.39 ± 0.06	0.4 ± 0.3	26.6 ± 0.4	0.3 ± 0.2	18.8 ± 7.3	24 ± 21
SHARDS10008335	12:37:34.11	62:15:42.27	4.78 ± 0.07	1.0 ± 0.3		0.9 ± 0.2		274 ± 397
SHARDS10006947	12:37:34.11	62:14:41.35	4.91 ± 0.08	—	26.7 ± 0.2	—	4.5 ± 1.0	—
SHARDS10005798	12:37:34.14	62:18:56.33	3.42 ± 0.07	—	25.9 ± 0.1	—	34.0 ± 4.5	—
SHARDS10006504	12:37:34.33	62:15:46.11	3.97 ± 0.06	—	25.8 ± 0.2	—	39.8 ± 7.2	—
SHARDS10006595	12:37:34.33	62:14:13.18	3.34 ± 0.06	—	27.1 ± 0.3	—	2.4 ± 0.8	—
SHARDS10006943	12:37:34.51	62:13:40.58	4.03 ± 0.06	0.2 ± 0.2	26.4 ± 0.3	0.2 ± 0.2	19.9 ± 6.0	21 ± 21
SHARDS10005662	12:37:34.54	62:18:07.39	3.67 ± 0.06	—	26.7 ± 0.6	—	7.3 ± 4.7	—
SHARDS10005725	12:37:34.61	62:15:58.78	3.57 ± 0.06	—	25.4 ± 0.1	—	57.3 ± 7.7	—
SHARDS10005928	12:37:34.76	62:15:29.00	3.36 ± 0.06	—	26.0 ± 0.3	—	133.4 ± 23.1	—
SHARDS10009797	12:37:34.95	62:14:58.70	3.33 ± 0.07	—	28.1 ± 0.4	—	8.7 ± 2.2	—
SHARDS10010730	12:37:34.97	62:13:41.38	4.65 ± 0.07	2.7 ± 0.2	28.0 ± 0.4	2.4 ± 0.2	1.1 ± 0.4	353 ± 202
SHARDS10011385	12:37:34.97	62:15:46.30	3.62 ± 0.06	—	26.5 ± 0.3	—	14.9 ± 4.9	—
SHARDS10007465	12:37:35.04	62:17:56.09	3.96 ± 0.06	—	25.4 ± 0.1	—	27.2 ± 3.4	—
SHARDS10005658	12:37:35.05	62:17:41.12	3.26 ± 0.07	—	27.1 ± 0.3	—	2.5 ± 0.6	—
SHARDS10008909	12:37:35.43	62:20:13.63	3.25 ± 0.07	—	27.3 ± 0.2	—	7.0 ± 1.5	98 ± 33
SHARDS10006117	12:37:35.56	62:20:12.95	3.27 ± 0.06	1.4 ± 0.2	26.3 ± 0.2	1.3 ± 0.2		
SHARDS10014880	12:37:36.33	62:14:52.99	3.57 ± 0.06	0.3 ± 0.2		0.3 ± 0.2		
SHARDS10004470	12:37:36.62	62:19:18.77	3.46 ± 0.07	—	25.6 ± 0.1	—	18.1 ± 2.1	—
SHARDS10007053	12:37:36.65	62:14:41.56	4.48 ± 0.07	—	25.7 ± 0.2	—	15 ± 2.3	—
SHARDS10008724	12:37:36.84	62:15:42.45	4.13 ± 0.07	1.2 ± 0.2	27.0 ± 0.2	1.1 ± 0.1	264.9 ± 63.2	113 ± 37
SHARDS10006575	12:37:36.98	62:13:31.53	3.73 ± 0.06	0.6 ± 0.2		0.5 ± 0.2		70 ± 46
SHARDS10005643	12:37:37.02	62:13:31.57	3.79 ± 0.06	0.9 ± 0.2	25.9 ± 0.2	0.8 ± 0.2	118.7 ± 24.7	39 ± 10
SHARDS10009625	12:37:37.03	62:13:30.92	3.70 ± 0.07	—	26.7 ± 0.2	—	19.3 ± 4.5	—
SHARDS10006422	12:37:37.31	62:15:05.83	3.09 ± 0.06	0.6 ± 0.2	26.6 ± 0.2	0.5 ± 0.2	2.8 ± 0.4	35 ± 18
SHARDS10010722	12:37:37.43	62:19:30.64	3.97 ± 0.06	—	27.5 ± 0.3	—	11.2 ± 12.5	—
SHARDS10005659	12:37:37.47	62:19:33.59	4.68 ± 0.06	—	25.6 ± 0.1	—	45.3 ± 6.5	—
SHARDS10006519	12:37:37.83	62:13:23.49	3.78 ± 0.06	—	26.5 ± 0.2	—	5.3 ± 1.1	—
SHARDS10007402	12:37:37.85	62:19:43.82	4.27 ± 0.07	—	26.3 ± 0.3	—	26.7 ± 8.0	—
SHARDS10009250	12:37:37.94	62:13:25.47	3.92 ± 0.06	—	26.2 ± 0.3	—	26.7 ± 8.0	—
SHARDS10008683	12:37:38.18	62:14:22.10	4.23 ± 0.07	—	27.5 ± 0.7	—	2.5 ± 1.0	—
SHARDS10007001	12:37:38.22	62:16:56.65	3.41 ± 0.07	—	24.9 ± 0.0	—	25.7 ± 16.3	—
SHARDS10006556	12:37:38.25	62:18:35.76	3.97 ± 0.06	1.1 ± 0.2	24.4 ± 0.3	1.0 ± 0.1	626.6 ± 59.4	
SHARDS10005435	12:37:38.35	62:15:24.90	4.09 ± 0.07	0.3 ± 0.2	26.4 ± 0.9	0.3 ± 0.2	4.2 ± 1.0	81 ± 23
SHARDS10013775	12:37:38.36	62:14:21.98	3.80 ± 0.06	—	27.2 ± 0.6	—	5.7 ± 1.0	25 ± 18
SHARDS10006277	12:37:38.57	62:19:11.83	3.56 ± 0.06	—	27.2 ± 0.2	—	8.2 ± 1.3	—
SHARDS10007323	12:37:38.87	62:19:46.03	4.52 ± 0.07	0.3 ± 0.2	26.1 ± 0.9	0.3 ± 0.2	24.7 ± 4.0	22 ± 15
SHARDS10007422	12:37:39.13	62:17:36.77	4.26 ± 0.07	—	26.0 ± 0.2	—	9.1 ± 7.8	
							35.7 ± 8.3	

Continued on next page

Table A.1 – *Continued from previous page*

Object Name	R.A. (J2000)	Dec. (J2000)	z	$L_{Ly\alpha}$ (10^{42} erg s^{-1})	m_{1500} (AB mag)	$SFR_{L_{Ly\alpha}}$ ($M_\odot$ yr^{-1})	$SFR_{L_{1500}}$ ($M_\odot$ yr^{-1})	EW_0 (Å)
SHARDS10009103	12:37:39.15	62:17:34.59	4.51 ± 0.07	–	26.6 ± 0.5	–	37.5 ± 18.3	–
SHARDS10014515	12:37:39.28	62:17:35.06	4.51 ± 0.07	0.5 ± 0.3	25.9 ± 0.3	0.4 ± 0.3	86.0 ± 22.2	14 ± 7
SHARDS10007188	12:37:39.38	62:17:34.55	4.51 ± 0.07	–	26.1 ± 0.3	–	111.1 ± 34.9	–
SHARDS10007963	12:37:39.47	62:17:35.47	4.51 ± 0.07	0.3 ± 0.2	27.1 ± 0.8	0.2 ± 0.1	33.7 ± 25.8	31 ± 23
SHARDS10008734	12:37:39.62	62:20:00.67	5.51 ± 0.07	1.9 ± 0.4	–	1.7 ± 0.4	–	143 ± 93
SHARDS10009758	12:37:39.71	62:16:03.46	3.54 ± 0.06	–	26.0 ± 0.1	–	34.8 ± 5.1	–
SHARDS10011904	12:37:39.89	62:19:59.35	6.07 ± 0.07	0.4 ± 0.5	26.2 ± 0.3	0.4 ± 0.5	9.7 ± 2.5	29 ± 45
SHARDS10009578	12:37:40.19	62:13:30.80	3.65 ± 0.06	–	26.6 ± 0.1	–	13.5 ± 1.7	–
SHARDS10007069	12:37:40.42	62:15:35.43	4.79 ± 0.07	–	25.9 ± 0.1	–	8.3 ± 1.1	–
SHARDS10010443	12:37:40.42	62:13:29.24	6.00 ± 0.07	–	25.5 ± 0.1	–	80.0 ± 7.2	–
SHARDS10005145	12:37:40.63	62:17:01.82	3.55 ± 0.06	–	25.0 ± 0.1	–	50.3 ± 4.5	–
SHARDS10005891	12:37:40.74	62:13:47.32	3.65 ± 0.06	–	26.1 ± 0.2	–	12.0 ± 2.4	–
SHARDS10006420	12:37:40.99	62:18:05.95	4.81 ± 0.07	0.3 ± 0.2	26.0 ± 0.1	0.3 ± 0.2	418.1 ± 56.9	21 ± 14
SHARDS10005568	12:37:41.01	62:15:03.90	3.67 ± 0.06	–	25.5 ± 0.1	–	20.3 ± 2.6	–
SHARDS10006420	12:37:41.03	62:18:05.37	4.81 ± 0.07	0.3 ± 0.3	26.0 ± 0.3	0.3 ± 0.3	41.2 ± 11.3	10 ± 7
SHARDS10005824	12:37:41.68	62:17:18.30	3.69 ± 0.06	–	25.6 ± 0.1	–	18.1 ± 2.5	–
SHARDS10008395	12:37:41.78	62:15:39.36	3.81 ± 0.06	1.2 ± 0.2	–	1.1 ± 0.2	–	110 ± 25
SHARDS10005948	12:37:41.83	62:17:30.40	3.97 ± 0.06	–	25.2 ± 0.1	–	25.9 ± 2.8	–
SHARDS10007735	12:37:41.99	62:17:37.26	3.69 ± 0.06	–	26.0 ± 0.2	–	43.1 ± 8.5	–
SHARDS10012166	12:37:42.20	62:17:21.36	4.26 ± 0.07	–	–	–	–	–
SHARDS10005984	12:37:42.30	62:17:29.61	3.69 ± 0.06	0.9 ± 0.2	26.1 ± 0.2	0.8 ± 0.1	375.0 ± 74.0	134 ± 65
SHARDS10011464	12:37:42.85	62:15:32.44	4.25 ± 0.07	0.3 ± 0.1	27.3 ± 0.4	–	4.6 ± 1.9	22 ± 10
SHARDS10005776	12:37:42.99	62:17:25.70	3.55 ± 0.06	–	25.4 ± 0.1	–	65.7 ± 7.5	–
SHARDS10005382	12:37:43.00	62:15:34.50	3.95 ± 0.06	–	25.2 ± 0.1	–	38.9 ± 4.2	–
SHARDS10006681	12:37:43.40	62:16:56.00	4.26 ± 0.07	–	26.0 ± 0.2	–	7.4 ± 1.2	–
SHARDS10008666	12:37:43.72	62:15:53.58	3.68 ± 0.06	–	26.8 ± 0.4	–	10.4 ± 3.6	–
SHARDS10007289	12:37:44.56	62:14:02.98	3.66 ± 0.06	–	25.9 ± 0.2	–	52.6 ± 10.4	–
SHARDS10008475	12:37:44.74	62:15:54.14	5.48 ± 0.07	0.4 ± 0.2	26.6 ± 0.5	0.4 ± 0.2	5.5 ± 2.4	47 ± 32
SHARDS10006493	12:37:44.84	62:18:17.25	5.09 ± 0.06	0.8 ± 0.2	26.1 ± 0.4	0.7 ± 0.2	14.5 ± 5.2	36 ± 14
SHARDS10008700	12:37:44.98	62:18:20.28	5.09 ± 0.06	1.4 ± 0.2	26.2 ± 0.4	1.2 ± 0.2	38.3 ± 14.5	98 ± 41
SHARDS10008759	12:37:45.07	62:17:34.81	3.42 ± 0.07	–	26.9 ± 0.3	–	14.9 ± 3.9	–
SHARDS10007908	12:37:45.24	62:16:20.60	4.11 ± 0.07	–	26.5 ± 0.3	–	140.1 ± 35.6	–
SHARDS10006737	12:37:45.84	62:17:56.51	3.56 ± 0.06	–	26.2 ± 0.2	–	67.9 ± 12.0	–
SHARDS10005452	12:37:46.82	62:16:54.84	4.11 ± 0.07	–	25.8 ± 0.3	–	59.3 ± 15.7	–
SHARDS10010687	12:37:47.00	62:14:49.74	3.25 ± 0.07	–	26.3 ± 0.2	–	318.0 ± 57.2	–
SHARDS10006143	12:37:47.27	62:17:59.37	3.56 ± 0.06	–	25.8 ± 0.1	–	19.4 ± 2.5	–
SHARDS10006844	12:37:47.66	62:18:47.39	3.70 ± 0.06	0.5 ± 0.2	26.4 ± 0.3	0.5 ± 0.2	10.1 ± 3.1	53 ± 28
SHARDS10010353	12:37:47.78	62:17:59.91	3.56 ± 0.06	–	26.7 ± 0.3	–	5.2 ± 1.4	–
SHARDS10009098	12:37:47.99	62:17:38.84	4.67 ± 0.07	–	–	–	–	–
SHARDS10009143	12:37:48.30	62:14:27.73	5.46 ± 0.07	0.3 ± 0.1	–	0.3 ± 0.1	–	–
SHARDS10005391	12:37:48.39	62:14:24.50	4.23 ± 0.07	1.4 ± 0.2	–	1.3 ± 0.2	–	130 ± 28
SHARDS10009493	12:37:48.54	62:17:48.20	4.27 ± 0.07	–	25.1 ± 0.1	–	15.2 ± 1.7	–
SHARDS10010344	12:37:48.61	62:14:54.73	4.24 ± 0.07	0.5 ± 0.2	26.0 ± 0.3	0.4 ± 0.2	110.2 ± 31.3	42 ± 27
SHARDS10012008	12:37:49.24	62:15:38.23	5.79 ± 0.06	0.8 ± 0.3	26.2 ± 0.4	0.7 ± 0.3	5.6 ± 1.9	60 ± 41
SHARDS10005365	12:37:49.75	62:19:05.10	4.12 ± 0.07	–	26.4 ± 0.2	–	38.1 ± 8.6	–
SHARDS10008004	12:37:49.78	62:17:22.39	5.50 ± 0.07	2.0 ± 0.2	26.2 ± 0.4	1.9 ± 0.2	84.9 ± 34.3	74 ± 15
SHARDS10006361	12:37:49.92	62:19:05.78	4.12 ± 0.07	0.4 ± 0.2	26.5 ± 0.4	0.3 ± 0.2	6.1 ± 2.5	22 ± 13
SHARDS10006843	12:37:50.08	62:17:32.03	3.97 ± 0.06	–	26.2 ± 0.2	–	11.4 ± 12.4	–
					27.5 ± 1.2		48.3 ± 11.6	

Continued on next page

Table A.1 – *Continued from previous page*

Object Name	R.A. (J2000)	Dec. (J2000)	z	$L_{Ly\alpha}$ (10^{42} erg s^{-1})	m_{1500} (AB mag)	$\mathrm{SFR}_{L_{Ly\alpha}}$ ($M_\odot$ yr^{-1})	$\mathrm{SFR}_{L_{1500}}$ ($M_\odot$ yr^{-1})	EW$_0$ (Å)
SHARDS10006875	12:37:50.63	62:18:46.36	4.27 ± 0.07	0.4 ± 0.2	27.2 ± 0.6	0.3 ± 0.1	9.3 ± 5.6	11 ± 4
SHARDS10002975	12:37:50.87	62:18:33.26	3.56 ± 0.06		25.3 ± 0.1		61.4 ± 6.2	
SHARDS10002976	12:37:50.93	62:18:32.07	3.42 ± 0.07	—	25.7 ± 0.1	—	35.7 ± 4.3	—
SHARDS10002022	12:37:51.07	62:18:27.64	3.34 ± 0.06	—	26.6 ± 0.3	—	300.2 ± 94.5	—
SHARDS10008376	12:37:51.20	62:18:49.07	4.39 ± 0.06	1.0 ± 0.2		0.9 ± 0.1		153 ± 61
SHARDS10005301	12:37:51.37	62:17:10.20	3.55 ± 0.06		25.8 ± 0.1		23.7 ± 3.1	
SHARDS10005246	12:37:51.65	62:18:00.51	3.56 ± 0.06	0.2 ± 0.3	25.2 ± 0.1	0.2 ± 0.2	52.7 ± 7.9	5 ± 6
SHARDS10006243	12:37:51.95	62:17:48.15	4.27 ± 0.07	—	25.7 ± 0.2	—	29.7 ± 5.7	—
SHARDS10006225	12:37:52.04	62:14:59.94	4.78 ± 0.07		26.4 ± 0.3		23.8 ± 7.8	
SHARDS10006826	12:37:52.42	62:15:50.85	5.07 ± 0.06	0.4 ± 0.2	25.7 ± 0.1	0.3 ± 0.2	71.7 ± 8.5	14 ± 7
SHARDS10006786	12:37:52.95	62:16:44.67	3.27 ± 0.07	—	25.8 ± 0.1	—	29.8 ± 4.1	—
SHARDS10005795	12:37:53.06	62:17:20.83	3.69 ± 0.06		26.5 ± 0.4		6.2 ± 2.1	
SHARDS10005785	12:37:53.09	62:16:54.44	3.27 ± 0.07	—	26.4 ± 0.2	—	14.4 ± 2.9	—
SHARDS10007046	12:37:53.22	62:18:39.14	3.25 ± 0.06	—	26.8 ± 0.4	—	2.8 ± 1.0	—
SHARDS10007802	12:37:53.35	62:16:32.46	4.25 ± 0.07	0.3 ± 0.2	27.3 ± 0.7	0.3 ± 0.1	3.6 ± 2.4	29 ± 18
SHARDS10012002	12:37:53.81	62:17:20.47	4.49 ± 0.07	0.7 ± 0.2		0.7 ± 0.2		132 ± 56
SHARDS10019053	12:37:54.10	62:17:30.80	4.35 ± 0.06	0.9 ± 0.2		0.8 ± 0.2		56 ± 21
SHARDS10006542	12:37:54.32	62:15:31.06	3.65 ± 0.06		25.6 ± 0.2		190.9 ± 32.0	
SHARDS10008031	12:37:54.50	62:17:05.75	3.49 ± 0.06	0.2 ± 0.2	26.6 ± 0.4	0.2 ± 0.2	16.4 ± 6.8	29 ± 35
SHARDS10006864	12:37:55.13	62:17:07.43	3.42 ± 0.07	—	26.2 ± 0.1	—	6.5 ± 1.0	—
SHARDS10005564	12:37:55.29	62:17:27.43	4.25 ± 0.07	—	25.2 ± 0.1	—	70.3 ± 9.7	—
SHARDS10007686	12:37:55.53	62:17:36.40	4.25 ± 0.07	—	26.6 ± 0.4	—	9.7 ± 3.5	—
SHARDS10007731	12:37:55.97	62:17:05.21	3.85 ± 0.06	—	24.7 ± 0.0	—	76.0 ± 5.8	—
SHARDS10005831	12:37:56.10	62:16:04.74	3.52 ± 0.06	—	25.7 ± 0.1	—	359.4 ± 54.8	—
SHARDS10008277	12:37:56.11	62:17:29.08	3.22 ± 0.06	—	25.5 ± 0.4	—	5.7 ± 2.3	—
SHARDS10008717	12:37:56.39	62:16:20.83	4.22 ± 0.07	—	25.8 ± 0.2	—	28.0 ± 5.2	—
SHARDS10006259	12:37:56.52	62:16:25.60	4.67 ± 0.07	—	26.3 ± 0.3	—	7.1 ± 1.8	—
SHARDS10007449	12:37:56.56	62:15:42.76	3.87 ± 0.06	—	26.1 ± 0.3	—	6.9 ± 1.7	—
SHARDS10004936	12:37:56.76	62:15:38.74	3.82 ± 0.07	—	26.3 ± 0.3	—	368.8 ± 26.4	—
SHARDS10010016	12:37:57.51	62:16:16.74	4.41 ± 0.07	—	27.6 ± 0.5	—	10.2 ± 4.6	—
SHARDS10007627	12:37:57.76	62:16:47.99	3.66 ± 0.07	—	27.6 ± 0.2	—	400.3 ± 75.9	—
SHARDS10005511	12:38:00.41	62:16:27.62	5.34 ± 0.07	—	25.8 ± 0.2	—	122.7 ± 10.6	—
SHARDS10006151	12:38:03.38	62:16:15.74	4.25 ± 0.07	0.7 ± 0.2	25.8 ± 0.2	0.6 ± 0.2	51.5 ± 10.6	32 ± 11

Table A.2: Main physical parameters derived from the best models fitted to each source. (1) Name of the object using the SHARDS identification. (2) Right ascension. (3) Declination. (4) Photometric redshift. (5) Stellar mass of the main SP. (6) Age of the main SP. (7) e-folding time of the main SP. (8) Stellar mass of the young SP. (9) Age of the young SP. (10) e-folding time of the young SP. The last three columns are left empty when the best solution does not require a second SP.

Object Name	R.A.	Dec.	z	$M_{\rm star,m}$	$\rm Age_m$	$\tau_{\rm m}$	$M_{\rm star,b}$	$\rm Age_b$	$\tau_{\rm b}$
	(J2000)	(J2000)		($10^9\ M_\odot$)	(Myr)	(Myr)	($10^9\ M_\odot$)	(Myr)	(Myr)
(1)	(2)	(3)	(4)	(5)	(6)	(7)	(8)	(9)	(10)
SHARDS20010117	12:35:48.1	62:12:02.4	4.28 ± 0.06	1.7 ± 1.1	68 ± 39	2.7 ± 1.4	–	–	–
SHARDS20007539	12:35:48.1	62:12:03.8	5.38 ± 0.07	9.7 ± 4.1	766 ± 240	3.0 ± 1.6	1.1 ± 1.5	16 ± 6	2.5 ± 1.6
SHARDS20012481	12:35:50.9	62:11:58.5	5.69 ± 0.06	2.6 ± 1.4	59 ± 27	2.5 ± 1.3	–	–	–
SHARDS20005927	12:35:51.5	62:12:16.5	3.22 ± 0.07	2.9 ± 0.5	48 ± 8	2.8 ± 1.4	–	–	–
SHARDS20005405	12:35:51.6	62:12:12.7	4.03 ± 0.07	6.7 ± 1.4	74 ± 20	2.8 ± 1.4	–	–	–
SHARDS20008074	12:35:52.2	62:11:20.8	5.53 ± 0.07	0.6 ± 0.3	20 ± 7	2.1 ± 1.2	–	–	–
SHARDS20008444	12:35:53.2	62:10:32.9	4.01 ± 0.07	5.7 ± 4.3	860 ± 450	3.0 ± 1.6	0.8 ± 1.0	32 ± 13	1.7 ± 1.3
SHARDS20010810	12:35:53.4	62:10:23.3	5.12 ± 0.06	1.3 ± 0.8	64 ± 39	2.6 ± 1.4	–	–	–
SHARDS20005669	12:35:54.1	62:10:32.9	3.36 ± 0.07	10.0 ± 5.9	318 ± 218	3.0 ± 1.6	0.5 ± 0.7	24 ± 10	2.5 ± 1.5
SHARDS20011405	12:35:54.3	62:10:18.8	5.37 ± 0.07	3.5 ± 1.4	73 ± 34	2.8 ± 1.4	–	–	–
SHARDS20006420	12:35:54.4	62:10:33.8	3.88 ± 0.06	6.6 ± 2.4	98 ± 46	2.9 ± 1.4	–	–	–
SHARDS20006258	12:35:54.5	62:12:14.6	3.48 ± 0.06	1.0 ± 0.4	16 ± 8	2.0 ± 1.2	–	–	–
SHARDS20013727	12:35:55.0	62:12:04.8	5.96 ± 0.07	20.0 ± 10.0	298 ± 199	3.0 ± 1.6	1.1 ± 1.4	24 ± 11	2.6 ± 1.5
SHARDS20009009	12:35:55.2	62:11:25.4	3.89 ± 0.06	1.6 ± 0.5	61 ± 25	2.7 ± 1.4	–	–	–
SHARDS20006827	12:35:55.7	62:10:19.0	4.28 ± 0.06	1.8 ± 0.6	38 ± 12	2.0 ± 1.1	–	–	–
SHARDS20008662	12:35:55.8	62:10:28.9	4.17 ± 0.07	2.1 ± 1.2	950 ± 420	3.0 ± 1.6	0.5 ± 0.4	26 ± 10	1.4 ± 1.1
SHARDS20008870	12:35:55.8	62:12:32.1	4.19 ± 0.07	34.0 ± 7.0	1070 ± 170	3.0 ± 1.6	1.2 ± 0.6	32 ± 11	1.5 ± 1.1
SHARDS20010887	12:35:56.2	62:11:45.4	5.14 ± 0.06	9.2 ± 3.2	59 ± 29	2.6 ± 1.3	–	–	–
SHARDS20010975	12:35:56.6	62:11:43.2	5.40 ± 0.07	1.9 ± 1.0	32 ± 15	2.5 ± 1.3	–	–	–
SHARDS20005559	12:35:57.2	62:10:39.0	4.17 ± 0.07	7.2 ± 3.0	65 ± 18	2.7 ± 1.4	–	–	–
SHARDS20003293	12:35:57.5	62:12:24.0	3.90 ± 0.06	0.8 ± 0.3	60 ± 20	2.6 ± 1.3	–	–	–
SHARDS20004834	12:35:57.7	62:11:30.0	3.37 ± 0.07	38.4 ± 19.4	660 ± 409	3.0 ± 1.6	6.8 ± 4.2	42 ± 11	1.9 ± 1.0
SHARDS20004871	12:35:58.2	62:11:05.5	3.62 ± 0.06	5.9 ± 0.8	64 ± 12	2.5 ± 1.2	–	–	–
SHARDS20009905	12:35:58.6	62:12:11.7	5.28 ± 0.07	0.2 ± 0.1	16 ± 5	2.7 ± 1.4	–	–	–
SHARDS20012586	12:35:58.9	62:10:17.3	5.69 ± 0.06	0.9 ± 0.5	19 ± 7	2.9 ± 1.4	–	–	–
SHARDS20010376	12:35:59.0	62:12:45.3	5.15 ± 0.06	6.7 ± 1.4	80 ± 13	2.9 ± 1.4	–	–	–
SHARDS20005220	12:35:59.5	62:09:49.7	4.29 ± 0.06	15.0 ± 4.0	102 ± 13	2.9 ± 1.4	–	–	–
SHARDS20005503	12:36:00.0	62:12:26.1	5.15 ± 0.06	1.5 ± 0.8	19 ± 6	1.7 ± 0.9	–	–	–
SHARDS20010137	12:36:00.6	62:12:20.0	4.20 ± 0.07	0.8 ± 0.2	49 ± 11	2.3 ± 1.2	–	–	–
SHARDS20011116	12:36:00.6	62:12:59.6	4.45 ± 0.07	1.3 ± 0.6	25 ± 11	3.0 ± 1.4	–	–	–
SHARDS20005166	12:36:00.8	62:12:52.4	3.50 ± 0.06	4.2 ± 0.7	67 ± 16	2.7 ± 1.4	–	–	–
SHARDS20005022	12:36:01.2	62:12:52.3	3.50 ± 0.06	7.6 ± 2.0	64 ± 13	2.7 ± 1.4	–	–	–
SHARDS20005185	12:36:01.2	62:12:53.7	3.50 ± 0.06	3.2 ± 1.0	50 ± 16	2.5 ± 1.2	–	–	–
SHARDS20005390	12:36:01.3	62:13:18.9	3.91 ± 0.06	1.8 ± 0.7	24 ± 8	2.6 ± 1.4	–	–	–
SHARDS20005748	12:36:01.4	62:09:44.7	3.61 ± 0.06	3.8 ± 1.9	100 ± 70	3.0 ± 1.6	0.1 ± 0.1	7 ± 4	3.3 ± 1.6
SHARDS20005027	12:36:01.5	62:09:43.1	3.36 ± 0.07	3.9 ± 0.9	63 ± 13	3.0 ± 1.4	–	–	–
SHARDS20006671	12:36:01.6	62:12:24.9	3.50 ± 0.06	15.0 ± 4.0	243 ± 216	3.0 ± 1.6	2.4 ± 1.7	33 ± 13	1.7 ± 1.3
SHARDS20005412	12:36:01.6	62:11:18.8	3.90 ± 0.06	13.0 ± 3.0	120 ± 40	2.9 ± 1.4	–	–	–

Continued on next page

Table A.2 – *Continued from previous page*

Object Name	R.A. (J2000)	Dec. (J2000)	z	$M_{\rm star,m}$ (10^9 $M_\odot$)	$\rm Age_m$ (Myr)	$\tau_{\rm m}$ (Myr)	$M_{\rm star,b}$ (10^9 $M_\odot$)	$\rm Age_b$ (Myr)	$\tau_{\rm b}$ (Myr)
SHARDS20004739	12:36:03.1	62:10:23.4	3.90 ± 0.06	7.1 ± 2.3	42 ± 10	2.0 ± 1.0	–	–	–
SHARDS20006276	12:36:04.1	62:09:22.0	3.75 ± 0.06	2.9 ± 0.4	26 ± 4	1.6 ± 0.7	–	–	–
SHARDS20005680	12:36:04.4	62:09:23.4	3.75 ± 0.06	1.1 ± 0.4	21 ± 8	2.9 ± 1.5	–	–	–
SHARDS20015119	12:36:04.6	62:12:27.8	5.73 ± 0.06	7.9 ± 2.7	87 ± 44	2.9 ± 1.4	–	–	–
SHARDS20005970	12:36:05.2	62:10:19.7	4.30 ± 0.06	7.3 ± 1.9	52 ± 16	2.6 ± 1.3	–	–	–
SHARDS20007405	12:36:05.3	62:13:23.6	4.06 ± 0.07	2.7 ± 0.5	38 ± 8	2.1 ± 1.1	–	–	–
SHARDS20005279	12:36:06.1	62:08:36.3	4.42 ± 0.07	13.0 ± 6.0	79 ± 32	2.8 ± 1.4	–	–	–
SHARDS20011335	12:36:06.6	62:14:04.0	3.65 ± 0.06	0.5 ± 0.2	57 ± 27	2.6 ± 1.4	–	–	–
SHARDS20009951	12:36:06.7	62:13:32.8	3.76 ± 0.06	0.4 ± 0.2	26 ± 12	2.5 ± 1.4	–	–	–
SHARDS20004883	12:36:07.4	62:13:40.1	3.65 ± 0.06	4.2 ± 0.9	40 ± 10	2.0 ± 1.1	–	–	–
SHARDS20008937	12:36:07.4	62:10:18.1	3.77 ± 0.06	1.0 ± 0.6	61 ± 32	2.7 ± 1.4	–	–	–
SHARDS20012287	12:36:07.5	62:11:05.4	3.77 ± 0.06	1.1 ± 0.4	70 ± 34	2.7 ± 1.4	–	–	–
SHARDS20010275	12:36:07.7	62:11:26.1	3.64 ± 0.06	0.3 ± 0.2	20 ± 11	3.1 ± 1.4	–	–	–
SHARDS20005404	12:36:07.9	62:09:30.1	3.62 ± 0.06	3.9 ± 0.2	60 ± 6	2.4 ± 1.2	–	–	–
SHARDS20005835	12:36:08.0	62:11:20.9	4.87 ± 0.08	10.0 ± 3.0	75 ± 23	2.8 ± 1.4	0.4 ± 0.2	18 ± 6	2.8 ± 1.6
SHARDS20006747	12:36:08.1	62:10:07.1	3.37 ± 0.07	9.9 ± 3.4	840 ± 260	3.0 ± 1.6	–	–	–
SHARDS20011097	12:36:08.4	62:10:57.6	4.58 ± 0.07	8.6 ± 1.7	88 ± 12	2.7 ± 1.4	0.4 ± 0.2	18 ± 6	2.8 ± 1.6
SHARDS20008566	12:36:08.4	62:09:01.7	3.89 ± 0.06	850.0 ± 310.0	1500 ± 100	3.0 ± 1.4	–	–	–
SHARDS20010119	12:36:08.5	62:10:16.3	3.90 ± 0.06	15.0 ± 6.0	919 ± 380	3.0 ± 1.6	1.1 ± 0.8	45 ± 10	2.5 ± 1.6
SHARDS20007130	12:36:08.6	62:08:40.6	3.75 ± 0.06	29.0 ± 8.0	660 ± 280	3.0 ± 1.6	2.0 ± 1.1	38 ± 12	1.8 ± 1.3
SHARDS20006314	12:36:08.6	62:10:18.7	4.59 ± 0.07	13.0 ± 1.0	103 ± 13	3.0 ± 1.4	–	–	–
SHARDS20008667	12:36:09.3	62:11:20.5	3.50 ± 0.06	1.6 ± 0.7	100 ± 400	3.0 ± 1.6	0.1 ± 0.1	12 ± 4	3.6 ± 1.4
SHARDS20005577	12:36:09.3	62:10:04.9	3.49 ± 0.06	9.4 ± 1.1	1200 ± 180	3.0 ± 1.6	0.3 ± 0.1	15 ± 4	2.8 ± 1.1
SHARDS20008093	12:36:09.5	62:14:03.5	4.22 ± 0.07	0.3 ± 0.1	33 ± 9	2.1 ± 1.1	–	–	–
SHARDS20005473	12:36:09.5	62:11:15.8	5.42 ± 0.07	5.8 ± 1.9	29 ± 9	2.1 ± 1.1	–	–	–
SHARDS20002083	12:36:09.7	62:09:10.7	3.91 ± 0.06	4.7 ± 1.0	50 ± 10	2.1 ± 1.1	–	–	–
SHARDS20008557	12:36:10.3	62:09:35.7	5.15 ± 0.06	4.8 ± 1.2	38 ± 13	2.2 ± 1.1	–	–	–
SHARDS20005273	12:36:10.4	62:09:09.9	3.89 ± 0.06	1.1 ± 0.2	16 ± 4	2.6 ± 1.2	–	–	–
SHARDS20013907	12:36:10.4	62:14:23.5	3.52 ± 0.06	0.2 ± 0.1	44 ± 16	2.4 ± 1.3	–	–	–
SHARDS20007147	12:36:10.4	62:08:56.6	3.65 ± 0.06	1.4 ± 0.5	48 ± 17	2.6 ± 1.3	–	–	–
SHARDS20007520	12:36:10.6	62:08:47.6	3.61 ± 0.06	2.0 ± 0.4	74 ± 24	2.8 ± 1.4	–	–	–
SHARDS20006199	12:36:10.7	62:12:42.7	3.79 ± 0.06	3.3 ± 1.6	34 ± 6	1.7 ± 0.8	–	–	–
SHARDS20006658	12:36:10.8	62:14:15.2	4.22 ± 0.07	39.0 ± 7.0	825 ± 208	3.0 ± 1.6	3.0 ± 1.3	44 ± 10	2.5 ± 1.3
SHARDS20007027	12:36:11.2	62:13:40.0	4.77 ± 0.07	5.7 ± 2.1	72 ± 32	2.8 ± 1.4	–	–	–
SHARDS20007071	12:36:11.2	62:08:23.1	4.02 ± 0.07	7.0 ± 1.9	87 ± 30	2.9 ± 1.4	–	–	–
SHARDS20015907	12:36:11.4	62:10:52.0	4.46 ± 0.07	29.0 ± 8.0	730 ± 300	3.0 ± 1.6	0.9 ± 0.4	22 ± 5	2.9 ± 1.2
SHARDS20006779	12:36:11.4	62:09:35.8	3.77 ± 0.06	1.7 ± 0.6	49 ± 10	2.5 ± 1.3	–	–	–
SHARDS20001577	12:36:11.5	62:09:31.1	3.37 ± 0.07	5.1 ± 0.8	39 ± 8	1.7 ± 0.8	–	–	–
SHARDS20007575	12:36:11.5	62:12:43.9	3.65 ± 0.06	0.4 ± 0.2	19 ± 7	2.6 ± 1.4	–	–	–
SHARDS20004520	12:36:11.9	62:09:10.5	4.30 ± 0.06	9.8 ± 2.8	37 ± 13	1.7 ± 0.8	–	–	–
SHARDS20007747	12:36:11.9	62:14:38.5	5.45 ± 0.07	23.0 ± 10.0	640 ± 260	3.0 ± 1.6	1.5 ± 1.6	18 ± 5	1.9 ± 1.0
SHARDS20010570	12:36:11.9	62:12:36.9	5.31 ± 0.07	0.3 ± 0.1	20 ± 7	2.3 ± 1.3	–	–	–
SHARDS20005294	12:36:12.0	62:09:39.7	3.91 ± 0.06	7.4 ± 0.7	79 ± 15	2.8 ± 1.4	–	–	–
SHARDS20010722	12:36:12.0	62:14:11.3	4.34 ± 0.06	0.4 ± 0.2	47 ± 23	2.4 ± 1.3	–	–	–
SHARDS20011388	12:36:12.2	62:09:35.0	4.59 ± 0.07	0.4 ± 0.1	24 ± 7	2.1 ± 1.2	–	–	–
SHARDS20007085	12:36:12.2	62:10:24.9	5.29 ± 0.07	4.4 ± 0.9	32 ± 8	1.8 ± 0.9	–	–	–
SHARDS20007508	12:36:12.3	62:10:20.9	3.63 ± 0.06	5.1 ± 1.8	990 ± 340	3.0 ± 1.6	0.2 ± 0.3	23 ± 6	2.0 ± 1.1
SHARDS20011200	12:36:12.4	62:14:17.5	4.23 ± 0.07	0.8 ± 0.5	53 ± 28	2.5 ± 1.3	–	–	–
SHARDS20005700	12:36:12.6	62:09:40.2	5.41 ± 0.07	14.0 ± 3.0	70 ± 20	2.7 ± 1.3	–	–	–

Continued on next page

Table A.2 – *Continued from previous page*

Object Name	R.A. (J2000)	Dec. (J2000)	z	$M_{\rm star,m}$ ($10^9\ M_\odot$)	$\rm Age_m$ (Myr)	$\tau_{\rm m}$ (Myr)	$M_{\rm star,b}$ ($10^9\ M_\odot$)	$\rm Age_b$ (Myr)	$\tau_{\rm b}$ (Myr)
SHARDS20013688	12:36:12.6	62:13:47.5	5.32 ± 0.07	2.1 ± 2.7	440 ± 330	3.0 ± 1.6	0.5 ± 0.7	21 ± 9	2.4 ± 1.5
SHARDS20007778	12:36:12.7	62:14:53.1	4.48 ± 0.07	13.0 ± 4.0	1000 ± 300	3.0 ± 1.6	0.7 ± 0.5	15 ± 6	2.1 ± 1.4
SHARDS20009967	12:36:13.2	62:13:32.7	4.62 ± 0.07	44.0 ± 9.0	471 ± 137	3.0 ± 1.6	1.7 ± 0.9	44 ± 10	2.3 ± 1.5
SHARDS20013579	12:36:13.2	62:14:20.6	4.08 ± 0.07	0.6 ± 0.3	60 ± 34	2.6 ± 1.4	–	–	–
SHARDS20007836	12:36:13.2	62:10:15.9	3.23 ± 0.07	0.8 ± 0.2	64 ± 15	2.7 ± 1.4	–	–	–
SHARDS20009758	12:36:13.3	62:10:39.0	5.02 ± 0.06	1.7 ± 1.1	71 ± 41	2.7 ± 1.4	–	–	–
SHARDS20006311	12:36:13.3	62:09:07.0	3.76 ± 0.06	11.0 ± 3.0	843 ± 249	3.0 ± 1.6	1.8 ± 1.2	49 ± 1	2.2 ± 1.0
SHARDS20005381	12:36:13.5	62:09:35.7	4.19 ± 0.07	6.8 ± 1.2	55 ± 13	2.5 ± 1.2	–	–	–
SHARDS20009956	12:36:13.5	62:09:31.0	3.77 ± 0.06	4.0 ± 1.1	1200 ± 300	3.0 ± 1.6	0.2 ± 0.2	28 ± 12	1.6 ± 1.2
SHARDS20014108	12:36:13.8	62:10:01.0	5.57 ± 0.07	4.1 ± 2.1	71 ± 41	2.7 ± 1.4	–	–	–
SHARDS20011916	12:36:13.9	62:14:21.4	5.88 ± 0.06	1.7 ± 1.0	34 ± 15	2.4 ± 1.3	–	–	–
SHARDS20007398	12:36:14.0	62:12:50.4	5.32 ± 0.07	1.4 ± 0.8	24 ± 10	2.1 ± 1.2	–	–	–
SHARDS20004841	12:36:14.1	62:10:22.8	3.64 ± 0.06	31.0 ± 7.0	290 ± 208	3.0 ± 1.6	4.6 ± 2.7	32 ± 11	1.4 ± 0.9
SHARDS20011037	12:36:14.1	62:09:38.3	4.31 ± 0.06	39.0 ± 10.0	393 ± 138	3.0 ± 1.6	5.9 ± 3.5	47 ± 8	1.9 ± 1.1
SHARDS20015984	12:36:14.3	62:10:48.4	5.99 ± 0.07	12.0 ± 4.0	70 ± 32	2.8 ± 1.4	–	–	–
SHARDS20007199	12:36:14.4	62:13:10.0	4.90 ± 0.08	6.5 ± 2.5	100 ± 40	2.9 ± 1.4	–	–	–
SHARDS20008483	12:36:14.5	62:10:39.4	3.78 ± 0.06	7.7 ± 2.2	1380 ± 160	3.0 ± 1.6	0.3 ± 0.2	24 ± 5	1.1 ± 0.5
SHARDS20005458	12:36:14.5	62:11:40.6	4.33 ± 0.06	5.7 ± 0.7	39 ± 5	1.9 ± 0.9	–	–	–
SHARDS20005148	12:36:14.8	62:10:49.8	3.38 ± 0.07	3.3 ± 0.4	67 ± 11	2.5 ± 1.3	–	–	–
SHARDS20008356	12:36:14.8	62:11:40.4	4.22 ± 0.07	2.7 ± 2.3	910 ± 390	3.0 ± 1.6	0.5 ± 0.6	20 ± 4	1.6 ± 0.9
SHARDS20008242	12:36:15.0	62:11:52.2	3.24 ± 0.07	18.0 ± 4.0	1280 ± 200	3.0 ± 1.6	0.7 ± 0.3	24 ± 6	1.1 ± 0.5
SHARDS20010508	12:36:15.1	62:13:13.0	4.90 ± 0.08	9.0 ± 6.0	869 ± 370	3.0 ± 1.6	0.5 ± 0.8	28 ± 12	2.8 ± 1.6
SHARDS20006670	12:36:15.3	62:11:10.4	4.21 ± 0.07	3.8 ± 0.6	36 ± 6	1.8 ± 0.8	–	–	–
SHARDS20004964	12:36:15.3	62:11:11.9	4.33 ± 0.06	10.1 ± 2.2	45 ± 10	2.2 ± 1.2	–	–	–
SHARDS20006780	12:36:15.4	62:15:07.3	4.63 ± 0.07	3.6 ± 1.4	51 ± 25	2.5 ± 1.3	–	–	–
SHARDS20005125	12:36:15.4	62:09:49.8	3.77 ± 0.06	11.0 ± 3.0	54 ± 13	2.7 ± 1.3	–	–	–
SHARDS20009668	12:36:15.5	62:13:26.7	4.90 ± 0.08	1.2 ± 0.7	63 ± 30	2.7 ± 1.4	–	–	–
SHARDS20005258	12:36:15.6	62:08:38.2	4.85 ± 0.08	11.8 ± 2.3	52 ± 11	2.6 ± 1.3	–	–	–
SHARDS20007856	12:36:15.6	62:15:09.3	4.23 ± 0.07	3.5 ± 1.7	57 ± 31	2.5 ± 1.3	–	–	–
SHARDS20011087	12:36:15.6	62:11:52.2	3.39 ± 0.07	1.1 ± 0.6	70 ± 42	2.7 ± 1.4	–	–	–
SHARDS20009704	12:36:15.7	62:10:56.5	3.92 ± 0.06	8.4 ± 5.8	530 ± 430	3.0 ± 1.6	1.4 ± 1.7	36 ± 13	1.7 ± 1.2
SHARDS20006191	12:36:16.1	62:14:55.8	3.40 ± 0.07	6.0 ± 1.4	860 ± 330	3.0 ± 1.6	0.2 ± 0.1	19 ± 6	3.5 ± 1.5
SHARDS20008109	12:36:16.2	62:09:06.3	4.59 ± 0.07	1.1 ± 0.6	40 ± 18	2.1 ± 1.2	–	–	–
SHARDS20009775	12:36:16.3	62:09:49.3	4.32 ± 0.06	47.4 ± 12.4	490 ± 250	3.0 ± 1.6	1.8 ± 1.2	41 ± 12	2.8 ± 1.6
SHARDS20006259	12:36:16.4	62:13:21.8	5.19 ± 0.06	17.0 ± 7.0	874 ± 210	3.0 ± 1.6	0.7 ± 0.5	19 ± 5	1.3 ± 0.7
SHARDS20008902	12:36:16.8	62:09:36.9	4.20 ± 0.07	11.0 ± 3.0	940 ± 290	3.0 ± 1.6	1.3 ± 0.8	24 ± 8	1.2 ± 0.7
SHARDS20008737	12:36:17.1	62:15:11.7	4.64 ± 0.07	6.8 ± 3.1	110 ± 70	2.9 ± 1.4	–	–	–
SHARDS20000642	12:36:17.3	62:08:36.9	3.90 ± 0.06	24.0 ± 6.0	969 ± 270	3.0 ± 1.6	0.6 ± 0.2	17 ± 7	2.7 ± 1.9
SHARDS20008636	12:36:17.3	62:09:00.1	4.59 ± 0.07	0.7 ± 0.3	40 ± 18	2.1 ± 1.2	–	–	–
SHARDS20004861	12:36:17.4	62:14:56.5	3.53 ± 0.06	5.4 ± 0.8	67 ± 16	2.7 ± 1.3	–	–	–
SHARDS20010163	12:36:17.5	62:10:22.4	5.30 ± 0.07	1.9 ± 0.9	27 ± 14	2.6 ± 1.4	–	–	–
SHARDS20007150	12:36:17.8	62:13:16.3	3.66 ± 0.06	1.1 ± 0.2	65 ± 18	2.7 ± 1.4	–	–	–
SHARDS20004728	12:36:17.9	62:14:21.9	4.24 ± 0.07	15.7 ± 1.6	111 ± 12	2.7 ± 1.6	0.9 ± 0.6	24 ± 5	1.0 ± 0.3
SHARDS20013550	12:36:18.1	62:14:34.7	4.24 ± 0.07	0.1 ± 0.0	15 ± 5	3.0 ± 1.4	–	–	–
SHARDS20006793	12:36:18.1	62:11:26.5	4.34 ± 0.06	12.0 ± 5.0	800 ± 320	3.0 ± 1.6	0.7 ± 0.8	21 ± 7	1.9 ± 1.1
SHARDS20006476	12:36:18.2	62:10:21.9	5.58 ± 0.07	31.0 ± 8.0	87 ± 30	2.9 ± 1.4	–	–	–
SHARDS20008202	12:36:18.6	62:08:14.3	4.30 ± 0.06	3.8 ± 3.2	570 ± 390	3.0 ± 1.6	0.8 ± 0.9	42 ± 12	2.3 ± 1.6
SHARDS20006130	12:36:18.6	62:14:21.4	4.36 ± 0.06	1.4 ± 0.3	47 ± 14	2.1 ± 1.1	–	–	–
SHARDS20008283	12:36:18.6	62:13:11.4	4.08 ± 0.07	1.0 ± 0.4	40 ± 16	2.2 ± 1.2	–	–	–

Continued on next page

Table A.2 – *Continued from previous page*

Object Name	R.A. (J2000)	Dec. (J2000)	z	$M_{\rm star,m}$ (10^9 $M_\odot$)	$\rm Age_m$ (Myr)	$\tau_{\rm m}$ (Myr)	$M_{\rm star,b}$ (10^9 $M_\odot$)	$\rm Age_b$ (Myr)	$\tau_{\rm b}$ (Myr)
SHARDS20007309	12:36:18.8	62:12:00.9	4.90 ± 0.08	5.8 ± 4.7	409 ± 360	3.0 ± 1.6	0.9 ± 1.1	24 ± 10	2.2 ± 1.4
SHARDS20006868	12:36:18.8	62:11:24.0	4.22 ± 0.07	19.0 ± 5.0	190 ± 60	3.0 ± 1.4	–	–	–
SHARDS20002379	12:36:18.9	62:11:33.3	3.93 ± 0.06	3.1 ± 0.4	40 ± 6	1.8 ± 0.9	–	–	–
SHARDS20008952	12:36:18.9	62:12:24.8	5.05 ± 0.06	8.5 ± 6.1	350 ± 280	3.0 ± 1.6	1.4 ± 1.6	25 ± 12	2.2 ± 1.4
SHARDS20006498	12:36:19.0	62:08:36.8	3.37 ± 0.07	12.0 ± 3.0	490 ± 330	3.0 ± 1.6	2.6 ± 1.3	39 ± 12	2.1 ± 1.4
SHARDS20006720	12:36:19.0	62:13:59.1	3.95 ± 0.06	3.5 ± 1.2	51 ± 23	2.3 ± 1.2	0.8 ± 1.0	12 ± 4	1.4 ± 0.9
SHARDS20009000	12:36:19.0	62:10:38.3	5.44 ± 0.07	5.8 ± 3.1	670 ± 270	3.0 ± 1.6	–	–	–
SHARDS20006040	12:36:19.0	62:09:32.4	3.91 ± 0.06	2.5 ± 0.9	33 ± 11	1.8 ± 0.9	0.8 ± 1.0	25 ± 10	1.8 ± 1.2
SHARDS20007567	12:36:19.2	62:10:49.7	4.33 ± 0.06	4.5 ± 3.5	530 ± 370	3.0 ± 1.6	–	–	–
SHARDS20016960	12:36:19.2	62:15:23.3	6.72 ± 0.14	17.0 ± 6.0	150 ± 60	3.0 ± 1.4	–	–	–
SHARDS20009201	12:36:19.2	62:13:08.8	3.95 ± 0.06	0.5 ± 0.2	17 ± 6	2.7 ± 1.4	–	–	–
SHARDS20006003	12:36:19.2	62:08:47.4	3.77 ± 0.06	7.0 ± 3.9	890 ± 409	3.0 ± 1.6	1.9 ± 1.6	36 ± 13	2.0 ± 1.4
SHARDS20010699	12:36:19.2	62:15:19.4	4.49 ± 0.07	1.2 ± 0.5	51 ± 23	2.5 ± 1.3	–	–	–
SHARDS20009747	12:36:19.3	62:08:39.2	3.90 ± 0.06	12.0 ± 4.0	1100 ± 300	3.0 ± 1.6	0.3 ± 0.1	23 ± 4	3.8 ± 1.5
SHARDS20013231	12:36:19.4	62:08:27.9	5.71 ± 0.06	26.7 ± 11.9	680 ± 250	3.0 ± 1.6	1.2 ± 1.2	39 ± 13	2.4 ± 1.6
SHARDS20007548	12:36:19.4	62:10:49.5	4.07 ± 0.07	4.4 ± 1.9	92 ± 49	2.9 ± 1.4	–	–	–
SHARDS20007432	12:36:19.6	62:10:50.9	4.34 ± 0.06	1.4 ± 0.8	54 ± 31	2.5 ± 1.3	–	–	–
SHARDS20014504	12:36:19.7	62:15:25.0	3.26 ± 0.07	0.2 ± 0.1	43 ± 22	2.4 ± 1.3	–	–	–
SHARDS20016872	12:36:19.8	62:12:21.9	3.40 ± 0.07	0.8 ± 0.4	69 ± 35	2.7 ± 1.4	–	–	–
SHARDS20005235	12:36:19.9	62:14:04.4	3.95 ± 0.06	3.0 ± 0.9	59 ± 23	2.4 ± 1.2	–	–	–
SHARDS20011850	12:36:20.1	62:14:13.7	5.33 ± 0.07	0.8 ± 0.4	48 ± 23	2.5 ± 1.3	–	–	–
SHARDS20013817	12:36:20.2	62:07:40.9	3.75 ± 0.06	2.0 ± 0.9	90 ± 48	2.9 ± 1.4	–	–	–
SHARDS20005304	12:36:20.3	62:12:11.2	4.08 ± 0.07	4.7 ± 3.9	800 ± 380	3.0 ± 1.6	1.4 ± 1.2	24 ± 3	1.0 ± 0.1
SHARDS20006306	12:36:20.3	62:13:59.3	3.81 ± 0.06	5.4 ± 2.0	1200 ± 300	3.0 ± 1.6	0.6 ± 0.5	22 ± 3	1.0 ± 0.1
SHARDS20008408	12:36:20.4	62:13:58.5	3.81 ± 0.06	5.2 ± 1.4	79 ± 29	2.8 ± 1.4	–	–	–
SHARDS20001139	12:36:20.4	62:09:37.7	3.50 ± 0.06	8.2 ± 0.9	45 ± 5	2.0 ± 0.8	–	–	–
SHARDS20007599	12:36:20.5	62:12:45.4	4.91 ± 0.08	4.1 ± 3.6	500 ± 360	3.0 ± 1.6	0.5 ± 0.8	15 ± 5	4.0 ± 1.4
SHARDS20007866	12:36:20.6	62:13:32.6	4.91 ± 0.08	1.0 ± 0.4	46 ± 18	2.3 ± 1.2	–	–	–
SHARDS20010067	12:36:20.7	62:08:37.9	5.28 ± 0.07	24.0 ± 7.0	457 ± 212	3.0 ± 1.6	0.7 ± 0.3	21 ± 4	4.3 ± 1.1
SHARDS20006845	12:36:20.7	62:13:30.6	4.91 ± 0.08	1.1 ± 0.6	23 ± 10	2.4 ± 1.4	–	–	–
SHARDS20004366	12:36:20.7	62:14:07.8	3.95 ± 0.06	3.2 ± 1.7	65 ± 18	2.5 ± 1.3	–	–	–
SHARDS20008963	12:36:20.8	62:08:29.5	4.04 ± 0.07	16.0 ± 6.0	750 ± 340	3.0 ± 1.6	0.9 ± 0.7	47 ± 9	2.2 ± 1.4
SHARDS20006203	12:36:20.9	62:15:05.7	3.41 ± 0.07	0.7 ± 0.2	38 ± 12	1.9 ± 1.0	–	–	–
SHARDS20007883	12:36:21.3	62:09:54.8	3.81 ± 0.06	2.7 ± 1.1	1200 ± 300	3.0 ± 1.6	0.3 ± 0.2	22 ± 6	1.1 ± 0.5
SHARDS20012642	12:36:21.3	62:09:02.7	4.20 ± 0.07	4.8 ± 3.5	540 ± 340	3.0 ± 1.6	0.8 ± 0.9	42 ± 12	2.3 ± 1.5
SHARDS20013414	12:36:21.4	62:09:04.4	5.73 ± 0.06	5.4 ± 3.2	94 ± 54	2.8 ± 1.4	–	–	–
SHARDS20008503	12:36:21.5	62:13:38.9	4.09 ± 0.07	2.4 ± 0.7	92 ± 38	2.9 ± 1.4	–	–	–
SHARDS20007440	12:36:21.6	62:12:04.1	3.52 ± 0.06	6.2 ± 2.0	18 ± 4	2.5 ± 1.2	–	–	–
SHARDS20004772	12:36:21.8	62:11:39.7	5.18 ± 0.06	12.9 ± 2.0	47 ± 10	2.3 ± 1.2	–	–	–
SHARDS20006586	12:36:21.9	62:14:30.9	4.09 ± 0.07	1.9 ± 0.6	37 ± 13	2.1 ± 1.1	–	–	–
SHARDS20007381	12:36:21.9	62:08:14.2	4.72 ± 0.07	0.5 ± 0.2	43 ± 15	2.3 ± 1.2	–	–	–
SHARDS20005050	12:36:21.9	62:15:16.8	4.92 ± 0.08	19.0 ± 5.0	67 ± 21	2.7 ± 1.4	–	–	–
SHARDS20012659	12:36:22.0	62:15:13.4	5.78 ± 0.06	0.4 ± 0.2	17 ± 6	2.8 ± 1.4	–	–	–
SHARDS20005714	12:36:22.1	62:09:57.5	4.33 ± 0.06	11.0 ± 7.0	350 ± 250	3.0 ± 1.6	2.9 ± 2.1	25 ± 7	1.1 ± 0.6
SHARDS20011578	12:36:22.2	62:15:49.4	4.36 ± 0.06	18.0 ± 5.0	563 ± 209	3.0 ± 1.6	0.8 ± 0.6	24 ± 8	1.2 ± 0.7
SHARDS20009182	12:36:22.2	62:09:42.3	3.78 ± 0.06	0.7 ± 0.2	18 ± 7	2.1 ± 1.3	–	–	–
SHARDS20009497	12:36:22.3	62:13:57.7	4.50 ± 0.07	0.7 ± 0.3	16 ± 6	2.4 ± 1.3	–	–	–
SHARDS20004970	12:36:22.4	62:13:36.5	4.36 ± 0.06	11.0 ± 3.0	66 ± 25	2.6 ± 1.3	–	–	–
SHARDS20001272	12:36:22.4	62:09:51.7	3.51 ± 0.06	1.6 ± 0.5	52 ± 23	2.2 ± 1.2	–	–	–

Continued on next page

Table A.2 – *Continued from previous page*

Object Name	R.A. (J2000)	Dec. (J2000)	z	$M_{\rm star,m}$ (10^9 $M_\odot$)	$\rm Age_m$ (Myr)	$\tau_{\rm m}$ (Myr)	$M_{\rm star,b}$ (10^9 $M_\odot$)	$\rm Age_b$ (Myr)	$\tau_{\rm b}$ (Myr)
SHARDS20012600	12:36:22.5	62:14:53.7	3.26 ± 0.07	0.2 ± 0.1	15 ± 6	3.0 ± 1.4	–	–	–
SHARDS20007135	12:36:22.5	62:07:12.9	3.36 ± 0.07	2.3 ± 0.5	77 ± 18	3.0 ± 1.4	–	–	–
SHARDS20008241	12:36:22.7	62:09:02.8	4.32 ± 0.06	0.9 ± 0.5	27 ± 13	2.6 ± 1.4	–	–	–
SHARDS20011383	12:36:22.8	62:14:21.9	5.34 ± 0.07	4.1 ± 0.9	40 ± 11	2.2 ± 1.1	–	–	–
SHARDS20006244	12:36:22.9	62:14:22.9	3.95 ± 0.06	1.2 ± 0.5	40 ± 16	2.1 ± 1.1	–	–	–
SHARDS20005080	12:36:22.9	62:10:02.7	3.79 ± 0.06	4.1 ± 1.6	46 ± 16	2.2 ± 1.1	–	–	–
SHARDS20007000	12:36:23.0	62:15:55.5	4.81 ± 0.08	16.0 ± 9.0	500 ± 300	3.0 ± 1.6	0.8 ± 1.1	18 ± 6	2.8 ± 1.7
SHARDS20006645	12:36:23.1	62:11:56.5	3.52 ± 0.06	0.9 ± 0.4	42 ± 21	2.0 ± 1.1	–	–	–
SHARDS20005265	12:36:23.2	62:12:35.5	4.36 ± 0.06	9.8 ± 3.8	607 ± 219	3.0 ± 1.6	0.3 ± 0.2	12 ± 5	3.2 ± 1.8
SHARDS20015020	12:36:23.3	62:13:10.7	4.49 ± 0.07	0.8 ± 0.4	59 ± 32	2.6 ± 1.4	–	–	–
SHARDS20015068	12:36:23.3	62:15:14.9	5.07 ± 0.06	0.5 ± 0.2	45 ± 18	2.4 ± 1.3	–	–	–
SHARDS20018787	12:36:23.4	62:16:03.2	5.07 ± 0.06	1.3 ± 1.0	58 ± 34	2.6 ± 1.3	–	–	–
SHARDS20013017	12:36:23.5	62:10:53.1	3.65 ± 0.06	8.6 ± 1.5	160 ± 50	3.0 ± 1.4	–	–	–
SHARDS20004838	12:36:23.5	62:08:47.5	3.38 ± 0.07	13.9 ± 1.8	66 ± 9	2.8 ± 1.4	–	–	–
SHARDS20006466	12:36:23.6	62:15:20.0	4.92 ± 0.08	25.0 ± 4.0	926 ± 127	3.0 ± 1.6	0.7 ± 0.2	19 ± 5	2.6 ± 1.4
SHARDS20005556	12:36:23.8	62:14:17.7	3.54 ± 0.06	2.2 ± 0.3	40 ± 6	2.0 ± 1.0	–	–	–
SHARDS20012395	12:36:24.0	62:15:43.4	4.65 ± 0.07	2.6 ± 1.3	120 ± 70	2.9 ± 1.4	–	–	–
SHARDS20010719	12:36:24.1	62:13:51.1	5.20 ± 0.06	2.0 ± 1.6	24 ± 19	2.8 ± 1.4	–	–	–
SHARDS20013820	12:36:24.1	62:11:43.2	5.61 ± 0.07	2.5 ± 1.3	50 ± 22	2.4 ± 1.3	–	–	–
SHARDS20009710	12:36:24.2	62:09:16.6	4.32 ± 0.06	1.1 ± 0.5	67 ± 33	2.7 ± 1.4	–	–	–
SHARDS20013918	12:36:24.2	62:14:24.6	5.34 ± 0.07	0.6 ± 0.3	45 ± 18	2.4 ± 1.3	–	–	–
SHARDS20010534	12:36:24.4	62:15:46.6	4.79 ± 0.07	0.3 ± 0.2	19 ± 12	2.4 ± 1.3	–	–	–
SHARDS20007585	12:36:24.5	62:09:21.3	3.38 ± 0.07	2.8 ± 0.9	79 ± 32	2.8 ± 1.4	–	–	–
SHARDS20009337	12:36:24.5	62:15:17.1	3.82 ± 0.06	10.0 ± 4.0	900 ± 350	3.0 ± 1.6	0.7 ± 0.9	26 ± 10	1.3 ± 0.9
SHARDS20007133	12:36:24.5	62:11:02.4	3.94 ± 0.06	0.7 ± 0.4	23 ± 10	2.3 ± 1.3	–	–	–
SHARDS20005602	12:36:24.6	62:07:39.5	4.30 ± 0.06	5.4 ± 1.5	51 ± 18	2.5 ± 1.3	–	–	–
SHARDS20007542	12:36:24.6	62:11:59.3	3.53 ± 0.06	8.6 ± 4.9	560 ± 459	3.0 ± 1.6	0.5 ± 0.5	19 ± 5	3.7 ± 1.4
SHARDS20010634	12:36:24.8	62:13:10.9	5.06 ± 0.06	2.8 ± 1.3	51 ± 28	2.9 ± 1.4	–	–	–
SHARDS20009655	12:36:25.0	62:12:34.8	3.81 ± 0.06	2.8 ± 1.2	78 ± 42	2.8 ± 1.4	–	–	–
SHARDS20005714	12:36:25.1	62:11:05.7	4.23 ± 0.07	5.5 ± 1.1	61 ± 19	2.6 ± 1.3	–	–	–
SHARDS20006463	12:36:25.3	62:09:09.6	4.32 ± 0.06	5.8 ± 2.2	66 ± 25	2.6 ± 1.3	–	–	–
SHARDS20010781	12:36:25.4	62:11:19.8	5.32 ± 0.07	8.2 ± 5.6	302 ± 246	3.0 ± 1.6	0.8 ± 1.1	22 ± 10	3.0 ± 1.6
SHARDS20014346	12:36:25.5	62:13:22.1	5.34 ± 0.07	1.4 ± 1.1	69 ± 45	2.7 ± 1.4	0.8 ± 0.7	23 ± 10	2.7 ± 1.4
SHARDS20014826	12:36:25.5	62:15:35.0	5.48 ± 0.07	19.0 ± 5.0	525 ± 235	3.0 ± 1.6	–	–	–
SHARDS20009609	12:36:25.6	62:07:06.5	5.38 ± 0.07	0.3 ± 0.1	16 ± 6	2.7 ± 1.4	–	–	–
SHARDS20010591	12:36:25.6	62:15:07.4	3.54 ± 0.06	18.0 ± 3.0	1280 ± 170	3.0 ± 1.6	0.5 ± 0.2	23 ± 4	1.0 ± 0.3
SHARDS20010751	12:36:25.6	62:13:10.5	3.95 ± 0.06	0.1 ± 0.1	18 ± 6	2.6 ± 1.4	–	–	–
SHARDS20004745	12:36:25.8	62:14:36.2	3.41 ± 0.07	12.3 ± 1.8	93 ± 4	3.1 ± 1.4	–	–	–
SHARDS20008284	12:36:25.9	62:14:58.9	4.25 ± 0.07	0.6 ± 0.1	29 ± 6	1.5 ± 0.7	–	–	–
SHARDS20007379	12:36:25.9	62:07:40.4	4.58 ± 0.07	9.4 ± 3.0	190 ± 80	3.0 ± 1.4	–	–	–
SHARDS20008577	12:36:25.9	62:16:10.3	3.68 ± 0.06	4.7 ± 2.7	770 ± 409	3.0 ± 1.6	0.3 ± 0.4	16 ± 5	3.4 ± 1.5
SHARDS20000859	12:36:25.9	62:09:03.6	4.32 ± 0.06	23.3 ± 1.2	60 ± 3	2.5 ± 1.0	–	–	–
SHARDS20008112	12:36:25.9	62:13:19.4	3.81 ± 0.06	2.2 ± 0.9	98 ± 50	2.9 ± 1.4	–	–	–
SHARDS20004779	12:36:26.0	62:08:59.4	4.32 ± 0.06	20.0 ± 4.0	79 ± 28	2.7 ± 1.6	2.0 ± 1.7	26 ± 8	1.2 ± 0.6
SHARDS20005242	12:36:26.0	62:09:00.3	4.32 ± 0.06	20.0 ± 7.0	257 ± 122	3.0 ± 1.6	4.7 ± 2.8	27 ± 7	1.1 ± 0.4
SHARDS20005536	12:36:26.1	62:09:13.2	4.21 ± 0.07	1.3 ± 0.2	37 ± 10	1.7 ± 0.8	–	–	–
SHARDS20007108	12:36:26.1	62:09:01.2	4.32 ± 0.06	16.0 ± 6.0	390 ± 250	3.0 ± 1.6	3.2 ± 2.4	32 ± 13	1.6 ± 1.1
SHARDS20014466	12:36:26.2	62:13:38.1	4.65 ± 0.07	1.7 ± 1.0	83 ± 58	2.8 ± 1.4	–	–	–
SHARDS20009028	12:36:26.2	62:10:32.5	5.45 ± 0.07	11.0 ± 7.0	262 ± 223	3.0 ± 1.6	1.3 ± 1.6	23 ± 10	2.1 ± 1.4

Continued on next page

Table A.2 – *Continued from previous page*

Object Name	R.A. (J2000)	Dec. (J2000)	z	$M_{\rm star,m}$ (10^9 $M_\odot$)	Age$_{\rm m}$ (Myr)	$\tau_{\rm m}$ (Myr)	$M_{\rm star,b}$ (10^9 $M_\odot$)	Age$_{\rm b}$ (Myr)	$\tau_{\rm b}$ (Myr)
SHARDS20008717	12:36:26.5	62:13:31.6	5.34 ± 0.07	1.6 ± 0.3	21 ± 4	1.9 ± 1.0	–	–	–
SHARDS20022686	12:36:26.5	62:12:07.4	5.20 ± 0.06	2.2 ± 1.0	46 ± 25	2.7 ± 1.4	–	–	–
SHARDS20007321	12:36:26.6	62:13:20.9	4.50 ± 0.07	0.2 ± 0.1	18 ± 5	2.3 ± 1.2	–	–	–
SHARDS20007074	12:36:26.6	62:06:21.1	3.60 ± 0.06	0.4 ± 0.5	12 ± 12	3.6 ± 1.3	–	–	–
SHARDS20003814	12:36:26.7	62:16:18.8	3.82 ± 0.06	1.9 ± 0.7	65 ± 33	2.7 ± 1.4	–	–	–
SHARDS20005090	12:36:26.8	62:08:25.4	3.91 ± 0.06	5.0 ± 0.8	76 ± 16	2.7 ± 1.4	–	–	–
SHARDS20005401	12:36:26.8	62:11:03.7	3.25 ± 0.07	5.2 ± 0.8	81 ± 16	3.1 ± 1.4	–	–	–
SHARDS20007167	12:36:26.9	62:10:06.2	5.04 ± 0.06	5.2 ± 1.2	47 ± 11	2.5 ± 1.3	–	–	–
SHARDS20008172	12:36:26.9	62:13:59.5	3.68 ± 0.06	8.4 ± 3.4	610 ± 320	3.0 ± 1.6	1.0 ± 0.9	41 ± 12	2.0 ± 1.4
SHARDS20015413	12:36:27.0	62:14:50.5	4.92 ± 0.08	3.0 ± 3.0	158 ± 128	2.9 ± 1.4	–	–	–
SHARDS20007619	12:36:27.1	62:15:17.9	4.65 ± 0.07	7.2 ± 2.5	790 ± 280	3.0 ± 1.6	1.0 ± 1.0	24 ± 7	1.1 ± 0.7
SHARDS20008187	12:36:27.1	62:12:41.6	4.36 ± 0.06	22.0 ± 6.0	1020 ± 180	3.0 ± 1.6	0.9 ± 0.5	34 ± 12	1.8 ± 1.4
SHARDS20007579	12:36:27.2	62:15:17.3	4.50 ± 0.07	8.9 ± 5.9	540 ± 350	3.0 ± 1.6	1.0 ± 1.3	23 ± 10	1.9 ± 1.2
SHARDS20012340	12:36:27.2	62:13:39.6	5.07 ± 0.06	5.1 ± 1.6	56 ± 28	2.6 ± 1.3	–	–	–
SHARDS20012246	12:36:27.4	62:16:01.9	4.65 ± 0.07	26.0 ± 7.0	387 ± 136	3.0 ± 1.4	–	–	–
SHARDS20015624	12:36:27.6	62:13:28.0	6.47 ± 0.11	4.4 ± 1.6	54 ± 26	2.5 ± 1.3	–	–	–
SHARDS20011533	12:36:27.7	62:14:32.1	4.10 ± 0.07	1.8 ± 0.7	54 ± 19	2.4 ± 1.3	–	–	–
SHARDS20014180	12:36:27.7	62:14:02.8	5.07 ± 0.06	0.4 ± 0.3	23 ± 13	2.9 ± 1.4	–	–	–
SHARDS20018314	12:36:27.8	62:14:32.9	3.54 ± 0.06	0.1 ± 0.1	18 ± 8	2.8 ± 1.4	–	–	–
SHARDS20010477	12:36:27.8	62:12:46.6	4.09 ± 0.07	0.1 ± 0.0	15 ± 4	2.8 ± 1.4	–	–	–
SHARDS20006528	12:36:27.9	62:14:56.7	3.41 ± 0.07	13.0 ± 3.0	220 ± 60	3.0 ± 1.4	–	–	–
SHARDS20005310	12:36:28.0	62:09:01.8	3.92 ± 0.06	2.8 ± 0.6	28 ± 5	4.2 ± 1.0	–	–	–
SHARDS20011786	12:36:28.1	62:13:19.5	5.34 ± 0.07	4.2 ± 2.6	81 ± 43	2.8 ± 1.4	–	–	–
SHARDS20011181	12:36:28.1	62:09:01.5	3.92 ± 0.06	3.7 ± 1.3	52 ± 18	2.3 ± 1.2	–	–	–
SHARDS20006518	12:36:28.2	62:09:07.8	4.33 ± 0.06	14.0 ± 6.0	700 ± 270	3.0 ± 1.6	1.8 ± 1.8	37 ± 13	1.9 ± 1.3
SHARDS20008735	12:36:28.3	62:08:50.9	4.21 ± 0.07	1.8 ± 0.8	53 ± 24	2.5 ± 1.3	–	–	–
SHARDS20017018	12:36:28.3	62:12:40.9	5.07 ± 0.06	2.8 ± 1.9	74 ± 40	2.7 ± 1.4	–	–	–
SHARDS20003920	12:36:28.4	62:15:37.2	3.41 ± 0.07	0.8 ± 0.3	53 ± 24	2.5 ± 1.3	–	–	–
SHARDS20010361	12:36:28.4	62:14:16.2	4.92 ± 0.08	22.0 ± 3.0	886 ± 148	3.0 ± 1.6	0.6 ± 0.2	18 ± 3	3.9 ± 1.0
SHARDS20007629	12:36:28.6	62:14:10.5	5.34 ± 0.07	1.9 ± 0.5	50 ± 15	2.4 ± 1.2	–	–	–
SHARDS20008303	12:36:28.6	62:08:51.4	4.32 ± 0.06	20.0 ± 3.0	1070 ± 220	3.0 ± 1.6	0.7 ± 0.4	24 ± 9	2.3 ± 1.3
SHARDS20011098	12:36:28.6	62:13:51.7	3.96 ± 0.06	9.8 ± 2.2	1250 ± 210	3.0 ± 1.6	0.3 ± 0.2	36 ± 13	2.2 ± 1.5
SHARDS20009271	12:36:28.7	62:14:23.8	5.63 ± 0.07	5.5 ± 1.9	57 ± 25	2.5 ± 1.3	–	–	–
SHARDS20005784	12:36:28.7	62:12:29.2	4.09 ± 0.07	1.3 ± 0.4	62 ± 19	2.6 ± 1.3	–	–	–
SHARDS20009880	12:36:28.7	62:14:18.8	5.48 ± 0.07	1.4 ± 0.7	24 ± 9	2.7 ± 1.4	–	–	–
SHARDS20008943	12:36:28.7	62:16:27.0	4.10 ± 0.07	1.1 ± 0.7	67 ± 45	2.6 ± 1.4	–	–	–
SHARDS20017665	12:36:28.7	62:16:15.3	3.54 ± 0.06	15.0 ± 4.0	1190 ± 220	3.0 ± 1.6	0.5 ± 0.3	37 ± 12	2.6 ± 1.6
SHARDS20004921	12:36:28.8	62:12:45.4	4.25 ± 0.07	6.6 ± 1.8	48 ± 12	2.3 ± 1.1	–	–	–
SHARDS20010811	12:36:28.8	62:14:19.2	5.79 ± 0.06	1.4 ± 0.7	43 ± 18	2.2 ± 1.2	–	–	–
SHARDS20009052	12:36:28.8	62:14:45.2	3.68 ± 0.06	0.2 ± 0.1	21 ± 7	2.4 ± 1.3	–	–	–
SHARDS20005934	12:36:29.0	62:12:00.3	4.36 ± 0.06	4.8 ± 1.6	52 ± 22	2.3 ± 1.2	–	–	–
SHARDS20004937	12:36:29.0	62:06:05.4	4.55 ± 0.07	9.6 ± 2.9	85 ± 33	2.8 ± 1.4	–	–	–
SHARDS20012975	12:36:29.2	62:12:38.3	4.92 ± 0.08	1.3 ± 0.8	75 ± 50	2.7 ± 1.4	–	–	–
SHARDS20015609	12:36:29.3	62:15:40.7	6.74 ± 0.14	0.2 ± 0.1	13 ± 4	3.1 ± 1.4	–	–	–
SHARDS20004011	12:36:29.4	62:15:13.0	3.68 ± 0.06	87.0 ± 8.0	138 ± 15	3.1 ± 1.6	4.6 ± 1.0	19 ± 1	2.9 ± 0.3
SHARDS20011663	12:36:29.5	62:14:48.3	4.25 ± 0.07	1.2 ± 0.5	52 ± 23	2.5 ± 1.3	–	–	–
SHARDS20006960	12:36:29.5	62:14:02.8	3.41 ± 0.07	0.5 ± 0.2	15 ± 5	3.0 ± 1.4	–	–	–
SHARDS20015849	12:36:29.7	62:12:55.8	5.48 ± 0.07	0.4 ± 0.7	21 ± 26	3.1 ± 1.4	–	–	–
SHARDS20011428	12:36:29.7	62:12:46.0	4.10 ± 0.07	1.3 ± 0.3	35 ± 10	2.1 ± 1.1	–	–	–

Continued on next page

Table A.2 – *Continued from previous page*

Object Name	R.A. (J2000)	Dec. (J2000)	z	$M_{\rm star,m}$ ($10^9\ M_\odot$)	$\rm Age_m$ (Myr)	$\tau_{\rm m}$ (Myr)	$M_{\rm star,b}$ ($10^9\ M_\odot$)	$\rm Age_b$ (Myr)	$\tau_{\rm b}$ (Myr)
SHARDS20014081	12:36:29.7	62:14:45.2	4.50 ± 0.07	3.5 ± 2.6	740 ± 390	3.0 ± 1.6	0.4 ± 0.6	33 ± 13	2.0 ± 1.5
SHARDS20013312	12:36:29.8	62:14:55.2	4.93 ± 0.08	0.9 ± 0.5	49 ± 20	2.4 ± 1.3	—	—	—
SHARDS20013937	12:36:29.8	62:14:32.0	5.48 ± 0.07	1.2 ± 0.6	22 ± 7	2.7 ± 1.5	—	—	—
SHARDS20009062	12:36:29.8	62:09:48.2	4.76 ± 0.07	0.4 ± 0.3	25 ± 12	2.7 ± 1.4	—	—	—
SHARDS20008220	12:36:29.9	62:12:34.0	3.54 ± 0.06	2.5 ± 2.1	980 ± 430	3.0 ± 1.6	0.7 ± 0.7	11 ± 4	1.3 ± 0.9
SHARDS20008664	12:36:29.9	62:16:56.0	4.69 ± 0.07	1.2 ± 0.6	60 ± 26	2.6 ± 1.3	—	—	—
SHARDS20006640	12:36:30.0	62:16:31.7	4.39 ± 0.06	12.0 ± 8.0	810 ± 409	3.0 ± 1.6	1.2 ± 1.4	19 ± 4	2.0 ± 1.1
SHARDS20008124	12:36:30.0	62:06:26.4	4.56 ± 0.07	2.0 ± 1.0	73 ± 37	2.8 ± 1.4	—	—	—
SHARDS20007258	12:36:30.0	62:15:45.1	3.54 ± 0.06	1.8 ± 0.8	58 ± 36	2.4 ± 1.3	—	—	—
SHARDS20007915	12:36:30.1	62:16:29.5	4.37 ± 0.06	3.9 ± 2.9	600 ± 380	3.0 ± 1.6	0.7 ± 0.8	40 ± 12	2.1 ± 1.5
SHARDS20012785	12:36:30.2	62:14:45.3	5.35 ± 0.07	4.5 ± 3.1	300 ± 260	3.0 ± 1.6	0.7 ± 0.8	26 ± 13	2.4 ± 1.5
SHARDS20006234	12:36:30.2	62:11:05.9	4.78 ± 0.07	7.9 ± 5.9	440 ± 370	3.0 ± 1.6	1.7 ± 1.8	25 ± 10	1.8 ± 1.3
SHARDS20006371	12:36:30.2	62:15:08.4	3.68 ± 0.06	0.5 ± 0.2	20 ± 7	2.9 ± 1.4	—	—	—
SHARDS20007936	12:36:30.2	62:13:45.0	5.35 ± 0.07	2.8 ± 1.0	41 ± 14	2.2 ± 1.2	—	—	—
SHARDS20011499	12:36:30.3	62:14:13.8	5.63 ± 0.07	1.0 ± 0.7	24 ± 9	2.4 ± 1.3	—	—	—
SHARDS20006583	12:36:30.4	62:06:59.2	4.18 ± 0.07	6.3 ± 2.5	430 ± 270	3.0 ± 1.6	0.7 ± 0.7	17 ± 5	3.3 ± 1.4
SHARDS20008593	12:36:30.4	62:09:43.1	4.34 ± 0.06	1.7 ± 0.8	50 ± 25	2.3 ± 1.3	—	—	—
SHARDS20007608	12:36:30.5	62:06:15.3	4.28 ± 0.06	0.6 ± 0.1	46 ± 11	2.3 ± 1.2	—	—	—
SHARDS20007578	12:36:30.5	62:15:41.3	3.42 ± 0.07	1.5 ± 0.5	84 ± 38	2.8 ± 1.4	—	—	—
SHARDS20006370	12:36:30.6	62:13:28.0	4.37 ± 0.06	7.3 ± 1.1	120 ± 30	3.0 ± 1.4	—	—	—
SHARDS20013374	12:36:30.6	62:12:58.3	3.26 ± 0.07	1.1 ± 0.4	56 ± 29	2.7 ± 1.4	—	—	—
SHARDS20010497	12:36:30.6	62:16:36.0	4.15 ± 0.07	2.9 ± 0.9	86 ± 32	2.9 ± 1.4	—	—	—
SHARDS20009182	12:36:30.7	62:09:21.4	4.88 ± 0.08	20.0 ± 8.0	930 ± 310	3.0 ± 1.6	0.7 ± 0.5	38 ± 13	3.0 ± 1.6
SHARDS20006461	12:36:30.8	62:14:46.6	4.10 ± 0.07	1.9 ± 0.3	41 ± 12	2.1 ± 1.1	—	—	—
SHARDS20014141	12:36:30.8	62:12:53.6	5.62 ± 0.07	1.3 ± 1.1	36 ± 33	3.0 ± 1.5	—	—	—
SHARDS20009549	12:36:30.9	62:16:44.0	3.20 ± 0.07	0.1 ± 0.1	15 ± 6	3.2 ± 1.4	—	—	—
SHARDS20011794	12:36:31.0	62:12:16.7	4.09 ± 0.07	2.3 ± 1.6	99 ± 80	3.0 ± 1.4	—	—	—
SHARDS20003443	12:36:31.0	62:12:15.6	3.54 ± 0.06	3.5 ± 1.1	49 ± 20	2.1 ± 1.1	—	—	—
SHARDS20005365	12:36:31.2	62:16:52.2	3.46 ± 0.06	10.3 ± 1.9	130 ± 30	3.1 ± 1.5	—	—	—
SHARDS20001522	12:36:31.2	62:10:17.5	3.52 ± 0.06	4.3 ± 2.5	940 ± 400	3.0 ± 1.6	0.5 ± 0.6	10 ± 2	1.1 ± 0.4
SHARDS20007926	12:36:31.3	62:08:52.3	4.06 ± 0.07	0.2 ± 0.1	14 ± 5	3.1 ± 1.4	—	—	—
SHARDS20005124	12:36:31.3	62:12:18.5	3.54 ± 0.06	49.5 ± 15.5	500 ± 250	3.0 ± 1.6	4.4 ± 1.9	48 ± 7	2.3 ± 1.2
SHARDS20005442	12:36:31.3	62:10:33.7	4.48 ± 0.07	2.2 ± 0.8	38 ± 7	1.9 ± 0.9	—	—	—
SHARDS20008033	12:36:31.4	62:15:43.2	4.83 ± 0.08	4.0 ± 1.4	76 ± 36	2.7 ± 1.4	—	—	—
SHARDS20009733	12:36:31.5	62:16:13.2	4.25 ± 0.07	1.4 ± 0.5	46 ± 17	2.2 ± 1.2	—	—	—
SHARDS20008713	12:36:31.6	62:10:35.3	4.23 ± 0.07	1.4 ± 0.7	59 ± 31	2.6 ± 1.3	—	—	—
SHARDS20018610	12:36:31.6	62:12:31.1	4.25 ± 0.07	0.1 ± 0.3	18 ± 31	3.0 ± 1.4	—	—	—
SHARDS20010033	12:36:31.7	62:09:23.8	5.30 ± 0.07	3.6 ± 1.6	83 ± 39	2.8 ± 1.4	—	—	—
SHARDS20005557	12:36:31.9	62:12:23.2	4.50 ± 0.07	4.7 ± 0.8	41 ± 12	2.2 ± 1.2	—	—	—
SHARDS20011759	12:36:32.0	62:16:05.1	3.82 ± 0.06	19.5 ± 10.4	430 ± 280	3.0 ± 1.6	0.7 ± 0.8	27 ± 11	3.3 ± 1.6
SHARDS20008719	12:36:32.0	62:13:39.0	4.37 ± 0.06	9.5 ± 2.1	110 ± 80	3.0 ± 1.4	—	—	—
SHARDS20003435	12:36:32.0	62:12:11.3	3.41 ± 0.07	17.0 ± 1.0	108 ± 11	2.9 ± 1.4	—	—	—
SHARDS20015534	12:36:32.1	62:14:41.9	6.05 ± 0.07	0.6 ± 1.2	33 ± 38	2.8 ± 1.4	—	—	—
SHARDS20009699	12:36:32.1	62:16:33.6	3.96 ± 0.06	2.2 ± 0.9	84 ± 41	2.8 ± 1.4	—	—	—
SHARDS20004892	12:36:32.1	62:14:32.7	3.69 ± 0.06	13.0 ± 3.0	98 ± 22	2.8 ± 1.4	—	—	—
SHARDS20014601	12:36:32.2	62:16:07.3	3.55 ± 0.06	28.0 ± 5.0	170 ± 40	3.1 ± 1.4	—	—	—
SHARDS20001223	12:36:32.2	62:09:46.4	3.65 ± 0.06	6.1 ± 4.3	530 ± 370	3.0 ± 1.6	1.6 ± 1.3	21 ± 3	1.7 ± 1.0
SHARDS20008098	12:36:32.3	62:06:23.1	4.28 ± 0.06	0.7 ± 0.3	47 ± 18	2.4 ± 1.3	—	—	—
SHARDS20003820	12:36:32.3	62:16:20.5	3.59 ± 0.06	26.0 ± 4.0	976 ± 210	3.0 ± 1.6	0.8 ± 0.3	22 ± 4	2.0 ± 1.1

Continued on next page

Table A.2 – *Continued from previous page*

Object Name	R.A. (J2000)	Dec. (J2000)	z	$M_{\rm star,m}$ (10^9 $M_\odot$)	$\rm Age_m$ (Myr)	$\tau_{\rm m}$ (Myr)	$M_{\rm star,b}$ (10^9 $M_\odot$)	$\rm Age_b$ (Myr)	$\tau_{\rm b}$ (Myr)
SHARDSJ001534.5	12:36:32.3	62:14:49.4	5.63 ± 0.07	2.1 ± 1.6	64 ± 40	2.6 ± 1.4	–	–	–
SHARDSJ000611.3	12:36:32.3	62:16:07.0	3.83 ± 0.06	43.0 ± 9.0	260 ± 100	3.0 ± 1.6	1.4 ± 0.7	14 ± 6	1.3 ± 0.7
SHARDSJ000711.5	12:36:32.5	62:13:31.3	5.35 ± 0.07	2.3 ± 0.5	52 ± 13	2.4 ± 1.2	–	–	–
SHARDSJ001060.0	12:36:32.6	62:12:17.3	3.54 ± 0.06	10.0 ± 2.9	950 ± 340	3.0 ± 1.6	0.3 ± 0.2	23 ± 8	2.7 ± 1.5
SHARDSJ000694.2	12:36:32.6	62:14:45.4	3.83 ± 0.06	0.6 ± 0.2	21 ± 5	2.3 ± 1.3	–	–	–
SHARDSJ000742.0	12:36:32.7	62:08:56.5	4.21 ± 0.07	9.0 ± 3.2	791 ± 272	3.0 ± 1.6	0.4 ± 0.6	12 ± 3	1.8 ± 1.1
SHARDSJ000644.1	12:36:32.7	62:16:44.2	3.87 ± 0.06	40.1 ± 12.6	907 ± 202	3.0 ± 1.6	1.8 ± 1.2	37 ± 12	1.9 ± 1.4
SHARDSJ000604.1	12:36:32.9	62:16:38.3	5.63 ± 0.07	6.7 ± 5.3	450 ± 370	3.0 ± 1.6	1.1 ± 1.2	20 ± 6	2.3 ± 1.3
SHARDSJ001483.7	12:36:32.9	62:09:13.5	4.22 ± 0.07	1.6 ± 0.5	47 ± 17	2.2 ± 1.2	–	–	–
SHARDSJ000609.8	12:36:33.1	62:12:30.3	3.54 ± 0.06	12.0 ± 3.0	72 ± 24	3.0 ± 1.4	–	–	–
SHARDSJ000457.6	12:36:33.1	62:05:54.3	4.01 ± 0.07	2.5 ± 0.8	73 ± 27	2.8 ± 1.4	–	–	–
SHARDSJ000674.5	12:36:33.2	62:15:04.4	3.69 ± 0.06	1.7 ± 0.4	33 ± 8	1.7 ± 0.8	–	–	–
SHARDSJ000907.4	12:36:33.2	62:13:02.2	4.25 ± 0.07	0.1 ± 0.0	15 ± 5	3.0 ± 1.4	–	–	–
SHARDSJ001848.1	12:36:33.2	62:18:17.5	4.25 ± 0.07	24.0 ± 5.0	86 ± 24	3.0 ± 1.4	–	–	–
SHARDSJ000512.2	12:36:33.4	62:09:07.0	4.33 ± 0.06	2.2 ± 2.3	83 ± 67	2.7 ± 1.4	–	–	–
SHARDSJ001785.4	12:36:33.4	62:12:32.4	4.79 ± 0.07	2.3 ± 1.2	74 ± 42	2.8 ± 1.4	–	–	–
SHARDSJ001365.2	12:36:33.4	62:12:15.9	5.49 ± 0.07	2.8 ± 2.0	70 ± 42	2.7 ± 1.4	–	–	–
SHARDSJ001496.7	12:36:33.4	62:16:40.8	5.48 ± 0.07	8.1 ± 3.3	82 ± 35	2.8 ± 1.4	–	–	–
SHARDSJ000747.5	12:36:33.4	62:06:40.4	5.12 ± 0.06	66.0 ± 6.0	902 ± 125	3.0 ± 1.6	3.3 ± 0.6	48 ± 7	2.3 ± 1.0
SHARDSJ000484.6	12:36:33.5	62:14:18.1	3.42 ± 0.07	4.8 ± 0.8	1200 ± 100	3.0 ± 1.6	0.1 ± 0.0	21 ± 3	1.1 ± 0.3
SHARDSJ001120.4	12:36:33.6	62:11:02.2	3.42 ± 0.07	1.6 ± 0.6	10 ± 3	2.5 ± 1.3	–	–	–
SHARDSJ000643.0	12:36:33.7	62:10:53.7	5.05 ± 0.06	6.2 ± 4.1	680 ± 390	3.0 ± 1.6	0.9 ± 1.1	23 ± 7	1.7 ± 1.1
SHARDSJ000632.9	12:36:33.7	62:12:30.9	3.54 ± 0.06	15.0 ± 3.0	60 ± 15	2.7 ± 1.3	–	–	–
SHARDSJ000362.8	12:36:33.8	62:16:30.4	3.60 ± 0.06	220.0 ± 40.0	918 ± 231	3.0 ± 1.6	25.0 ± 5.0	50 ± 0	2.6 ± 0.8
SHARDSJ000752.3	12:36:33.8	62:14:33.8	4.11 ± 0.07	0.1 ± 0.3	14 ± 23	3.2 ± 1.4	–	–	–
SHARDSJ001873.4	12:36:33.9	62:14:04.5	3.69 ± 0.06	0.5 ± 0.2	15 ± 5	3.2 ± 1.5	–	–	–
SHARDSJ001032.4	12:36:34.0	62:11:25.0	5.62 ± 0.07	1.3 ± 0.9	54 ± 41	3.0 ± 1.4	–	–	–
SHARDSJ001162.2	12:36:34.0	62:15:30.2	4.83 ± 0.08	3.0 ± 1.1	40 ± 18	2.7 ± 1.4	–	–	–
SHARDSJ000781.0	12:36:34.2	62:17:08.5	5.22 ± 0.06	1.2 ± 0.6	50 ± 29	2.5 ± 1.3	–	–	–
SHARDSJ001660.6	12:36:34.2	62:12:28.2	3.41 ± 0.07	0.4 ± 0.2	70 ± 41	2.7 ± 1.4	–	–	–
SHARDSJ001172.7	12:36:34.4	62:15:56.4	3.42 ± 0.07	26.1 ± 12.1	493 ± 248	3.0 ± 1.6	2.6 ± 2.8	33 ± 13	1.8 ± 1.4
SHARDSJ001404.5	12:36:34.4	62:05:47.5	5.61 ± 0.07	9.5 ± 5.7	61 ± 51	3.8 ± 1.4	–	–	–
SHARDSJ000515.9	12:36:34.4	62:05:46.5	3.59 ± 0.06	0.6 ± 0.3	13 ± 7	2.2 ± 1.5	–	–	–
SHARDSJ000709.9	12:36:34.4	62:13:15.6	4.10 ± 0.07	0.2 ± 0.1	20 ± 8	2.8 ± 1.4	–	–	–
SHARDSJ000982.2	12:36:34.4	62:13:23.1	3.97 ± 0.06	1.3 ± 0.5	73 ± 35	2.8 ± 1.4	–	–	–
SHARDSJ000801.6	12:36:34.5	62:16:50.0	4.28 ± 0.06	0.5 ± 0.3	50 ± 24	2.5 ± 1.3	–	–	–
SHARDSJ001402.2	12:36:34.5	62:14:18.3	4.38 ± 0.06	38.1 ± 10.8	577 ± 162	3.0 ± 1.6	8.4 ± 4.3	50 ± 1	2.3 ± 1.0
SHARDSJ000490.7	12:36:34.8	62:07:47.3	4.31 ± 0.06	18.0 ± 5.0	618 ± 243	3.0 ± 1.6	1.1 ± 0.8	39 ± 13	2.2 ± 1.5
SHARDSJ000946.7	12:36:34.9	62:12:25.3	4.37 ± 0.06	0.6 ± 0.3	47 ± 21	2.4 ± 1.3	–	–	–
SHARDSJ001593.3	12:36:34.9	62:13:27.4	4.66 ± 0.07	12.3 ± 12.4	350 ± 250	3.0 ± 1.6	1.8 ± 2.6	20 ± 10	2.5 ± 1.5
SHARDSJ001350.2	12:36:35.0	62:13:51.3	5.35 ± 0.07	0.2 ± 0.1	17 ± 3	3.1 ± 1.4	–	–	–
SHARDSJ000820.8	12:36:35.1	62:18:15.3	3.41 ± 0.07	6.1 ± 3.1	450 ± 350	3.0 ± 1.6	2.1 ± 1.3	41 ± 12	2.1 ± 1.4
SHARDSJ000814.7	12:36:35.1	62:16:10.5	3.55 ± 0.06	7.5 ± 1.0	48 ± 6	2.5 ± 0.6	–	–	–
SHARDSJ000544.4	12:36:35.1	62:13:55.8	4.25 ± 0.07	6.3 ± 0.9	32 ± 7	1.5 ± 0.2	–	–	–
SHARDSJ000274.5	12:36:35.1	62:13:29.8	3.69 ± 0.06	1.7 ± 1.3	45 ± 17	2.2 ± 1.1	–	–	–
SHARDSJ000321.1	12:36:35.2	62:07:43.0	4.31 ± 0.06	4.1 ± 1.3	420 ± 42	2.2 ± 1.1	1.2 ± 1.2	20 ± 6	1.4 ± 0.9
SHARDSJ000536.1	12:36:35.3	62:15:04.6	3.97 ± 0.06	6.5 ± 4.3	850 ± 420	3.0 ± 1.6			
SHARDSJ000884.1	12:36:35.4	62:16:45.0	5.39 ± 0.07	0.3 ± 0.1	19 ± 6	2.2 ± 1.2	1.4 ± 1.2	21 ± 2	1.0 ± 0.1
SHARDSJ000868.3	12:36:35.4	62:13:51.0	4.38 ± 0.06	5.2 ± 3.0	969 ± 310	3.0 ± 1.6			

Continued on next page

Table A.2 – *Continued from previous page*

Object Name	R.A. (J2000)	Dec. (J2000)	z	$M_{\rm star,m}$ ($10^9\ M_\odot$)	$\rm Age_m$ (Myr)	$\tau_{\rm m}$ (Myr)	$M_{\rm star,b}$ ($10^9\ M_\odot$)	$\rm Age_b$ (Myr)	$\tau_{\rm b}$ (Myr)
SHARDS20006033	12:36:35.5	62:13:57.9	4.11 ± 0.07	14.0 ± 5.0	1100 ± 400	3.0 ± 1.6	1.8 ± 1.3	23 ± 5	1.1 ± 0.4
SHARDS20005252	12:36:35.5	62:13:50.0	4.51 ± 0.07	5.8 ± 0.5	62 ± 9	2.3 ± 1.1	–	–	–
SHARDS20008556	12:36:35.5	62:13:13.0	4.10 ± 0.07	0.2 ± 0.1	17 ± 5	2.6 ± 1.4	–	–	–
SHARDS20017681	12:36:35.6	62:14:17.0	6.74 ± 0.14	0.5 ± 0.3	18 ± 6	3.0 ± 1.4	–	–	–
SHARDS20007052	12:36:35.7	62:15:26.1	3.55 ± 0.06	0.6 ± 0.2	18 ± 5	3.0 ± 1.4	–	–	–
SHARDS20008325	12:36:35.8	62:14:28.0	4.83 ± 0.08	1.8 ± 0.5	73 ± 21	2.9 ± 1.4	–	–	–
SHARDS20005944	12:36:35.8	62:12:27.0	3.68 ± 0.06	16.0 ± 1.0	1230 ± 20	3.0 ± 1.6	0.4 ± 0.0	24 ± 1	4.9 ± 0.5
SHARDS20009748	12:36:35.9	62:13:54.7	5.35 ± 0.07	2.9 ± 1.1	27 ± 11	2.6 ± 1.4	–	–	–
SHARDS20005134	12:36:36.1	62:11:54.2	3.54 ± 0.06	94.8 ± 10.9	320 ± 30	2.9 ± 1.6	2.6 ± 0.6	50 ± 0	2.6 ± 1.4
SHARDS20005504	12:36:36.1	62:06:02.2	4.16 ± 0.07	2.8 ± 0.6	66 ± 16	2.7 ± 1.3	–	–	–
SHARDS20005728	12:36:36.1	62:08:01.3	3.91 ± 0.06	18.0 ± 7.0	930 ± 430	3.0 ± 1.6	2.8 ± 1.7	49 ± 5	2.3 ± 1.4
SHARDS20017781	12:36:36.2	62:15:50.4	5.11 ± 0.06	1.8 ± 1.0	73 ± 38	2.7 ± 1.4	–	–	–
SHARDS20010038	12:36:36.3	62:12:40.7	4.65 ± 0.07	0.2 ± 0.1	16 ± 5	2.7 ± 1.5	–	–	–
SHARDS20006167	12:36:36.4	62:12:17.0	3.54 ± 0.06	10.7 ± 2.3	120 ± 30	3.0 ± 1.4	–	–	–
SHARDS20005489	12:36:36.4	62:16:20.0	4.02 ± 0.07	24.1 ± 2.1	1200 ± 100	3.0 ± 1.6	0.6 ± 0.1	15 ± 1	5.0 ± 0.2
SHARDS20000244	12:36:36.5	62:07:24.8	4.19 ± 0.07	0.9 ± 0.3	24 ± 8	2.5 ± 1.3	–	–	–
SHARDS20017150	12:36:36.5	62:15:34.7	6.75 ± 0.14	18.0 ± 9.0	432 ± 174	3.0 ± 1.6	0.8 ± 0.9	21 ± 6	3.1 ± 1.4
SHARDS20009692	12:36:36.7	62:05:55.7	3.87 ± 0.06	1.6 ± 0.7	43 ± 21	2.2 ± 1.2	–	–	–
SHARDS20007149	12:36:36.8	62:06:49.4	3.62 ± 0.06	0.4 ± 0.2	12 ± 4	1.8 ± 1.1	–	–	–
SHARDS20009506	12:36:36.8	62:16:47.5	4.28 ± 0.06	63.0 ± 27.0	433 ± 140	3.0 ± 1.6	3.3 ± 2.5	42 ± 11	2.2 ± 1.5
SHARDS20010086	12:36:36.9	62:14:32.4	3.55 ± 0.06	1.1 ± 0.4	70 ± 33	2.8 ± 1.4	–	–	–
SHARDS20009072	12:36:37.0	62:14:58.8	5.09 ± 0.06	0.3 ± 0.1	25 ± 10	2.5 ± 1.4	–	–	–
SHARDS20013821	12:36:37.1	62:14:48.4	4.38 ± 0.06	0.5 ± 0.4	48 ± 28	2.5 ± 1.3	–	–	–
SHARDS20007136	12:36:37.2	62:10:47.5	4.64 ± 0.07	2.3 ± 1.0	65 ± 31	2.7 ± 1.4	–	–	–
SHARDS20012571	12:36:37.2	62:15:57.9	3.36 ± 0.07	1.2 ± 0.7	81 ± 49	2.7 ± 1.4	–	–	–
SHARDS20008722	12:36:37.2	62:07:41.7	4.20 ± 0.07	8.7 ± 3.7	170 ± 80	3.0 ± 1.4	–	–	–
SHARDS20018981	12:36:37.2	62:15:32.4	4.26 ± 0.07	0.4 ± 0.3	60 ± 39	2.6 ± 1.4	–	–	–
SHARDS20013416	12:36:37.2	62:15:54.7	4.67 ± 0.07	0.3 ± 0.2	46 ± 20	2.5 ± 1.3	–	–	–
SHARDS20016999	12:36:37.3	62:17:11.3	6.49 ± 0.11	4.4 ± 2.6	95 ± 58	2.9 ± 1.4	–	–	–
SHARDS20005023	12:36:37.3	62:16:10.5	4.02 ± 0.07	16.7 ± 1.7	106 ± 15	2.9 ± 1.4	–	–	–
SHARDS20010716	12:36:37.3	62:11:51.5	5.62 ± 0.07	26.0 ± 38.0	650 ± 370	3.0 ± 1.6	3.9 ± 7.0	40 ± 13	2.3 ± 1.6
SHARDS20012081	12:36:37.5	62:14:07.0	3.97 ± 0.06	4.4 ± 0.7	1230 ± 120	3.0 ± 1.6	0.1 ± 0.0	19 ± 4	4.1 ± 1.1
SHARDS20009737	12:36:37.5	62:12:36.0	5.21 ± 0.06	1.5 ± 0.9	48 ± 24	2.4 ± 1.3	–	–	–
SHARDS20011958	12:36:37.5	62:11:51.8	5.63 ± 0.07	3.2 ± 1.9	31 ± 16	1.6 ± 0.9	–	–	–
SHARDS20010441	12:36:37.6	62:13:39.2	4.11 ± 0.07	6.5 ± 3.4	560 ± 370	3.0 ± 1.6	0.3 ± 0.3	20 ± 7	2.9 ± 1.6
SHARDS20006108	12:36:37.7	62:06:22.2	4.57 ± 0.07	8.7 ± 6.0	350 ± 300	3.0 ± 1.6	4.3 ± 2.8	46 ± 10	2.2 ± 1.4
SHARDS20011333	12:36:37.8	62:16:25.0	5.69 ± 0.06	6.3 ± 5.0	610 ± 310	3.0 ± 1.6	0.6 ± 0.9	20 ± 5	2.8 ± 1.4
SHARDS20010952	12:36:37.8	62:10:35.4	5.78 ± 0.06	4.7 ± 1.9	70 ± 31	2.7 ± 1.4	–	–	–
SHARDS20011853	12:36:37.8	62:15:33.5	3.55 ± 0.06	1.0 ± 0.4	74 ± 32	2.8 ± 1.4	–	–	–
SHARDS20010554	12:36:38.0	62:14:42.7	3.55 ± 0.06	1.3 ± 0.4	40 ± 10	2.3 ± 1.2	–	–	–
SHARDS20018746	12:36:38.0	62:16:42.3	6.26 ± 0.14	2.1 ± 3.3	372 ± 246	3.0 ± 1.6	0.4 ± 0.6	16 ± 6	3.5 ± 1.6
SHARDS20011004	12:36:38.0	62:12:57.5	3.55 ± 0.06	0.3 ± 0.2	22 ± 16	2.9 ± 1.4	–	–	–
SHARDS20000132	12:36:38.2	62:06:55.7	3.62 ± 0.06	7.9 ± 1.3	44 ± 10	1.8 ± 0.9	–	–	–
SHARDS20016319	12:36:38.2	62:16:01.7	4.41 ± 0.06	77.4 ± 22.6	310 ± 60	3.0 ± 1.4	–	–	–
SHARDS20013533	12:36:38.3	62:07:16.7	3.76 ± 0.06	5.2 ± 1.2	45 ± 13	2.3 ± 1.2	–	–	–
SHARDS20008360	12:36:38.4	62:15:27.2	5.22 ± 0.06	2.3 ± 1.0	45 ± 24	2.3 ± 1.2	–	–	–
SHARDS20015718	12:36:38.5	62:16:34.4	4.03 ± 0.07	17.0 ± 3.0	1200 ± 100	3.0 ± 1.6	0.5 ± 0.1	23 ± 4	3.0 ± 1.6
SHARDS20009925	12:36:38.6	62:11:38.2	3.82 ± 0.06	0.1 ± 0.1	17 ± 7	3.0 ± 1.4	–	–	–

Continued on next page

Table A.2 – *Continued from previous page*

Object Name	R.A. (J2000)	Dec. (J2000)	z	$M_{\rm star,m}$ (10^9 $M_\odot$)	$\rm Age_m$ (Myr)	$\tau_{\rm m}$ (Myr)	$M_{\rm star,b}$ (10^9 $M_\odot$)	$\rm Age_b$ (Myr)	$\tau_{\rm b}$ (Myr)
SHARDS2001961	12:36:38.8	62:15:24.9	4.67 ± 0.07	1.3 ± 1.1	86 ± 59	2.8 ± 1.4	–	–	–
SHARDS2006289	12:36:38.8	62:16:26.4	4.29 ± 0.07	2.8 ± 1.1	39 ± 14	2.0 ± 1.1	–	–	–
SHARDS2008424	12:36:38.9	62:08:31.2	3.78 ± 0.06	1.1 ± 0.5	44 ± 20	2.2 ± 1.2	–	–	–
SHARDS2001674	12:36:38.9	62:15:49.7	6.26 ± 0.14	50.2 ± 23.4	368 ± 211	3.0 ± 1.6	6.8 ± 5.6	48 ± 6	2.2 ± 1.3
SHARDS2001977	12:36:39.2	62:14:16.2	4.67 ± 0.07	21.0 ± 7.0	690 ± 270	3.0 ± 1.6	1.0 ± 0.8	34 ± 13	1.9 ± 1.4
SHARDS2009701	12:36:39.2	62:12:32.9	4.66 ± 0.07	1.0 ± 0.6	39 ± 28	2.7 ± 1.4	–	–	–
SHARDS2006131	12:36:39.2	62:11:02.1	4.24 ± 0.07	1.6 ± 0.5	49 ± 17	2.3 ± 1.2	–	–	–
SHARDS2011505	12:36:39.3	62:14:40.1	4.51 ± 0.07	0.7 ± 0.3	53 ± 21	2.5 ± 1.3	–	–	–
SHARDS2007965	12:36:39.3	62:15:26.4	3.97 ± 0.06	0.4 ± 0.2	17 ± 6	2.8 ± 1.4	–	–	–
SHARDS1010677	12:36:39.3	62:17:51.3	4.43 ± 0.07	0.6 ± 0.5	62 ± 41	2.6 ± 1.4	–	–	–
SHARDS2006502	12:36:39.3	62:09:03.2	4.22 ± 0.07	0.6 ± 0.2	13 ± 5	2.5 ± 1.4	–	–	–
SHARDS2008538	12:36:39.4	62:12:16.2	3.68 ± 0.06	0.7 ± 0.2	24 ± 7	3.3 ± 1.3	–	–	–
SHARDS2025308	12:36:39.4	62:17:30.1	3.62 ± 0.06	1.8 ± 0.2	26 ± 3	1.5 ± 0.6	–	–	–
SHARDS2005445	12:36:39.6	62:12:30.5	3.41 ± 0.07	100.0 ± 10.0	560 ± 50	3.0 ± 1.6	5.5 ± 0.3	49 ± 1	2.2 ± 1.0
SHARDS1001190	12:36:39.6	62:18:00.7	6.64 ± 0.14	2.9 ± 1.7	60 ± 32	2.6 ± 1.4	–	–	–
SHARDS2011322	12:36:39.7	62:14:06.8	5.08 ± 0.06	4.7 ± 3.1	640 ± 290	3.0 ± 1.6	0.5 ± 0.6	18 ± 6	2.1 ± 1.3
SHARDS2006896	12:36:39.7	62:11:47.4	4.10 ± 0.07	9.7 ± 4.7	439 ± 290	3.0 ± 1.6	1.2 ± 1.2	43 ± 11	2.3 ± 1.5
SHARDS2018964	12:36:39.8	62:11:07.8	4.92 ± 0.08	0.2 ± 0.1	15 ± 6	3.0 ± 1.4	–	–	–
SHARDS2014454	12:36:39.9	62:13:55.5	3.55 ± 0.06	0.2 ± 0.1	27 ± 19	2.8 ± 1.4	–	–	–
SHARDS2005752	12:36:40.0	62:11:11.8	4.37 ± 0.06	4.0 ± 1.2	61 ± 23	2.5 ± 1.3	–	–	–
SHARDS2007090	12:36:40.0	62:07:38.8	4.05 ± 0.07	7.3 ± 2.5	120 ± 40	3.0 ± 1.6	–	–	–
SHARDS2013998	12:36:40.1	62:16:04.1	5.94 ± 0.07	20.0 ± 9.0	688 ± 165	3.0 ± 1.6	0.8 ± 0.9	35 ± 13	2.3 ± 1.6
SHARDS2009272	12:36:40.1	62:12:01.2	4.50 ± 0.07	3.6 ± 2.8	560 ± 380	3.0 ± 1.6	0.8 ± 0.9	36 ± 13	2.0 ± 1.5
SHARDS1007510	12:36:40.2	62:18:01.7	4.43 ± 0.07	0.6 ± 0.3	33 ± 15	2.9 ± 1.4	–	–	–
SHARDS2011183	12:36:40.2	62:14:28.8	5.21 ± 0.06	0.4 ± 0.2	14 ± 6	3.1 ± 1.4	–	–	–
SHARDS2012402	12:36:40.2	62:09:42.2	4.51 ± 0.07	0.7 ± 0.4	43 ± 18	2.2 ± 1.2	–	–	–
SHARDS2013477	12:36:40.3	62:09:36.7	5.32 ± 0.07	8.9 ± 6.0	530 ± 300	3.0 ± 1.6	0.8 ± 1.2	20 ± 7	2.7 ± 1.5
SHARDS2012613	12:36:40.3	62:13:54.0	4.51 ± 0.07	12.3 ± 2.0	1200 ± 100	3.0 ± 1.6	0.6 ± 0.3	22 ± 5	1.2 ± 0.7
SHARDS2015077	12:36:40.3	62:13:31.1	3.42 ± 0.07	0.8 ± 0.7	159 ± 132	2.9 ± 1.4	–	–	–
SHARDS2018778	12:36:40.5	62:11:33.0	5.48 ± 0.07	0.3 ± 2.0	20 ± 44	3.1 ± 1.4	–	–	–
SHARDS2007251	12:36:40.5	62:10:43.2	3.53 ± 0.06	4.1 ± 0.8	72 ± 24	2.9 ± 1.4	–	–	–
SHARDS2006327	12:36:40.6	62:06:33.7	3.89 ± 0.06	3.9 ± 1.7	68 ± 48	3.0 ± 1.4	–	–	–
SHARDS2008030	12:36:40.7	62:16:36.1	5.20 ± 0.06	0.9 ± 0.4	16 ± 6	2.9 ± 1.4	–	–	–
SHARDS2015721	12:36:40.7	62:16:37.4	5.92 ± 0.06	0.5 ± 3.6	36 ± 28	2.5 ± 1.4	–	–	–
SHARDS2006417	12:36:40.8	62:16:38.3	4.99 ± 0.06	12.0 ± 3.0	78 ± 28	2.9 ± 1.4	–	–	–
SHARDS2005144	12:36:40.8	62:16:54.8	3.76 ± 0.06	6.6 ± 1.4	62 ± 18	2.6 ± 1.3	–	–	–
SHARDS2009559	12:36:40.8	62:09:17.9	4.76 ± 0.07	2.0 ± 1.4	79 ± 42	2.8 ± 1.4	–	–	–
SHARDS2011570	12:36:40.8	62:13:10.5	4.85 ± 0.08	1.5 ± 1.0	75 ± 43	2.8 ± 1.4	–	–	–
SHARDS2008514	12:36:40.8	62:17:36.4	3.69 ± 0.06	0.7 ± 0.3	39 ± 16	2.1 ± 1.1	–	–	–
SHARDS1006201	12:36:40.8	62:17:28.7	3.37 ± 0.07	4.8 ± 0.9	43 ± 8	2.3 ± 1.1	–	–	–
SHARDS2005343	12:36:40.9	62:06:42.4	4.18 ± 0.07	5.9 ± 0.7	92 ± 15	2.6 ± 1.4	–	–	–
SHARDS2012567	12:36:40.9	62:15:16.9	4.34 ± 0.06	0.4 ± 0.2	51 ± 21	2.5 ± 1.3	–	–	–
SHARDS2009026	12:36:41.0	62:09:25.6	3.39 ± 0.07	7.3 ± 1.8	60 ± 7	2.8 ± 1.3	–	–	–
SHARDS2002929	12:36:41.1	62:17:09.0	3.37 ± 0.07	3.6 ± 0.5	30 ± 5	1.8 ± 0.8	–	–	–
SHARDS2008983	12:36:41.2	62:17:50.0	3.62 ± 0.06	4.2 ± 1.4	95 ± 39	2.9 ± 1.4	–	–	–
SHARDS1012656	12:36:41.3	62:17:40.0	3.62 ± 0.06	103.3 ± 1.8	1250 ± 140	3.0 ± 1.6	0.3 ± 0.1	22 ± 3	4.0 ± 1.4
SHARDS2012839	12:36:41.4	62:09:25.5	5.32 ± 0.07	50.0 ± 12.2	844 ± 176	3.0 ± 1.6	1.8 ± 0.9	42 ± 11	2.4 ± 1.6
SHARDS2006019	12:36:41.4	62:16:41.9	4.18 ± 0.07	4.2 ± 1.3	82 ± 34	2.8 ± 1.4	–	–	–
SHARDS1003055	12:36:41.5	62:18:22.5	3.49 ± 0.06	2.3 ± 2.0	700 ± 459	3.0 ± 1.6	0.4 ± 0.5	16 ± 5	1.9 ± 1.3

Continued on next page

Table A.2 – *Continued from previous page*

Object Name	R.A. (J2000)	Dec. (J2000)	z	$M_{\rm star,m}$ (10^9 $M_\odot$)	Age_m (Myr)	τ_m (Myr)	$M_{\rm star,b}$ (10^9 $M_\odot$)	Age_b (Myr)	τ_b (Myr)
SHARDS10012391	12:36:41.5	62:17:47.2	5.40 ± 0.07	1.7 ± 0.8	48 ± 23	2.3 ± 1.3	–	–	–
SHARDS20008622	12:36:41.5	62:06:54.3	4.19 ± 0.07	9.8 ± 3.2	170 ± 80	3.0 ± 1.4	–	–	–
SHARDS20013003	12:36:41.7	62:11:58.5	4.50 ± 0.07	26.0 ± 8.0	749 ± 240	3.0 ± 1.6	1.3 ± 0.9	29 ± 11	1.5 ± 1.1
SHARDS20017400	12:36:41.7	62:15:45.9	5.50 ± 0.07	0.2 ± 0.1	11 ± 4	3.2 ± 1.4	–	–	–
SHARDS10008308	12:36:41.7	62:17:41.2	3.90 ± 0.06	0.5 ± 0.2	18 ± 7	3.0 ± 1.4	–	–	–
SHARDS10005829	12:36:41.8	62:18:07.4	4.19 ± 0.07	1.1 ± 0.4	29 ± 9	1.6 ± 0.8	–	–	–
SHARDS20015979	12:36:42.0	62:11:24.5	6.25 ± 0.14	18.0 ± 8.0	487 ± 188	3.0 ± 1.6	0.6 ± 0.4	20 ± 4	4.4 ± 1.1
SHARDS20005917	12:36:42.0	62:07:30.6	5.01 ± 0.06	6.5 ± 2.1	88 ± 34	2.9 ± 1.4	–	–	–
SHARDS20016073	12:36:42.0	62:16:56.2	6.16 ± 0.14	7.0 ± 4.6	80 ± 40	2.8 ± 1.4	–	–	–
SHARDS20013075	12:36:42.1	62:07:01.2	3.76 ± 0.06	0.8 ± 0.2	60 ± 20	2.6 ± 1.3	–	–	–
SHARDS20014836	12:36:42.1	62:16:31.0	5.80 ± 0.06	11.0 ± 7.0	475 ± 243	3.0 ± 1.6	1.2 ± 1.6	33 ± 14	1.9 ± 1.4
SHARDS20007667	12:36:42.2	62:11:12.2	5.48 ± 0.07	7.3 ± 1.1	72 ± 53	3.0 ± 1.6	0.6 ± 0.6	20 ± 4	3.4 ± 1.5
SHARDS20004868	12:36:42.2	62:15:23.0	4.28 ± 0.06	33.0 ± 9.0	120 ± 30	3.1 ± 1.4	–	–	–
SHARDS10006528	12:36:42.3	62:17:19.0	3.37 ± 0.07	2.1 ± 0.7	61 ± 29	2.6 ± 1.4	–	–	–
SHARDS20011168	12:36:42.5	62:09:02.6	5.59 ± 0.07	12.0 ± 5.0	150 ± 70	3.0 ± 1.4	–	–	–
SHARDS20010845	12:36:42.5	62:15:16.2	4.02 ± 0.06	1.7 ± 0.8	80 ± 37	2.8 ± 1.4	–	–	–
SHARDS20008900	12:36:42.6	62:11:04.4	5.62 ± 0.07	1.8 ± 0.9	39 ± 18	2.0 ± 1.1	–	–	–
SHARDS20008670	12:36:42.7	62:15:55.3	4.12 ± 0.07	0.9 ± 0.3	20 ± 7	3.3 ± 1.4	–	–	–
SHARDS20015099	12:36:42.7	62:13:25.4	6.50 ± 0.11	4.2 ± 2.7	110 ± 70	2.9 ± 1.4	–	–	–
SHARDS20016040	12:36:42.9	62:07:58.1	5.84 ± 0.06	17.0 ± 6.0	100 ± 40	3.0 ± 1.4	–	–	–
SHARDS20006187	12:36:42.9	62:09:58.5	3.67 ± 0.06	225.0 ± 13.0	560 ± 10	3.0 ± 1.6	5.8 ± 0.3	50 ± 0	1.0 ± 0.2
SHARDS20005617	12:36:43.0	62:09:57.5	3.67 ± 0.06	210.0 ± 30.0	1060 ± 250	3.0 ± 1.6	5.4 ± 0.8	50 ± 0	1.7 ± 1.3
SHARDS20022661	12:36:43.0	62:10:18.3	4.78 ± 0.07	1.3 ± 0.5	45 ± 19	2.2 ± 1.2	–	–	–
SHARDS20016349	12:36:43.0	62:16:33.2	6.75 ± 0.14	18.4 ± 11.5	329 ± 206	3.0 ± 1.6	2.9 ± 3.3	27 ± 13	2.0 ± 1.4
SHARDS20006281	12:36:43.0	62:10:55.2	4.09 ± 0.07	9.9 ± 5.7	830 ± 480	3.0 ± 1.6	0.8 ± 0.8	20 ± 4	2.3 ± 1.2
SHARDS10007206	12:36:43.0	62:17:33.1	5.41 ± 0.07	13.0 ± 5.0	723 ± 245	3.0 ± 1.6	0.7 ± 0.8	15 ± 9	3.1 ± 1.6
SHARDS20007272	12:36:43.0	62:07:10.1	4.19 ± 0.07	2.8 ± 0.7	79 ± 23	2.9 ± 1.4	–	–	–
SHARDS20006911	12:36:43.0	62:07:12.6	4.04 ± 0.07	1.1 ± 0.4	61 ± 19	2.7 ± 1.3	–	–	–
SHARDS20003769	12:36:43.1	62:16:36.0	3.48 ± 0.06	6.3 ± 0.9	46 ± 8	2.0 ± 1.0	–	–	–
SHARDS20007839	12:36:43.1	62:11:05.1	4.50 ± 0.07	1.1 ± 0.4	55 ± 20	2.5 ± 1.3	–	–	–
SHARDS20005338	12:36:43.1	62:10:44.8	3.67 ± 0.06	17.0 ± 3.0	128 ± 21	3.3 ± 1.4	–	–	–
SHARDS10005604	12:36:43.2	62:17:29.1	3.90 ± 0.06	2.0 ± 0.4	25 ± 4	3.6 ± 0.8	–	–	–
SHARDS20007846	12:36:43.3	62:14:11.5	3.83 ± 0.06	6.1 ± 2.5	1100 ± 400	3.0 ± 1.6	0.2 ± 0.2	17 ± 4	3.1 ± 1.3
SHARDS20025361	12:36:43.4	62:16:56.1	5.40 ± 0.07	2.2 ± 1.4	42 ± 26	2.8 ± 1.4	–	–	–
SHARDS10005410	12:36:43.4	62:18:15.9	4.44 ± 0.07	8.6 ± 4.6	790 ± 290	3.0 ± 1.6	0.9 ± 1.1	15 ± 2	1.1 ± 0.3
SHARDS10016909	12:36:43.5	62:18:16.5	4.44 ± 0.07	0.1 ± 0.0	15 ± 5	2.7 ± 1.4	–	–	–
SHARDS20004706	12:36:43.5	62:11:21.4	3.54 ± 0.06	24.7 ± 1.6	78 ± 9	2.5 ± 1.3	–	–	–
SHARDS20017692	12:36:43.6	62:13:53.7	3.97 ± 0.06	0.4 ± 0.2	44 ± 18	2.4 ± 1.3	–	–	–
SHARDS20004872	12:36:43.8	62:12:41.5	4.51 ± 0.07	13.0 ± 8.0	470 ± 260	3.0 ± 1.6	4.5 ± 2.7	25 ± 1	1.0 ± 0.1
SHARDS10011362	12:36:43.9	62:18:31.7	4.59 ± 0.07	0.6 ± 0.4	26 ± 17	2.6 ± 1.4	–	–	–
SHARDS20008756	12:36:44.0	62:15:07.3	3.75 ± 0.06	2.0 ± 0.7	83 ± 39	2.8 ± 1.4	–	–	–
SHARDS20013486	12:36:44.0	62:13:14.2	5.64 ± 0.07	0.9 ± 0.6	50 ± 27	2.5 ± 1.3	–	–	–
SHARDS10008371	12:36:44.2	62:17:09.3	4.19 ± 0.07	1.6 ± 1.6	600 ± 380	3.0 ± 1.6	0.3 ± 0.4	16 ± 5	2.7 ± 1.6
SHARDS20011466	12:36:44.2	62:07:00.4	4.19 ± 0.07	9.5 ± 1.6	915 ± 166	3.0 ± 1.6	0.3 ± 0.1	21 ± 4	1.0 ± 0.3
SHARDS10003454	12:36:44.2	62:17:41.4	3.38 ± 0.07	6.4 ± 5.6	520 ± 380	3.0 ± 1.6	5.2 ± 1.7	44 ± 10	1.9 ± 1.0
SHARDS20006730	12:36:44.3	62:11:17.6	3.96 ± 0.06	3.8 ± 0.8	36 ± 9	1.7 ± 0.8	–	–	–
SHARDS20014151	12:36:44.3	62:11:44.8	5.35 ± 0.07	24.4 ± 16.3	319 ± 212	3.0 ± 1.6	1.0 ± 1.3	29 ± 13	3.1 ± 1.6
SHARDS20012331	12:36:44.3	62:16:23.9	4.43 ± 0.07	70.1 ± 12.4	537 ± 231	3.0 ± 1.6	2.1 ± 0.8	36 ± 12	2.7 ± 1.6
SHARDS20005215	12:36:44.4	62:10:03.7	3.81 ± 0.06	36.0 ± 9.0	250 ± 136	3.0 ± 1.6	5.8 ± 3.5	32 ± 11	1.3 ± 0.7

Continued on next page

Table A.2 – *Continued from previous page*

Object Name	R.A. (J2000)	Dec. (J2000)	z	$M_{\rm star,m}$ ($10^9\ M_\odot$)	$\rm Age_m$ (Myr)	$\tau_{\rm m}$ (Myr)	$M_{\rm star,b}$ ($10^9\ M_\odot$)	$\rm Age_b$ (Myr)	$\tau_{\rm b}$ (Myr)
SHARDS20000232	12:36:44.4	62:07:22.7	4.20 ± 0.07	21.0 ± 4.0	110 ± 30	3.0 ± 1.4	—	—	—
SHARDS20018507	12:36:44.4	62:09:20.2	5.18 ± 0.06	0.5 ± 0.6	25 ± 18	2.6 ± 1.4	—	—	—
SHARDS20010705	12:36:44.5	62:15:17.4	4.29 ± 0.06	0.3 ± 0.1	38 ± 11	2.1 ± 1.1	—	—	—
SHARDS20013762	12:36:44.5	62:14:19.5	3.42 ± 0.07	0.3 ± 0.2	61 ± 35	2.7 ± 1.4	—	—	—
SHARDS20008158	12:36:44.5	62:07:04.4	4.19 ± 0.07	13.0 ± 3.0	1200 ± 0	3.0 ± 1.6	0.4 ± 0.1	21 ± 3	1.0 ± 0.3
SHARDS20014762	12:36:44.5	62:12:36.1	5.36 ± 0.07	0.4 ± 0.2	40 ± 16	2.3 ± 1.2	—	—	—
SHARDS20011324	12:36:44.6	62:10:40.0	3.54 ± 0.06	0.5 ± 0.3	21 ± 15	3.0 ± 1.4	—	—	—
SHARDS20005176	12:36:44.7	62:11:50.5	4.66 ± 0.07	39.0 ± 7.0	120 ± 30	3.0 ± 1.4	—	—	—
SHARDS20008534	12:36:44.7	62:13:52.5	3.42 ± 0.07	0.6 ± 0.2	30 ± 10	1.8 ± 1.0	—	—	—
SHARDS20018297	12:36:44.7	62:12:05.9	5.91 ± 0.06	0.4 ± 0.4	23 ± 15	2.9 ± 1.4	—	—	—
SHARDS20008064	12:36:44.8	62:12:05.7	3.77 ± 0.06	2.0 ± 0.7	76 ± 39	2.8 ± 1.4	—	—	—
SHARDS20006062	12:36:45.0	62:07:42.9	3.78 ± 0.06	5.3 ± 0.9	120 ± 80	3.0 ± 1.6	0.2 ± 0.2	24 ± 9	3.2 ± 1.6
SHARDS20011766	12:36:45.0	62:14:20.8	4.62 ± 0.07	5.8 ± 4.0	120 ± 80	2.9 ± 1.4	—	—	—
SHARDS20006942	12:36:45.1	62:11:06.8	4.10 ± 0.07	54.8 ± 13.3	450 ± 270	3.0 ± 1.6	1.5 ± 0.5	30 ± 10	4.3 ± 1.2
SHARDS20010821	12:36:45.1	62:14:16.3	4.39 ± 0.06	0.8 ± 0.4	56 ± 30	2.6 ± 1.3	—	—	—
SHARDS20009323	12:36:45.2	62:14:14.6	3.82 ± 0.06	1.3 ± 0.5	61 ± 28	2.6 ± 1.4	—	—	—
SHARDS20009185	12:36:45.2	62:09:32.2	3.94 ± 0.06	1.0 ± 0.5	68 ± 36	2.7 ± 1.4	—	—	—
SHARDS20005675	12:36:45.2	62:09:33.7	4.35 ± 0.06	21.0 ± 4.0	1000 ± 300	3.0 ± 1.6	0.8 ± 0.3	20 ± 6	3.8 ± 1.6
SHARDS20008968	12:36:45.2	62:09:38.0	3.25 ± 0.07	0.2 ± 0.1	14 ± 5	3.0 ± 1.5	—	—	—
SHARDS20005675	12:36:45.2	62:09:34.1	4.35 ± 0.06	3.0 ± 1.2	49 ± 16	2.4 ± 1.2	—	—	—
SHARDS20006879	12:36:45.2	62:11:07.4	3.22 ± 0.07	28.0 ± 4.0	370 ± 60	3.0 ± 1.6	1.3 ± 0.4	44 ± 10	2.8 ± 1.6
SHARDS20022705	12:36:45.3	62:16:11.7	5.54 ± 0.07	3.3 ± 3.5	480 ± 340	3.0 ± 1.6	0.9 ± 1.0	33 ± 14	1.7 ± 1.3
SHARDS20012658	12:36:45.4	62:18:02.4	5.42 ± 0.07	0.8 ± 0.6	35 ± 26	2.7 ± 1.4	—	—	—
SHARDS20010734	12:36:45.7	62:14:11.8	3.97 ± 0.06	0.3 ± 0.1	17 ± 6	3.0 ± 1.5	—	—	—
SHARDS20009632	12:36:45.7	62:11:33.7	3.77 ± 0.06	11.7 ± 1.9	1230 ± 120	3.0 ± 1.6	0.3 ± 0.1	20 ± 4	4.0 ± 1.3
SHARDS20004663	12:36:45.8	62:14:21.9	3.42 ± 0.07	12.2 ± 11.9	660 ± 380	3.0 ± 1.6	9.9 ± 3.7	50 ± 0	2.0 ± 1.0
SHARDS20012625	12:36:45.8	62:11:58.3	5.63 ± 0.07	5.9 ± 4.7	530 ± 310	3.0 ± 1.6	0.7 ± 1.0	18 ± 6	2.8 ± 1.5
SHARDS20009303	12:36:45.9	62:11:11.1	4.65 ± 0.07	4.0 ± 1.3	46 ± 16	2.4 ± 1.2	—	—	—
SHARDS20009104	12:36:46.0	62:15:36.9	4.27 ± 0.07	3.1 ± 1.2	110 ± 60	2.9 ± 1.4	5.4 ± 0.4	50 ± 0	2.1 ± 1.0
SHARDS20007885	12:36:46.1	62:13:48.9	3.75 ± 0.06	212.0 ± 15.0	570 ± 60	3.0 ± 1.6	—	—	—
SHARDS20015308	12:36:46.1	62:14:17.0	5.22 ± 0.06	1.3 ± 1.2	65 ± 47	2.6 ± 1.4	—	—	—
SHARDS20004843	12:36:46.2	62:07:01.5	4.44 ± 0.07	13.0 ± 4.0	95 ± 32	2.9 ± 1.4	—	—	—
SHARDS20017518	12:36:46.2	62:16:40.9	3.22 ± 0.07	0.1 ± 0.0	16 ± 6	2.9 ± 1.4	—	—	—
SHARDS20009131	12:36:46.2	62:11:28.5	3.91 ± 0.06	0.4 ± 0.2	51 ± 26	2.5 ± 1.3	—	—	—
SHARDS20008584	12:36:46.3	62:11:34.5	3.41 ± 0.07	14.0 ± 4.0	1300 ± 300	3.0 ± 1.6	0.5 ± 0.5	25 ± 7	1.1 ± 0.6
SHARDS20005302	12:36:46.3	62:16:12.6	3.62 ± 0.06	9.0 ± 1.6	75 ± 17	2.8 ± 1.4	—	—	—
SHARDS20009371	12:36:46.4	62:15:10.2	4.29 ± 0.06	1.0 ± 0.4	58 ± 24	2.6 ± 1.3	—	—	—
SHARDS20005562	12:36:46.4	62:15:13.4	4.03 ± 0.07	1.0 ± 0.4	17 ± 6	2.8 ± 1.5	—	—	—
SHARDS20017780	12:36:46.4	62:18:11.7	4.88 ± 0.08	0.1 ± 0.0	13 ± 5	3.1 ± 1.4	—	—	—
SHARDS20015666	12:36:46.4	62:13:48.0	3.42 ± 0.07	0.4 ± 0.2	71 ± 42	2.7 ± 1.4	—	—	—
SHARDS20012701	12:36:46.5	62:11:58.4	4.20 ± 0.07	0.9 ± 0.0	11 ± 4	3.0 ± 1.4	—	—	—
SHARDS20009665	12:36:46.7	62:12:30.1	3.83 ± 0.06	0.2 ± 0.1	13 ± 5	2.8 ± 1.4	—	—	—
SHARDS20004982	12:36:46.7	62:12:57.1	3.36 ± 0.07	1.1 ± 0.2	13 ± 3	1.6 ± 1.0	—	—	—
SHARDS20007144	12:36:46.7	62:06:28.3	4.33 ± 0.06	13.0 ± 5.0	913 ± 224	3.0 ± 1.6	0.8 ± 1.0	27 ± 10	1.3 ± 0.9
SHARDS20002930	12:36:46.8	62:07:07.8	3.22 ± 0.07	10.9 ± 2.3	53 ± 13	2.5 ± 1.2	—	—	—
SHARDS20008739	12:36:46.8	62:07:02.5	3.90 ± 0.06	1.4 ± 0.8	41 ± 21	2.2 ± 1.2	—	—	—
SHARDS20005085	12:36:46.9	62:15:39.2	3.41 ± 0.07	24.0 ± 4.0	170 ± 40	3.0 ± 1.4	0.6 ± 0.1	50 ± 1	2.8 ± 1.6
SHARDS20018693	12:36:46.9	62:15:27.6	4.27 ± 0.07	24.0 ± 4.0	1200 ± 100	2.9 ± 1.6	—	—	—
SHARDS20006064	12:36:46.9	62:07:06.7	4.31 ± 0.06	14.0 ± 3.0	150 ± 50	2.9 ± 1.4	—	—	—

Continued on next page

Table A.2 – *Continued from previous page*

Object Name	R.A. (J2000)	Dec. (J2000)	z	$M_{\rm star,m}$ (10^9 $M_\odot$)	$\rm Age_m$ (Myr)	$\tau_{\rm m}$ (Myr)	$M_{\rm star,b}$ (10^9 $M_\odot$)	$\rm Age_b$ (Myr)	$\tau_{\rm b}$ (Myr)
SHARDS20011356	12:36:47.0	62:11:18.1	4.10 ± 0.07	0.5 ± 0.2	53 ± 19	2.6 ± 1.3	–	–	–
SHARDS20000360	12:36:47.0	62:07:50.0	3.23 ± 0.07	3.1 ± 0.5	86 ± 15	2.9 ± 1.4	–	–	–
SHARDS20006145	12:36:47.0	62:07:16.8	4.44 ± 0.07	27.0 ± 3.0	132 ± 22	2.9 ± 1.4	–	–	–
SHARDS10005856	12:36:47.0	62:18:43.7	3.38 ± 0.07	13.0 ± 3.0	130 ± 40	2.9 ± 1.4	–	–	–
SHARDS20007155	12:36:47.1	62:13:08.2	3.97 ± 0.06	13.0 ± 3.0	1200 ± 300	3.0 ± 1.6	0.6 ± 0.3	23 ± 3	1.0 ± 0.1
SHARDS20016717	12:36:47.1	62:07:53.1	5.29 ± 0.07	0.4 ± 0.2	18 ± 6	2.7 ± 1.4	–	–	–
SHARDS10007641	12:36:47.3	62:17:04.2	5.41 ± 0.07	1.3 ± 0.7	27 ± 12	2.5 ± 1.4	–	–	–
SHARDS10010013	12:36:47.3	62:16:07.4	4.58 ± 0.07	1.2 ± 0.6	71 ± 38	2.8 ± 1.4	–	–	–
SHARDS20010619	12:36:47.4	62:15:13.6	3.61 ± 0.06	1.8 ± 0.7	120 ± 60	2.9 ± 1.4	–	–	–
SHARDS20010488	12:36:47.4	62:10:38.1	4.09 ± 0.07	9.3 ± 1.3	1200 ± 120	3.0 ± 1.6	0.2 ± 0.0	18 ± 2	4.9 ± 0.4
SHARDS20016530	12:36:47.4	62:13:37.2	5.23 ± 0.06	5.0 ± 1.9	130 ± 60	3.0 ± 1.4	–	–	–
SHARDS10006982	12:36:47.4	62:18:57.9	3.64 ± 0.06	1.9 ± 0.6	63 ± 28	2.6 ± 1.4	–	–	–
SHARDS20009830	12:36:47.5	62:11:00.3	3.54 ± 0.06	7.8 ± 3.1	730 ± 360	3.0 ± 1.6	0.5 ± 0.5	41 ± 12	2.3 ± 1.6
SHARDS20015743	12:36:47.5	62:11:59.9	5.91 ± 0.07	0.4 ± 0.3	26 ± 16	2.6 ± 1.4	–	–	–
SHARDS20006335	12:36:47.6	62:10:23.8	3.40 ± 0.07	11.0 ± 3.0	110 ± 30	3.2 ± 1.4	–	–	–
SHARDS20018017	12:36:47.6	62:15:08.0	4.52 ± 0.07	0.6 ± 0.4	46 ± 20	2.4 ± 1.3	–	–	–
SHARDS10012882	12:36:47.7	62:17:16.9	4.31 ± 0.06	16.0 ± 3.0	1050 ± 210	3.0 ± 1.6	0.7 ± 0.4	31 ± 12	1.7 ± 1.4
SHARDS20008709	12:36:47.7	62:15:09.2	4.57 ± 0.07	8.5 ± 1.0	91 ± 18	2.8 ± 1.4	–	–	–
SHARDS20005017	12:36:47.7	62:11:35.1	3.54 ± 0.06	12.0 ± 5.0	340 ± 290	3.0 ± 1.6	3.8 ± 2.0	41 ± 12	2.0 ± 1.2
SHARDS20007137	12:36:47.9	62:09:25.6	4.08 ± 0.07	2.8 ± 0.9	98 ± 45	2.9 ± 1.4	–	–	–
SHARDS20004537	12:36:48.0	62:09:41.4	5.19 ± 0.06	92.4 ± 24.1	919 ± 143	3.0 ± 1.6	5.2 ± 2.0	23 ± 3	2.6 ± 0.8
SHARDS20011472	12:36:48.0	62:12:00.7	4.93 ± 0.08	0.4 ± 0.2	16 ± 7	3.0 ± 1.4	–	–	–
SHARDS20009288	12:36:48.1	62:13:45.8	4.52 ± 0.07	26.0 ± 5.0	778 ± 212	3.0 ± 1.6	1.9 ± 1.6	29 ± 10	1.3 ± 0.8
SHARDS10010985	12:36:48.1	62:19:02.5	3.64 ± 0.06	0.1 ± 0.1	12 ± 4	3.1 ± 1.4	–	–	–
SHARDS20008788	12:36:48.1	62:15:34.0	5.54 ± 0.07	32.0 ± 4.0	936 ± 111	3.0 ± 1.6	0.8 ± 0.1	19 ± 1	4.8 ± 0.5
SHARDS20007738	12:36:48.2	62:14:43.6	3.56 ± 0.06	44.0 ± 8.0	567 ± 223	3.0 ± 1.6	2.0 ± 0.6	45 ± 10	2.7 ± 1.6
SHARDS10012429	12:36:48.2	62:16:37.4	3.38 ± 0.07	0.3 ± 0.2	61 ± 36	2.6 ± 1.4	–	–	–
SHARDS10013979	12:36:48.2	62:16:30.7	3.63 ± 0.06	4.3 ± 2.4	147 ± 109	2.9 ± 1.4	–	–	–
SHARDS20015260	12:36:48.3	62:09:39.4	4.63 ± 0.07	1.0 ± 0.5	50 ± 20	2.4 ± 1.3	–	–	–
SHARDS20009821	12:36:48.3	62:13:20.4	3.56 ± 0.06	1.0 ± 0.5	50 ± 36	3.1 ± 1.4	–	–	–
SHARDS20018558	12:36:48.3	62:15:03.7	5.93 ± 0.06	0.2 ± 0.5	21 ± 30	3.0 ± 1.4	–	–	–
SHARDS20008926	12:36:48.4	62:15:31.1	3.76 ± 0.06	0.6 ± 0.2	39 ± 15	2.2 ± 1.2	–	–	–
SHARDS20009870	12:36:48.4	62:12:17.3	5.36 ± 0.07	52.0 ± 45.0	434 ± 245	3.0 ± 1.6	7.0 ± 9.8	34 ± 12	1.7 ± 1.2
SHARDS20017589	12:36:48.4	62:09:45.5	3.53 ± 0.06	0.5 ± 0.2	47 ± 24	2.4 ± 1.3	–	–	–
SHARDS10005025	12:36:48.4	62:16:43.0	4.19 ± 0.07	11.4 ± 1.8	55 ± 7	2.4 ± 1.2	–	–	–
SHARDS10007239	12:36:48.5	62:19:05.7	4.61 ± 0.07	30.0 ± 6.0	900 ± 280	3.0 ± 1.6	0.8 ± 0.2	29 ± 11	3.4 ± 1.5
SHARDS10010315	12:36:48.5	62:18:13.6	3.50 ± 0.06	0.1 ± 0.1	17 ± 7	3.1 ± 1.4	–	–	–
SHARDS20012717	12:36:48.6	62:11:20.0	4.66 ± 0.07	0.2 ± 0.1	16 ± 4	2.1 ± 1.3	–	–	–
SHARDS10016735	12:36:48.6	62:16:31.8	6.65 ± 0.14	18.0 ± 13.1	470 ± 236	3.0 ± 1.6	1.3 ± 1.8	41 ± 12	2.5 ± 1.6
SHARDS20013849	12:36:48.7	62:15:16.7	4.04 ± 0.07	0.4 ± 0.2	52 ± 23	2.5 ± 1.3	–	–	–
SHARDS20007005	12:36:48.7	62:08:10.3	4.88 ± 0.08	15.2 ± 1.9	130 ± 40	2.8 ± 1.4	–	–	–
SHARDS20019079	12:36:48.8	62:11:25.3	4.25 ± 0.07	0.7 ± 0.5	64 ± 43	2.6 ± 1.4	–	–	–
SHARDS20014914	12:36:48.8	62:07:20.6	5.15 ± 0.06	46.5 ± 13.8	727 ± 208	3.0 ± 1.6	1.3 ± 0.7	25 ± 8	2.8 ± 1.4
SHARDS20016700	12:36:48.8	62:07:40.7	6.19 ± 0.14	19.0 ± 7.0	120 ± 50	3.0 ± 1.4	–	–	–
SHARDS20009301	12:36:48.9	62:12:44.4	4.67 ± 0.07	0.6 ± 0.2	45 ± 13	2.3 ± 1.2	–	–	–
SHARDS20011033	12:36:48.9	62:11:25.8	4.66 ± 0.07	1.4 ± 0.7	60 ± 30	2.6 ± 1.3	–	–	–
SHARDS10003033	12:36:48.9	62:18:25.5	3.38 ± 0.07	2.4 ± 0.5	62 ± 16	2.6 ± 1.3	–	–	–
SHARDS20006572	12:36:48.9	62:09:08.9	3.66 ± 0.06	0.5 ± 0.2	16 ± 6	2.9 ± 1.5	–	–	–
SHARDS10008432	12:36:48.9	62:18:53.8	4.89 ± 0.08	2.4 ± 2.2	800 ± 370	3.0 ± 1.6	0.4 ± 0.6	17 ± 4	4.0 ± 1.3

Continued on next page

Table A.2 – *Continued from previous page*

Object Name	R.A. (J2000)	Dec. (J2000)	z	$M_{\rm star,m}$ (10^9 $M_\odot$)	$\rm Age_m$ (Myr)	$\tau_{\rm m}$ (Myr)	$M_{\rm star,b}$ (10^9 $M_\odot$)	$\rm Age_b$ (Myr)	$\tau_{\rm b}$ (Myr)
SHARDS20006140	12:36:49.0	62:11:52.9	4.66 ± 0.07	7.2 ± 2.6	594 ± 236	3.0 ± 1.6	1.1 ± 1.0	24 ± 6	1.1 ± 0.5
SHARDS20011008	12:36:49.0	62:15:22.3	4.52 ± 0.07	0.5 ± 0.2	45 ± 14	2.3 ± 1.2	—	—	—
SHARDS20007006	12:36:49.1	62:13:30.6	4.39 ± 0.06	14.0 ± 3.0	180 ± 60	3.0 ± 1.4	—	—	—
SHARDS20011601	12:36:49.1	62:10:22.1	3.81 ± 0.06	0.7 ± 0.8	50 ± 60	2.9 ± 1.4	—	—	—
SHARDS20025409	12:36:49.1	62:15:52.0	3.90 ± 0.06	0.5 ± 0.4	57 ± 37	2.6 ± 1.6	0.6 ± 0.8	28 ± 12	1.4 ± 1.1
SHARDS20010215	12:36:49.2	62:09:47.2	3.94 ± 0.06	2.6 ± 3.2	680 ± 450	3.0 ± 1.6	0.6 ± 0.8	28 ± 12	1.4 ± 1.1
SHARDS20005370	12:36:49.2	62:15:38.6	5.14 ± 0.06	6.0 ± 1.1	64 ± 14	2.6 ± 1.3	3.5 ± 0.2	50 ± 0	2.0 ± 1.3
SHARDS20010078	12:36:49.3	62:07:34.7	5.02 ± 0.06	140.0 ± 10.0	960 ± 90	3.0 ± 1.6			
SHARDS20005850	12:36:49.5	62:14:21.2	3.36 ± 0.07	0.4 ± 0.2	13 ± 5	2.6 ± 1.4			
SHARDS20011401	12:36:49.6	62:08:55.8	3.52 ± 0.06	1.3 ± 0.5	51 ± 26	2.5 ± 1.3			
SHARDS20006578	12:36:49.6	62:07:57.8	4.88 ± 0.08	9.4 ± 0.8	89 ± 13	2.8 ± 1.4			
SHARDS20006571	12:36:49.6	62:15:24.4	4.18 ± 0.07	2.2 ± 0.8	52 ± 19	2.5 ± 1.3			
SHARDS20013746	12:36:49.6	62:10:39.0	5.79 ± 0.06	28.9 ± 10.3	385 ± 77	3.0 ± 1.6	1.2 ± 0.8	20 ± 8	2.3 ± 1.2
SHARDS10009609	12:36:49.7	62:18:13.3	3.23 ± 0.07	0.3 ± 0.1	18 ± 7	3.1 ± 1.5	—	—	—
SHARDS20002756	12:36:49.7	62:13:28.7	3.42 ± 0.07	4.8 ± 0.7	74 ± 22	2.8 ± 1.4			
SHARDS20013107	12:36:49.8	62:10:45.0	5.21 ± 0.06	25.0 ± 4.0	901 ± 147	3.0 ± 1.6	0.7 ± 0.2	19 ± 4	4.2 ± 1.0
SHARDS10008730	12:36:49.8	62:15:52.0	4.30 ± 0.06	6.4 ± 2.1	183 ± 101	3.0 ± 1.4	—	—	—
SHARDS20011530	12:36:49.9	62:12:47.7	5.36 ± 0.07	41.5 ± 16.1	200 ± 60	3.0 ± 1.4			
SHARDS10008771	12:36:49.9	62:12:24.1	3.64 ± 0.06	2.4 ± 1.0	60 ± 33	2.6 ± 1.4			
SHARDS20008753	12:36:49.9	62:08:05.0	3.65 ± 0.06	3.1 ± 1.2	92 ± 36	2.9 ± 1.4			
SHARDS20011732	12:36:49.9	62:09:30.1	5.46 ± 0.07	5.7 ± 2.3	88 ± 42	2.9 ± 1.6	0.5 ± 0.6	19 ± 6	2.5 ± 1.4
SHARDS20014293	12:36:50.0	62:13:55.7	5.81 ± 0.06	2.4 ± 2.5	409 ± 270	3.0 ± 1.6			
SHARDS20008210	12:36:50.0	62:09:33.6	5.33 ± 0.07	1.4 ± 0.7	20 ± 9	2.7 ± 1.4	3.9 ± 1.2	46 ± 9	2.5 ± 1.5
SHARDS20008207	12:36:50.0	62:07:34.4	5.16 ± 0.06	150.0 ± 30.0	891 ± 133	3.0 ± 1.6			
SHARDS10012647	12:36:50.1	62:18:00.5	3.50 ± 0.06	0.7 ± 0.4	64 ± 38	2.7 ± 1.4	—	—	—
SHARDS20010714	12:36:50.1	62:14:33.8	3.61 ± 0.06	0.8 ± 0.4	33 ± 18	3.2 ± 1.4			
SHARDS10006314	12:36:50.2	62:16:25.2	3.38 ± 0.07	1.1 ± 0.3	56 ± 20	2.5 ± 1.3			
SHARDS20006375	12:36:50.2	62:11:19.1	3.96 ± 0.06	2.0 ± 0.4	70 ± 16	2.8 ± 1.4			
SHARDS10008675	12:36:50.3	62:16:23.2	4.05 ± 0.07	0.1 ± 0.1	17 ± 6	2.7 ± 1.4			
SHARDS20009900	12:36:50.3	62:12:26.1	5.49 ± 0.07	1.1 ± 0.4	48 ± 14	2.4 ± 1.2	—	—	—
SHARDS10007578	12:36:50.4	62:18:57.9	4.21 ± 0.07	1.9 ± 0.8	67 ± 41	3.0 ± 1.4			
SHARDS20011658	12:36:50.5	62:12:50.4	4.38 ± 0.06	2.8 ± 1.2	640 ± 330	3.0 ± 1.6	0.1 ± 0.1	18 ± 5	4.1 ± 1.3
SHARDS10017724	12:36:50.5	62:18:16.9	3.64 ± 0.06	0.2 ± 0.1	45 ± 16	2.4 ± 1.3	—	—	—
SHARDS20012497	12:36:50.6	62:09:32.4	4.92 ± 0.08	35.2 ± 11.0	500 ± 290	3.0 ± 1.4			
SHARDS20005660	12:36:50.7	62:09:32.5	4.24 ± 0.07	1.5 ± 0.5	46 ± 17	2.2 ± 1.2			
SHARDS20010568	12:36:50.8	62:11:08.3	4.37 ± 0.06	1.9 ± 0.8	56 ± 35	2.9 ± 1.4	—	—	—
SHARDS20017030	12:36:50.9	62:11:26.6	3.82 ± 0.06	0.3 ± 0.2	51 ± 26	2.5 ± 1.3			
SHARDS20007436	12:36:50.9	62:09:04.7	3.80 ± 0.06	11.0 ± 3.0	265 ± 206	3.0 ± 1.6	2.1 ± 1.4	41 ± 12	2.3 ± 1.6
SHARDS20007244	12:36:50.9	62:08:49.5	3.52 ± 0.06	1.2 ± 0.6	51 ± 23	2.4 ± 1.3	—	—	—
SHARDS10012082	12:36:50.9	62:19:15.3	4.61 ± 0.07	4.4 ± 2.2	24 ± 10	2.7 ± 1.4			
SHARDS20007645	12:36:51.0	62:13:38.8	3.98 ± 0.06	12.0 ± 5.0	1000 ± 400	3.0 ± 1.6	0.6 ± 0.4	19 ± 5	2.2 ± 1.1
SHARDS20011342	12:36:51.1	62:09:43.1	3.79 ± 0.06	0.2 ± 0.1	20 ± 4	2.7 ± 1.4			
SHARDS20009490	12:36:51.1	62:09:35.6	4.24 ± 0.07	7.4 ± 4.8	610 ± 360	3.0 ± 1.6	1.3 ± 1.4	40 ± 12	2.0 ± 1.4
SHARDS10011621	12:36:51.1	62:08:48.0	3.79 ± 0.06	0.4 ± 0.2	56 ± 29	2.6 ± 1.4	—	—	—
SHARDS20011536	12:36:51.2	62:09:20.9	4.77 ± 0.07	0.3 ± 0.3	21 ± 10	2.9 ± 1.4			
SHARDS20012099	12:36:51.2	62:15:24.1	3.62 ± 0.06	2.6 ± 2.7	1210 ± 210	3.0 ± 1.6	0.1 ± 0.0	19 ± 4	4.1 ± 1.3
SHARDS20009241	12:36:51.2	62:13:49.0	4.71 ± 0.07	51.8 ± 24.7	303 ± 242	3.0 ± 1.6	1.5 ± 1.0	29 ± 11	4.1 ± 1.3
SHARDS20007340	12:36:51.2	62:14:53.2	4.52 ± 0.07	5.8 ± 1.5	42 ± 14	2.2 ± 1.1	—	—	—
SHARDS10003147	12:36:51.3	62:18:14.8	3.51 ± 0.06	7.8 ± 1.4	42 ± 6	1.8 ± 0.9	—	—	—

Continued on next page

Table A.2 – *Continued from previous page*

Object Name	R.A. (J2000)	Dec. (J2000)	z	$M_{\rm star,m}$ (10^9 $M_\odot$)	$\rm Age_m$ (Myr)	$\tau_{\rm m}$ (Myr)	$M_{\rm star,b}$ (10^9 $M_\odot$)	$\rm Age_b$ (Myr)	$\tau_{\rm b}$ (Myr)
SHARDS20005336	12:36:51.3	62:14:59.5	4.58 ± 0.07	2.9 ± 0.2	26 ± 1	1.6 ± 0.6	–	–	–
SHARDS20007294	12:36:51.4	62:08:56.6	5.45 ± 0.07	2.2 ± 0.8	24 ± 7	3.5 ± 1.4	–	–	–
SHARDS10010803	12:36:51.4	62:19:04.8	4.33 ± 0.06	5.1 ± 3.9	409 ± 320	3.0 ± 1.6	0.6 ± 0.8	24 ± 12	2.4 ± 1.5
SHARDS20006072	12:36:51.5	62:11:49.0	3.96 ± 0.06	3.7 ± 0.6	39 ± 8	2.0 ± 1.0	–	–	–
SHARDS10005640	12:36:51.6	62:16:37.2	3.91 ± 0.06	6.7 ± 3.0	156 ± 126	3.0 ± 1.6	0.5 ± 0.6	22 ± 9	2.8 ± 1.5
SHARDS10012394	12:36:51.7	62:19:11.3	3.79 ± 0.06	0.4 ± 0.2	49 ± 24	2.5 ± 1.3	–	–	–
SHARDS20008477	12:36:51.7	62:12:15.1	3.97 ± 0.06	1.2 ± 0.4	51 ± 23	2.4 ± 1.3	–	–	–
SHARDS10013447	12:36:51.7	62:19:08.0	4.61 ± 0.07	4.3 ± 3.3	390 ± 330	3.0 ± 1.6	0.5 ± 0.7	28 ± 13	2.7 ± 1.5
SHARDS20010543	12:36:51.7	62:13:26.3	3.98 ± 0.06	2.3 ± 0.9	1100 ± 300	3.0 ± 1.6	0.1 ± 0.0	11 ± 3	4.5 ± 1.0
SHARDS20009191	12:36:51.8	62:11:11.3	5.63 ± 0.07	1.9 ± 1.0	25 ± 11	2.3 ± 1.3	–	–	–
SHARDS10004575	12:36:51.8	62:19:05.8	3.39 ± 0.07	18.0 ± 3.0	102 ± 19	3.0 ± 1.4	–	–	–
SHARDS10006854	12:36:51.8	62:19:10.4	3.93 ± 0.06	2.7 ± 0.8	51 ± 16	3.0 ± 1.4	–	–	–
SHARDS20004816	12:36:51.9	62:15:15.7	3.37 ± 0.07	3.5 ± 2.8	260 ± 290	3.0 ± 1.6	2.7 ± 0.9	23 ± 3	2.7 ± 0.8
SHARDS20006419	12:36:51.9	62:15:14.5	3.37 ± 0.07	5.5 ± 0.6	100 ± 30	2.9 ± 1.6	0.2 ± 0.1	21 ± 5	4.3 ± 1.2
SHARDS20009653	12:36:51.9	62:12:55.6	4.67 ± 0.07	23.0 ± 3.0	1150 ± 160	3.0 ± 1.6	0.8 ± 0.3	20 ± 3	1.0 ± 0.2
SHARDS20006542	12:36:52.0	62:11:04.7	3.96 ± 0.06	6.4 ± 2.5	1200 ± 300	3.0 ± 1.6	0.9 ± 0.8	23 ± 5	1.1 ± 0.4
SHARDS20007868	12:36:52.0	62:11:44.9	5.35 ± 0.07	5.5 ± 1.1	82 ± 19	2.9 ± 1.4	–	–	–
SHARDS10009061	12:36:52.1	62:15:46.2	4.19 ± 0.07	2.4 ± 1.8	600 ± 420	3.0 ± 1.6	4.5 ± 2.0	26 ± 4	1.0 ± 0.3
SHARDS10006579	12:36:52.2	62:18:31.5	3.24 ± 0.07	3.2 ± 0.6	100 ± 30	3.0 ± 1.4	0.7 ± 0.9	34 ± 13	1.9 ± 1.5
SHARDS20024707	12:36:52.3	62:15:25.2	4.43 ± 0.07	0.3 ± 0.2	21 ± 7	2.8 ± 1.4	–	–	–
SHARDS20007044	12:36:52.3	62:08:44.0	3.93 ± 0.06	0.7 ± 0.3	20 ± 7	2.3 ± 1.4	–	–	–
SHARDS10007560	12:36:52.3	62:16:05.1	5.29 ± 0.07	4.1 ± 0.8	67 ± 16	2.7 ± 1.4	–	–	–
SHARDS20002671	12:36:52.4	62:13:37.8	3.56 ± 0.06	5.4 ± 0.8	38 ± 4	1.9 ± 0.8	–	–	–
SHARDS10003357	12:36:52.5	62:17:50.9	3.79 ± 0.06	13.0 ± 7.0	960 ± 350	3.0 ± 1.6	4.5 ± 2.0	26 ± 4	1.0 ± 0.3
SHARDS10011513	12:36:52.5	62:18:17.7	4.75 ± 0.07	6.7 ± 4.6	770 ± 360	3.0 ± 1.6	0.7 ± 0.9	34 ± 13	1.9 ± 1.5
SHARDS10013390	12:36:52.5	62:16:01.7	3.38 ± 0.07	4.9 ± 1.6	120 ± 40	3.0 ± 1.4	–	–	–
SHARDS20009536	12:36:52.6	62:15:04.7	4.58 ± 0.07	15.0 ± 5.0	1050 ± 210	3.0 ± 1.6	0.6 ± 0.4	37 ± 13	2.1 ± 1.5
SHARDS20006394	12:36:52.7	62:11:38.0	4.66 ± 0.07	20.0 ± 4.0	1040 ± 210	3.0 ± 1.6	1.2 ± 0.8	38 ± 13	1.9 ± 1.4
SHARDS20006394	12:36:52.7	62:11:37.3	3.96 ± 0.06	2.7 ± 0.9	62 ± 20	2.8 ± 1.4	–	–	–
SHARDS20002663	12:36:52.7	62:13:39.1	3.42 ± 0.07	1.8 ± 0.3	34 ± 6	1.7 ± 0.7	–	–	–
SHARDS20006425	12:36:52.8	62:09:24.8	3.53 ± 0.06	11.0 ± 3.0	305 ± 139	3.0 ± 1.6	1.6 ± 1.2	45 ± 10	2.4 ± 1.5
SHARDS10006082	12:36:52.9	62:17:24.0	4.06 ± 0.07	0.4 ± 0.1	14 ± 4	3.1 ± 1.3	–	–	–
SHARDS20013378	12:36:53.0	62:11:08.6	5.21 ± 0.06	27.0 ± 6.0	645 ± 220	3.0 ± 1.6	0.9 ± 0.6	24 ± 9	2.0 ± 1.1
SHARDS20015076	12:36:53.1	62:11:53.6	3.42 ± 0.07	1.2 ± 0.6	75 ± 43	2.8 ± 1.4	–	–	–
SHARDS10012815	12:36:53.1	62:15:43.3	3.49 ± 0.06	1.2 ± 0.6	73 ± 50	2.7 ± 1.4	–	–	–
SHARDS20011455	12:36:53.1	62:12:59.5	5.23 ± 0.06	4.2 ± 2.6	580 ± 290	3.0 ± 1.6	0.8 ± 0.9	16 ± 6	2.3 ± 1.5
SHARDS20005331	12:36:53.1	62:13:31.7	3.56 ± 0.06	4.8 ± 0.9	54 ± 16	2.6 ± 1.3	–	–	–
SHARDS20012201	12:36:53.3	62:11:12.3	3.96 ± 0.06	1.1 ± 0.6	91 ± 52	2.9 ± 1.4	–	–	–
SHARDS10008463	12:36:53.3	62:18:44.9	3.93 ± 0.06	0.9 ± 0.4	55 ± 26	2.6 ± 1.3	–	–	–
SHARDS10009196	12:36:53.3	62:18:33.5	4.22 ± 0.07	34.0 ± 5.0	855 ± 218	3.0 ± 1.6	1.1 ± 0.6	23 ± 6	1.1 ± 0.5
SHARDS20018112	12:36:53.4	62:13:10.2	3.84 ± 0.06	1.1 ± 0.8	71 ± 53	2.6 ± 1.4	–	–	–
SHARDS20008406	12:36:53.5	62:08:44.9	3.66 ± 0.06	2.5 ± 1.2	83 ± 41	2.8 ± 1.4	–	–	–
SHARDS20011830	12:36:53.5	62:14:53.1	4.58 ± 0.07	14.0 ± 5.0	750 ± 270	3.0 ± 1.6	1.1 ± 1.1	38 ± 13	2.0 ± 1.4
SHARDS20011676	12:36:53.5	62:11:50.0	4.66 ± 0.07	1.6 ± 1.0	73 ± 54	2.7 ± 1.4	–	–	–
SHARDS10012561	12:36:53.7	62:17:36.0	4.75 ± 0.07	0.6 ± 0.2	46 ± 14	2.4 ± 1.2	–	–	–
SHARDS20013642	12:36:53.9	62:14:55.9	5.82 ± 0.06	1.5 ± 0.8	40 ± 20	2.2 ± 1.2	–	–	–
SHARDS10017061	12:36:54.0	62:19:00.1	3.51 ± 0.06	0.3 ± 0.2	53 ± 25	2.6 ± 1.3	–	–	–
SHARDS10014221	12:36:54.0	62:15:33.7	3.23 ± 0.07	0.1 ± 0.0	15 ± 6	2.3 ± 1.4	–	–	–
SHARDS20004616	12:36:54.0	62:08:55.1	4.23 ± 0.07	28.0 ± 4.0	74 ± 7	3.0 ± 1.4	–	–	–

Continued on next page

Table A.2 – *Continued from previous page*

Object Name	R.A. (J2000)	Dec. (J2000)	z	$M_{\rm star,m}$ (10^9 $M_\odot$)	$\rm Age_m$ (Myr)	$\tau_{\rm m}$ (Myr)	$M_{\rm star,b}$ (10^9 $M_\odot$)	$\rm Age_b$ (Myr)	$\tau_{\rm b}$ (Myr)
SHARDS20000798	12:36:54.1	62:08:56.1	3.94 ± 0.06	8.6 ± 4.8	750 ± 380	3.0 ± 1.6	0.9 ± 1.2	16 ± 5	1.3 ± 0.7
SHARDS10003545	12:36:54.1	62:17:33.8	3.65 ± 0.06	3.9 ± 0.9	74 ± 25	2.7 ± 1.3	–	–	–
SHARDS20241556	12:36:54.1	62:15:06.3	4.58 ± 0.07	5.4 ± 3.7	880 ± 340	3.0 ± 1.6	1.7 ± 1.3	22 ± 3	1.0 ± 0.2
SHARDS20241337	12:36:54.2	62:15:07.0	4.30 ± 0.06	3.3 ± 1.3	85 ± 46	2.9 ± 1.4	–	–	–
SHARDS20012559	12:36:54.2	62:13:19.6	5.50 ± 0.07	1.4 ± 0.7	36 ± 20	2.5 ± 1.4	–	–	–
SHARDS10006446	12:36:54.3	62:16:12.7	3.91 ± 0.06	4.7 ± 0.5	37 ± 4	1.8 ± 0.8	–	–	–
SHARDS10011651	12:36:54.3	62:16:21.1	4.45 ± 0.07	0.8 ± 0.4	49 ± 30	2.5 ± 1.3	–	–	–
SHARDS10008601	12:36:54.3	62:15:30.8	4.44 ± 0.07	0.5 ± 0.2	44 ± 15	2.3 ± 1.2	–	–	–
SHARDS20011498	12:36:54.3	62:12:42.9	5.92 ± 0.06	3.2 ± 1.2	55 ± 21	2.5 ± 1.3	–	–	–
SHARDS20007869	12:36:54.5	62:08:24.9	4.76 ± 0.07	13.0 ± 6.0	840 ± 290	3.0 ± 1.6	1.0 ± 1.1	38 ± 13	2.0 ± 1.5
SHARDS20023948	12:36:54.5	62:14:58.4	4.72 ± 0.07	2.5 ± 0.4	22 ± 3	1.3 ± 0.5	–	–	–
SHARDS20023901	12:36:54.6	62:15:05.2	4.58 ± 0.07	7.0 ± 1.9	65 ± 21	2.8 ± 1.4	–	–	–
SHARDS20025252	12:36:54.6	62:15:12.0	3.49 ± 0.06	3.8 ± 0.6	56 ± 6	2.0 ± 0.9	–	–	–
SHARDS10002257	12:36:54.6	62:16:26.9	3.78 ± 0.06	1.5 ± 0.6	58 ± 26	2.6 ± 1.3	–	–	–
SHARDS10007859	12:36:54.7	62:16:22.1	3.91 ± 0.06	7.3 ± 0.7	177 ± 19	2.8 ± 1.4	–	–	–
SHARDS20012408	12:36:54.7	62:13:32.9	4.70 ± 0.07	65.2 ± 15.9	589 ± 165	3.0 ± 1.6	2.1 ± 1.1	27 ± 10	1.3 ± 0.9
SHARDS20009233	12:36:54.8	62:08:30.2	4.76 ± 0.07	9.6 ± 5.6	700 ± 330	3.0 ± 1.6	1.0 ± 1.2	36 ± 13	2.0 ± 1.5
SHARDS20010396	12:36:54.8	62:08:27.0	4.62 ± 0.07	12.0 ± 6.0	730 ± 320	3.0 ± 1.6	0.9 ± 1.0	41 ± 12	2.3 ± 1.6
SHARDS20016398	12:36:54.9	62:12:54.4	6.75 ± 0.14	1.3 ± 0.7	20 ± 7	2.3 ± 1.3	–	–	–
SHARDS10008547	12:36:55.0	62:16:27.3	4.60 ± 0.07	2.1 ± 1.1	79 ± 44	2.8 ± 1.4	–	–	–
SHARDS10011476	12:36:55.0	62:19:01.1	3.52 ± 0.06	0.9 ± 0.6	90 ± 65	2.8 ± 1.4	–	–	–
SHARDS20022974	12:36:55.1	62:14:59.8	3.49 ± 0.06	1.0 ± 0.5	81 ± 53	2.8 ± 1.4	–	–	–
SHARDS10013882	12:36:55.1	62:19:49.9	3.52 ± 0.06	0.5 ± 0.2	47 ± 23	2.4 ± 1.3	–	–	–
SHARDS20022674	12:36:55.2	62:10:34.0	4.37 ± 0.06	1.1 ± 0.5	58 ± 28	2.6 ± 1.3	–	–	–
SHARDS20022647	12:36:55.2	62:10:36.2	4.25 ± 0.07	1.5 ± 0.6	48 ± 21	2.4 ± 1.2	–	–	–
SHARDS20004751	12:36:55.4	62:12:13.4	5.08 ± 0.06	14.6 ± 1.3	58 ± 7	2.5 ± 1.2	–	–	–
SHARDS20007964	12:36:55.4	62:10:18.4	4.09 ± 0.07	11.0 ± 4.0	1100 ± 400	3.0 ± 1.6	2.2 ± 1.6	34 ± 13	1.8 ± 1.3
SHARDS10002758	12:36:55.4	62:17:07.3	3.51 ± 0.06	8.9 ± 1.8	45 ± 10	2.2 ± 1.1	–	–	–
SHARDS10008550	12:36:55.4	62:15:48.8	5.15 ± 0.06	1.3 ± 0.7	60 ± 29	2.6 ± 1.4	–	–	–
SHARDS20025422	12:36:55.4	62:15:08.4	5.97 ± 0.07	0.6 ± 0.4	23 ± 10	2.8 ± 1.4	–	–	–
SHARDS10005512	12:36:55.5	62:13:32.8	5.15 ± 0.06	3.1 ± 0.8	23 ± 6	3.1 ± 1.4	–	–	–
SHARDS20009588	12:36:55.6	62:14:12.9	3.70 ± 0.06	2.4 ± 0.9	150 ± 60	3.0 ± 1.4	–	–	–
SHARDS20006499	12:36:55.6	62:11:50.3	4.80 ± 0.07	4.6 ± 1.6	58 ± 27	2.5 ± 1.3	–	–	–
SHARDS10017446	12:36:55.7	62:17:26.1	3.92 ± 0.06	7.2 ± 3.0	869 ± 380	3.0 ± 1.6	0.2 ± 0.2	20 ± 6	3.7 ± 1.5
SHARDS20007020	12:36:55.8	62:13:51.0	3.98 ± 0.06	10.2 ± 2.5	1250 ± 220	3.0 ± 1.6	0.3 ± 0.1	19 ± 6	3.6 ± 1.5
SHARDS10006179	12:36:55.8	62:19:18.7	3.24 ± 0.07	7.2 ± 0.9	101 ± 15	3.1 ± 1.4	–	–	–
SHARDS20010482	12:36:55.8	62:15:01.4	4.36 ± 0.06	2.1 ± 1.1	85 ± 55	2.8 ± 1.4	–	–	–
SHARDS10016877	12:36:55.8	62:15:38.7	4.45 ± 0.07	0.4 ± 0.2	18 ± 7	2.8 ± 1.4	–	–	–
SHARDS20006029	12:36:55.9	62:08:46.0	3.80 ± 0.06	5.6 ± 0.8	78 ± 18	2.8 ± 1.4	–	–	–
SHARDS20005223	12:36:55.9	62:11:46.8	3.42 ± 0.07	2.6 ± 1.9	57 ± 30	2.5 ± 1.3	–	–	–
SHARDS20004544	12:36:55.9	62:14:12.4	4.03 ± 0.07	33.0 ± 5.0	120 ± 30	2.8 ± 1.6	4.8 ± 4.0	27 ± 7	1.1 ± 0.4
SHARDS10009979	12:36:56.0	62:16:38.9	4.33 ± 0.06	0.9 ± 0.5	52 ± 26	2.5 ± 1.3	–	–	–
SHARDS20011261	12:36:56.0	62:11:57.4	3.55 ± 0.06	8.9 ± 3.2	450 ± 260	3.0 ± 1.6	0.7 ± 0.6	35 ± 14	2.0 ± 1.5
SHARDS10013243	12:36:56.1	62:19:12.7	4.76 ± 0.07	86.0 ± 7.0	500 ± 90	3.0 ± 1.6	2.3 ± 0.4	26 ± 4	1.1 ± 0.5
SHARDS20025278	12:36:56.1	62:15:00.9	3.22 ± 0.07	8.0 ± 1.8	62 ± 17	2.9 ± 1.4	–	–	–
SHARDS20005742	12:36:56.1	62:14:54.8	3.97 ± 0.06	3.1 ± 0.3	52 ± 5	2.1 ± 1.0	–	–	–
SHARDS20007301	12:36:56.2	62:09:26.4	3.94 ± 0.06	1.2 ± 0.5	34 ± 16	3.0 ± 1.4	–	–	–
SHARDS10010961	12:36:56.4	62:12:31.8	3.24 ± 0.07	0.6 ± 0.3	63 ± 32	2.7 ± 1.4	–	–	–
SHARDS10008567	12:36:56.4	62:15:27.0	5.56 ± 0.07	5.1 ± 0.8	52 ± 8	1.9 ± 1.0	–	–	–

Continued on next page

Table A.2 – *Continued from previous page*

Object Name	R.A. (J2000)	Dec. (J2000)	z	$M_{\rm star,m}$ ($10^9\,M_\odot$)	$\rm Age_m$ (Myr)	$\tau_{\rm m}$ (Myr)	$M_{\rm star,b}$ ($10^9\,M_\odot$)	$\rm Age_b$ (Myr)	$\tau_{\rm b}$ (Myr)
SHARDS10007601	12:36:56.4	62:19:30.0	3.52 ± 0.06	1.5 ± 0.6	81 ± 40	2.8 ± 1.4	–	–	–
SHARDS20007191	12:36:56.5	62:13:39.9	3.36 ± 0.07	1.5 ± 0.5	51 ± 21	2.6 ± 1.3	–	–	–
SHARDS20007330	12:36:56.5	62:09:22.8	3.67 ± 0.06	5.4 ± 2.6	980 ± 390	3.0 ± 1.6	1.2 ± 1.1	39 ± 12	2.1 ± 1.5
SHARDS10004758	12:36:56.5	62:18:46.8	3.65 ± 0.06	1.6 ± 0.5	63 ± 24	2.6 ± 1.3	–	–	–
SHARDS20010724	12:36:56.5	62:13:13.6	5.23 ± 0.06	6.1 ± 3.9	509 ± 290	3.0 ± 1.6	0.4 ± 0.6	18 ± 6	3.3 ± 1.6
SHARDS10006882	12:36:56.5	62:17:34.6	4.07 ± 0.07	6.1 ± 3.6	490 ± 380	3.0 ± 1.6	2.5 ± 1.3	32 ± 12	1.6 ± 1.2
SHARDS10009123	12:36:56.6	62:17:58.5	3.39 ± 0.07	5.7 ± 1.2	1100 ± 300	3.0 ± 1.6	0.2 ± 0.1	19 ± 4	4.0 ± 1.4
SHARDS10009362	12:36:56.6	62:18:40.2	4.34 ± 0.06	0.8 ± 0.5	62 ± 34	2.6 ± 1.4	–	–	–
SHARDS20008777	12:36:56.7	62:09:30.5	5.19 ± 0.06	0.2 ± 0.1	16 ± 5	2.9 ± 1.4	–	–	–
SHARDS10006367	12:36:56.7	62:19:56.3	4.23 ± 0.07	3.7 ± 1.3	77 ± 35	2.7 ± 1.4	–	–	–
SHARDS20016256	12:36:56.8	62:13:05.0	6.27 ± 0.14	9.1 ± 1.6	52 ± 17	2.6 ± 1.3	–	–	–
SHARDS20009828	12:36:56.8	62:11:16.5	3.83 ± 0.06	1.4 ± 0.6	72 ± 36	2.8 ± 1.4	–	–	–
SHARDS20010968	12:36:56.9	62:14:20.8	3.89 ± 0.06	7.0 ± 3.8	660 ± 390	3.0 ± 1.6	1.2 ± 1.2	29 ± 12	1.5 ± 1.1
SHARDS20006102	12:36:57.0	62:12:04.8	3.42 ± 0.07	6.7 ± 1.7	1250 ± 200	3.0 ± 1.6	0.3 ± 0.1	19 ± 4	1.9 ± 1.1
SHARDS20014909	12:36:57.0	62:13:41.2	5.93 ± 0.06	1.0 ± 0.6	32 ± 16	2.5 ± 1.4	–	–	–
SHARDS20006946	12:36:57.0	62:11:51.0	3.69 ± 0.06	0.2 ± 0.1	11 ± 4	3.2 ± 1.4	–	–	–
SHARDS10005479	12:36:57.0	62:17:06.6	4.07 ± 0.07	7.0 ± 2.0	52 ± 18	2.5 ± 1.3	–	–	–
SHARDS20015545	12:36:57.1	62:14:02.7	5.82 ± 0.06	1.9 ± 2.0	66 ± 45	2.6 ± 1.4	–	–	–
SHARDS20011891	12:36:57.1	62:10:56.3	4.10 ± 0.07	0.5 ± 0.2	19 ± 7	2.7 ± 1.4	–	–	–
SHARDS20005588	12:36:57.2	62:08:13.2	4.76 ± 0.07	8.5 ± 1.9	39 ± 11	1.9 ± 1.0	–	–	–
SHARDS20005741	12:36:57.2	62:12:34.4	3.42 ± 0.07	5.7 ± 1.0	55 ± 12	2.8 ± 1.4	–	–	–
SHARDS10012500	12:36:57.2	62:16:46.8	4.46 ± 0.07	0.5 ± 0.2	48 ± 17	2.4 ± 1.3	–	–	–
SHARDS10008187	12:36:57.2	62:18:53.7	3.52 ± 0.06	7.5 ± 1.6	1230 ± 110	2.9 ± 1.6	0.2 ± 0.1	23 ± 4	3.4 ± 1.5
SHARDS20008432	12:36:57.3	62:11:32.8	4.66 ± 0.07	1.2 ± 0.5	53 ± 21	2.5 ± 1.3	–	–	–
SHARDS20009044	12:36:57.3	62:11:15.5	4.80 ± 0.07	11.0 ± 6.0	750 ± 370	3.0 ± 1.6	2.6 ± 1.8	25 ± 7	1.1 ± 0.6
SHARDS20008932	12:36:57.3	62:12:49.4	5.23 ± 0.06	19.0 ± 5.0	813 ± 181	3.0 ± 1.6	0.5 ± 0.2	20 ± 4	2.7 ± 1.1
SHARDS20025450	12:36:57.3	62:14:55.1	4.31 ± 0.06	0.5 ± 0.5	53 ± 34	2.5 ± 1.3	–	–	–
SHARDS20006088	12:36:57.3	62:12:56.3	3.56 ± 0.06	6.6 ± 1.7	64 ± 22	2.6 ± 1.3	–	–	–
SHARDS20017397	12:36:57.3	62:13:08.4	3.98 ± 0.06	15.0 ± 3.0	1200 ± 300	3.0 ± 1.6	0.5 ± 0.3	37 ± 13	2.2 ± 1.5
SHARDS20005313	12:36:57.4	62:11:52.9	3.42 ± 0.07	5.6 ± 2.6	300 ± 270	3.0 ± 1.6	2.1 ± 0.8	25 ± 3	1.0 ± 0.3
SHARDS20008481	12:36:57.4	62:10:12.1	3.67 ± 0.06	0.6 ± 0.3	42 ± 17	2.3 ± 1.2	–	–	–
SHARDS10007458	12:36:57.5	62:16:50.5	4.61 ± 0.07	3.2 ± 1.6	44 ± 24	3.1 ± 1.4	–	–	–
SHARDS20009578	12:36:57.6	62:11:39.0	3.27 ± 0.07	1.2 ± 0.4	73 ± 35	2.8 ± 1.4	–	–	–
SHARDS20005956	12:36:57.7	62:09:17.9	4.08 ± 0.07	13.0 ± 6.0	490 ± 360	3.0 ± 1.6	3.4 ± 2.2	38 ± 13	1.9 ± 1.3
SHARDS20006837	12:36:57.8	62:14:25.0	3.37 ± 0.07	0.6 ± 0.2	31 ± 10	1.6 ± 0.8	–	–	–
SHARDS20007749	12:36:57.8	62:10:45.2	4.50 ± 0.07	1.1 ± 0.4	50 ± 18	2.4 ± 1.3	–	–	–
SHARDS10006061	12:36:57.8	62:15:02.6	4.44 ± 0.07	7.4 ± 1.6	1050 ± 230	3.0 ± 1.6	0.2 ± 0.2	15 ± 3	1.2 ± 0.6
SHARDS20018568	12:36:57.8	62:14:33.5	5.96 ± 0.07	6.0 ± 6.6	170 ± 134	2.9 ± 1.4	–	–	–
SHARDS10001620	12:36:57.8	62:15:34.3	3.50 ± 0.06	6.1 ± 0.5	76 ± 10	2.6 ± 1.4	–	–	–
SHARDS10006084	12:36:57.9	62:15:24.9	4.44 ± 0.07	6.1 ± 1.7	50 ± 20	2.5 ± 1.3	–	–	–
SHARDS10007794	12:36:57.9	62:18:04.9	4.34 ± 0.06	4.2 ± 2.0	730 ± 330	3.0 ± 1.6	0.9 ± 0.8	38 ± 13	2.2 ± 1.6
SHARDS20009778	12:36:58.0	62:13:50.3	4.18 ± 0.07	6.7 ± 1.4	1000 ± 300	3.0 ± 1.6	0.2 ± 0.1	13 ± 3	4.2 ± 1.0
SHARDS10007538	12:36:58.1	62:17:39.2	3.65 ± 0.06	5.2 ± 3.1	950 ± 440	3.0 ± 1.6	0.8 ± 0.8	43 ± 11	2.2 ± 1.4
SHARDS20006121	12:36:58.1	62:11:14.8	4.51 ± 0.07	8.8 ± 1.0	48 ± 5	2.4 ± 1.1	–	–	–
SHARDS10010421	12:36:58.2	62:15:10.3	4.05 ± 0.07	2.2 ± 0.9	57 ± 33	2.5 ± 1.3	–	–	–
SHARDS20009401	12:36:58.2	62:12:06.7	4.67 ± 0.07	14.0 ± 6.0	650 ± 290	3.0 ± 1.6	1.7 ± 1.6	39 ± 13	2.1 ± 1.5
SHARDS10013643	12:36:58.2	62:15:11.5	3.23 ± 0.07	0.6 ± 0.3	87 ± 57	2.8 ± 1.4	–	–	–
SHARDS20007501	12:36:58.3	62:11:20.4	3.96 ± 0.06	0.3 ± 0.1	15 ± 5	2.8 ± 1.4	–	–	–
SHARDS10017054	12:36:58.3	62:14:58.2	3.63 ± 0.06	5.2 ± 2.6	710 ± 420	3.0 ± 1.6	0.4 ± 0.4	40 ± 13	2.4 ± 1.6

Continued on next page

Table A.2 – *Continued from previous page*

Object Name	R.A. (J2000)	Dec. (J2000)	z	$M_{\rm star,m}$ (10^9 $M_\odot$)	$\rm Age_m$ (Myr)	$\tau_{\rm m}$ (Myr)	$M_{\rm star,b}$ (10^9 $M_\odot$)	$\rm Age_b$ (Myr)	$\tau_{\rm b}$ (Myr)
SHARDS20009570	12:36:58.3	62:11:17.4	3.41 ± 0.07	0.4 ± 0.2	54 ± 23	2.5 ± 1.3	–	–	–
SHARDS10010385	12:36:58.4	62:16:15.0	5.16 ± 0.06	1.7 ± 0.8	22 ± 10	2.6 ± 1.4	–	–	–
SHARDS10001876	12:36:58.5	62:15:55.6	3.50 ± 0.06	2.3 ± 0.8	46 ± 15	2.1 ± 1.0	–	–	–
SHARDS20014339	12:36:58.6	62:12:44.1	6.27 ± 0.14	0.1 ± 0.1	11 ± 4	3.2 ± 1.4	–	–	–
SHARDS20014001	12:36:58.6	62:10:11.8	4.92 ± 0.08	3.2 ± 1.7	100 ± 53	2.9 ± 1.4	–	–	–
SHARDS10010637	12:36:58.6	62:17:06.7	4.22 ± 0.07	0.4 ± 0.1	40 ± 13	2.2 ± 1.2	–	–	–
SHARDS10011777	12:36:58.8	62:17:53.7	3.65 ± 0.06	0.1 ± 0.0	16 ± 7	3.0 ± 1.4	–	–	–
SHARDS10007531	12:36:58.8	62:17:10.4	4.46 ± 0.07	0.6 ± 0.2	19 ± 7	2.8 ± 1.5	–	–	–
SHARDS20011706	12:36:58.9	62:09:17.6	5.46 ± 0.07	1.1 ± 0.8	42 ± 32	2.7 ± 1.4	–	–	–
SHARDS20006444	12:36:59.0	62:12:29.1	4.52 ± 0.07	0.7 ± 0.3	19 ± 6	2.9 ± 1.3	–	–	–
SHARDS20011056	12:36:59.1	62:13:35.7	3.21 ± 0.07	0.1 ± 0.0	40 ± 12	2.2 ± 1.2	–	–	–
SHARDS20005661	12:36:59.1	62:09:25.6	3.53 ± 0.06	3.8 ± 0.9	47 ± 13	1.9 ± 1.0	–	–	–
SHARDS20005706	12:36:59.1	62:12:23.7	4.12 ± 0.07	2.8 ± 1.3	37 ± 3	4.6 ± 0.7	0.4 ± 0.2	22 ± 6	1.1 ± 0.4
SHARDS10007548	12:36:59.3	62:17:22.9	4.22 ± 0.07	11.9 ± 2.0	1060 ± 170	3.0 ± 1.6	–	–	–
SHARDS10005590	12:36:59.4	62:19:05.4	3.80 ± 0.06	3.5 ± 0.7	35 ± 6	1.8 ± 0.8	–	–	–
SHARDS10013023	12:36:59.5	62:15:01.5	3.63 ± 0.06	1.2 ± 0.5	63 ± 39	2.6 ± 1.4	–	–	–
SHARDS10005569	12:36:59.5	62:15:14.4	3.38 ± 0.07	5.8 ± 1.1	54 ± 11	2.6 ± 1.3	–	–	–
SHARDS20007303	12:36:59.7	62:14:27.9	3.76 ± 0.06	2.7 ± 0.7	89 ± 36	2.9 ± 1.4	5.4 ± 4.1	46 ± 9	2.2 ± 1.3
SHARDS10009008	12:36:59.7	62:14:54.4	5.56 ± 0.07	36.7 ± 14.4	576 ± 229	3.0 ± 1.6	–	–	–
SHARDS10005202	12:36:59.8	62:18:54.3	3.94 ± 0.06	6.1 ± 0.7	51 ± 6	2.3 ± 1.2	–	–	–
SHARDS10006208	12:36:59.8	62:15:13.1	4.20 ± 0.07	4.2 ± 0.9	30 ± 10	1.7 ± 0.8	–	–	–
SHARDS20006282	12:36:59.8	62:12:18.9	5.36 ± 0.07	37.0 ± 5.0	59 ± 11	2.9 ± 1.4	–	–	–
SHARDS10014349	12:36:59.8	62:16:36.2	3.39 ± 0.07	0.3 ± 0.1	47 ± 22	2.4 ± 1.3	–	–	–
SHARDS20009598	12:36:59.8	62:11:37.6	4.11 ± 0.07	2.0 ± 0.9	85 ± 46	2.8 ± 1.4	–	–	–
SHARDS10007109	12:36:59.9	62:14:58.3	4.59 ± 0.07	0.9 ± 0.5	34 ± 18	1.9 ± 1.1	–	–	–
SHARDS20015155	12:36:59.9	62:10:12.7	4.65 ± 0.07	1.6 ± 1.0	70 ± 42	2.7 ± 1.4	–	–	–
SHARDS10014300	12:37:00.2	62:18:03.5	4.23 ± 0.07	0.1 ± 0.1	17 ± 10	3.0 ± 1.4	–	–	–
SHARDS20012043	12:37:00.2	62:11:13.4	5.35 ± 0.07	11.1 ± 2.8	58 ± 36	2.6 ± 1.4	–	–	–
SHARDS20008701	12:37:00.2	62:10:08.4	3.95 ± 0.06	22.0 ± 3.0	1200 ± 100	2.6 ± 1.6	0.6 ± 0.1	24 ± 1	4.4 ± 1.1
SHARDS10014756	12:37:00.3	62:14:47.2	3.49 ± 0.06	1.8 ± 1.1	162 ± 113	2.9 ± 1.4	–	–	–
SHARDS20013362	12:37:00.3	62:16:54.1	4.10 ± 0.07	1.1 ± 0.7	78 ± 46	2.8 ± 1.4	–	–	–
SHARDS10012558	12:37:00.3	62:16:36.7	5.31 ± 0.07	0.2 ± 0.1	17 ± 6	3.0 ± 1.4	–	–	–
SHARDS20006915	12:37:00.4	62:13:41.8	4.42 ± 0.07	1.3 ± 0.5	52 ± 20	2.4 ± 1.3	–	–	–
SHARDS10007325	12:37:00.5	62:09:04.5	4.47 ± 0.07	7.8 ± 2.5	770 ± 280	3.0 ± 1.6	0.8 ± 0.8	24 ± 8	1.1 ± 0.7
SHARDS20009314	12:37:00.6	62:09:56.0	3.54 ± 0.06	14.0 ± 4.0	49 ± 20	1.9 ± 1.1	–	–	–
SHARDS10013351	12:37:00.6	62:16:58.6	4.22 ± 0.07	0.8 ± 0.4	49 ± 22	2.4 ± 1.3	–	–	–
SHARDS10005366	12:37:00.7	62:17:56.0	4.23 ± 0.07	15.0 ± 4.0	97 ± 18	2.8 ± 1.4	–	–	–
SHARDS10014778	12:37:00.7	62:18:38.2	6.22 ± 0.14	0.4 ± 0.2	13 ± 4	3.2 ± 1.4	–	–	–
SHARDS10017788	12:37:00.8	62:18:47.0	3.49 ± 0.06	0.3 ± 0.2	57 ± 34	2.6 ± 1.4	–	–	–
SHARDS20007141	12:37:00.9	62:09:28.3	3.40 ± 0.07	0.2 ± 0.1	14 ± 5	3.0 ± 1.4	–	–	–
SHARDS10010226	12:37:00.9	62:17:32.4	3.26 ± 0.07	1.7 ± 0.5	74 ± 30	2.8 ± 1.4	–	–	–
SHARDS10007065	12:37:01.0	62:17:16.2	3.52 ± 0.06	1.5 ± 0.5	66 ± 26	2.7 ± 1.4	–	–	–
SHARDS10012026	12:37:01.0	62:15:39.9	5.43 ± 0.07	0.4 ± 0.3	24 ± 17	2.9 ± 1.4	–	–	–
SHARDS10015429	12:37:01.0	62:16:58.7	6.00 ± 0.07	3.5 ± 2.5	78 ± 52	2.7 ± 1.4	–	–	–
SHARDS20006656	12:37:01.0	62:09:16.8	4.35 ± 0.06	2.7 ± 0.8	57 ± 21	2.6 ± 1.3	–	–	–
SHARDS10017226	12:37:01.1	62:16:14.5	3.24 ± 0.07	0.2 ± 0.1	45 ± 22	2.4 ± 1.3	–	–	–
SHARDS10006025	12:37:01.1	62:20:20.9	4.23 ± 0.07	1.4 ± 1.6	18 ± 7	2.8 ± 1.5	–	–	–
SHARDS20005678	12:37:01.2	62:09:36.3	3.40 ± 0.07	16.0 ± 4.0	509 ± 320	3.0 ± 1.6	3.2 ± 1.5	37 ± 12	1.8 ± 1.2
SHARDS20014132	12:37:01.4	62:11:39.4	5.36 ± 0.07	23.0 ± 3.0	886 ± 143	3.0 ± 1.6	0.8 ± 0.3	20 ± 5	1.2 ± 0.5

Continued on next page

Table A.2 – *Continued from previous page*

Object Name	R.A. (J2000)	Dec. (J2000)	z	$M_{\rm star,m}$ ($10^9\ M_\odot$)	$\rm Age_m$ (Myr)	$\tau_{\rm m}$ (Myr)	$M_{\rm star,b}$ ($10^9\ M_\odot$)	$\rm Age_b$ (Myr)	$\tau_{\rm b}$ (Myr)
SHARDS20009678	12:37:01.4	62:10:05.2	3.95 ± 0.06	1.5 ± 0.4	38 ± 9	2.1 ± 1.1	–	–	–
SHARDS20009174	12:37:01.4	62:09:10.0	4.35 ± 0.06	0.4 ± 0.2	41 ± 18	2.3 ± 1.2	–	–	–
SHARDS20010462	12:37:01.4	62:13:30.5	4.57 ± 0.07	6.1 ± 4.0	120 ± 70	2.9 ± 1.4	–	–	–
SHARDS20005711	12:37:01.5	62:11:57.2	3.42 ± 0.07	8.4 ± 1.6	86 ± 23	2.9 ± 1.4	–	–	–
SHARDS20004977	12:37:01.5	62:12:11.4	5.08 ± 0.06	4.6 ± 0.5	35 ± 3	1.7 ± 0.8	–	–	–
SHARDS20011028	12:37:01.5	62:13:46.5	4.43 ± 0.07	1.6 ± 0.6	73 ± 31	2.8 ± 1.4	–	–	–
SHARDS10006205	12:37:01.6	62:19:42.9	4.09 ± 0.07	3.5 ± 0.7	68 ± 16	2.8 ± 1.4	–	–	–
SHARDS10012078	12:37:01.7	62:15:45.7	4.46 ± 0.07	7.1 ± 3.4	700 ± 320	3.0 ± 1.6	0.2 ± 0.3	21 ± 6	4.0 ± 1.4
SHARDS20016052	12:37:01.7	62:10:02.5	6.03 ± 0.07	8.4 ± 4.1	150 ± 90	3.0 ± 1.4	–	–	–
SHARDS10006053	12:37:01.9	62:19:16.7	4.35 ± 0.06	3.4 ± 1.1	35 ± 15	1.9 ± 1.0	–	–	–
SHARDS20003315	12:37:02.0	62:12:25.3	3.42 ± 0.07	3.6 ± 0.9	44 ± 12	2.1 ± 1.1	–	–	–
SHARDS10009585	12:37:02.0	62:17:32.8	3.80 ± 0.06	0.5 ± 0.2	53 ± 23	2.5 ± 1.3	–	–	–
SHARDS20005919	12:37:02.0	62:10:17.6	3.96 ± 0.06	17.0 ± 5.0	1200 ± 300	3.0 ± 1.6	1.6 ± 0.9	23 ± 3	1.0 ± 0.2
SHARDS10012416	12:37:02.1	62:18:13.0	4.35 ± 0.06	0.5 ± 0.2	41 ± 14	2.2 ± 1.2	–	–	–
SHARDS10003989	12:37:02.2	62:20:50.3	3.81 ± 0.06	1.8 ± 0.5	22 ± 7	3.2 ± 1.3	–	–	–
SHARDS10008844	12:37:02.2	62:15:07.0	3.63 ± 0.06	3.0 ± 2.1	170 ± 112	2.9 ± 1.4	–	–	–
SHARDS20011503	12:37:02.3	62:10:19.5	3.54 ± 0.06	9.6 ± 2.0	1100 ± 300	3.0 ± 1.6	0.4 ± 0.2	23 ± 9	1.3 ± 0.9
SHARDS10006994	12:37:02.3	62:20:12.8	4.09 ± 0.07	1.3 ± 0.6	46 ± 19	2.2 ± 1.2	–	–	–
SHARDS20006060	12:37:02.3	62:12:39.9	3.88 ± 0.06	2.0 ± 0.6	36 ± 13	2.9 ± 1.5	2.7 ± 2.5	29 ± 9	1.2 ± 0.7
SHARDS20005484	12:37:02.3	62:13:40.0	3.89 ± 0.06	16.0 ± 6.0	700 ± 320	3.0 ± 1.6	–	–	–
SHARDS10008108	12:37:02.4	62:19:21.4	4.09 ± 0.07	2.6 ± 1.2	55 ± 33	2.4 ± 1.3	–	–	–
SHARDS20011174	12:37:02.4	62:11:33.0	5.35 ± 0.07	3.9 ± 1.5	71 ± 27	2.8 ± 1.4	–	–	–
SHARDS20007604	12:37:02.4	62:11:09.4	4.51 ± 0.07	4.6 ± 2.4	63 ± 33	2.5 ± 1.3	–	–	–
SHARDS10008039	12:37:02.5	62:17:13.4	3.65 ± 0.06	1.3 ± 0.8	39 ± 29	2.9 ± 1.4	–	–	–
SHARDS10013113	12:37:02.5	62:18:07.0	4.23 ± 0.07	0.3 ± 0.2	23 ± 14	2.9 ± 1.4	–	–	–
SHARDS10015202	12:37:02.5	62:17:25.1	3.93 ± 0.06	6.2 ± 2.9	490 ± 340	3.0 ± 1.6	0.2 ± 0.2	15 ± 5	4.2 ± 1.2
SHARDS20015702	12:37:02.5	62:13:58.0	5.37 ± 0.07	1.4 ± 1.1	73 ± 46	2.7 ± 1.4	–	–	–
SHARDS20006821	12:37:02.5	62:11:55.0	3.83 ± 0.06	3.3 ± 0.8	39 ± 11	2.0 ± 1.0	–	–	–
SHARDS10009504	12:37:02.5	62:16:05.8	5.43 ± 0.07	0.8 ± 0.4	25 ± 9	2.4 ± 1.3	–	–	–
SHARDS10015291	12:37:02.6	62:16:38.1	6.21 ± 0.14	22.0 ± 32.0	400 ± 270	3.0 ± 1.6	4.6 ± 7.0	35 ± 13	1.9 ± 1.4
SHARDS20001613	12:37:02.6	62:10:27.5	3.41 ± 0.07	1.5 ± 0.2	78 ± 21	2.9 ± 1.4	–	–	–
SHARDS10008415	12:37:02.7	62:17:02.2	4.22 ± 0.07	0.2 ± 0.1	18 ± 6	2.2 ± 1.3	–	–	–
SHARDS10010885	12:37:02.7	62:18:21.5	3.40 ± 0.07	2.6 ± 2.2	660 ± 430	3.0 ± 1.6	0.2 ± 0.4	17 ± 5	3.0 ± 1.6
SHARDS20012654	12:37:02.7	62:13:55.1	5.55 ± 0.07	5.7 ± 3.5	703 ± 247	3.0 ± 1.6	0.3 ± 0.5	18 ± 3	4.2 ± 1.1
SHARDS20023318	12:37:02.7	62:12:28.9	5.24 ± 0.07	5.0 ± 1.8	54 ± 24	2.9 ± 1.4	–	–	–
SHARDS20011267	12:37:02.8	62:11:41.7	5.36 ± 0.07	0.4 ± 0.2	22 ± 9	2.7 ± 1.4	–	–	–
SHARDS20010427	12:37:02.8	62:09:15.5	3.94 ± 0.06	1.4 ± 0.5	52 ± 20	2.4 ± 1.3	–	–	–
SHARDS20005951	12:37:02.9	62:13:06.7	4.29 ± 0.06	7.9 ± 3.3	211 ± 197	3.0 ± 1.6	2.1 ± 1.8	35 ± 13	1.9 ± 1.4
SHARDS10005684	12:37:02.9	62:16:13.3	3.79 ± 0.06	160.0 ± 10.0	1200 ± 100	3.0 ± 1.6	4.0 ± 0.2	50 ± 0	1.5 ± 1.0
SHARDS10009682	12:37:03.0	62:15:03.1	4.74 ± 0.07	0.6 ± 0.3	46 ± 18	2.4 ± 1.3	–	–	–
SHARDS10010010	12:37:03.0	62:20:44.4	3.67 ± 0.06	3.2 ± 1.6	214 ± 150	3.0 ± 1.4	–	–	–
SHARDS20009724	12:37:03.1	62:11:37.9	3.55 ± 0.06	0.2 ± 0.1	13 ± 5	2.9 ± 1.4	–	–	–
SHARDS10008872	12:37:03.1	62:16:08.1	4.61 ± 0.07	1.9 ± 0.8	68 ± 37	2.7 ± 1.4	–	–	–
SHARDS10008355	12:37:03.1	62:17:54.0	4.23 ± 0.07	0.9 ± 0.3	48 ± 17	2.3 ± 1.2	–	–	–
SHARDS20012491	12:37:03.2	62:10:25.4	4.10 ± 0.07	16.0 ± 4.0	1200 ± 300	3.0 ± 1.6	0.8 ± 0.5	33 ± 13	1.8 ± 1.4
SHARDS20005736	12:37:03.3	62:13:00.6	4.29 ± 0.06	2.7 ± 0.6	69 ± 20	2.7 ± 1.4	–	–	–
SHARDS20007270	12:37:03.3	62:10:06.4	4.37 ± 0.06	1.2 ± 0.4	53 ± 17	2.4 ± 1.3	–	–	–
SHARDS20007459	12:37:03.3	62:13:31.5	5.27 ± 0.07	2.0 ± 0.6	39 ± 14	2.0 ± 1.1	–	–	–
SHARDS10006713	12:37:03.4	62:17:03.2	3.93 ± 0.06	2.0 ± 0.6	62 ± 22	2.6 ± 1.3	–	–	–

Continued on next page

Table A.2 – *Continued from previous page*

Object Name	R.A. (J2000)	Dec. (J2000)	z	$M_{\rm star,m}$ (10^9 $M_\odot$)	$\rm Age_m$ (Myr)	$\tau_{\rm m}$ (Myr)	$M_{\rm star,b}$ (10^9 $M_\odot$)	$\rm Age_b$ (Myr)	$\tau_{\rm b}$ (Myr)
SHARDS10006271	12:37:03.4	62:16:16.2	3.93 ± 0.06	1.3 ± 0.6	30 ± 15	2.8 ± 1.4			
SHARDS10007662	12:37:03.4	62:19:21.9	3.81 ± 0.06	2.9 ± 2.7	620 ± 480	3.0 ± 1.6	0.7 ± 0.8	42 ± 12	2.3 ± 1.5
SHARDS20024698	12:37:03.5	62:14:29.7	4.31 ± 0.06	8.4 ± 2.5	81 ± 33	3.0 ± 1.4	—	—	—
SHARDS20004993	12:37:03.6	62:14:22.7	3.37 ± 0.07	7.4 ± 2.0	101 ± 15	3.0 ± 1.4	—	—	—
SHARDS20013448	12:37:03.6	62:11:58.5	5.22 ± 0.06	1.4 ± 0.5	15 ± 5	3.2 ± 1.4	—	—	—
SHARDS20006714	12:37:03.6	62:12:53.5	4.41 ± 0.06	1.4 ± 0.4	58 ± 18	2.5 ± 1.3			
SHARDS10010965	12:37:03.7	62:17:06.0	3.52 ± 0.06	1.4 ± 0.7	1100 ± 400	3.0 ± 1.6	0.3 ± 0.2	28 ± 12	1.6 ± 1.2
SHARDS10006438	12:37:03.7	62:14:54.5	4.20 ± 0.07	6.2 ± 1.9	83 ± 34	2.9 ± 1.4	—	—	—
SHARDS20011532	12:37:03.7	62:10:46.6	3.82 ± 0.06	2.7 ± 1.3	150 ± 80	3.0 ± 1.4	—	—	—
SHARDS20012876	12:37:03.7	62:11:57.7	5.22 ± 0.06	1.0 ± 0.4	18 ± 6	3.0 ± 1.4	—	—	—
SHARDS20025317	12:37:03.8	62:14:30.3	4.20 ± 0.07	7.8 ± 0.9	87 ± 16	2.8 ± 1.4	—	—	—
SHARDS20024717	12:37:03.8	62:14:29.5	4.44 ± 0.06	1.5 ± 0.7	59 ± 30	2.6 ± 1.4	—	—	—
SHARDS20011816	12:37:03.8	62:13:30.6	4.04 ± 0.06	0.1 ± 0.0	13 ± 5	2.9 ± 1.4	—	—	—
SHARDS10007523	12:37:03.9	62:15:02.9	4.45 ± 0.07	0.2 ± 0.1	13 ± 4	1.6 ± 0.9	—	—	—
SHARDS20002484	12:37:03.9	62:11:41.7	3.55 ± 0.06	8.2 ± 1.7	45 ± 12	2.2 ± 1.1			
SHARDS10012723	12:37:03.9	62:14:52.1	4.45 ± 0.07	133.0 ± 13.0	491 ± 142	3.0 ± 1.6	3.4 ± 0.3	28 ± 8	1.4 ± 0.9
SHARDS20005129	12:37:04.0	62:12:33.0	5.79 ± 0.06	1.4 ± 0.5	16 ± 6	1.5 ± 1.0			
SHARDS20004383	12:37:04.0	62:11:57.5	3.42 ± 0.07	27.0 ± 8.0	310 ± 50	3.0 ± 1.6	0.7 ± 0.2	15 ± 1	5.0 ± 0.0
SHARDS10011163	12:37:04.0	62:12:00.1	4.35 ± 0.06	27.7 ± 23.3	496 ± 235	3.0 ± 1.6	2.4 ± 3.9	33 ± 13	1.9 ± 1.4
SHARDS10007044	12:37:04.0	62:26:49.3	4.24 ± 0.07	6.0 ± 2.1	99 ± 41	3.0 ± 1.4			
SHARDS20012005	12:37:04.1	62:13:40.2	3.62 ± 0.06	4.8 ± 2.7	360 ± 300	3.0 ± 1.6	0.4 ± 0.6	27 ± 13	2.9 ± 1.6
SHARDS20009776	12:37:04.2	62:09:43.6	4.64 ± 0.07	1.3 ± 0.7	50 ± 26	2.4 ± 1.3	—	—	—
SHARDS10017960	12:37:04.2	62:16:36.1	3.79 ± 0.06	0.1 ± 0.0	13 ± 5	3.1 ± 1.4	—	—	—
SHARDS10007812	12:37:04.3	62:15:59.3	5.03 ± 0.06	8.7 ± 2.3	74 ± 24	2.8 ± 1.4			
SHARDS20002017	12:37:04.3	62:11:04.8	3.27 ± 0.07	12.4 ± 2.3	1230 ± 20	2.9 ± 1.6	0.3 ± 0.1	24 ± 1	3.5 ± 1.6
SHARDS10008370	12:37:04.4	62:16:19.4	4.34 ± 0.06	0.8 ± 0.3	34 ± 9	2.0 ± 1.1	—	—	—
SHARDS20007025	12:37:04.4	62:12:26.6	3.88 ± 0.06	0.7 ± 0.5	21 ± 25	2.4 ± 1.5			
SHARDS10011495	12:37:04.4	62:14:54.1	3.50 ± 0.06	11.0 ± 3.0	1300 ± 150	3.0 ± 1.6	0.4 ± 0.3	28 ± 9	1.3 ± 0.8
SHARDS10008398	12:37:04.5	62:17:20.1	4.77 ± 0.07	4.9 ± 1.7	97 ± 48	2.9 ± 1.4	—	—	—
SHARDS20012459	12:37:04.5	62:13:54.7	3.98 ± 0.06	0.7 ± 0.3	64 ± 32	2.7 ± 1.4			
SHARDS20010077	12:37:04.6	62:12:47.7	3.60 ± 0.06	7.3 ± 3.6	730 ± 420	3.0 ± 1.6	0.4 ± 0.4	17 ± 6	2.5 ± 1.6
SHARDS20007051	12:37:04.6	62:10:46.2	3.41 ± 0.07	0.4 ± 0.2	16 ± 6	2.9 ± 1.4	—	—	—
SHARDS20022732	12:37:04.8	62:14:17.6	3.90 ± 0.06	0.4 ± 0.3	23 ± 16	3.1 ± 1.5	—	—	—
SHARDS10007674	12:37:04.8	62:15:04.1	4.23 ± 0.07	1.3 ± 0.7	56 ± 31	2.5 ± 1.3	—	—	—
SHARDS10006795	12:37:04.9	62:13:00.1	4.45 ± 0.07	0.5 ± 0.2	20 ± 6	2.5 ± 1.4	—	—	—
SHARDS20022653	12:37:04.9	62:14:23.0	3.77 ± 0.06	6.2 ± 1.4	150 ± 50	3.0 ± 1.4	—	—	—
SHARDS10006417	12:37:04.9	62:15:44.1	3.51 ± 0.06	6.9 ± 0.8	85 ± 14	2.9 ± 1.4			
SHARDS10005494	12:37:05.0	62:15:05.7	4.60 ± 0.07	6.7 ± 2.3	869 ± 320	3.0 ± 1.6	1.1 ± 0.9	17 ± 4	1.3 ± 0.7
SHARDS20011722	12:37:05.0	62:11:44.7	5.36 ± 0.07	0.9 ± 0.1	14 ± 5	3.0 ± 1.4			
SHARDS20007194	12:37:05.0	62:13:45.4	3.76 ± 0.06	19.0 ± 4.0	538 ± 224	3.0 ± 1.6	1.3 ± 0.8	39 ± 12	2.3 ± 1.5
SHARDS10015749	12:37:05.0	62:16:22.3	4.47 ± 0.07	0.5 ± 0.5	29 ± 26	2.9 ± 1.4	—	—	—
SHARDS10003566	12:37:05.0	62:17:37.0	3.94 ± 0.06	10.3 ± 1.5	40 ± 6	1.9 ± 0.9	—	—	—
SHARDS20007957	12:37:05.1	62:13:07.4	4.18 ± 0.07	1.9 ± 0.7	60 ± 27	2.7 ± 1.4	—	—	—
SHARDS20006240	12:37:05.1	62:13:15.8	4.29 ± 0.06	1.4 ± 0.3	50 ± 7	1.5 ± 0.6	—	—	—
SHARDS10006378	12:37:05.1	62:16:43.5	4.34 ± 0.06	2.0 ± 0.7	24 ± 8	2.6 ± 1.3	—	—	—
SHARDS10004141	12:37:05.1	62:26:09.6	3.67 ± 0.06	0.8 ± 0.3	15 ± 5	2.2 ± 1.2	—	—	—
SHARDS20010628	12:37:05.3	62:12:23.9	4.27 ± 0.07	0.5 ± 0.2	45 ± 17	2.4 ± 1.3	—	—	—
SHARDS20007116	12:37:05.3	62:10:16.4	3.41 ± 0.07	1.7 ± 0.2	54 ± 4	3.3 ± 1.3	—	—	—
SHARDS10017828	12:37:05.3	62:16:09.7	4.46 ± 0.07	0.5 ± 0.3	49 ± 27	2.5 ± 1.3	—	—	—

Continued on next page

Table A.2 – *Continued from previous page*

Object Name	R.A. (J2000)	Dec. (J2000)	z	$M_{\rm star,m}$ ($10^9\,M_\odot$)	Age_m (Myr)	τ_m (Myr)	$M_{\rm star,b}$ ($10^9\,M_\odot$)	Age_b (Myr)	τ_b (Myr)
SHARDS10006400	12:37:05.4	62:16:11.0	4.46 ± 0.07	7.6 ± 6.6	610 ± 360	3.0 ± 1.6	5.0 ± 2.6	48 ± 7	2.5 ± 1.4
SHARDS20008799	12:37:05.4	62:13:13.2	4.87 ± 0.08	1.1 ± 0.5	46 ± 22	2.3 ± 1.3	–	–	–
SHARDS10006400	12:37:05.4	62:16:10.7	4.47 ± 0.07	30.0 ± 6.0	308 ± 120	3.0 ± 1.6	3.9 ± 2.6	30 ± 12	1.4 ± 1.0
SHARDS10007002	12:37:05.5	62:20:54.1	3.95 ± 0.06	1.9 ± 0.6	59 ± 22	2.6 ± 1.3	–	–	–
SHARDS10011501	12:37:05.5	62:16:01.3	5.17 ± 0.06	0.2 ± 0.1	16 ± 5	3.0 ± 1.4	–	–	–
SHARDS20002483	12:37:05.5	62:11:41.6	3.55 ± 0.06	9.2 ± 1.0	70 ± 8	2.9 ± 1.4	–	–	–
SHARDS10006027	12:37:05.5	62:20:09.0	4.24 ± 0.07	2.2 ± 0.8	63 ± 28	2.6 ± 1.3	–	–	–
SHARDS10006560	12:37:05.6	62:19:31.0	4.24 ± 0.07	3.5 ± 1.6	60 ± 32	2.6 ± 1.3	–	–	–
SHARDS10007841	12:37:05.6	62:16:03.9	6.21 ± 0.14	0.8 ± 0.3	20 ± 6	2.4 ± 1.3	–	–	–
SHARDS20014176	12:37:05.6	62:13:40.6	3.62 ± 0.06	7.1 ± 1.4	1230 ± 150	3.0 ± 1.6	0.2 ± 0.1	18 ± 3	4.5 ± 1.0
SHARDS10007944	12:37:05.6	62:20:38.1	3.81 ± 0.06	1.8 ± 0.4	85 ± 34	2.9 ± 1.4	–	–	–
SHARDS20008105	12:37:05.6	62:11:34.0	4.51 ± 0.07	3.6 ± 1.0	33 ± 10	1.8 ± 0.9	–	–	–
SHARDS20009084	12:37:05.7	62:13:42.3	5.27 ± 0.07	3.8 ± 0.8	39 ± 10	2.2 ± 1.1	–	–	–
SHARDS10009208	12:37:05.9	62:18:49.6	4.09 ± 0.07	0.1 ± 0.1	11 ± 3	3.4 ± 1.3	–	–	–
SHARDS20003052	12:37:06.0	62:12:52.0	3.36 ± 0.07	4.8 ± 0.6	89 ± 16	2.9 ± 1.4	–	–	–
SHARDS20007226	12:37:06.1	62:09:17.7	3.67 ± 0.06	0.7 ± 0.4	21 ± 12	3.3 ± 1.4	–	–	–
SHARDS20005167	12:37:06.1	62:10:00.1	3.54 ± 0.06	6.4 ± 0.8	47 ± 5	2.7 ± 1.2	–	–	–
SHARDS10002183	12:37:06.2	62:16:21.2	3.93 ± 0.06	0.5 ± 0.3	16 ± 6	2.3 ± 1.3	–	–	–
SHARDS20009961	12:37:06.2	62:09:42.0	5.06 ± 0.06	7.0 ± 2.4	60 ± 31	2.5 ± 1.3	–	–	–
SHARDS20017868	12:37:06.2	62:11:44.9	6.50 ± 0.11	3.1 ± 3.8	330 ± 250	3.0 ± 1.6	0.8 ± 1.0	21 ± 9	2.4 ± 1.4
SHARDS10009642	12:37:06.3	62:20:21.0	4.24 ± 0.07	1.0 ± 0.6	54 ± 31	2.5 ± 1.3	–	–	–
SHARDS10014162	12:37:06.4	62:16:55.8	4.34 ± 0.06	9.4 ± 1.2	1160 ± 170	3.0 ± 1.6	0.2 ± 0.0	23 ± 3	4.9 ± 0.4
SHARDS20018366	12:37:06.4	62:11:56.3	4.67 ± 0.07	23.0 ± 4.0	1080 ± 170	3.0 ± 1.6	0.6 ± 0.1	50 ± 0	2.3 ± 1.5
SHARDS20007435	12:37:06.5	62:13:20.5	3.62 ± 0.06	3.2 ± 2.4	740 ± 490	3.0 ± 1.6	0.9 ± 0.8	18 ± 5	3.7 ± 1.3
SHARDS10006812	12:37:06.5	62:15:22.8	5.30 ± 0.07	5.7 ± 4.4	267 ± 233	3.0 ± 1.6	0.7 ± 1.0	3 ± 2	3.3 ± 1.6
SHARDS10001631	12:37:06.5	62:15:35.4	3.51 ± 0.06	1.9 ± 0.5	21 ± 6	2.7 ± 1.3	–	–	–
SHARDS20004742	12:37:06.6	62:13:49.0	3.22 ± 0.07	12.0 ± 1.0	92 ± 5	3.2 ± 1.4	–	–	–
SHARDS20006584	12:37:06.7	62:13:48.3	3.37 ± 0.07	9.6 ± 1.8	97 ± 23	2.9 ± 1.4	–	–	–
SHARDS20008740	12:37:06.8	62:11:10.5	3.55 ± 0.06	7.8 ± 1.7	1310 ± 190	3.0 ± 1.6	0.3 ± 0.2	24 ± 6	1.1 ± 0.5
SHARDS20010093	12:37:06.8	62:10:28.5	3.82 ± 0.06	1.8 ± 0.7	86 ± 45	2.9 ± 1.4	–	–	–
SHARDS20011103	12:37:06.9	62:11:51.4	4.11 ± 0.07	0.7 ± 0.4	75 ± 44	2.8 ± 1.4	–	–	–
SHARDS20012384	12:37:06.9	62:12:11.6	5.24 ± 0.07	1.9 ± 1.0	61 ± 28	2.6 ± 1.4	–	–	–
SHARDS20010764	12:37:06.9	62:10:49.8	3.96 ± 0.06	0.7 ± 0.4	60 ± 31	2.6 ± 1.4	–	–	–
SHARDS20009601	12:37:06.9	62:10:38.3	3.41 ± 0.07	1.0 ± 0.4	72 ± 32	2.7 ± 1.4	–	–	–
SHARDS20005013	12:37:07.1	62:10:32.7	3.54 ± 0.06	41.0 ± 4.0	240 ± 40	3.0 ± 1.6	2.2 ± 0.9	25 ± 4	1.0 ± 0.3
SHARDS10006050	12:37:07.1	62:15:07.4	3.38 ± 0.07	1.7 ± 0.5	53 ± 19	2.7 ± 1.3	–	–	–
SHARDS10011034	12:37:07.1	62:17:21.6	3.80 ± 0.06	0.8 ± 0.4	73 ± 39	2.8 ± 1.4	–	–	–
SHARDS10013254	12:37:07.1	62:15:00.9	3.64 ± 0.06	0.2 ± 0.3	37 ± 42	2.9 ± 1.4	–	–	–
SHARDS10010974	12:37:07.2	62:17:23.4	3.80 ± 0.06	8.3 ± 2.5	1160 ± 240	3.0 ± 1.6	0.2 ± 0.1	24 ± 7	4.0 ± 1.4
SHARDS10017890	12:37:07.2	62:15:10.9	4.21 ± 0.07	1.3 ± 1.5	101 ± 119	3.0 ± 1.4	–	–	–
SHARDS20008806	12:37:07.3	62:13:31.1	3.90 ± 0.06	3.9 ± 1.4	120 ± 60	3.0 ± 1.4	–	–	–
SHARDS10016620	12:37:07.3	62:16:04.6	4.47 ± 0.07	0.4 ± 0.2	40 ± 19	2.2 ± 1.2	–	–	–
SHARDS20007684	12:37:07.3	62:11:24.6	4.11 ± 0.07	5.2 ± 1.6	130 ± 60	3.0 ± 1.4	–	–	–
SHARDS20004680	12:37:07.4	62:13:53.4	3.63 ± 0.06	63.0 ± 5.0	851 ± 109	3.0 ± 1.6	3.2 ± 0.5	25 ± 1	1.0 ± 0.1
SHARDS20008879	12:37:07.4	62:13:34.6	4.04 ± 0.07	7.2 ± 4.1	440 ± 360	3.0 ± 1.6	0.7 ± 0.9	30 ± 14	2.6 ± 1.6
SHARDS20007333	12:37:07.5	62:11:25.2	3.83 ± 0.06	1.8 ± 0.9	44 ± 23	2.2 ± 1.1	–	–	–
SHARDS20017009	12:37:07.6	62:12:38.1	4.29 ± 0.06	77.5 ± 15.0	1200 ± 100	3.0 ± 1.4	–	–	–
SHARDS10007935	12:37:07.7	62:16:35.3	3.93 ± 0.06	0.3 ± 0.1	16 ± 6	2.6 ± 1.4	–	–	–
SHARDS10014265	12:37:07.7	62:15:37.4	5.86 ± 0.06	8.4 ± 6.9	412 ± 237	3.0 ± 1.6	1.5 ± 1.8	15 ± 6	1.6 ± 1.0

Continued on next page

Table A.2 – *Continued from previous page*

Object Name	R.A. (J2000)	Dec. (J2000)	z	$M_{\rm star,m}$ ($10^9\ M_\odot$)	$\rm Age_m$ (Myr)	$\tau_{\rm m}$ (Myr)	$M_{\rm star,b}$ ($10^9\ M_\odot$)	$\rm Age_b$ (Myr)	$\tau_{\rm b}$ (Myr)
SHARDS20014756	12:37:07.8	62:10:35.4	3.41 ± 0.07	6.9 ± 1.9	909 ± 400	3.0 ± 1.6	0.4 ± 0.3	22 ± 9	2.8 ± 1.6
SHARDS20018464	12:37:07.8	62:14:02.8	3.49 ± 0.06	7.9 ± 1.3	1200 ± 100	2.9 ± 1.6	0.2 ± 0.0	23 ± 3	4.8 ± 0.7
SHARDS20006889	12:37:08.0	62:14:33.9	3.68 ± 0.06	1.4 ± 0.4	27 ± 8	3.1 ± 1.5	–	–	–
SHARDS20006636	12:37:08.0	62:12:10.9	5.50 ± 0.07	30.0 ± 10.0	480 ± 290	3.0 ± 1.6	1.9 ± 1.8	27 ± 10	2.4 ± 1.5
SHARDS10009030	12:37:08.0	62:15:47.7	4.22 ± 0.07	3.3 ± 1.1	78 ± 30	2.9 ± 1.4	1.2 ± 1.4	22 ± 8	2.2 ± 1.3
SHARDS10006921	12:37:08.1	62:14:34.9	4.60 ± 0.07	9.8 ± 6.0	570 ± 350	3.0 ± 1.6	–	–	–
SHARDS10010910	12:37:08.3	62:14:40.3	3.23 ± 0.07	0.6 ± 0.2	55 ± 29	2.6 ± 1.3	0.9 ± 1.1	25 ± 12	2.0 ± 1.3
SHARDS10015239	12:37:08.3	62:17:15.0	6.02 ± 0.07	4.2 ± 3.7	330 ± 260	3.0 ± 1.6	0.2 ± 0.1	22 ± 6	3.2 ± 1.6
SHARDS10010490	12:37:08.4	62:11:14.5	3.68 ± 0.06	7.4 ± 1.4	1180 ± 220	3.0 ± 1.6	–	–	–
SHARDS10008970	12:37:08.5	62:15:05.1	5.30 ± 0.07	0.6 ± 0.3	24 ± 8	2.6 ± 1.4	1.1 ± 1.1	33 ± 13	1.8 ± 1.3
SHARDS20013235	12:37:08.5	62:09:32.6	3.81 ± 0.06	8.0 ± 2.9	990 ± 380	3.0 ± 1.6	0.4 ± 0.4	23 ± 8	1.2 ± 0.8
SHARDS20009681	12:37:08.6	62:13:33.2	4.19 ± 0.07	2.9 ± 1.2	880 ± 320	3.0 ± 1.6	1.2 ± 0.6	20 ± 1	1.8 ± 1.0
SHARDS10000381	12:37:08.6	62:14:26.3	3.91 ± 0.06	34.0 ± 9.0	1300 ± 300	3.0 ± 1.6	–	–	–
SHARDS20009051	12:37:08.7	62:09:51.6	4.24 ± 0.07	0.4 ± 0.1	37 ± 14	2.1 ± 1.1	0.1 ± 0.4	7 ± 7	3.4 ± 1.6
SHARDS10017359	12:37:08.8	62:14:17.4	4.45 ± 0.07	0.7 ± 2.9	430 ± 360	3.0 ± 1.6	–	–	–
SHARDS20013188	12:37:08.8	62:12:03.6	3.74 ± 0.06	1.3 ± 0.5	24 ± 9	2.6 ± 1.4	–	–	–
SHARDS20006923	12:37:08.8	62:12:42.7	3.96 ± 0.06	0.1 ± 0.1	18 ± 6	2.6 ± 1.4	–	–	–
SHARDS20008463	12:37:08.9	62:11:39.7	3.42 ± 0.07	1.0 ± 0.3	37 ± 11	2.1 ± 1.1	–	–	–
SHARDS10003587	12:37:09.0	62:11:29.4	3.67 ± 0.06	0.7 ± 0.2	15 ± 5	2.5 ± 1.2	–	–	–
SHARDS20012347	12:37:09.1	62:10:11.2	4.65 ± 0.07	0.2 ± 0.1	22 ± 10	2.6 ± 1.4	–	–	–
SHARDS10006899	12:37:09.1	62:15:18.7	4.61 ± 0.07	9.7 ± 4.8	710 ± 310	3.0 ± 1.6	1.2 ± 1.2	43 ± 11	2.3 ± 1.5
SHARDS10007913	12:37:09.1	62:13:01.5	3.81 ± 0.06	37.0 ± 5.0	433 ± 115	3.0 ± 1.6	1.5 ± 0.9	37 ± 12	1.7 ± 1.3
SHARDS10008659	12:37:09.2	62:15:15.9	4.46 ± 0.07	14.0 ± 6.0	610 ± 280	3.0 ± 1.6	1.3 ± 1.4	24 ± 7	1.1 ± 0.6
SHARDS20009757	12:37:09.2	62:10:41.6	4.37 ± 0.06	1.0 ± 0.5	62 ± 32	2.6 ± 1.4	–	–	–
SHARDS20009608	12:37:09.3	62:13:29.7	3.62 ± 0.06	0.3 ± 0.2	18 ± 8	2.7 ± 1.4	–	–	–
SHARDS10014616	12:37:09.3	62:16:18.5	5.87 ± 0.06	7.9 ± 6.1	408 ± 244	3.0 ± 1.6	1.0 ± 1.3	18 ± 5	2.4 ± 1.3
SHARDS10007012	12:37:09.3	62:16:00.7	3.93 ± 0.06	7.0 ± 2.1	1000 ± 370	3.0 ± 1.6	0.3 ± 0.2	15 ± 5	2.8 ± 1.6
SHARDS10010257	12:37:09.4	62:19:04.7	4.93 ± 0.08	2.4 ± 1.6	93 ± 63	2.8 ± 1.4	–	–	–
SHARDS20008657	12:37:09.5	62:13:42.4	4.31 ± 0.06	1.4 ± 0.6	66 ± 30	2.7 ± 1.4	–	–	–
SHARDS20009264	12:37:09.5	62:09:56.4	4.65 ± 0.07	3.2 ± 1.4	52 ± 26	2.5 ± 1.3	–	–	–
SHARDS10009202	12:37:09.6	62:14:57.0	3.64 ± 0.06	17.0 ± 6.0	258 ± 113	3.0 ± 1.6	1.3 ± 0.7	16 ± 5	2.0 ± 1.1
SHARDS20002042	12:37:09.6	62:11:07.3	3.42 ± 0.07	6.0 ± 0.8	39 ± 7	1.8 ± 0.9	–	–	–
SHARDS10004461	12:37:09.7	62:12:07.1	3.96 ± 0.06	27.0 ± 4.0	636 ± 176	3.0 ± 1.6	2.8 ± 0.6	24 ± 2	2.7 ± 0.8
SHARDS20001516	12:37:09.7	62:20:16.5	3.41 ± 0.07	5.6 ± 1.9	61 ± 60	2.6 ± 1.3	–	–	–
SHARDS10009342	12:37:09.8	62:20:35.7	3.41 ± 0.07	2.4 ± 0.9	130 ± 60	3.0 ± 1.4	–	–	–
SHARDS10011820	12:37:09.8	62:14:09.5	3.91 ± 0.06	0.5 ± 0.2	19 ± 8	3.3 ± 1.4	–	–	–
SHARDS20024692	12:37:09.8	62:14:00.3	3.63 ± 0.06	20.2 ± 1.2	960 ± 100	3.0 ± 1.6	0.6 ± 0.3	25 ± 3	1.1 ± 0.5
SHARDS10010161	12:37:09.8	62:16:07.2	4.62 ± 0.07	2.9 ± 1.5	60 ± 34	2.7 ± 1.4	–	–	–
SHARDS10005946	12:37:09.8	62:21:11.3	5.07 ± 0.06	24.4 ± 2.5	108 ± 14	2.9 ± 1.4	–	–	–
SHARDS10001004	12:37:09.8	62:14:29.4	3.38 ± 0.07	20.0 ± 4.0	69 ± 15	2.8 ± 1.4	–	–	–
SHARDS20025321	12:37:09.8	62:14:01.9	3.91 ± 0.06	1.2 ± 0.4	16 ± 6	1.8 ± 1.2	–	–	–
SHARDS10005528	12:37:09.8	62:14:39.4	4.32 ± 0.06	54.0 ± 8.0	557 ± 134	3.0 ± 1.6	2.6 ± 0.7	20 ± 1	1.0 ± 0.0
SHARDS10011670	12:37:09.9	62:15:31.0	5.17 ± 0.06	1.1 ± 0.7	60 ± 32	2.6 ± 1.4	–	–	–
SHARDS10013088	12:37:09.9	62:16:08.9	3.65 ± 0.06	0.6 ± 0.3	65 ± 34	2.7 ± 1.4	–	–	–
SHARDS20008810	12:37:10.0	62:13:48.3	3.63 ± 0.06	2.4 ± 0.6	67 ± 21	2.8 ± 1.4	–	–	–
SHARDS10013903	12:37:10.0	62:15:39.4	3.65 ± 0.06	0.3 ± 0.3	35 ± 34	2.9 ± 1.4	–	–	–
SHARDS10006039	12:37:10.0	62:20:48.0	4.92 ± 0.08	123.0 ± 16.0	482 ± 123	3.0 ± 1.6	3.2 ± 0.4	50 ± 0	3.0 ± 1.6
SHARDS10006603	12:37:10.2	62:20:01.0	4.25 ± 0.07	3.5 ± 0.7	40 ± 8	2.2 ± 1.1	–	–	–
SHARDS20015541	12:37:10.2	62:12:18.3	5.69 ± 0.06	85.2 ± 13.4	902 ± 113	3.0 ± 1.6	2.2 ± 0.3	50 ± 0	2.6 ± 1.6

Continued on next page

Table A.2 – *Continued from previous page*

Object Name	R.A. (J2000)	Dec. (J2000)	z	$M_{\rm star,m}$ (10^9 $M_\odot$)	Age_m (Myr)	τ_m (Myr)	$M_{\rm star,b}$ (10^9 $M_\odot$)	Age_b (Myr)	τ_b (Myr)
SHARDS10010350	12:37:10.2	62:16:50.5	4.63 ± 0.07	4.0 ± 2.6	790 ± 380	3.0 ± 1.6	1.2 ± 1.0	23 ± 7	1.2 ± 0.7
SHARDS10009059	12:37:10.4	62:14:48.6	3.78 ± 0.06	0.5 ± 0.2	29 ± 13	2.6 ± 1.4	–	–	–
SHARDS20024706	12:37:10.5	62:13:58.5	4.59 ± 0.07	0.3 ± 0.1	20 ± 8	2.5 ± 1.4	–	–	–
SHARDS20009275	12:37:10.5	62:11:58.0	4.02 ± 0.07	0.8 ± 0.3	51 ± 19	2.5 ± 1.3	–	–	–
SHARDS20009738	12:37:10.6	62:10:27.6	4.50 ± 0.07	0.3 ± 0.1	13 ± 4	3.0 ± 1.3	–	–	–
SHARDS10005835	12:37:10.6	62:14:52.6	3.64 ± 0.06	5.9 ± 1.5	86 ± 19	3.0 ± 1.4	–	–	–
SHARDS20004928	12:37:10.7	62:12:39.0	3.83 ± 0.06	12.0 ± 3.0	44 ± 7	1.8 ± 0.9	–	–	–
SHARDS10005433	12:37:10.7	62:16:10.0	4.6 ± 0.07	13.8 ± 8.0	400 ± 330	3.0 ± 1.6	6.0 ± 3.0	35 ± 12	1.5 ± 1.0
SHARDS10001648	12:37:10.9	62:15:36.8	3.51 ± 0.06	0.8 ± 0.2	39 ± 11	1.9 ± 1.0	–	–	–
SHARDS20001484	12:37:10.9	62:10:13.4	3.41 ± 0.07	8.9 ± 3.0	58 ± 24	2.3 ± 1.3	–	–	–
SHARDS10005647	12:37:10.9	62:20:59.8	4.25 ± 0.07	40.7 ± 11.1	541 ± 154	3.0 ± 1.6	3.4 ± 1.4	23 ± 2	1.0 ± 0.0
SHARDS20001899	12:37:11.0	62:10:54.8	3.41 ± 0.07	4.9 ± 0.8	81 ± 16	2.8 ± 1.4	–	–	–
SHARDS10010091	12:37:11.1	62:15:34.9	4.47 ± 0.07	4.3 ± 2.6	110 ± 80	2.9 ± 1.4	–	–	–
SHARDS10008299	12:37:11.1	62:16:38.6	5.19 ± 0.06	9.8 ± 3.4	174 ± 227	3.0 ± 1.6	1.9 ± 2.2	29 ± 14	3.3 ± 1.6
SHARDS10006279	12:37:11.1	62:15:04.7	4.46 ± 0.07	0.6 ± 0.1	20 ± 3	1.2 ± 0.4	–	–	–
SHARDS20022683	12:37:11.1	62:12:43.5	3.89 ± 0.06	81.1 ± 14.8	1100 ± 300	3.0 ± 1.6	2.5 ± 0.9	43 ± 11	2.6 ± 1.6
SHARDS10005969	12:37:11.1	62:16:14.0	3.52 ± 0.06	1.8 ± 0.6	280 ± 330	3.0 ± 1.6	0.4 ± 0.3	18 ± 7	3.8 ± 1.6
SHARDS10006745	12:37:11.5	62:20:20.7	4.25 ± 0.07	2.4 ± 0.3	58 ± 10	2.5 ± 1.2	–	–	–
SHARDS10004929	12:37:11.5	62:21:55.5	4.10 ± 0.07	41.0 ± 6.0	61 ± 9	2.5 ± 1.2	–	–	–
SHARDS10012240	12:37:11.6	62:20:54.2	3.82 ± 0.06	52.0 ± 7.0	1420 ± 140	3.0 ± 1.6	1.4 ± 0.3	50 ± 1	3.2 ± 1.6
SHARDS20024273	12:37:11.6	62:12:54.3	4.42 ± 0.07	28.0 ± 5.0	860 ± 250	3.0 ± 1.6	1.5 ± 0.8	43 ± 11	2.4 ± 1.5
SHARDS10007484	12:37:11.7	62:15:07.2	4.46 ± 0.07	0.8 ± 0.4	26 ± 11	2.5 ± 1.4	–	–	–
SHARDS10008124	12:37:11.7	62:18:27.2	5.20 ± 0.06	1.9 ± 0.5	62 ± 15	2.7 ± 1.4	–	–	–
SHARDS20010003	12:37:11.9	62:11:52.6	5.22 ± 0.06	0.6 ± 0.3	28 ± 12	2.5 ± 1.3	–	–	–
SHARDS10005600	12:37:11.9	62:14:35.0	4.45 ± 0.07	3.4 ± 1.2	34 ± 10	1.7 ± 0.9	–	–	–
SHARDS20007787	12:37:11.9	62:10:02.9	4.49 ± 0.07	3.9 ± 1.6	65 ± 32	2.6 ± 1.4	–	–	–
SHARDS20008760	12:37:12.0	62:11:37.0	4.80 ± 0.07	0.5 ± 0.2	27 ± 10	2.3 ± 1.3	–	–	–
SHARDS20008702	12:37:12.1	62:10:54.1	5.21 ± 0.06	0.5 ± 0.2	18 ± 6	2.8 ± 1.4	–	–	–
SHARDS10006628	12:37:12.1	62:20:39.6	3.96 ± 0.06	4.7 ± 3.2	710 ± 430	3.0 ± 1.6	0.8 ± 0.9	17 ± 6	2.2 ± 1.4
SHARDS10006574	12:37:12.3	62:14:36.1	4.33 ± 0.06	0.3 ± 0.1	21 ± 6	2.1 ± 1.2	–	–	–
SHARDS10006858	12:37:12.3	62:14:16.5	4.60 ± 0.07	1.9 ± 0.6	59 ± 20	2.6 ± 1.3	–	–	–
SHARDS10008529	12:37:12.3	62:16:26.0	4.35 ± 0.06	0.2 ± 0.1	18 ± 5	2.7 ± 1.4	–	–	–
SHARDS10007096	12:37:12.3	62:15:32.9	3.65 ± 0.06	3.8 ± 2.6	1000 ± 400	3.0 ± 1.6	1.2 ± 1.0	23 ± 5	1.1 ± 0.4
SHARDS10005562	12:37:12.3	62:16:07.6	4.08 ± 0.07	5.2 ± 2.0	74 ± 13	2.9 ± 1.4	–	–	–
SHARDS10014170	12:37:12.4	62:18:28.1	6.24 ± 0.14	15.0 ± 10.0	459 ± 250	3.0 ± 1.6	2.5 ± 2.9	18 ± 5	2.3 ± 1.2
SHARDS10018196	12:37:12.5	62:15:21.1	5.17 ± 0.06	0.1 ± 0.1	12 ± 4	3.2 ± 1.4	–	–	–
SHARDS20011614	12:37:12.5	62:10:23.5	3.54 ± 0.06	0.1 ± 0.1	13 ± 4	3.1 ± 1.4	–	–	–
SHARDS10007175	12:37:12.6	62:21:37.7	4.37 ± 0.06	0.3 ± 0.2	16 ± 6	2.4 ± 1.3	–	–	–
SHARDS10005464	12:37:12.6	62:21:59.3	4.65 ± 0.07	45.0 ± 8.0	704 ± 198	3.0 ± 1.6	2.9 ± 2.1	28 ± 10	1.3 ± 0.7
SHARDS10009762	12:37:12.6	62:15:04.2	6.00 ± 0.07	17.0 ± 10.0	318 ± 204	3.0 ± 1.6	1.1 ± 1.4	23 ± 11	2.2 ± 1.4
SHARDS10012105	12:37:12.6	62:14:53.2	3.51 ± 0.06	1.0 ± 0.4	66 ± 33	2.7 ± 1.4	–	–	–
SHARDS20008527	12:37:12.7	62:10:48.8	4.66 ± 0.07	5.3 ± 2.7	68 ± 39	2.7 ± 1.4	–	–	–
SHARDS10006379	12:37:12.8	62:16:58.7	4.36 ± 0.06	2.9 ± 0.9	47 ± 19	2.2 ± 1.2	–	–	–
SHARDS20007254	12:37:12.8	62:11:32.0	5.10 ± 0.06	4.8 ± 1.4	69 ± 26	2.7 ± 1.4	–	–	–
SHARDS10006522	12:37:12.8	62:21:27.3	4.25 ± 0.07	2.4 ± 0.9	46 ± 18	2.3 ± 1.2	–	–	–
SHARDS10006064	12:37:12.9	62:21:36.7	3.41 ± 0.07	8.6 ± 1.8	110 ± 30	2.3 ± 1.4	–	–	–
SHARDS10005830	12:37:13.0	62:21:42.4	3.68 ± 0.06	4.8 ± 0.9	81 ± 16	2.9 ± 1.4	–	–	–
SHARDS10005728	12:37:13.0	62:20:26.8	3.26 ± 0.07	1.8 ± 0.5	43 ± 14	2.2 ± 1.1	–	–	–
SHARDS10005007	12:37:13.0	62:21:11.2	4.25 ± 0.07	29.4 ± 23.3	530 ± 290	3.0 ± 1.6	23.0 ± 7.0	48 ± 7	2.5 ± 0.9

Continued on next page

Table A.2 – *Continued from previous page*

Object Name	R.A. (J2000)	Dec. (J2000)	z	$M_{\rm star,m}$ (10^9 $M_\odot$)	$\rm Age_m$ (Myr)	$\tau_{\rm m}$ (Myr)	$M_{\rm star,b}$ (10^9 $M_\odot$)	$\rm Age_b$ (Myr)	$\tau_{\rm b}$ (Myr)
SHARDS2001691918	12:37:13.1	62:12:06.7	6.61 ± 0.14	6.3 ± 3.5	150 ± 80	2.9 ± 1.4	—	—	—
SHARDS1006384	12:37:13.1	62:16:06.7	3.94 ± 0.06	3.3 ± 0.9	29 ± 8	3.2 ± 1.4	—	—	—
SHARDS1011694	12:37:13.1	62:18:24.1	4.25 ± 0.07	2.8 ± 0.9	50 ± 20	2.6 ± 1.3	—	—	—
SHARDS1007072	12:37:13.2	62:18:44.6	3.68 ± 0.06	1.1 ± 0.5	60 ± 28	2.6 ± 1.4	—	—	—
SHARDS2007630	12:37:13.2	62:21:08.9	4.26 ± 0.07	4.7 ± 1.2	80 ± 30	2.9 ± 1.4	—	—	—
SHARDS1006128	12:37:13.2	62:21:21.4	4.25 ± 0.07	5.0 ± 2.9	60 ± 32	2.4 ± 1.3	—	—	—
SHARDS1006324	12:37:13.2	62:15:47.8	4.62 ± 0.07	49.3 ± 16.1	354 ± 111	3.0 ± 1.6	15.0 ± 4.0	49 ± 6	2.1 ± 1.1
SHARDS1010954	12:37:13.3	62:16:06.4	3.52 ± 0.06	2.9 ± 0.4	59 ± 10	2.5 ± 1.2	—	—	—
SHARDS1005737	12:37:13.4	62:21:39.2	5.26 ± 0.07	3.5 ± 0.8	42 ± 12	2.0 ± 1.0	—	—	—
SHARDS1007421	12:37:13.7	62:21:02.9	5.26 ± 0.07	1.5 ± 0.6	55 ± 23	2.5 ± 1.3	—	—	—
SHARDS1007446	12:37:13.8	62:18:48.8	4.50 ± 0.07	1.1 ± 0.6	30 ± 14	1.7 ± 0.9	—	—	—
SHARDS1014567	12:37:13.8	62:15:38.7	4.35 ± 0.06	0.6 ± 0.4	44 ± 27	2.3 ± 1.3	—	—	—
SHARDS2002400	12:37:13.8	62:11:35.2	3.60 ± 0.06	3.6 ± 0.7	32 ± 6	4.1 ± 1.1	—	—	—
SHARDS1011575	12:37:14.0	62:14:14.1	3.64 ± 0.06	0.2 ± 0.2	19 ± 15	3.1 ± 1.4	—	—	—
SHARDS2010744	12:37:14.0	62:11:35.0	4.27 ± 0.07	1.2 ± 1.6	77 ± 42	2.8 ± 1.6	1.8 ± 1.1	39 ± 13	2.0 ± 1.5
SHARDS1007654	12:37:14.0	62:18:39.2	3.96 ± 0.06	27.0 ± 7.0	$1\,100 \pm 400$	3.0 ± 1.6	—	—	—
SHARDS1007983	12:37:14.0	62:16:31.6	4.63 ± 0.07	7.5 ± 1.6	110 ± 30	2.9 ± 1.4	—	—	—
SHARDS1011747	12:37:14.1	62:14:45.7	3.79 ± 0.06	0.3 ± 0.2	28 ± 19	2.8 ± 1.4	—	—	—
SHARDS1010712	12:37:14.1	62:15:51.9	4.47 ± 0.07	0.3 ± 0.2	47 ± 26	2.5 ± 1.3	—	—	—
SHARDS2004562	12:37:14.2	62:11:03.8	3.82 ± 0.06	16.6 ± 2.5	71 ± 11	3.0 ± 1.4	—	—	—
SHARDS1009188	12:37:14.3	62:17:09.7	4.24 ± 0.07	0.8 ± 0.2	49 ± 16	2.4 ± 1.2	—	—	—
SHARDS2002641	12:37:14.4	62:12:18.1	3.75 ± 0.06	0.8 ± 0.3	57 ± 21	2.6 ± 1.3	—	—	—
SHARDS1007197	12:37:14.4	62:15:18.9	4.34 ± 0.06	2.8 ± 1.1	96 ± 43	2.9 ± 1.4	—	—	—
SHARDS1007532	12:37:14.4	62:19:48.9	5.35 ± 0.07	12.0 ± 6.0	580 ± 270	3.0 ± 1.6	0.6 ± 0.8	20 ± 6	2.4 ± 1.2
SHARDS1008210	12:37:14.5	62:15:32.4	5.18 ± 0.06	6.9 ± 3.6	52 ± 34	2.3 ± 1.2	—	—	—
SHARDS1011225	12:37:14.6	62:13:19.0	5.56 ± 0.07	1.8 ± 0.9	43 ± 21	2.2 ± 1.2	—	—	—
SHARDS1005807	12:37:14.6	62:14:33.5	3.78 ± 0.06	4.3 ± 1.2	58 ± 19	3.0 ± 1.4	—	—	—
SHARDS1005754	12:37:14.7	62:18:39.4	3.41 ± 0.07	148.0 ± 12.0	670 ± 80	3.0 ± 1.6	3.8 ± 0.3	50 ± 0	3.9 ± 1.4
SHARDS1010276	12:37:14.8	62:20:14.8	5.48 ± 0.07	9.0 ± 7.0	440 ± 310	3.0 ± 1.6	1.8 ± 2.0	37 ± 13	2.0 ± 1.5
SHARDS1009652	12:37:14.8	62:15:25.8	3.24 ± 0.07	1.1 ± 0.3	48 ± 23	2.5 ± 1.3	—	—	—
SHARDS1004426	12:37:15.0	62:19:25.5	3.82 ± 0.06	5.5 ± 0.9	32 ± 6	1.7 ± 0.7	—	—	—
SHARDS2009644	12:37:15.1	62:13:38.2	3.60 ± 0.06	7.2 ± 2.1	19 ± 10	2.8 ± 1.4	—	—	—
SHARDS1007280	12:37:15.1	62:13:42.5	4.44 ± 0.07	7.1 ± 2.2	120 ± 40	3.0 ± 1.4	—	—	—
SHARDS1005201	12:37:15.1	62:20:31.0	3.68 ± 0.06	14.7 ± 1.6	60 ± 5	2.8 ± 1.4	—	—	—
SHARDS1005986	12:37:15.1	62:20:46.2	4.11 ± 0.07	1.0 ± 0.3	41 ± 14	2.0 ± 1.1	—	—	—
SHARDS2008507	12:37:15.1	62:20:40.4	5.63 ± 0.07	29.5 ± 13.4	353 ± 227	3.0 ± 1.6	5.2 ± 4.4	43 ± 11	2.2 ± 1.4
SHARDS2009005	12:37:15.2	62:11:19.9	4.68 ± 0.07	0.1 ± 0.0	15 ± 4	2.6 ± 1.4	—	—	—
SHARDS2016927	12:37:15.2	62:12:03.1	5.33 ± 0.07	0.3 ± 0.2	33 ± 5	3.0 ± 1.4	—	—	—
SHARDS1005399	12:37:15.2	62:19:14.5	4.37 ± 0.06	4.8 ± 0.7	29 ± 5	1.6 ± 0.7	—	—	—
SHARDS1013708	12:37:15.3	62:13:35.5	5.45 ± 0.07	9.9 ± 5.9	570 ± 300	3.0 ± 1.6	1.2 ± 1.4	24 ± 11	1.8 ± 1.2
SHARDS1006852	12:37:15.5	62:14:11.3	4.45 ± 0.07	19.2 ± 2.2	780 ± 40	2.9 ± 1.4	—	—	—
SHARDS2022654	12:37:15.5	62:12:08.6	4.03 ± 0.07	15.0 ± 3.0	795 ± 210	3.0 ± 1.6	1.2 ± 0.5	49 ± 1	2.1 ± 1.1
SHARDS1006557	12:37:15.6	62:16:23.6	5.19 ± 0.06	3.1 ± 1.1	96 ± 15	2.7 ± 1.4	—	—	—
SHARDS1006572	12:37:15.6	62:16:47.8	4.36 ± 0.06	4.3 ± 1.2	70 ± 28	2.7 ± 1.4	—	—	—
SHARDS1011518	12:37:15.7	62:13:49.8	5.45 ± 0.07	2.0 ± 0.9	52 ± 21	2.4 ± 1.3	—	—	—
SHARDS2010726	12:37:15.7	62:10:57.2	3.54 ± 0.06	0.3 ± 0.2	26 ± 20	3.0 ± 1.4	—	—	—
SHARDS1012250	12:37:15.8	62:12:53.9	5.27 ± 0.07	1.5 ± 0.7	48 ± 22	2.4 ± 1.3	—	—	—
SHARDS1007152	12:37:15.8	62:16:47.4	4.24 ± 0.07	1.2 ± 0.8	84 ± 55	2.8 ± 1.4	—	—	—
SHARDS1005443	12:37:15.8	62:16:49.2	4.09 ± 0.07	1.2 ± 0.1	36 ± 4	1.8 ± 0.8	—	—	—

Continued on next page

Table A.2 – *Continued from previous page*

Object Name	R.A. (J2000)	Dec. (J2000)	z	$M_{\rm star,m}$ (10^9 $M_\odot$)	$\rm Age_m$ (Myr)	$\tau_{\rm m}$ (Myr)	$M_{\rm star,b}$ (10^9 $M_\odot$)	$\rm Age_b$ (Myr)	$\tau_{\rm b}$ (Myr)
SHARDS10006107	12:37:15.9	62:18:22.9	4.25 ± 0.07	9.3 ± 3.7	883 ± 249	3.0 ± 1.6	1.4 ± 1.2	41 ± 12	2.1 ± 1.3
SHARDS10006353	12:37:16.1	62:19:27.8	3.54 ± 0.06	7.9 ± 3.2	450 ± 409	3.0 ± 1.6	2.0 ± 1.5	37 ± 13	2.2 ± 1.6
SHARDS20008439	12:37:16.2	62:10:50.3	3.41 ± 0.07	1.0 ± 0.5	46 ± 23	2.3 ± 1.3	–	–	–
SHARDS10008541	12:37:16.2	62:13:35.5	5.01 ± 0.06	0.2 ± 0.1	19 ± 6	2.6 ± 1.4	–	–	–
SHARDS10010911	12:37:16.3	62:14:59.5	4.76 ± 0.07	1.1 ± 0.5	55 ± 25	2.5 ± 1.3	–	–	–
SHARDS20015851	12:37:16.3	62:10:53.4	5.80 ± 0.06	65.0 ± 346.0	51 ± 149	2.9 ± 1.4	–	–	–
SHARDS10014767	12:37:16.3	62:13:37.3	4.20 ± 0.07	3.8 ± 1.6	90 ± 57	2.9 ± 1.4	–	–	–
SHARDS10007889	12:37:16.3	62:22:17.4	3.42 ± 0.07	13.0 ± 5.0	990 ± 400	3.0 ± 1.6	0.7 ± 0.7	20 ± 6	2.2 ± 1.2
SHARDS10006452	12:37:16.4	62:16:58.8	3.40 ± 0.07	0.5 ± 0.2	17 ± 6	2.7 ± 1.5	–	–	–
SHARDS10015417	12:37:16.4	62:14:57.3	6.21 ± 0.14	0.1 ± 0.1	15 ± 5	2.9 ± 1.4	–	–	–
SHARDS10007736	12:37:16.5	62:20:07.3	4.80 ± 0.07	16.0 ± 4.0	160 ± 50	3.0 ± 1.4	–	–	–
SHARDS10011638	12:37:16.6	62:15:51.9	3.94 ± 0.06	0.3 ± 0.1	45 ± 20	2.4 ± 1.3	–	–	–
SHARDS10005186	12:37:16.6	62:13:53.4	3.50 ± 0.06	3.7 ± 0.6	74 ± 25	2.7 ± 1.3	–	–	–
SHARDS10007051	12:37:16.7	62:19:27.2	3.54 ± 0.06	6.0 ± 2.1	120 ± 50	2.9 ± 1.4	–	–	–
SHARDS20022719	12:37:16.7	62:12:04.0	4.57 ± 0.07	25.5 ± 10.1	670 ± 250	3.0 ± 1.6	4.1 ± 3.2	48 ± 8	2.1 ± 1.2
SHARDS10008600	12:37:16.7	62:16:17.7	3.66 ± 0.06	0.4 ± 0.2	18 ± 6	2.9 ± 1.4	–	–	–
SHARDS10007105	12:37:16.7	62:17:50.0	3.95 ± 0.06	3.4 ± 1.4	65 ± 32	2.6 ± 1.4	–	–	–
SHARDS20011741	12:37:16.7	62:11:16.6	3.73 ± 0.06	12.0 ± 4.0	1000 ± 400	3.0 ± 1.6	0.6 ± 0.4	41 ± 12	2.3 ± 1.6
SHARDS10005719	12:37:16.8	62:20:44.7	3.83 ± 0.06	0.5 ± 0.2	15 ± 6	2.2 ± 1.5	–	–	–
SHARDS10006981	12:37:16.9	62:14:00.4	5.29 ± 0.07	15.0 ± 4.0	66 ± 23	2.9 ± 1.4	–	–	–
SHARDS10008733	12:37:17.0	62:21:44.8	3.55 ± 0.06	16.0 ± 3.0	1250 ± 180	3.0 ± 1.6	0.5 ± 0.2	27 ± 10	1.4 ± 1.1
SHARDS10003104	12:37:17.1	62:18:19.8	3.68 ± 0.06	56.0 ± 8.0	432 ± 142	3.0 ± 1.6	3.8 ± 1.5	32 ± 11	1.2 ± 0.7
SHARDS10003900	12:37:17.1	62:21:10.3	3.27 ± 0.07	11.0 ± 1.6	58 ± 9	2.8 ± 1.3	–	–	–
SHARDS20011164	12:37:17.2	62:11:01.5	4.25 ± 0.07	1.5 ± 0.9	800 ± 350	3.0 ± 1.6	0.3 ± 0.3	26 ± 11	1.4 ± 1.1
SHARDS10007056	12:37:17.2	62:18:59.3	3.96 ± 0.06	0.2 ± 0.1	16 ± 6	2.6 ± 1.4	–	–	–
SHARDS10014408	12:37:17.2	62:14:59.8	4.22 ± 0.07	0.3 ± 0.2	16 ± 6	3.1 ± 1.4	–	–	–
SHARDS10007661	12:37:17.3	62:20:05.9	4.38 ± 0.06	4.0 ± 1.4	99 ± 40	2.9 ± 1.4	–	–	–
SHARDS10007224	12:37:17.3	62:14:02.5	3.92 ± 0.06	13.0 ± 3.0	1280 ± 230	3.0 ± 1.6	0.7 ± 0.4	22 ± 4	1.0 ± 0.3
SHARDS10008525	12:37:17.3	62:13:25.3	5.15 ± 0.06	3.0 ± 1.1	66 ± 27	2.7 ± 1.4	–	–	–
SHARDS10005633	12:37:17.5	62:16:38.5	4.49 ± 0.07	22.0 ± 4.0	101 ± 23	2.6 ± 1.4	–	–	–
SHARDS10005716	12:37:17.6	62:19:26.3	4.11 ± 0.07	11.8 ± 2.3	73 ± 18	3.0 ± 1.4	–	–	–
SHARDS10006402	12:37:17.6	62:13:28.1	3.50 ± 0.06	6.0 ± 2.6	1000 ± 400	3.0 ± 1.6	0.3 ± 0.3	17 ± 4	3.1 ± 1.5
SHARDS10000432	12:37:17.6	62:13:09.7	3.37 ± 0.07	1.2 ± 0.5	42 ± 23	2.3 ± 1.2	–	–	–
SHARDS10003772	12:37:17.7	62:21:49.4	3.27 ± 0.07	5.2 ± 0.9	52 ± 9	2.4 ± 1.2	–	–	–
SHARDS10004588	12:37:17.7	62:19:04.6	3.96 ± 0.06	4.4 ± 0.6	66 ± 9	2.7 ± 1.3	–	–	–
SHARDS10007493	12:37:17.7	62:20:30.7	3.83 ± 0.06	11.0 ± 6.0	660 ± 380	3.0 ± 1.6	2.6 ± 2.1	49 ± 5	2.2 ± 1.3
SHARDS10005275	12:37:17.8	62:13:04.1	4.31 ± 0.06	5.7 ± 0.5	74 ± 6	2.6 ± 1.3	–	–	–
SHARDS10012747	12:37:17.9	62:15:40.8	5.88 ± 0.06	0.6 ± 0.4	23 ± 8	2.3 ± 1.3	–	–	–
SHARDS10010884	12:37:17.9	62:17:59.1	5.62 ± 0.07	0.8 ± 0.4	19 ± 6	3.0 ± 1.4	–	–	–
SHARDS10005406	12:37:17.9	62:17:15.6	4.25 ± 0.07	14.0 ± 1.0	111 ± 10	3.0 ± 1.4	–	–	–
SHARDS20025351	12:37:18.0	62:11:57.3	4.17 ± 0.07	0.1 ± 0.0	15 ± 5	2.5 ± 1.4	–	–	–
SHARDS10007010	12:37:18.0	62:13:09.7	4.31 ± 0.06	0.8 ± 0.3	48 ± 16	2.3 ± 1.2	–	–	–
SHARDS10005802	12:37:18.1	62:16:41.3	4.78 ± 0.07	16.0 ± 6.0	459 ± 320	3.0 ± 1.6	2.4 ± 1.9	32 ± 13	2.3 ± 1.6
SHARDS10009075	12:37:18.1	62:20:14.1	4.66 ± 0.07	1.1 ± 0.6	61 ± 29	2.6 ± 1.4	–	–	–
SHARDS10007498	12:37:18.3	62:15:47.1	4.48 ± 0.07	29.0 ± 9.0	395 ± 184	3.0 ± 1.6	2.0 ± 1.6	31 ± 12	1.6 ± 1.2
SHARDS20007547	12:37:18.3	62:10:59.6	3.35 ± 0.07	0.8 ± 0.2	36 ± 7	1.9 ± 1.0	–	–	–
SHARDS10001627	12:37:18.3	62:15:35.2	3.40 ± 0.07	3.3 ± 0.8	57 ± 17	2.3 ± 1.2	–	–	–
SHARDS10008374	12:37:18.4	62:18:19.2	3.82 ± 0.06	0.7 ± 0.3	54 ± 32	2.5 ± 1.3	–	–	–
SHARDS10006456	12:37:18.5	62:22:27.7	4.11 ± 0.07	8.2 ± 2.5	1100 ± 400	3.0 ± 1.6	1.0 ± 0.8	36 ± 13	1.8 ± 1.2

Continued on next page

Table A.2 – *Continued from previous page*

Object Name	R.A. (J2000)	Dec. (J2000)	z	$M_{\rm star,m}$ ($10^9\ M_\odot$)	$\rm Age_m$ (Myr)	$\tau_{\rm m}$ (Myr)	$M_{\rm star,b}$ ($10^9\ M_\odot$)	$\rm Age_b$ (Myr)	$\tau_{\rm b}$ (Myr)
SHARDS10006488	12:37:18.7	62:22:28.1	4.50 ± 0.07	0.8 ± 0.4	20 ± 6	1.9 ± 1.2	—	—	—
SHARDS20025355	12:37:18.7	62:11:56.4	4.17 ± 0.07	1.0 ± 0.6	89 ± 55	2.8 ± 1.4	—	—	—
SHARDS10006597	12:37:18.8	62:15:22.7	5.45 ± 0.07	13.0 ± 5.0	53 ± 24	3.4 ± 1.4	—	—	—
SHARDS10006000	12:37:18.8	62:12:19.4	3.89 ± 0.06	20.0 ± 9.0	560 ± 310	3.0 ± 1.6	0.8 ± 1.0	19 ± 5	1.8 ± 1.1
SHARDS10006145	12:37:18.8	62:15:17.5	3.93 ± 0.06	4.7 ± 2.6	1100 ± 400	3.0 ± 1.6	0.4 ± 0.5	18 ± 3	4.4 ± 1.0
SHARDS10005595	12:37:19.0	62:22:29.7	4.25 ± 0.07	7.4 ± 1.9	53 ± 15	2.6 ± 1.3	—	—	—
SHARDS10004376	12:37:19.0	62:19:33.5	4.26 ± 0.07	7.6 ± 0.8	70 ± 7	3.0 ± 1.4	—	—	—
SHARDS10016579	12:37:19.1	62:12:49.9	4.30 ± 0.06	1.3 ± 0.6	56 ± 22	2.5 ± 1.3	1.0 ± 0.7	34 ± 12	1.5 ± 0.9
SHARDS10005784	12:37:19.2	62:19:47.9	3.42 ± 0.07	10.8 ± 1.9	1000 ± 300	3.0 ± 1.6	—	—	—
SHARDS10006640	12:37:19.3	62:14:15.7	3.38 ± 0.07	1.9 ± 0.4	59 ± 9	2.1 ± 1.1	—	—	—
SHARDS10009329	12:37:19.5	62:17:27.0	4.10 ± 0.07	3.3 ± 0.5	28 ± 3	1.4 ± 0.6	—	—	—
SHARDS10008605	12:37:19.6	62:17:29.9	4.37 ± 0.06	0.8 ± 0.5	64 ± 39	2.7 ± 1.4	—	—	—
SHARDS10006108	12:37:19.6	62:16:35.2	5.47 ± 0.07	1.5 ± 0.8	23 ± 10	3.4 ± 1.4	—	—	—
SHARDS10005808	12:37:19.6	62:22:36.1	4.25 ± 0.07	13.0 ± 3.0	786 ± 194	3.0 ± 1.6	1.8 ± 1.0	47 ± 8	2.1 ± 1.1
SHARDS10006734	12:37:19.7	62:22:23.4	4.66 ± 0.07	1.6 ± 0.6	38 ± 23	2.6 ± 1.3	—	—	—
SHARDS10012165	12:37:19.7	62:16:02.9	5.88 ± 0.06	4.6 ± 4.2	459 ± 250	3.0 ± 1.6	0.9 ± 1.1	20 ± 8	1.7 ± 1.1
SHARDS10009880	12:37:19.8	62:14:13.3	5.24 ± 0.07	75.0 ± 9.0	350 ± 40	3.0 ± 1.6	3.9 ± 0.5	49 ± 2	2.5 ± 1.1
SHARDS10017072	12:37:19.8	62:13:21.1	3.23 ± 0.07	0.1 ± 0.1	16 ± 12	3.2 ± 1.4	—	—	—
SHARDS10008388	12:37:19.8	62:19:58.7	4.38 ± 0.06	2.3 ± 1.2	81 ± 46	2.8 ± 1.4	—	—	—
SHARDS10011201	12:37:19.8	62:18:58.6	3.42 ± 0.07	0.8 ± 0.3	82 ± 40	2.9 ± 1.4	—	—	—
SHARDS10008885	12:37:19.9	62:19:55.8	3.83 ± 0.06	8.3 ± 2.3	360 ± 148	3.0 ± 1.4	—	—	—
SHARDS10010067	12:37:20.0	62:12:00.6	5.26 ± 0.07	0.1 ± 0.0	11 ± 4	3.0 ± 1.4	—	—	—
SHARDS10015867	12:37:20.0	62:14:53.4	6.00 ± 0.07	4.9 ± 3.2	74 ± 56	2.9 ± 1.4	—	—	—
SHARDS10006058	12:37:20.0	62:21:23.8	4.93 ± 0.08	4.2 ± 1.6	31 ± 13	1.8 ± 1.0	—	—	—
SHARDS10010672	12:37:20.2	62:13:23.5	3.63 ± 0.06	0.4 ± 0.3	62 ± 39	2.6 ± 1.4	—	—	—
SHARDS10009269	12:37:20.3	62:14:47.9	3.79 ± 0.06	2.8 ± 1.3	890 ± 409	3.0 ± 1.6	0.2 ± 0.3	19 ± 7	2.7 ± 1.6
SHARDS10015428	12:37:20.3	62:17:10.1	6.72 ± 0.14	0.4 ± 0.6	18 ± 19	3.0 ± 1.4	—	—	—
SHARDS10009118	12:37:20.4	62:18:35.3	3.68 ± 0.06	1.1 ± 0.5	68 ± 35	2.7 ± 1.4	—	—	—
SHARDS10006944	12:37:20.4	62:22:55.7	4.10 ± 0.07	0.9 ± 0.3	37 ± 13	2.0 ± 1.0	—	—	—
SHARDS10005080	12:37:20.4	62:22:14.9	4.26 ± 0.07	18.0 ± 3.0	60 ± 10	2.8 ± 1.4	—	—	—
SHARDS10007306	12:37:20.5	62:17:33.0	3.41 ± 0.07	2.5 ± 0.7	72 ± 26	2.8 ± 1.4	—	—	—
SHARDS20004592	12:37:20.6	62:11:05.8	4.40 ± 0.07	19.0 ± 6.0	66 ± 19	2.6 ± 1.2	—	—	—
SHARDS10010449	12:37:20.6	62:17:31.4	4.37 ± 0.06	0.9 ± 0.5	51 ± 29	2.5 ± 1.3	—	—	—
SHARDS10007656	12:37:20.6	62:19:00.8	3.69 ± 0.06	17.0 ± 5.0	919 ± 360	3.0 ± 1.6	0.5 ± 0.2	22 ± 6	3.6 ± 1.4
SHARDS10015156	12:37:20.6	62:15:46.7	3.55 ± 0.06	25.0 ± 8.0	400 ± 290	3.0 ± 1.6	5.7 ± 2.7	42 ± 11	1.7 ± 1.1
SHARDS10005301	12:37:20.8	62:13:01.2	3.80 ± 0.06	10.9 ± 1.5	96 ± 23	3.2 ± 1.4	—	—	—
SHARDS10009199	12:37:20.8	62:14:12.9	4.61 ± 0.07	0.7 ± 0.4	34 ± 20	2.7 ± 1.4	—	—	—
SHARDS10007282	12:37:20.8	62:16:10.3	4.24 ± 0.07	2.8 ± 0.8	99 ± 40	3.0 ± 1.4	—	—	—
SHARDS10005491	12:37:20.8	62:18:43.2	4.11 ± 0.07	3.5 ± 0.6	28 ± 2	1.6 ± 0.7	—	—	—
SHARDS10009034	12:37:20.9	62:18:27.8	5.63 ± 0.07	2.9 ± 0.2	20 ± 2	1.6 ± 0.7	—	—	—
SHARDS10005733	12:37:20.9	62:14:07.6	3.24 ± 0.07	5.2 ± 1.5	83 ± 23	3.0 ± 1.4	—	—	—
SHARDS10016750	12:37:21.0	62:12:05.7	6.63 ± 0.14	2.2 ± 1.7	58 ± 44	2.8 ± 1.4	—	—	—
SHARDS20008477	12:37:21.0	62:11:16.3	3.60 ± 0.06	0.4 ± 0.2	13 ± 5	2.2 ± 1.2	—	—	—
SHARDS10014441	12:37:21.0	62:13:56.6	5.46 ± 0.07	2.2 ± 1.1	15 ± 9	3.1 ± 1.4	—	—	—
SHARDS10015320	12:37:21.1	62:19:27.1	5.22 ± 0.06	62.0 ± 8.0	990 ± 70	3.0 ± 1.6	1.6 ± 0.2	15 ± 1	1.0 ± 0.3
SHARDS10013087	12:37:21.1	62:22:21.0	4.51 ± 0.07	6.6 ± 3.6	640 ± 340	3.0 ± 1.6	1.1 ± 1.2	35 ± 13	1.9 ± 1.4
SHARDS10000066	12:37:21.2	62:11:45.9	4.03 ± 0.07	2.6 ± 0.7	59 ± 18	2.5 ± 1.3	—	—	—

Continued on next page

Table A.2 – *Continued from previous page*

Object Name	R.A. (J2000)	Dec. (J2000)	z	$M_{\rm star,m}$ (10^9 $M_\odot$)	$\rm Age_m$ (Myr)	$\tau_{\rm m}$ (Myr)	$M_{\rm star,b}$ (10^9 $M_\odot$)	$\rm Age_b$ (Myr)	$\tau_{\rm b}$ (Myr)
SHARDS20010936	12:37:21.2	62:11:17.2	4.11 ± 0.07	0.8 ± 0.4	63 ± 31	2.6 ± 1.4	–	–	–
SHARDS10012627	12:37:21.2	62:13:59.3	4.90 ± 0.08	1.3 ± 0.8	86 ± 55	2.8 ± 1.4	–	–	–
SHARDS20015171	12:37:21.2	62:11:25.7	3.36 ± 0.07	0.3 ± 0.2	380 ± 380	3.0 ± 1.6	0.0 ± 0.0	6 ± 3	3.4 ± 1.6
SHARDS10005608	12:37:21.3	62:13:10.3	3.38 ± 0.07	9.8 ± 1.2	79 ± 15	3.0 ± 1.4	–	–	–
SHARDS10009097	12:37:21.3	62:12:21.7	4.58 ± 0.07	0.8 ± 0.6	40 ± 30	2.8 ± 1.4	–	–	–
SHARDS10006728	12:37:21.4	62:17:38.5	4.10 ± 0.07	0.6 ± 0.2	35 ± 12	1.9 ± 1.0	–	–	–
SHARDS10000371	12:37:21.4	62:12:59.2	3.63 ± 0.06	3.6 ± 0.6	35 ± 7	1.7 ± 0.7	–	–	–
SHARDS10005492	12:37:21.5	62:12:17.6	4.58 ± 0.07	14.0 ± 6.0	570 ± 310	3.0 ± 1.6	4.2 ± 2.8	49 ± 4	2.1 ± 1.2
SHARDS10007376	12:37:21.5	62:13:41.3	3.78 ± 0.06	26.0 ± 8.0	1100 ± 300	3.0 ± 1.6	1.4 ± 0.8	42 ± 11	2.1 ± 1.3
SHARDS10008057	12:37:21.5	62:13:00.1	3.63 ± 0.06	2.9 ± 0.4	50 ± 6	2.2 ± 1.1	–	–	–
SHARDS10009068	12:37:21.6	62:19:12.0	5.36 ± 0.07	7.1 ± 2.5	130 ± 70	3.0 ± 1.4	–	–	–
SHARDS10014866	12:37:21.6	62:17:23.4	3.26 ± 0.07	0.3 ± 0.2	62 ± 45	2.7 ± 1.4	–	–	–
SHARDS10008856	12:37:21.6	62:16:32.4	3.67 ± 0.06	0.7 ± 0.5	61 ± 35	2.6 ± 1.4	–	–	–
SHARDS10010894	12:37:21.7	62:13:11.0	3.50 ± 0.06	0.1 ± 0.0	13 ± 4	3.3 ± 1.4	–	–	–
SHARDS10010379	12:37:21.7	62:15:05.0	5.04 ± 0.06	56.4 ± 10.5	703 ± 177	3.0 ± 1.4	–	–	–
SHARDS10011292	12:37:21.8	62:14:41.4	5.31 ± 0.07	1.2 ± 0.6	56 ± 26	2.6 ± 1.3	–	–	–
SHARDS10010964	12:37:22.0	62:19:01.1	4.66 ± 0.07	15.0 ± 6.0	530 ± 290	3.0 ± 1.6	1.3 ± 1.3	38 ± 13	2.1 ± 1.5
SHARDS10007478	12:37:22.0	62:14:37.4	3.79 ± 0.06	3.4 ± 0.7	72 ± 18	2.8 ± 1.4	–	–	–
SHARDS10011669	12:37:22.1	62:13:55.4	5.99 ± 0.07	1.3 ± 0.3	43 ± 12	2.2 ± 1.1	–	–	–
SHARDS10003185	12:37:22.1	62:18:12.4	3.68 ± 0.06	5.3 ± 0.5	75 ± 6	3.0 ± 1.4	–	–	–
SHARDS10006133	12:37:22.1	62:13:57.9	3.38 ± 0.07	0.3 ± 0.1	16 ± 5	3.2 ± 1.4	–	–	–
SHARDS10009690	12:37:22.1	62:15:53.8	4.92 ± 0.08	0.1 ± 0.0	18 ± 6	2.6 ± 1.4	–	–	–
SHARDS10007821	12:37:22.1	62:15:46.2	5.46 ± 0.07	23.0 ± 9.0	110 ± 40	3.0 ± 1.4	–	–	–
SHARDS10007626	12:37:22.3	62:21:47.3	3.97 ± 0.06	9.1 ± 1.8	1160 ± 240	3.0 ± 1.6	0.2 ± 0.1	18 ± 3	4.7 ± 0.8
SHARDS10007454	12:37:22.4	62:14:14.8	3.79 ± 0.06	2.1 ± 0.4	40 ± 8	2.2 ± 1.1	–	–	–
SHARDS10016659	12:37:22.8	62:12:28.4	3.62 ± 0.06	0.2 ± 0.2	18 ± 17	3.1 ± 1.4	–	–	–
SHARDS10008257	12:37:22.9	62:21:43.8	4.93 ± 0.08	2.0 ± 1.1	70 ± 42	2.7 ± 1.4	–	–	–
SHARDS10005822	12:37:22.9	62:18:11.5	3.54 ± 0.06	4.0 ± 1.0	47 ± 13	2.6 ± 1.3	–	–	–
SHARDS10010177	12:37:23.0	62:14:03.9	3.92 ± 0.06	2.6 ± 2.4	700 ± 450	3.0 ± 1.6	0.3 ± 0.5	17 ± 5	2.8 ± 1.6
SHARDS10008652	12:37:23.0	62:14:11.9	6.00 ± 0.07	8.6 ± 2.8	95 ± 50	2.9 ± 1.4	–	–	–
SHARDS10007803	12:37:23.0	62:11:57.7	4.71 ± 0.07	8.0 ± 3.6	500 ± 270	3.0 ± 1.6	1.6 ± 1.6	27 ± 10	1.3 ± 1.0
SHARDS10005889	12:37:23.1	62:15:17.4	4.08 ± 0.07	1.9 ± 0.7	41 ± 15	2.0 ± 1.1	–	–	–
SHARDS10006109	12:37:23.2	62:14:00.7	4.33 ± 0.06	17.0 ± 4.0	401 ± 136	3.0 ± 1.6	1.0 ± 1.0	23 ± 7	1.1 ± 0.5
SHARDS10009361	12:37:23.4	62:12:10.4	3.37 ± 0.07	0.6 ± 0.2	65 ± 30	2.7 ± 1.4	–	–	–
SHARDS10009152	12:37:23.4	62:13:49.7	4.21 ± 0.07	2.8 ± 0.9	45 ± 18	2.2 ± 1.2	–	–	–
SHARDS10015293	12:37:23.5	62:14:59.5	6.01 ± 0.07	33.8 ± 10.7	544 ± 166	3.0 ± 1.6	0.9 ± 0.4	22 ± 5	3.3 ± 1.1
SHARDS10011610	12:37:23.5	62:14:29.1	4.22 ± 0.07	1.1 ± 0.5	49 ± 30	2.9 ± 1.4	–	–	–
SHARDS10005473	12:37:23.6	62:20:38.4	4.51 ± 0.07	17.8 ± 12.3	690 ± 310	3.0 ± 1.6	2.7 ± 3.3	20 ± 3	1.8 ± 1.0
SHARDS10000941	12:37:23.6	62:14:21.2	3.51 ± 0.06	9.6 ± 1.4	77 ± 13	3.0 ± 1.4	–	–	–
SHARDS10006333	12:37:23.7	62:13:29.4	3.38 ± 0.07	24.0 ± 6.0	565 ± 216	3.0 ± 1.6	2.6 ± 1.1	48 ± 7	2.4 ± 1.2
SHARDS10003916	12:37:23.7	62:21:13.0	3.55 ± 0.06	70.7 ± 19.8	160 ± 50	2.9 ± 1.6	3.5 ± 2.2	18 ± 3	4.1 ± 1.2
SHARDS10000377	12:37:23.8	62:13:00.6	3.38 ± 0.07	14.0 ± 3.0	857 ± 220	3.0 ± 1.6	1.9 ± 1.3	25 ± 2	1.0 ± 0.1
SHARDS10007352	12:37:23.8	62:16:27.1	4.49 ± 0.07	130.0 ± 10.0	1100 ± 100	3.0 ± 1.6	3.3 ± 0.2	50 ± 0	2.3 ± 1.4
SHARDS10006257	12:37:23.9	62:18:15.0	3.41 ± 0.07	2.3 ± 0.8	53 ± 19	2.2 ± 1.2	–	–	–
SHARDS10006257	12:37:23.9	62:18:15.4	3.42 ± 0.07	8.3 ± 5.6	720 ± 400	3.0 ± 1.6	1.5 ± 1.5	21 ± 6	1.9 ± 1.1
SHARDS10011421	12:37:23.9	62:15:56.4	3.67 ± 0.06	0.1 ± 0.0	12 ± 4	3.5 ± 1.3	–	–	–
SHARDS10008105	12:37:24.0	62:18:32.7	3.42 ± 0.07	22.0 ± 4.0	450 ± 90	3.0 ± 1.4	–	–	–
SHARDS10010331	12:37:24.0	62:11:45.4	4.42 ± 0.07	0.6 ± 0.2	18 ± 5	3.2 ± 1.2	–	–	–
SHARDS10005314	12:37:24.1	62:18:33.5	3.42 ± 0.07	51.3 ± 11.4	290 ± 90	3.0 ± 1.6	3.8 ± 1.8	33 ± 12	1.7 ± 1.1

Continued on next page

Table A.2 – *Continued from previous page*

Object Name	R.A. (J2000)	Dec. (J2000)	z	$M_{\rm star,m}$ (10^9 $M_\odot$)	$\rm Age_m$ (Myr)	$\tau_{\rm m}$ (Myr)	$M_{\rm star,b}$ (10^9 $M_\odot$)	$\rm Age_b$ (Myr)	$\tau_{\rm b}$ (Myr)
SHARDS10013381	12:37:24.1	62:18:34.2	3.42 ± 0.07	41.0 ± 5.0	200 ± 30	3.0 ± 1.6	3.3 ± 1.4	46 ± 9	2.1 ± 1.3
SHARDS10009011	12:37:24.2	62:12:37.6	3.76 ± 0.06	0.4 ± 0.4	27 ± 25	3.1 ± 1.4	—	—	—
SHARDS10008696	12:37:24.2	62:12:54.3	3.77 ± 0.06	0.4 ± 0.2	42 ± 16	2.2 ± 1.2	—	—	—
SHARDS10006700	12:37:24.5	62:19:35.4	4.11 ± 0.07	9.6 ± 2.1	1180 ± 200	3.0 ± 1.6	0.3 ± 0.1	20 ± 4	3.2 ± 1.1
SHARDS10007705	12:37:24.5	62:12:25.8	4.72 ± 0.07	1.2 ± 0.4	55 ± 18	2.5 ± 1.3	0.3 ± 0.3	23 ± 8	1.2 ± 0.7
SHARDS10011003	12:37:24.6	62:14:58.0	3.66 ± 0.06	5.2 ± 1.4	1100 ± 300	3.0 ± 1.6	—	—	—
SHARDS10007395	12:37:24.6	62:12:54.1	3.63 ± 0.06	0.8 ± 0.3	33 ± 21	2.5 ± 1.3	—	—	—
SHARDS10006160	12:37:24.7	62:18:50.5	3.69 ± 0.06	6.8 ± 0.9	520 ± 30	3.2 ± 1.4	—	—	—
SHARDS10008695	12:37:25.0	62:14:07.8	4.22 ± 0.07	3.0 ± 1.2	93 ± 46	2.8 ± 1.4	—	—	—
SHARDS10009285	12:37:25.2	62:18:45.3	5.64 ± 0.07	4.4 ± 0.8	53 ± 9	2.0 ± 1.0	—	—	—
SHARDS10010541	12:37:25.3	62:13:19.3	3.64 ± 0.06	1.9 ± 0.5	34 ± 9	1.9 ± 1.0	—	—	—
SHARDS10012056	12:37:25.3	62:20:48.3	5.36 ± 0.07	41.1 ± 12.0	681 ± 217	3.0 ± 1.6	4.9 ± 4.4	31 ± 11	1.4 ± 0.9
SHARDS10006159	12:37:25.4	62:20:48.1	3.55 ± 0.06	6.2 ± 1.9	520 ± 50	2.9 ± 1.4	—	—	—
SHARDS10010265	12:37:25.4	62:11:58.6	4.03 ± 0.07	1.9 ± 0.7	86 ± 42	2.9 ± 1.4	—	—	—
SHARDS10018093	12:37:25.5	62:21:25.7	6.22 ± 0.14	2.0 ± 2.7	131 ± 148	2.9 ± 1.4	—	—	—
SHARDS10007020	12:37:25.5	62:13:33.2	4.06 ± 0.07	2.3 ± 0.9	50 ± 21	2.3 ± 1.3	—	—	—
SHARDS10005179	12:37:25.5	62:13:39.2	3.78 ± 0.06	17.0 ± 10.0	380 ± 300	3.0 ± 1.6	6.7 ± 3.0	39 ± 12	1.7 ± 1.0
SHARDS10015064	12:37:25.7	62:17:43.2	6.74 ± 0.14	19.3 ± 11.3	379 ± 208	3.0 ± 1.6	4.4 ± 4.1	21 ± 9	1.7 ± 1.1
SHARDS10006968	12:37:25.7	62:20:47.9	3.69 ± 0.06	3.4 ± 1.5	49 ± 22	2.3 ± 1.3	—	—	—
SHARDS10013230	12:37:25.7	62:13:26.1	5.16 ± 0.06	0.9 ± 0.6	60 ± 33	2.6 ± 1.4	—	—	—
SHARDS10007410	12:37:25.9	62:20:01.9	4.51 ± 0.07	1.3 ± 0.4	61 ± 17	2.7 ± 1.4	—	—	—
SHARDS10015413	12:37:26.0	62:21:27.5	6.64 ± 0.14	0.4 ± 0.3	14 ± 8	3.0 ± 1.4	—	—	—
SHARDS10006087	12:37:26.1	62:21:07.6	3.97 ± 0.06	4.8 ± 1.3	49 ± 16	2.5 ± 1.3	—	—	—
SHARDS10008449	12:37:26.1	62:20:11.2	4.67 ± 0.07	1.3 ± 0.5	60 ± 21	2.6 ± 1.4	—	—	—
SHARDS10003542	12:37:26.2	62:17:34.1	3.68 ± 0.06	1.5 ± 0.7	69 ± 32	2.7 ± 1.4	—	—	—
SHARDS10007287	12:37:26.5	62:20:17.2	4.67 ± 0.07	2.1 ± 1.2	74 ± 43	2.7 ± 1.4	—	—	—
SHARDS10011338	12:37:26.5	62:14:11.8	3.93 ± 0.06	6.1 ± 3.5	850 ± 450	3.0 ± 1.6	0.7 ± 0.9	37 ± 13	2.0 ± 1.5
SHARDS10008081	12:37:26.5	62:15:27.2	5.46 ± 0.07	1.2 ± 0.4	46 ± 16	2.3 ± 1.2	—	—	—
SHARDS10006489	12:37:26.5	62:20:16.0	4.94 ± 0.08	1.9 ± 1.6	23 ± 7	3.8 ± 1.4	—	—	—
SHARDS10010774	12:37:26.5	62:18:36.3	5.64 ± 0.07	10.0 ± 3.0	100 ± 50	3.0 ± 1.4	—	—	—
SHARDS10000237	12:37:26.5	62:14:36.5	3.49 ± 0.06	3.7 ± 0.6	71 ± 18	2.7 ± 1.4	—	—	—
SHARDS10008945	12:37:26.5	62:14:41.3	3.52 ± 0.06	0.3 ± 0.1	46 ± 16	2.4 ± 1.3	—	—	—
SHARDS10005727	12:37:26.5	62:13:10.5	3.38 ± 0.07	4.3 ± 1.9	65 ± 17	2.9 ± 1.4	—	—	—
SHARDS10010263	12:37:26.6	62:13:54.0	4.90 ± 0.08	14.0 ± 5.0	919 ± 300	3.0 ± 1.6	0.4 ± 0.3	24 ± 3	4.8 ± 0.8
SHARDS10013791	12:37:26.6	62:18:08.1	5.49 ± 0.07	1.8 ± 0.8	56 ± 27	2.6 ± 1.3	—	—	—
SHARDS10009297	12:37:26.7	62:13:02.1	4.73 ± 0.07	0.7 ± 0.1	16 ± 3	2.8 ± 1.4	—	—	—
SHARDS10005481	12:37:26.8	62:12:34.3	3.50 ± 0.06	3.7 ± 2.5	36 ± 4	1.7 ± 0.8	—	—	—
SHARDS10016008	12:37:26.8	62:14:39.8	6.74 ± 0.14	6.4 ± 2.4	70 ± 34	2.7 ± 1.4	—	—	—
SHARDS10006956	12:37:26.9	62:14:47.1	5.04 ± 0.06	14.0 ± 3.0	927 ± 133	3.0 ± 1.6	0.5 ± 0.2	19 ± 5	3.7 ± 1.2
SHARDS10008381	12:37:26.9	62:20:07.4	4.94 ± 0.08	0.5 ± 0.3	24 ± 12	2.8 ± 1.4	—	—	—
SHARDS10006163	12:37:27.0	62:15:24.5	3.83 ± 0.06	2.7 ± 0.6	54 ± 7	1.8 ± 0.8	—	—	—
SHARDS10008662	12:37:27.1	62:15:49.5	4.09 ± 0.07	0.5 ± 0.2	46 ± 19	2.4 ± 1.3	—	—	—
SHARDS10015434	12:37:27.3	62:17:54.5	5.91 ± 0.06	1.1 ± 0.7	45 ± 23	2.4 ± 1.3	—	—	—
SHARDS10009552	12:37:27.3	62:14:23.7	4.62 ± 0.07	1.9 ± 1.1	82 ± 48	2.8 ± 1.4	—	—	—
SHARDS10011078	12:37:27.4	62:12:05.2	4.58 ± 0.07	0.7 ± 0.5	50 ± 24	2.5 ± 1.3	—	—	—
SHARDS10005951	12:37:27.5	62:18:00.5	3.69 ± 0.06	1.1 ± 0.2	25 ± 5	3.5 ± 1.2	—	—	—
SHARDS10006478	12:37:27.5	62:17:22.3	4.37 ± 0.06	34.0 ± 5.0	762 ± 183	3.0 ± 1.6	1.0 ± 0.3	22 ± 3	1.0 ± 0.0
SHARDS10008518	12:37:27.5	62:18:39.0	5.36 ± 0.07	3.4 ± 1.3	50 ± 23	2.5 ± 1.3	—	—	—
SHARDS10006234	12:37:27.6	62:14:55.0	4.35 ± 0.06	2.5 ± 0.9	42 ± 17	2.1 ± 1.1	—	—	—

Continued on next page

Table A.2 – *Continued from previous page*

Object Name	R.A. (J2000)	Dec. (J2000)	z	$M_{\rm star,m}$ (10^9 $M_\odot$)	$\rm Age_m$ (Myr)	$\tau_{\rm m}$ (Myr)	$M_{\rm star,b}$ (10^9 $M_\odot$)	$\rm Age_b$ (Myr)	$\tau_{\rm b}$ (Myr)
SHARDS10009872	12:37:27.7	62:20:05.2	4.67 ± 0.07	0.1 ± 0.1	13 ± 4	3.1 ± 1.4	–	–	–
SHARDS10005476	12:37:27.7	62:12:34.2	3.90 ± 0.06	6.9 ± 3.2	1200 ± 300	3.0 ± 1.6	0.9 ± 0.7	19 ± 3	4.4 ± 1.2
SHARDS10006517	12:37:28.1	62:12:29.0	3.49 ± 0.06	0.9 ± 0.3	50 ± 19	2.3 ± 1.2	–	–	–
SHARDS10008777	12:37:28.2	62:20:11.3	4.39 ± 0.06	3.5 ± 1.0	42 ± 16	2.3 ± 1.2	–	–	–
SHARDS10007497	12:37:28.2	62:14:30.4	3.52 ± 0.06	22.0 ± 3.0	350 ± 90	3.0 ± 1.6	1.0 ± 0.5	41 ± 11	2.3 ± 1.6
SHARDS10008558	12:37:28.2	62:13:10.8	3.64 ± 0.06	0.6 ± 0.3	18 ± 7	3.0 ± 1.4	–	–	–
SHARDS10010843	12:37:28.3	62:18:14.3	4.38 ± 0.06	9.1 ± 5.3	570 ± 310	3.0 ± 1.6	0.8 ± 1.1	30 ± 13	1.7 ± 1.3
SHARDS10005254	12:37:28.4	62:17:35.4	4.26 ± 0.07	6.0 ± 0.8	77 ± 10	2.6 ± 1.3	–	–	–
SHARDS10009498	12:37:28.4	62:20:35.4	4.39 ± 0.06	2.1 ± 1.1	50 ± 26	2.4 ± 1.3	–	–	–
SHARDS10001215	12:37:28.5	62:14:52.4	3.66 ± 0.06	7.1 ± 2.4	45 ± 8	2.0 ± 1.0	–	–	–
SHARDS10010951	12:37:28.6	62:14:41.3	5.76 ± 0.06	14.0 ± 6.0	509 ± 219	3.0 ± 1.6	1.0 ± 1.2	27 ± 12	2.0 ± 1.3
SHARDS10006613	12:37:28.7	62:15:03.9	3.52 ± 0.06	1.0 ± 0.3	37 ± 12	2.1 ± 1.1	–	–	–
SHARDS10006221	12:37:28.8	62:14:17.1	3.65 ± 0.06	1.8 ± 1.0	64 ± 36	2.5 ± 1.3	–	–	–
SHARDS10000918	12:37:28.8	62:14:18.9	3.52 ± 0.06	2.9 ± 1.0	36 ± 11	1.7 ± 0.8	–	–	–
SHARDS10008196	12:37:28.9	62:14:19.7	3.52 ± 0.06	20.0 ± 8.0	600 ± 459	3.0 ± 1.6	5.2 ± 3.1	42 ± 11	1.9 ± 1.2
SHARDS10007842	12:37:29.0	62:19:13.1	3.27 ± 0.07	0.7 ± 0.3	59 ± 27	2.6 ± 1.3	–	–	–
SHARDS10010134	12:37:29.1	62:12:08.0	4.43 ± 0.07	0.2 ± 0.1	23 ± 8	2.5 ± 1.4	–	–	–
SHARDS10000943	12:37:29.2	62:14:22.2	3.65 ± 0.06	14.8 ± 2.0	85 ± 16	3.0 ± 1.4	–	–	–
SHARDS10007953	12:37:29.2	62:15:03.2	3.66 ± 0.06	4.9 ± 1.9	890 ± 400	3.0 ± 1.6	0.5 ± 0.5	20 ± 8	2.3 ± 1.4
SHARDS10010123	12:37:29.2	62:14:02.6	3.51 ± 0.06	6.2 ± 1.8	1200 ± 300	3.0 ± 1.6	0.4 ± 0.2	23 ± 7	1.2 ± 0.7
SHARDS10006758	12:37:29.3	62:18:04.4	4.66 ± 0.07	5.2 ± 2.5	459 ± 330	3.0 ± 1.6	0.5 ± 0.6	22 ± 7	2.4 ± 1.4
SHARDS10007431	12:37:29.4	62:14:16.1	3.39 ± 0.07	2.1 ± 0.6	91 ± 44	2.9 ± 1.4	–	–	–
SHARDS10013955	12:37:29.5	62:13:16.0	3.64 ± 0.06	1.0 ± 0.6	86 ± 65	2.8 ± 1.4	–	–	–
SHARDS10000864	12:37:29.6	62:14:11.2	3.51 ± 0.06	6.1 ± 1.3	82 ± 18	3.1 ± 1.4	–	–	–
SHARDS10004019	12:37:29.7	62:20:33.1	3.42 ± 0.07	2.6 ± 0.8	54 ± 22	2.3 ± 1.2	–	–	–
SHARDS10010203	12:37:29.8	62:13:34.5	3.78 ± 0.06	2.2 ± 1.2	120 ± 80	2.9 ± 1.4	–	–	–
SHARDS10010812	12:37:29.8	62:19:41.1	4.27 ± 0.07	33.0 ± 10.0	786 ± 231	3.0 ± 1.6	1.6 ± 0.9	43 ± 11	2.3 ± 1.5
SHARDS10000761	12:37:29.8	62:13:58.4	3.79 ± 0.06	3.6 ± 0.6	79 ± 14	2.7 ± 1.4	–	–	–
SHARDS10009339	12:37:29.9	62:13:40.4	3.39 ± 0.07	0.9 ± 0.4	64 ± 41	2.6 ± 1.3	–	–	–
SHARDS10002620	12:37:29.9	62:16:56.4	3.26 ± 0.07	6.4 ± 0.8	63 ± 17	2.6 ± 1.3	–	–	–
SHARDS10005513	12:37:30.1	62:12:16.8	3.90 ± 0.06	1.3 ± 0.4	17 ± 6	2.2 ± 1.3	–	–	–
SHARDS10005930	12:37:30.1	62:12:18.3	4.19 ± 0.07	2.9 ± 0.5	38 ± 5	1.8 ± 0.9	–	–	–
SHARDS10008400	12:37:30.1	62:17:58.5	3.69 ± 0.06	28.0 ± 5.0	1190 ± 160	3.0 ± 1.6	0.8 ± 0.2	25 ± 6	3.3 ± 1.4
SHARDS10007860	12:37:30.4	62:13:23.8	3.64 ± 0.06	6.2 ± 4.6	350 ± 300	3.0 ± 1.6	0.6 ± 0.8	26 ± 13	2.7 ± 1.6
SHARDS10009893	12:37:30.4	62:14:48.8	4.23 ± 0.07	0.4 ± 0.2	54 ± 25	2.6 ± 1.3	–	–	–
SHARDS10011676	12:37:30.5	62:19:39.3	4.39 ± 0.06	53.0 ± 9.0	592 ± 167	3.0 ± 1.6	1.6 ± 0.6	49 ± 2	2.6 ± 1.5
SHARDS10007584	12:37:30.6	62:13:07.9	3.38 ± 0.07	0.8 ± 0.3	56 ± 27	2.5 ± 1.3	–	–	–
SHARDS10015342	12:37:30.9	62:15:32.8	6.23 ± 0.14	11.0 ± 7.0	275 ± 245	3.0 ± 1.6	3.0 ± 2.8	37 ± 13	2.0 ± 1.5
SHARDS10006394	12:37:30.9	62:15:22.7	3.53 ± 0.06	2.7 ± 0.8	80 ± 28	2.9 ± 1.4	–	–	–
SHARDS10005836	12:37:30.9	62:14:03.2	3.93 ± 0.06	12.0 ± 4.0	198 ± 124	3.0 ± 1.6	4.0 ± 0.8	25 ± 3	1.0 ± 0.3
SHARDS10010822	12:37:31.0	62:12:54.2	4.73 ± 0.07	18.0 ± 3.0	860 ± 270	3.0 ± 1.6	0.6 ± 0.3	23 ± 8	3.1 ± 1.5
SHARDS10007062	12:37:31.1	62:15:25.9	3.95 ± 0.06	7.6 ± 4.1	500 ± 340	3.0 ± 1.6	0.3 ± 0.2	20 ± 10	3.9 ± 1.4
SHARDS10007336	12:37:31.1	62:17:24.4	4.94 ± 0.08	1.1 ± 0.8	26 ± 12	2.6 ± 1.4	–	–	–
SHARDS10008585	12:37:31.2	62:15:11.3	4.92 ± 0.08	0.4 ± 0.2	20 ± 7	2.5 ± 1.4	–	–	–
SHARDS10011285	12:37:31.4	62:15:31.9	5.47 ± 0.07	0.6 ± 0.4	18 ± 7	2.7 ± 1.4	–	–	–
SHARDS10008216	12:37:31.4	62:13:31.4	3.64 ± 0.06	2.4 ± 2.0	400 ± 380	3.0 ± 1.6	0.3 ± 0.4	21 ± 10	3.0 ± 1.6
SHARDS10009535	12:37:31.5	62:17:08.3	5.35 ± 0.07	3.7 ± 1.7	110 ± 60	2.9 ± 1.4	–	–	–
SHARDS10012794	12:37:31.7	62:16:16.7	5.20 ± 0.06	51.5 ± 10.8	772 ± 178	3.0 ± 1.6	1.4 ± 0.5	50 ± 3	2.8 ± 1.6
SHARDS10006716	12:37:31.7	62:12:46.8	3.23 ± 0.07	1.6 ± 0.7	42 ± 20	2.1 ± 1.1	–	–	–

Continued on next page

Table A.2 – *Continued from previous page*

Object Name	R.A. (J2000)	Dec. (J2000)	z	$M_{\rm star,m}$ ($10^9\ M_\odot$)	$\rm Age_m$ (Myr)	$\tau_{\rm m}$ (Myr)	$M_{\rm star,b}$ ($10^9\ M_\odot$)	$\rm Age_b$ (Myr)	$\tau_{\rm b}$ (Myr)
SHARDS10008779	12:37:31.9	62:15:41.0	3.40 ± 0.07	3.0 ± 0.9	93 ± 39	2.9 ± 1.4	—	—	—
SHARDS10006433	12:37:31.9	62:20:31.7	4.39 ± 0.06	2.8 ± 1.4	60 ± 32	2.5 ± 1.3	—	—	—
SHARDS10008612	12:37:32.0	62:17:08.9	4.66 ± 0.07	3.2 ± 1.7	75 ± 41	2.8 ± 1.4	—	—	—
SHARDS10005576	12:37:32.0	62:16:43.3	4.65 ± 0.07	9.9 ± 1.3	94 ± 13	3.0 ± 1.4	—	—	—
SHARDS10011819	12:37:32.1	62:15:01.2	3.25 ± 0.07	0.5 ± 0.2	55 ± 32	2.6 ± 1.4	6.8 ± 4.4	28 ± 10	1.3 ± 0.9
SHARDS10008639	12:37:32.3	62:15:02.2	5.61 ± 0.07	19.3 ± 11.5	540 ± 280	3.0 ± 1.6	—	—	—
SHARDS10014561	12:37:32.3	62:18:48.3	3.42 ± 0.07	0.8 ± 0.4	92 ± 54	2.9 ± 1.4	—	—	—
SHARDS10011091	12:37:32.3	62:15:44.5	4.24 ± 0.07	1.4 ± 0.7	50 ± 26	2.4 ± 1.3	—	—	—
SHARDS10010895	12:37:32.6	62:13:57.3	3.65 ± 0.06	0.2 ± 0.2	20 ± 14	3.0 ± 1.4	—	—	—
SHARDS10008703	12:37:32.6	62:12:47.0	3.63 ± 0.06	12.0 ± 5.0	590 ± 300	3.0 ± 1.6	0.4 ± 0.3	20 ± 6	3.0 ± 1.5
SHARDS10013032	12:37:32.7	62:14:16.2	6.01 ± 0.07	41.7 ± 16.8	399 ± 191	3.0 ± 1.6	3.5 ± 2.7	44 ± 10	2.4 ± 1.5
SHARDS10008570	12:37:32.8	62:12:39.6	3.63 ± 0.06	0.5 ± 0.2	49 ± 16	2.4 ± 1.3	—	—	—
SHARDS10008396	12:37:32.8	62:14:11.9	4.47 ± 0.07	1.7 ± 0.7	74 ± 32	2.8 ± 1.4	—	—	—
SHARDS10018257	12:37:32.9	62:14:42.1	3.66 ± 0.06	2.1 ± 0.9	150 ± 90	3.0 ± 1.4	—	—	—
SHARDS10008154	12:37:33.1	62:14:23.2	4.34 ± 0.06	13.0 ± 3.0	911 ± 237	3.0 ± 1.6	0.9 ± 0.7	35 ± 12	1.8 ± 1.3
SHARDS10013675	12:37:33.1	62:18:04.2	6.26 ± 0.14	18.0 ± 8.0	608 ± 204	3.0 ± 1.6	0.9 ± 1.0	19 ± 5	2.6 ± 1.4
SHARDS10006591	12:37:33.2	62:13:47.8	3.79 ± 0.06	3.0 ± 0.7	69 ± 22	2.8 ± 1.4	—	—	—
SHARDS10011085	12:37:33.2	62:17:51.5	4.51 ± 0.07	15.9 ± 1.9	809 ± 210	3.0 ± 1.6	0.4 ± 0.1	24 ± 4	4.8 ± 0.7
SHARDS10006026	12:37:33.2	62:17:40.0	4.51 ± 0.07	2.9 ± 0.5	31 ± 6	1.7 ± 0.8	—	—	—
SHARDS10010332	12:37:33.2	62:14:07.4	4.34 ± 0.06	1.7 ± 1.0	100 ± 70	2.9 ± 1.4	1.0 ± 1.2	26 ± 11	1.3 ± 1.0
SHARDS10008588	12:37:33.3	62:14:44.6	5.46 ± 0.07	6.8 ± 4.8	650 ± 290	3.0 ± 1.6	—	—	—
SHARDS10009010	12:37:33.4	62:14:07.1	3.65 ± 0.06	2.3 ± 1.0	65 ± 41	3.1 ± 1.4	—	—	—
SHARDS10006184	12:37:33.8	62:19:44.1	3.42 ± 0.07	1.7 ± 1.8	86 ± 23	2.9 ± 1.4	—	—	—
SHARDS10015108	12:37:33.9	62:15:19.2	3.25 ± 0.07	0.7 ± 0.3	63 ± 36	2.6 ± 1.4	—	—	—
SHARDS10010038	12:37:33.9	62:20:16.5	4.39 ± 0.06	9.9 ± 3.2	680 ± 310	3.0 ± 1.6	0.3 ± 0.2	19 ± 5	4.0 ± 1.4
SHARDS10009335	12:37:34.1	62:15:42.3	4.78 ± 0.07	0.3 ± 0.2	16 ± 5	3.0 ± 1.4	—	—	—
SHARDS10018047	12:37:34.1	62:14:41.4	4.91 ± 0.08	1.1 ± 0.6	51 ± 17	2.4 ± 1.3	—	—	—
SHARDS10005798	12:37:34.1	62:18:55.5	3.42 ± 0.07	6.5 ± 1.0	96 ± 26	3.0 ± 1.4	3.4 ± 2.0	42 ± 12	2.4 ± 1.5
SHARDS10006564	12:37:34.3	62:15:46.1	3.67 ± 0.06	6.6 ± 3.8	350 ± 360	3.0 ± 1.6	—	—	—
SHARDS10016395	12:37:34.3	62:14:13.2	4.34 ± 0.06	1.3 ± 0.7	74 ± 45	2.8 ± 1.4	0.4 ± 0.5	18 ± 9	3.0 ± 1.6
SHARDS10006843	12:37:34.5	62:15:40.6	3.53 ± 0.06	6.0 ± 5.0	290 ± 310	3.0 ± 1.6	—	—	—
SHARDS10006962	12:37:34.5	62:13:37.6	4.07 ± 0.07	0.9 ± 0.2	43 ± 13	2.1 ± 1.1	—	—	—
SHARDS10005725	12:37:34.6	62:13:07.4	3.67 ± 0.06	3.6 ± 0.9	66 ± 21	2.6 ± 1.3	—	—	—
SHARDS10005928	12:37:34.7	62:14:58.7	3.53 ± 0.06	3.9 ± 0.3	75 ± 6	2.9 ± 1.4	—	—	—
SHARDS10009797	12:37:34.8	62:15:29.0	5.36 ± 0.07	1.9 ± 0.7	54 ± 21	2.6 ± 1.3	—	—	—
SHARDS10010730	12:37:35.0	62:13:42.0	4.36 ± 0.06	2.2 ± 2.2	610 ± 380	3.0 ± 1.6	0.5 ± 0.6	26 ± 12	1.6 ± 1.2
SHARDS10011385	12:37:35.0	62:13:41.4	4.62 ± 0.07	0.1 ± 0.0	5 ± 1	3.4 ± 1.3	—	—	—
SHARDS10007468	12:37:35.0	62:15:56.3	3.67 ± 0.06	2.3 ± 1.2	100 ± 60	2.9 ± 1.4	—	—	—
SHARDS10005658	12:37:35.1	62:17:47.1	3.96 ± 0.06	6.6 ± 1.0	75 ± 10	2.8 ± 1.4	—	—	—
SHARDS10008909	12:37:35.4	62:17:41.5	4.26 ± 0.07	1.4 ± 1.6	84 ± 43	2.8 ± 1.4	—	—	—
SHARDS10006717	12:37:35.9	62:20:12.9	3.27 ± 0.07	11.3 ± 1.4	1200 ± 140	3.0 ± 1.6	0.3 ± 0.1	15 ± 1	5.0 ± 0.2
SHARDS10014850	12:37:36.3	62:14:53.0	5.77 ± 0.06	3.5 ± 2.9	261 ± 221	3.0 ± 1.6	0.6 ± 0.7	23 ± 11	2.5 ± 1.5
SHARDS10004470	12:37:36.6	62:19:18.8	3.56 ± 0.06	1.5 ± 0.3	67 ± 20	2.7 ± 1.4	—	—	—
SHARDS10007053	12:37:36.7	62:14:41.6	4.48 ± 0.07	14.0 ± 5.0	700 ± 270	3.0 ± 1.6	1.2 ± 1.4	28 ± 11	1.4 ± 1.1
SHARDS10008724	12:37:36.8	62:15:43.5	4.10 ± 0.07	0.2 ± 0.1	11 ± 4	2.9 ± 1.4	—	—	—
SHARDS10006655	12:37:37.0	62:13:07.5	3.53 ± 0.06	9.6 ± 5.2	720 ± 360	3.0 ± 1.6	0.5 ± 0.7	18 ± 6	3.0 ± 1.6
SHARDS10006575	12:37:37.0	62:13:31.6	3.79 ± 0.06	6.7 ± 6.4	393 ± 280	3.0 ± 1.6	0.2 ± 0.1	19 ± 3	4.4 ± 1.0
SHARDS10005648	12:37:37.0	62:13:10.1	4.21 ± 0.07	9.7 ± 6.0	710 ± 280	3.0 ± 1.6	2.5 ± 2.1	23 ± 3	1.0 ± 0.1
SHARDS10009625	12:37:37.1	62:13:30.9	3.79 ± 0.06	7.9 ± 1.1	1260 ± 200	3.0 ± 1.6	0.2 ± 0.1	22 ± 5	1.1 ± 0.4

Continued on next page

Table A.2 – *Continued from previous page*

Object Name	R.A. (J2000)	Dec. (J2000)	z	$M_{\rm star,m}$ (10^9 $M_\odot$)	$\rm Age_m$ (Myr)	$\tau_{\rm m}$ (Myr)	$M_{\rm star,b}$ (10^9 $M_\odot$)	$\rm Age_b$ (Myr)	$\tau_{\rm b}$ (Myr)
SHARDS10006422	12:37:37.3	62:15:05.8	4.09 ± 0.07	1.4 ± 0.7	20 ± 10	3.1 ± 1.6	–	–	–
SHARDS10010725	12:37:37.3	62:18:05.6	3.97 ± 0.06	3.7 ± 1.0	1200 ± 300	3.0 ± 1.6	0.2 ± 0.2	30 ± 13	1.8 ± 1.4
SHARDS10005659	12:37:37.5	62:19:37.2	4.68 ± 0.07	8.7 ± 2.4	84 ± 26	2.9 ± 1.4	–	–	–
SHARDS10000519	12:37:37.8	62:13:23.6	3.78 ± 0.06	2.2 ± 0.6	33 ± 7	1.7 ± 0.8	–	–	–
SHARDS10007402	12:37:37.9	62:19:45.8	4.27 ± 0.07	2.5 ± 0.9	44 ± 21	2.2 ± 1.2	–	–	–
SHARDS10009250	12:37:37.9	62:13:22.5	3.92 ± 0.06	0.5 ± 0.2	36 ± 14	2.3 ± 1.3	–	–	–
SHARDS10008683	12:37:38.2	62:14:22.1	4.23 ± 0.07	1.5 ± 0.9	47 ± 36	2.2 ± 1.2	–	–	–
SHARDS10007001	12:37:38.2	62:16:56.7	3.41 ± 0.07	1.6 ± 0.3	44 ± 11	2.2 ± 1.1	–	–	–
SHARDS10006556	12:37:38.2	62:18:32.8	3.97 ± 0.06	8.1 ± 1.1	1100 ± 240	3.0 ± 1.6	0.2 ± 0.1	18 ± 3	4.2 ± 1.3
SHARDS10005435	12:37:38.3	62:15:24.9	4.09 ± 0.07	5.0 ± 2.2	270 ± 280	3.0 ± 1.6	0.6 ± 0.8	26 ± 11	2.8 ± 1.6
SHARDS10013772	12:37:38.4	62:14:22.0	3.80 ± 0.06	0.6 ± 0.6	71 ± 63	2.6 ± 1.4	–	–	–
SHARDS10006277	12:37:38.6	62:19:11.8	3.56 ± 0.06	4.2 ± 0.5	88 ± 13	2.8 ± 1.4	–	–	–
SHARDS10007323	12:37:38.9	62:19:46.0	4.52 ± 0.07	20.0 ± 8.0	730 ± 310	3.0 ± 1.6	0.8 ± 0.6	21 ± 6	1.9 ± 1.1
SHARDS10007422	12:37:39.1	62:17:36.8	4.26 ± 0.07	70.4 ± 10.0	560 ± 80	3.0 ± 1.6	1.9 ± 0.5	25 ± 3	1.0 ± 0.2
SHARDS10009103	12:37:39.1	62:17:34.6	4.51 ± 0.07	20.0 ± 7.0	840 ± 220	3.0 ± 1.6	1.2 ± 1.2	31 ± 12	1.5 ± 1.1
SHARDS10014515	12:37:39.3	62:17:35.1	4.51 ± 0.07	38.0 ± 6.0	229 ± 90	3.0 ± 1.6	2.0 ± 1.7	22 ± 7	3.2 ± 1.3
SHARDS10007188	12:37:39.4	62:17:34.6	4.51 ± 0.07	16.3 ± 10.7	390 ± 280	3.0 ± 1.6	4.5 ± 3.3	28 ± 9	1.2 ± 0.8
SHARDS10007963	12:37:39.5	62:17:35.5	4.51 ± 0.07	0.9 ± 0.3	19 ± 6	3.2 ± 1.4	–	–	–
SHARDS10008734	12:37:39.6	62:20:00.7	5.51 ± 0.07	13.0 ± 7.0	450 ± 270	3.0 ± 1.6	0.6 ± 0.6	16 ± 5	4.1 ± 1.3
SHARDS10009758	12:37:39.7	62:16:03.5	3.54 ± 0.06	7.0 ± 1.6	1200 ± 300	3.0 ± 1.6	0.2 ± 0.1	21 ± 3	1.0 ± 0.2
SHARDS10011904	12:37:39.9	62:19:59.4	6.07 ± 0.07	27.0 ± 9.0	618 ± 184	3.0 ± 1.6	1.1 ± 1.1	20 ± 6	2.1 ± 1.2
SHARDS10009578	12:37:40.2	62:13:30.8	3.65 ± 0.06	6.3 ± 3.9	670 ± 420	3.0 ± 1.6	0.9 ± 1.0	36 ± 13	2.0 ± 1.5
SHARDS10007069	12:37:40.4	62:15:35.4	4.79 ± 0.07	27.0 ± 6.0	553 ± 233	3.0 ± 1.6	2.1 ± 1.4	41 ± 12	2.4 ± 1.6
SHARDS10010443	12:37:40.4	62:13:29.2	6.00 ± 0.07	22.1 ± 13.9	537 ± 233	3.0 ± 1.6	4.5 ± 4.5	32 ± 11	1.4 ± 0.9
SHARDS10005145	12:37:40.6	62:17:01.8	3.55 ± 0.06	17.0 ± 5.0	842 ± 237	3.0 ± 1.6	3.9 ± 2.1	46 ± 9	2.1 ± 1.0
SHARDS10005891	12:37:40.7	62:13:47.3	3.65 ± 0.06	5.1 ± 2.9	380 ± 340	3.0 ± 1.6	2.0 ± 1.4	46 ± 9	2.4 ± 1.5
SHARDS10006420	12:37:41.0	62:18:05.9	4.81 ± 0.07	33.0 ± 9.0	830 ± 280	3.0 ± 1.6	0.9 ± 0.4	22 ± 8	2.1 ± 1.2
SHARDS10005568	12:37:41.0	62:15:03.9	3.67 ± 0.06	3.5 ± 0.8	42 ± 13	2.0 ± 1.1	–	–	–
SHARDS10006420	12:37:41.0	62:18:05.4	4.81 ± 0.07	19.0 ± 6.0	780 ± 280	3.0 ± 1.6	0.7 ± 0.4	19 ± 5	1.9 ± 1.1
SHARDS10005824	12:37:41.7	62:17:18.3	3.69 ± 0.06	4.4 ± 1.4	57 ± 26	2.5 ± 1.3	–	–	–
SHARDS10008395	12:37:41.8	62:15:39.4	3.81 ± 0.06	2.8 ± 2.4	420 ± 390	3.0 ± 1.6	0.4 ± 0.5	14 ± 6	3.7 ± 1.5
SHARDS10005948	12:37:41.8	62:17:30.4	3.97 ± 0.06	5.0 ± 0.8	52 ± 9	2.6 ± 1.3	–	–	–
SHARDS10007735	12:37:42.0	62:17:37.3	3.69 ± 0.06	15.0 ± 4.0	1000 ± 300	3.0 ± 1.6	1.6 ± 0.7	26 ± 6	1.1 ± 0.5
SHARDS10012166	12:37:42.2	62:17:21.4	4.26 ± 0.07	3.8 ± 2.9	710 ± 380	3.0 ± 1.6	0.1 ± 0.2	14 ± 5	4.2 ± 1.2
SHARDS10005984	12:37:42.3	62:17:29.6	3.69 ± 0.06	1.4 ± 0.5	25 ± 10	3.2 ± 1.3	–	–	–
SHARDS10011464	12:37:42.9	62:15:32.4	4.25 ± 0.07	44.0 ± 4.0	910 ± 235	3.0 ± 1.6	1.4 ± 0.5	31 ± 11	1.6 ± 1.3
SHARDS10005776	12:37:43.0	62:17:25.7	3.55 ± 0.06	10.2 ± 1.6	74 ± 16	2.9 ± 1.4	–	–	–
SHARDS10005382	12:37:43.0	62:15:34.5	3.95 ± 0.06	8.6 ± 1.9	81 ± 15	2.9 ± 1.4	–	–	–
SHARDS10006681	12:37:43.4	62:16:56.0	4.26 ± 0.07	17.0 ± 3.0	717 ± 227	3.0 ± 1.6	1.0 ± 0.6	25 ± 6	1.1 ± 0.5
SHARDS10008866	12:37:43.7	62:15:53.6	3.68 ± 0.06	3.3 ± 1.1	140 ± 60	3.0 ± 1.4	–	–	–
SHARDS10007289	12:37:44.6	62:14:03.0	3.66 ± 0.06	6.1 ± 0.8	120 ± 50	2.7 ± 1.4	–	–	–
SHARDS10008475	12:37:44.7	62:15:54.1	5.48 ± 0.07	5.2 ± 3.5	610 ± 300	3.0 ± 1.6	1.1 ± 1.2	16 ± 6	2.6 ± 1.6
SHARDS10006493	12:37:44.8	62:18:17.2	5.09 ± 0.06	1.1 ± 0.5	18 ± 5	3.5 ± 1.2	–	–	–
SHARDS10008700	12:37:45.0	62:18:20.3	5.09 ± 0.06	0.3 ± 0.1	7 ± 1	3.5 ± 1.3	–	–	–
SHARDS10008759	12:37:45.1	62:17:34.8	3.42 ± 0.07	1.2 ± 0.5	69 ± 39	2.7 ± 1.4	–	–	–
SHARDS10007908	12:37:45.2	62:16:20.6	4.11 ± 0.07	6.1 ± 2.2	1100 ± 400	3.0 ± 1.6	0.6 ± 0.7	26 ± 10	1.3 ± 0.9
SHARDS10006737	12:37:45.8	62:17:56.5	3.56 ± 0.06	1.1 ± 0.4	56 ± 20	2.5 ± 1.3	–	–	–
SHARDS10005452	12:37:46.8	62:16:54.8	4.11 ± 0.07	38.0 ± 8.0	382 ± 159	3.0 ± 1.6	4.5 ± 3.0	41 ± 12	1.7 ± 1.1
SHARDS10010687	12:37:47.0	62:14:49.7	3.25 ± 0.07	2.0 ± 0.6	96 ± 36	3.0 ± 1.4	–	–	–

Continued on next page

Table A.2 – *Continued from previous page*

Object Name	R.A. (J2000)	Dec. (J2000)	z	$M_{\rm star,m}$ (10^9 $M_\odot$)	$\rm Age_m$ (Myr)	$\tau_{\rm m}$ (Myr)	$M_{\rm star,b}$ (10^9 $M_\odot$)	$\rm Age_b$ (Myr)	$\tau_{\rm b}$ (Myr)
SHARDS10006143	12:37:47.3	62:17:59.4	3.56 ± 0.06	1.8 ± 0.4	26 ± 7	1.4 ± 0.6	—	—	—
SHARDS10006844	12:37:47.7	62:18:47.4	3.70 ± 0.06	0.2 ± 0.1	17 ± 6	2.5 ± 1.3	—	—	—
SHARDS10010353	12:37:47.8	62:17:59.9	3.56 ± 0.06	1.0 ± 0.4	80 ± 43	2.8 ± 1.4	0.7 ± 0.4	21 ± 6	2.8 ± 1.0
SHARDS10009098	12:37:48.0	62:17:38.8	4.67 ± 0.07	25.0 ± 8.0	600 ± 310	3.0 ± 1.6	0.4 ± 0.5	16 ± 5	3.5 ± 1.5
SHARDS10009143	12:37:48.3	62:14:27.7	5.46 ± 0.07	2.3 ± 1.9	509 ± 300	3.0 ± 1.6	—	—	—
SHARDS10005391	12:37:48.4	62:14:24.5	4.23 ± 0.07	2.7 ± 0.7	36 ± 7	1.8 ± 0.8	—	—	—
SHARDS10009493	12:37:48.5	62:17:48.2	4.27 ± 0.07	0.3 ± 0.2	10 ± 3	2.9 ± 1.5	0.3 ± 0.3	17 ± 4	3.8 ± 1.4
SHARDS10010344	12:37:48.6	62:14:54.7	4.24 ± 0.07	7.0 ± 2.6	850 ± 310	3.0 ± 1.6	—	—	—
SHARDS10012008	12:37:49.2	62:13:38.2	5.79 ± 0.06	8.1 ± 3.1	100 ± 46	2.9 ± 1.4	—	—	—
SHARDS10005365	12:37:49.8	62:19:05.1	4.12 ± 0.07	1.5 ± 0.5	15 ± 5	2.8 ± 1.5	—	—	—
SHARDS10008004	12:37:49.8	62:17:22.4	5.50 ± 0.07	11.0 ± 5.0	720 ± 247	3.0 ± 1.6	0.6 ± 0.6	17 ± 5	1.5 ± 0.9
SHARDS10006361	12:37:49.9	62:19:05.8	4.12 ± 0.07	5.5 ± 2.0	94 ± 69	2.9 ± 1.4	—	—	—
SHARDS10006843	12:37:50.1	62:17:32.9	3.97 ± 0.06	9.1 ± 2.8	140 ± 50	3.0 ± 1.4	—	—	—
SHARDS10006875	12:37:50.6	62:18:46.4	4.27 ± 0.07	6.9 ± 2.1	99 ± 46	3.0 ± 1.4	—	—	—
SHARDS10002975	12:37:50.9	62:18:33.3	3.56 ± 0.06	2.8 ± 1.0	27 ± 9	2.8 ± 1.4	—	—	—
SHARDS10002976	12:37:50.9	62:18:32.1	3.42 ± 0.07	2.0 ± 0.4	31 ± 7	1.6 ± 0.7	—	—	—
SHARDS10008022	12:37:51.1	62:18:27.8	3.84 ± 0.06	2.2 ± 1.0	99 ± 66	2.8 ± 1.4	—	—	—
SHARDS10006376	12:37:51.2	62:18:49.1	4.39 ± 0.06	16.0 ± 4.0	377 ± 165	3.0 ± 1.6	0.5 ± 0.2	19 ± 5	4.0 ± 1.3
SHARDS10008351	12:37:51.4	62:17:10.2	3.55 ± 0.06	4.6 ± 1.1	93 ± 27	3.0 ± 1.4	—	—	—
SHARDS10005306	12:37:51.7	62:18:00.5	3.56 ± 0.06	2.5 ± 0.5	22 ± 4	2.4 ± 1.0	—	—	—
SHARDS10005243	12:37:51.9	62:17:48.7	4.27 ± 0.07	8.7 ± 1.9	35 ± 9	1.7 ± 0.9	—	—	—
SHARDS10006925	12:37:52.0	62:14:59.9	4.78 ± 0.07	1.9 ± 1.0	52 ± 21	2.4 ± 1.3	—	—	—
SHARDS10006086	12:37:52.4	62:13:50.9	5.07 ± 0.06	41.0 ± 8.0	652 ± 225	3.0 ± 1.6	1.5 ± 0.9	15 ± 5	1.6 ± 0.9
SHARDS10005768	12:37:52.9	62:16:44.7	3.27 ± 0.07	5.3 ± 0.9	115 ± 23	3.0 ± 1.4	—	—	—
SHARDS10008785	12:37:53.1	62:17:20.8	3.69 ± 0.06	0.9 ± 0.5	61 ± 33	2.6 ± 1.4	—	—	—
SHARDS10006046	12:37:53.1	62:16:54.4	3.27 ± 0.07	1.4 ± 0.4	37 ± 13	2.0 ± 1.0	—	—	—
SHARDS10007862	12:37:53.2	62:18:39.1	3.98 ± 0.06	1.4 ± 0.7	100 ± 50	2.9 ± 1.4	—	—	—
SHARDS10006804	12:37:53.6	62:16:09.3	4.25 ± 0.07	0.7 ± 0.4	20 ± 10	2.8 ± 1.5	—	—	—
SHARDS10012002	12:37:53.8	62:16:32.5	5.49 ± 0.07	8.6 ± 5.4	370 ± 250	2.8 ± 1.6	0.6 ± 0.8	18 ± 6	3.1 ± 1.6
SHARDS10019053	12:37:54.0	62:17:20.1	4.38 ± 0.06	70.9 ± 19.0	1200 ± 100	3.0 ± 1.6	1.8 ± 0.5	47 ± 8	3.6 ± 1.6
SHARDS10006542	12:37:54.3	62:15:31.8	3.95 ± 0.06	8.7 ± 9.6	100 ± 14	2.9 ± 1.4	—	—	—
SHARDS10008031	12:37:54.5	62:16:28.1	3.69 ± 0.06	4.6 ± 2.0	130 ± 100	3.0 ± 1.4	—	—	—
SHARDS10006864	12:37:55.1	62:17:05.7	3.42 ± 0.07	1.1 ± 0.4	65 ± 22	2.7 ± 1.4	—	—	—
SHARDS10005566	12:37:55.3	62:17:27.3	4.26 ± 0.07	7.5 ± 1.9	49 ± 16	2.4 ± 1.2	—	—	—
SHARDS10007686	12:37:55.5	62:15:36.4	4.25 ± 0.07	2.2 ± 1.0	37 ± 14	2.0 ± 1.1	—	—	—
SHARDS10002731	12:37:56.0	62:17:05.2	3.55 ± 0.06	9.2 ± 1.3	44 ± 10	1.9 ± 1.0	—	—	—
SHARDS10005327	12:37:56.1	62:16:04.7	3.82 ± 0.06	4.8 ± 2.1	67 ± 28	2.6 ± 1.4	—	—	—
SHARDS10008277	12:37:56.1	62:17:21.0	5.22 ± 0.06	0.6 ± 0.2	37 ± 16	2.1 ± 1.2	—	—	—
SHARDS10006259	12:37:56.4	62:16:25.6	4.26 ± 0.07	2.9 ± 0.8	72 ± 28	2.8 ± 1.4	—	—	—
SHARDS10007449	12:37:56.5	62:15:42.9	4.67 ± 0.07	0.7 ± 0.2	44 ± 12	2.2 ± 1.2	—	—	—
SHARDS10004816	12:37:56.9	62:15:39.8	3.82 ± 0.06	4.5 ± 2.7	860 ± 409	3.0 ± 1.6	0.7 ± 0.8	36 ± 12	1.7 ± 1.2
SHARDS10010016	12:37:57.5	62:17:18.7	4.81 ± 0.07	29.8 ± 10.9	66 ± 23	2.6 ± 1.2	—	—	—
SHARDS10007627	12:37:58.4	62:16:09.4	3.41 ± 0.07	7.6 ± 1.5	100 ± 80	2.8 ± 1.4	—	—	—
SHARDS10005511	12:38:00.8	62:15:47.2	4.66 ± 0.07	7.9 ± 6.9	87 ± 13	3.1 ± 1.4	—	—	—
SHARDS10006151	12:38:03.4	62:16:26.0	5.34 ± 0.07	24.0 ± 6.0	55 ± 18	2.5 ± 1.2	—	—	—
		62:16:15.7	4.25 ± 0.07	1.1 ± 0.4	17 ± 6	2.9 ± 1.5	—	—	—

Table A.3: Overview of the galaxies found in close groups. (1) Group identification. (2) SHARDS identification. (3) Right ascension. (4) Declination. (5) Distance between the objects in the group. In case of more than two objects in a group, the distance shown is the largest between the central object and the rest. (6) Photometric redshift.

Group (1)	Source ID (2)	R.A. (J2000) (3)	Dec. (J2000) (4)	Distance (kpc) (5)	Redshift (6)
G1	SHARDS10005314	12:37:24.06	62:18:33.45	6.57 ± 0.09	3.42 ± 0.07
G1	SHARDS10008105	12:37:24.01	62:18:32.67	6.57 ± 0.09	3.42 ± 0.07
G1	SHARDS10013381	12:37:24.10	62:18:34.25	6.57 ± 0.09	3.42 ± 0.07
G2	SHARDS10004588	12:37:17.72	62:19:04.59	45.65 ± 2.85	3.96 ± 0.06
G2	SHARDS10007056	12:37:17.21	62:18:59.31	45.65 ± 2.85	3.96 ± 0.06
G3	SHARDS20005310	12:36:28.03	62:09:01.82	5.86 ± 0.08	3.92 ± 0.06
G3	SHARDS20011181	12:36:28.14	62:09:01.52	5.86 ± 0.08	3.92 ± 0.06
G4	SHARDS20005660	12:36:50.68	62:09:32.47	30.26 ± 1.13	4.24 ± 0.07
G4	SHARDS20009490	12:36:51.10	62:09:35.58	30.26 ± 1.13	4.24 ± 0.07
G5	SHARDS10006493	12:37:44.84	62:18:17.25	20.56 ± 0.73	5.09 ± 0.06
G5	SHARDS10008700	12:37:44.98	62:18:20.28	20.56 ± 0.73	5.09 ± 0.06
G6	SHARDS10009103	12:37:39.15	62:17:34.59	9.15 ± 0.13	4.51 ± 0.07
G6	SHARDS10007188	12:37:39.38	62:17:34.55	9.15 ± 0.13	4.51 ± 0.07
G6	SHARDS10007963	12:37:39.47	62:17:35.47	9.15 ± 0.13	4.51 ± 0.07
G6	SHARDS10014515	12:37:39.28	62:17:35.06	9.15 ± 0.13	4.51 ± 0.07
G7	SHARDS20009174	12:37:01.39	62:09:09.95	50.23 ± 4.24	4.35 ± 0.06
G7	SHARDS20006656	12:37:01.04	62:09:16.78	50.23 ± 4.24	4.35 ± 0.06
G8	SHARDS20006276	12:36:04.10	62:09:21.99	18.50 ± 0.35	3.75 ± 0.06
G8	SHARDS20005680	12:36:04.40	62:09:23.37	18.50 ± 0.35	3.75 ± 0.06
G9	SHARDS20008735	12:36:28.26	62:08:50.89	17.45 ± 0.26	4.21 ± 0.07
G9	SHARDS20008303	12:36:28.60	62:08:51.41	17.45 ± 0.26	4.32 ± 0.06
G10	SHARDS20005675	12:36:45.20	62:09:33.70	3.26 ± 0.03	4.35 ± 0.06
G10	SHARDS20005675	12:36:45.20	62:09:33.70	3.26 ± 0.03	4.35 ± 0.06
G11	SHARDS20006187	12:36:42.88	62:09:58.50	8.47 ± 0.11	3.67 ± 0.06
G11	SHARDS20005617	12:36:42.96	62:09:57.51	8.47 ± 0.11	3.67 ± 0.06
G12	SHARDS20022647	12:36:55.16	62:10:36.18	14.97 ± 0.44	4.25 ± 0.07
G12	SHARDS20022674	12:36:55.16	62:10:34.05	14.97 ± 0.44	4.37 ± 0.06
G13	SHARDS20006868	12:36:18.83	62:11:23.97	38.25 ± 1.02	4.22 ± 0.07
G13	SHARDS20006793	12:36:18.14	62:11:26.48	38.25 ± 1.02	4.34 ± 0.06
G14	SHARDS20011174	12:37:02.37	62:11:32.96	59.64 ± 3.63	5.35 ± 0.07
G14	SHARDS20011267	12:37:02.81	62:11:41.66	59.64 ± 3.63	5.36 ± 0.07
G14	SHARDS20014132	12:37:01.36	62:11:39.36	59.64 ± 3.63	5.36 ± 0.07
G15	SHARDS20009724	12:37:03.09	62:11:37.87	50.53 ± 1.73	3.55 ± 0.06
G15	SHARDS20002484	12:37:03.87	62:11:41.75	50.53 ± 1.73	3.55 ± 0.06
G16	SHARDS20005458	12:36:14.51	62:11:40.62	14.02 ± 0.18	4.33 ± 0.06
G16	SHARDS20008356	12:36:14.80	62:11:40.40	14.02 ± 0.18	4.22 ± 0.07
G17	SHARDS20010716	12:36:37.34	62:11:51.53	8.50 ± 0.11	5.62 ± 0.07
G17	SHARDS20011958	12:36:37.54	62:11:51.78	8.50 ± 0.11	5.63 ± 0.07
G18	SHARDS20012876	12:37:03.71	62:11:57.72	6.50 ± 0.08	5.22 ± 0.06
G18	SHARDS20013448	12:37:03.61	62:11:58.46	6.50 ± 0.08	5.22 ± 0.06
G19	SHARDS20003443	12:36:31.05	62:12:15.59	26.07 ± 0.84	3.54 ± 0.06
G19	SHARDS20005124	12:36:31.31	62:12:18.50	26.07 ± 0.84	3.54 ± 0.06
G20	SHARDS10005492	12:37:21.48	62:12:17.60	29.42 ± 1.70	4.58 ± 0.07
G20	SHARDS10009097	12:37:21.29	62:12:21.74	29.42 ± 1.70	4.58 ± 0.07

Continued on next page

Table A.3 – *Continued from previous page*

Group	Source ID	R.A. (J2000)	Dec. (J2000)	Distance (kpc)	Redshift
G21	SHARDS20016606	12:36:34.22	62:12:28.22	36.38 ± 0.58	3.41 ± 0.07
G21	SHARDS20006329	12:36:33.74	62:12:30.87	36.38 ± 0.58	3.54 ± 0.06
G21	SHARDS20004876	12:36:33.07	62:12:30.30	36.38 ± 0.58	3.54 ± 0.06
G22	SHARDS20022683	12:37:11.11	62:12:43.55	40.44 ± 2.18	3.89 ± 0.06
G22	SHARDS20004928	12:37:10.66	62:12:38.99	40.44 ± 2.18	3.83 ± 0.06
G23	SHARDS20006306	12:36:20.29	62:13:59.32	54.85 ± 1.82	3.81 ± 0.06
G23	SHARDS20008408	12:36:20.39	62:13:58.54	54.85 ± 1.82	3.81 ± 0.06
G23	SHARDS20007883	12:36:21.32	62:13:54.84	54.85 ± 1.82	3.81 ± 0.06
G24	SHARDS20010722	12:36:12.05	62:14:11.31	46.91 ± 3.52	4.34 ± 0.06
G24	SHARDS20011200	12:36:12.44	62:14:17.49	46.91 ± 3.52	4.23 ± 0.07
G25	SHARDS10008703	12:37:32.62	62:12:47.02	56.32 ± 5.07	3.63 ± 0.06
G25	SHARDS10008870	12:37:32.80	62:12:39.58	56.32 ± 5.07	3.63 ± 0.06
G26	SHARDS20005166	12:36:00.84	62:12:52.37	16.98 ± 0.20	3.50 ± 0.06
G26	SHARDS20005022	12:36:01.16	62:12:52.33	16.98 ± 0.20	3.50 ± 0.06
G26	SHARDS20005185	12:36:01.25	62:12:53.70	16.98 ± 0.20	3.50 ± 0.06
G27	SHARDS10000371	12:37:21.45	62:12:59.19	7.04 ± 0.08	3.63 ± 0.06
G27	SHARDS10008057	12:37:21.49	62:13:00.07	7.04 ± 0.08	3.63 ± 0.06
G28	SHARDS10005275	12:37:17.84	62:13:04.08	40.52 ± 2.88	4.31 ± 0.06
G28	SHARDS10007010	12:37:18.05	62:13:09.71	40.52 ± 2.88	4.31 ± 0.06
G29	SHARDS20005951	12:37:02.90	62:13:06.65	51.46 ± 4.49	4.29 ± 0.06
G29	SHARDS20005736	12:37:03.28	62:13:00.55	51.46 ± 4.49	4.29 ± 0.06
G29	SHARDS20006714	12:37:03.61	62:12:53.55	51.46 ± 4.49	4.41 ± 0.06
G30	SHARDS20007199	12:36:14.43	62:13:10.04	34.76 ± 1.22	4.90 ± 0.08
G30	SHARDS20010508	12:36:15.06	62:13:12.99	34.76 ± 1.22	4.90 ± 0.08
G31	SHARDS10005608	12:37:21.28	62:13:10.25	23.81 ± 0.40	3.38 ± 0.07
G31	SHARDS10010894	12:37:21.71	62:13:10.97	23.81 ± 0.40	3.50 ± 0.06
G32	SHARDS20008556	12:36:35.52	62:13:12.99	56.89 ± 1.33	4.10 ± 0.07
G32	SHARDS20007099	12:36:34.43	62:13:15.61	56.89 ± 1.33	4.10 ± 0.07
G33	SHARDS20005240	12:37:05.07	62:13:15.80	58.90 ± 6.42	4.29 ± 0.06
G33	SHARDS20007957	12:37:05.04	62:13:07.35	58.90 ± 6.42	4.18 ± 0.07
G34	SHARDS20005331	12:36:53.14	62:13:31.73	59.76 ± 3.57	3.56 ± 0.06
G34	SHARDS20002671	12:36:52.41	62:13:37.81	59.76 ± 3.57	3.56 ± 0.06
G35	SHARDS10000575	12:37:37.02	62:13:31.57	7.38 ± 0.09	3.79 ± 0.06
G35	SHARDS10009625	12:37:37.13	62:13:30.92	7.38 ± 0.09	3.79 ± 0.06
G36	SHARDS20006720	12:36:18.99	62:13:59.08	57.66 ± 3.09	3.95 ± 0.06
G36	SHARDS20005235	12:36:19.85	62:14:04.36	57.66 ± 3.09	3.95 ± 0.06
G36	SHARDS20004366	12:36:20.74	62:14:07.82	57.66 ± 3.09	3.95 ± 0.06
G37	SHARDS20025321	12:37:09.83	62:14:01.94	55.10 ± 5.52	3.91 ± 0.06
G37	SHARDS10011820	12:37:09.76	62:14:09.52	55.10 ± 5.52	3.91 ± 0.06
G38	SHARDS10000864	12:37:29.65	62:14:11.24	39.60 ± 2.14	3.51 ± 0.06
G38	SHARDS10007431	12:37:29.35	62:14:16.06	39.60 ± 2.14	3.39 ± 0.07
G38	SHARDS10000918	12:37:28.84	62:14:18.88	39.60 ± 2.14	3.52 ± 0.06
G38	SHARDS10008196	12:37:28.88	62:14:19.65	39.60 ± 2.14	3.52 ± 0.06
G39	SHARDS10006221	12:37:28.79	62:14:17.06	43.60 ± 2.55	3.65 ± 0.06
G39	SHARDS10000943	12:37:29.19	62:14:22.22	43.60 ± 2.55	3.65 ± 0.06
G40	SHARDS20006130	12:36:18.64	62:14:21.42	34.45 ± 0.46	4.36 ± 0.06
G40	SHARDS20004728	12:36:17.94	62:14:21.93	34.45 ± 0.46	4.24 ± 0.07
G41	SHARDS20024698	12:37:03.53	62:14:29.70	10.09 ± 0.14	4.31 ± 0.06
G41	SHARDS20025317	12:37:03.71	62:14:30.34	10.09 ± 0.14	4.20 ± 0.07
G42	SHARDS10005600	12:37:11.89	62:14:35.01	18.70 ± 0.32	4.45 ± 0.07
G42	SHARDS10006574	12:37:12.25	62:14:36.07	18.70 ± 0.32	4.33 ± 0.06
G43	SHARDS20007340	12:36:51.25	62:14:53.23	42.91 ± 3.60	4.52 ± 0.07
G43	SHARDS20005336	12:36:51.32	62:14:59.51	42.91 ± 3.60	4.58 ± 0.07

Continued on next page

Table A.3 – *Continued from previous page*

Group	Source ID	R.A. (J2000)	Dec. (J2000)	Distance (kpc)	Redshift
G44	SHARDS10007523	12:37:03.87	62:15:02.89	51.11 ± 1.33	4.45 ± 0.07
G44	SHARDS10006795	12:37:04.85	62:15:00.05	51.11 ± 1.33	4.45 ± 0.07
G45	SHARDS10006279	12:37:11.11	62:15:04.73	32.37 ± 0.89	4.46 ± 0.07
G45	SHARDS10007484	12:37:11.68	62:15:07.23	32.37 ± 0.89	4.46 ± 0.07
G46	SHARDS20023901	12:36:54.59	62:15:05.23	46.33 ± 4.55	4.58 ± 0.07
G46	SHARDS20024156	12:36:54.12	62:15:06.34	46.33 ± 4.55	4.58 ± 0.07
G46	SHARDS20022948	12:36:54.56	62:14:58.39	46.33 ± 4.55	4.72 ± 0.07
G47	SHARDS20006371	12:36:30.21	62:15:08.38	52.64 ± 2.30	3.68 ± 0.06
G47	SHARDS20004011	12:36:29.44	62:15:12.99	52.64 ± 2.30	3.68 ± 0.06
G48	SHARDS20008709	12:36:47.74	62:15:09.17	10.23 ± 0.19	4.57 ± 0.07
G48	SHARDS20018017	12:36:47.60	62:15:07.97	10.23 ± 0.19	4.52 ± 0.07
G49	SHARDS20006419	12:36:51.88	62:15:14.53	9.24 ± 0.17	3.37 ± 0.07
G49	SHARDS20004816	12:36:51.85	62:15:15.71	9.24 ± 0.17	3.37 ± 0.07
G50	SHARDS20006845	12:36:20.72	62:15:30.57	13.95 ± 0.42	4.91 ± 0.08
G50	SHARDS20007866	12:36:20.61	62:15:32.56	13.95 ± 0.42	4.91 ± 0.08
G51	SHARDS20012395	12:36:24.01	62:15:43.37	28.37 ± 1.19	4.65 ± 0.07
G51	SHARDS20010534	12:36:24.39	62:15:46.64	28.37 ± 1.19	4.79 ± 0.07
G52	SHARDS10005433	12:37:10.66	62:16:010.0	45.08 ± 1.31	4.62 ± 0.07
G52	SHARDS10010161	12:37:09.79	62:16:07.16	45.08 ± 1.31	4.62 ± 0.07
G53	SHARDS10006400	12:37:05.36	62:16:11.03	9.32 ± 0.17	4.46 ± 0.07
G53	SHARDS10006400	12:37:05.36	62:16:11.03	9.32 ± 0.17	4.46 ± 0.07
G53	SHARDS10017828	12:37:05.33	62:16:09.68	9.32 ± 0.17	4.46 ± 0.07
G54	SHARDS10006572	12:37:15.65	62:16:47.76	9.48 ± 0.13	4.36 ± 0.06
G54	SHARDS10017152	12:37:15.84	62:16:47.40	9.48 ± 0.13	4.24 ± 0.07
G55	SHARDS20004779	12:36:25.97	62:08:59.41	67.41 ± 8.29	4.32 ± 0.06
G55	SHARDS20000859	12:36:25.92	62:09:03.62	67.41 ± 8.29	4.32 ± 0.06
G55	SHARDS20007108	12:36:26.12	62:09:01.16	67.41 ± 8.29	4.32 ± 0.06
G55	SHARDS20005242	12:36:25.99	62:09:00.29	67.41 ± 8.29	4.32 ± 0.06
G55	SHARDS20006463	12:36:25.34	62:09:09.58	67.41 ± 8.29	4.32 ± 0.06
G55	SHARDS20005536	12:36:26.11	62:09:13.23	67.41 ± 8.29	4.21 ± 0.07
G56	SHARDS10007735	12:37:41.99	62:17:37.26	58.86 ± 5.35	3.69 ± 0.06
G56	SHARDS10005984	12:37:42.30	62:17:29.61	58.86 ± 5.35	3.69 ± 0.06
G57	SHARDS10015064	12:37:25.65	62:17:43.16	47.94 ± 2.45	6.74 ± 0.14
G57	SHARDS10016008	12:37:26.80	62:17:39.80	47.94 ± 2.45	6.74 ± 0.14
G58	SHARDS10005366	12:37:00.66	62:17:56.02	57.12 ± 5.57	4.23 ± 0.07
G58	SHARDS10014300	12:37:00.21	62:18:03.54	57.12 ± 5.57	4.23 ± 0.07
G59	SHARDS10006143	12:37:47.27	62:17:59.37	26.86 ± 0.33	3.56 ± 0.06
G59	SHARDS10010353	12:37:47.78	62:17:59.91	26.86 ± 0.33	3.56 ± 0.06
G60	SHARDS10011163	12:37:04.03	62:18:00.13	47.06 ± 1.82	4.35 ± 0.06
G60	SHARDS10007674	12:37:04.82	62:18:04.12	47.06 ± 1.82	4.23 ± 0.07
G61	SHARDS10006420	12:37:40.99	62:18:05.95	4.27 ± 0.04	4.81 ± 0.07
G61	SHARDS10006420	12:37:40.99	62:18:05.95	4.27 ± 0.04	4.81 ± 0.07
G62	SHARDS10005822	12:37:22.93	62:18:11.51	59.96 ± 1.90	3.54 ± 0.06
G62	SHARDS10006257	12:37:23.92	62:18:15.43	59.96 ± 1.90	3.42 ± 0.07
G63	SHARDS10016909	12:36:43.53	62:18:16.46	5.78 ± 0.07	4.44 ± 0.07
G63	SHARDS10005410	12:36:43.44	62:18:15.89	5.78 ± 0.07	4.44 ± 0.07
G64	SHARDS20006670	12:36:15.30	62:11:10.44	10.23 ± 0.20	4.21 ± 0.07
G64	SHARDS20004964	12:36:15.33	62:11:11.88	10.23 ± 0.20	4.33 ± 0.06
G65	SHARDS10005595	12:37:18.98	62:22:29.66	55.81 ± 4.30	4.25 ± 0.07
G65	SHARDS10006108	12:37:19.65	62:22:36.14	55.81 ± 4.30	4.25 ± 0.07
G66	SHARDS10006522	12:37:12.83	62:21:27.28	45.65 ± 3.49	4.25 ± 0.07
G66	SHARDS10006128	12:37:13.22	62:21:21.36	45.65 ± 3.49	4.25 ± 0.07

Continued on next page

Table A.3 – *Continued from previous page*

Group	Source ID	R.A. (J2000)	Dec. (J2000)	Distance (kpc)	Redshift
G67	SHARDS10006489	12:37:26.47	62:20:15.96	59.25 ± 7.33	4.94 ± 0.08
G67	SHARDS10008381	12:37:26.89	62:20:07.37	59.25 ± 7.33	4.94 ± 0.08
G68	SHARDS10008388	12:37:19.80	62:19:58.69	52.47 ± 2.74	4.38 ± 0.06
G68	SHARDS10004376	12:37:19.00	62:19:53.52	52.47 ± 2.74	4.26 ± 0.07
G69	SHARDS10006353	12:37:16.13	62:19:27.76	29.24 ± 0.37	3.54 ± 0.06
G69	SHARDS10007051	12:37:16.68	62:19:27.19	29.24 ± 0.37	3.54 ± 0.06
G70	SHARDS20005381	12:36:13.47	62:09:35.74	36.38 ± 1.01	4.19 ± 0.07
G70	SHARDS20011037	12:36:14.11	62:09:38.28	36.38 ± 1.01	4.31 ± 0.06
G71	SHARDS10005365	12:37:49.75	62:19:05.10	9.57 ± 0.14	4.12 ± 0.07
G71	SHARDS10006361	12:37:49.92	62:19:05.78	9.57 ± 0.14	4.12 ± 0.07
G72	SHARDS10006982	12:36:47.42	62:18:57.89	47.92 ± 2.24	3.64 ± 0.06
G72	SHARDS10010985	12:36:48.06	62:19:02.53	47.92 ± 2.24	3.64 ± 0.06
G73	SHARDS10006875	12:37:50.63	62:18:46.36	33.36 ± 1.01	4.27 ± 0.07
G73	SHARDS10006376	12:37:51.20	62:18:49.07	33.36 ± 1.01	4.39 ± 0.06
G74	SHARDS20007869	12:36:54.51	62:08:24.88	21.30 ± 1.01	4.76 ± 0.07
G74	SHARDS20009233	12:36:54.81	62:08:30.23	21.30 ± 1.01	4.76 ± 0.07
G74	SHARDS20010396	12:36:54.83	62:08:27.03	21.30 ± 1.01	4.62 ± 0.07
G75	SHARDS20025351	12:37:18.02	62:11:57.33	32.51 ± 0.51	4.17 ± 0.07
G75	SHARDS20025355	12:37:18.66	62:11:56.42	32.51 ± 0.51	4.17 ± 0.07
G76	SHARDS10017788	12:37:00.80	62:14:46.95	28.65 ± 0.34	3.49 ± 0.06
G76	SHARDS10014756	12:37:00.26	62:14:47.23	28.65 ± 0.34	3.49 ± 0.06
G77	SHARDS10010712	12:37:14.14	62:15:51.95	49.60 ± 4.30	4.47 ± 0.07
G77	SHARDS10014567	12:37:13.77	62:15:58.72	49.60 ± 4.30	4.35 ± 0.06
G78	SHARDS10011034	12:37:07.14	62:17:21.55	13.20 ± 0.30	3.80 ± 0.06
G78	SHARDS10010974	12:37:07.15	62:17:23.35	13.20 ± 0.30	3.80 ± 0.06
G79	SHARDS10013113	12:37:02.49	62:18:07.01	46.66 ± 3.58	4.23 ± 0.07
G79	SHARDS10012416	12:37:02.07	62:18:12.99	46.66 ± 3.58	4.35 ± 0.06
G80	SHARDS10007287	12:37:26.46	62:20:17.24	43.36 ± 3.54	4.67 ± 0.07
G80	SHARDS10008049	12:37:26.12	62:20:11.23	43.36 ± 3.54	4.67 ± 0.07
G81	SHARDS10017061	12:36:53.97	62:19:00.13	53.84 ± 0.71	3.51 ± 0.06
G81	SHARDS10011476	12:36:54.98	62:19:01.15	53.84 ± 0.71	3.52 ± 0.06
G82	SHARDS20005143	12:36:32.34	62:16:07.04	23.38 ± 0.53	3.83 ± 0.06
G82	SHARDS20011759	12:36:31.97	62:16:05.15	23.38 ± 0.53	3.82 ± 0.06
G83	SHARDS20012717	12:36:48.60	62:11:20.03	41.04 ± 3.26	4.66 ± 0.07
G83	SHARDS20011033	12:36:48.89	62:11:25.80	41.04 ± 3.26	4.66 ± 0.07
G84	SHARDS20004843	12:36:46.16	62:07:01.52	50.22 ± 2.83	4.44 ± 0.07
G84	SHARDS20006064	12:36:46.89	62:07:06.71	50.22 ± 2.83	4.31 ± 0.06
G85	SHARDS20004907	12:36:34.85	62:07:47.34	35.33 ± 1.79	4.31 ± 0.06
G85	SHARDS20000321	12:36:35.23	62:07:43.05	35.33 ± 1.79	4.31 ± 0.06
G86	SHARDS10010812	12:37:29.77	62:19:41.09	35.48 ± 0.74	4.27 ± 0.07
G86	SHARDS10011676	12:37:30.45	62:19:39.29	35.48 ± 0.74	4.39 ± 0.06
G87	SHARDS20005122	12:36:33.35	62:09:06.98	47.18 ± 3.81	4.33 ± 0.06
G87	SHARDS20006098	12:36:33.06	62:09:13.45	47.18 ± 3.81	4.22 ± 0.07
G88	SHARDS20006640	12:36:29.96	62:16:31.71	17.80 ± 0.51	4.39 ± 0.06
G88	SHARDS20007915	12:36:30.14	62:16:29.46	17.80 ± 0.51	4.37 ± 0.06
G89	SHARDS20007258	12:36:30.03	62:15:45.14	38.75 ± 1.50	3.54 ± 0.06
G89	SHARDS20007578	12:36:30.53	62:15:41.32	38.75 ± 1.50	3.42 ± 0.07
G90	SHARDS20007432	12:36:19.58	62:10:50.89	22.07 ± 0.37	4.34 ± 0.06
G90	SHARDS20007567	12:36:19.16	62:10:49.67	22.07 ± 0.37	4.33 ± 0.06
G91	SHARDS20008158	12:36:44.50	62:07:04.36	31.69 ± 1.60	4.19 ± 0.07
G91	SHARDS20011466	12:36:44.19	62:07:00.43	31.69 ± 1.60	4.19 ± 0.07
G92	SHARDS20009601	12:37:06.93	62:10:38.31	51.45 ± 1.63	3.41 ± 0.07
G92	SHARDS20014756	12:37:07.79	62:10:35.35	51.45 ± 1.63	3.41 ± 0.07

B

Monte Carlo Schechter function fit to the SMF

In this appendix we show the confidence intervals of the Schechter parameters obtained using Monte Carlo simulations to fit the SMF. The perturbations in the measurements are implemented injecting a Gaussian noise to each point consistent with its own Poissonian error. Additionally, the $M_{\rm star}$ bins are also perturbed, both in size and centre value. In particular, the bin size is perturbed between 0.2-0.3 dex in intervals of 0.025 dex. The central $M_{\rm star}$ value of each bin is as well shifted 0.1 dex in intervals of 0.025 dex.

At $z \sim 6$, using the SMF points up to the estimated stellar mass 90% completeness limit results in the inclusion of actually incomplete points close to the characteristic M^* knee for several $M_{\rm star}$ bin perturbations, obtaining positive values for the low mass slope. To solve this issue, only strictly increasing SMF points are considered for the Schechter function fit as we move to lower stellar masses up to our $M_{\rm star,lim}$, since further points are considered incomplete. The α slope is also constrained to $-2.8 < \alpha < -1.0$ for the fit. We are aware that this approach could bias our $z \sim 6$ low mass slope estimation towards steeper values, as warned in the text. This uncertainty is, in any case, reflected by the errors associated to the best-fit α value obtained at $z \sim 6$.

The significance contours of the three Schechter parameters at $z \sim 4$, 5 and 6 are shown in Figs. B.1, B.2 and B.3, respectively.

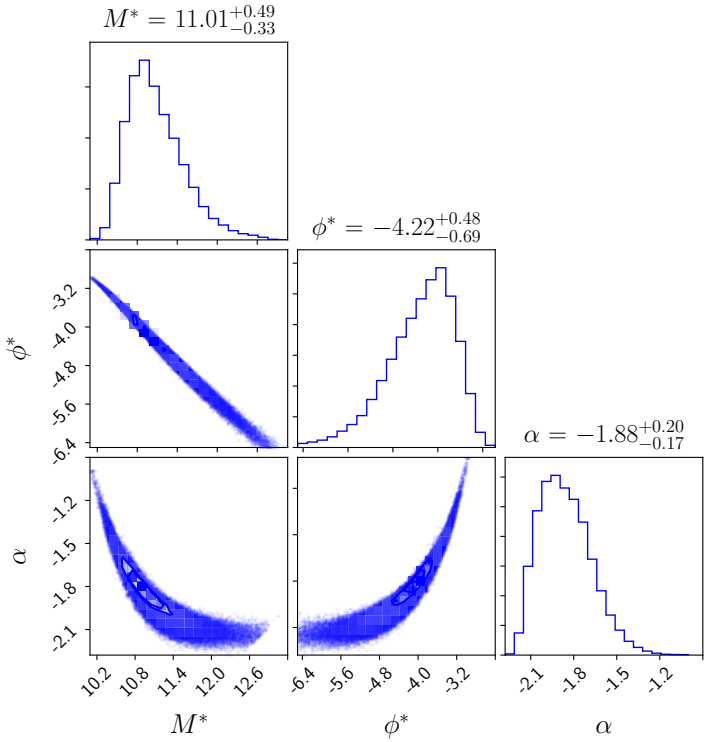

Figure B.1: Confidence intervals of the Schechter parameters from the SMF Monte Carlo fitting at $z \sim 4$. The inner and outer contours correspond to the 1σ and 3σ significance, respectively.

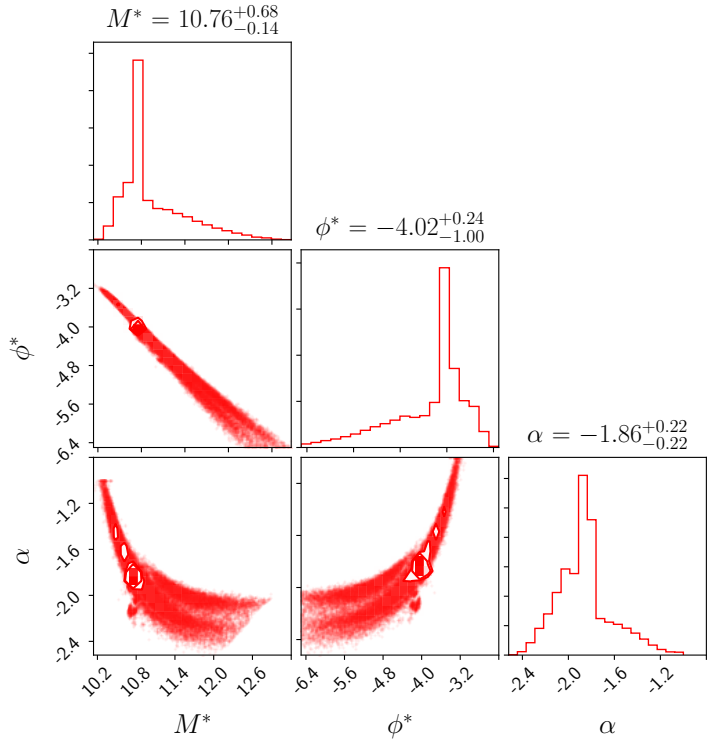

Figure B.2: Confidence intervals of the Schechter parameters from the SMF Monte Carlo fitting at $z \sim 5$. The inner and outer contours correspond to the 1σ and 3σ significance, respectively.

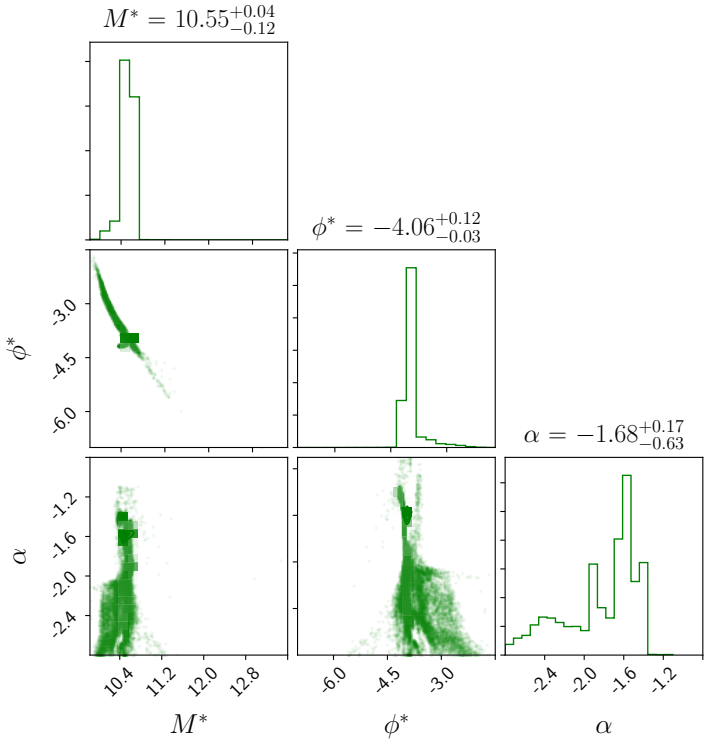

Figure B.3: Confidence intervals of the Schechter parameters from the SMF Monte Carlo fitting at $z \sim 6$. The inner and outer contours correspond to the 1σ and 3σ significance, respectively.

C

MOS spectra of observed $z \sim 5.2$ overdensity candidates

This appendix collects the 1D and 2D spectra obtained from the MOS observation described in Sec. 4.2. We show here the spectra of all the detected galaxies, 13 out of the 24 sources targeted during the observation. The quality flag of each detection, position, photometric and spectroscopic redshift of each object is summarised in Table 4.2.

Fig. C.1 corresponds to three detected sources from the Walter et al. (2012) original overdensity. Figs. C.2, C.3 and C.4 present the 8 newly discovered proto-cluster members. Two initial candidates found out of $z = 5.20 \pm 0.03$ are shown in Fig. C.5. Note, however, that the measured spectroscopic redshift of these galaxies is consistent with the previously estimated photo-z within the errors (see Table 4.2). Finally, Figs. C.6 and C.7 correspond to the four mask fillers detected.

For every image, the upper thinner horizontal frame shows the 2D spectrum, with a red circle around the source. In the lower panel, the 1D spectrum of the galaxy is represented with a solid black histogram. The solid vertical red line indicates the peak center of the Lyα emission line. The dashed blue histogram shows the sky lines spectrum rescaled down for visibility, and the zero flux is delimited by the horizontal dashed green line.

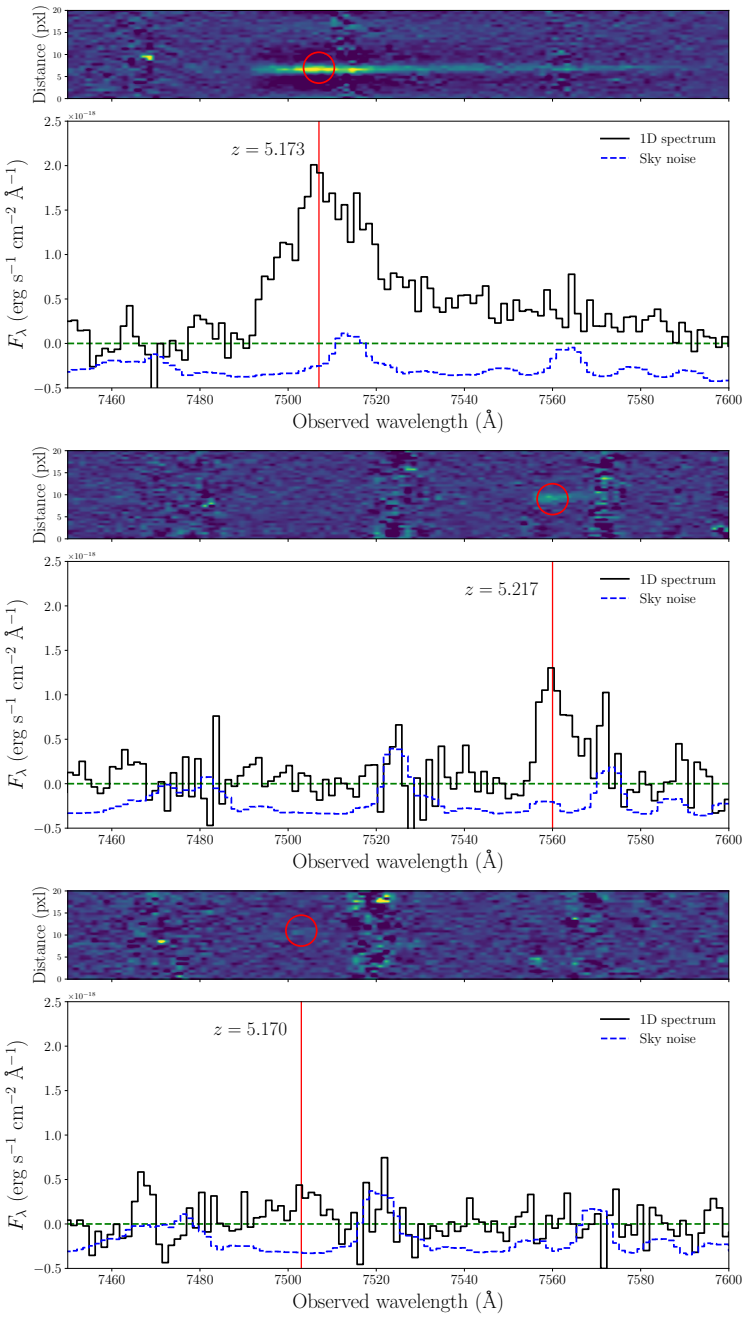

Figure C.1: 2D and 1D spectra of SHARDS20004537, SHARDS20007459 and SHARDS10006357, overdensity members also found in Walter et al. (2012).

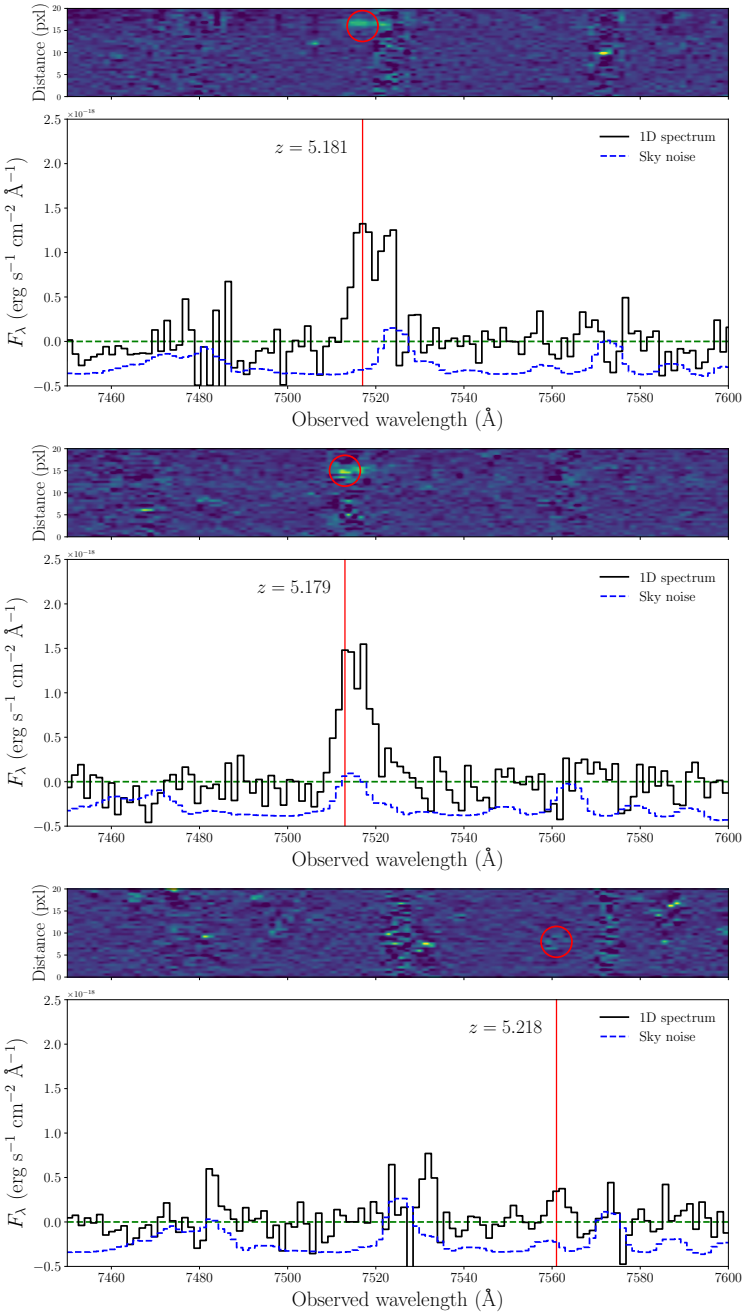

Figure C.2: 2D and 1D spectra of SHARDS20008777, SHARDS20013107 and SHARDS10006522, three newly found overdensity members.

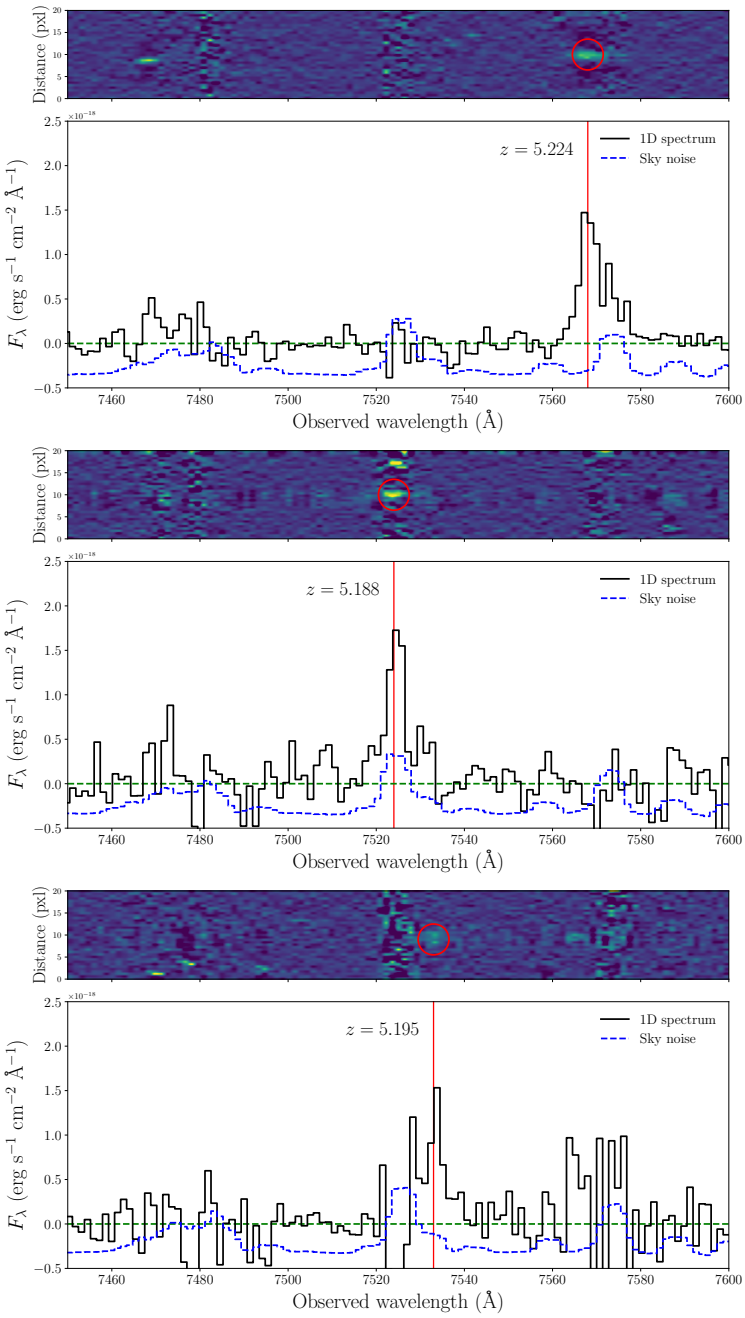

Figure C.3: 2D and 1D spectra of SHARDS20013448, SHARDS20010724 and SHARDS10018196, three newly found overdensity members.

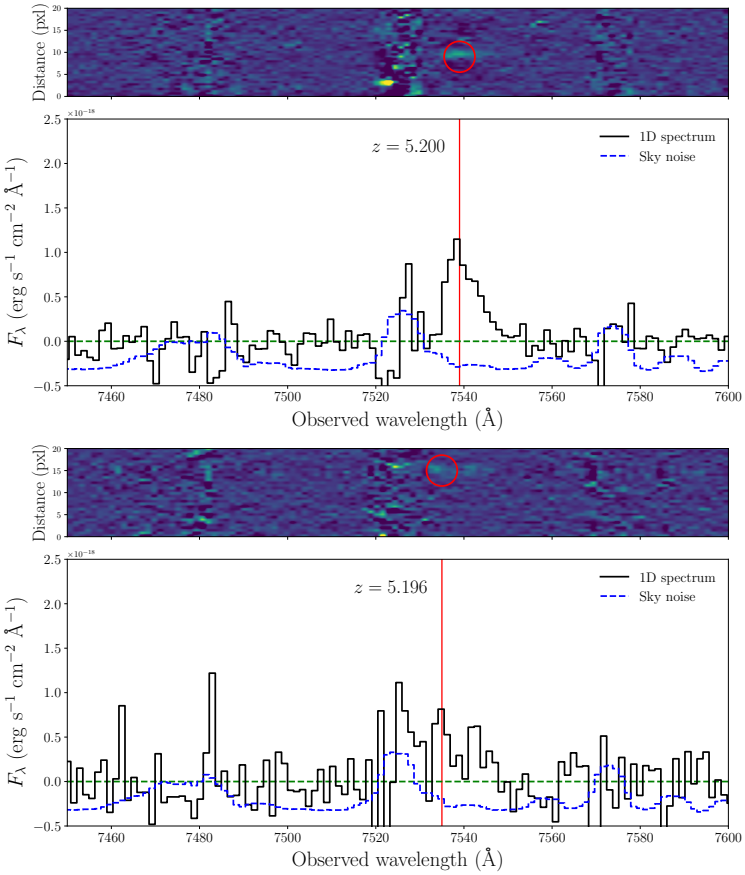

Figure C.4: 2D and 1D spectra of SHARDS10011501 and SHARDS10010385, two newly found overdensity members.

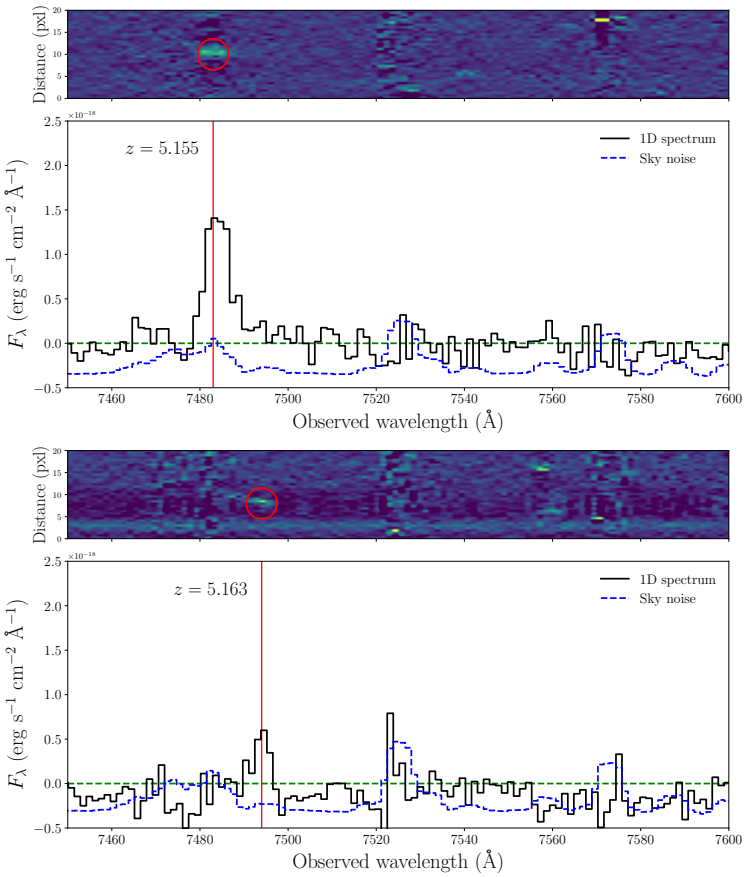

Figure C.5: 2D and 1D spectra of SHARDS20008702 and SHARDS10008210, two overdensity candidates found out of the proto-cluster.

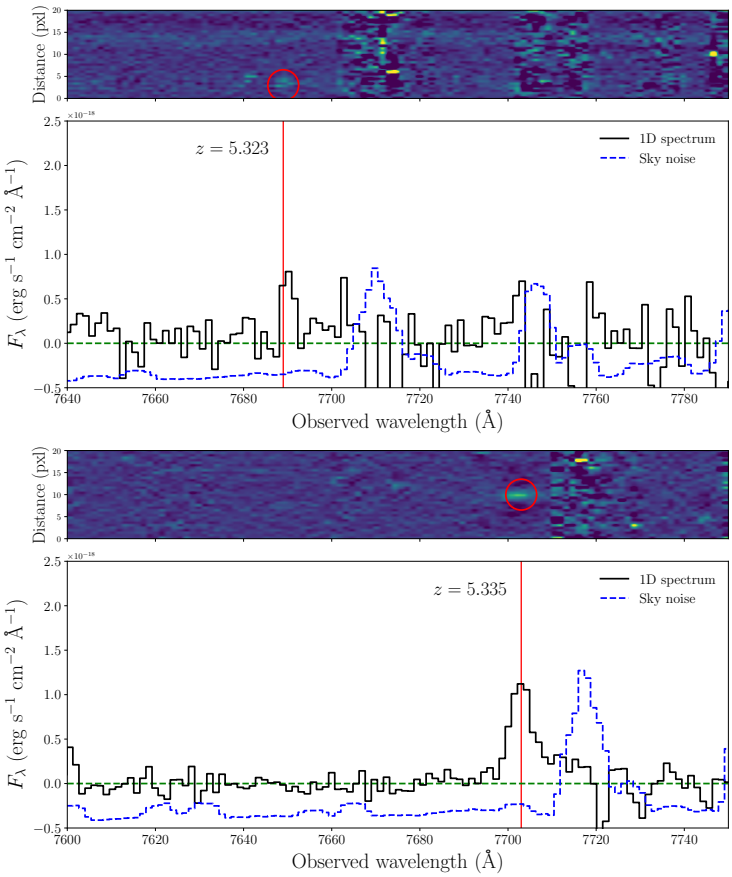

Figure C.6: 2D and 1D spectrum of SHARDS20007667 and SHARDS20011722, two mask fillers at different redshifts.

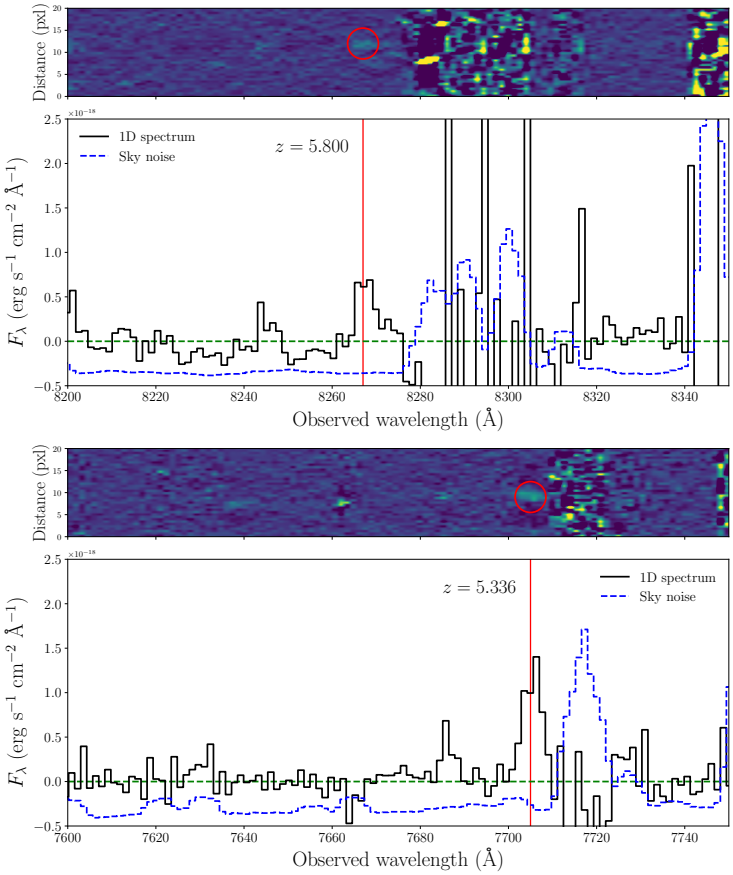

Figure C.7: 2D and 1D spectrum of SHARDS20013642 and SHARDS10008970, two mask fillers at different redshifts.

D

Machine learning clusters summary

This appendix presents a summary of the results obtained from the best GM clustering models for the SHARDS and SC4K samples at all redshift intervals. The GM clustering algorithm employed is run for a hundred initial random seeds using a diagonal covariance matrix. The optimal number of classes in each situation is determined by a minimisation of the BIC (see Sec. 5.3.1). From the models producing the best amount of classes, that presenting the highest silhouette coefficient is taken as the best clustering model.

Table D.1: Median physical properties of the sources within each ML-derived class for the SHARDS sample at $z \sim 4$. The errors shown correspond to the standard error of the medians.

Cluster ID	$M_{\rm star}$ (10^9 $M_\odot$)	Age (Myr)	Lyα EW$_0$ (Å)	β	LAEs fraction	N
0	3.6 ± 5.0	296 ± 236	114.8 ± 11.8	-2.23 ± 0.23	1.0	6
1	5.6 ± 4.1	80 ± 36	0.0 ± 0.0	-1.55 ± 0.12	0.0	82
2	2.7 ± 1.2	52 ± 325	16.6 ± 1.5	-1.76 ± 0.13	1.0	3
3	3.4 ± 2.3	61 ± 42	0.0 ± 1.3	-1.62 ± 0.07	0.28	127
4	5.5 ± 0.8	67 ± 34	0.0 ± 0.0	-1.69 ± 0.05	0.0	105
5	1.3 ± 1.1	23 ± 157	59.6 ± 10.9	-2.26 ± 0.25	1.0	16
6	2.3 ± 6.3	60 ± 66	24.4 ± 2.8	-1.87 ± 0.10	0.85	67

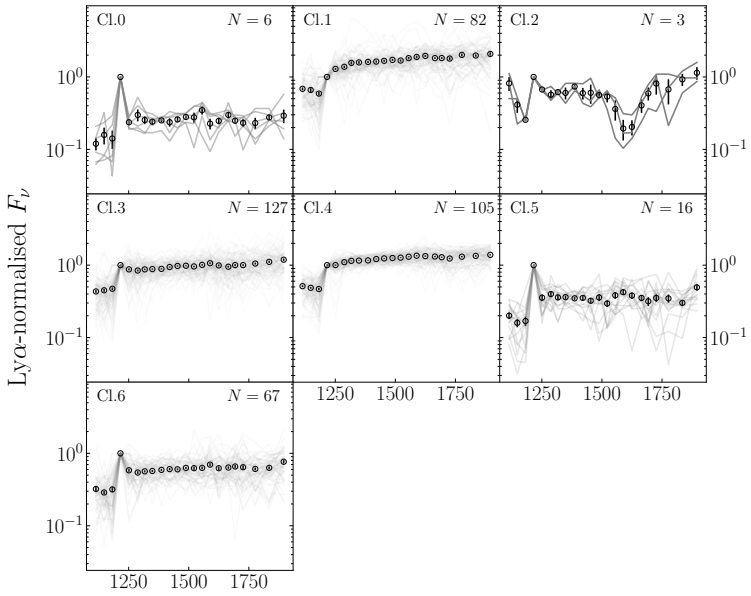

Figure D.1: Best GM clustering model for the SHARDS sample at $z \sim 4$. The open circles show the mean SED of the objects in the cluster. The error bars of the circles correspond to the standard error of the mean. Every individual SED belonging to each class is represented by a faded grey line.

Table D.2: Median physical properties of the sources within each ML-derived class for the SHARDS sample at $z \sim 5$. The errors shown correspond to the standard error of the medians.

Cluster ID	$M_{\rm star}$ ($10^9\ M_\odot$)	Age (Myr)	Lyα EW$_0$ (Å)	β	LAEs fraction	N
0	3.9 ± 6.2	139 ± 103	16.4 ± 11.2	-2.07 ± 0.29	0.90	10
1	7.0 ± 1.5	70 ± 37	0.0 ± 15.4	-1.82 ± 0.10	0.11	81
2	10.9 ± 7.1	575 ± 93	20.8 ± 8.0	-2.04 ± 0.24	0.70	20

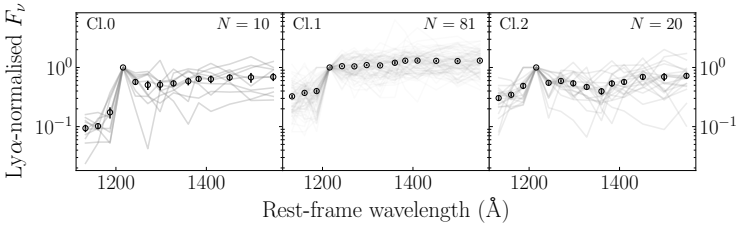

Figure D.2: Best GM clustering model for the SHARDS sample at $z \sim 5$. The open circles show the mean SED of the objects in the cluster. The error bars of the circles correspond to the standard error of the mean. Every individual SED belonging to each class is represented by a faded grey line.

Table D.3: Median physical properties of the sources within each ML-derived class for the SHARDS sample at $z \sim 6$. The errors shown correspond to the standard error of the medians.

Cluster ID	$M_{\rm star}$ (10^9 $M_\odot$)	Age (Myr)	Lyα EW$_0$ (Å)	β	LAEs fraction	N
0	4.0 ± 2.6	316 ± 258	30.1 ± 13.9	-2.38 ± 0.14	1.00	2
1	7.9 ± 5.3	79 ± 61	0.0 ± 55.3	-1.80 ± 0.18	0.36	22

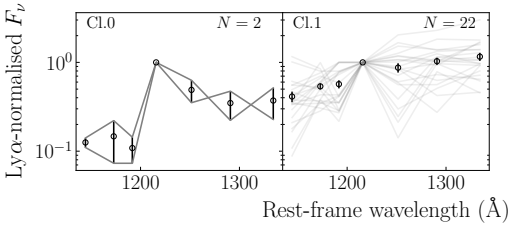

Figure D.3: Best GM clustering model for the SHARDS sample at $z \sim 6$. The open circles show the mean SED of the objects in the cluster. The error bars of the circles correspond to the standard error of the mean. Every individual SED belonging to each class is represented by a faded grey line.

Table D.4: Median physical properties of the sources within each ML-derived class for the SC4K-COSMOS sample at $z \sim 3$. The errors shown correspond to the standard error of the medians.

Cluster ID	$M_{\rm star}$ (10^9 $M_\odot$)	Age (Myr)	$F(\mathrm{Ly}\alpha)$ (10^{-17} erg s^{-1} cm^{-2})	β	N
0	0.3 ± 6.1	8 ± 12	0.1 ± 38.6	-2.44 ± 0.01	548
1	3.7 ± 9.0	263 ± 10	8.2 ± 97.4	-2.00 ± 0.02	656
2	9.6 ± 6.4	217 ± 15	7.8 ± 1.3	-1.57 ± 0.12	324
3	1.1 ± 6.0	150 ± 10	8.7 ± 50.9	-2.44 ± 0.04	745
4	5.1 ± 4.4	267 ± 24	0.1 ± 3.9	-1.89 ± 0.24	248
5	0.1 ± 42.0	7 ± 18	8.4 ± 31.9	-2.44 ± 0.11	284
6	20.9 ± 561	282 ± 157	7.6 ± 68.5	-2.12 ± 0.99	6

Table D.5: Median physical properties of the sources within each ML-derived class for the SC4K-COSMOS sample at $z \sim 4$. The errors shown correspond to the standard error of the medians.

Cluster ID	$M_{\rm star}$ (10^9 $M_\odot$)	Age (Myr)	$F(\mathrm{Ly}\alpha)$ (10^{-17} erg s^{-1} cm^{-2})	β	N
0	91.5 ± 215	136 ± 142	6.1 ± 82.1	-0.88 ± 1.13	5
1	0.9 ± 12.1	9 ± 30	6.5 ± 43.0	-2.44 ± 0.04	58
2	0.5 ± 18.9	9 ± 34	7.4 ± 41.6	-2.44 ± 0.03	61
3	2.9 ± 69.9	16 ± 33	7.4 ± 1.1	-2.44 ± 0.14	32
4	687 ± 231	244 ± 35	6.6 ± 1.3	-2.44 ± 1.00	27
5	32.8 ± 484	215 ± 76	5.9 ± 1.1	-1.69 ± 0.20	14
6	10.7 ± 91.2	205 ± 39	6.3 ± 60.6	-2.27 ± 0.66	36

Table D.6: Median physical properties of the sources within each ML-derived class for the SC4K-COSMOS sample at $z \sim 5$. The errors shown correspond to the standard error of the medians.

Cluster ID	$M_{\rm star}$ (10^9 $M_\odot$)	Age (Myr)	$F(\mathrm{Ly}\alpha)$ (10^{-17} erg s^{-1} cm^{-2})	β	N
0	3.9 ± 42.5	11 ± 20	7.2 ± 33.2	-2.44 ± 0.33	98
1	5.0 ± 18.0	58 ± 23	6.9 ± 63.8	-2.27 ± 0.11	67
2	3.6 ± 32.7	19 ± 20	7.0 ± 56.8	-2.44 ± 0.12	108
3	5.0 ± 20.0	10 ± 78	4.3 ± 94.0	-2.44 ± 0.00	5
4	53.7 ± 675	11 ± 66	5.6 ± 1.4	-2.44 ± 3.00	7
5	484 ± 252	67 ± 31	7.6 ± 1.3	-2.44 ± 1.60	18

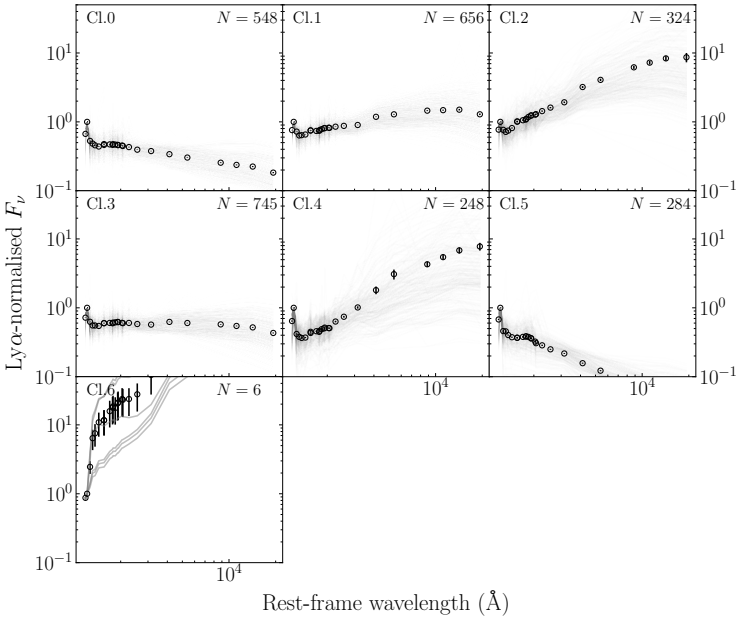

Figure D.4: Best GM clustering model for the SC4K-COSMOS sample at $z \sim 3$. The open circles show the mean SED of the objects in the cluster. The error bars of the circles correspond to the standard error of the mean. Every individual SED belonging to each class is represented by a grey line faded in proportion to the number of objects within the class.

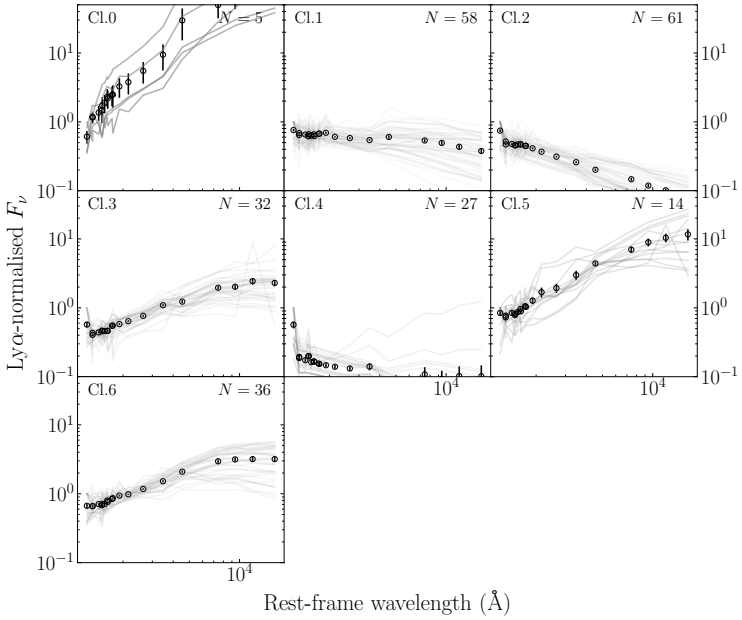

Figure D.5: Best GM clustering model for the SC4K-COSMOS sample at $z \sim 4$. The open circles show the mean SED of the objects in the cluster. The error bars of the circles correspond to the standard error of the mean. Every individual SED belonging to each class is represented by a grey line faded in proportion to the number of objects within the class.

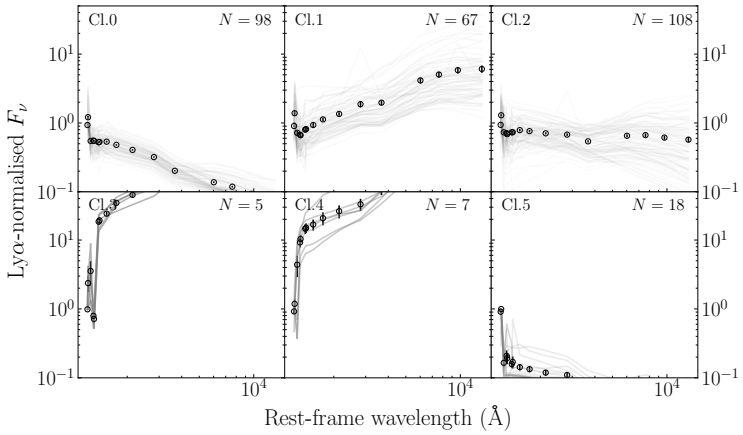

Figure D.6: Best GM clustering model for the SC4K-COSMOS sample at $z \sim 5$. The open circles show the mean SED of the objects in the cluster. The error bars of the circles correspond to the standard error of the mean. Every individual SED belonging to each class is represented by a grey line faded in proportion to the number of objects within the class.

Table D.7: Median physical properties of the sources within each ML-derived class for the SC4K-COSMOS sample at $z \sim 6$. The errors shown correspond to the standard error of the medians.

Cluster ID	$M_{\rm star}$ (10^{10} $M_\odot$)	Age (Myr)	F(Lyα) (10^{-17} erg s^{-1} cm^{-2})	β	N
0	46.5 ± 238	41 ± 46	6.0 ± 1.9	-1.88 ± 1.76	21
1	398 ± 312	48 ± 30	3.7 ± 1.1	-1.30 ± 4.98	10
2	1151 ± 1249	190 ± 115	3.4 ± 44.0	-1.78 ± 0.37	6
3	17.9 ± 215	56 ± 34	2.0 ± 46.5	-1.93 ± 1.68	45
4	169 ± 3239	309 ± 173	3.4 ± 2.3	-2.11 ± 0.23	4
5	9.5 ± 1916	17 ± 97	3.4 ± 1.4	-2.44 ± 0.12	11
6	30.5 ± 1127	121 ± 78	1.6 ± 3.2	-2.08 ± 8.81	3

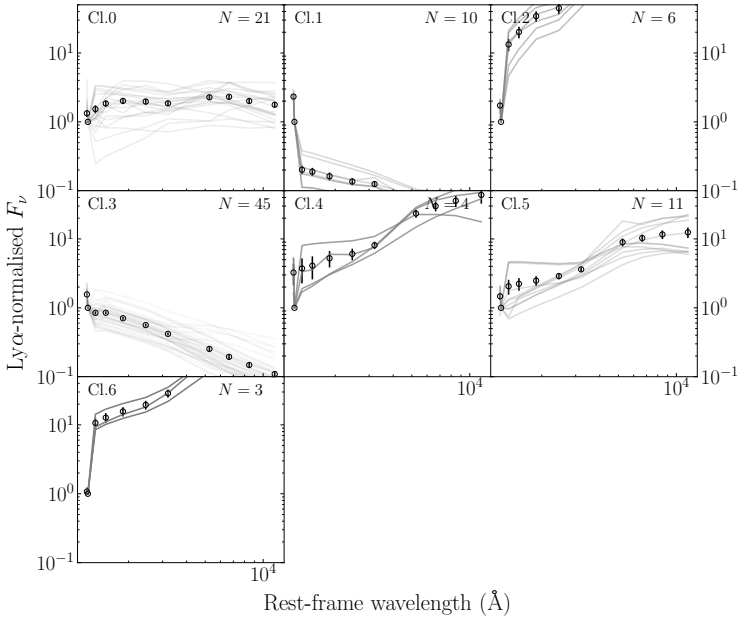

Figure D.7: Best GM clustering model for the SC4K-COSMOS sample at $z \sim 6$. The open circles show the mean SED of the objects in the cluster. The error bars of the circles correspond to the standard error of the mean. Every individual SED belonging to each class is represented by a grey line faded in proportion to the number of objects within the class.

Acknowledgements

When people ask what pushes us to do a Ph.D. in Astrophysics, we often think of the thirst for knowledge and the curiosity to unveil (or at least contribute to) the yet unknown mysteries of the Cosmos. Alternatively, we answer that we love the overwhelming feeling that comes from looking to the vastness of the Universe. Nothing is more humbling than working with galaxies of billions of solar masses to relativise your existence and problems. But, above all, I decided to do a Ph.D. in Astrophysics to challenge myself.

These last years have been such an adventure. I first arrived at the IAC as the young blacksmith's son who leaves his little village to learn magic in the mightiest citadel of the kingdom and suddenly finds himself surrounded by great wizards whose fascinating abilities escape his knowledge. I'm not going to pretend that at the end of his trip the blacksmith's son has become an archmage. We could say I now know some tricks, but that's also because this isn't the end of the trip but only of the first chapter.

As in all the adventures, there has been dark and bright times, restless searches in the ancient manuscripts and joyful discoveries, doubts, inquisitor referees and benevolent tutors, long travels to far away lands, small defeats and great victories. But the protagonist of our tale wouldn't have been able to achieve his exploit without the help of many other characters.

First of all, of course, I want to thank my supervisors, Drs. José Miguel Rodríguez Espinosa and Casiana Muñoz Tuñón. I've always felt incredibly comfortable with you since the very first day, and, besides your good guidance, I really appreciate that you've been so respectful with my work, meal and training schedule. You'll always be my scientific parents.

Apart from my direct supervisors, there are many other great scientists I've met during these years who have made me a better researcher in one way or another. In fact, too many to name them all here, but there are a few to whom I'd like to show special gratefulness. To Dr. Ángel Bongiovanni, for always

being helpful and inspiring, transmitting calm and at the same time passion for what we do. To Dr. Helmut Dannerbauer, for introducing me in the world of proto-clusters, moving me towards one of my favourite findings of this thesis and giving me some good tips regarding academic life. And to Dr. David Sobral, for his support, patience, humility and priceless help during the last year of work. It has been a pleasure to collaborate with you all and I really hope to keep doing so in the upcoming years.

But despite all I've learned from those erudite people, no one has been more important for this sorcerer's apprentice than the Doctorandos brotherhood, with a deserved special mention for Alejandro Lumbreras, who has been a loyal companion all along our personal crusade against the 25-headed SHARDS hydra. You guys have been my brothers and sisters in the IAC catacombs. Lunches with you have been an incredibly fun and enriching experience, both in serious discussions and hilarious jokes. You're undoubtedly the greatest loot I take from this journey. Wherever I go now, I know I'll miss you.

From outside of academia, I have to acknowledge my parents for having given me an exceptional education at home, a bunch of opportunities that have taken me here and, above all, much love. To my siblings, you're the three single human beings I love the most in this entire low-z galaxy. Life seems much easier knowing that no matter what sinuous path I take, I got the luck of being part of this unbreakable group of six clowns that we call family, or as they say in Japanese: "¡Al turrón!".

Among the people who have helped me to endure this epoch of my life, I have to give special acknowledgements to the Bulbo Raquídeo, for providing me laughs and a good rest defending the tower every other weekend; to Cárceles for being always there in the shadows and, not mattering when we meet, making it look like if I had never left Málaga; and to my beloved Captain "No Sé Cuántos", for being the person that makes me laugh the most at the end of many hard days while having dinner and playing card games at the other side of the magic mirror. Special thanks to all the people from "3 príncipes" and "Athenea" gyms for making it possible to move my mind from the hydrogen to the irons every day. You've been an important part of my life these years. I'll not forget you.

Last, but certainly not least, I'd like to thank the entire Haro and Arrabal families for being always so supportive and enthusiastic with my work, it's for me a blessing having such "fronic" relatives and an honour wearing you in my surnames every time my name appears in a work.

Thank you all.